INFECTION, INFLAMMATION, CARDIOVASCULAR DISEASES AND NEURODEGENERATION

EDITED BY: Deng-Feng Zhang, Gjumrakch Aliev, Feiqi Zhu and Xian-Le Bu
PUBLISHED IN: Frontiers in Aging Neuroscience, Frontiers in Neuroscience and Frontiers in Cellular Neuroscience

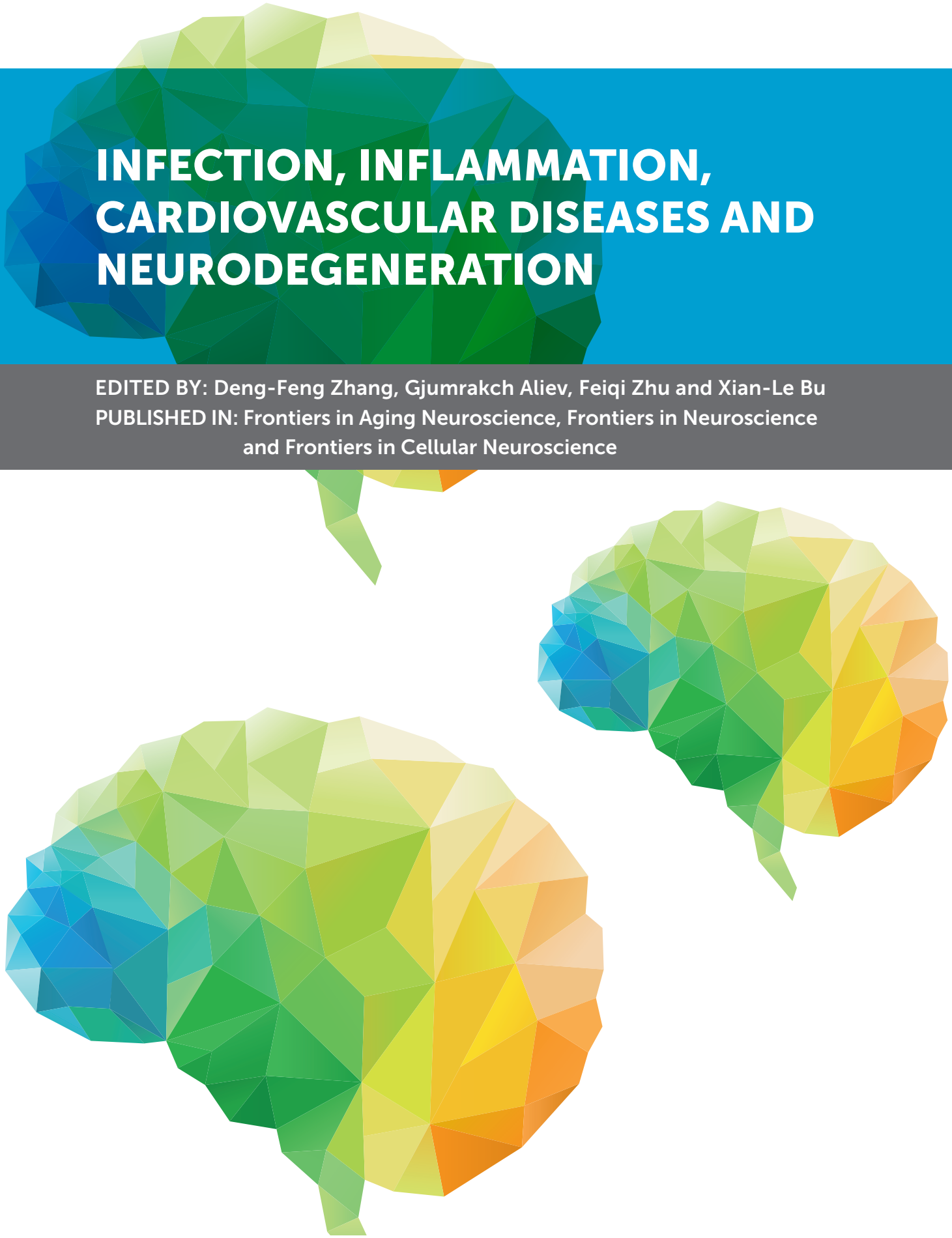

frontiers Research Topics

frontiers

ISSN 1664-8714
ISBN 978-2-88971-543-5
DOI 10.3389/978-2-88971-543-5

About Frontiers

Frontiers is more than just an open-access publisher of scholarly articles: it is a pioneering approach to the world of academia, radically improving the way scholarly research is managed. The grand vision of Frontiers is a world where all people have an equal opportunity to seek, share and generate knowledge. Frontiers provides immediate and permanent online open access to all its publications, but this alone is not enough to realize our grand goals.

Frontiers Journal Series

The Frontiers Journal Series is a multi-tier and interdisciplinary set of open-access, online journals, promising a paradigm shift from the current review, selection and dissemination processes in academic publishing. All Frontiers journals are driven by researchers for researchers; therefore, they constitute a service to the scholarly community. At the same time, the Frontiers Journal Series operates on a revolutionary invention, the tiered publishing system, initially addressing specific communities of scholars, and gradually climbing up to broader public understanding, thus serving the interests of the lay society, too.

Dedication to Quality

Each Frontiers article is a landmark of the highest quality, thanks to genuinely collaborative interactions between authors and review editors, who include some of the world's best academicians. Research must be certified by peers before entering a stream of knowledge that may eventually reach the public - and shape society; therefore, Frontiers only applies the most rigorous and unbiased reviews.
Frontiers revolutionizes research publishing by freely delivering the most outstanding research, evaluated with no bias from both the academic and social point of view. By applying the most advanced information technologies, Frontiers is catapulting scholarly publishing into a new generation.

What are Frontiers Research Topics?

Frontiers Research Topics are very popular trademarks of the Frontiers Journals Series: they are collections of at least ten articles, all centered on a particular subject. With their unique mix of varied contributions from Original Research to Review Articles, Frontiers Research Topics unify the most influential researchers, the latest key findings and historical advances in a hot research area! Find out more on how to host your own Frontiers Research Topic or contribute to one as an author by contacting the Frontiers Editorial Office: frontiersin.org/about/contact

INFECTION, INFLAMMATION, CARDIOVASCULAR DISEASES AND NEURODEGENERATION

Topic Editors:
Deng-Feng Zhang, Kunming Institute of Zoology (CAS), China
Gjumrakch Aliev, GALLY International Biomedical Research, United States
Feiqi Zhu, Shenzhen University, China
Xian-Le Bu, Third Military Medical University, China

Citation: Zhang, D.-F., Aliev, G., Zhu, F., Bu, X.-L., eds. (2021). Infection, Inflammation, Cardiovascular diseases and Neurodegeneration. Lausanne: Frontiers Media SA. doi: 10.3389/978-2-88971-543-5

Table of Contents

frontiers in Neuroscience

EDITORIAL
published: 09 September 2021
doi: 10.3389/fnins.2021.750172

Editorial: Infection, Inflammation, Cardiovascular Diseases, and Neurodegeneration

Deng-Feng Zhang[1]*, *Xian-Le Bu*[2], *Gjumrakch Aliev*[3] and *Feiqi Zhu*[4]*

[1] Key Laboratory of Animal Models and Human Disease Mechanisms, Kunming Institute of Zoology, Chinese Academy of Sciences, Kunming, China, [2] Department of Neurology and Centre for Clinical Neuroscience, Daping Hospital, Third Military Medical University, Chongqing, China, [3] GALLY International Biomedical Research Institute, San Antonio, TX, United States, [4] Department of Neurology, The Third Affiliated Hospital, Shenzhen University, Shenzhen, China

Keywords: infection, inflammation, neurodegeneration, immune, vasculature

Editorial on the Research Topic

Infection, Inflammation, Cardiovascular Diseases, and Neurodegeneration

The global burden of neurodegenerative disorders, such as Alzheimer's disease (AD), Parkinson's disease (PD), vascular dementia, and stroke increases rapidly (GBD Neurology Collaborators, 2019). Great efforts are needed to promote the understanding, treatment, and prevention of these diseases. Although remarkable progress have been made in the comprehension of the pathophysiology of neurodegeneration, the etiology is not yet completely understood. Immune system is highly involved in the development of neurodegeneration, since immune genes play a prominent part in genetic risk of typical neurodegenerative diseases (Jonsson et al., 2013; Zhang et al., 2019; Harding et al., 2021). Investigation of immune imbalance, infection and inflammation in neurodegeneration has been a major focus of the field. In this Research Topic, a dozen papers has been compiled, covering multiple aspects regarding inflammation in neurodegeneration.

Microglia activation has been a major process during the development of neurodegeneration. Understanding the activation and regulation of microglia is essential for the management of neuroinflammation. Singh et al. showed that Japanese encephalitis virus (JEV) infection increases chemokines (C-C motif) receptor 2 (CCR2) mediated microglia activation. CCR2 inhibition reduces microglia activation and neurotoxic proinflammatory mediators after JEV infection. Their results provided an important therapeutic target for regulating the microglia activation in pathogenesis of neurodegenerative diseases. In addition to virus infection, bacterial infection such as Chronic Periodontitis (CP) was supposed to be involved in the development of AD (Kamer et al., 2015; Chen et al., 2017). To explore the cross-links between periodontitis and AD, Rong et al. analyzed serum proteins from CP patients and controls using the two-dimensional differential in-gel electrophoresis proteomic approach. They found that 10 serum proteins including cathepsin B (CTSB) were altered in CP patients, and serum concentration of CTSB has a negative correlation with cognition. Importantly, in human neuroblastoma SK-N-SH cells overexpressing wild-type APP695, Porphyromonas gingivalis treatment increases the protein level of CTSB in a TNF-α dependent manner. The increase of CTSB then leads to a prominent increase in $A\beta_{1-40}$ and $A\beta_{1-42}$ in the cell lysates, which could be rescued by CTSB inhibition. Their results provided a TNF-α-CTSB based molecular mechanism underlying the increased risk of AD in CP patients.

Besides pathogens, it has been demonstrated that neurological changes correlated with changes in the gut microbiota. Jeon et al. investigated the changes in the gut microbiota composition and diversity of the middle cerebral artery occlusion ischemic stroke pig model. They found elevated systemic inflammation and reduced microbial diversity at acute stage of stroke. For

Edited and reviewed by:
Wendy Noble,
King's College London,
United Kingdom

***Correspondence:**
Deng-Feng Zhang
zhangdengfeng@mail.kiz.ac.cn
Feiqi Zhu
Zfqzsu2004@aliyun.com

Specialty section:
This article was submitted to Neurodegeneration, a section of the journal Frontiers in Neuroscience

Received: *30 July 2021*
Accepted: *17 August 2021*
Published: *09 September 2021*

Citation:
Zhang D-F, Bu X-L, Aliev G and Zhu F (2021) Editorial: Infection, Inflammation, Cardiovascular Diseases, and Neurodegeneration. Front. Neurosci. 15:750172. doi: 10.3389/fnins.2021.750172

instance, abundance of the Proteobacteria was significantly increased, while Firmicutes and Lactobacillus decreased poststroke. Interestingly, the microbial pattern of poststroke model returned to prestroke-like status at late stage of stroke, suggesting the plasticity of gut microbiome in the course of stroke. Their findings might benefit the assessment of stroke pathology and the development of therapeutic targets.

Systemic inflammation might be the potential link between infection and neurological alterations, as indicated by Yan et al. and Liu et al.. The long-term administration of levodopa (L-dopa), the gold-standard treatment for PD, may lead to L-dopa-induced dyskinesia (LID). Yan et al. investigated how systemic inflammation exacerbates LID. They constructed a LID rat model under stimulation of lipopolysaccharides (LPS) and long-term treatment of L-dopa. Dyskinesia-related phenotypes, glia activation, and inflammatory responses were then evaluated at several time points. They found that the LPS injection activated the glia and inflammatory response in the striatum of LID rats, and the systemic inflammation exacerbated the intensity of abnormal involuntary movements induced by L-dopa treatment. Inhibition of the inflammatory response improved the behavioral dysfunction. This study suggests that control of systemic inflammation is crucial for management of drug reaction and complications in neurodegenerative diseases. In another study, Liu et al. assessed the effect of LPS-induced systemic inflammation on brain functional connectivity in aged rats. They found that rats with intraperitoneal injected LPS showed higher levels of inflammatory cytokines and astrocyte activation in the hippocampus, which leads to decreased functional connectivity on the right orbital cortex, right olfactory bulb, and left hippocampus, and finally impaired memory performance. Inhibition of the inflammatory activation in the hippocampus improved the memory performance and functional connectivity. These data demonstrated that inhibiting neuroinflammation improves the brain functional connectivity.

Sepsis-associated delirium (SAD) is another good model for investigating the interaction between brain dysfunction and inflammatory responses. Li et al. performed a retrospective study analyzing the association between SAD and lymphocyte counts in the peripheral blood, alongside a prospective trial evaluating the predictive value of lymphocyte for early diagnosis of SAD. In the retrospective analysis, they showed that lymphocyte counts in the SAD group were significantly higher than in non-delirious counterparts. Importantly, they found that an NK cell count cut-off value of 87 cells/ml in septic patients at ICU admission was predictive of delirium with a sensitivity of 80.2% and specificity of 80.8%. These preliminary but promising data showed the value of measuring peripheral lymphocyte for monitoring the pathophysiological process in the central nerve system.

The blood-brain barrier (BBB), which is consisted of vascular, immune, and neural cells, is the key for the interaction between immune system and the central nervous system. BBB dysfunction are frequently observed in the pathology and progression of neurological diseases (Xiao et al., 2020). Since elevated pulse pressure can cause BBB dysfunction that may drive or contribute to adverse neurological changes, Levin et al. reviewed the impact of elevated pulse pressure on microvascular damage and discussed efforts to repurpose blood pressure medications to prevent or treat dementia. They proposed that new drugs or devices should be developed to safely reduce elevated pulse pressure specifically to the brain. As indicated by Levin et al., vascular risk factors such as hypertension and diabetes are associated with cognitive decline and the risk of dementia (Purnell et al., 2009). To investigate whether the aggregation of vascular risk factors modulates the spontaneous brain activity, Zhuang et al. performed a resting-state functional MRI scanning of patients with mild cognitive impairment (MCI). They found that MCI patients with high vascular risk showed decreased amplitude of low-frequency fluctuation in the left hippocampus compared to that of healthy subjects with high vascular risk. This preliminary data highlighted a potential imaging mechanism underlying vascular contribution to brain activity.

As shown above, cytokines such as interleukins and chemokines such as CCR2 play pivotal and comprehensive roles in neurodegenerative diseases, however, the exact activating pathways and cell-type specificities of such inflammatory molecules remained unclear. Chen et al. reviewed the way how microglia, astrocyte, and oligodendrocyte respond to a typical interleukin, the IL-17A, and summarized plant compounds targeting IL-17A. Considering the complicated activation and regulation pattern of cytokines, more focused and fine-grained examination of the exact roles of cytokines in neurodegenerative diseases is needed.

The pathogen hypothesis, which postulates a causal role of infectious agents (e.g., herpes virus) in the development of AD, has been a non-negligible topic, whereas amyloid beta is recognized to be an antimicrobial peptide that protects against fungal, bacterial, and viral infection (Gosztyla et al., 2018). However, it is unclear when the hypothesis will benefit the clinical practice. Nevertheless, it is time to "Connect the Dots," as proposed by Ethan R. Roy and Wei Cao from Baylor College of Medicine. In their Perspective, they summarized the actions and roles of Aβ in AD neuropathogenesis, especially in the microbial entrapment related processes. They also described the activation of the IFN antiviral pathway and depict a multilayered connection between antiviral immune response and other agents and factors relevant to AD. Regardless of the unclear molecular mechanism underlying the antiviral immune response in both the CNS and peripheral system, taking anti-infection into consideration for the development of AD therapy might be a crucial step.

In summary, the articles and reviews in this Research Topic covered multiple aspects including key molecules, pathways, cell types, and brain regions in typical neurodegeneration regarding viral and bacterial infection, gut microbiota, and systemic inflammation. These scattered but diverse studies broadened the boundary of discipline of neuroinflammation. Nevertheless, there are much broader unknown area regarding inflammation and neurodegeneration. Hopefully, more and more studies and projects are ongoing to uncover the intricate relationship between immunogical and vascular factors and neurodegenerative disorders.

AUTHOR CONTRIBUTIONS

All authors listed have made a substantial, direct and intellectual contribution to the work, and approved it for publication.

FUNDING

This work was supported by the National Natural Science Foundation of China (82022017 and 31970965), the Youth Innovation Promotion Association of Chinese Academy of Sciences, the Applied Basic Research Foundation of Yunnan Province (2019FA009 and 2019FI015), the Sanming Project of Medicine in Shenzhen (SZSM201801014), and the Key project of Shenzhen Science and Technology Innovation Committee (JCYJ20200109143431341).

ACKNOWLEDGMENTS

We would like to thank all authors, reviewers, and editors of this Research Topic.

REFERENCES

Chen, C., Wu, Y., and Chang, Y. (2017). Association between chronic periodontitis and the risk of Alzheimer's disease: a retrospective, population-based, matched-cohort study. *Alzheimers Res. Ther*. 9:56. doi: 10.1186/s13195-017-0282-6

GBD Neurology Collaborators (2019). Global, regional, and national burden of neurological disorders, 1990-2016: a systematic analysis for the Global Burden of Disease Study 2016. *Lancet Neurol*. 18, 459–480. doi: 10.1016/S1474-4422(18)30499-X

Gosztyla, M., Brothers, H., and Robinson, S. (2018). Alzheimer's Amyloid-beta is an antimicrobial peptide: a review of the evidence. *J. Alzheimers Dis.* 62, 1495–1506. doi: 10.3233/JAD-171133

Harding, O., Evans, C., Ye, J., Cheung, J., Maniatis, T., and Holzbaur, E. L. (2021). ALS- and FTD-associated missense mutations in TBK1 differentially disrupt mitophagy. *Proc. Natl. Acad. Sci. U.S.A*. 118:e2025053118. doi: 10.1073/pnas.2025053118

Jonsson, T., Stefansson, H., Steinberg, S., Jonsdottir, I., Jonsson, P., Snaedal, J., et al. (2013). Variant of TREM2 associated with the risk of Alzheimer's disease. *N. Engl. J. Med*. 368, 107–116. doi: 10.1056/NEJMoa1211103

Kamer, A., Pirraglia, E., Tsui, W., Rusinek, H., Vallabhajosula, S., Mosconi, L., et al. (2015). Periodontal disease associates with higher brain amyloid load in normal elderly. *Neurobiol. Aging* 36, 627–633. doi: 10.1016/j.neurobiolaging.2014.10.038

Purnell, C., Gao, S., Callahan, C., and Hendrie, H. (2009). Cardiovascular risk factors and incident Alzheimer disease: a systematic review of the literature. *Alzheimer Dis. Assoc. Disord.* 23, 1–10. doi: 10.1097/WAD.0b013e318187541c

Xiao, M., Xiao, Z., Yang, B., Lan, Z., and Fang, F. (2020). Blood-brain barrier: more contributor to disruption of central nervous system homeostasis than victim in neurological disorders. *Front. Neurosci*. 14:764. doi: 10.3389/fnins.2020.00764

Zhang, D., Fan, Y., Xu, M., Wang, G., Wang, D., Li, J., et al. (2019). Complement C7 is a novel risk gene for Alzheimer's disease in Han Chinese. *Natl. Sci. Rev*. 6, 257–274. doi: 10.1093/nsr/nwy127

Conflict of Interest: The authors declare that the research was conducted in the absence of any commercial or financial relationships that could be construed as a potential conflict of interest.

Publisher's Note: All claims expressed in this article are solely those of the authors and do not necessarily represent those of their affiliated organizations, or those of the publisher, the editors and the reviewers. Any product that may be evaluated in this article, or claim that may be made by its manufacturer, is not guaranteed or endorsed by the publisher.

frontiers in Neuroscience

PERSPECTIVE
published: 24 June 2020
doi: 10.3389/fnins.2020.00669

Pulse Pressure: An Emerging Therapeutic Target for Dementia

Rachel A. Levin[1,2], Mark H. Carnegie[1,2] and David S. Celermajer[1,3]**

[1] The Brain Protection Company, Sydney, NSW, Australia, [2] M.H. Carnegie & Co., Sydney, NSW, Australia, [3] The Heart Research Institute, Sydney, NSW, Australia

Elevated pulse pressure can cause blood-brain barrier dysfunction and subsequent adverse neurological changes that may drive or contribute to the development of dementia with age. In short, elevated pulse pressure dysregulates cerebral endothelial cells and increases cellular production of oxidative and inflammatory molecules. The resulting cerebral microvascular damage, along with excessive pulsatile mechanical force, can induce breakdown of the blood-brain barrier, which in turn triggers brain cell impairment and death. We speculate that elevated pulse pressure may also reduce the efficacy of other therapeutic strategies for dementia. For instance, BACE1 inhibitors and anti-amyloid-β biologics reduce amyloid-β deposits in the brain that are thought to be a cause of Alzheimer's disease, the most prevalent form of dementia. However, upregulation of oxidative and inflammatory molecules and increased amyloid-β secretion by cerebral endothelial cells exposed to elevated pulse pressure may hinder cognitive improvements with these drugs. Additionally, stem or progenitor cell therapy has the potential to repair blood-brain barrier damage, but chronic oxidative and inflammatory stress due to elevated pulse pressure can inhibit stem and progenitor cell regeneration. Finally, we discuss current efforts to repurpose blood pressure medications to prevent or treat dementia. We propose that new drugs or devices should be developed to safely reduce elevated pulse pressure specifically to the brain. Such novel technologies may alleviate an entire downstream pathway of cellular dysfunction, oxidation, inflammation, and amyloidogenesis, thereby preventing pulse-pressure-induced cognitive decline. Furthermore, these technologies may also enhance efficacy of other dementia therapeutics when used in combination.

Keywords: pulse pressure, carotid wave intensity, blood brain barrier, inflammation, oxidation, amyloidogenesis, microbleed, cognitive decline and dementia

OPEN ACCESS

Edited by:
Feiqi Zhu,
Third Affiliated Hospital, Shenzhen University, China

Reviewed by:
Peiying Li,
Renji Hospital, School of Medicine Shanghai Jiaotong University, China
Nataliya G. Kolosova,
Institute of Cytology and Genetics, Russian Academy of Sciences, Russia

****Correspondence:***
Rachel A. Levin
rachel.levin@mhcarnegie.com
David S. Celermajer
David.Celermajer@health.nsw.gov.au

Specialty section:
This article was submitted to Neurodegeneration, a section of the journal Frontiers in Neuroscience

Received: *14 April 2020*
Accepted: *02 June 2020*
Published: *24 June 2020*

Citation:
Levin RA, Carnegie MH and Celermajer DS (2020) Pulse Pressure: An Emerging Therapeutic Target for Dementia. Front. Neurosci. 14:669. doi: 10.3389/fnins.2020.00669

INTRODUCTION

Force from ventricular ejection produces a pulse pressure in the arterial tree. Pulse pressure (systolic minus diastolic blood pressure) is normally dampened by the elastic properties of central arteries. However, pulse pressure can become elevated in some circumstances, especially with increased age (Pinto, 2007). Two mechanisms that lead to a chronic increase in pulse pressure are (i) progressive stiffening of central vessels from changes in endothelial cell and vessel wall structure (Lee and Oh, 2010; Wagenseil and Mecham, 2012) and (ii) excessive wave reflection from high resistance peripheral vessels (Safar, 2008). Age-related elevation of pulse pressure is typically due to increased systolic pressure, while diastolic pressure is unchanged or slightly decreased (Pinto, 2007; Steppan et al., 2011). High systolic pressure increases the workload on the left ventricle, which can result

in left ventricular hypertrophy and heart failure (Chae et al., 1999; Steppan et al., 2011). The kidneys and brain are also adversely affected by arterial stiffening and high pulse pressure, as these organs share the key characteristic of having low resistance microvasculature that allows for deep penetration of the pulse (O'Rourke and Safar, 2005). Thus, both organs are susceptible to damage of their delicate microvessels, which in turn damages the organ tissue (Arulkumaran et al., 2010; Stone et al., 2015). Elevated pulse pressure can therefore lead to comorbidities such as chronic kidney disease and cognitive decline (Townsend, 2015). In this perspective article, we will focus on the impact of high pulse pressure on the brain.

Throughout the human brain, over 600 kilometers of blood vessels supply the brain tissue with oxygen and nutrients, while also removing metabolic by-products from the brain (Zlokovic, 2008; Pardridge, 2015; Iadecola, 2017; Kisler et al., 2017). Cerebral microvessels lack external elastic laminae, making them more fragile than other systemic vessels (Lee, 1995). Neuronal health and signaling rely on precise chemical homeostasis; hence, blood vessels in the brain are specialized to form the blood-brain barrier, a structure that restricts non-selective passage of molecules and cells. The blood-brain barrier is composed of endothelial cells connected by tight junctions and pericytes that encircle the microvessels, which together are sheathed by astrocyte end feet (Ballabh et al., 2004). Tight junctions block the leakage of blood-based molecules in between individual cerebral endothelial cells; pericytes regulate endothelial cell gene expression and polarize astrocyte end feet; and astrocytes secrete factors that support the development and maintenance of cellular interactions within the blood-brain barrier and between the blood-brain barrier and neurons (Armulik et al., 2010; Alvarez et al., 2013). Breakdown of the blood-brain barrier is widely believed to drive several neurodegenerative diseases such as Parkinson's disease, Huntington's disease, and dementia, including Alzheimer's disease (Ballabh et al., 2004; Desai et al., 2007; Drouin-Ouellet et al., 2015; Wardlaw et al., 2017; Sweeney et al., 2018).

Development of dementia with age is likely driven by numerous distinct and multifactorial pathologies. As the discovery and understanding of underlying mechanisms advances, we expect new sub-types of dementia to be defined. This may enable development of therapeutic strategies that are efficacious for specific patient groups. A rapidly growing body of research studies and epidemiologic evidence indicate that elevated pulse pressure is a potential key contributor to blood-brain barrier breakdown and cognitive impairment in many individuals (Stone et al., 2015; Thorin-Trescases et al., 2018). High pulse pressure correlates with cerebral microvascular damage (Triantafyllidi et al., 2009) as well as white matter structural differences in elderly patient brains (Tsao et al., 2013; Purkayastha et al., 2014; Tarumi et al., 2014). In multiple large population studies considering thousands of individuals, high pulse pressure has been a strong, independent risk factor and predictor of cognitive decline later in life (Waldstein et al., 2008; Mitchell et al., 2011; Meyer et al., 2017). Most recently, Chiesa et al. (2019) linked progressive cognitive impairment to carotid wave intensity, a surrogate marker of arterial stiffness and pulse pressure directly delivered to the brain. Middle-aged adults with top-quartile carotid wave intensity values were found to have a 50% increased risked of future cognitive decline, compared to those with "control value" carotid wave intensity. Further, de Montgolfier et al. (2019) demonstrated that high pulse pressure in wild-type mice and Alzheimer's disease model mice increased the prevalence of microbleeds, which is characteristic of individuals with Alzheimer's disease (Brundel et al., 2012). Taken together, these findings highlight pulse pressure as a new pathogenetic factor for cognitive decline.

There are nearly 50 million people living with dementia worldwide, and this number is expected to triple by 2050 (World Health Organization, 2017). Therapeutic development efforts to date have largely focused on directly reducing amyloid-β, a marker of Alzheimer's disease, in the brain. Yet, despite billions of dollars spent on R&D, no cure or preventative solution has earned FDA approval, emphasizing the urgent need for novel approaches. Here, we discuss the impacts of elevated pulse pressure on the blood-brain barrier and cognition, and we propose that pulse pressure is a promising therapeutic target for a potential new sub-type of dementia.

PULSE PRESSURE, ENDOTHELIAL CELL DYSFUNCTION, AND BLOOD-BRAIN BARRIER DAMAGE

Endothelial cell dysfunction is thought to be critically involved in development and progression of several diseases such as atherosclerosis, heart failure, kidney disease, and certain neurological conditions (Su et al., 2006; Malyszko, 2010; Rajendran et al., 2013; Vanhoutte et al., 2017; Giannitsi et al., 2019). Pulse pressure regulates endothelial cells in diverse ways, ranging from the individual cell level to the greater microvascular integrity level. Elevated pulse pressure (>70 mmHg) causes blood vessels to be cyclically stretched ∼15–20% (pathological stretch) compared to normal pulse pressure (30–50 mmHg) that causes blood vessels to be cyclically stretched only ∼5% (physiological stretch) (Anwar et al., 2012; Gao et al., 2014; Jufri et al., 2015). Physiological stretch is essential for maintaining proper endothelial cell gene expression and function such as signal transduction, balanced reactive oxygen species generation and cellular structure. Conversely, pathological stretch has been shown to cause oxidative stress, inflammation, and apoptosis of endothelial cells (Jufri et al., 2015) that could compromise the blood-brain barrier.

Pathological stretch increases production of reactive oxygen species and inflammatory cytokines by endothelial cells. Increased O_2^- promotes oxidative tissue damage and increases H_2O_2 that activates the NF-κB inflammatory pathway. Inflammatory cytokines, including VCAM-1, ICAM-1, TNFα, IL-6, and IL-8, further activate NF-κB and inflammation in blood vessels (Jufri et al., 2015). Blood concentrations of VCAM-1, TNFα, and IL-6 are higher in people with Alzheimer's disease compared to healthy individuals (Swardfager et al., 2010; Lai et al., 2017). Chronic inflammation of the blood-brain barrier can lead to apoptosis of cerebral endothelial cells, astrocytes,

and pericytes (van Kralingen et al., 2013; Jufri et al., 2017; Sweeney et al., 2018). Loss of these cells may permanently impair blood-brain barrier integrity since NF-κB activation, chronic inflammation, and oxidative stress also cause stem/progenitor cell dysfunction (Yao et al., 2006; Shao et al., 2011; Lin et al., 2013; Josephson et al., 2019) that could diminish regenerative potential in the blood-brain barrier. Additionally, the NF-κB pathway upregulates amyloidogenesis (Ju Hwang et al., 2019). Upregulated β-secretase 1 (BACE1) and amyloid precursor protein (APP) expression and increased amyloid-β (specifically Aβ42) secretion have all been directly observed from cerebral endothelial cells in response to pathological stretch (Gangoda et al., 2018). Amyloid-β decreases tight junction proteins, increases IL-6, and increases matrix metalloproteinases that degrade the extracellular matrix (Vukic et al., 2009; Hartz et al., 2012; Weekman and Wilcock, 2016). TNFα also upregulates matrix metalloproteinase expression in endothelial cells under pathological stretch (Wang et al., 2003). Thus, pathological stretch modulates numerous molecules that result in chronic oxidative stress, inflammation, amyloidogenesis, and damage of the blood-brain barrier.

Pathological stretch can also impact blood-brain barrier integrity through non-oxidative and non-inflammatory pathways. Pathological stretch upregulates integrin β3 and downregulates titin in cerebral endothelial cells, which may reduce cellular elasticity, consequently damaging the blood-brain barrier. Furthermore, downregulation of eukaryotic translation initiation factor 4 gamma 3 in these cerebral endothelial cells under excess stretch attenuates global protein synthesis and therefore cell proliferation (Jufri et al., 2017). Sorting nexin-1, a protein that recycles cell-surface receptors (Haft et al., 1998), is also substantially downregulated in cerebral endothelial cells exposed to pathological stretch (Jufri et al., 2017). While the specific interaction between sorting nexin-1 and cerebral endothelial cell receptors is not yet defined, dysregulation of sorting nexins often results in abnormal receptor expression and cellular signaling that disrupts homeostasis (Zhao et al., 2012; Wang et al., 2013; Yang et al., 2014). Thus, decreased sorting nexin-1 due to pathological stretch has the potential to dysregulate key endothelial cell receptors that may exacerbate microvascular damage. For example, sorting nexin downregulation decreases expression of the endothelial cell surface receptor FEEL-1/stabilin-1 (Adachi and Tsujimoto, 2010), which can reduce endothelial cell-cell interaction and angiogenesis (Adachi and Tsujimoto, 2002).

Blood-brain barrier breakdown due to elevated pulse pressure may result in microbleeds in the brain from cumulative pulse-pressure-induced cellular damage over time as well as from the excessive direct mechanical force of the pulse. As briefly mentioned earlier, a recent mechanistic study in wild-type mice and Alzheimer's disease model (APP/PS1) mice has reinforced the importance of high pulse pressure in the pathogenesis of dementia-related cerebral changes. de Montgolfier et al. (2019) studied mice following transverse aortic constriction surgery that increased pulse pressure in only the right side of the brain, while the left side of the brain experienced normal pulse pressure and served as an internal control. In addition to causing more microbleeds, elevated pulse pressure led to blood-brain barrier dysfunction, loss of cerebral microvessel density, and hypoperfusion in both wild-type and APP/PS1 mice. Notably, the right hemisphere that was exposed to high pulse pressure in APP/PS1 mice also had more amyloid-β deposition compared to the left hemisphere that experienced normal pulse pressure.

BLOOD-BRAIN BARRIER DAMAGE AND COGNITIVE DECLINE

Elevated pulse pressure compromises the blood-brain barrier through several processes, including oxidation, inflammation, and apoptosis. However, this damage does not stay confined to the blood-brain barrier (**Figure 1**). Reactive oxygen species, inflammatory cytokines, amyloid-β, and blood leak into the neural tissue from the injured blood-brain barrier triggering neuron dysfunction and death that may drive the development of certain dementias (Lynch, 2010; Sharma and Sharma, 2010; Van der Flier and Cordonnier, 2012; Lyman et al., 2014; Martinez-Ramirez et al., 2014; Huang et al., 2016; Sweeney et al., 2018). Resultant oxidative stress and inflammation in the brain following blood-brain barrier leakage can also upregulate brain cell production of amyloid-β (Tong et al., 2005; Lee et al., 2008). This increase in amyloid-β, coupled with the increased amyloid-β secretion from cerebral endothelial cells exposed to elevated pulsatile stretch (Gangoda et al., 2018), accelerates the formation of amyloid-β plaques (Alasmari et al., 2018; Cheignon et al., 2018). Amyloid-β deposition in the brain disrupts neuronal synapses and breaks neuronal branches (Tsai et al., 2004) and further exacerbates oxidative stress, neuroinflammation, and apoptosis (Miranda et al., 2000; Xie et al., 2013; Dorey et al., 2014). Moreover, loss of pericytes due to blood-brain barrier inflammation contributes amyloid-β build-up since pericytes can remove amyloid-β from the brain (Sagare et al., 2013).

Blood-brain barrier microbleeds from elevated pulse pressure allow for systemic molecules and circulating cells to enter the sensitive neural tissue. For example, hemoglobin is a vital systemic protein that carries oxygen in blood, but it can damage neural tissue. Breakdown of hemoglobin in the brain leads to release of redox-active iron and production of reactive oxygen species resulting in oxidative damage (Robinson et al., 2009). Heme-deposits colocalize with amyloid-β plaques, indicating that microbleeds are involved in amyloid-β pathology (Cullen et al., 2006). Another important systemic protein is fibrinogen, which is a clotting factor in blood. However, upon vascular injury, fibrinogen is enzymatically converted to fibrin, which can also damage neural tissue. Brain deposition of fibrinogen originating from blood is increased in Alzheimer's disease patients (Narayan et al., 2015). The resulting fibrin is linked to neuroinflammation, neuron dysfunction, and neuron death, as well as reduced blood-brain barrier integrity (Paul et al., 2007; Cortes-Canteli et al., 2015). Fibrin can bind to amyloid-β, which prevents fibrin clearance from both the blood-brain barrier and the brain leading to more microbleeds and neurodegeneration (Cortes-Canteli et al., 2012; Ahn et al., 2017). Microbleeds also recruit circulating immune cells that infiltrate the brain (Fiala et al., 2002; Cullen

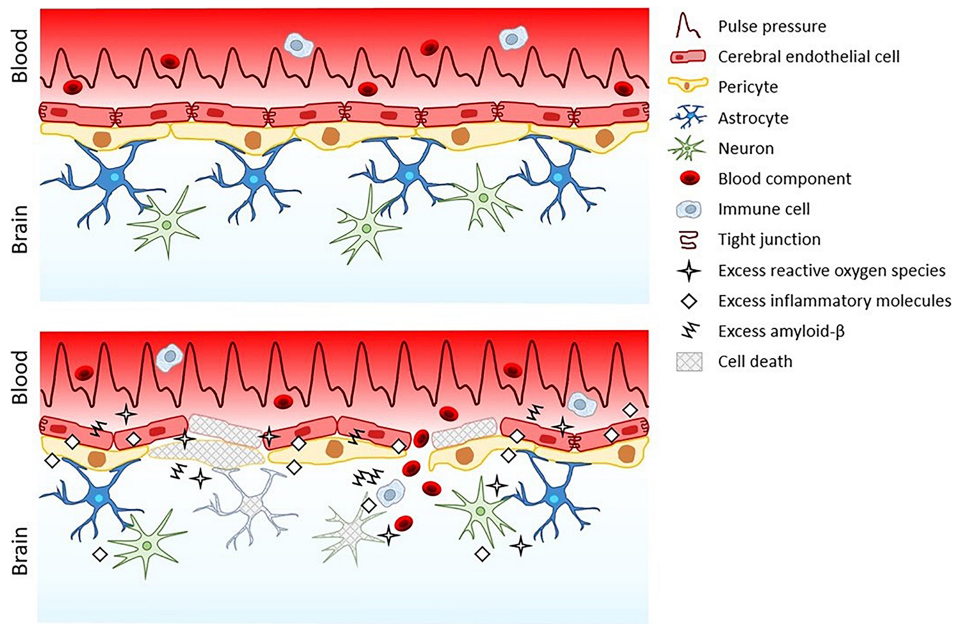

FIGURE 1 | The blood-brain barrier and neuropil under normal pulse pressure (top) versus elevated pulse pressure (bottom).

et al., 2005) and activate the brain-resident microglia (Xue and Del Bigio, 2000), which in turn activate neurotoxic reactive astrocytes that are implicated in neurodegeneration (Liddelow et al., 2017). However, even in the absence of microbleeds, pulse-pressure-induced endothelial dysfunction alone may be sufficient to drive wide-spread degeneration of the blood-brain barrier and neural tissue.

In summary, elevated pulse pressure delivers initial and continuous insults to the blood-brain barrier. Chronic oxidation and inflammation in the blood-brain barrier and upregulated secretion of amyloid-β from the blood-brain barrier causes persistent brain oxidative stress, neuroinflammation, amyloid-β deposition, and consequential neurodegeneration. This new pathological pathway of pulse-pressure-induced cognitive decline in dementia (**Figure 2**) may shed light on previous disappointments in therapeutic development for dementia, as well as reveal future opportunities.

POTENTIAL PULSE PRESSURE IMPACTS ON THERAPEUTIC STRATEGIES FOR DEMENTIA

Amyloid-β has been a primary focus of R&D for Alzheimer's disease. Despite over two decades of work and numerous clinical-stage drug candidates, no BACE1 inhibitors or anti-amyloid-β therapeutics have been demonstrated to improve cognitive function, thus none have achieved regulatory approval (Panza et al., 2019). Considering the pulse pressure paradigm of dementia (**Figures 1**, **2**), drug targeting of only amyloid-β might be insufficient as a stand-alone therapy. Alternatively, anti-inflammatory agents have been proposed to treat Alzheimer's disease. Anti-inflammatory agents like enetercept (a TNFα inhibitor approved for several types of arthritis) have been suggested to treat Alzheimer's disease (Decourt et al., 2017). However, a phase II trial of enterecept failed to show any significant improvements in cognitive ability (Butchart et al., 2015). Other anti-inflammatory agents currently in clinical trials for Alzheimer's disease include a RIPK1 inhibitor (DNL747, phase I; Denali Therapeutics), a TREM2 activator (AL002, phase I; Alector), and a non-steroidal anti-inflammatory (Salsalate, phase I; University of California San Francisco). Ultimately, targeting inflammatory-mediating molecules or amyloid-β to treat dementia may be an uphill battle since elevated pulse pressure will continue to broadly activate various inflammatory processes and increase amyloid-β throughout the blood-brain barrier and neural tissue. Thus, lowering elevated pulse pressure in certain dementia patients may be an essential first step to limit the production of inflammatory molecules and amyloid-β (as well as reactive oxygen species) before administering drugs, if necessary, to inhibit any remaining disease activity. Reduction of pulse pressure may therefore also allow for lower doses of these drugs to improve their safety profiles.

Another challenge for many neurological drug candidates, including anti-inflammatory and anti-amyloid-β biologics, is the inability to readily cross blood-brain barrier; only molecules that have a molecular weight under 400 Da and form fewer than eight hydrogen bonds are expected to passively diffuse (Pardridge, 2012). Hence, blood-brain barrier damage has been hypothesized as an avenue for larger drugs to enter the brain. Abulrob et al. (2008) showed that biologics can pass through blood-brain barrier lesions but do not widely distribute in neural tissue. Also, leakage is not uniform across the entire blood-brain barrier (Bien-Ly et al., 2015; Gyanwali et al., 2019), so drug delivery

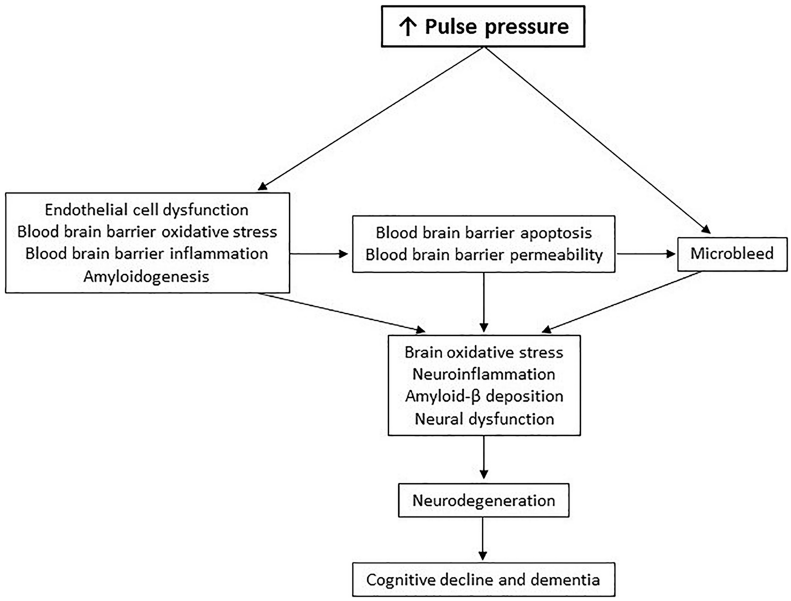

FIGURE 2 | The pulse-pressure-induced cognitive decline pathway.

throughout the brain may be inadequate. Moreover, while blood-brain barrier disruption from elevated pulse pressure may enable some locally confined penetration of certain dementia drugs into the brain, it also allows for entry of toxic blood components that harm neurons. Hence, promoting blood-brain barrier health and integrity through the reduction of elevated pulse pressure alone may be a superior solution for treating certain dementias, and only if still required, drug candidates that can passively diffuse through the intact blood-brain barrier could be trialed.

A different drug delivery approach utilizes endogenous cerebral endothelial cell receptors that innately transport specific molecules from the systemic circulation into the brain. One such receptor is the insulin receptor that transports insulin from blood into the brain to support neuron function and metabolism (Bilotta et al., 2017). Molecular trojan horse technology is being developed to exploit various transport receptors. Molecular trojan horses are comprised of a therapeutic domain (e.g., an enzyme, an antibody fragment, or neurotrophin) fused to a receptor-binding domain (e.g., an insulin receptor antibody) to facilitate active transport by receptors across the blood-brain barrier (Pardridge, 2017). However, elevated pulse pressure causes endothelial cell dysfunction (Jufri et al., 2015; Jufri et al., 2017), which could impact receptor expression and activity. Therefore, it may be critical to first resolve elevated pulse pressure before administering therapies that have been designed in consideration of healthy blood-brain barrier dynamics.

Stem and progenitor cell therapies are also gaining attention as a strategy to repair blood-brain barrier damage and treat dementia (Cheng et al., 2018; Zhang et al., 2018; Alipour et al., 2019). Autologous and allogeneic stem cells are currently in clinical trials for Alzheimer's disease (Hope Biosciences; Nature Cell Co; Medipost Co; CHA Biotech Co; Stemedica Cell Technologies; Longeveron; and University of Miami). However, elevated pulse pressure chronically induces NF-κB, inflammation, and reactive oxygen species production that can limit the regenerative potential of stem and progenitor cells (Yao et al., 2006; Shao et al., 2011; Lin et al., 2013; Josephson et al., 2019). Accordingly, reduction of elevated pulse pressure may be necessary to enhance stem and progenitor cell efficacy.

PULSE PRESSURE AS A THERAPEUTIC TARGET FOR DEMENTIA

As discussed above, elevated pulse pressure may initiate a cascade of oxidation, inflammation, amyloidogenesis, blood-brain barrier damage, and neurodegeneration. Therefore, novel therapeutics could be developed to target pulse pressure as a potential preventative solution or treatment for certain dementias. A relevant approach currently under investigation is the repurposing of blood pressure medications. In the SPRINT-MIND study of 9361 individuals, aggressive antihypertensive therapy was shown to significantly reduce the risk of cognitive decline (Williamson et al., 2019) but was also linked to serious adverse events, such as hypotension and acute kidney failure (Group, 2015). Currently, Losartan and Telmisartan are in phase III (University of Texas Southwestern) and phase I (Emory University) trials for Alzheimer's disease, respectively. Both are angiotensin II receptor antagonists that induce blood vessel dilation to lower blood pressure, which may reduce the incidence, progression, and pathology of Alzheimer's disease (Li et al., 2010, 2012). However, Losartan, Telmisartan, and the antihypertensive drugs in the SRPINT-MIND study lower both systolic and diastolic blood pressure. Lowering diastolic blood pressure is potentially dangerous in dementia patients if cerebral autoregulation fails in the elderly (Toth et al., 2017;

Zhou et al., 2019) since this may result in decreased blood flow, which can exacerbate cognitive decline (Benedictus et al., 2017; Leijenaar et al., 2017). Considering the safety profiles and effect on diastolic blood pressure, these drugs may be difficult to apply in practice for treating older patients with stiff vessels.

When developing new technologies to restore healthier pulse pressure, minimizing adverse events will be paramount due to the elderly patient population in dementia. Accordingly, an appealing therapy would lower systolic but not diastolic blood pressure. If feasible, therapeutic targeting of the brain, instead of the whole systemic circulation, may further benefit safety. For example, reducing pulse wave intensity at and distal to the carotid artery may be particularly useful for alleviating pulse pressure impacts on the brain specifically. A technology that safely lowers elevated pulse pressure could also improve efficacy of potentially synergistic therapies when used in combination. Future therapeutic development could explore reducing carotid/cerebral artery stiffness, restoring carotid/cerebral artery elasticity, or reducing peripheral wave reflection. These approaches may produce a novel drug or device to prevent or treat cognitive decline in certain dementias.

AUTHOR CONTRIBUTIONS

The authors conceived the scope of the manuscript together. RL drafted the manuscript. All authors critically revised the manuscript. RL finalized the manuscript for publication. All authors approved the submitted version.

REFERENCES

Abulrob, A., Brunette, E., Slinn, J., Baumann, E., and Stanimirovic, D. (2008). Dynamic analysis of the blood-brain barrier disruption in experimental stroke using time domain in vivo fluorescence imaging. *Mol. Imaging* 7, 248–262.

Adachi, H., and Tsujimoto, M. (2002). FEEL-1, a novel scavenger receptor with in vitro bacteria-binding and angiogenesis-modulating activities. *J. Biol. Chem.* 277, 34264–34270. doi: 10.1074/jbc.m204277200

Adachi, H., and Tsujimoto, M. (2010). Adaptor protein sorting nexin 17 interacts with the scavenger receptor FEEL-1/stabilin-1 and modulates its expression on the cell surface. *Biochim. Biophys. Acta* 1803, 553–563. doi: 10.1016/j.bbamcr.2010.02.011

Ahn, H. J., Chen, Z.-L., Zamolodchikov, D., Norris, E. H., and Strickland, S. (2017). Interactions of β-amyloid peptide with fibrinogen and coagulation factor XII may contribute to Alzheimer's disease. *Curr. Opin. Hematol.* 24, 427–431. doi: 10.1097/moh.0000000000000368

Alasmari, F., Alshammari, M. A., Alasmari, A. F., Alanazi, W. A., and Alhazzani, K. (2018). Neuroinflammatory cytokines induce amyloid beta neurotoxicity through modulating amyloid precursor protein levels/metabolism. *Biomed Res. Int.* 2018:3087475.

Alipour, M., Nabavi, S. M., Arab, L., Vosough, M., Pakdaman, H., Ehsani, E., et al. (2019). Stem cell therapy in Alzheimer's disease: possible benefits and limiting drawbacks. *Mol. Biol. Rep.* 46, 1425–1446. doi: 10.1007/s11033-018-4499-7

Alvarez, J. I., Katayama, T., and Prat, A. (2013). Glial influence on the blood brain barrier. *Glia* 61, 1939–1958. doi: 10.1002/glia.22575

Anwar, M., Shalhoub, J., Lim, C., Gohel, M., and Davies, A. (2012). The effect of pressure-induced mechanical stretch on vascular wall differential gene expression. *J. Vasc. Res.* 49, 463–478. doi: 10.1159/000339151

Armulik, A., Genové, G., Mäe, M., Nisancioglu, M. H., Wallgard, E., Niaudet, C., et al. (2010). Pericytes regulate the blood–brain barrier. *Nature* 468, 557–561.

Arulkumaran, N., Diwakar, R., Tahir, Z., Mohamed, M., Carlos Kaski, J., and Banerjee, D. (2010). Pulse pressure and progression of chronic kidney disease. *J. Nephrol.* 23, 189–193.

Ballabh, P., Braun, A., and Nedergaard, M. (2004). The blood–brain barrier: an overview: structure, regulation, and clinical implications. *Neurobiol. Dis.* 16, 1–13.

Benedictus, M. R., Leeuwis, A. E., Binnewijzend, M. A., Kuijer, J. P., Scheltens, P., Barkhof, F., et al. (2017). Lower cerebral blood flow is associated with faster cognitive decline in Alzheimer's disease. *Eur. Radiol.* 27, 1169–1175. doi: 10.1007/s00330-016-4450-z

Bien-Ly, N., Boswell, C. A., Jeet, S., Beach, T. G., Hoyte, K., Luk, W., et al. (2015). Lack of widespread BBB disruption in Alzheimer's disease models: focus on therapeutic antibodies. *Neuron* 88, 289–297. doi: 10.1016/j.neuron.2015.09.036

Bilotta, F., Lauretta, M., Tewari, A., Haque, M., Hara, N., Uchino, H., et al. (2017). Insulin and the brain: a sweet relationship with intensive care. *J. Intensive Care Med.* 32, 48–58. doi: 10.1177/0885066615594341

Brundel, M., Heringa, S. M., De Bresser, J., Koek, H. L., Zwanenburg, J. J., Kappelle, L. J., et al. (2012). High prevalence of cerebral microbleeds at 7Tesla MRI in patients with early Alzheimer's disease. *J. Alzheimers Dis.* 31, 259–263. doi: 10.3233/jad-2012-120364

Butchart, J., Brook, L., Hopkins, V., Teeling, J., Püntener, U., Culliford, D., et al. (2015). Etanercept in Alzheimer disease: a randomized, placebo-controlled, double-blind, phase 2 trial. *Neurology* 84, 2161–2168. doi: 10.1212/wnl.0000000000001617

Chae, C. U., Pfeffer, M. A., Glynn, R. J., Mitchell, G. F., Taylor, J. O., and Hennekens, C. H. (1999). Increased pulse pressure and risk of heart failure in the elderly. *JAMA* 281, 634–643.

Cheignon, C., Tomas, M., Bonnefont-Rousselot, D., Faller, P., Hureau, C., and Collin, F. (2018). Oxidative stress and the amyloid beta peptide in Alzheimer's disease. *Redox Biol.* 14, 450–464.

Cheng, Z., Wang, L., Qu, M., Liang, H., Li, W., Li, Y., et al. (2018). Mesenchymal stem cells attenuate blood-brain barrier leakage after cerebral ischemia in mice. *J. Neuroinflammation* 15:135.

Chiesa, S. T., Masi, S., Shipley, M. J., Ellins, E. A., Fraser, A. G., Hughes, A. D., et al. (2019). Carotid artery wave intensity in mid-to late-life predicts cognitive decline: the Whitehall II study. *Eur. Heart J.* 40, 2300–2309. doi: 10.1093/eurheartj/ehz189

Cortes-Canteli, M., Mattei, L., Richards, A. T., Norris, E. H., and Strickland, S. (2015). Fibrin deposited in the Alzheimer's disease brain promotes neuronal degeneration. *Neurobiol. Aging* 36, 608–617. doi: 10.1016/j.neurobiolaging.2014.10.030

Cortes-Canteli, M., Zamolodchikov, D., Ahn, H. J., Strickland, S., and Norris, E. H. (2012). Fibrinogen and altered hemostasis in Alzheimer's disease. *J. Alzheimers Dis.* 32, 599–608. doi: 10.3233/jad-2012-120820

Cullen, K. M., Kócsi, Z., and Stone, J. (2005). Pericapillary haem-rich deposits: evidence for microhaemorrhages in aging human cerebral cortex. *J. Cereb. Blood Flow Metab.* 25, 1656–1667. doi: 10.1038/sj.jcbfm.9600155

Cullen, K. M., Kócsi, Z., and Stone, J. (2006). Microvascular pathology in the aging human brain: evidence that senile plaques are sites of microhaemorrhages. *Neurobiol. Aging* 27, 1786–1796. doi: 10.1016/j.neurobiolaging.2005.10.016

de Montgolfier, O., Pinçon, A., Pouliot, P., Gillis, M.-A., Bishop, J., Sled, J. G., et al. (2019). High systolic blood pressure induces cerebral microvascular endothelial dysfunction, neurovascular unit damage, and cognitive decline in mice. *Hypertension* 73, 217–228. doi: 10.1161/hypertensionaha.118.12048

Decourt, B., Lahiri, K. D., and Sabbagh, M. N. (2017). Targeting tumor necrosis factor alpha for Alzheimer's disease. *Curr. Alzheimer Res.* 14, 412–425.

Desai, B. S., Monahan, A. J., Carvey, P. M., and Hendey, B. (2007). Blood–brain barrier pathology in Alzheimer's and Parkinson's disease: implications for drug therapy. *Cell Transplant.* 16, 285–299. doi: 10.3727/000000007783464731

Dorey, E., Chang, N., Liu, Q. Y., Yang, Z., and Zhang, W. (2014). Apolipoprotein E, amyloid-beta, and neuroinflammation in Alzheimer's disease. *Neurosci. Bull.* 30, 317–330. doi: 10.1007/s12264-013-1422-z

Drouin-Ouellet, J., Sawiak, S. J., Cisbani, G., Lagacé, M., Kuan, W. L., Saint-Pierre, M., et al. (2015). Cerebrovascular and blood–brain barrier impairments in Huntington's disease: potential implications for its pathophysiology. *Ann. Neurol.* 78, 160–177. doi: 10.1002/ana.24406

Fiala, M., Liu, Q., Sayre, J., Pop, V., Brahmandam, V., Graves, M., et al. (2002). Cyclooxygenase-2-positive macrophages infiltrate the Alzheimer's disease brain and damage the blood–brain barrier. *Eur. J. Clin. Investig.* 32, 360–371. doi: 10.1046/j.1365-2362.2002.00994.x

Gangoda, S. V., Avadhanam, B., Jufri, N. F., Sohn, E. H., Butlin, M., Gupta, V., et al. (2018). Pulsatile stretch as a novel modulator of amyloid precursor protein processing and associated inflammatory markers in human cerebral endothelial cells. *Sci. Rep.* 8:1689.

Gao, J., Huang, T., Zhou, L.-J., Ge, Y.-L., Lin, S.-Y., and Dai, Y. (2014). Preconditioning effects of physiological cyclic stretch on pathologically mechanical stretch-induced alveolar epithelial cell apoptosis and barrier dysfunction. *Biochem. Biophys. Res. Commun.* 448, 342–348. doi: 10.1016/j.bbrc.2014.03.063

Giannitsi, S., Maria, B., Bechlioulis, A., and Naka, K. (2019). Endothelial dysfunction and heart failure: a review of the existing bibliography with emphasis on flow mediated dilation. *JRSM Cardiovasc. Dis.* 8:2048004019843047.

Group, S. R. (2015). A randomized trial of intensive versus standard blood-pressure control. *N. Engl. J. Med.* 373, 2103–2116.

Gyanwali, B., Shaik, M. A., Venketasubramanian, N., Chen, C., and Hilal, S. (2019). Mixed-location cerebral microbleeds: an imaging biomarker for cerebrovascular pathology in cognitive impairment and dementia in a memory clinic population. *J. Alzheimers Dis.* 71, 1309–1320. doi: 10.3233/jad-190540

Haft, C. R., De La Luz Sierra, M., Barr, V. A., Haft, D. H., and Taylor, S. I. (1998). Identification of a family of sorting nexin molecules and characterization of their association with receptors. *Mol. Cell. Biol.* 18, 7278–7287. doi: 10.1128/mcb.18.12.7278

Hartz, A. M., Bauer, B., Soldner, E. L., Wolf, A., Boy, S., Backhaus, R., et al. (2012). Amyloid-β contributes to blood–brain barrier leakage in transgenic human amyloid precursor protein mice and in humans with cerebral amyloid angiopathy. *Stroke* 43, 514–523. doi: 10.1161/strokeaha.111.627562

Huang, W. J., Zhang, X., and Chen, W. W. (2016). Role of oxidative stress in Alzheimer's disease. *Biomed. Rep.* 4, 519–522.

Iadecola, C. (2017). The neurovascular unit coming of age: a journey through neurovascular coupling in health and disease. *Neuron* 96, 17–42. doi: 10.1016/j.neuron.2017.07.030

Josephson, A. M., Bradaschia-Correa, V., Lee, S., Leclerc, K., Patel, K. S., Lopez, E. M., et al. (2019). Age-related inflammation triggers skeletal stem/progenitor cell dysfunction. *Proc. Natl. Acad. Sci. U.S.A.* 116, 6995–7004. doi: 10.1073/pnas.1810692116

Ju Hwang, C., Choi, D.-Y., Park, M. H., and Hong, J. T. (2019). NF-KB as a key mediator of brain inflammation in Alzheimer's disease. *CNS Neurol. Disord. Drug Targets* 18, 3–10. doi: 10.2174/1871527316666170807130011

Jufri, N. F., Mohamedali, A., Ahn, S. B., Avolio, A., and Baker, M. S. (2017). Effects of acute and chronic biomechanical strain on human cerebral endothelial cells in altering their proteome profile. *Curr. Proteomics* 14, 214–223.

Jufri, N. F., Mohamedali, A., Avolio, A., and Baker, M. S. (2015). Mechanical stretch: physiological and pathological implications for human vascular endothelial cells. *Vasc. Cell* 7:8.

Kisler, K., Nelson, A. R., Montagne, A., and Zlokovic, B. V. (2017). Cerebral blood flow regulation and neurovascular dysfunction in Alzheimer disease. *Nat. Rev. Neurosci.* 18, 419–434. doi: 10.1038/nrn.2017.48

Lai, K. S. P., Liu, C. S., Rau, A., Lanctôt, K. L., Köhler, C. A., Pakosh, M., et al. (2017). Peripheral inflammatory markers in Alzheimer's disease: a systematic review and meta-analysis of 175 studies. *J. Neurol. Neurosurg. Psychiatry* 88, 876–882. doi: 10.1136/jnnp-2017-316201

Lee, H.-Y., and Oh, B.-H. (2010). Aging and arterial stiffness. *Circ. J.* 74, 2257–2262.

Lee, J. W., Lee, Y. K., Yuk, D. Y., Choi, D. Y., Ban, S. B., Oh, K. W., et al. (2008). Neuro-inflammation induced by lipopolysaccharide causes cognitive impairment through enhancement of beta-amyloid generation. *J. Neuroinflammation* 5:37. doi: 10.1186/1742-2094-5-37

Lee, R. M. (1995). Morphology of cerebral arteries. *Pharmacol. Ther.* 66, 149–173. doi: 10.1016/0163-7258(94)00071-a

Leijenaar, J. F., Van Maurik, I. S., Kuijer, J. P., Van Der Flier, W. M., Scheltens, P., Barkhof, F., et al. (2017). Lower cerebral blood flow in subjects with Alzheimer's dementia, mild cognitive impairment, and subjective cognitive decline using two-dimensional phase-contrast magnetic resonance imaging. *Alzheimers Dement.* 9, 76–83. doi: 10.1016/j.dadm.2017.10.001

Li, N.-C., Lee, A., Whitmer, R. A., Kivipelto, M., Lawler, E., Kazis, L. E., et al. (2010). Use of angiotensin receptor blockers and risk of dementia in a predominantly male population: prospective cohort analysis. *BMJ* 340:b5465. doi: 10.1136/bmj.b5465

Li, W., Zhang, J., Lu, F., Ma, M., Wang, J., Suo, A., et al. (2012). Effects of telmisartan on the level of Aβ1-42, interleukin-1β, tumor necrosis factor α and cognition in hypertensive patients with Alzheimer's disease. *Zhonghua Yi Xue Za Zhi* 92, 2743–2746.

Liddelow, S. A., Guttenplan, K. A., Clarke, L. E., Bennett, F. C., Bohlen, C. J., Schirmer, L., et al. (2017). Neurotoxic reactive astrocytes are induced by activated microglia. *Nature* 541, 481–487.

Lin, C.-P., Lin, F.-Y., Huang, P.-H., Chen, Y.-L., Chen, W.-C., Chen, H.-Y., et al. (2013). Endothelial progenitor cell dysfunction in cardiovascular diseases: role of reactive oxygen species and inflammation. *Biomed Res. Int.* 2013: 845037.

Lyman, M., Lloyd, D. G., Ji, X., Vizcaychipi, M. P., and Ma, D. (2014). Neuroinflammation: the role and consequences. *Neurosci. Res.* 79, 1–12. doi: 10.1016/j.neures.2013.10.004

Lynch, M. A. (2010). Age-related neuroinflammatory changes negatively impact on neuronal function. *Front. Aging Neurosci.* 1:6. doi: 10.3389/neuro.24.006.2009

Malyszko, J. (2010). Mechanism of endothelial dysfunction in chronic kidney disease. *Clin. Chim. Acta* 411, 1412–1420. doi: 10.1016/j.cca.2010.06.019

Martinez-Ramirez, S., Greenberg, S. M., and Viswanathan, A. (2014). Cerebral microbleeds: overview and implications in cognitive impairment. *Alzheimers Res. Ther.* 6:33. doi: 10.1186/alzrt263

Meyer, M. L., Palta, P., Tanaka, H., Deal, J. A., Wright, J., Knopman, D. S., et al. (2017). Association of central arterial stiffness and pressure pulsatility with mild cognitive impairment and dementia: the Atherosclerosis Risk in Communities Study-Neurocognitive Study (ARIC-NCS). *J. Alzheimers Dis.* 57, 195–204. doi: 10.3233/jad-161041

Miranda, S., Opazo, C., Larrondo, L. F., Muñoz, F. J., Ruiz, F., Leighton, F., et al. (2000). The role of oxidative stress in the toxicity induced by amyloid β-peptide in Alzheimer's disease. *Prog. Neurobiol.* 62, 633–648. doi: 10.1016/s0301-0082(00)00015-0

Mitchell, G. F., Van Buchem, M. A., Sigurdsson, S., Gotal, J. D., Jonsdottir, M. K., Kjartansson, O., et al. (2011). Arterial stiffness, pressure and flow pulsatility and brain structure and function: the Age, Gene/Environment Susceptibility–Reykjavik study. *Brain* 134, 3398–3407. doi: 10.1093/brain/awr253

Narayan, P. J., Kim, S.-L., Lill, C., Feng, S., Faull, R. L., Curtis, M. A., et al. (2015). Assessing fibrinogen extravasation into Alzheimer's disease brain using high-content screening of brain tissue microarrays. *J. Neurosci. Methods* 247, 41–49. doi: 10.1016/j.jneumeth.2015.03.017

O'Rourke, M. F., and Safar, M. E. (2005). Relationship between aortic stiffening and microvascular disease in brain and kidney: cause and logic of therapy. *Hypertension* 46, 200–204. doi: 10.1161/01.hyp.0000168052.00426.65

Panza, F., Lozupone, M., Logroscino, G., and Imbimbo, B. P. (2019). A critical appraisal of amyloid-β-targeting therapies for Alzheimer disease. *Nat. Rev. Neurol.* 15, 73–88. doi: 10.1038/s41582-018-0116-6

Pardridge, W. (2015). Targeted delivery of protein and gene medicines through the blood–brain barrier. *Clin. Pharmacol. Ther.* 97, 347–361. doi: 10.1002/cpt.18

Pardridge, W. M. (2012). Drug transport across the blood–brain barrier. *J. Cereb. Blood Flow Metab.* 32, 1959–1972.

Pardridge, W. M. (2017). Delivery of biologics across the blood–brain barrier with molecular Trojan horse technology. *Biodrugs* 31, 503–519. doi: 10.1007/s40259-017-0248-z

Paul, J., Strickland, S., and Melchor, J. P. (2007). Fibrin deposition accelerates neurovascular damage and neuroinflammation in mouse models of Alzheimer's disease. *J. Exp. Med.* 204, 1999–2008. doi: 10.1084/jem.20070304

Pinto, E. (2007). Blood pressure and ageing. *Postgrad. Med. J.* 83, 109–114. doi: 10.1136/pgmj.2006.048371

Purkayastha, S., Fadar, O., Mehregan, A., Salat, D. H., Moscufo, N., Meier, D. S., et al. (2014). Impaired cerebrovascular hemodynamics are associated with cerebral white matter damage. *J. Cereb. Blood Flow Metab.* 34, 228–234. doi: 10.1038/jcbfm.2013.180

Rajendran, P., Rengarajan, T., Thangavel, J., Nishigaki, Y., Sakthisekaran, D., Sethi, G., et al. (2013). The vascular endothelium and human diseases. *Int. J. Biol. Sci.* 9, 1057–1069.

Robinson, S. R., Dang, T. N., Dringen, R., and Bishop, G. M. (2009). Hemin toxicity: a preventable source of brain damage following hemorrhagic stroke. *Redox Rep.* 14, 228–235. doi: 10.1179/135100009x12525712409931

Safar, M. E. (2008). Pulse pressure, arterial stiffness and wave reflections (augmentation index) as cardiovascular risk factors in hypertension. *Ther. Adv. Cardiovasc. Dis.* 2, 13–24. doi: 10.1177/1753944707086652

Sagare, A. P., Bell, R. D., Zhao, Z., Ma, Q., Winkler, E. A., Ramanathan, A., et al. (2013). Pericyte loss influences Alzheimer-like neurodegeneration in mice. *Nat. Commun.* 4:2932.

Shao, L., Li, H., Pazhanisamy, S. K., Meng, A., Wang, Y., and Zhou, D. (2011). Reactive oxygen species and hematopoietic stem cell senescence. *Int. J. Hematol.* 94, 24–32. doi: 10.1007/s12185-011-0872-1

Sharma, H. S., and Sharma, A. (2010). "Breakdown of the blood-brain barrier in stress alters cognitive dysfunction and induces brain pathology: new perspectives for neuroprotective strategies," in *Brain Protection in Schizophrenia, Mood and Cognitive Disorders*, ed. M. Ritsner (Dordrecht: Springer), 243–303. doi: 10.1007/978-90-481-8553-5_9

Steppan, J., Barodka, V., Berkowitz, D. E., and Nyhan, D. (2011). Vascular stiffness and increased pulse pressure in the aging cardiovascular system. *Cardiol. Res. Pract.* 2011:263585.

Stone, J., Johnstone, D. M., Mitrofanis, J., and O'rourke, M. (2015). The mechanical cause of age-related dementia (Alzheimer's disease): the brain is destroyed by the pulse. *J. Alzheimers Dis.* 44, 355–373. doi: 10.3233/jad-141884

Su, T. C., Chien, K. L., Jeng, J. S., Chang, C. J., Hsu, H. C., Chen, M. F., et al. (2006). Pulse pressure, aortic regurgitation and carotid atherosclerosis: a comparison between hypertensives and normotensives. *Int. J. Clin. Pract.* 60, 134–140. doi: 10.1111/j.1742-1241.2006.00777.x

Swardfager, W., Lanctôt, K., Rothenburg, L., Wong, A., Cappell, J., and Herrmann, N. (2010). A meta-analysis of cytokines in Alzheimer's disease. *Biol. Psychiatry* 68, 930–941.

Sweeney, M. D., Sagare, A. P., and Zlokovic, B. V. (2018). Blood–brain barrier breakdown in Alzheimer disease and other neurodegenerative disorders. *Nat. Rev. Neurol.* 14, 133–150. doi: 10.1038/nrneurol.2017.188

Tarumi, T., Khan, M. A., Liu, J., Tseng, B. M., Parker, R., Riley, J., et al. (2014). Cerebral hemodynamics in normal aging: central artery stiffness, wave reflection, and pressure pulsatility. *J. Cereb. Blood Flow Metab.* 34, 971–978. doi: 10.1038/jcbfm.2014.44

Thorin-Trescases, N., De Montgolfier, O., Pinçon, A., Raignault, A., Caland, L., Labbé, P., et al. (2018). Impact of pulse pressure on cerebrovascular events leading to age-related cognitive decline. *Am. J. Physiol. Heart Circ. Physiol.* 314, H1214–H1224.

Tong, Y., Zhou, W., Fung, V., Christensen, M., Qing, H., Sun, X., et al. (2005). Oxidative stress potentiates BACE1 gene expression and Aβ generation. *J. Neural Transm.* 112, 455–469. doi: 10.1007/s00702-004-0255-3

Toth, P., Tarantini, S., Csiszar, A., and Ungvari, Z. (2017). Advances in cardiovascular geroscience: functional vascular contributions to cognitive impairment and dementia: mechanisms and consequences of cerebral autoregulatory dysfunction, endothelial impairment, and neurovascular uncoupling in aging. *Am. J. Physiol. Heart Circ. Physiol.* 312, H1–H20.

Townsend, R. R. (2015). Arterial stiffness and chronic kidney disease: lessons from the Chronic Renal Insufficiency Cohort study. *Curr. Opin. Nephrol. Hypertens.* 24, 47–53. doi: 10.1097/mnh.0000000000000086

Triantafyllidi, H., Arvaniti, C., Lekakis, J., Ikonomidis, I., Siafakas, N., Tzortzis, S., et al. (2009). Cognitive impairment is related to increased arterial stiffness and microvascular damage in patients with never-treated essential hypertension. *Am. J. Hypertens.* 22, 525–530. doi: 10.1038/ajh.2009.35

Tsai, J., Grutzendler, J., Duff, K., and Gan, W.-B. (2004). Fibrillar amyloid deposition leads to local synaptic abnormalities and breakage of neuronal branches. *Nat. Neurosci.* 7, 1181–1183. doi: 10.1038/nn1335

Tsao, C. W., Seshadri, S., Beiser, A. S., Westwood, A. J., Decarli, C., Au, R., et al. (2013). Relations of arterial stiffness and endothelial function to brain aging in the community. *Neurology* 81, 984–991. doi: 10.1212/wnl.0b013e3182a43e1c

Van der Flier, W. M., and Cordonnier, C. (2012). Microbleeds in vascular dementia: clinical aspects. *Exp. Gerontol.* 47, 853–857. doi: 10.1016/j.exger.2012.07.007

van Kralingen, C., Kho, D. T., Costa, J., Angel, C. E., and Graham, E. S. (2013). Exposure to inflammatory cytokines IL-1β and TNFα induces compromise and death of astrocytes; implications for chronic neuroinflammation. *PLoS One* 8:e84269. doi: 10.1371/journal.pone.0084269

Vanhoutte, P., Shimokawa, H., Feletou, M., and Tang, E. (2017). Endothelial dysfunction and vascular disease–a 30th anniversary update. *Acta Physiol.* 219, 22–96. doi: 10.1111/apha.12646

Vukic, V., Callaghan, D., Walker, D., Lue, L.-F., Liu, Q. Y., Couraud, P.-O., et al. (2009). Expression of inflammatory genes induced by beta-amyloid peptides in human brain endothelial cells and in Alzheimer's brain is mediated by the JNK-AP1 signaling pathway. *Neurobiol. Dis.* 34, 95–106. doi: 10.1016/j.nbd.2008.12.007

Wagenseil, J. E., and Mecham, R. P. (2012). Elastin in large artery stiffness and hypertension. *J. Cardiovasc. Trans. Res.* 5, 264–273. doi: 10.1007/s12265-012-9349-8

Waldstein, S. R., Rice, S. C., Thayer, J. F., Najjar, S. S., Scuteri, A., and Zonderman, A. B. (2008). Pulse pressure and pulse wave velocity are related to cognitive decline in the Baltimore Longitudinal Study of Aging. *Hypertension* 51, 99–104. doi: 10.1161/hypertensionaha.107.093674

Wang, B.-W., Chang, H., Lin, S., Kuan, P., and Shyu, K.-G. (2003). Induction of matrix metalloproteinases-14 and-2 by cyclical mechanical stretch is mediated by tumor necrosis factor-α in cultured human umbilical vein endothelial cells. *Cardiovasc. Res.* 59, 460–469. doi: 10.1016/s0008-6363(03)00428-0

Wang, X., Zhao, Y., Zhang, X., Badie, H., Zhou, Y., Mu, Y., et al. (2013). Loss of sorting nexin 27 contributes to excitatory synaptic dysfunction by modulating glutamate receptor recycling in Down's syndrome. *Nat. Med.* 19, 473–480. doi: 10.1038/nm.3117

Wardlaw, J. M., Makin, S. J., Hernández, M. C. V., Armitage, P. A., Heye, A. K., Chappell, F. M., et al. (2017). Blood-brain barrier failure as a core mechanism in cerebral small vessel disease and dementia: evidence from a cohort study. *Alzheimers Dement.* 13, 634–643. doi: 10.1016/j.jalz.2016.09.006

Weekman, E. M., and Wilcock, D. M. (2016). Matrix metalloproteinase in blood-brain barrier breakdown in dementia. *J. Alzheimers Dis.* 49, 893–903. doi: 10.3233/jad-150759

Williamson, J. D., Pajewski, N. M., Auchus, A. P., Bryan, R. N., Chelune, G., Cheung, A. K., et al. (2019). Effect of intensive vs standard blood pressure control on probable dementia: a randomized clinical trial. *JAMA* 321, 553–561.

World Health Organization (2017). *Dementia. Fact sheet, Updated December* 2017. Geneva: WHO.

Xie, H., Hou, S., Jiang, J., Sekutowicz, M., Kelly, J., and Bacskai, B. J. (2013). Rapid cell death is preceded by amyloid plaque-mediated oxidative stress. *Proc. Natl. Acad. Sci. U.S.A.* 110, 7904–7909. doi: 10.1073/pnas.1217938110

Xue, M., and Del Bigio, M. R. (2000). Intracerebral injection of autologous whole blood in rats: time course of inflammation and cell death. *Neurosci. Lett.* 283, 230–232. doi: 10.1016/s0304-3940(00)00971-x

Yang, J., Villar, V. A., Jones, J. E., Guo, Y., Asico, L. D., Armando, I., et al. (2014). Sorting nexin 19: a novel regulator of renal dopamine D1 receptor. *Hypertension* 64:A296.

Yao, E.-H., Yu, Y., and Fukuda, N. (2006). Oxidative stress on progenitor and stem cells in cardiovascular diseases. *Curr. Pharm. Biotechnol.* 7, 101–108. doi: 10.2174/138920106776597685

Zhang, S., Zhi, Y., Li, F., Huang, S., Gao, H., Han, Z., et al. (2018). Transplantation of in vitro cultured endothelial progenitor cells repairs the blood-brain barrier

and improves cognitive function of APP/PS1 transgenic AD mice. *J. Neurol. Sci.* 387, 6–15. doi: 10.1016/j.jns.2018.01.019

Zhao, Y., Wang, Y., Yang, J., Wang, X., Zhao, Y., Zhang, X., et al. (2012). Sorting nexin 12 interacts with BACE1 and regulates BACE1-mediated APP processing. *Mol. Neurodegener.* 7:30. doi: 10.1186/1750-1326-7-30

Zhou, G., Zhao, X., Lou, Z., Zhou, S., Shan, P., Zheng, N., et al. (2019). Impaired cerebral autoregulation in Alzheimer's disease: a transcranial doppler study. *J. Alzheimers Dis.* 72, 623–631. doi: 10.3233/jad-190296

Zlokovic, B. V. (2008). The blood-brain barrier in health and chronic neurodegenerative disorders. *Neuron* 57, 178–201. doi: 10.1016/j.neuron.2008.01.003

Conflict of Interest: The Brain Protection Company is a clinical-stage company developing novel therapies for cognitive decline. DC is the Founder and Chief Medical Officer of The Brain Protection Company and holds equity in The Brain Protection Company. RL and MC are from M.H. Carnegie & Co, which holds equity in The Brain Protection Company.

frontiers in Neuroscience

ORIGINAL RESEARCH
published: 29 July 2020
doi: 10.3389/fnins.2020.00745

^{18}F-Florbetaben Amyloid PET Imaging: A Chinese Study in Cognitive Normal Controls, Mild Cognitive Impairment, and Alzheimer's Disease Patients

Yan Chang[1†], Can Li[1†], Hui Yang[1], Yue Wu[2], Baixuan Xu[1], Jinming Zhang[1] and Ruimin Wang[1]*

[1] Department of Nuclear Medicine, The First Medical Centre, Chinese PLA General Hospital, Beijing, China, [2] Siemens Healthineers Ltd., Beijing, China

OPEN ACCESS

Edited by:
Xian-Le Bu,
Third Military Medical University, China

Reviewed by:
Behrooz Hooshyar Yousefi,
Philipps University of Marburg, Germany
Cristina Lanni,
The University of Pavia, Italy

****Correspondence:***
Ruimin Wang
wrm@yeah.net

[†]These authors have contributed equally to this work and share first authorship

Specialty section:
This article was submitted to Neurodegeneration, a section of the journal Frontiers in Neuroscience

Received: *11 April 2020*
Accepted: *24 June 2020*
Published: *29 July 2020*

Citation:
Chang Y, Li C, Yang H, Wu Y, Xu B, Zhang J and Wang R (2020) ^{18}F-Florbetaben Amyloid PET Imaging: A Chinese Study in Cognitive Normal Controls, Mild Cognitive Impairment, and Alzheimer's Disease Patients. Front. Neurosci. 14:745. doi: 10.3389/fnins.2020.00745

Objective: To evaluate amyloid-β deposition with ^{18}F-florbetaben (FBB) PET imaging against ^{11}C-PIB PET in cognitive normal controls (NC), mild cognitive impairment (MCI), and Alzheimer's disease (AD) patients.

Methods: We recruited 45 subjects (15 in each group of NC, MCI, and mild/moderate AD) who had undergone dynamic ^{18}F-FBB amyloid PET imaging. For comparison study, 17 participants, including six NC, five MCI, and six AD patients, also underwent ^{11}C-PIB PET imaging on separate days. Standardized uptake value ratios (SUVR) were calculated using the cerebellar cortex as the reference region with regions of interest (ROI) manually defined on co-registered CT. Quantitative analysis of mean cortical uptake was calculated using global SUVR. Spearman correlation analysis between MMSE scores and SUVR of 18F-FBB and 11C-PIB images were calculated.

Results: One (7%) of the 15 NC participants, nine (60%) of 15 MCI patients, and 12 (80%) of 15 AD patients had amyloid-positive lesions on ^{18}F-FBB PET images. In AD patients, global SUVR was significantly higher than those of MCI patients (1.73 ± 0.62 vs. 1.55 ± 0.11, $P < 0.001$) and NC subjects (1.73 ± 0.62 vs. 1.13 ± 0.43, $P < 0.001$). In the comparison study, one NC participant, five MCI patients, and five AD patients had amyloid-positive lesions on ^{11}C-PIB PET images. There was a significant linear correlation ($r^2 = 0.81$, $P < 0.001$) between ^{18}F-FBB and PIB global SUVR values. MMSE scores had negative correlations with SUVR on ^{11}C-PIB PET ($r_1 = -0.650$, $P = 0.005$) or SUVR on ^{18}F-FBB PET ($r_2 = -0.754$, $P < 0.0001$).

Conclusion: Our study suggests that ^{18}F-FBB is a useful tracer for the evaluation of amyloid-β deposition in vivo and that global SUVR of ^{18}F-FBB PET might be a reliable tool in the diagnosis of AD.

Keywords: Alzheimer's disease, amyloid imaging, florbetaben, PET, amyloid beta

INTRODUCTION

Alzheimer's disease (AD) is the most common form and the most common cause of dementia in elderly. China has the largest population of patients with AD in the world, accounting for approximately 25% of the entire population with AD worldwide (Jia et al., 2019). Extracellular β-amyloid (Aβ) plaques and intracellular neurofibrillary tangles (NFTs) have been used as AD neuropathologic hallmarks. The regional evolution of AD pathology in terms of Aβ and NFTs has been described in postmortem brain tissue (Braak and Braak, 1991). Aβ load can be quantified using ^{11}C-labeled Pittsburgh compound-B (PIB) PET. Neuropathological studies reported that the initial plaques are located in the temporal and orbitofrontal cortices, extending later to the cingulate, frontal, and parietal cortices (Braak and Braak, 1997). In 2011, the National Institute on Aging and Alzheimer's Association (NIA-AA) created diagnostic guidelines for the preclinical, mild cognitive impairment (MCI), and dementia stages of AD and supported the use of imaging and biomarkers (McKhann et al., 2011). In 2018, NIA-AA updated and unified the new research framework for observational and interventional research of AD. In this research framework, AD is defined by its underlying pathologic processes that can be documented *in vivo* by biomarkers (Jack et al., 2018). Aβ imaging *in vivo* with PET not only allows assessment of Aβ deposition in the brain but also provides an important new tool for the evaluation of the causes, diagnosis, and treatment of dementia (Rowe and Villemagne, 2011).

The most widely used PET Aβ ligand, ^{11}C-PIB, was a major breakthrough that provided the first non-invasive *in vivo* detection of cortical deposition and had shown extensive cortical binding in almost all AD patients, indicating that Aβ imaging may help in distinguishing AD patients from healthy elderly controls (Rowe et al., 2007) and differential diagnosis of the dementias (Rabinovici et al., 2007; Rowe et al., 2007). However, the 20-min radioactive half-life of ^{11}C limits the use of ^{11}C-PIB in research and clinic. To overcome its limitation, a fluorine-18 [18F]-labeled molecule with a radioactive half-life of 110 min is more suitable, which allows widespread distribution from a production facility to multiple sites for research and clinical use. Three ^{18}F-labeled Aβ PET tracers have been granted by the US Food and Drug Administration (FDA) and the European Medicines Association (EMA): florbetapir (Amyvid, Eli Lilly), florbetaben (FBB, Neuraceq, Piramal Imaging Ltd.), and flutemetamol (GE Healthcare). The three FDA-approved tracers exhibited different kinetic behaviors and varying levels of specificity with amyloid-β and off-target white matter binding (Landau et al., 2014).

Among the three ^{18}F-labeled Aβ PET tracers, ^{18}F-FBB was proved to have high in vitro affinity and specificity to amyloid-β, which brought our strong interest. The first human experimental study with FBB for its potential to assess amyloid-β plaques in mild AD patients was carried out in Australia by Rowe et al. (2008). In this study, 15 mild AD patients, 15 healthy elderly controls, and five patients with frontotemporal lobar degeneration (FTLD) underwent ^{18}F-FBB PET imaging. Images were analyzed both by visual interpretation (all patients with FTLD and 13 of the 15 HCs as Aβ negative) and by simple semi-quantitative measurement (compared to HCs or FTLD patients, higher neocortical SUVR was observed in AD patients). The results showed a robust separation of patients with AD from healthy elderly controls and FTLD patients (Rowe et al., 2008). In a pivotal histopathology phase 3 study, which validated ^{18}F-FBB by comparing *in vivo* PET imaging with postmortem histopathology, the results showed high sensitivity (97.9%) and specificity (88.9%) and high predictive values for the detection of histopathology-confirmed neuritic amyloid-β plaques (Sabri et al., 2015). Results from previous studies (Villemagne et al., 2012; Becker et al., 2013) also support the value of ^{18}F-FBB PET as a diagnostic marker.

In China, to the best of our knowledge, such validation of ^{18}F-FBB has not been achieved to date, especially for differentiation diagnosis of cognitive normal controls (NC), MCI patients, and AD patients, although ^{11}C-PIB and ^{18}F-florbetapir were relatively widely used. In our study, the aim was to evaluate and validate brain Aβ deposition in NC and MCI and AD patients using amyloid PET imaging with ^{18}F-FBB and in the comparative study using ^{11}C-PIB.

MATERIALS AND METHODS

Participants

A total of 45 subjects (15 in each group of NC, MCI, and mild/moderate AD) aged 55–86 years were enrolled in this study. Recruitment and evaluation of NC, MCI, and AD patients were performed at the Department of Neurologic Medicine, Chinese PLA General Hospital. Participants underwent a comprehensive clinical examination including medical history, neurological assessment, routine blood analysis, electrocardiography, psychometric examination, and amyloid PET imaging using ^{18}F-FBB and ^{11}C-PIB. All participants were given the Mini-Mental State Examination (MMSE) and the Clinical Dementia Rating (CDR) score to evaluate the cognitive status. Of these participants, all NC participants had no impairment in cognition and subjective complaint of memory decline with an MMSE score range of 28 or more and a CDR scale of 0. 15 patients with MCI had objective cognitive impairment and had no disability in their daily lives. The MMSE score was 24–28 and a CDR score of at least 0.5; 15 AD patients met the National Institute of Neurological and Communicative Disorders and Stroke and the Alzheimer's Disease and Related Disorders Association Alzheimer's criteria for probable AD and the Diagnostic and Statistical Manual of Mental Disorders-IV criteria for dementia of Alzheimer's type. Varying from moderate to mild, AD patients were reported with an MMSE score ranging from 18 to 25 and a CDR scale of 0.5 to 2. All participants had completed at least 9 years of education.

All participants underwent structural MRI examinations on a 3T Siemens MRI scanner (MAGNETOM Skyra, Siemens Medical Solutions, Erlangen, Germany). Participants with cerebral infarctions, history of significant head trauma, or brain diseases as well as participants with psychiatric disorders including serious depression and schizophrenia were excluded. Current or recent

drug or chronic alcohol dependence or use or any significant other systemic disease or unstable medical conditions were also excluded. The study was approved by the Chinese PLA General Hospital Human Ethics Committee (S2018-166-01). Written informed consent was obtained from all participants or their caregivers before participation. Safety monitoring consisted of clinical symptom observation and intermittent measurement of vital signs. Adverse events and side effects were evaluated 24 h, 48 h, and 2 weeks after injection.

Tracer Synthesis

^{18}F-FBB and ^{11}C-PIB were labeled and produced in the Department of Nuclear Medicine, Chinese PLA General Hospital. Xiantong International Pharmaceuticals, Inc. (Beijing, China) supplied the precursor and cold standard for production of ^{18}F-FBB. In brief, ^{18}F-FBB was synthesized by a PET-MF-2V-IT-I homemade fluoride module. The total synthesis time is about 38 min. The final product had an average specific activity of 337.5 GBq/μmol (222–453 GBq/μmol). The radiochemical purity is over 95%. ^{11}C-PIB was synthesized from its corresponding precursors as described elsewhere (Philippe et al., 2011). It was synthesized by ^{11}CH3-triflate and 6-OH-BTA-0, then purified by semi-preparative HPLC, and reformulated with a radiochemical purity of >95%.

PET/CT Imaging

All participants underwent ^{18}F-FBB PET/CT in a random order within 6 months after comprehensive clinical examination. PET/CT was performed using a 3D imaging consisting of a PET scanner and a multislice CT (μMl 510, United lmaging, China) in the Department of Nuclear Medicine. A spiral CT for the brain was acquired with CT parameters of 120 kV, 110 mAs, and slice thickness 3.00 mm, equal to those of PET. A vacuum cushion was used to minimize head movement during the scanning.

Participants underwent a dynamic PET emission scan in the three-dimensional mode. Dynamic brain PET images were collected continuously for 20 min. ^{11}C-PIB PET/CT images were obtained at 40–70 min after intravenous injection (3.7–5.5 MBq/kg), while ^{18}F-FBB PET/CT images were acquired at 90–110 min after injection (3.7–5.5 MBq/kg). Data obtained from the CT scans were used to correct the attenuation for PET emission data.

In a dual-tracer study, ^{18}F-FBB and ^{11}C-PIB were used in six NC participants and five patients with MCI and six with AD. ^{18}F-FBB and ^{11}C-PIB PET/CT were performed in all participants on separate days, independently.

Image Analysis

Regions of interest (ROI) analysis was performed on individual PET images and the co-registered CT images. The standardized uptake value ratio (SUVR) was calculated using the cerebellar cortex as a reference region, due to lack of amyloid plaque. To obtain quantitative regional SUVR values of ^{18}F-FBB and ^{11}C-PIB PET, circular ROI with a diameter of 1–1.5 cm was placed on eight bilateral cortical regions of the PET images corresponding to anatomic CT scans. The eight bilateral cortical regions were as follows: precuneus cortex (Pre), parietal cortex (PC), anterior cingulate gyrus (ACG), posterior cingulate gyrus (PCG), frontal cortex (FC), temporal cortex (TC), occipital cortex (OC), and cerebellar cortex. Global SUVR was defined as the arithmetic mean of the PC, ACG, PCG, FC, OC, and TC SUVR (Barthel et al., 2011).

For visual analysis of ^{18}F-FBB and ^{11}C-PIB PET, blind to clinical diagnosis and other clinical data, two independent nuclear medicine physicians with experience in interpretation of ^{18}F-FBB and ^{11}C-PIB PET images classified the ^{18}F-FBB and ^{11}C-PIB images as "amyloid positive" or "amyloid negative." A scan was read as positive if the tracer deposited was visible in one cortical region. A "negative scan" was defined when there was no increased tracer uptake in any cortical region (Marchant et al., 2011). ^{18}F-FBB images were generated from the 90–110-min data for visual inspection on a MedEx workstation and displayed with a rainbow color scale. Reading ^{18}F-FBB images starting at the cerebellum, scrolling upward to the TC and FC, then to the PCG and Pre, and finally to the PC (Sabri et al., 2015).

Statistical Analysis

All the data analyses were performed using SPSS (version 25.0; IBM). The normality of the distributions for all continuous variables was tested using the Shapiro–Wilk test. Continuous data for the three groups were evaluated using one-way ANOVA for normally distributed values. For comparisons of SUVR among NC participants, AD and MCI patients were performed using independent-sample *t*-tests. Spearman correlation coefficients and significance levels were used to evaluate correlations between SUVR values of ^{18}F-FBB PET vs. ^{11}C-PIB PET and MMSE. The effect size was calculated with Cohen *d*. Statistics were considered significant at $p < 0.05$. Data were presented as means ± standard deviations (SDs).

RESULTS

Cognitive Function

Fifteen NC, 15 MCI, and 15 AD patients were enrolled in our clinical study between May and October 2019. All the participants completed the study and were included in the final analysis. The participants' demographic characteristics are summarized in **Table 1**. There was no significant difference in gender among the NC, MCI, and AD groups. MCI and AD patients were significantly older than NC participants. MMSE and CDR scores were statistically significant among the three groups (**Table 1**).

TABLE 1 | Demographic information of study participants.

	AD (*n* = 15)	MCI (*n* = 15)	NC (*n* = 15)	*P*-value
Age (years)	74.40 ± 8.33	71.93 ± 7.35	64.07 ± 6.10	–
Gender (M/F)	8/7	7/8	8/7	–
MMSE score	20.80 ± 2.62	25.93 ± 1.28	29.27 ± 0.80	<0.001
CDR score	1.01 ± 0.42	0.47 ± 0.13	0.00 ± 0.00	<0.001

Data are reported as means ± standard deviation. Abbreviations: AD, Alzheimer's disease; MCI, mild cognitive impairment; NC, cognitive normal controls; MMSE, Mini-Mental State Examination; CDR, Clinical Dementia Rating Score.

Remarkably lower MMSE scores (20.80 ± 2.62) and higher CDR scores (1.01 ± 0.42) were observed in AD patients compared with NC participants or MCI patients, while MCI patients showed notably lower mean MMSE scores (25.93 ± 1.28) and higher CDR scores (0.47 ± 0.13) than NC participants.

Safety Analysis

No serious adverse reaction related to the study drug were observed and reported after the ^{18}F-FBB and PIB PET/CT scan and during at least the 2-week follow-up period.

Visual Analysis

The ^{18}F-FBB uptake was more extensive in Pre, PC, ACG, PCG, FC, TC, and OC (**Table 2**). A lot of the MCI patients also exhibited extensive Aβ deposition, especially in PCG, FC, and PC. The typical images in AD, positive (and negative) MCI, and NC patients are shown in **Figure 1**. Compared to the ^{11}C-PIB images, higher non-specific binding in the white matter was seen in the ^{18}F-FBB images (**Figure 1**).

Fourteen of the 15 NC participants were amyloid-negative and clearly distinguishable from patients with AD. One NC participant, a 75-year-old man, with no family history of dementia and no subjective or objective memory decline complaints, with mild positive ^{18}F-FBB PET signal, showed increased uptakes in the orbitofrontal cortex and lateral TC as observed in positive ^{11}C-PIB PET images. Of the 15 MCI patients, nine (60.0%) had positive scans on ^{18}F-FBB PET. Seven of the nine amyloid-positive MCI patients had typical positive scans. The remaining two patients showed focal positive scans: one patient was amyloid-positive in PC, FC, and TC, while the other was amyloid-positive in FC and PC. Among the nine MCI patients, five MCI patients underwent a dual-tracer (^{18}F-FBB and ^{11}C-PIB) study producing amyloid-positive images in both PET scans. Twelve of the 15 AD patients showed widespread cortical ^{18}F-FBB deposition; the proportion of patients with negative scans is consistent with previous clinical samples in AD (Villemagne et al., 2012). Six patients that underwent ^{11}C-PIB PET showed an almost identical cortical distribution compared to ^{18}F-FBB images. Both ^{11}C-PIB and ^{18}F-FBB-positive PET images showed highly increased uptakes in CG, FC, TC, PC, and OC, with no appreciable binding in the cerebellar cortex. In three AD patients, a 68-year-old man, a 69-year-old man, and a 72-year-old man, no amyloid plaques deposits were found.

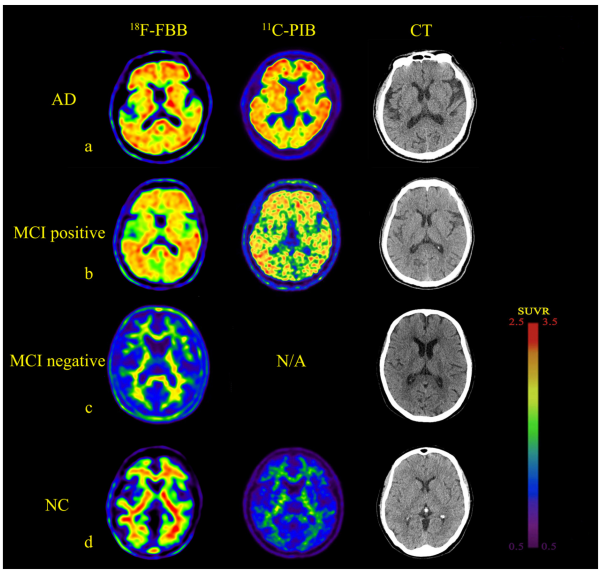

FIGURE 1 | Comparison of brain axial PET images of ^{18}F-FBB and ^{11}C-PIB in NC, MCI, and AD for example. **(a)** NC participant (75-years-old, male, MMSE = 28). **(b)** MCI patient (73-years-old, male, MMSE = 27). **(c)** MCI patient (67-years-old, female, MMSE = 24). **(d)** Early stage AD patient (78-years-old, male, MMSE = 24). Both ^{18}F-FBB PET/CT and ^{11}C-PIB PET/CT images showed no amyloid deposition **(a,c)**. Amyloid deposition in widespread cortical was almost identical in ^{18}F-FBB PET/CT and ^{11}C-PIB PET/CT **(b,d)**.

TABLE 2 | Regional and global ^{18}F-FBB SUVR and effect size in MCI and AD patients and NC participants.

	^{18}F-FBB		
Region	**NC**	**MCI (effect size)**	**AD (effect size)**
Precuneus cortex	1.20 ± 0.28	1.58 ± 0.60(0.92)	1.81 ± 0.43(1.68)
Parietal cortex	1.19 ± 0.20	1.48 ± 0.59(0.65)**	1.75 ± 0.37(1.88)*
Anterior cingulate gyrus	1.08 ± 0.36	1.42 ± 0.69(0.61)**	1.62 ± 0.33(1.56)*
Posterior cingulate gyrus	1.16 ± 0.28	1.63 ± 0.70(0.88)**	1.78 ± 0.41(1.76)*
Frontal cortex	1.01 ± 0.18	1.68 ± 0.93(1.00)**	1.7 ± 0.32(2.65)*
Temporal cortex	1.10 ± 0.26	1.66 ± 0.83(0.91)**	1.76 ± 0.35(2.71)*
Occipital cortex	1.13 ± 0.20	1.48 ± 0.54(0.85)**	1.78 ± 0.34(2.33)*
Global[a]	1.13 ± 0.43	1.55 ± 0.11(1.34)**	1.73 ± 0.62(1.12)*
Cerebellar cortex (reference region)	0.92 ± 0.14	0.97 ± 0.34(0.07)	0.99 ± 0.16(0.19)

*Data are presented as means ± standard deviation. Abbreviations: AD, Alzheimer's disease; MCI, mild cognitive impairment; NC, cognitive normal controls; SUVR, standardized uptake value ratio. *Significantly different from HC (P < 0.05). **Significantly different from MCI (P < 0.05). [a]Arithmetic mean of anterior cingulate and posterior cingulate gyrus, parietal cortex, frontal cortex, lateral temporal cortex, and occipital cortex SUVR.*

Quantitative Analysis

The mean values of ^{18}F-FBB SUVR and effect size by brain regions for the three groups are summarized in **Table 2**. For ^{18}F-FBB PET, the SUVR was significantly higher in AD patients in all cortical regions as well as the global cortex (1.73 ± 0.62; $P < 0.001$) than those of NC participants. There was a significant difference between the global SUVR of MCI patients and NC participants (**Figure 2** and **Table 2**). In ^{18}F-FBB PET, MCI patients yielded a slightly higher effect size than did AD patients ($d = 1.34$ and 1.12 for MCI and AD, respectively; **Table 2**).

Comparisons of characteristics in each group are illustrated in **Table 3**. Seventeen subjects underwent both ^{18}F-FBB and ^{11}C-PIB PET/CT studies on separate days, respectively. The final diagnosis was as follows: NC: $n = 6$, MCI: $n = 5$; early AD: $n = 5$; moderate AD: $n = 1$. Global SUVRs in the ^{18}F-FBB and ^{11}C-PIB PET/CT

studies were similar (1.46 ± 0.32 vs. 1.47 ± 0.41, respectively), while ^{18}F-FBB SD was slightly wider (**Figure 3A**). **Figure 3A** shows between SUVR of ^{18}F-FBB PET and global SUVR of PIB PET. A strong positive linear correlation (r^2 = 0.81, P < 0.001) of global SUVR between ^{18}F-FBB and ^{11}C-PIB was observed. Spearman correlation analysis was performed between MMSE scores and SUVR of ^{18}F-FBB and ^{11}C-PIB images. We found that MMSE scores had negative correlations with SUVR on ^{11}C-PIB PET (r_1 = −0.650, P = 0.005) or SUVR on ^{18}F-FBB PET (r_2 = −0.754, P < 0.0001). That is, the higher the MMSE scores were, the smaller the SUVR on ^{11}C-PIB PET or ^{18}F-FBB PET was. Furthermore, the correlation of the MMSE score with SUVR on ^{18}F-FBB PET was detected larger than that with SUVR on ^{11}C-PIB PET (| r_2| >| r_1|) (**Figure 3B**).

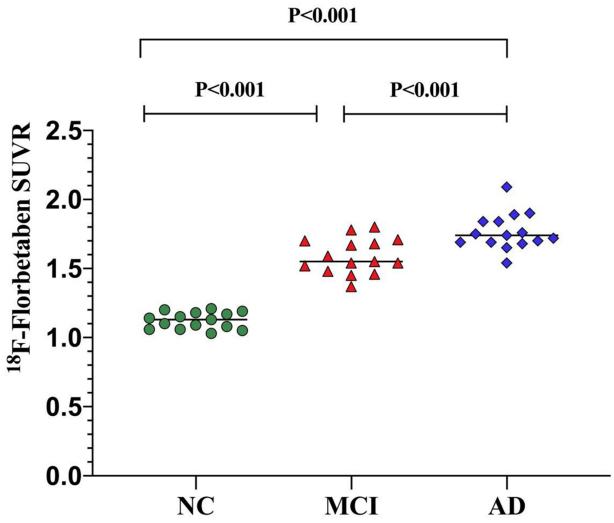

FIGURE 2 | Global SUVR of ^{18}F-FBB analyses in NC participants and patients with MCI and AD. Global SUVR of AD patients (1.73 ± 0.62) were significantly higher than those of MCI patients (1.55 ± 0.11) and NC (1.13 ± 0.43) participants.

DISCUSSION

The aim of this study was to evaluate amyloid positivity by visual analysis and quantitative analysis of ^{18}F-FBB SUVR in the NC participants and MCI and AD patients as well as comparing its correlation with ^{11}C-PIB PET. As expected, we demonstrated that ^{18}F-FBB is a useful amyloid PET tracer with excellent linear correlation in the detectability of amyloid deposition, compared to ^{11}C-PIB.

In our study, the AD patients and amyloid-positive MCI patients showed higher cortical uptake than amyloid-negative MCI patients and NC participants in ^{18}F-FBB PET/CT. It is important to note in this study that one NC participant was deemed to be amyloid-positive. In addition, the proportion of amyloid-positive patients is lower than in some previous studies (Villemagne et al., 2012; Landau et al., 2014). The prevalence of scans positive of ^{18}F-FBB and PIB reported in our study is slightly lower than that of positive scans in NC participants in the previous study (Villemagne et al., 2012). This may be related to the younger age of the participants in the NC group.

In the dual-tracer study, ^{18}F-FBB and ^{11}C-PIB images were similar to the progression of Aβ deposition categorized by Braak staging (Braak and Braak, 1991, 1997). In the AD spectrum (both MCI and AD), Aβ deposition was seen in FC, ACG, PCG, PC, Pre, and TC in the majority of patients; dual-tracer images may correspond to Braak C stages. There was no significant Aβ deposition in nine patients, which may correspond to Braak stage 0. Visual analysis proved the diagnostic ability of ^{18}F-FBB to be comparable to other amyloid PET tracers (**Figure 1**). The quantification comparison between ^{18}F-FBB and ^{11}C-PIB exhibited an excellent linear correlation, which further illustrated the diagnostic value of ^{18}F-FBB (**Figure 3A**). Moreover, we found that the threshold of global SUVR was about 1.4 in ^{18}F-FBB, which closely corresponded to a global SUVR of 1.5 in ^{11}C-PIB. We also found that there was a negative correlation between MMSE score and SUVR values of ^{18}F-FBB PET vs. ^{11}C-PIB PET in three groups, indicating that the severity of the disease is associated with the significance of cognitive decline.

^{18}F-FBB images (**Figure 1**) showed an excellent differentiation diagnosis possibility in NC, MCI, and AD. The results convince us to believe that this radiotracer provided a robust separation of AD patients from MCI and NC participants. SUVR comparison between three groups verified our hypothesis (**Figure 2**). This separation was performed by visual image analysis and a quantitative measure derived from a short PET scan. In visual analysis, cortical uptake and global SUVR of ^{18}F-FBB were slightly higher in MCI patients than in NC participants in PET scans. The threshold value of global SUVR 1.4 could clearly distinguish between MCI and NC participants. However, several patients with MCI showed amyloid-negative deposition and one patient with amyloid deposition was found in the NC group. It is reported that about 10–30% of healthy aged persons showed high amyloid deposition (Cohen et al., 2012). So, this is reasonable to have an amyloid-positive patient in 15 NC participants. Moreover, for the MCI group, 60% of ^{18}F-FBB scans are positive, consistent with the previous study (Anna et al., 2018). Follow-up studies have reported that 70% of amyloid-positive MCI patients will progress to dementia due to AD over 3 years (Okello et al., 2009; Villemagne et al., 2011). Further deep research is needed. As we mentioned above, our clinical diagnosis of AD was not confirmed with pathology due to the unavailability of autopsy.

For visual diagnosis, as shown in **Figure 1**, a distinct feature was the higher degree of non-specific binding of ^{18}F-FBB to white matter, which is a common feature of ^{18}F-florbetapir and ^{18}F-flutemetamol (Vandenberghe et al., 2010; Wong et al., 2010). Due to the higher non-specific binding in white matter, the visual readouts of ^{18}F-FBB and all the other novel ^{18}F-labeled amyloid radiotracers seem to be challenging in clinical application. The spillover effect of white matter might result in higher measurement of cortical uptake than its actual value. In NC participants, white matter uptake of ^{18}F-FBB was significantly higher than that of ^{11}C-PIB. ^{11}C-PIB PET images usually show

TABLE 3 | Characteristics of 17 participants examined by ^{18}F-FBB and by ^{11}C-PIB.

Participants	Age	Sex	Clinical diagnosis	MMSE score	CDR score	FBB SUVR	PIB SUVR
1	57	M	NC	29	0	1.03	0.69
2	67	F	NC	29	0	1.18	1.16
3	75	M	NC[a]	28	0	1.13	0.75
4	64	F	NC	28	0	1.06	0.90
5	63	F	NC	30	0	1.14	1.05
6	59	F	NC	30	0	1.09	0.94
7	64	M	MCI	25	0.5	1.37	1.14
8	71	M	MCI	26	0.5	1.52	1.69
9	73	M	MCI[b]	27	0.5	1.59	1.81
10	85	F	MCI	28	0.5	1.54	1.73
11	76	F	MCI	27	0.5	1.48	1.39
12	86	M	Early AD	21	1	1.84	1.71
13	78	M	Early AD[c]	24	1	1.69	2.10
14	76	F	Early AD	23	1	1.54	1.67
15	70	F	Early AD	21	1	1.89	1.74
16	60	F	Early AD	21	0.5	1.70	1.48
17	83	M	Moderate AD	18	2	2.09	2.30
Total	71.0 ± 9.10			25.59 ± 3.66	0.53 ± 0.54	1.46 ± 0.32	1.47 ± 0.41

*Data are reported as means ± standard deviation. Abbreviations: AD, Alzheimer's disease; MCI, mild cognitive impairment; NC, cognitive normal controls; MMSE, Mini-Mental State Examination; CDR, Clinical Dementia Rating Score; SUVR, standardized uptake value ratio. [a]Case d, [b]Case b, and [c]Case a in **Figure 1**.*

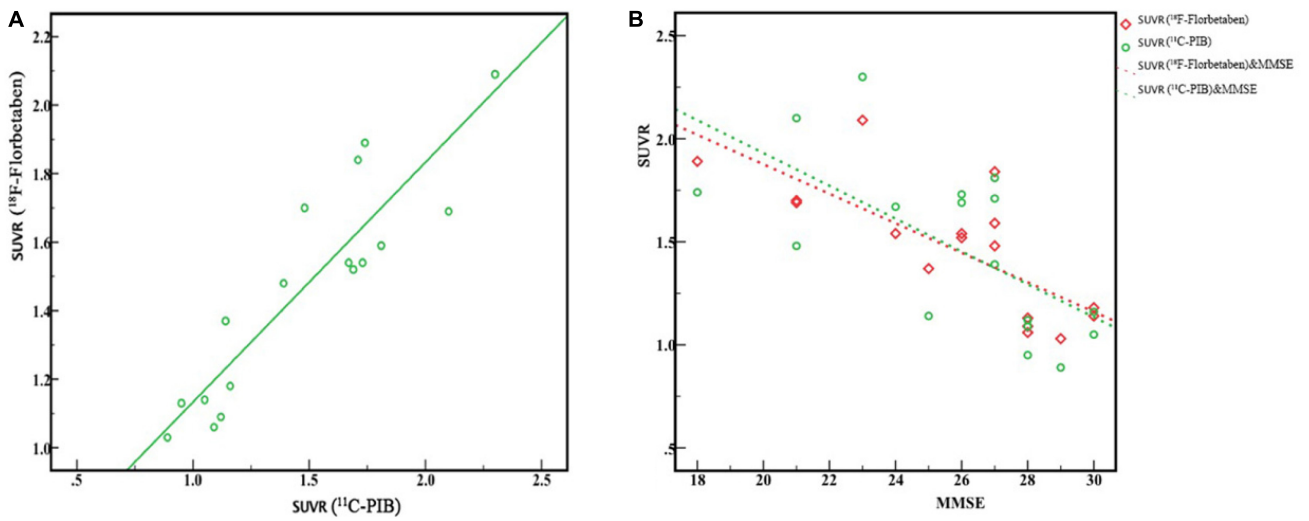

FIGURE 3 | Correlation between ^{18}F-FBB and ^{11}C-PIB global SUVR from six AD and five MCI patients and six NC participants. **(A)** Excellent linear correlation was observed ($r^2 = 0.81$, $P < 0.0001$). **(B)** MMSE scores had a negative correlation with SUVR of PIB PET ($r_1 = 0.650$, $P < 0.005$) and SUVR of ^{18}F-FBB PET ($r_2 = 0.754$, $P < 0.0001$).

deposition in gray matter in excess of that in white matter in AD. While the ^{18}F-labeled amyloid radiotracers all show a distinctive white matter pattern in those with no or low Aβ deposition, in AD patients, these ^{18}F-labeled novel tracers frequently show loss of the gray–white matter demarcation with a consequent loss of the normal white matter pattern as the predominant evidence of cortical Aβ deposition (Rowe and Villemagne, 2011). However, each of the FDA-approved agents provides a nearly identical qualitative evaluation of the presence of cortical Aβ deposition and diagnostic abilities (Vandenberghe et al., 2010; Wong et al., 2010; Sabri et al., 2015). Despite this, both radiotracers provided a robust separation of AD patients from MCI-negative patients and NC participants. White matter hyperintensities (WMHs or leukoareosis) are commonly seen in AD patients, and MRI often shows focal hyperintensities in the deep and subcortical white matter. Pietroboni et al. reported that WM damage represents a crucial feature in AD pathogenesis. Moreover, the correlation between CSF Aβ levels and WM-lesion load suggests a confirmed link between Aβ pathology and WM macrostructural and microstructural damage. A further

limitation of this study is the lack of structural MRI data, which would allow us to evaluate WM macrostructural and microstructural damage and adjust for volume loss. Besides, SUVR in amyloid PET was calculated using the cerebellum as a reference region in most studies (Barthel et al., 2011; Villemagne et al., 2012; Hatashita et al., 2014) which is known to have very little accumulation of Aβ (Svedberg et al., 2009) leading to a higher SUVR. There was a significant correlation between ^{18}F-FBB and ^{11}C-PIB in the global SUVR. The slope of the linear correlation was 0.43. This slope is similar to or lower than other ^{18}F-labeled Aβ radiopharmaceuticals, such as ^{18}F-flutemetamol (slope of 0.81) (Landau et al., 2014), ^{18}F-florbetapir (slopes ranging from 0.33 to 0.64) (Wolk et al., 2012; Landau et al., 2013), and ^{18}F-FC119S (slope of 0.41) (Byun et al., 2017).

For ^{18}F-FBB, PET images are obtained 90 min after injection, similar to ^{18}F-flutemetamol (90 min after injection) (Byun et al., 2017) or longer than other ^{18}F-labeled Aβ radiopharmaceuticals, such as ^{18}F-FC119S (30 min after injection) (Byun et al., 2017) and ^{18}F-florbetapir (30–50 min after injection) (Wolk et al., 2012; Landau et al., 2013). Anyway, the total time spent for PET imaging after injection of ^{18}F-FBB (110 min) is similar to other ^{18}F-labeled Aβ radiopharmaceuticals (40–150 min).

Furthermore, research efforts that have more broadly measured amyloid burden antemortem with amyloid PET imaging might have the potential to be helpful for differential diagnosis in neurodegenerative dementia, including dementia with Lewy bodies (DLB), Parkinson disease with dementia (PDD), and vascular dementia (VaD). Despite these dementias being similar and the overlapping clinical, neuropsychological, and neuropathological features, DLB, VaD, PD, and PDD could be differentiated by their degree of cortical deposition of amyloid and cognitive ability (Rik et al., 2015; Donaghy et al., 2018; Melzer et al., 2019). Some studies found Aβ to be consistently higher among Down's syndrome (DS); however, the association between Aβ1-40 and Aβ1-42 concentrations among DS and AD dementia was inconsistent (Iulita et al., 2016; Lee et al., 2016; Fortea et al., 2018; O'Bryant et al., 2018). This was the initial study on ^{18}F-FBB in China. With little experience for differential diagnosis in neurodegeneration, our future work will explore the role amyloid PET and blood-based biomarkers play in AD and other neurodegeneration dementias during the process of the study and literatures review.

Our study has several certain limitations that should be noted. First, the relatively small number of our study population and the use of correlation instead of regression analysis to interpret data cannot indicate causality between variables, leading to a limited statistical power. Our results should be interpreted with caution. Second, the clinical diagnosis of patients with AD was performed before PET study by certified physicians in a comprehensive diagnosis applying DSM-IV and the NINCDS-ADRDA criteria. No autopsy or histopathological confirmation of amyloid plaque accumulation or biomarkers in cerebrospinal fluids [such as Aβ40, Aβ42, and phosphorylated Tau (pTau)] was performed. Finally, we have not evaluated MCI potential progression to AD. It is possible that several amyloid-positive patients will develop AD in future. Future studies and follow-up study would be required.

CONCLUSION

Our clinical study demonstrated that ^{18}F-FBB could reliably detect Aβ deposition *in vivo* and discriminating NC and AD patients, which is significantly correlated with ^{11}C-PIB. Although ^{18}F-FBB showed higher non-specific binding to white matter in participants, we could obtain images similar to ^{11}C-PIB PET. The total time spent for ^{18}F-FBB imaging is similar to other ^{18}F-labeled Aβ radiotracers. In addition, all of these results suggest ^{18}F-FBB to be a useful and suitable tool for Aβ deposition imaging *in vivo*. We would like to expand the utilization of this tracer further in various fields of research and clinical practice.

DATA AVAILABILITY STATEMENT

All datasets presented in this study are included in the article/supplementary material.

ETHICS STATEMENT

The studies involving human participants were reviewed and approved by the Chinese PLA General Hospital Human Ethics Committee. The patients/participants provided their written informed consent to participate in this study. Written informed consent was obtained from the individual(s) and/or minor(s)' legal guardian/next of kin for the publication of any potentially identifiable images or data included in this article.

AUTHOR CONTRIBUTIONS

YC and CL contributed to the conception and design of the study and wrote the first draft of the manuscript. HY performed the statistical analysis. YW revised the manuscript. BX, JZ, and RW ensured that the questions related to the accuracy or integrity of any part of the work are appropriately investigated and resolved. All authors contributed to the manuscript revision and read and approved the submitted version.

FUNDING

RW has received research grants from the Capital Clinical Special Application (Z121107001012116), Medical Big Data Project of Chinese PLA General Hospital (2019MBD-007), and National Natural Science Foundation of China (11975249).

ACKNOWLEDGMENTS

We thank Dr. Shulin Yao from the Department of Nuclear Medicine, Chinese PLA General Hospital, for the technical support regarding this work.

REFERENCES

Anna, M., Pietroboni, H., Marta, S., and Tiziana, C. (2018). CSF β-amyloid and white matter damage: a new perspective on Alzheimer's disease. *J. Neurol. Neurosurg. Psychiatry* 89, 352–357. doi: 10.1136/jnnp-2017-316603

Barthel, H., Gertz, H. J., and Dresel, S. (2011). Cerebral amyloid-beta PET with florbetaben (18F) in patients with Alzheimer's disease and healthy controls: a multicentre phase 2 diagnostic study. *Lancet Neurol.* 10, 424–435. doi: 10.1016/S1474-4422(11)70077-1

Becker, G. A., Ichise, M., and Barthek, H. (2013). PET quantification of 18F-florbetaben binding to beta-amyloid deposits in human brains. *J. Nucl. Med.* 54, 723–731. doi: 10.2967/jnumed.112.107185

Braak, H., and Braak, E. (1991). Neuropathological staging of Alzheimer-related changes. *Acta Neuropathol.* 82, 239–259. doi: 10.1007/BF00308809

Braak, H., and Braak, E. (1997). Frequency of stages of Alzheimer-related lesions in different age categories. neurobiol aging. *Neurobiol. Aging* 18, 351–357. doi: 10.1016/s0197-4580(97)00056-0

Byun, B. H., Kim, B. I., and Park, S. Y. (2017). Head-to-head comparison of 11C-PiB and 18F-FC119S for Aβ imaging in healthy subjects, mild cognitive impairment patients, and Alzheimer's disease patients. *Medicine* 96:e6441. doi: 10.1097/MD.0000000000006441

Cohen, A. D., Rabinovici, G. D., and Mathis, C. A. (2012). Using Pittsburgh compound B for in vivo PET imaging of fibrillar amyloid-beta. *Adv. Pharmacol.* 64, 27–81. doi: 10.1016/B978-0-12-394816-8.00002-7

Donaghy, P. C., Firbank, M. J., Thomas, A. J., Lloyd, J., Petrides, G., Barnett, N., et al. (2018). Clinical and imaging correlates of amyloid deposition in dementia with lewy bodies. *Mov. Disord.* 3, 1130–1138. doi: 10.1002/mds.27403

Fortea, J., Carmona-Iragui, M., and Benejam, B. (2018). Plasma and CSF biomarkers for the diagnosis of Alzheimer's disease in adults with down syndrome: a cross-sectional study. *Lancet Neurol.* 17, 860–869. doi: 10.1016/s1474-4422(18)30285-0

Hatashita, S., Yamasaki, H., and Suzuki, Y. (2014). [18F]Flutemetamol amyloid-beta PET imaging compared with [11C]PIB across the spectrum of Alzheimer's disease. *Eur. J. Nucl. Med. Mol. Imaging* 41, 290–300. doi: 10.1007/s00259-013-2564-y

Iulita, M. F., Ower, A., and Barone, C. (2016). An inflammatory and trophic disconnect biomarker profile revealed in down syndrome plasma: relation to cognitive decline and longitudinal evaluation. *Alzheimer's Dementia J. Alzheimer's Assoc.* 12, 1132–1148. doi: 10.1016/j.jalz.2016.05.001

Jack, C. R., Bennett, D. A., and Blennow, K. (2018). NIA-AA research framework: toward a biological definition of Alzheimer's disease. *Alzheimer's Dement.* 14, 535–562. doi: 10.1016/j.jalz.2018.02.018

Jia, L., Quan, M., and Fu, Y. (2019). Dementia in China: epidemiology, clinical management, and research advances. *Lancet Neurol.* 19, 81–92. doi: 10.1016/S1474-4422(19)30290-X

Landau, S. M., Breault, C., and Joshi, A. D. (2013). Amyloid-beta imaging with Pittsburgh compound B and florbetapir: comparing radiotracers and quantification methods. *J. Nucl. Med.* 54, 70–77. doi: 10.2967/jnumed.112.109009

Landau, S. M., Thomas, B. A., and Thurfjell, L. (2014). Amyloid PET imaging in Alzheimer's disease: a comparison of three radiotracers. *Eur. J. Nucl. Med. Mol. Imaging* 41, 1398–1407. doi: 10.1007/s00259-014-2753-3

Lee, N. C., Yang, S. Y., and Chieh, J. J. (2016). Blood beta-amyloid and tau in Down syndrome: a comparison with Alzheimer's disease. *Front. Aging Neurosci.* 8:316.

Marchant, N. L., Reed, B. R., and Decarli, C. S. (2011). Cerebrovascular disease, beta-amyloid, and cognition in aging. *Neurobiol. Aging* 33:1006.e25–36. doi: 10.1016/j.neurobiolaging.2011.10.001

McKhann, G. M., Knopman, D. S., and Chertkow, H. (2011). The diagnosis of dementia due to Alzheimer's disease: recommendations from the National Institute on aging and the Alzheimer's assocation workgroup. *Alzheimer's Dement.* 7, 263–269. doi: 10.1016/j.jalz.2011.03.005

Melzer, T. R., Stark, M. R., Keenan, R. J., Myall, D. J., MacAskill, M. R., Pitcher, T. L., et al. (2019). Beta Amyloid deposition is not associated with cognitive impairment in Parkinson's Disease. *Front. Neurol.* 10:391. doi: 10.3389/fneur.2019.00391

O'Bryant, S., Zhang, F., and Lee, J. (2018). "Proteomic biomarkers for detecting and predicting AD risk among adults with Down syndrome," in *FRS Presentation at the 2018 Alzheimer's Association International Conference*, Chicago, IL.

Okello, A., Koivunen, J., and Edison, P. (2009). Conversion of amyloid positive and negative MCI to AD over 3 years: an 11C-PIB PET study. *Neurology* 73, 754–760. doi: 10.1212/WNL.0b013e3181b23564

Philippe, C., Haeusler, D., and Mitterhauser, M. (2011). Optimization of the radiosynthesis of the Alzheimer tracer 2-(4-N-[11C]methylaminophenyl)-6-hydroxybenzothiazole ([11C]PIB). *Appl. Radiat. Isot.* 69, 1212–1217. doi: 10.1016/j.apradiso.2011.04.010

Rabinovici, G. D., Furst, A. J., and O'Neil, J. P. (2007). 11C-PIB PET imaging in Alzheimer disease and frontotemporal lobar degeneration. *Neurology* 68, 1205–1212. doi: 10.1212/01.wnl.0000259035.98480.ed

Rik, O., Willemijn, J. J., and Gil, D. (2015). Prevalence of amyloid PET positivity in dementia syndromes: a meta-analysis. *JAMA* 313, 1939–1949. doi: 10.1001/jama.2015.4669

Rowe, C. C., Ackerman, U., and Browne, W. (2008). Imaging of amyloid beta in Alzheimer's disease with (18)F-BAY94-9172, a novel PET tracer: proof of mechanism. *Lancet Neurol.* 7, 129–135. doi: 10.1016/S1474-4422(08)70001-2

Rowe, C. C., Ng, S., and Ackermann, U. (2007). Imaging beta-amyloid burden in aging and dementia. *Neurology* 68, 1718–1725. doi: 10.1212/01.wnl.0000261919.22630.ea

Rowe, C. C., and Villemagne, V. L. (2011). Brain amyloid imaging. *J. Nucl. Med.* 52, 1733–1740. doi: 10.2967/jnumed.110.076315

Sabri, O., Sabbagh, M. N., and Seibyl, J. (2015). Florbetaben PET imaging to detect amyloid beta plaques in Alzheimer's disease: phase 3 study. *Alzheimer's Dement.* 11, 964–974. doi: 10.1016/j.jalz.2015.02.004

Svedberg, M. M., Hall, H., and Hellstrom-Lindahl, E. (2009). [(11)C]PIB-amyloid binding and levels of Abeta40 and Abeta42 in postmortem brain tissue from Alzheimer patients. *Neurochem. Int.* 54, 347–357. doi: 10.1016/j.jalz.2010.05.383

Vandenberghe, R., Van Laere, K., Ivanoiu, A., and Salmon, E. (2010). 18F-flutemetamol amyloid imaging in Alzheimer disease and mild cognitive impairment: a phase 2 trial. *Ann. Neurol.* 68, 319–329. doi: 10.1002/ana.22068

Villemagne, V. L., Mulligan, R. S., and Pejoska, S. (2012). Comparison of 11C-PiB and 18F-florbetaben for Aβ imaging in ageing and Alzheimer's disease. *Eur. J. Nucl. Med. Mol. Imaging* 39, 983–989. doi: 10.1007/s00259-012-2088-x

Villemagne, V. L., Pike, K. E., and Chetelat, G. (2011). Longitudinal assessment of Abeta and cognition in aging and Alzheimer disease. *Ann. Neurol.* 69, 181–192. doi: 10.1002/ana.22248

Wolk, D. A., Zhang, Z., and Boudhar, S. (2012). Amyloid imaging in Alzheimer's disease: comparison of florbetapir and Pittsburgh compound-B positron emission tomography. *J. Neurol. Neurosurg. Psychiatry* 83, 923–926. doi: 10.1136/jnnp-2012-302548

Wong, D. F., Rosenberg, P. B., and Zhou, Y. (2010). In vivo imaging of amyloid deposition in Alzheimer disease using the radioligand 18F-AV-45 (flobetapir F 18). *J. Nucl. Med.* 51, 913–920. doi: 10.2967/jnumed.109.069088

Conflict of Interest: YW was employed by company Siemens Healthineers Ltd., Beijing, China.

The remaining authors declare that the research was conducted in the absence of any commercial or financial relationships that could be construed as a potential conflict of interest.

frontiers in Cellular Neuroscience

BRIEF RESEARCH REPORT
published: 13 August 2020
doi: 10.3389/fncel.2020.00230

CCR2 Inhibition Reduces Neurotoxic Microglia Activation Phenotype After Japanese Encephalitis Viral Infection

*Swati Singh†, Gajendra Singh†, Swasti Tiwari and Alok Kumar**

Department of Molecular Medicine and Biotechnology, Sanjay Gandhi Postgraduate Institute of Medical Sciences (SGPGIMS), Lucknow, India

Controlling the proinflammatory response of microglia by targeting chemokines (C-C motif) receptor 2 (CCR2) could be an important therapeutic approach for Japanese encephalitis virus (JEV) infection. Here, through JEV infection to BV2 microglia and young BALB/c mice, we investigated that CCR2 is highly upregulated after JEV infection and plays a key role in determining microglia activation phenotype and associated with neurotoxic proinflammatory mediators of TNF-α and IFNγ. In addition, we found JEV infection to BV2 microglia causes an increase in microglial proliferation and cell body area at day 1 and day 3. Using the agonist molecule of CCR2 inhibition; RS102895, significantly reduces microglia reactive phenotype and nitric oxide production. Further, to define the role of CCR2 in functional responses of microglia and their activation phenotype, we performed *in vitro* cell scratch functional assay and ImageJ analysis. When compared with control, microglia cells showed a significant increase in elongated or rod-like activated phenotype in JEV-infected cells at 24 h post-infection and CCR2 inhibition significantly reduced the elongated activation phenotype induced by JEV infection, suggesting that CCR2 acts as a critical regulator for microglia activation phenotype after JEV infection. We found that JEV-infected mice treated with RS102895 had less microglia activation and reduced mRNA expression of CCR2 and proinflammatory mediators such as IFN-γ in cortical tissue. Collectively, our data indicate that CCR2 drives reactive phenotype of microglia and its inhibition reduces microglia activation and neurotoxic proinflammatory mediators after JEV infection.

Keywords: japanese encephalitis virus infection, microglia activation, proinflammatory markers, CCR2 chemokine receptor, CCR2 chemokine receptor inhibition

OPEN ACCESS

Edited by:
Gjumrakch Aliev, GALLY International Biomedical Research, United States

Reviewed by:
Bin Zhou, Nanjing Agricultural University, China
Chun-Jung Chen, Taichung Veterans General Hospital, Taiwan

****Correspondence:***
Alok Kumar
dralokkumar03@gmail.com

†These authors have contributed equally to this work

Specialty section:
This article was submitted to Non-Neuronal Cells, a section of the journal Frontiers in Cellular Neuroscience

Received: *15 April 2020*
Accepted: *30 June 2020*
Published: *13 August 2020*

Citation:
Singh S, Singh G, Tiwari S and Kumar A (2020) CCR2 Inhibition Reduces Neurotoxic Microglia Activation Phenotype After Japanese Encephalitis Viral Infection. Front. Cell. Neurosci. 14:230. doi: 10.3389/fncel.2020.00230

INTRODUCTION

Recently, both experimental and clinical studies demonstrated that uncontrolled neuroinflammatory responses of central nervous system in Japanese encephalitis virus (JEV) infection is a major contributor to cell death and neurological dysfunction (Chen et al., 2012). JEV infection induced a neuroinflammatory response including microglia activation that further found engaged in release of proinflammatory mediators (e.g., TNF-α, IFN-γ) along with production of reactive oxygen species that contribute to neuronal cell death in bystander fashion (Das et al., 2008; Thongtan et al., 2010; Chen et al., 2012). However, the underlying molecular mechanism of dysregulated proinflammatory responses of microglia after JEV infection is not well understood.

Though, in some studies, of microglia migration dynamics, alteration in their morphology including activation from resting phenotype, and adaptation of phagocytic morphologies are observed in association with their neuroinflammatory responses and neuronal cell death after JEV infection (Kreutzberg, 1996; Ghoshal et al., 2007; Kettenmann et al., 2011; Sips et al., 2012).

Chemokines are found to play an important role in recruitment of leukocytes and other immune cells in the specific area of the JEV-infected brain. For instance, chemokines (C-C motif) ligand-2 (CCL-2) and its receptor chemokines (C-C motif) 2 (CCR2) were found upregulated in brain cortex, striatum, thalamus, hippocampus, sub-ventricular zone, and midbrain area in JEV infection (Swarup et al., 2008; Das et al., 2011; Srivastava et al., 2012; Han et al., 2014) and associated with infiltration of monocytes, T-lymphocytes, and natural killer cells in inflamed brain areas (Rollins, 1991; Getts et al., 2008; Semple et al., 2010). CCR2 expression was also found to be significantly increased in resident immune cells of human microglia followed by JEV infection (Lannes et al., 2017), suggesting that CCR2 plays a key role in the regulation of microglia function and JEV pathogenesis. In recent study, it is also elucidated that CCR2 inhibition attenuates microglia activation and proinflammatory response to kainic acid (KA)-induced injury and reduces microglia-mediated neuronal cell death pathways (Tian et al., 2017). But, CCR2-dependent changes in microglia phenotype and their response followed by JEV infection need to be elucidated further. Here, we set out to investigate the cellular mechanism that drives proinflammatory response of microglia after JEV infection and to establish the role of CCR2 in JEV pathogenesis. The aims of the current study are: (1) to test the hypothesis that CCR2 activation is associated with proinflammatory response of microglia, and (2) to determine that systemic administration of CCR2 antagonist molecule RS102895 reduces proinflammatory response of microglia in JEV-infected mice.

MATERIALS AND METHODS

Virus

An Indian neurovirulent, GP78 (GP 78668A) strain of JEV was used in the study. Virus was propagated in 2–3 weeks old suckling mice brain. A total of 25 μl from stock was inoculated intracerebrally in 2–3 weeks old suckling mice. After 4 days of infection; the mice were deeply anesthetized with chloroform, sacrificed, and brain tissue was homogenized in sterile phosphate-buffered saline (PBS) and virus titer was determined by the standard plaque assay (Yang et al., 2004).

Animal

BALB/c mice 2–3 weeks old were used throughout the study. Mice were procured and housed at the animal care facility of SGPGIMS, Lucknow. Mice were fed with protein-rich diet and water *ad libitum*. The animals were maintained in an air-conditioned room (25 ± 2°C) with 12 h light (7:00–19:00) and dark cycle. All the experiments were performed during the daylight cycle.

JEV Inoculation

BALB/c mice were inoculated with 3×10^6 plaque-forming units (PFU) resuspended in 20 μl of PBS by using stereotaxic intracerebral injection with bregma and lambda on the same horizontal plane as described before Shukla et al. (2016). Control mice were inoculated with sterile 1× PBS (Sigma, USA). Mice were monitored daily and were sacrificed at days 3 and 7 post-inoculation. The brains were excised aseptically and were processed for biochemical analysis.

Study 1

Sham and JEV-infected mice (n = 4/group) were used for immunohistochemistry studies. At 7 days post-infection, mice were transcardially perfused with ice-cold 0.9% saline (100 ml), followed by 300 ml of 4% paraformaldehyde. Brains were removed and post-fixed in 4% paraformaldehyde overnight, and cryoprotected in 30% sucrose and were processed for microglia analysis.

Study 2

Sham and JEV-infected (n = 7/time point/group) mice were transcardially perfused with ice-cold 0.9% saline (100 ml) at 3 and 7 days post-infection. Ipsilateral cortical tissue was rapidly dissected and snap-frozen on liquid nitrogen for RNA extraction and western blotting.

Study 3

A CCR2 antagonist, RS102895, was intraperitoneally (i.p.) injected by giving a dose of 5 mg/kg at 72 h before JEV infection (n = 6) or control (n = 6) and once daily for the following 5 days. Mice were transcardially perfused with ice-cold 0.9% saline (100 ml), and ipsilateral cortical tissue was rapidly dissected and processed for snap-freezing on liquid nitrogen for RNA extraction and western blot analysis.

BV2 Microglia Cell Culture, Cell Body Area, and Proliferation Analysis

BV2 microglia (murine microglial cell line) were grown on poly-L-lysine (Sigma–Aldrich) coated with or without coverslips in a 24-well plate and were maintained in Dulbecco's modified Eagle's medium (DMEM; Invitrogen, Carlsbad, CA, USA) supplemented with 10% fetal equine serum (HyClone, Logan, UT, USA) and 1% penicillin and streptomycin (Invitrogen) at 37°C with 5% CO_2. Mock or JEV (at a multiplicity of infection of 10 TCID50/cell) infections were introduced for various time periods and cell body area, and proliferation analysis was performed as described before (Flora et al., 2019; Verdonk et al., 2016). Briefly, bright-field high-magnification images were acquired at constant light intensity and exposure. Images were exported to ImageJ software, where cell body area was analyzed using selection drawing tools. Similarly, for cell proliferation assay, BV2 microglia cells were treated with mock or JEV infection at 37°C with 5% CO_2 for the time period of 3, 24, and 72 h. Cells were trypsinized and were incubated with equal mixture of trypan blue and viable cells were counted using a hemocytometer.

RS102895 Treatment and Scratch Analysis

For CCR2 inhibitor treatment, cells were pre-treated with CCR2 antagonist, RS102895 (100 ng/ml), for 4 h before mock or JEV infection for various time periods and were processed for mRNA analysis and scratch experiment for the phenotypic and functional characterization. For the functional experiment, a cross-pattern scratch was introduced into the microglia cell culture and the activated number of microglia cells within the scratch area was counted at twelve fields per well. All experiments were repeated three times.

Cell Viability Assay

Cell viability was determined using a tetrazolium salt 3-(4,5-dimethylthiazol-2-yl)-2,5-diphenyltetrazolium bromide (MTT; Millipore Sigma) colorimetric assay. BV2 microglia cells were incubated in 96-well plates in DMEM containing 10% fetal calf serum and 1% penicillin and streptomycin (40 U/ml and 40 mg/ml, respectively). Ten microliters of MTT at a final concentration of 0.5 mg/ml was added to each well. After 3 h incubation in 5% CO_2 at 37°C, media was discarded and formazan crystals were dissolved by adding 100 ml of DMSO to each well. The absorbance was measured at 540 nm using an absorbance microplate reader and cell viability was expressed as a percentage of surviving cells compared with the control cells.

Nitric Oxide Assay

Nitric oxide (NO) release into BV2 microglia condition media was assayed using a Greiss reagent assay (Invitrogen; G7921), as per the manufacturer's instructions. NO concentration was calculated using standard curves generated from a nitrite stock, and results were expressed in micromoles.

Real-Time PCR

Total RNA was extracted from snap-frozen samples using an RNeasy isolation kit (Qiagen, Valencia, CA, USA) with on-column DNase treatment (Qiagen). cDNA synthesis was performed on 1 μg of total RNA using a Verso cDNA RT kit (Thermo Scientific, Pittsburg, PA, USA); the protocols used were according to the manufacturer's instructions. Real-time PCR was performed using an ABI 7500 Sequence Detection System (Applied Biosystems) in the presence of SYBR Green. Standard PCR conditions were used as prescribed in SYBR Green I core reagent protocol. PCR was performed using nucleotide primers of CD11b, CCR2, TNF-α, and IFNγ (obtained from Integrated DNA Technology, Coralville, IA, USA). Gene expression was calculated relative to the endogenous control sample (GAPDH) to determine relative expression values, using the $2^{-\Delta\Delta Ct}$ method (where Ct is the threshold cycle). All experiments were repeated three times.

Quantification of Virus

Quantification of viral RNA from brain tissue homogenate was performed by using Geno Sen real-time RT-PCR kit for JEV (Genome Diagnostics). Analysis was performed on an ABI 7500 real-time PCR system (Applied Biosystems). Virus copy number in the samples were determined by using pre-quantified JEV-specific RNA standards with known copy numbers, provided with the kit.

Western Blotting

Proteins from ipsilateral cortical tissue were extracted using RIPA buffer, equalized, and loaded onto 5–20% gradient gels for SDS-PAGE (Bio-Rad, Hercules, CA, USA). Proteins were transferred onto nitrocellulose membranes and then blocked overnight in 5% milk in 1× TBS containing 0.05% Tween-20 (TBS-T). The membrane was incubated in rabbit anti-IBA1 (1:1,000; BD Transduction Laboratories), mouse anti-caspase 12 (1:1,000; Cell Signaling Technology), mouse anti-ubiquitin (1:1,000; Cell Signaling Technology), mouse anti-phospho-H2AX (1:1,000; Cell Signaling Technology), and rabbit anti-GAPDH (1:2,000; Sigma) overnight at 4°C, then washed three times in TBS-T and incubated in appropriate HRP-conjugated secondary antibodies for 2 h at room temperature. Membranes were washed three times in TBS-T, and proteins were visualized using Super Signal West Dura Extended Duration Substrate (Thermo Scientific, Rockford, IL, USA). Chemiluminescence was captured using ChemiDoc XRS + System (Bio-Rad), and protein bands were quantified by densitometric analysis using Bio-Rad Molecular Imaging Software. The data are normalized with endogenous control of GAPDH and expressed in arbitrary units. All experiments were repeated three times.

Lipid Peroxidation Assay

Lipid peroxidation (LPO) was measured in tissue homogenate by assaying the level of thiobarbituric acid reactive substances as an index of peroxidation of lipids by using the method of Ohkawa et al. (1979).

Immunohistochemistry

Twenty-micrometer coronal brain sections were selected, and standard immunostaining techniques were employed as described before (Kumar et al., 2016). Briefly, sections were incubated primary antibody rabbit anti-IBA1 (1:1,000; BD Transduction Laboratories) overnight at 4°C, then washed three times in 1× PBS and incubated with biotinylated anti-rabbit IgG antibody (Vector Laboratories, Burlingame, CA, USA) for 2 h at room temperature and avidin–biotin–horseradish peroxidase solution (Vectastain elite ABC kit; Vector Laboratories) for 1 h and then reacted with 3,30-diaminobenzidine (Vector Laboratories) for color development. Images were acquired using a fluorescent Nikon Ti-E inverted microscope, at ×10 (Plan APO 10× NA 0.45) or ×20 (Plan APO 20× NA 0.75) magnification. Exposure times were kept constant for all sections in each experiment. All experiments were repeated three times.

Statistical Analysis

Quantitative data were expressed as mean standard errors of the mean (SEM). RT-PCR relative expression, nitric oxide production, activated microglia cell number, microglia cell body area, and proliferation were analyzed by one-way analysis of variance (ANOVA), followed by *post hoc* adjustments using Student–Newman–Keuls test. Remaining data were analyzed using Student's *t*-test. Statistical tests were performed using GraphPad Prism program V.5 for Windows (GraphPad Software, San Diego, CA, USA). A p-value < 0.05 was considered statistically significant.

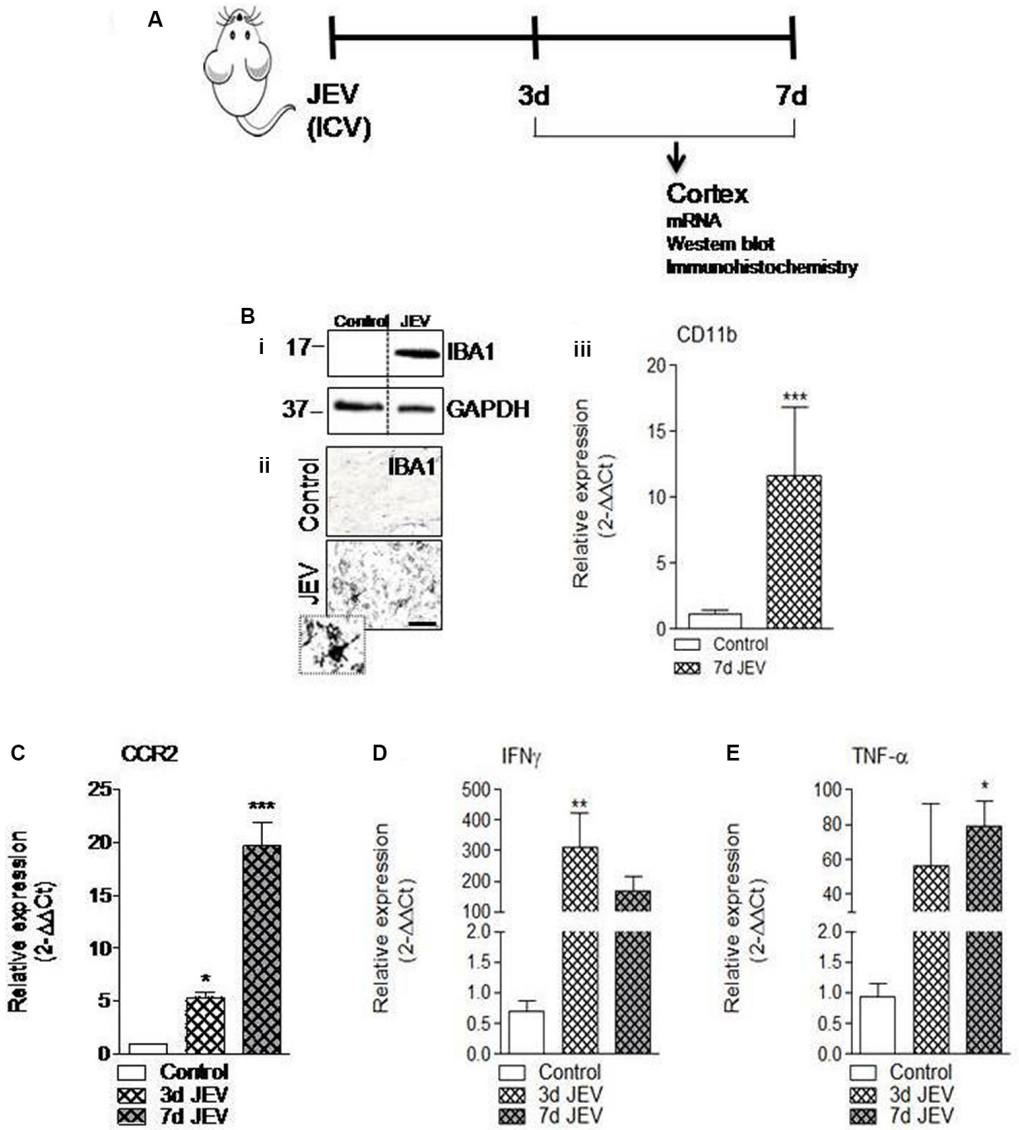

FIGURE 1 | Microglia activation and its proinflammatory mediators significantly increases in cortex after Japanese encephalitis virus (JEV) infection. **(A)** JEV infection was intracerebrally (ICV) injected and tissue cortex were collected for mRNA, western blot, and immunohistochemistry analysis. **(Bi)** IBA1 protein expression at 7 days post-infection in the cortex tissue samples followed by JEV infection compared with control. **(ii)** Representative images for immunohistochemistry of Iba1 positive microglia cell at 7 days post-infection in cortex of JEV-infected tissue compared with control animals. Scale bars = 50 μm. **(iii)** qPCR analysis of microglia gene CD11b in the cortex of control and JEV-infected mice at 7 days post-infection. **(C–E)** JEV infection–induced expression of CCR2 and proinflammatory genes, TNF-α, and IFNγ in JEV-infected mice compared with control animals. One-way ANOVA; data = mean ± SEM; n = 3–7/group; $^{*}p < 0.05$, $^{**}p < 0.01$, and $^{***}p < 0.001$ vs. control group.

RESULTS

JEV Infection Induces Microglia Activation, CCR2 Expression, and Classical Proinflammatory Mediators of TNF-α and IFNγ

Consistent with previous finding (Wang and Deubel, 2011), we also noted that mRNA copy of JE viral infection significantly increases over time (1.4×10^5, 4×10^5, and 6×10^5 copies/ml at 1, 3, and 7 days, respectively), which suggested that JE viral infection progresses over time. Moreover, increased microglia cell activation has been reported in the JEV-infected brain and found associated with neurological dysfunction and increased neurodegeneration (Chen et al., 2010). In the current study, we set out to investigate the mechanism that drives proinflammatory response of microglia activation after JEV infection and to establish the role of CCR2 in JEV pathology. For this, JEV infection was introduced into mice and cortical tissue was isolated at 3 and 7 days for mRNA, western blot, and immunohistochemistry analysis (**Figure 1A**). Our western

blot analysis revealed that JEV infection robustly induced Iba1 protein expression in JEV-infected animals compared with control, suggesting that microglia activation significantly increases in JEV-infected cortical tissue (**Figure 1Bi**). On the basis of cell morphological analysis (as we have described in a previous publication Kumar et al., 2013), we further noted that hypertrophy-activated microglia, which is characterized by larger cell body area with thicker, shorter, and highly branched processes, significantly increases at day 7 in JEV-infected cortical tissue compared with control animals cortical tissue (**Figure 1Bii**). Next, our mRNA gene expression analysis of CCR2, CD11b, and classical proinflammatory markers of TNF-α and IFNγ suggests that JEV infection significantly increased mRNA level of CCR2 receptor, CD11b, TNF-α, and IFNγ when compared with control animals [$p < 0.05$ (TNF-α, CCR2 at 3 days), $p < 0.01$ (IFNγ at 3 days), $p < 0.001$ (CD11b at 7 days and CCR2 at 7 days); **Figures 1Biii–E**].

JEV Infection Alters Microglia Phenotype, Increases Microglia Cell Body Area and Proliferation *in vitro*

The cell number and morphological analysis were performed using a hemocytometer and ImageJ software at different cell culture times of 3, 24, and 72 h in BV2 microglia after JEV infection and control cells. There was an increase in microglia cell body area [$^{*}p < 0.05$ (when compared with 24 h control), $^{\wedge}p < 0.05$ (when compared with 72 h control); **Figures 2A,B**] and microglia cell number [$^{*}p < 0.05$, $^{**}p < 0.01$ (when compared with 3 h control); **Figure 2C**], suggesting that JEV infection increased activated microglia cellular phenotype and proliferation when compared with control microglia cells.

CCR2 Inhibition Reduces Microglia Activation and Nitric Oxide Production in Microglia Cell Culture After JEV Infection

CCR2 regulation was thought to regulate redox signaling and neuroinflammatory responses in CNS (Brune et al., 2013). Therefore, in the current study, we hypothesized that CCR2 drives neurotoxic microglia neuroinflammatory response after JEV infection. To test this hypothesis, we inhibited CCR2 by using CCR2 inhibitor, RS102895, in microglia cell culture of both JEV-infected microglia cell and control microglia cells, and analyzed nitric oxide production using a spectrophotometer and microglia activation phenotype. Note that *in vitro* study experiments, we used 100 ng/ml concentration of RS102895 after determining 100% of cell viability level for CCR2 and JEV infection to microglia cells. JEV infection significantly increases CCR2 expression and nitric oxide production in JEV-infected microglia cells when compared with levels in control microglia [$^{**}p < 0.01$ (CCR2), $^{**}p < 0.01$ (nitric oxide) vs. control microglia cells; **Figures 3A,B**]. In contrast, CCR2 treatment in JEV infection group resulted in a significant reduction of CCR2 expression and nitric oxide production [$^{\wedge\wedge}p < 0.01$ (CCR2), $^{\wedge\wedge}p < 0.01$ (nitric oxide) vs. control microglia cells; **Figures 3A,B**], indicative of a reduced neurotoxic response of microglia in CCR2-treated JEV microglia when compared with control microglia cells. We then expanded our analysis to functional response of microglia and their activation phenotype analysis by performing *in vitro* scratch functional assay and ImageJ analysis as described before (**Figure 3C**). When compared with control microglia cells, there was a significant increase in elongated or rod-like activated phenotype of microglia in

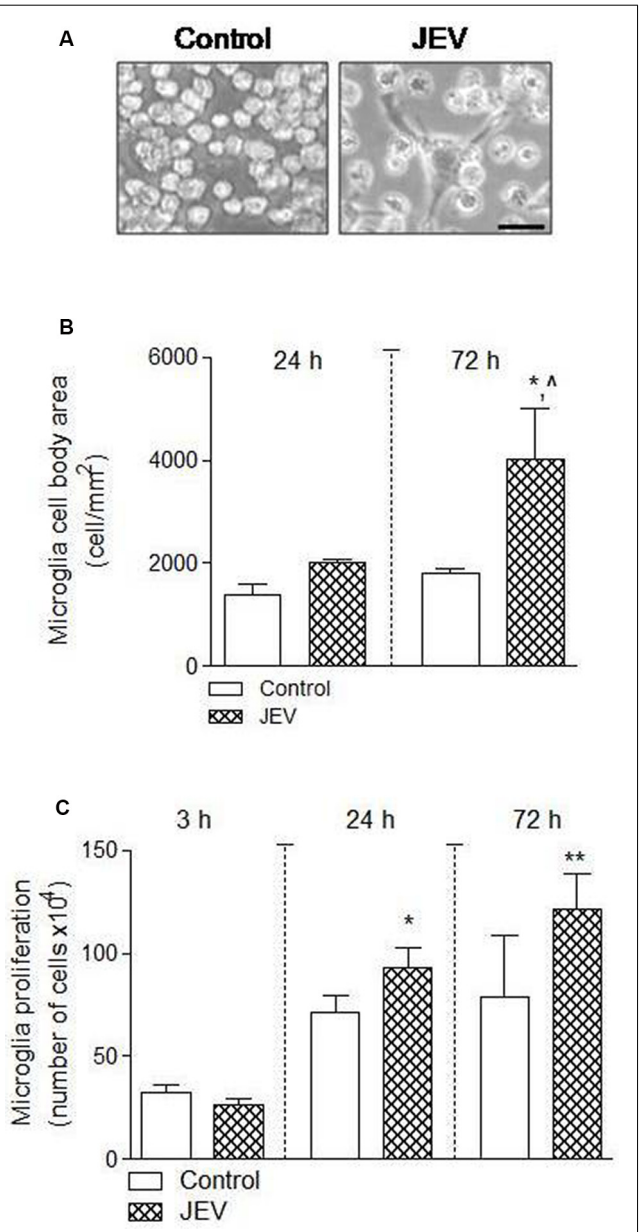

FIGURE 2 | Microglia proliferation and cell body area increases after JEV infection compared with control cells. BV2 microglia cells were infected with JEV and microglia morphology was observed at different times of 24 and 72 h. **(A–C)** Microscopic morphometric analysis and microglia cell number analysis showed that microglia cell body area and proliferation significantly increases after JEV infection compared with control microglia cells. Data are expressed as mean ± SEM; n = 3–4/group; $^{*}p < 0.05$, $^{\wedge}p < 0.05$ vs. control group at 72 h for microglia cell body area **(B)** and $^{*}p < 0.05$ and $^{**}p < 0.01$ vs. control group at 24 and 72 h for microglia proliferation **(C)**. One-way ANOVA.

JEV-infected microglia cells at 24 h post-infection ($p < 0.001$ vs. control microglia cells; **Figures 3D,E**). Notably, CCR2 treatment significantly reduced the elongated activation phenotype induced by JEV infection ($p < 0.01$ vs. JEV-infected microglia cells; **Figure 3E**).

CCR2 Inhibition Reduces Proinflammatory-Neurotoxic Mediators of Microglia After JEV Infection

To investigate the effect of CCR2 inhibition in JEV infection, we used CCR2 inhibitor RS102895 in JEV mice model as shown in **Figure 4A**. We assessed mRNA expression of CCR2, microglial CD11b expression, proinflammatory mediators of TNF-α, IFNγ, and neuronal cell death markers of LPO, poly-ubiquitin, H2AX, and caspase 12 in cortical tissue at day 5 in JEV-infected, RS102895-treated JEV-infected animals, and respective control animals to establish the effect of CCR2 on microglia activation and neuronal cell death pathways. As predicted, JEV infection significantly increases CCR2, CD11b, TNF-α, IFNγ, LPO, and poly-ubiquitin in JEV-infected cortical tissue when compared with levels in control tissue [$^{**}p < 0.01$ (CCR2), $^{**}p < 0.01$ (CD11b), $^{*}p < 0.05$ (TNF-α), $^{*}p < 0.05$ (IFNγ), $^{*}p < 0.05$ (LPO); **Figures 4B–E**, **Supplementary Figures S2A,B**]. In contrast, CCR2 treatment in JEV-infected animals resulted in significantly reduced CCR2 and microglial CD11b mRNA expression along with proinflammatory marker of IFNγ expression at day 5 post-JEV infection, indicating reduced expression of CCR2 associated with reduced expression of proinflammatory neurotoxic mediators of microglia in the cortex of CCR2-treated JEV-infected mice when compared with JEV-infected mice alone [$p < 0.01$ (CCR2), $p < 0.05$ (CD11b, IFNγ); **Figures 4B–E**].

DISCUSSION

In the current study, we delineated the role of CCR2 in determining morphology of microglia and neuroinflammatory response in JEV pathogenesis. We found that post-JEV infection, CCR2 expression is significantly increased and associated with reactive phenotype of microglia and subsequent production of proinflammatory mediators of TNF-α and IFNγ. Furthermore, our results demonstrated that CCR2 inhibition is an important target for controlling reactive microglia morphology and neuroinflammatory response of JEV infection.

A number of preclinical and clinical human studies suggest that exaggerated neuroinflammatory response of microglia contributes to JEV pathologies (Ghoshal et al., 2007; Sips et al., 2012). However, limited information is available for the alteration of microglial morphological features after JEV infection. Under normal physiological conditions, microglia exist in resting phenotype (inactivated) and continuously screen the CNS microenvironment for the maintenance of homeostatic condition. In immune challenge condition of viral infection or injury to CNS, these microglia cells rapidly transform into an activated state, proliferate, migrate to challenge site, and participate in the presentation of antigens, phagocytosis, and promote the resolution process (Hanisch and Kettenmann, 2007; Ransohoff and Perry, 2009). However, in case of larger extent of immune challenge, microglia cell body transforms to amoeboid cell body which is characterized by lesser processes and large cell body, and adopt a very similar morphology to bloodborne macrophages (Hanisch and Kettenmann, 2007). Similarly, in our JEV study, we observed that microglia morphology transformed into a highly reactive phenotype and cell body area; proliferation largely increases after JEV infection compared with control microglia cells (Ghoshal et al., 2007). Moreover, by performing *in vitro* functional scratch analysis, we observed that microglia adopted elongated/rod-like morphology after JEV at scratch area compared with control microglia cells. We observed that these rod microglia cells have few and polar processes that is entirely polarized and have a narrow cell soma. Similarly, these changes have also been noted and found associated with infection such as typhus, syphilis, and sleeping sickness (Spielmeyer, 1922; Ziebell et al., 2012; Au and Ma, 2017). Along with this, we noted that CCR2 inhibitor treatment causes a decrease in activated/elongated morphology of microglia, suggesting that CCR2 chemokine signaling plays a key role in microglia morphology transformation and JEV-mediated pathogenesis. To determine the further role of this unique morphology in inflammatory response, we also evaluated the production of nitric oxide and found that CCR2 inhibition significantly decreases nitric oxide production in CCR2 inhibitor-treated JEV-infected microglia cells. The following findings are consistent with previous findings in which changes in microglia morphologies after viral infection are noted, and with treatment of anti-inflammatory molecules such as minocycline, activation morphology of microglia was found decreased (Mishra and Basu, 2008; Quick et al., 2017). However, the role and morphological attribute of elongated microglia by using a specific antibody, which discriminates these morphologies in JEV pathogenesis, needs to be explored further. Nevertheless, our findings represent that alteration in elongated microglia morphology is a general response rather than JE specific, although these findings highlight the fact that the following understanding about key pathologies can be helpful in controlling the immunopathological response against JEV.

In phagocytic cells such as microglia, CCR2 is a G protein-coupled seven-transmembrane spanning receptor (GPCR). CCR2 signals through these GPCRs, specifically Gi to activate extracellular signal-regulated kinase ERK1/2 signal pathways (Jimenez-Sainz et al., 2003). The increased expression of CCR2 is associated with increased infiltration of inflammatory monocytes NK and T cells at sites of inflammation, which are key components of proinflammatory cascade after JEV infection (Liu et al., 2018; Zhang et al., 2019). Microglia is a key player in neuroinflammation, and proinflammatory cytokine production responsible for progressive neuron damage and CCR2 on microglia has been implicated as a key player for proinflammatory response in many neurodegenerative diseases and thus important in regulating microglia-mediated neurotoxicity (Ghoshal et al., 2007; Terry et al., 2012; Kim et al., 2016; Chauhan et al., 2017; Käufer et al., 2018; Zhang et al., 2019).

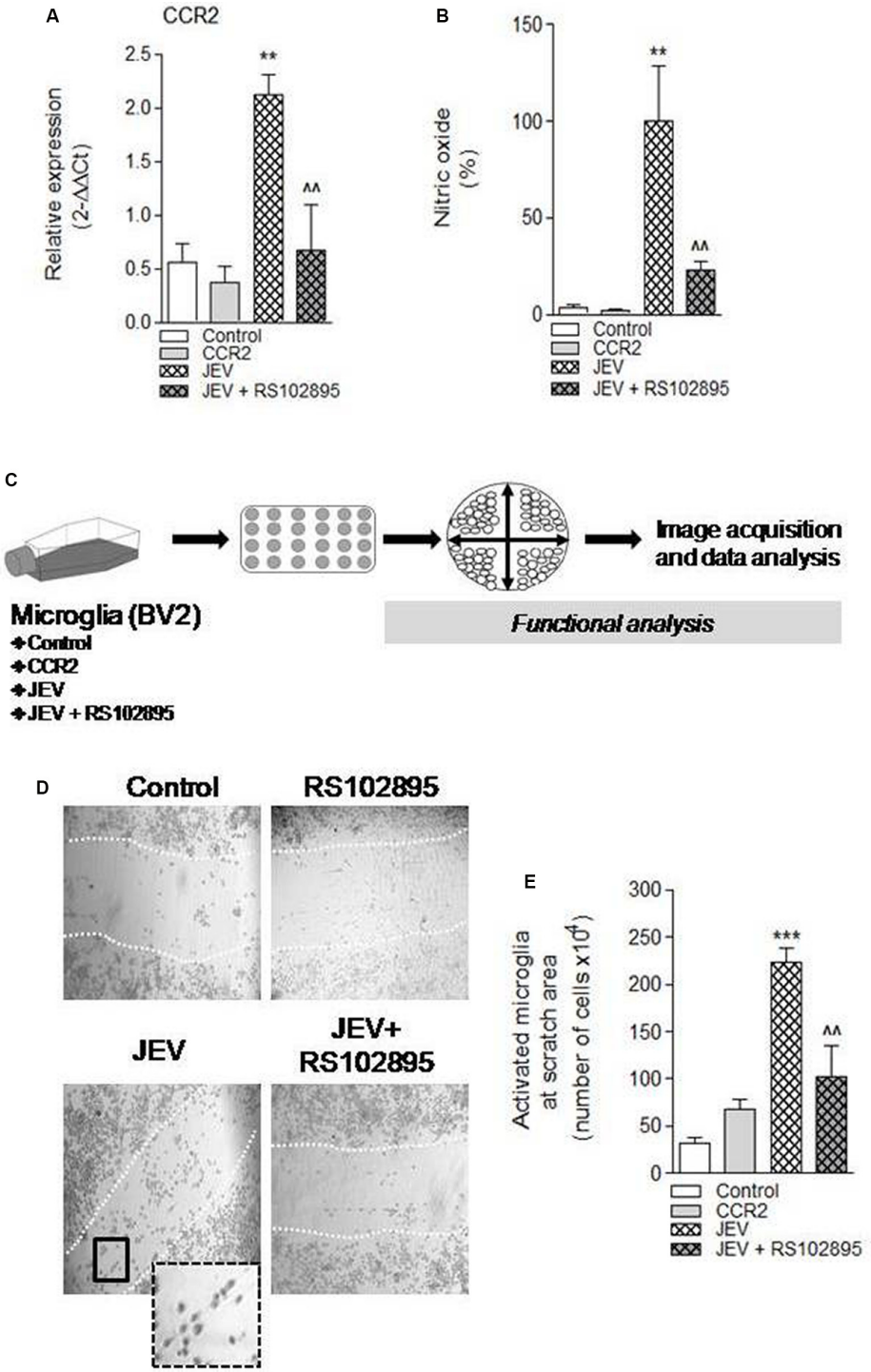

FIGURE 3 | Chemokines (C-C motif) receptor 2 (CCR2) inhibition, by using molecular inhibitor RS102895, to BV2 microglia cell culture after JEV infection alters function response and reduces microglia activation phenotype. **(A)** Consistent with our JEV infection into mice model study, we further found that JEV infection–induced expression of CCR2 into BV2 microglia cell culture compared with control cells and RS102895 treatment significantly reduces its expression. **(B)** Similarly, nitric oxide (NO) analysis was also performed in supernatant of control, JEV-infected, and RS102895-treated JEV-infected microglia cells, and reduction in NO response was observed. Data are expressed as mean ± SEM; n = 3–5/group; $^{**}p < 0.01$ vs. control and $^{\wedge\wedge}p < 0.01$ vs. JEV-infected microglia cells at 24 h. One-way ANOVA. **(C)** Further for the functional assays, microglia cells were seeded and cross-pattern scratch was performed after JEV infection and CCR2 treatment and migration analysis was performed. **(D,E)** After 24 h, images were acquired and were analyzed for their phenotypic analysis. At the scratch area, we observed that the elongated phenotype of microglia (activated) significantly reduces after CCR2 treatment compared with JEV-infected microglia cells and control microglia cells. Data are expressed as mean ± SEM; n = 3/group; $^{***}p < 0.001$ vs. control and $^{\wedge\wedge}p < 0.01$ vs. JEV-infected microglia cells at 24 h. One-way ANOVA.

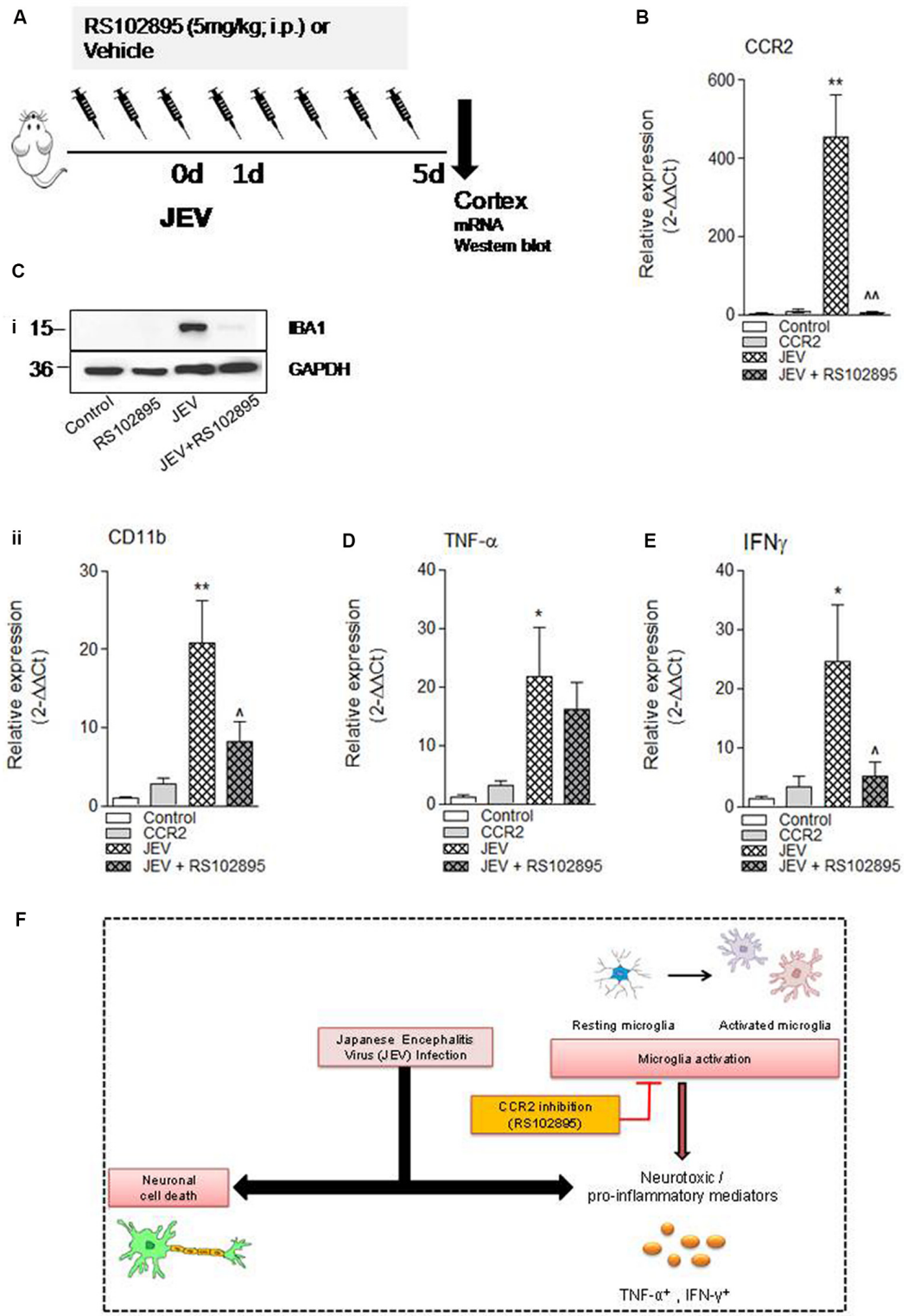

FIGURE 4 | CCR2 inhibitor treatment reduces neuroinflammation and cell death markers after JEV infection. **(A)** RS102895 was intraperitoneally (i.p.) injected by giving a dose of 5 mg/kg at 72 h before JEV infection and once daily for the following 5 days. **(B–E)** mRNA and **(Ci)** protein western blot analyses were performed at 5 days post-JEV infection in JEV-infected and RS102895-treated JEV-infected animals. Data are expressed as mean ± SEM; n = 3–6/group; $^{*}p < 0.05$ and $^{**}p < 0.01$ vs. control group and $^{\wedge}p < 0.05$, $^{\wedge\wedge}p < 0.01$ vs. JEV-infected animals. One-way ANOVA. **(F)** Graphical abstract summarizing interaction of CCR2 with neuroinflammation after JEV infection.

In the present study, we provide evidence that CCR2 plays a key role in strong inflammatory response and disease pathogenesis after JEV infection (Ghoshal et al., 2007). Furthermore, we used CCR2 antagonist molecule RS102895 to inhibit CCR2 expression during JEV infection both *in vivo* and *in vitro* and observed the key disease outcome measures so that JEV-induced brain pathologies can be understood. RS102895 has been previously used to interfere with CCR2 signaling in the brain (Hung et al., 2013) and also highlighted the block of enhancement of phosphorylation of NFkappaB (NF-kB/p65), and involved in modulation of LPS-mediated inflammation-induced pathologies (Cerri et al., 2016).

Increased level of CCR2 expression in our study is consistent with a previous finding in which upregulation of CCR2 level is reported in JEV infection (Chowdhury and Khan, 2017). Moreover, there is a direct relationship between increased CCR2 expression and proinflammatory response after JEV infection (Liu et al., 2018). We show increased CCR2 expression and classical proinflammatory markers of TNF-α and IFNγ in cortical tissue of JEV-infected animals. When we blocked CCR2 expression by using CCR2 inhibitor, proinflammatory markers such as IFNγ reduced (He et al., 2016), but there was no significant change observed in TNF-α compared with JEV-infected animals. In a previous study, it has been shown that mice deficient in CCL2 can only block 40–50% monocyte movement from bone marrow (Jia et al., 2008). This could be one of the reasons why CCR2 inhibitor treatment cannot do complete inhibition of inflammation during JEV infection. However further study for trafficking of $CCR2^+$ inflammatory immune cells such as monocytes from bone marrow to the CNS, their interaction with microglia cells, functional response toward either protective or pathological role, and their inhibition by genetic knockdown such as by using siRNA needs to be explored further.

Finally, in our study, we aim to assess if CCR2 inhibitor treatment could be a potential target for reduction of JEV-induced cell death pathways. We investigated the impact of RS102895 on neuronal cell death after JEV infection. Surprisingly, we did not observe any significant reduction in neuronal cell death pathways upon RS102895 treatment except for a trend in decrease of cell death markers of lipid peroxidation (LPO) and poly-ubiquitin (**Supplementary Figure S2A**). The following results suggest that JEV infection triggers CCR2-independent neuronal cell death pathways, associated with bystander direct virus-mediated injury (**Figure 4F**). A potential caveat to the interpretation of the present neuronal cell death data is the lack of observation of cell death–related marker changes beyond 7 days as JE disease progressed to severity and the mice death rate significantly increased after JEV infection. Moreover, in our study, we could not include JE viral load analysis followed by CCR2 inhibitor treatment because of disease severity; however, a previous study had demonstrated that CCR2 deficiency in mice leads to decreased susceptibility against lethal infection of JEV, but there is no difference in viral load in the brain (Kim et al., 2016). However, we did perform key outcome measures such as changes in body weight and survival rate after JEV infection (data not shown) to ascertain the level of disease severity and determine whether CCR2 inhibitor treatment reduces the effect of post-JEV infection. We found that there is no change in body weight and survival rate in CCR2-treated JEV-infected brain at 7 days. On the contrary, a previous study of Liu et al. (2018), in which JEV infection was introduced through intraperitoneal injection, demonstrated that mice treated with CCR2 antagonists had a higher survival rate (about 60%); this also suggests that treatment of CCR2 inhibitor and disease outcome is also dependent on the loss of integrity of blood–brain barrier and severity of JEV infection.

Overall, the following study confirms the role of CCR2 in JEV pathogenesis. We have demonstrated that JEV infection causes an increase in the level of CCR2 and key neuroinflammatory mediators such as TNF-α and IFNγ, which reflects a deleterious effect and skewed microglia activation phenotype toward a more reactive phenotype. These observations highlighted the role of JEV-induced CCR2 activation in neuroinflammation. Nevertheless, further studies are required to affirm the biochemical mechanisms involved in the inflammatory regulation of CCR2 pathways as it is also possible that JEV infection could upregulate the CCR2 expression in astrocytes, infiltrating other immune cells such as neutrophils and leukocytes, and initiate the downstream cross-talk signaling cascades.

DATA AVAILABILITY STATEMENT

The raw data supporting the conclusions of this article will be made available by the authors, without undue reservation.

ETHICS STATEMENT

The animal study was reviewed and approved by SGPGIMS institutional ethics committee.

AUTHOR CONTRIBUTIONS

AK: conceptualization, methodology, validation, formal analysis, investigation, data curation, visualization, and writing—original draft. SS and GS: methodology, data curation, and validation. ST: resources and supervision. All authors contributed to the article and approved the submitted version.

FUNDING

This study was supported by the Ramalingaswami re-entry fellowship (BT/RLF/Re-entry/13/2014) from the Department of Biotechnology, Ministry of Science and Technology, Government of India, to AK.

SUPPLEMENTARY MATERIAL

The Supplementary Material for this article can be found online at: https://www.frontiersin.org/articles/10.3389/fncel.2020.00230/full#supplementary-material.

REFERENCES

Au, N. P. B., and Ma, C. H. E. (2017). Recent advances in the study of bipolar/rod-shaped microglia and their roles in neurodegeneration. *Front. Aging Neurosci.* 9:128. doi: 10.3389/fnagi.2017.00128

Brune, B., Dehne, N., Grossmann, N., Jung, M., Namgaladze, D., Schmid, T., et al (2013). Redox control of inflammation in macrophages. *Antioxid. Redox Signal.* 19, 595–637. doi: 10.1089/ars.2012.4785

Cerri, C., Genovesi, S., Allegra, M., Pistillo, F., Puntener, U., Guglielmotti, A., et al (2016). The chemokine CCL2 mediates the seizure-enhancing effects of systemic inflammation. *J. Neurosci.* 36, 3777–3788. doi: 10.1523/jneurosci.0451-15.2016

Chauhan, P. S., Khanna, V. K., Kalita, J., and Misra, U. K. (2017). Japanese encephalitis virus infection results in transient dysfunction of memory learning and cholinesterase inhibition. *Mol. Neurobiol.* 54, 4705–4715. doi: 10.1007/s12035-016-9963-6

Chen, C. J., Ou, Y. C., Chang, C. Y., Pan, H. C., Liao, S. L., Chen, S. Y., et al (2012). Glutamate released by japanese encephalitis virus-infected microglia involves TNF-alpha signaling and contributes to neuronal death. *Glia* 60, 487–501. doi: 10.1002/glia.22282

Chen, C.-J., Ou, Y.-C., Lin, S.-Y., Raung, S.-L., Liao, S.-L., Lai, C.-Y., et al (2010). Glial activation involvement in neuronal death by japanese encephalitis virus infection. *J. Gen. Virol.* 91, 1028–1037. doi: 10.1099/vir.0.013565-0

Chowdhury, P., and Khan, S. A. (2017). Significance of CCL2, CCL5 and CCR2 polymorphisms for adverse prognosis of japanese encephalitis from an endemic population of India. *Sci. Rep.* 7:13716. doi: 10.1038/s41598-017-14091-8

Das, S., Dutta, K., Kumawat, K. L., Ghoshal, A., Adhya, D., and Basu, A. (2011). Abrogated inflammatory response promotes neurogenesis in a murine model of japanese encephalitis. *PLoS One* 6:e17225. doi: 10.1371/journal.pone.0017225

Das, S., Mishra, M. K., Ghosh, J., and Basu, A. (2008). Japanese encephalitis virus infection induces IL-18 and IL-1β in microglia and astrocytes: correlation with *in vitro* cytokine responsiveness of glial cells and subsequent neuronal death. *J. Neuroimmunol.* 195, 60–72. doi: 10.1016/j.jneuroim.2008.01.009

Flora, G. K., Anderton, R. S., Meloni, B. P., Guillemin, G. J., Knuckey, N. W., MacDougall, G., et al (2019). Microglia are both a source and target of extracellular cyclophilin A. *Heliyon* 5:e02390. doi: 10.1016/j.heliyon.2019.e02390

Getts, D. R., Terry, R. L., Getts, M. T., Muller, M., Rana, S., Shrestha, B., et al (2008). Ly6c^{+} "inflammatory monocytes" are microglial precursors recruited in a pathogenic manner in West Nile virus encephalitis. *J. Exp. Med.* 205, 2319–2337. doi: 10.1084/jem.20080421

Ghoshal, A., Das, S., Ghosh, S., Mishra, M. K., Sharma, V., Koli, P., et al (2007). Proinflammatory mediators released by activated microglia induces neuronal death in japanese encephalitis. *Glia* 55, 483–496. doi: 10.1002/glia.20474

Han, Y. W., Choi, J. Y., Uyangaa, E., Kim, S. B., Kim, J. H., Kim, B. S., et al (2014). Distinct dictation of japanese encephalitis virus-induced neuroinflammation and lethality *via* triggering TLR3 and TLR4 signal pathways. *PLoS Pathog.* 10:e1004319. doi: 10.1371/journal.ppat.1004319

Hanisch, U. K., and Kettenmann, H. (2007). Microglia: active sensor and versatile effector cells in the normal and pathologic brain. *Nat. Neurosci.* 10, 1387–1394. doi: 10.1038/nn1997

He, M., Dong, H., Huang, Y., Lu, S., Zhang, S., Qian, Y., et al (2016). Astrocyte-derived CCL2 is associated with M1 activation and recruitment of cultured microglial cells. *Cell. Physiol. Biochem.* 38, 859–870. doi: 10.1159/000443040

Hung, Y. W., Lai, M. T., Tseng, Y. J., Chou, C. C., and Lin, Y. Y. (2013). Monocyte hemoattractant protein-1 affects migration of hippocampal neural progenitors following status epilepticus in rats. *J. Neuroinflammation* 10:11. doi: 10.1186/1742-2094-10-11

Jia, T., Serbina, N. V., Brandl, K., Zhong, M. X., Leiner, I. M., Charo, I. F., et al (2008). Additive roles for MCP-1 and MCP-3 in CCR2-mediated recruitment of inflammatory monocytes during listeria monocytogenes infection. *J. Immunol.* 180, 6846–6853. doi: 10.4049/jimmunol.180.10.6846

Jimenez-Sainz, M. C., Fast, B., Mayor, F. Jr., and Aragay, A. M. (2003). Signaling pathways for monocyte chemoattractant protein 1-mediated extracellular signal-regulated kinase activation. *Mol. Pharmacol.* 64, 773–782. doi: 10.1124/mol.64.3.773

Käufer, C., Chhatbar, C., Broer, S., Waltl, I., Ghita, L., Gerhauser, I., et al (2018). Chemokine receptors CCR2 and CX3CR1 regulate viral encephalitis-induced hippocampal damage but not seizures. *Proc. Natl. Acad. Sci. U S A.* 115, E8929–E8938. doi: 10.1073/pnas.1806754115

Kettenmann, H., Hanisch, U.-K., Noda, M., and Verkhratsky, A. (2011). Physiology of microglia. *Physiol. Rev.* 91, 461–553. doi: 10.1152/physrev.00011.2010

Kim, J. H., Patil, A. M., Choi, J. Y., Kim, S. B., Uyangaa, E., Hossain, F. M., et al (2016). CCL2, but not its receptor, is essential to restrict immune privileged central nervous system-invasion of japanese encephalitis virus *via* regulating accumulation of CD11b(+) Ly-6C(hi) monocytes. *Immunology* 149, 186–203. doi: 10.1111/imm.12626

Kreutzberg, G. W. (1996). Microglia: a sensor for pathological events in the CNS. *Trends Neurosci.* 19, 312–318. doi: 10.1016/0166-2236(96)10049-7

Kumar, A., Alvarez-Croda, D. M., Stoica, B. A., Faden, A. I., and Loane, D. J. (2016). Microglial/macrophage polarization dynamics following traumatic brain injury. *J. Neurotrauma* 33, 1732–1750. doi: 10.1089/neu.2015.4268

Kumar, A., Stoica, B. A., Sabirzhanov, B., Burns, M. P., Faden, A. I., and Loane, D. J. (2013). Traumatic brain injury in aged animals increases lesion size and chronically alters microglial/macrophage classical and alternative activation states. *Neurobiol. Aging* 34, 1397–1411. doi: 10.1016/j.neurobiolaging.2012.11.013

Lannes, N., Neuhaus, V., Scolari, B., Kharoubi-Hess, S., Walch, M., Summerfield, A., et al (2017). Interactions of human microglia cells with japanese encephalitis virus. *Virol. J.* 14:8. doi: 10.1186/s12985-016-0675-3

Liu, K., Xiao, C., Wang, F., Xiang, X., Ou, A., Wei, J., et al (2018). Chemokine receptor antagonist block inflammation and therapy japanese encephalitis virus infection in mouse model. *Cytokine* 110, 70–77. doi: 10.1016/j.cyto.2018.04.022

Mishra, M. K., and Basu, A. (2008). Minocycline neuroprotects, reduces microglial activation, inhibits caspase 3 induction and viral replication following japanese encephalitis. *J Neurochem* 105, 1582–1595. doi: 10.1111/j.1471-4159.2008.05238.x

Ohkawa, H., Ohishi, N., and Yagi, K. (1979). Assay for lipid peroxides in animal tissues by thiobarbituric acid reaction. *Anal. Biochem.* 95, 351–358. doi: 10.1016/0003-2697(79)90738-3

Quick, E. D., Seitz, S., Clarke, P., and Tyler, K. L. (2017). Minocycline has anti-inflammatory effects and reduces cytotoxicity in an ex vivo spinal cord slice culture model of west nile virus infection. *J. Virol.* 91:e00569–17. doi: 10.1128/JVI.00569-17

Ransohoff, R. M., and Perry, V. H. (2009). Microglial physiology: unique stimuli, specialized responses. *Annu. Rev. Immunol.* 27, 119–145. doi: 10.1146/annurev.immunol.021908.132528

Rollins, B. J. (1991). JE/MCP-1: an early-response gene encodes a monocyte-specific cytokine. *Cancer Cells* 3, 517–524.

Semple, B. D., Kossmann, T., and Morganti-Kossmann, M. C. (2010). Role of chemokines in CNS health and pathology: a focus on the CCL2/CCR2 and CXCL8/CXCR2 networks. *J. Cereb. Blood Flow Metab.* 30, 459–473. doi: 10.1038/jcbfm.2009.240

Shukla, V., Shakya, A. K., Shukla, M., Kumari, N., Krishnani, N., Dhole, T. N., et al (2016). Circulating levels of matrix metalloproteinases and tissue inhibitors of matrix metalloproteinases during japanese encephalitis virus infection. *Virusdisease* 27, 63–76. doi: 10.1007/s13337-015-0301-9

Sips, G. J., Wilschut, J., and Smit, J. M. (2012). Neuroinvasive flavivirus infections. *Rev. Med. Virol.* 22, 69–87. doi: 10.1002/rmv.712

Spielmeyer, W. (1922). *Histopathologie Des Nervensystems.* Berlin: Verlag vonJulius Springer.

Srivastava, R., Kalita, J., Khan, M. Y., and Misra, U. K. (2012). Status of proinflammatory and anti-inflammatory cytokines in different brain regions of a rat model of japanese encephalitis. *Inflamm. Res.* 61, 381–389. doi: 10.1007/s00011-011-0423-5

Swarup, V., Ghosh, J., Das, S., and Basu, A. (2008). Tumor necrosis factor receptor-associated death domain mediated neuronal death contributes to the glial activation and subsequent neuroinflammation in japanese encephalitis. *Neurochem Int* 52, 1310–1321. doi: 10.1016/j.neuint.2008.01.014

Terry, R. L., Getts, D. R., Deffrasnes, C., van Vreden, C., Campbell, I. L., and King, N. J. (2012). Inflammatory monocytes and the pathogenesis of viral encephalitis. *J. Neuroinflammation* 9:270. doi: 10.1186/1742-2094-9-270

Thongtan, T., Cheepsunthorn, P., Chaiworakul, V., Rattanarungsan, C., Wikan, N., and Smith, D. R. (2010). Highly permissive infection of microglial cells by japanese encephalitis virus: a possible role as a viral reservoir. *Microbes Infect.* 12, 37–45. doi: 10.1016/j.micinf.2009.09.013

Tian, D. S., Peng, J., Murugan, M., Feng, L. J., Liu, J. L., Eyo, U. B., et al (2017). Chemokine CCL2-CCR2 signaling induces neuronal cell death *via* STAT3 activation and IL-1β production after status epilepticus. *J. Neurosci.* 37, 7878–7892. doi: 10.1523/jneurosci.0315-17.2017

Verdonk, F., Roux, P., Flamant, P., Fiette, L., Bozza, F. A., Simard, S., et al (2016). Phenotypic clustering: a novel method for microglial morphology analysis. *J. Neuroinflammation* 13:153. doi: 10.1186/s12974-016-0614-7

Wang, K., and Deubel, V. (2011). Mice with different susceptibility to japanese encephalitis virus infection show selective neutralizing antibody response and myeloid cell infectivity. *PLoS One* 6:e24744. doi: 10.1371/journal.pone.0024744

Yang, K. D., Yeh, W. T., Chen, R. F., Chuon, H. L., Tsai, H. P., Yao, C. W., et al (2004). A model to study neurotropism and persistency of japanese encephalitis virus infection in human neuroblastoma cells and leukocytes. *J. Gen. Virol.* 85, 635–642. doi: 10.1099/vir.0.19426-0

Zhang, F., Qi, L., Li, T., Li, X., Yang, D., Cao, S., et al (2019). $PD1^{+}$ $CCR2^{+}$ $CD8^{+}$ T cells infiltrate the central nervous system during acute japanese encephalitis virus infection. *Virol. Sin.* 34, 538–548. doi: 10.1007/s12250-019-00134-z

Ziebell, J. M., Taylor, S. E., Cao, T., Harrison, J. L., and Lifshitz, J. (2012). Rod microglia: elongation, alignment and coupling to form trains across the somatosensory cortex after experimental diffuse brain injury. *J. Neuroinflammation* 9:247. doi: 10.1186/1742-2094-9-247

Conflict of Interest: The authors declare that the research was conducted in the absence of any commercial or financial relationships that could be construed as a potential conflict of interest.

frontiers in Aging Neuroscience

ORIGINAL RESEARCH
published: 21 August 2020
doi: 10.3389/fnagi.2020.00248

Chronic Periodontitis and Alzheimer Disease: A Putative Link of Serum Proteins Identification by 2D-DIGE Proteomics

Xianfang Rong[1†], Liping Xiang[1†], Yanfen Li[1], Hongfa Yang[2], Weijian Chen[1], Lei Li[1], Defeng Liang[1] and Xincai Zhou[1]*

[1]*Department of Stomatology, Shenzhen Baoan Women's and Children's Hospital, Jinan University, Shenzhen, China,*
[2]*Department of Cardiology, The Second Affiliated Hospital of the University of South China, Hengyang, China*

Increasing evidence indicates Chronic Periodontitis (CP) is a comorbidity of Alzheimer's disease (AD), which is the most common form of age-related dementia, and for the latter, effective diagnostic and treatment strategies are lacking. Although inflammation is present in both diseases, the exact mechanisms and cross-links between CP and AD are poorly understood; and a direct association between the two has not been reported. This study aimed to identify a direct serum proteins link between AD and CP. Two-dimensional differential in-gel electrophoresis was employed to analyze serum samples from 12 CP patients and 12 age-matched controls. Furthermore, to determine the molecular link between CP and AD, neuroblastoma SK-N-SH APPwt cells were treated with 1 μg/ml of lipopolysaccharide from *Porphyromonas gingivalis* (P.g-LPS). Ten differentially expressed proteins were identified in CP patients. Among them, nine proteins were up-regulated, and one protein was down-regulated. Of the 10 differentially expressed proteins, five proteins were reportedly involved in the pathology of AD: Cofilin-2, Cathepsin B, Clusterin, Triosephosphate isomerase, and inter-alpha-trypsin inhibitor heavy chain H4 (ITI-H4). Western blotting indicated significantly higher expression of Cofilin-2, Cathepsin B, and Clusterin and lower expression of ITI-H4 in the CP group than in the Control group. The serum concentration of Cathepsin B has a good correlation with MMSE scores. Moreover, the protein level of Cathepsin B (but not that of ADAM10 and BACE1) increased significantly along with a prominent increase in $A\beta_{1-40}$ and $A\beta_{1-42}$ in the cell lysates of P.g-LPS-treated SK-N-SH APPwt cells. Cathepsin B inhibition resulted in a sharp decrease in $A\beta_{1-40}$ and $A\beta_{1-42}$ in the cell lysates. Furthermore, TNF-α was one of the most important inflammatory cytokines for the P.g-LPS-induced Cathepsin B upregulation in SK-N-SH APPwt cells. These results show that CP and AD share an association, while Cathepsin B could be a key link between the two diseases. The discovery of the identical serum proteins provides a potential mechanism underlying the increased risk of AD in CP patients, which could be critical for elucidating the pathophysiology of AD.

Keywords: chronic periodontitis, Alzheimer's disease, two-dimensional differential in-gel electrophoresis, biomarker, Cathepsin B

OPEN ACCESS

Edited by:
Feiqi Zhu,
Shenzhen University, China

Reviewed by:
Michael Malek-Ahmadi,
Banner Alzheimer's Institute, United States
Qian Liu,
Northwest University, China

***Correspondence:**
Xincai Zhou
zhouxcmoya@sina.com

[†]These authors have contributed equally to this work

Received: *26 May 2020*
Accepted: *20 July 2020*
Published: *21 August 2020*

Citation:
Rong X, Xiang L, Li Y, Yang H, Chen W, Li L, Liang D and Zhou X (2020) Chronic Periodontitis and Alzheimer Disease: A Putative Link of Serum Proteins Identification by 2D-DIGE Proteomics. Front. Aging Neurosci. 12:248. doi: 10.3389/fnagi.2020.00248

INTRODUCTION

Alzheimer's disease (AD) is one of the most common forms of dementia among elderly people and is pathologically characterized by senile plaques and neuro-fibrillary tangles and clinically characterized by progressive deterioration of episodic memory and cognitive decline (Hardy and Higgins, 1992). The acknowledged history of AD spans almost a century, starting with its first description by Alois Alzheimer in 1907 (Alzheimer et al., 1995). During recent decades, the sequential events that occur in the development and pathology of AD have been extensively studied, yet the precise etiology of the disease remains elusive, and current preventative and curative strategies are largely unsuccessful (Rong et al., 2017; Rasmussen and Langerman, 2019). Considering the complexity of AD pathology, it is apparent that other risk factors also exist besides those known, such as gender, education, smoking, dietary habit, depression, hypertension, diabetes mellitus, obesity, and head injury (Shinohara et al., 2014; Dursun et al., 2016; Badea et al., 2019; Jackson et al., 2019; Tapiainen et al., 2020).

Chronic Periodontitis (CP) is an oral chronic infection/inflammatory disease that affects a considerable worldwide population (López and Baelum, 2015). CP comprises both gingivitis and periodontitis; for the latter, inflammation is localized in the gingival tissues or the inflammatory process reaches deeper connective and bone tissue, causing bone and attachment loss that may ultimately lead to tooth loss (Lang et al., 2009). This local inflammatory process may induce a systemic inflammatory state *via* mechanisms including dissemination of pro-inflammatory cytokines or bacteria or both from oral to extra-oral sites or even to blood circulation, which may contribute to the exacerbation of several diseases (Martins et al., 2016).

The following two findings support that comorbidity exists between CP and AD: first, AD patients have greater impairment of oral health because of their progressive cognitive impairment, which affects their oral hygiene habits; second, chronic CP can trigger or exacerbate the neuro-inflammatory process observed in AD (Kamer et al., 2015; Pazos et al., 2018). However, interventional studies reporting a direct association between CP and AD are still lacking (Teixeira et al., 2017; Olsen and Singhrao, 2020).

The vascular channel is reported to be the primary link between oral bacteria or pro-inflammatory molecules and the brain (Balan et al., 2011; Maurer et al., 2018). Accordingly, the serum is the preferred specimen for the study of comorbidity of the two diseases. Approximately 500 ml of cerebrospinal fluid is absorbed into the blood daily; thus, the serum may offer a rich source of brain-related disease biomarkers (Asgari et al., 2015). As an improvement of 2D-PAGE, two-dimensional differential in-gel electrophoresis (2D-DIGE) provides a novel opportunity to identify biomarkers or therapeutic targets (Murphy and Dowling, 2018). DIGE incorporates three types of fluorescent molecules (CyDyes), which are used to pre-label samples before separation by 2-DIGE. Proteins of interest are identified by tandem mass spectrometry [liquid chromatography-mass spectrometry/mass spectrometry (LC-MS/MS); Pasquali et al., 2017].

In this study, we aimed to: (i) identify and validate differentially expressed proteins in CP patients and controls ($n = 23$ for CP patients; $n = 45$ for age-matched healthy controls); and (ii) explore the molecular mechanism of Cathepsin B as a link between CP and AD *in vitro*.

MATERIALS AND METHODS

Human Serum Sample Collection

The study was approved by the Medical Ethics Committee of Shenzhen Baoan Women's and Children's Hospital and all subjects signed informed consent before enrolment in the study. Detailed demographic information of CP patients and age-matched controls are presented in **Table 1**. A serum sample from 23 CP patients and 45 age-matched controls were collected. Blood samples were collected into evacuated collection tubes with no anticoagulant and were allowed to clot for 2 h on ice before centrifugation at 3,000 g for 10 min and 4°C. Serum was collected and stored in Eppendorf tubes at −80°C until utilized for the study.

Serum Pre-fractionation

The process of depletion and desalination was performed according to the protocol described previously. The Agilent Human 14 Multiple Affinity Removal Column (Hu-14, 4.6 × 50 mm) was used to remove the most abundant proteins from the serum, which include IgG, IgA, IgM, albumin, antitrypsin, transthyretin, haptoglobin, transferrin, fibrinogen, alpha1-acid glycoprotein, alpha2-macroglobulin, apolipoproteinAII, apolipoprotein AI and complement C3. After depletion, the centrifugal concentrators (YM-3, MWCO3 kDa, Millipore) were used to desalt and concentrate the samples (Lu et al., 2014).

2D-DIGE Analysis and Image Analysis

The standard of 2D-DIGE analysis was performed according to the protocol described previously (Dowling and Ohlendieck, 2018). Most importantly, to reduce the variation of signal in gels, the photomultiplier tube (PMT) was set to ensure maximum pixel intensity values for all gel images within a range of 40,000–60,000 pixels. DeCyder 7.0 (GE Healthcare) was used to analyze the images. In the DIA module, each spot was detected, matched, and normalized; in the BVA module, spot statistics were reviewed. The spots with an average ratio of more than

TABLE 1 | Characteristics of Chronic Periodontal disease (CP) patients and control subjects.

	Subjects	
	Control	**CP**
Numbers	45	23
Mean age (years)	62.5 ± 3.4	63.2 ± 4.1
Sex, M/F	21/24	10/13
Mean MMSE score	27.8 ± 1.6	20.4 ± 3.3
Mean duration of disease (years)		10.8 ± 0.5

MMSE, Mini-Mental State Examination; Data are displayed as the mean ± SEM.

+1.5 or less than −1.5 and with a statistical difference ($p < 0.05$) were isolated for further investigation.

Identification of Candidate Protein Biomarkers by LC-MS/MS

The standard LC-MS/MS and database searching were performed according to the protocol described previously (Sun et al., 2015). Briefly, LC-MS analysis was carried out using a Surveyor MS Pump Plus HPLC system coupled to a Thermo Fisher Finnigan LTQ linear ion trap mass spectrometer (Thermo Fisher Corporation, San Jose, CA, USA) using nano-electrospray ionization. Tryptic peptides were loaded onto a trap column (300SB-C18, 5 × 0.3 mm, 5 μm particle size; Agilent Technologies, Santa Clara, CA, USA) connected through a zero dead volume union to the self-packed analytical column (C18, 100 × 0.1 mm, 3 μm particle size; SunChrom, Germany). The peptides were then separated by linear gradient elution involving 0–45% B over 55 min followed by 45–100% B over 10 min (B is 80% acetonitrile, 0.1% formic acid) at a flow rate of 500 nL/min. MS data were analyzed using SEQUEST against the National Center for Biotechnology Information (NCBI) human protein database and the results filtered, sorted, and displayed using Bioworks 3.2. Returned protein lists were filtered using the parameters: Peptide Xcorr value >1.90 (for +1 charge), >2.75 (for +2 charge), >3.75 (for +3 charge); peptide Delt CN >0.1; protein probabilities <0.001. At least two unique peptides were required for each identified protein.

Western Blot Analysis

Western blot was performed as described before (Sun et al., 2015). Briefly, the PVDF membranes were incubated with anti-Cofilin-2 (Santa Cruz, sc-166985), anti-Cathepsin B (Cell Signal Technology, 31718), anti-Triosephosphate isomerase (Abcam, ab28760), anti-Clusterin (CST, 34642), anti-ITI-H4 (Santa Cruz, sc-515353), anti-APP (Cell Signal Technology, 29765), Anti-sAPPα (IBL, 11088), Anti-sAPPβ (IBL, 18957) Anti-BACE1 (Abcam, ab2077), anti-ADAM10 (Cell Signal Technology, 14194) and anti-β-actin (Cell Signal Technology, 3700) overnight at 4°C. After washed with TBST, HRP-conjugated secondary antibodies (1:10,000) were applied at room temperature for 1 h. The signals were detected by a ChemiDoc MP system (Bio-Rad) and analyzed by ImageJ software.

Enzyme-Linked Immunosorbent Assay (ELISA)

ELISA was performed according to the instruction of each kit: Human Amyloid beta (aa1–40) ELISA Kit (DAB140B, R&D Systems), Human Amyloid beta (aa1–42) ELISA Kit (DAB142, R&D Systems) and Human Cathepsin B ELISA Kit (ab119584, Abcam). Each sample was performed in duplicate. Briefly, Serum (or diluted serum) at 100 μl was added to the plate and incubated for 2 h at 2–8°C. After a total of four washes, Conjugate was added and incubated for another 2 h at 2–8°C. After another four washes, Substrate Solution was added to each well and incubated for 30 min at room temperature. For signal detection, each well was determined using 450 nm as a primary wavelength and 630 nm as a reference wavelength.

Cell Culture

Human neuroblastoma SK-N-SH cells overexpressing wild-type APP695 (SK-N-SH APPwt) were a gift from Dr. Dennis Selkoe (Boston, MA, USA). SK-N-SH APPwt cells were grown in DMEM, plus10% fetal bovine serum (Hyclone, Los Angeles, CA, USA), 100 U/ml penicillin/streptomycin. Also, cells were supplemented with 200 μg/ml G418. Cell cultures were maintained at 37°C in a humidified atmosphere containing 5% CO2 and passed every 2–4 days based on 85% confluence. P.g-LPS was obtained from Invivo Gen (San Diego, CA, USA), and applied to the supernatant of SK-N-SH APPwt cells with the final concentration 1 μg/ml for a total of 7 days to mimic CP *in vitro* (P.g-LPS was incubated for 4 days initially. At confluence, SK-N-SH APPwt cells were passaged and new P.g-LPS were applied to the supernatant immediately and incubated for another 3 days). For Cathepsin B inhibition, a final concentration of 75 μM CA-074 methyl ester (Sigma-Aldrich, USA) was applied to the supernatant of SK-N-SH APPwt cells 1 h before P.g-LPS. For Cathepsin B activation, IL-6 (10 ng/ml, Genscript, Z03134), IL-1β(100 pg/ml, Genscript, Z02978), TNF-α (10 ng/ml, Genscript, Z01001) and recombinant Human CRP protein (1 mg/L, Abcam ab171471) were applied to SK-N-SH APPwt cells for 24 h. For TNF-α inhibition, pomalidomide (2 μM, Selleck, S1567) was applied to P.g-LPS treated SK-N-SH APPwt cells 24 h before cell harvest.

Statistical Analysis

For the 2D-DIGE experiment study, DeCyder 7.0 (GE Healthcare) was used to analysis data from DIGE (DIA and BVA model). Spots with $p < 0.05$ and variation ratio >1.5-fold between groups were considered as the differential spots. For Western blot data, comparison between the groups was made using a two-tailed unpaired Student's *t*-test. The Control group was normalized to 100%. All data were shown as mean ± SD, and prism software (GraphPad Prism5, La Jolla, CA, USA) was used to create the graphs. A value of $p < 0.05$ was considered to be statistically significant. The correlation between Cathepsin B level and MMSE scores were performed with the Spearman correlation coefficient.

RESULTS

Clinical Data

The clinical data from each subject are summarized in **Table 1**. No significant differences were found in age, sex, and education between the two groups in either the 2-DIGE study or the validation study ($p > 0.05$).

Serum Aβ Measurements in the Clinical Cohort

Whole serum from the CP group and Control group were analyzed to determine the concentration of $A\beta_{1-40}$ and $A\beta_{1-42}$. The serum levels of $A\beta_{1-40}$ and $A\beta_{1-42}$ did not differ significantly between the groups, with observed serum levels of 216.9 ± 44.0 and 237.0 ± 66.6 pg/ml for $A\beta_{1-40}$ in the CP and Control groups, respectively ($p = 0.142$) and 22.5 ± 6.0 and 19.8 ± 4.8 pg/ml for $A\beta_{1-42}$ in the CP group and Control

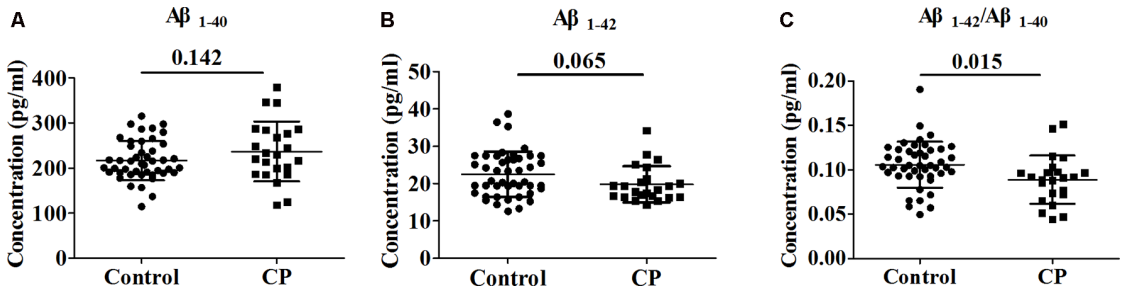

FIGURE 1 | Comparison of $A\beta_{1-40}$, $A\beta_{1-42}$ and $A\beta_{1-42}/A\beta_{1-40}$ between Chronic Periodontitis (CP) group and Control group. **(A)** The concentration of $A\beta_{1-40}$ between CP group and Control group. **(B)** The concentration of between CP group and Control group. **(C)** The concentration of $A\beta_{1-42}/A\beta_{1-40}$ between CP group and Control group. No significant difference between the CP group and Control group in $A\beta_{1-40}$ ($p = 0.142$), $A\beta_{1-42}$ ($p = 0.065$) were observed. $A\beta_{1-42}/A\beta_{1-40}$ was significantly decreased in the CP group compared to the Control group ($p = 0.009$).

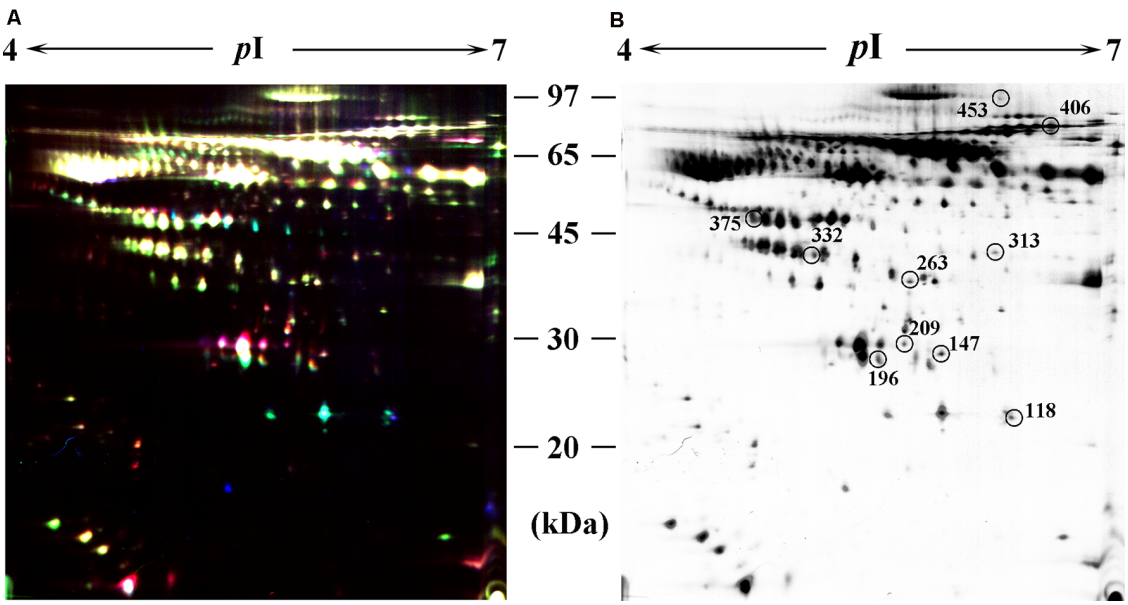

FIGURE 2 | Identification of differentially expressed spots by using two-dimensional differential in-gel electrophoresis (2D-DIGE). Abundant protein depleted serum was subjected to 2D-DIGE quantitative analysis to identify proteins with differing abundance between the CP group and Control group. **(A)** Over-lay of cy2-marked loading control, cy3-marked, and cy5-marked serum sample from CP patient and age-matched controls ($n = 12$). **(B)** Distribution of differentially expressed protein spots. The samples were separated using IPG gel (pH 4–7, 18 cm) in the first phase and 12.5% SDS-PAGE; 150 ug of protein was used in each gel. The spots showing significant differences between CP patients and controls (see **Table 2**) were labeled in a 2D-DIGE gel.

group, respectively ($p = 0.065$). However, the $A\beta_{1-42}/A\beta_{1-40}$ ratio was notably lower ($p = 0.009$) in the CP group than in the Control group, with serum levels of 0.1057 ± 0.0258 and 0.0889 ± 0.0271 pg/ml, respectively (**Figure 1**).

Identification of Differentially Expressed Proteins in CP Patients Using 2D-DIGE

In the differential in-gel analysis (DIA) workspace, approximately500 spots were detected in each gel by the Decyder software. In the Biological variation analysis (BVA) module, the Cy2 image from gel number five was selected as the master gel, as it had the maximum number of spots. Overall, 10 spots were found to be differentially expressed with the criteria (**Figure 2B**). The 10 spots of interest were manually excised from colloidal Coomassie-stained preparative gels of the pooled CP patients' and age-matched controls' depleted serum for in-gel trypsin proteolysis and subsequent LC-MS/MS (LTQ) analysis (**Table 2**). All 10 differentially expressed protein spots corresponded to 10 different proteins; Cofilin-2 (118 spots), Heat shock protein beta-1 (147 spots), Retinol-binding protein 4 (196 spots), Triosephosphate isomerase (209 spots), Cathepsin B (263 spots), Haptoglobin (313 spots), Alpha-1-antitrypsin (332 spots), Clusterin(375 spots), Complement factor B (406 spots), and inter-alpha-trypsin inhibitor heavy chain H4 (ITI-H4; 453 spots). These proteins were consistent with the theoretical

TABLE 2 | Differentially expressed serum proteins in CP patients as compared with controls.

Spot No.[a]	Protein definition	Accession GI No.	Score	Sequence coverage (%)	pI[b]	MW[c]	Variation ratio	*p*-value
118	Cofilin-2	6671746	110.26	33.9	6.77	18709.5	+9.46	0.0014
147	Heat shock protein beta-1	4504517	40.20	11.7	5.98	22782.5	+5.23	0.0064
196	Retinol-binding protein 4	18088326	63.16	33.7	5.76	23010.0	+5.45	0.0011
209	Triosephosphate isomerase	1906326	170.29	57.1	5.65	30791.7	+25.37	0.0354
263	Cathepsin B	6681089	50.39	76.1	5.88	37821.6	+10,000	0.0217
313	Haptoglobin	292156	30.27	15.9	6.13	45861.5	+5.20	0.0016
332	Alpha-1-antitrypsin	189163542	150.21	61.4	5.37	46736.5	+2.27	0.0004
375	Clusterin	355594753	80.21	22.5	4.68	52494.5	+2.63	0.0434
406	Complement factor B	4261689	110.63	36.5	6.67	85532.9	+10,000	0.0059
453	ITI-H4	262050538	80.26	23.2	6.53	103358.1	−43.52	0.0036

Serum proteins from CP patients and controls were separated by DIGE and compared DeCyder 7.0 (GE Healthcare). Spots with $p < 0.05$ and variation ratio >1.5-fold between groups were considered as the differential spots. "Ratio = 10,000" means the spot presented only in one group. Their identities were determined by LC-MS/MS as described in "Materials and Methods" section. Spot numbers correspond to those in ***Figure 2****. [a]Spot numbers correspond to those in* ***Figure 2B****. [b]pI is the theoretical calculated from the amino acid sequence of the predicted mature protein. [c]MW refers to the theoretical molecular mass is kDa calculated from the amino acid sequence.*

molecular weights and *p*I ranges based on the positions of the spots on the gel.

Protein Validation of the Differential Proteins Using Whole Serum

Whole serum was used in the validation study by western blot analysis, in line with clinical practice. In the validation study, five differential proteins were selected for validation by western blot analysis because of their well-established relationship with AD (**Figure 3A**). In line with the 2D-DIGE study, the expression of Cofilin-2, Cathepsin B, and Clusterin was respectively increased by 58.3, 42.6, and 27.5% (**Figures 3B,E,F**), whereas the expression of ITI-H4 was reduced by 60.8% (**Figure 3C**) in whole serum from the CP group. In contrast to the 2D-DIGE results, the expression of Triosephosphate isomerase remained unchanged (**Figure 3D**). Cathepsin B was selected for further validation by ELISA. The results showed a huge increase of Cathepsin B serum concentration in CP patients (39.7 ± 2.5) as compared to controls (15.2 ± 1.2; **Figure 3G**). The serum concentration of Cathepsin B correlated well with MMSE scores ($r = -0.874$, $p < 0.001$; **Figure 3H**).

Cathepsin B in SK-N-SH APPwt Cells

To determine the molecular link between CP and AD, neuroblastoma SK-N-SH APPwt cells were treated with 1 μg/ml of P.g-LPS for 7 days. Results show that P.g-LPS treatment significantly increased both the $A\beta_{1-40}$ ($p < 0.01$) and $A\beta_{1-42}$ ($p < 0.05$) levels in the cell lysates of SK-N-SH APPwt cells (**Figures 4A–C**). To identify the underlying mechanism, we investigated the effect of P.g-LPS on the APP-processing enzymes ADAM10, BACE1, and Cathepsin B and APP cleavage fragments using western blotting. P.g-LPS treatment significantly increased the protein level of sAPPβ ($p < 0.01$) and Cathepsin B ($p < 0.01$), with a considerable decrease of sAPPα ($p < 0.01$; **Figures 4D,E**). To further verify our results, a specific Cathepsin B inhibitor CA074Me was applied to assess Cathepsin B inhibition on the $A\beta_{1-40}$ and $A\beta_{1-42}$ levels in SK-N-SH APPwt cells. The results indicated a robust decrease in the $A\beta_{1-40}$ ($p < 0.05$) and $A\beta_{1-42}$ levels in P.g-LPS-treated-SK-N-SH APPwt cells after Cathepsin B inhibition (**Figures 4G–I**).

Inflammatory Cytokines in P.g-LPS Treated SK-N-SH APPwt Cells

To elucidate the underlying mechanism of P.g-LPS-induced Cathepsin B up-regulation in SK-N-SH APPwt cells, the well-known inflammatory cytokines in CP including IL-6, IL-1β, and TNF-α, and CRP were applied to the supernatant of SK-N-SH APPwt cells. Only TNF-α treatment could significantly raise the protein level of Cathepsin B ($p < 0.01$; **Figures 5A,B**). Furthermore, pomalidomide, a specific TNF-α inhibitor was applied. The results showed in the context of TNF-α inhibition, P.g-LPS could not up-regulate the protein expression of Cathepsin B, which confirmed it was TNF-α which was responsible for P.g-LPS induced Cathepsin B up-regulation in SK-N-SH APPwt cells (**Figures 5C,D**).

DISCUSSION

Several studies have indicated that patients with AD have poorer dental health than age-matched controls, while other studies have also confirmed that patients with CP have cognitive defects and even dementia (Pritchard et al., 2017; Dominy et al., 2019). However, the mechanism underlying the relationship between periodontitis and cognitive decline remains unclear (Gaur and Agnihotri, 2015; Chen et al., 2017). In this study, for the first time, we examined the correlation between CP and AD, regarding proteomics.

Approximately 500 protein spots were successfully matched between the two groups on each gel, and 10 proteins that underwent significant changes (nine up-regulated and one down-regulated) were identified (**Table 2**). Of the 10 proteins, three have been previously reported to play a positive role in the inflammatory process: Haptoglobin, Alpha-1-antitrypsin, and Complement factor B, which supports our findings (Chou et al., 2012; Ostvik et al., 2014; Yang et al., 2017; Cholette et al., 2018; Balbi et al., 2019; Reeves et al., 2019). It is proposed that inflammation, originated from CP, might add to the inflammatory pool in the serum by contributing several pro-inflammatory mediators, such as C-reactive protein, interleukin (IL)-1, IL-6, and TNF-α, which cause cell apoptosis, tumor genesis, neuro-inflammation, and a systemic immune response (Rapone et al., 2019; Wang et al., 2019).

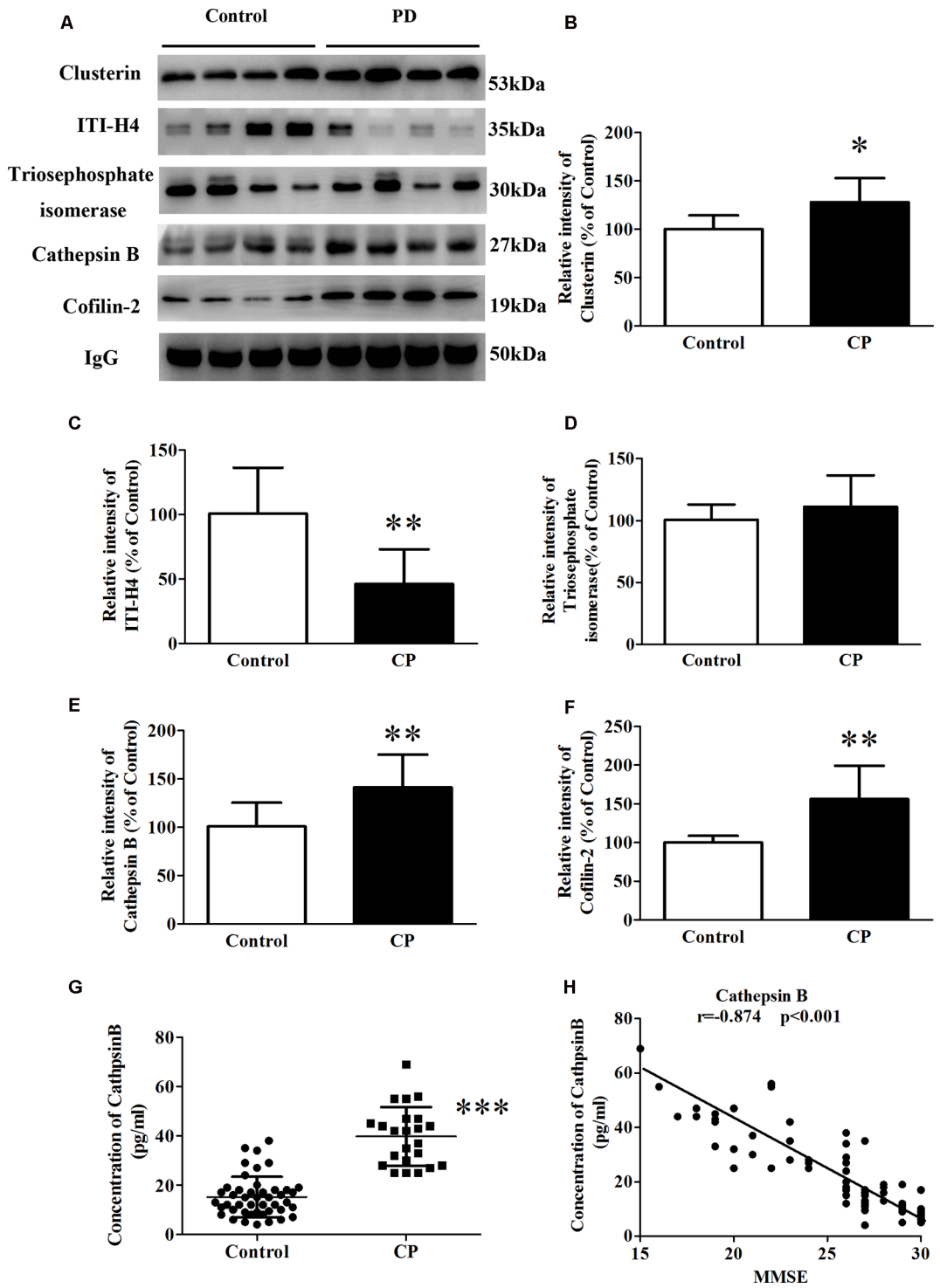

FIGURE 3 | The expression of Clusterin, ITI-H4, Triosephosphate isomerase, Cathepsin B, and Cofilin-2 between Control subjects and CP patients. **(A)** A representative panel of Western blots of Clusterin, ITI-H4, Triosephosphate isomerase, Cathepsin B and Cofilin-2. **(B)** Quantitative comparison of the Western blot of Clusterin. **(C)** Quantitative comparison of the Western blot of ITI-H4. **(D)** Quantitative comparison of the Western blot of Triosephosphate isomerase. **(E)** Quantitative comparison of the Western blot of Cathepsin B. **(F)** Quantitative comparison of the Western blot of Cofilin-2. **(G)** The serum concentration of Cathepsin B for each individual was measured by ELISA. **(H)** The correlation between serum Cathepsin B and MMSE score. Data represent mean ± SEM for 16 individual subjects per group. $^{*}p < 0.05$ compared with the Control group, $^{**}p < 0.01$ compared with the Control group, $^{***}p < 0.001$ compared with Control group, student's *t*-test.

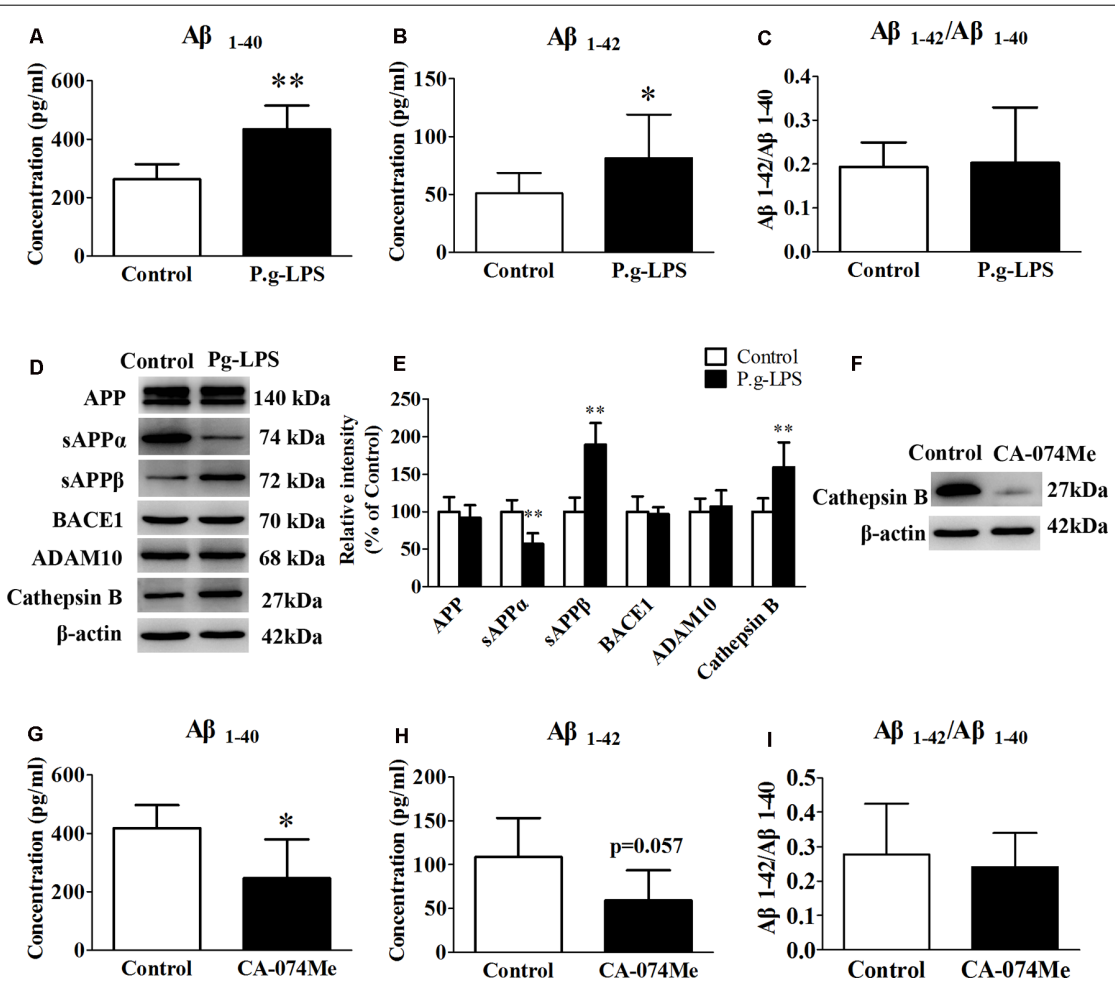

FIGURE 4 | Cathepsin B inhibition could decrease the concentration of $A\beta_{1-40}$ and $A\beta_{1-42}$ in P.g-LPS-treated SK-N-SH APPwt cells. **(A–C)** $A\beta_{1-40}$, $A\beta_{1-42}$, $A\beta_{1-42}/A\beta_{1-40}$ concentration in SK-N-SH APPwt cells and P.g-LPS-treated SK-N-SH APPwt cells. **(D,E)** Representative panel and Quantitative comparison of the Western blot of APP, sAPPα, sAPPβ, BACE1, ADAM10, and Cathepsin B in the cell lysates of SK-N-SH APPwt cells and P.g-LPS-treated SK-N-SH APPwt cells. **(F)** A representative panel of the Western blot of Cathepsin B in the cell lysates of P.g-LPS-treated SK-N-SH APPwt cells after CA-074Me application. **(G–I)** $A\beta_{1-40}$, $A\beta_{1-42}$ and $A\beta_{1-42}/A\beta_{1-40}$ concentration after Cathepsin B inhibition in P.g-LPS-treated SK-N-SH APPwt cells. $^{*}p < 0.05$ compared with Control group, $^{**}p < 0.01$ compared with Control group, student's *t*-test.

Recently, an association between CP and AD was hypothesized. It was suggested that CP worsened the inflammatory processes of AD in the brain. This was mainly attributed to increased levels of pro-inflammatory mediators, which activate the already primed microglial cells within the central nervous system and hasten the neuro-degeneration process (Wu and Nakanishi, 2015; Gil Montoya et al., 2020). In this study, of the 10 differentially expressed proteins, five have been extensively studied concerning the pathology of AD: Cofilin-2, Triosephosphate isomerase, Cathepsin B, Clusterin, and ITI-H4, which strengthens the possibility of an association between the two diseases. To further validate our results, these five proteins were analyzed by western blot. Cofilin-2, Cathepsin B, and Clusterin levels were increased and ITI-H4 levels were robustly reduced in the whole serum from CP patients. Although Triosephosphate isomerase was observed to be altered on 2D-DIGE, western blot detected no significant alteration. Of the five AD-related proteins above, Cathepsin B was chosen for further study with the highest correlation with the MMSE score ($r = -0.874$, $p < 0.001$).

Nowadays, as there is still no effective treatment or curable drugs for AD, early and accurate diagnosis has become a prime requirement for the management of AD. CSF diagnosis (by invasive means) may not always be feasible, and better non-invasive diagnostic techniques are needed. This is especially important since many AD patients are elder people, whose body is relatively poor and cannot bear the impact of spinal puncture. A large part of CSF proteins is draining out of the brain, which makes serum as a protein pool at the forefront for diagnosis. For Cathepsin B, our future study was to check if their quantity varies during aging and/or as periodontitis diagnosis timeline increases. Usually, it takes 10 years from diagnosis of periodontitis to become a risk factor for AD, so there could be a steady increase in Cathepsin B overtime after the initial diagnosis of periodontal

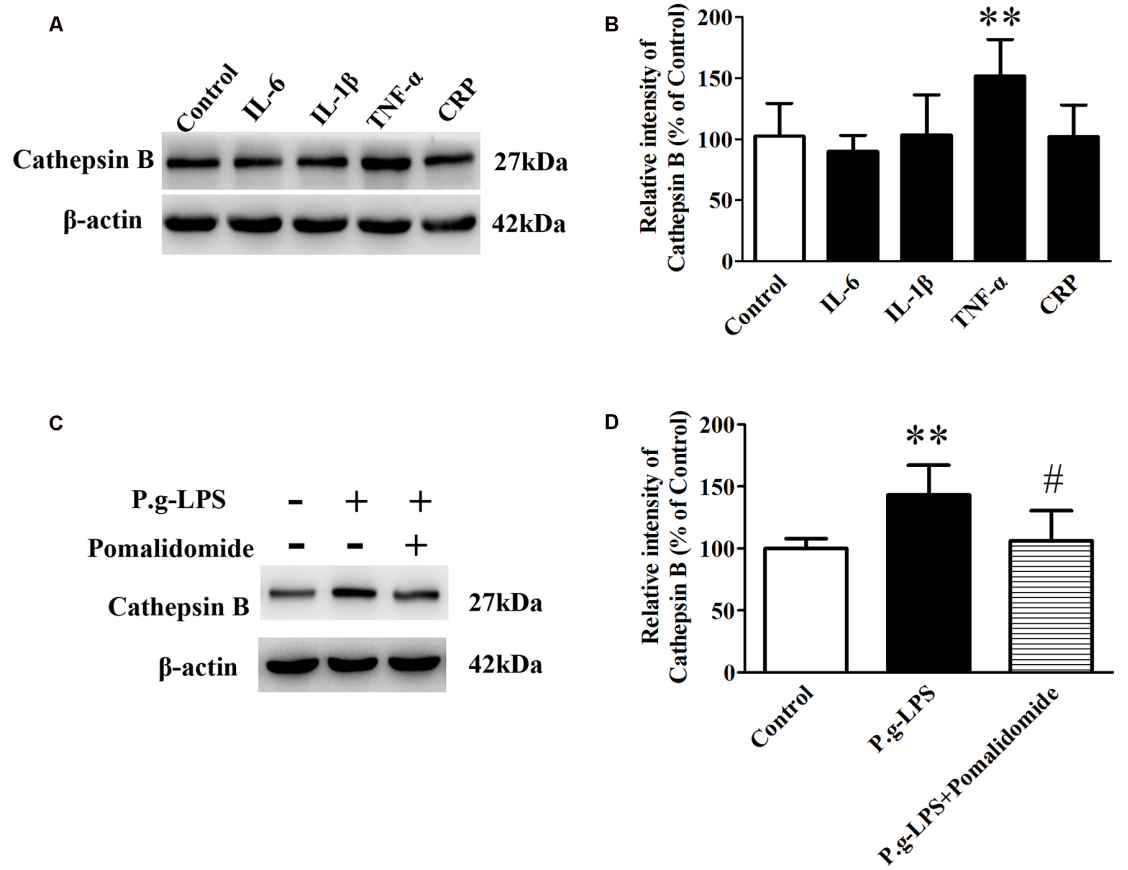

FIGURE 5 | TNF-α is responsible for the increase of Cathepsin B in P.g-LPS-treated SK-N-SH APPwt cells. **(A,B)** Representative panel and quantitative comparison of the Western blot of Cathepsin B in IL-6-treated group, IL-1β-treated group, TNF-α-treated group, and recombinant Human CRP-treated group and Control group. **(C,D)** Representative panel and quantitative comparison of the Western blot of cathepsin B in Control group, P.g-LPS-treated group, and P.g-LPS plus pomalidomide-treated group. $^{\#}p < 0.05$ compared to P.g-LPS group, $^{**}p < 0.01$ compared with Control group, student's *t*-test.

disease. Cathepsin B could be a potential biomarker to make stronger associations with periodontitis and AD.

Evidence also indicates that Cathepsin B has β-secretase activity, participating in APP-processing and cutting to Aβ (Perlenfein and Murphy, 2017; Batkulwar et al., 2018; Sun et al., 2018). Therefore, the molecular mechanism of Cathepsin B in the pathology of AD is interesting. There are two sources of serum Cathepsin B, peripheral organs leaking and brain penetration. It has been reported that macrophages-produced Cathepsin B involves in peripheral Aβ production both *in vitro* and *in vivo*. Cathepsin B but not BACE1 could cut the wild-type β-secretase site effectively and further into $A\beta_{1-42}$ and $A\beta_{3-42}$ (Nie et al., 2019). In the central nervous system, Cathepsin B is mainly secreted by microglia and packaged into neuronal secretory vesicles with its signal peptide, which will either be captured by neurons or circulate into the CSF. Upon BBB damage, Cathepsin B is absorbed into the serum. Our results also showed at least part of the serum Cathepsin B comes from brain penetration (data not shown). Cathepsin B has been also confirmed to promote mature IL-lβ processing and secretion *via* activated microglia. Our results demonstrated that the protein level of Cathepsin B was significantly increased along with drastic augmentation in both $A\beta_{1-40}$ and $A\beta_{1-42}$ levels in SK-N-SH APPwt cells treated with 1 μg/ml P.g-LPS for 7 days. Furthermore, inhibition of Cathepsin B could result in a significant reduction in both the $A\beta_{1-40}$ and the $A\beta_{1-42}$ levels (**Figures 4G,H**). This is important because, despite evidence indicating the comorbidity of CP and AD, no studies demonstrate the causal link between CP and AD (Harding et al., 2017). Our study, for the first time, demonstrated that Cathepsin B might be a key link between the two diseases.

Clarified by several other studies, the pathology of CP is accompanied with the outbreak of inflammatory mediators, especially pro-inflammatory cytokines such as IL-6, IL-1β, TNF-α, Human NF-κB p65, and CRP (Singhrao et al., 2015; Teixeira et al., 2017; Ranjan et al., 2018; Singhrao and Olsen, 2018, 2019). Wu et al. (2017) found IL-1β, which was produced by microglia, could increase the level of Cathepsin B APP through IL-1R signaling in primary neurons after P.g-LPS treatment. IL-1β was the key inflammatory mediators that link CP and AD (Wu et al., 2017). Nevertheless, our results showed that only TNF-α treatment could significantly upregulate the

protein level of Cathepsin B. TNF-α could be an intermediate between P.g-LPS treatment and the production of Cathepsin B and APP. These different results were probably due to the source of inflammatory mediators: microglia-derived IL-1β and exogenous TNF-α. Future microglia and primary neuron co-culture systems are needed to confirm the results of this study.

There are also arguments for this work. Our clinical serum study showed $A\beta_{1-42}/A\beta_{1-40}$ ratio was notably lower ($p = 0.009$) in the CP group, which is different from the previous report. Elevated plasma $A\beta_{1-42}/A\beta_{1-40}$ ratio was observed in severe periodontitis group than in other groups (moderate/mild/absent; Gil-Montoya et al., 2017). Those differences were most likely attributed to the source and degree of patients. Because after we separated the participants into severe, moderate, mild, and control, we also got similar results as what Gil-Montoya et al. (2017) have reported. However, only three CP patients were detected as severe periodontitis, which made the results of subgroup unreliable (date not shown). Anyway, it is well-known that lower serum $A\beta_{1-42}$ level and $A\beta_{1-42}/A\beta_{1-40}$ ratio could be found in AD patients as compared to age-matched normal controls, which strongly supports our findings.

In conclusion, in our exploration study, 10 differential expressed proteins were identified between CP and Control groups, while, in the validation study, Cofilin-2, Cathepsin B, Clusterin, and ITI-H4 exhibited a significant alteration in the whole serum samples. Also, Cathepsin B might be a link between CP and AD. Our study represents a new hope for therapeutic interventions that could prevent the progression and worsening of AD.

DATA AVAILABILITY STATEMENT

The raw data supporting the conclusions of this article will be made available by the authors, without undue reservation.

ETHICS STATEMENT

The studies involving human participants were reviewed and approved by Lian Zhang Medical Ethics Committee, Shenzhen Baoan Women's and Children's Hospital. The patients/participants provided their written informed consent to participate in this study.

AUTHOR CONTRIBUTIONS

XR finished 2D-dige and wrote the article. LX contributed to the *in vitro* study. YL contributed to cell culture. HY was in charge of sample collection. WC and LL contributed to western blot and ELISA. DL revised the article. XZ provided the idea and funding of the study.

ACKNOWLEDGMENTS

We would like to thank Editage (www.editage.cn) for English language editing.

SUPPLEMENTARY MATERIAL

The Supplementary Material for this article can be found online at: https://www.frontiersin.org/articles/10.3389/fnagi.2020.00248/full#supplementary-material.

REFERENCES

Alzheimer, A., Stelzmann, R. A., Schnitzlein, H. N., and Murtagh, F. R. (1995). An English translation of Alzheimer's 1907 paper, "Uber eine eigenartige Erkankung der Hirnrinde". *Clin. Anat.* 8, 429–431. doi: 10.1002/ca.980080612

Asgari, N., Berg, C. T., Morch, M. T., Khorooshi, R., and Owens, T. (2015). Cerebrospinal fluid aquaporin-4-immunoglobulin G disrupts blood brain barrier. *Ann. Clin. Transl. Neurol.* 2, 857–863. doi: 10.1002/acn3.221

Badea, A., Wu, W., Shuff, J., Wang, M., Anderson, R. J., Qi, Y., et al. (2019). Identifying vulnerable brain networks in mouse models of genetic risk factors for late onset alzheimer's disease. *Front. Neuroinform.* 13:72. doi: 10.3389/fninf.2019.00072

Balan, H., Popescu, E., and Angelescu, G. (2011). Pathologic crossroads: cardiovascular diseases, periodontal diseases and calcium antagonists. *J. Med. Life* 4, 2–10.

Balbi, B., Sangiorgi, C., Gnemmi, I., Ferrarotti, I., Vallese, D., Paracchini, E., et al. (2019). Bacterial load and inflammatory response in sputum of α-1 antitrypsin deficiency patients with COPD. *Int. J. Chron. Obstruct. Pulmon. Dis.* 14, 1879–1893. doi: 10.2147/COPD.S207203

Batkulwar, K., Godbole, R., Banarjee, R., Kassaar, O., Williams, R. J., and Kulkarni, M. J. (2018). Advanced glycation end products modulate amyloidogenic APP processing and tau phosphorylation: a mechanistic link between glycation and the development of Alzheimer's disease. *ACS Chem. Neurosci.* 9, 988–1000. doi: 10.1021/acschemneuro.7b00410

Chen, C. K., Wu, Y. T., and Chang, Y. C. (2017). Association between chronic periodontitis and the risk of Alzheimer's disease: a retrospective, population-based, matched-cohort study. *Alzheimers Res. Ther.* 9:56. doi: 10.1186/s13195-017-0282-6

Cholette, J. M., Pietropaoli, A. P., Henrichs, K. F., Alfieris, G. M., Powers, K. S., Gensini, F., et al. (2018). Elevated free hemoglobin and decreased haptoglobin levels are associated with adverse clinical outcomes, unfavorable physiologic measures and altered inflammatory markers in pediatric cardiac surgery patients. *Transfusion* 58, 1631–1639. doi: 10.1111/trf.14601

Chou, W. W., Wang, Y. S., Chen, K. C., Wu, J. M., Liang, C. L., and Juo, S. H. (2012). Tannic acid suppresses ultraviolet B-induced inflammatory signaling and complement factor B on human retinal pigment epithelial cells. *Cell Immunol.* 273, 79–84. doi: 10.1016/j.cellimm.2011.11.003

Dominy, S. S., Lynch, C., Ermini, F., Benedyk, M., Marczyk, A., Konradi, A., et al. (2019). *Porphyromonas gingivalis* in Alzheimer's disease brains: evidence for disease causation and treatment with small-molecule inhibitors. *Sci. Adv.* 5:eaau3333. doi: 10.1126/sciadv.aau3333

Dowling, P., and Ohlendieck, K. (2018). DIGE analysis of immunodepleted plasma. *Methods Mol. Biol.* 1664, 245–257. doi: 10.1007/978-1-4939-7268-5_19

Dursun, E., Alaylioglu, M., Bilgic, B., Hanagasi, H., Lohmann, E., Atasoy, I. L., et al. (2016). Vitamin D deficiency might pose a greater risk for ApoEvarepsilon4 non-carrier Alzheimer's disease patients. *Neurol. Sci.* 37, 1633–1643. doi: 10.1007/s10072-016-2647-1

Gaur, S., and Agnihotri, R. (2015). Alzheimer's disease and chronic periodontitis: is there an association? *Geriatr. Gerontol. Int.* 15, 391–404. doi: 10.1111/ggi.12425

Gil Montoya, J. A., Barrios, R., Sanchez-Lara, I., Ramos, P., Carnero, C., Fornieles, F., et al. (2020). Systemic inflammatory impact of periodontitis on cognitive impairment. *Gerodontology* 37, 11–18. doi: 10.1111/ger.12431

Gil-Montoya, J. A., Barrios, R., Santana, S., Sanchez-Lara, I., Pardo, C. C., Fornieles-Rubio, F., et al. (2017). Association between periodontitis

and amyloid β peptide in elderly people with and without cognitive impairment. *J. Periodontol.* 88, 1051–1058. doi: 10.1902/jop.2017.170071

Harding, A., Robinson, S., Crean, S., and Singhrao, S. K. (2017). Can better management of periodontal disease delay the onset and progression of Alzheimer's disease? *J. Alzheimers Dis.* 58, 337–348. doi: 10.3233/jad-170046

Hardy, J. A., and Higgins, G. A. (1992). Alzheimer's disease: the amyloid cascade hypothesis. *Science* 256, 184–185. doi: 10.1126/science.1566067

Jackson, R. J., Rose, J., Tulloch, J., Henstridge, C., Smith, C., and Spires-Jones, T. L. (2019). Clusterin accumulates in synapses in Alzheimer's disease and is increased in apolipoprotein E4 carriers. *Brain Commun.* 1:fcz003. doi: 10.1093/braincomms/fcz003

Kamer, A. R., Pirraglia, E., Tsui, W., Rusinek, H., Vallabhajosula, S., Mosconi, L., et al. (2015). Periodontal disease associates with higher brain amyloid load in normal elderly. *Neurobiol. Aging* 36, 627–633. doi: 10.1016/j.neurobiolaging.2014.10.038

Lang, N. P., Schätzle, M. A., and Löe, H. (2009). Gingivitis as a risk factor in periodontal disease. *J. Clin. Periodontol.* 36, 3–8. doi: 10.1038/sj.bdj.2009.818

López, R., and Baelum, V. (2015). Periodontal disease classifications revisited. *Eur. J. Oral Sci.* 123, 385–389. doi: 10.1111/eos.12227

Lu, W., Wan, X., Liu, B., Rong, X., Zhu, L., Li, P., et al. (2014). Specific changes of serum proteins in Parkinson's disease patients. *PLoS One* 9:e95684. doi: 10.1371/journal.pone.0095684

Martins, M. D., Jiao, Y., Larsson, L., Almeida, L. O., Garaicoa-Pazmino, C., Le, J. M., et al. (2016). Epigenetic modifications of histones in periodontal disease. *J. Dent. Res.* 95, 215–222. doi: 10.1177/0022034515611876

Maurer, K., Rahming, S., and Prvulovic, D. (2018). Dental health in advanced age and Alzheimer's disease: a possible link with bacterial toxins entering the brain? *Psychiatry Res. Neuroimaging* 282, 132–133. doi: 10.1016/j.pscychresns.2018.06.009

Murphy, S., and Dowling, P. (2018). DIGE analysis of proteominer(TM) fractionated serum/plasma samples. *Methods Mol. Biol.* 1664, 109–114. doi: 10.1007/978-1-4939-7268-5_10

Nie, R., Wu, Z., Ni, J., Zeng, F., Yu, W., Zhang, Y., et al. (2019). Porphyromonas gingivalis infection induces Amyloid-β accumulation in monocytes/macrophages. *J. Alzheimers Dis.* 72, 479–494. doi: 10.3233/jad-190298

Olsen, I., and Singhrao, S. K. (2020). Is there a link between genetic defects in the complement cascade and Porphyromonas gingivalis in Alzheimer's disease? *J. Oral Microbiol.* 12:1676486. doi: 10.1080/20002297.2019.1676486

Ostvik, A. E., Granlund, A., Gustafsson, B. I., Torp, S. H., Espevik, T., Mollnes, T. E., et al. (2014). Mucosal toll-like receptor 3-dependent synthesis of complement factor B and systemic complement activation in inflammatory bowel disease. *Inflamm. Bowel Dis.* 20, 995–1003. doi: 10.1097/mib.0000000000000035

Pasquali, M., Serchi, T., Planchon, S., and Renaut, J. (2017). 2D-DIGE in proteomics. *Methods Mol. Biol.* 1654, 245–254. doi: 10.1007/978-1-4939-7231-9_17

Pazos, P., Leira, Y., Dominguez, C., Pias-Peleteiro, J. M., Blanco, J., and Aldrey, J. M. (2018). Association between periodontal disease and dementia: a literature review. *Neurologia* 33, 602–613. doi: 10.1016/j.nrl.2016.07.013

Perlenfein, T. J., and Murphy, R. M. (2017). A mechanistic model to predict effects of cathepsin B and cystatin C on β-amyloid aggregation and degradation. *J. Biol. Chem.* 292, 21071–21082. doi: 10.1074/jbc.m117.811448

Pritchard, A. B., Crean, S., Olsen, I., and Singhrao, S. K. (2017). Periodontitis, microbiomes and their role in Alzheimer's disease. *Front. Aging Neurosci.* 9:336. doi: 10.3389/fnagi.2017.00336

Ranjan, R., Abhinay, A., and Mishra, M. (2018). Can oral microbial infections be a risk factor for neurodegeneration? A review of the literature. *Neurol. India* 66, 344–351. doi: 10.4103/0028-3886.227315

Rapone, B., Converti, I., Santacroce, L., Cesarano, F., Vecchiet, F., Cacchio, L., et al. (2019). Impact of periodontal inflammation on nutrition and inflammation markers in hemodialysis patients. *Antibiotics* 8:209. doi: 10.3390/antibiotics8040209

Rasmussen, J., and Langerman, H. (2019). Alzheimer's disease—why we need early diagnosis. *Degener Neurol. Neuromuscul. Dis.* 9, 123–130. doi: 10.2147/dnnd.s228939

Reeves, E. P., Dunlea, D. M., McQuillan, K., O'Dwyer, C. A., Carroll, T. P., Saldova, R., et al. (2019). Circulating truncated α-1 antitrypsin glycoprotein in patient plasma retains anti-inflammatory capacity. *J. Immunol.* 202, 2240–2253. doi: 10.4049/jimmunol.1801045

Rong, X. F., Sun, Y. N., Liu, D. M., Yin, H. J., Peng, Y., Xu, S. F., et al. (2017). The pathological roles of NDRG2 in Alzheimer's disease, a study using animal models and APPwt-overexpressed cells. *CNS Neurosci. Ther.* 23, 667–679. doi: 10.1111/cns.12716

Shinohara, M., Sato, N., Shimamura, M., Kurinami, H., Hamasaki, T., Chatterjee, A., et al. (2014). Possible modification of Alzheimer's disease by statins in midlife: interactions with genetic and non-genetic risk factors. *Front. Aging Neurosci.* 6:71. doi: 10.3389/fnagi.2014.00071

Singhrao, S. K., Harding, A., Poole, S., Kesavalu, L., and Crean, S. (2015). Porphyromonas gingivalis periodontal infection and its putative links with Alzheimer's disease. *Mediators Inflamm.* 2015:137357. doi: 10.1155/2015/137357

Singhrao, S. K., and Olsen, I. (2018). Are *Porphyromonas gingivalis* outer membrane vesicles microbullets for sporadic Alzheimer's disease manifestation? *J. Alzheimers Dis. Rep.* 2, 219–228. doi: 10.3233/adr-180080

Singhrao, S. K., and Olsen, I. (2019). Assessing the role of Porphyromonas gingivalis in periodontitis to determine a causative relationship with Alzheimer's disease. *J. Oral Microbiol.* 11:1563405. doi: 10.1080/20002297.2018.1563405

Sun, B., Fan, P., Liao, M., and Zhang, Y. (2018). Modeling endophilin-mediated Aβ disposal in glioma cells. *Biochim. Biophys. Acta Mol. Cell Res.* 1865, 1385–1396. doi: 10.1016/j.bbamcr.2018.06.015

Sun, Y., Rong, X., Lu, W., Peng, Y., Li, J., Xu, S., et al. (2015). Translational study of Alzheimer's disease (AD) biomarkers from brain tissues in AβPP/PS1 mice and serum of AD patients. *J. Alzheimers Dis.* 45, 269–282. doi: 10.3233/jad-142805

Tapiainen, V., Lavikainen, P., Koponen, M., Taipale, H., Tanskanen, A., Tiihonen, J., et al. (2020). The risk of head injuries associated with antipsychotic use among persons With Alzheimer's disease. *J. Am. Geriatr. Soc.* 68, 595–602. doi: 10.1111/jgs.16275

Teixeira, F. B., Saito, M. T., Matheus, F. C., Prediger, R. D., Yamada, E. S., Maia, C. S. F., et al. (2017). Periodontitis and Alzheimer's disease: a possible comorbidity between oral chronic inflammatory condition and neuroinflammation. *Front. Aging Neurosci.* 9:327. doi: 10.3389/fnagi.2017.00327

Wang, R. P., Ho, Y. S., Leung, W. K., Goto, T., and Chang, R. C. (2019). Systemic inflammation linking chronic periodontitis to cognitive decline. *Brain Behav. Immun.* 81, 63–73. doi: 10.1016/j.bbi.2019.07.002

Wu, Z., and Nakanishi, H. (2015). Lessons from microglia aging for the link between inflammatory bone disorders and Alzheimer's disease. *J. Immunol. Res.* 2015:471342. doi: 10.1155/2015/471342

Wu, Z., Ni, J., Liu, Y., Teeling, J. L., Takayama, F., Collcutt, A., et al. (2017). Cathepsin B plays a critical role in inducing Alzheimer's disease-like phenotypes following chronic systemic exposure to lipopolysaccharide from Porphyromonas gingivalis in mice. *Brain Behav. Immun.* 65, 350–361. doi: 10.1016/j.bbi.2017.06.002

Yang, H., Wang, H., Wang, Y., Addorisio, M., Li, J., Postiglione, M. J., et al. (2017). The haptoglobin β subunit sequesters HMGB1 toxicity in sterile and infectious inflammation. *J. Intern. Med.* 282, 76–93. doi: 10.1111/joim.12619

Conflict of Interest: The authors declare that the research was conducted in the absence of any commercial or financial relationships that could be construed as a potential conflict of interest.

frontiers in Aging Neuroscience

REVIEW
published: 29 September 2020
doi: 10.3389/fnagi.2020.566922

Interleukin-17A: The Key Cytokine in Neurodegenerative Diseases

Junjue Chen, Xiaohong Liu and Yisheng Zhong**

Department of Ophthalmology, Ruijin Hospital, Shanghai Jiao Tong University School of Medicine, Shanghai, China

Neurodegenerative diseases are characterized by the loss of neurons and/or myelin sheath, which deteriorate over time and cause dysfunction. Interleukin 17A is the signature cytokine of a subset of $CD4^+$ helper T cells known as Th17 cells, and the IL-17 cytokine family contains six cytokines and five receptors. Recently, several studies have suggested a pivotal role for the interleukin-17A (IL-17A) cytokine family in human inflammatory or autoimmune diseases and neurodegenerative diseases, including psoriasis, rheumatoid arthritis (RA), Alzheimer's disease (AD), Parkinson's disease (PD), multiple sclerosis (MS), amyotrophic lateral sclerosis (ALS), and glaucoma. Studies in recent years have shown that the mechanism of action of IL-17A is more subtle than simply causing inflammation. Although the specific mechanism of IL-17A in neurodegenerative diseases is still controversial, it is generally accepted now that IL-17A causes diseases by activating glial cells. In this review article, we will focus on the function of IL-17A, in particular the proposed roles of IL-17A, in the pathogenesis of neurodegenerative diseases.

Keywords: interleukin-17A, neurodegenerative diseases, microglia, astrocytes, oligodendrocytes, glaucoma

OPEN ACCESS

Edited by:
Feiqi Zhu,
Shenzhen University, China

Reviewed by:
Sachchida Nand Rai,
University of Allahabad, India
Merja Jaronen,
University of Eastern Finland, Finland

****Correspondence:***
Xiaohong Liu
hong203103@163.com
Yisheng Zhong
yszhong68@126.com

Received: *29 May 2020*
Accepted: *31 August 2020*
Published: *29 September 2020*

Citation:
Chen J, Liu X and Zhong Y (2020) Interleukin-17A: The Key Cytokine in Neurodegenerative Diseases. Front. Aging Neurosci. 12:566922. doi: 10.3389/fnagi.2020.566922

INTRODUCTION

Interleukin-17A (IL-17A) is the signature cytokine of a subset of $CD4^+$ helper T cells known as Th17 cells (McGeachy et al., 2019). The feature of Th17 cells is the expression of the RAR-related orphan receptor γ (RORγt) transcription factor (Ivanov et al., 2006). Initially termed CTLA8, IL-17A was cloned firstly in 1993 from a cDNA library of subtractive rodents and the IL-17-binding receptor was first reported in 1995 (Rouvier et al., 1993; Gaffen, 2011a). Researchers were interested because the sequences of the receptor and ligand of this molecule are different from those of other known cytokines in mammals (McGeachy et al., 2019). In human inflammatory or autoimmune diseases and neurodegenerative diseases, the

Abbreviations: IL-17A, Interleukin-17A; Th cells, helper T cells; AD, Alzheimer's disease; PD, Parkinson's disease; MS, Multiple sclerosis; RORκt, transcription factor RAR-related orphan receptor gamma; NKT cells, natural killer T; LC3s, group 3 innate lymphoid cells; CNS, central nervous system; DLB, Dementia with Lewy Bodies; IOP, intraocular pressure; RGCs, retinal ganglion cells; CSF, cerebrospinal fluid; NGF, nerve growth factor; PDGF, platelet-derived growth factor; ORF13, open reading frame 13; iPSC, induced pluripotent stem cell; MBNs, midbrain neurons; TRAF6, TNF-receptor associated factor 6; NF-κB, nuclear factor κB; Bcl3, B cell lymphoma 3-encoded protein; AS, ankylosing spondylitis; RA, rheumatoid arthritis; IgE, immunoglobin E; IL, interleukin; SFB, segmented filamentous bacterium; REG3A, regenerating islet-derived protein 3-alpha; KKS, Kallikrein-Kinin System; Del-1, developmental endothelial locus-1; ICH, intracerebral hemeorrhage;BBB, blood-brain barrier; EAE, experimental autoimmune encephalomyelitis; TLR, Toll-like receptors; ALS, Amyotrophic lateral sclerosis; IR, ischemia-reperfusion; TNF-α, tumor necrosis factor-α; LPS, lipopolysaccharide; SERIF, SEF/IL-17 receptor; IL-17RB, IL-17 receptor B; ERK, extracellular regulated protein kinases; GM-CSF, granulocyte-macrophage colony stimulating factor; CXCL1, chemokine (C-X-C motif) ligand 1; G-CSF, granulocyte colony stimulating factor.

IL-17A cytokine family has been reported to play a crucial function (Infante-Duarte et al., 2000; Luzza et al., 2000). IL-17A is produced by Th17 cells and other variable sources. In different conditions, the sources may be immune cells, including CD8+(Tc17) cells, "natural" Th17 cells, group 3 innate lymphoid cells (LC3s) and natural killer T (NKT) cells, or resident cells of the central nervous system (CNS), such as microglia (Cua and Tato, 2010).

Neurodegenerative diseases are characterized by progressive loss of selectively vulnerable populations of neurons, which progressively worsens over time and eventually leads to dysfunction (Hammond et al., 2019). There is a convincing body of evidence that protein aggregation, neuronal loss, and immune pathway dysregulation are common features of neurodegeneration (Hammond et al., 2019). These diseases include AD, PD, dementia with Lewy Bodies (DLB), multiple sclerosis (MS), and glaucoma. Glaucoma is characterized by visual field loss and progressive damage to the optic nerve axon and retinal ganglion cells (RGCs; Tian et al., 2015). The elevated intraocular pressure (IOP) is thought to be a major risk factor (Quigley and Broman, 2006; Wei and Cho, 2019). Studies have shown that IL-17A is involved in the pathogenesis of CNS neurodegenerative diseases. Levels of IL-17A in cerebrospinal fluid (CSF) and plasma are significantly increased in patients with MS, AD, and PD, and the expression levels are related to the severity and progress of diseases (Gu et al., 2013; Zhang et al., 2013; Kostic et al., 2014). Although the function of IL-17A in CNS neurodegenerative diseases is less understood and remains somewhat controversial, IL-17A is described to induce the occurrence and development of diseases by activating glial cells (especially microglia; Gu et al., 2013; Kolbinger et al., 2016). Therefore, for this review article, we mainly focused on recent studies on IL-17A and its role in neurodegenerative diseases.

IL-17A AND IL-17 FAMILY CYTOKINES

There are six cytokines and five receptors in the IL-17 family (Gaffen, 2011b). The cytokines include IL-17A to IL-17F, and the receptors included IL-17RA to IL-17RE. These cytokines are dimer molecules, and they contain 163–202 amino acids with molecular weights ranging from 23 to 36 kDa (Gaffen, 2011b). The structures of these cytokines are similar to those of platelet-derived growth factor (PDGF) and nerve growth factor (NGF), which involve a special cystine knot fold architecture (Hymowitz et al., 2001). In the IL-17 family, IL-17A is the most studied cytokine, and it has the 57% sequence homology with the open reading frame 13 (ORF13) of Herpesvirus saimiri, a T cell tropic-herpesvirus that causes a lymphoproliferative syndrome (Gaffen, 2011b). Although they have a similar ORF13 sequence, the 3′ UTR of IL-17A has an adenylate-uridylate-rich (AU-rich) instability sequence, a common characteristic of growth factor and cytokine genes, and IL-17A can induce cytokine secretion in certain cells (Gaffen, 2011b). Thus, IL-17A is considered a cytokine (McGeachy et al., 2019). It has been shown that IL-17A exerts functions in the process of immune inflammation, neovascularization, and tumor development (Zhu et al., 2016; Kuwabara et al., 2017).

IL-17B through IL-17F was discovered when researchers screened for the homologous genes of IL-17A. IL-17B has been reported to play an important role in cancer and inflammation. The proliferation and migration of gastric carcinoma cells are facilitated by IL-17B through activating mesenchymal stem cells *in vitro* (Bie et al., 2017b). The resistance to the treatment of paclitaxel in breast cancer is promoted by IL-17B through activation of the extracellular regulated protein kinases 1/2 (ERK1/2) pathway (Laprevotte et al., 2017). IL-17B exerts a dual function in the development and progression of inflammation. In mucosal inflammation, IL-17B plays an anti-inflammation role (Reynolds et al., 2015). In rat models with indomethacin-induced intestinal inflammation, however, IL-17RB levels are increased, and intraperitoneal injection of IL-17B promotes the migration of neutrophils in normal mice, indicating that IL-17B has a pro-inflammatory function (Shi et al., 2000; Bie et al., 2017a). The source of IL-17C is different from IL-17A as IL-17C is produced by different cells, such as epithelial cells (Ramirez-Carrozzi et al., 2011). A recent study has shown that the peripheral nerve neurons are protected by IL-17C, which acts as a neurotrophic cytokine, during Herpes simplex virus reactivation (Peng et al., 2017). Also, through the expression of antimicrobial peptides, chemokines, and pro-inflammatory cytokines, epithelial inflammatory responses are stimulated by IL-17C. Although IL-17C plays a proinflammatory role in a skin inflammation model induced by imiquimod, it has a protective function in colitis elicited by dextran sodium sulfate (Ramirez-Carrozzi et al., 2011). IL-17D is preferentially expressed in some tissues, such as adipose tissue and skeletal muscle, as well as some organs, including lung, heart, and pancreas (Starnes et al., 2002). IL-17D has some effect during inflammation, tumors, and viral infection. Stimulation of endothelial cells with IL-17D induces a classic pro-inflammatory cytokine response, including granulocyte-macrophage colony-stimulating factor (GM-CSF), IL-6, and IL-8 and the increased expression of IL-8 is dependent on nuclear factor B (NF-κB)-dependent (Starnes et al., 2002). Compared to wild-type animals, IL-17D$^{(-/-)}$ mice showed a higher incidence of cancer and exacerbated viral infections, indicating that the expression of IL-17D after viral infection and tumors is essential for the protection of the host (Saddawi-Konefka et al., 2016). Moreover, IL-17D plays a role in tumors and virus surveillance mediated by NK-cells (Saddawi-Konefka et al., 2016). There are some differences between IL-17E (now called IL-25) and other family members of IL-17. IL-25 is associated with type 2 immune response marked by increased serum Immunoglobin E (IgE), IgG, and IgA levels as well as pathological changes in the gastrointestinal tract and lungs. In the digestive tract, IL-25 limits chronic inflammation and regulates type 2 immune response (Owyang et al., 2006). IL-25 induces IL-4, IL-5, and IL-13 gene expression (Fort et al., 2001). An early study indicated that IL-25 exerts an opposite function in the pathogenesis of organ-specific autoimmunity compared to IL-17A (Kleinschek et al., 2007). IL-17F and IL-17A are similar in terms of function and source. These two cytokines are not only the result of gene replication, as they are located next to each other on the same chromosome, but are also co-produced by Th17 cells (Waisman et al., 2015). Similar

to IL-17A, IL-17F contributes to inflammatory responses and barrier surface protection (Puel et al., 2011).

RECEPTORS AND SIGNALING PATHWAYS OF IL-17

There are five receptors (IL-17RA to IL-17RE) in the IL-17 receptor family and these receptors are composed of two chains (Waisman et al., 2015). Among these receptors, IL-17A and IL-17F bind to the same receptor, which is a heterodimer composed of IL-17RA and IL-17RC (Ely et al., 2009; Hu Y. et al., 2010). The heterodimeric receptor composed of IL-17RA and IL-17RC is express in CNS resident cells, such as microglia and astrocytes, as well as CNS endothelial cells (Kebir et al., 2007; Das Sarma et al., 2009). However, the expression of the IL-17 receptor expresses on neurons remains controversial. Early studies have shown that rat dorsal root ganglion neurons and mouse neural stem cells express IL-17 receptors (Li et al., 2013; Segond von Banchet et al., 2013). Recently, human PD- induced pluripotent stem cell (iPSC)-derived midbrain neurons (MBNs) have been described to express IL-17 receptors (Kawanokuchi et al., 2008; Sommer et al., 2018).

The IL-17 receptor family has one thing in common, namely, it shares a cytoplasmic motif termed "SEFIR" (SEF/IL-17 receptor; Novatchkova et al., 2003). After contact with IL-17 family cytokines and the IL-17R complex, Act1) an adaptor protein) is recruited to the SEFIR domain of the receptor complex (Qian et al., 2007; Liu et al., 2011; Waisman et al., 2015). The intracellular SEFIR domain then interacts with a corresponding SEFIR motif on the Act1 adaptor. Act1 then rapidly ubiquitinates another E3 ubiquitin ligase, namely TNF-receptor associated factor 6 (TRAF6; Schwandner et al., 2000; Qian et al., 2007). Ultimately, IL-17 signaling triggers the activation of the canonical NF-κB cascade response (Qian et al., 2007). Collectively, transcriptional induction of target genes is triggered by these factors (McGeachy et al., 2019; **Figure 1**). When the NF-κB cascade response is activated, IL-17- NF-κB signaling induces several positive and negative feedback circuits to control related physiological function. NF-κB upregulates the expression of B cell lymphoma 3-encoded protein (Bcl3) and then, in turn, facilitates the expression of multiple IL-17-NF-κB-driven anti-microbial and proinflammatory genes (Ruddy et al., 2004; Karlsen et al., 2010). However, IL-17- NF-κB signaling induces several negative feedback circuits to restrain the activation of NF-κB, such as deubiquitination (Garg et al., 2013; Cruz et al., 2017). Among the above signaling pathways, Act1 is an essential activator. The absence of the Act1 gene has been shown to cause complete failure in the response of cells to IL-17 (Qian et al., 2007; Liu et al., 2011).

FUNCTION OF IL-17A

Induction of the expression of chemokines, such as chemokine (C-X-C motif) ligand 1 (CXCL1), CXCL2, and CXCL8, is an important function of IL-17A. These chemokines can attract myeloid cells to injured or infected tissues (Onishi and Gaffen, 2010). IL-17A also induces the expression of IL-6 and granulocyte colony-stimulating factor (G-CSF), which promotes myeloid-driven innate inflammation (Gaffen et al., 2014). When encountering acute microbial invasion, IL-17A induces responses to protect the host. Overwhelming data suggest that IL-17A has a specific function in the prevention of Candida albicans. Antifungal immunity is regulated by IL-17A through upregulating antimicrobial peptides (e.g., defensins) and proinflammatory cytokines (e.g., CXCL1 and CXCL5; Conti and Gaffen, 2015; Drummond and Lionakis, 2019). The increased expression of proinflammatory cytokines and antimicrobial peptides has a synergistic effect on limiting fungal overgrowth (Conti and Gaffen, 2015; Drummond and Lionakis, 2019).

In injured psoriatic skin tissue, dysregulated IL-17 signaling promotes pathogenic inflammation. A phase 2 clinical trial has shown that inhibitory treatment of IL-17A is effective, indicating the pathogenic role of IL-17A in mediating important inflammatory pathways in psoriasis (Chiricozzi and Krueger, 2013). In ankylosing spondylitis (AS), another autoimmune disease, IL-17A has been shown to contribute to pathogenic inflammation. Two double-blinded phase-3 trials have reported that the use of secukinumab (an anti-IL-17A monoclonal antibody) to treat AS is effective (Baeten et al., 2015). However, researchers have failed to identify evidence of meaningful clinical efficacy with brodalumab (a human anti-IL-17A monoclonal antibody) treatment in rheumatoid arthritis (RA) at least when compared to treatment with methotrexate (Pavelka et al., 2015). Taken together, these data indicate that further studies are required to clearly understand the role of IL-17A in the pathogenesis of autoimmune diseases.

In healthy skin, commensal microflora induces the production of IL-17A, which provides anti-fungal protection (McGeachy et al., 2019). When injury destroys the epithelial barrier of the skin, IL-17A promotes epithelial-cell proliferation and can clear the pathogenic agents (Naik et al., 2015). Production of IL-17A from the local epithelium is driven by the microbiota, resulting in the anti-microbial function. Colonization with the segmented filamentous bacterium (SFB), a single commensal microbe, is sufficient to induce the production of IL-17A in the lamina propria of the small intestine of mice. SFB and Th17 cells mediate the protection from pathogenic microorganisms (Ivanov et al., 2009). A previous study has suggested that IL-17A is beneficial in controlling dysbiosis and maintaining a homeostatic balance in the gut. The predisposition to neuroinflammation is enhanced by abolishing the intestinal IL-17RA pathway, thus confirming the crucial role of the IL-17R pathway in mediating the protection of epithelial surface and interaction of host and microbiome (Ivanov et al., 2009; Kumar et al., 2016).

IL-17A promotes the repair of tissue. A crucial part of wound repair is the proliferation of epithelial keratinocytes. In keratinocytes, the expression of regenerating islet-derived protein 3-alpha (REG3A), an intestinal anti-microbial protein, is increased during psoriasis. IL-17A induces keratinocytes to express REG3A, and this process promotes the proliferation of keratinocytes after injury in psoriasis (Lai et al., 2012).

IL-17A and transcription factors that regulate adipocyte differentiation have been reported to act in concert to contribute

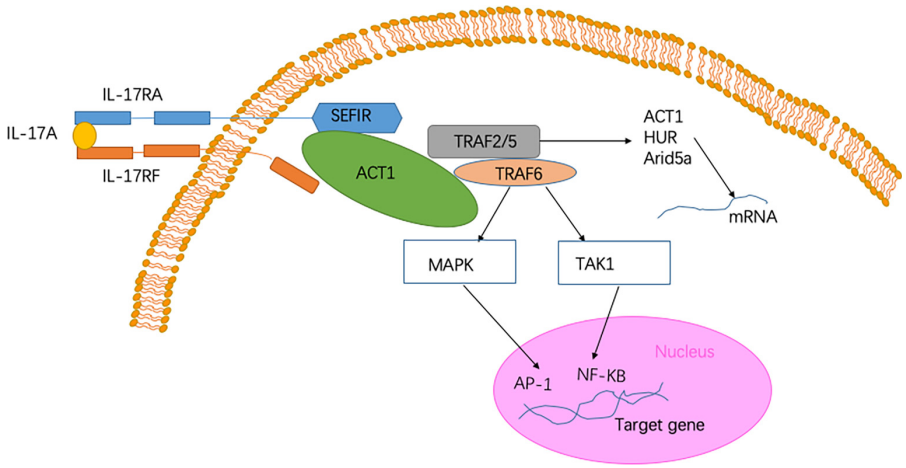

FIGURE 1 | Signaling pathway of Interleukin-17A (IL-17A). The heterodimer receptor consists of two subunits, IL-17RA and IL-17RF, which bind to IL-17A, IL-17F, and IL-17AF ligands. The intracellular SEF/IL-17 receptor (SEFIR) domains interact with a corresponding SEFIR motif on the Act1 adaptor (Novatchkova et al., 2003). TNF-receptor associated factor 6 (TRAF6) and TRAF2/5 proteins bind to the TRAF-binding site in Act1. After binding to Act1, TRAF6 mediates the activation of the classical nuclear factor-κB (NF-KB) pathway of MAPK:AP-1. Collectively, these pathways trigger the transcriptional induction of target genes (Qian et al., 2007). In the IL-17 signaling pathway, a pathway of post-transcriptional mRNA stabilization is promoted through the recruitment of TRAF2 and TRAF5 by Act1 (Schwandner et al., 2000). This physiological process is achieved by controlling multiple RNA-binding proteins, such as HuR and Arid5a.

to the suppression of adipogenesis (Ahmed and Gaffen, 2013). Mice with deficiency of both IL-17A and IL-17RA gain increased fat with age, and IL-17A suppresses the maturation of cells with adipogenic potential, indicating that IL-17A inhibits adipogenesis (Ahmed and Gaffen, 2013). In a healthy state, IL-17A directly influences the metabolic function of adipocytes. IL-17A produced by γδT cells controls the homeostasis of regulatory T cells and adaptive thermogenesis in adipose tissue (Kohlgruber et al., 2018).

These abovementioned findings show that IL-17A is not just an inflammatory factor. IL-17A usually protects the body during the acute injury, but when a wound takes a long time to heal and turns to a chronic injury, the effect of IL-17A may turn into erosion or hyperproliferation of the wound, ultimately leading to the loss of function (McGeachy et al., 2019).

ROLE OF IL-17A IN NEURODEGENERATIVE DISEASES

There are several divergent and shared pathological and clinical features of age-related CNS neurodegenerative diseases, such as diverse protein aggregation and selective vulnerability of the brain that impact the clinical presentation and immune responses of diseases (Hammond et al., 2019). Neurodegenerative diseases lead to impairments of a person's memory and cognitive ability, and some of these diseases affect patients' ability to speak, move, and breathe. Neurodegenerative disease is a multifactorial disease that included aging, mitochondrial defects, dysfunctions in autophagic lysosomal pathways, neurovascular toxicity, synaptic toxicity, accumulation of misfolded proteins, and liquid-phase transitions in pathological protein aggregation (Focus on Neurodegenerative Disease, 2018).

Neuroinflammation contributes, in part, to the occurrence of neurodegenerative diseases. Neuroinflammation in diseases, such as PD, AD, and ALS, is characterized by a reactive morphology of glial cells and increased levels of inflammatory mediators in the parenchyma (Ransohoff, 2016). To date, most pieces of evidence point to a pathogenic role for IL-17A in the CNS neurodegenerative diseases. IL-17A acts on multiple CNS resident cells to potentiate inflammation (Qian et al., 2007; Stromnes et al., 2008; Kang et al., 2010; Ji et al., 2013; Kang Z. et al., 2013; Liu et al., 2015; Rodgers et al., 2015; Liu Z. et al., 2019; **Figure 2**). It has been reported that IL-17A plays a regulatory factor in the induced cytokine network rather than as a direct role to mediate tissue damage during neuroinflammation (Zimmermann et al., 2013). Also, several studies have been reported the impact of medicinal plants on the level of IL-17A in neurodegenerative diseases (**Table 1**).

AD is the most common type of late-onset dementia, and it is a complex molecular and genetic disease. The features of AD are neuronal and extensive synaptic loss, which leads to brain volume loss. Subsequently, the pathological changes of brain structure lead to a decline in patients' memory and cognitive function that results in an inability to take care of themselves in daily life (Hammond et al., 2019). In recent years, the understanding of the pathological mechanism of AD has been constantly improved. The important pathological features of AD include intracellular neurofibrillary tangles resulting from the aggregation of hyperphosphorylated tau and deposition of extracellular neurotoxic plaques primarily composed of amyloid-β (Aβ; Holtzman et al., 2011). The aggregation of amyloid and tau eventually impacts the hippocampal, entorhinal cortex, and neocortical regions (Montine et al., 2012). Furthermore, Bussian et al. (2018) found that senescent microglia and astroglia

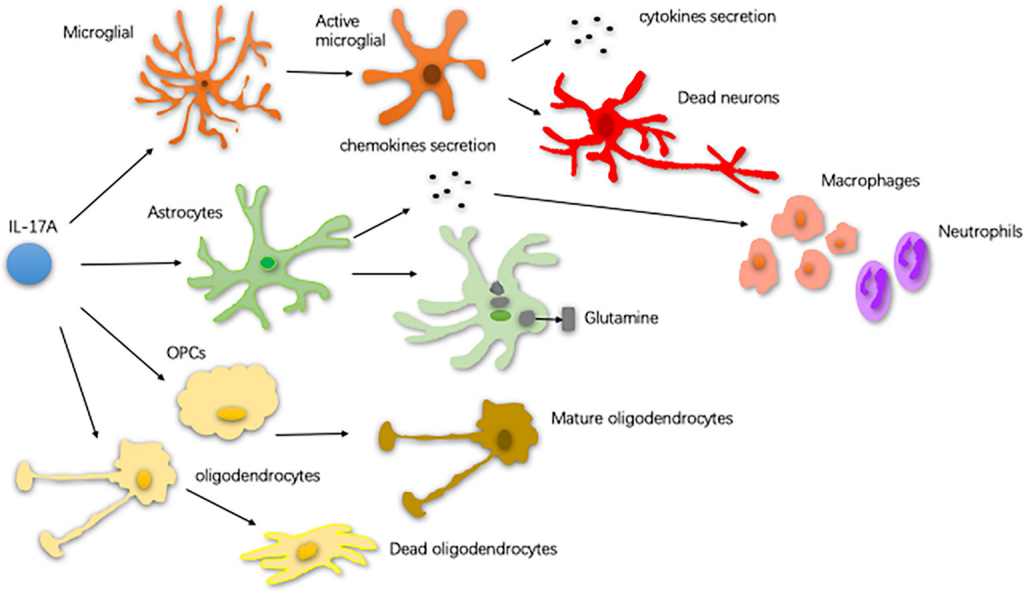

FIGURE 2 | The way of glial cells respond to IL-17A. In central nervous system (CNS) neurodegenerative diseases, IL-17A binds to the receptor on the surface of microglia and activates microglia. Activated microglia secrete cytokines, exacerbating dopaminergic neurons loss. Astrocytes respond to IL-17A through generating chemokines to promote the recruitment of inflammatory cells, such as macrophages and neutrophils. IL-17A reduces the ability of astrocytes to absorb and transform glutamate as well as enhance the excitotoxicity of glutamate. IL-17A inhibits the maturation of oligodendrocyte lineage cells (OPCs) and exacerbates the TNF-α-induced oligodendrocyte apoptosis (Qian et al., 2007; Stromnes et al., 2008; Kang et al., 2010; Ji et al., 2013; Kang Z. et al., 2013; Liu et al., 2015; Rodgers et al., 2015; Liu Z. et al., 2019).

TABLE 1 | The impact of medicinal plants on the level of interleukin-17A (IL-17A) in neurodegenerative diseases.

Authors	Disease	Medicinal plant	Effects on the level of IL-17A
Zhang Y. et al. (2015)	AD	Matrine	Reduction
Fragoulis et al. (2017)	AD	Kavalactones methysticin	Reduction
Chen et al. (2019)	AD	Oxymatrine	Reduction
Sanadgol et al. (2017)	MS	Ellagic acid	Reduction[a]
Zhang J. et al. (2015)/Wang et al. (2008)	MS	Tripchlorolide	Reduction[b]
Wang et al. (2012)	MS	Huperzine A	Reduction[c]
Zhao et al. (2011)	MS	Matrine	Reduction
Singh et al. (2007)	MS	Resveratrol	Reduction

AD, Alzheimer's disease; MS, Multiple sclerosis; [a] Ellagic acid decreases IL-17A is dose-dependent; [b] Tripchlorolide suppressed the mRNA levels of IL-17A; [c] Huperzine A down-regulates mRNA and protein levels of IL-17A.

influence neurofibrillary tangle formation and intraneuronal tau phosphorylation.

IL-17A may play a significant role in the pathogenesis of AD. In terms of clinical manifestations, elevated levels of IL-17A in plasma and CSF have been reported in patients with AD. For example, Chen et al. (2014) showed that IL-17A level in serum is increased in Chinese patients, and Hu W. T. et al. (2010) reported that the CSF level of IL-17A increases in patients. Also, Behairi et al. (2015) found that the baseline level of IL-17A is markedly higher in AD patients compared to controls. At the cellular and genetic level, there is also evidence of the correlation between IL-17A and the pathogenesis of AD. It has been reported that TH17 cell differentiation and activation as well as associated transcription factors are increased in patients with AD (Saresella et al., 2011). The induction and expression of IL-17A may be due to the polymorphism of Th17-related genes (Zota et al., 2009). BACE1 is a transmembrane asparty1 protease that plays a role in forming plaques in AD (Vassar, 2004). BACE1-deficient T cells have reduced IL-17A expression under Th17 conditions in AD mouse models (Hernandez-Mir et al., 2019). However, the effect of IL-17A on the pathogenesis of AD is controversial. Yang generated an AD mouse model with IL-17A overexpression and Yang et al. (2017) reported that IL-17A does not exacerbate neuroinflammation, and Yang also demonstrated that IL-17A overexpression decreases the level of soluble Aβ in the CSF and hippocampus as well as improves the metabolism of glucose (Yang et al., 2017). Two distinct human cohort studies have reported that the IL-17A level is decreased in AD patients compared to healthy controls (Doecke et al., 2012; Hu et al., 2013).

PD is the second most frequent form of neurodegenerative disease. PD is characterized by motor symptoms, including

tremor, rigidity, and bradykinesia (Moustafa et al., 2016). A key pathological finding in PD is the aggregation of hallmark proteins (known as Lewy bodies), primarily composed of protein α-synuclein (Hamilton, 2000). There are certain routes for degeneration and aggregation of proteins generally spreading from the brain stem to the substantia nigra and other midbrain regions and then to the neocortex (Braak et al., 2004). Before the onset of symptoms, there is a massive loss of dopamine-producing neurons in the substantia nigra (Cheng et al., 2010). Recently, Sommer et al. (2018) have reported that T lymphocytes increase cell death in PD. iPSC-derived MBNs are mediated by IL-17A, indicating that IL-17A may be involved in PD pathogenesis. Liu et al. (2017) have demonstrated that Th17 cells infiltrated into the brain parenchyma through the disrupted blood-brain barrier (BBB) in PD. It has also been confirmed in animal experiments that IL-17A plays a role in the development of PD. Dopaminergic neurodegeneration, motor impairment, and BBB disruption are alleviated in mice with a deficiency of IL-17A (Liu Z. et al., 2019). However, the decreased plasma level of IL-17A is found in PD patients compared to controls (Rocha et al., 2018).

MS is an inflammatory demyelinating disorder of the CNS (Kostic et al., 2014), and susceptible genes and environmental factors are involved in disease pathogenesis. MS is characterized by the onset of recurring clinical symptoms followed by partial or total recovery. After 10–15 years of the disease, progressive deterioration is observed in up to 50% of untreated patients (Kolbinger et al., 2016). In approximately 15% of MS patients, the disease deteriorates from its onset (Gold et al., 2010). At present, the pathophysiology of MS has not been elucidated. MS may be primarily a neurodegenerative disease in which inflammation occurs as a secondary response that amplifies the state of progression (Kassmann et al., 2007). Compared to other neurodegenerative diseases, IL-17A has been mostly studied in MS. A possible pathogenic function of IL-17A in the pathogenesis of MS has been suggested. Kostic et al. (2014) demonstrated that the IL-17A level is increased in MS patients. In human MS brain tissue, the IL-17A-producing cells have been found but not in noninflamed brain tissue or normal white matter (Tzartos et al., 2008). In human MS plaques samples, an increase of IL-17A mRNA has been detected (Lock et al., 2002), and it has been reported that IL-17A content is related to BBB disruption and neutrophil expansion in CSF (Kostic et al., 2017). In terms of pathogenesis, Th17 cells may utilize the excitotoxicity of glutamate as an effector mechanism in MS. In MS, IL-17A is directly related to glutamate levels and may stimulate the Ca^{2+}-dependent release of glutamate (Kostic et al., 2017). In the experimental autoimmune encephalomyelitis (an animal model of MS, EAE), IL-17RA expression is significantly increased in the CNS (Das Sarma et al., 2009). After binding to the IL-17RA complex in the CNS, IL-17A participates in the pathogenesis of EAE by promoting CD4 cell migration and secreting chemokines (Liu G. et al., 2014).

Amyotrophic lateral sclerosis (ALS) is another chronic neurodegenerative diseases of the CNS. The feature of ALS is the loss of upper and lower motor neurons, leading to motor and extra-motor symptoms. The neuropathological feature of this disease is the aggregation and accumulation of ubiquitylated proteinaceous inclusions in the motor neurons. In most subtypes of ALS, TAR DNA-binding protein 43 (TDP43) is the main component of these inclusions, but other abnormal protein aggregates are also present, including neurofilamentous hyaline conglomerate and misfolded superoxide dismutase (SOD1; Hardiman et al., 2017). The potential culprits of this disease may be the high-molecular-weight complexes that appear before protein aggregation, and the high-molecular-weight protein might contribute to the cell-to-cell spread of disease (Marino et al., 2015). Microglia have some impact on ALS disease. In the SOD1 mouse model of ALS, microglia have been found to contribute to the severity and progression of the disease. In contrast, microglial plays a neuroprotective role in the TDP43-dependent mouse model of ALS (Spiller et al., 2018). Together, these data indicate that microglial may exert different roles depending on the specific animal model and stimulus in ALS. In ALS, the IL-17A-mediated pathway may play a critical role. It has been reported that IL-17A serum concentrations in sporadic ALS and familial ALS patients are significantly higher than control subjects without autoimmune disorders (Fiala et al., 2010; Rentzos et al., 2010).

Glaucoma is also known as a neurodegenerative disorder characterized by RGCs death and axonal damage of the optic nerve, and ultimately leading to irreversible blindness (Levin et al., 2017). Glaucoma is considered as a disease caused by multiple factors, including high IOP mechanical injury, neurotrophic factor deprivation, ischemia/reperfusion injury, oxidative stress injury, excitatory glutamate toxicity, and abnormal immune-inflammatory response (Burgoyne, 2011; Rieck, 2013; Križaj et al., 2014). Studies have shown that immune dysfunctions, such as changes in cytokine signaling, immune cell proliferation, migration, and phagocytosis, as well as reactive gliosis, are common features of neurodegenerative diseases (Hammond et al., 2019). Autoimmunity is related to the pathogenesis of glaucoma as evidenced by large amounts of serum autoantibodies in glaucoma patients and animal models (Wax et al., 2008; Bell et al., 2013). In glaucoma, the elevated IOP is thought to be a major risk factor (Wei and Cho, 2019). However, increasing pieces of evidence have shown that the immune response plays a part in the pathogenesis of glaucoma. In recent years, some researchers have studied the IL-17A levels in patients with glaucoma. Yang et al. (2019) reported that the plasma levels of IL-17A are comparable in glaucoma patients and healthy people, and they demonstrated that the average frequencies of Th17 cells in patients with glaucoma is not significantly higher than that in the control group. In another study, however, researchers have demonstrated that the frequency of IL-17A-secreting cells and IL-17A$^+$ CD4 T cells is significantly higher in patients with glaucoma than in controls (Ren et al., 2019). Using a retinal ischemia-reperfusion (IR) mouse model caused by acute elevated IOP, researchers have reported that elevated IOP increases the expression of IL-17A (Li et al., 2018). Because these studies measured IL-17A in peripheral blood in human patients and glaucoma is a complex disease whose pathogenesis has not been fully understood, further studies are needed to understand the role of IL-17A in glaucoma.

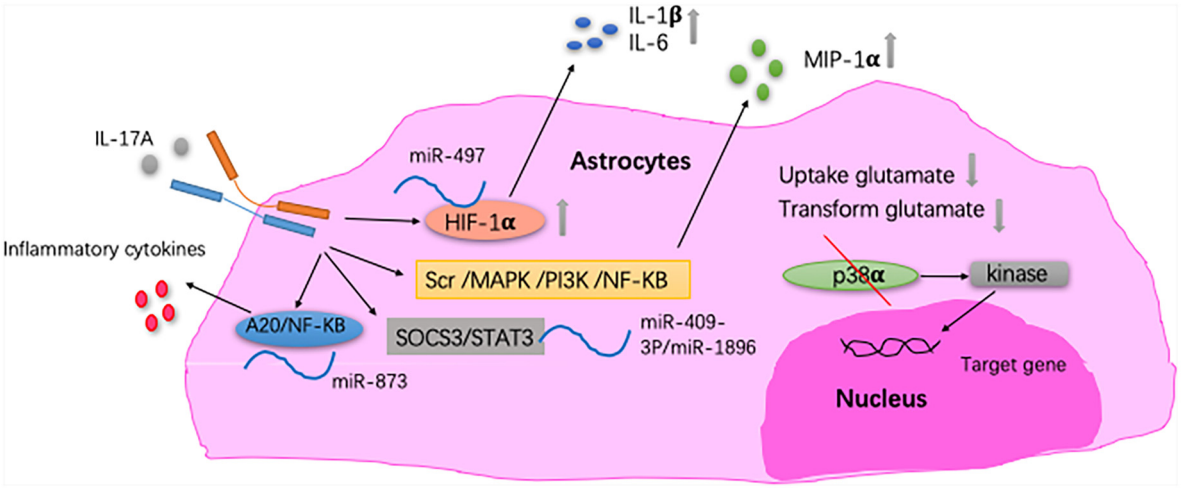

FIGURE 3 | The relationship between IL-17A and astrocytes. In astrocytes, IL-17A induces expression of macrophage inflammatory protein-α (MIP-1α) through Src/MAPK/PI3K/NF-KB pathways (Yi et al., 2014). IL-17A enhances the excitotoxicity of glutamate by reducing the ability of astrocyte to absorb and transform glutamate (Kostic et al., 2017). In EAE mice, IL-17A triggers the downregulation of miR-497, thereby upregulating the hypoxia-inducible factor-1α (HIF-1α) transcription factor in astrocytes as well as IL-1β and IL-6 secretion by astrocytes. MiR-409-3p and MiR-1896 are involved in the process of IL-17A-mediated secretion of inflammatory cytokines by astrocytes by targeting the SOCS3/STAT3 signaling pathway in EAE mice. Under IL-17A stimulation, miR-873 participates in inflammatory cytokine production in astrocytes through the A20/NF-KB pathway in EAE mice (Liu X. et al., 2014; Shan et al., 2017; Liu X. et al., 2019). In EAE mice, proinflammatory gene expression induced by IL-17A is diminished through the abrogation of p38α in astrocytes, which was *via* the defective activation of MAPK-activated protein kinase 2 (Huang et al., 2015).

THE ROLE OF IL-17A IN A DIFFERENT MODEL SYSTEM OF NEURODEGENERATIVE DISEASES

Some animal models are used for the research of neurodegenerative diseases. In APP/PS1 mice, a transgenic mouse model of AD that overexpresses amyloid precursor protein (APP) with the Swedish mutation and exon-9-deleted presenilin 1, IL-17A is reported to play a key role in the induction and development of AD (Browne et al., 2013). IL-17A-producing T cell infiltrates in the brains of APP/PS1 mice which enhances the activation of glial cells and exacerbates neurodegeneration (McManus et al., 2014; Ahuja et al., 2017). IL-17A overexpression in this transgenic mouse model reduces soluble Aβ levels, decreases cerebral amyloid angiopathy, and improves glucose metabolism (Yang et al., 2017). IL-17A does not exacerbate neuroinflammation and significantly improves learning and anxiety deficits in this IL-17A overexpressing APP/PS1 mice (Yang et al., 2017). In 5XFAD mice, another animal model of AD, the production of IL-17A is decreased in the gut-residing immune cells (Saksida et al., 2018). In another animal models of AD including hAPP mice, 3xTg-AD mice, Mo/Hu APPswe PS1dE9 mice and Aβ1–42-Induced AD rat model, the level of IL-17A shows a significant upregulation compared with wild type mice (Jin et al., 2008; Zhang et al., 2013; Zhang Y. et al., 2015; Chen et al., 2015, 2019; Yang et al., 2015; St-Amour et al., 2019). In MPTP (1-methyl-4-phenyl-1,2,3,6-tetrahydropyridine) treaded mouse and MPP+ (1-methyl-4-phenylpyridinium) treated rats (animal models of PD), the levels of IL-17A are upregulated in the substantia nigra, spleen, serum, and mesenteric lymph nodes. Furthermore, IL-17A promotes neurodegeneration in PD depending on microglial activation and partly TNF-α release (Huang et al., 2014; Dutta et al., 2019; Liu Z. et al., 2019). The pathological role of IL-17A in EAE, an animal model of MS, has been demonstrated. A monoclonal anti-IL-17A Ab (MM17F3) autovaccination is reported to prevent histological and clinical manifestations of EAE (Uyttenhove et al., 2007). In the EAE mouse model with TnC−/−, the reduced ability of Th17 cells to produce IL-17 is observed in spleens (Momčilović et al., 2017). Also, IL-17A mRNA and protein levels increase in the cup-induced mouse model of MS (Sanadgol et al., 2017). For ALS, the SOD1G93A mice model is established and in this model, IL-17A is found to gradually increase with aging (Noh et al., 2014).

THE RELATIONSHIP BETWEEN IL-17A AND GLIAL CELLS IN NEURODEGENERATIVE DISEASES

Microglial cells are an important part of the glial population of the CNS, and they account for approximately 10% of the total number of cells and are the largest number of mononuclear phagocytes in the CNS (Colonna and Butovsky, 2017). Microglial cells play a key role in CNS development and maintenance of CNS homeostasis. During CNS injury, microglial cells play a neuroprotective role by morphologically changing, proliferating, and migrating to the damaged site to phagocytose and eliminate microbes, protein aggregates, and dead cells (Colonna and Butovsky, 2017). Also, microglial

cells secrete many soluble factors, such as neurotrophic factors and neurotrophic factors, which are involved in the immune response of the CNS. Aberrations in the normal phenotype or functions of microglial cells may lead to excessive synapse loss, contributing to the pathogenic mechanism of neurodegenerative diseases of the CNS. For example, microglial cells are induced to engulf neurons by recognizing phosphatidylserine exposed on tau-laden neurons, produce nitric oxide, and release of the MFGE8 opsonin. MFGE8 is required for engulfment and uptake of neurons (Brelstaff et al., 2018). Molecules expressed on the surface of microglial cells, such as LRRC33 and TREM2, affect relevant cellular pathways by binding to specific proteins (Qin et al., 2018; Li et al., 2019). These biological processes play a role in the pathogenesis of neurodegenerative diseases.

Although the specific mechanism of IL-17A in neurodegenerative diseases is still controversial, it is generally accepted that IL-17A causes diseases by activating glial cells (especially microglia). In a PD model, IL-17A activates microglia *in vitro* and accelerates the death of dopamine neurons through activating microglial cells (Liu Z. et al., 2019). Consistently, the IL-17A effect is abrogated after inhibition of the IL-17RA signaling pathway in microglia (Liu Z. et al., 2019), confirming the pathogenic relevance of microglial cells in mediating neurodegeneration in PD. Compared to controls, the expression of IL-17RA is increased in microglial cells of the CNS in EAE mice, which may be due to Toll-like receptors (TLR) signaling inducing IL-17RA expression in neuroglial cells (Liu G. et al., 2014). In EAE, IL-17A treatment induces the upregulation of chemokine secretion by microglial cells (Das Sarma et al., 2009). In aged rats, IL-17A participates in the process of neuroinflammation and cognitive impairment induced by lipopolysaccharide (LPS) through microglia activation (Sun et al., 2015). In acute glaucoma mouse models, inhibition of microglial activation reduces the secretion of IL-17A (Li et al., 2018). However, the relationship between IL-17A and microglia in neurodegenerative diseases has not been elucidated. Yang et al. (2017) reported that IL-17A overexpression in the mouse brain does not promote activation of microglia in AD mouse models. The evidence above suggests that further studies are needed.

Astrocytes play a central role in maintaining homeostasis of CNS, including regulation of synapse formation and maintenance, preserving neurological function, supplying energy to neurons, and maintaining the function of BBB (Pellerin and Magistretti, 2004; Molofsky and Deneen, 2015; Almad and Maragakis, 2018). Astrocytes are not homogeneous but can be specialized according to different regions of the CNS in which they reside (Pekny and Pekna, 2016). These glial cells of the CNS affect the structure and function of surrounding neurons. In the tripartite synapse, astrocytes can modulate synaptic activity by gliotransmission (Haydon, 2016). In the CNS, astrocytes communicate with surrounding neurons, microglia, and oligodendrocytes through hemichannels, which act in concert to maintain the normal function of CNS (Almad and Maragakis, 2018). During the disease course of the CNS, phenotypic conversion of microglial cells is induced by signals from astrocytes (Locatelli et al., 2018). An astrocyte that loses its function (termed A1 astrocyte) is induced by activated neuroinflammatory microglia (Liddelow et al., 2017). Taken together these data highlight the crucial role of astrocyte-microglia communication in neurodegenerative diseases of CNS.

Astrocytes and IL-17A have been mainly studied in MS. One of the pathological features of MS is increased astrogliosis-associated neuroinflammation. Astrogliosis is a process by which astrocytes activate, proliferate, and upregulate the expression of the glial fibrillary acidic protein, and it is the main cause of MS plaque formation (Yi et al., 2014). By reducing the ability of astrocytes to absorb and transform glutamate, IL-17A enhances the excitotoxicity of glutamate (Kostic et al., 2017). Thus, astrocytes may act as a potential target for the neuroprotective effect of MS. In the CNS of EAE mice, the expression of IL-17RA is increased in astrocytes (Das Sarma et al., 2009; Colombo et al., 2014). Macrophage inflammatory protein-α (MIP-1α) is the β-chemokine that induces the directed migration of eosinophils, T lymphocytes and monoctyes, and it contributes to the pathogenesis of EAE. In primary astrocytes, IL-17A induces the expression of MIP-1α (Yi et al., 2014). Furthermore, miRNAs are involved in the pathogenesis mediated by IL-17A-expressing astrocytes in EAE (Liu X. et al., 2014, 2019; Shan et al., 2017). Under IL-17A stimulation, miRNAs participate in inflammatory cytokine production in astrocytes and, in turn, aggravate EAE development. Collectively, these findings suggest that the pathogenic role of the IL-17A-miRNA-astrocytes axis in EAE and may indicate a therapeutic target for treating MS. IL-17A blockade by Act1 ablation in astrocytes inhibits the induction of EAE and has a therapeutic effect (Kang et al., 2010; Yan et al., 2012). Also, in a mouse model of MS, proinflammatory gene expression induced by IL-17A is diminished through the abrogation of p38α in astrocytes (Huang et al., 2015; **Figure 3**). *In vitro* studies have shown that IL-17A secreted by activated astrocytes plays a neuroprotective role in acute neuroinflammation (Hu et al., 2014).

Oligodendrocytes are a group of glial cells in the CNS and have a supporting role for neuron migration, terminal differentiation, axon wrapping, axon recognition, myelin production, and myelin maintenance (Cai and Xiao, 2016). The main function of oligodendrocytes is the formation of myelin, which benefits nerve repair by maintaining myelin restoration (Bradl and Lassmann, 2010). Oligodendrocytes perform their physiological functions by communicating with neighboring astrocytes and neurons (Orthmann-Murphy et al., 2007). The loss or dysfunction of oligodendrocytes contributes to the vulnerability of the human brain to neurodegenerative diseases. For example, in AD and Huntington's disease (HD), disturbances of myelin integrity are exacerbated compared to normal controls (Bartzokis et al., 2004, 2007). Increased numbers of oligodendrocyte progenitor cells (OPCs) are observed in ALS patients, indicating the failure of myelin regeneration (Kang S. H. et al., 2013). Recently, it has been reported that oligodendrocyte heterogeneity in human MS brain tissue may contribute to the disease progression (Jäkel et al., 2019). IL-17A plays a role in the development of oligodendrocyte lineage cells. IL-17A inhibits the maturation of oligodendrocyte lineage cells *in vitro* (Kang Z. et al., 2013) and it exacerbates the TNF-α-induced

oligodendrocyte apoptosis (Paintlia et al., 2011). In EAE, mature oligodendrocytes and OPCs have different effects on the progression of the disease. Kang Z. et al. (2013) reported that the deletion of Act1, the adaptor protein required for IL-17 signaling, from mature oligodendrocytes does not affect the course of EAE. However, elimination of IL-17A signaling in OPCs (referred to as NG2 glia) reduces EAE severity.

CONCLUSION

IL-17A is a signature of a key T helper cell population and evidence suggests a crucial role for IL-17A in the pathogenesis of autoimmune diseases and neurodegenerative diseases. The function of IL-17A has been proven to be varied as it not only contributes to pathogenic inflammation but also induces innate-like acute immune defenses. Thus, IL-17A is not simply an inflammatory factor. Although the specific mechanism of IL-17A in neurodegenerative diseases is still controversial, it is generally accepted that IL-17A causes diseases by activating glial cells. The functions of IL-17A have proven to be more adaptable and diverse than initially discovered. IL-17A may also play a key role in tissue damage. Our understanding of these processes is still lacking, particularly in the role of IL-17A in the pathogenesis of glaucoma. Also, we are still in the early stages of understandin how IL-17A interacts with different cytokines and how IL-17A signals are transmitted in response to microbial stimuli. Understanding how IL-17A interacts with different cells and cytokines is important. Uncovering the molecular pathways may allow the identification of better targets to modulate these cellular processes. Novel therapeutic strategies may be discovered by such studies.

AUTHOR CONTRIBUTIONS

JC wrote and edited the manuscript. XL and YZ edited the manuscript. All authors read and approved the final manuscript. All authors contributed to the article and approved the submitted version.

ACKNOWLEDGMENTS

The authors would like to thank Huan Yu and Jun Sun for their support of this work.

REFERENCES

Ahmed, M., and Gaffen, S. L. (2013). IL-17 inhibits adipogenesis in part *via* C/EBPα, PPARγ and Kruppel-like factors. *Cytokine* 61, 898–905. doi: 10.1016/j.cyto.2012.12.007

Ahuja, M., Buabeid, M., Abdel-Rahman, E., Majrashi, M., Parameshwaran, K., Amin, R., et al. (2017). Immunological alteration and toxic molecular inductions leading to cognitive impairment and neurotoxicity in transgenic mouse model of Alzheimer's disease. *Life Sci.* 177, 49–59. doi: 10.1016/j.lfs.2017.03.004

Almad, A., and Maragakis, N. J. (2018). A stocked toolbox for understanding the role of astrocytes in disease. *Nat. Rev. Neurol.* 14, 351–362. doi: 10.1038/s41582-018-0010-2

Baeten, D., Sieper, J., Braun, J., Baraliakos, X., Dougados, M., Emery, P., et al. (2015). Secukinumab, an interleukin-17A inhibitor, in ankylosing spondylitis. *N Engl. J. Med.* 373, 2534–2548. doi: 10.1056/NEJMoa1505066

Bartzokis, G., Lu, P. H., and Mintz, J. (2004). Quantifying age-related myelin breakdown with MRI: novel therapeutic targets for preventing cognitive decline and Alzheimer's disease. *J. Alzheimers Dis.* 6, S53–S59. doi: 10.3233/jad-2004-6s604

Bartzokis, G., Lu, P. H., Tishler, T. A., Fong, S. M., Oluwadara, B., Finn, J. P., et al. (2007). Myelin breakdown and iron changes in Huntington's disease: pathogenesis and treatment implications. *Neurochem. Res.* 32, 1655–1664. doi: 10.1007/s11064-007-9352-7

Behairi, N., Belkhelfa, M., Mesbah-Amroun, H., Rafa, H., Belarbi, S., Tazir, M., et al. (2015). All-trans-retinoic acid modulates nitric oxide and interleukin-17A production by peripheral blood mononuclear cells from patients with Alzheimer's disease. *Neuroimmunomodulation* 22, 385–393. doi: 10.1159/000435885

Bell, K., Gramlich, O. W., Von Thun Und Hohenstein-Blaul, N., Beck, S., Funke, S., Wilding, C., et al. (2013). Does autoimmunity play a part in the pathogenesis of glaucoma? *Prog. Retin. Eye Res.* 36, 199–216. doi: 10.1016/j.preteyeres.2013.02.003

Bie, Q., Jin, C., Zhang, B., and Dong, H. (2017a). IL-17B: a new area of study in the IL-17 family. *Mol. Immunol.* 90, 50–56. doi: 10.1016/j.molimm.2017.07.004

Bie, Q., Zhang, B., Sun, C., Ji, X., Barnie, P. A., Qi, C., et al. (2017b). IL-17B activated mesenchymal stem cells enhance proliferation and migration of gastric cancer cells. *Oncotarget* 8, 18914–18923. doi: 10.18632/oncotarget.14835

Braak, H., Ghebremedhin, E., Rüb, U., Bratzke, H., and Del Tredici, K. (2004). Stages in the development of Parkinson's disease-related pathology. *Cell Tissue Res.* 318, 121–134. doi: 10.1007/s00441-004-0956-9

Bradl, M., and Lassmann, H. (2010). Oligodendrocytes: biology and pathology. *Acta Neuropathol.* 119, 37–53. doi: 10.1007/s00401-009-0601-5

Brelstaff, J., Tolkovsky, A. M., Ghetti, B., Goedert, M., and Spillantini, M. G. (2018). Living neurons with tau filaments aberrantly expose phosphatidylserine and are phagocytosed by microglia. *Cell Rep.* 24, 1939.e4–1948.e4. doi: 10.1016/j.celrep.2018.07.072

Browne, T. C., McQuillan, K., McManus, R. M., O'Reilly, J. A., Mills, K. H., and Lynch, M. A. (2013). IFN-γ production by amyloid β-specific Th1 cells promotes microglial activation and increases plaque burden in a mouse model of Alzheimer's disease. *J. Immunol.* 190, 2241–2251. doi: 10.4049/jimmunol.1200947

Burgoyne, C. F. (2011). A biomechanical paradigm for axonal insult within the optic nerve head in aging and glaucoma. *Exp. Eye Res.* 93, 120–132. doi: 10.1016/j.exer.2010.09.005

Bussian, T. J., Aziz, A., Meyer, C. F., Swenson, B. L., van Deursen, J. M., and Baker, D. J. (2018). Clearance of senescent glial cells prevents tau-dependent pathology and cognitive decline. *Nature* 562, 578–582. doi: 10.1038/s41586-018-0543-y

Cai, Z., and Xiao, M. (2016). Oligodendrocytes and Alzheimer's disease. *Int. J. Neurosci.* 126, 97–104. doi: 10.1186/s40478-018-0515-3

Chen, J. M., Jiang, G. X., Li, Q. W., Zhou, Z. M., and Cheng, Q. (2014). Increased serum levels of interleukin-18, -23 and -17 in Chinese patients with Alzheimer's disease. *Dement. Geriatr. Cogn. Disord.* 38, 321–329. doi: 10.1159/000360606

Chen, J. H., Ke, K. F., Lu, J. H., Qiu, Y. H., and Peng, Y. P. (2015). Protection of TGF-β1 against neuroinflammation and neurodegeneration in Aβ1–42-induced Alzheimer's disease model rats. *PLoS One* 10:e0116549. doi: 10.1371/journal.pone.0116549

Chen, Y., Qi, Z., Qiao, B., Lv, Z., Hao, Y., and Li, H. (2019). Oxymatrine can attenuate pathological deficits of Alzheimer's disease mice through regulation of neuroinflammation. *J. Neuroimmunol.* 334:576978. doi: 10.1016/j.jneuroim.2019.576978

Cheng, H. C., Ulane, C. M., and Burke, R. E. (2010). Clinical progression in Parkinson disease and the neurobiology of axons. *Ann. Neurol.* 67, 715–725. doi: 10.1002/ana.21995

Chiricozzi, A., and Krueger, J. G. (2013). IL-17 targeted therapies for psoriasis. *Expert Opin. Investig. Drugs* 22, 993–1005. doi: 10.1517/13543784.2013.806483

Colombo, E., Di Dario, M., Capitolo, E., Chaabane, L., Newcombe, J., Martino, G., et al. (2014). Fingolimod may support neuroprotection *via* blockade of astrocyte nitric oxide. *Ann. Neurol.* 76, 325–337. doi: 10.1002/ana.24217

Colonna, M., and Butovsky, O. (2017). Microglia function in the central nervous system during health and neurodegeneration. *Annu. Rev. Immunol.* 35, 441–468. doi: 10.1146/annurev-immunol-051116-052358

Conti, H. R., and Gaffen, S. L. (2015). IL-17-mediated immunity to the opportunistic fungal pathogen candida albicans. *J. Immunol.* 195, 780–788. doi: 10.4049/jimmunol.1500909

Cruz, J. A., Childs, E. E., Amatya, N., Garg, A. V., Beyaert, R., Kane, L. P., et al. (2017). Interleukin-17 signaling triggers degradation of the constitutive NF-κB inhibitor ABIN-1. *Immunohorizons* 1, 133–141. doi: 10.4049/immunohorizons.1700035

Cua, D. J., and Tato, C. M. (2010). Innate IL-17-producing cells: the sentinels of the immune system. *Nat. Rev. Immunol.* 10, 479–489. doi: 10.1038/nri2800

Das Sarma, J., Ciric, B., Marek, R., Sadhukhan, S., Caruso, M. L., Shafagh, J., et al. (2009). Functional interleukin-17 receptor A is expressed in central nervous system glia and upregulated in experimental autoimmune encephalomyelitis. *J. Neuroinflammation* 6:14. doi: 10.1186/1742-2094-6-14

Doecke, J. D., Laws, S. M., Faux, N. G., Wilson, W., Burnham, S. C., Lam, C. P., et al. (2012). Blood-based protein biomarkers for diagnosis of Alzheimer disease. *Arch. Neurol.* 69, 1318–1325. doi: 10.1001/archneurol.2012.1282

Drummond, R. A., and Lionakis, M. S. (2019). Organ-specific mechanisms linking innate and adaptive antifungal immunity. *Semin. Cell Dev. Biol.* 89, 78–90. doi: 10.1016/j.semcdb.2018.01.008

Dutta, D., Kundu, M., Mondal, S., Roy, A., Ruehl, S., Hall, D. A., et al. (2019). RANTES-induced invasion of Th17 cells into substantia nigra potentiates dopaminergic cell loss in MPTP mouse model of Parkinson's disease. *Neurobiol. Dis.* 132:104575. doi: 10.1016/j.nbd.2019.104575

Ely, L. K., Fischer, S., and Garcia, K. C. (2009). Structural basis of receptor sharing by interleukin 17 cytokines. *Nat. Immunol.* 10, 1245–1251. doi: 10.1038/ni.1813

Fiala, M., Chattopadhay, M., La Cava, A., Tse, E., Liu, G., Lourenco, E., et al. (2010). IL-17A is increased in the serum and in spinal cord CD8 and mast cells of ALS patients. *J. Neuroinflammation* 7:76. doi: 10.1186/1742-2094-7-76

Focus on Neurodegenerative Disease. (2018). Focus on neurodegenerative disease. *Nat. Neurosci.* 21:1293. doi: 10.1038/s41593-018-0250-x

Fort, M. M., Cheung, J., Yen, D., Li, J., Zurawski, S. M., Lo, S., et al. (2001). IL-25 induces IL-4, IL-5, and IL-13 and Th2-associated pathologies *in vivo*. *Immunity* 15, 985–995. doi: 10.1016/s1074-7613(01)00243-6

Fragoulis, A., Siegl, S., Fendt, M., Jansen, S., Soppa, U., Brandenburg, L. O., et al. (2017). Oral administration of methysticin improves cognitive deficits in a mouse model of Alzheimer's disease. *Redox Biol.* 12, 843–853. doi: 10.1016/j.redox.2017.04.024

Gaffen, S. L. (2011a). Life before seventeen: cloning of the IL-17 receptor. *J. Immunol.* 187, 4389–4391. doi: 10.4049/jimmunol.1102576

Gaffen, S. L. (2011b). Recent advances in the IL-17 cytokine family. *Curr. Opin. Immunol.* 23, 613–619. doi: 10.1016/j.coi.2011.07.006

Gaffen, S. L., Jain, R., Garg, A. V., and Cua, D. J. (2014). The IL-23-IL-17 immune axis: from mechanisms to therapeutic testing. *Nat. Rev. Immunol.* 14, 585–600. doi: 10.1038/nri3707

Garg, A. V., Ahmed, M., Vallejo, A. N., Ma, A., and Gaffen, S. L. (2013). The deubiquitinase A20 mediates feedback inhibition of interleukin-17 receptor signaling. *Sci. Signal.* 6:ra44. doi: 10.1126/scisignal.2003699

Gold, R., Wolinsky, J. S., Amato, M. P., and Comi, G. (2010). Evolving expectations around early management of multiple sclerosis. *Ther. Adv. Neurol. Disord.* 3, 351–367. doi: 10.1177/1756285610385608

Gu, C., Wu, L., and Li, X. (2013). IL-17 family: cytokines, receptors and signaling. *Cytokine* 64, 477–485. doi: 10.1016/j.cyto.2013.07.022

Hamilton, R. L. (2000). Lewy bodies in Alzheimer's disease: a neuropathological review of 145 cases using α-synuclein immunohistochemistry. *Brain Pathol.* 10, 378–384. doi: 10.1111/j.1750-3639.2000.tb00269.x

Hammond, T. R., Marsh, S. E., and Stevens, B. (2019). Immune signaling in neurodegeneration. *Immunity* 50, 955–974. doi: 10.1016/j.immuni.2019.03.016

Hardiman, O., Al-Chalabi, A., Chio, A., Corr, E. M., Logroscino, G., Robberecht, W., et al. (2017). Amyotrophic lateral sclerosis. *Nat. Rev. Dis. Primers* 3:17071. doi: 10.1056/NEJMra1603471

Haydon, P. G. (2016). The evolving view of astrocytes. *Cerebrum* 2016:cer-12-16. doi: 10.1002/2016gc006279

Hernandez-Mir, G., Raphael, I., Revu, S., Poholek, C. H., Avery, L., Hawse, W. F., et al. (2019). The Alzheimer's disease-associated protein BACE1 modulates T cell activation and Th17 function. *J. Immunol.* 203, 665–675. doi: 10.4049/jimmunol.1800363

Holtzman, D. M., Morris, J. C., and Goate, A. M. (2011). Alzheimer's disease: the challenge of the second century. *Sci. Transl. Med.* 3:77sr71. doi: 10.1126/scitranslmed.3002369

Hu, M. H., Zheng, Q. F., Jia, X. Z., Li, Y., Dong, Y. C., Wang, C. Y., et al. (2014). Neuroprotection effect of interleukin (IL)-17 secreted by reactive astrocytes is emerged from a high-level IL-17-containing environment during acute neuroinflammation. *Clin. Exp. Immunol.* 175, 268–284. doi: 10.1111/cei.12219

Hu, W. T., Chen-Plotkin, A., Grossman, M., Arnold, S. E., Clark, C. M., Shaw, L. M., et al. (2010). Novel CSF biomarkers for frontotemporal lobar degenerations. *Neurology* 75, 2079–2086. doi: 10.1212/WNL.0b013e318200d78d

Hu, Y., Ota, N., Peng, I., Refino, C. J., Danilenko, D. M., Caplazi, P., et al. (2010). IL-17RC is required for IL-17A- and IL-17F-dependent signaling and the pathogenesis of experimental autoimmune encephalomyelitis. *J. Immunol.* 184, 4307–4316. doi: 10.4049/jimmunol.0903614

Hu, W. T., Watts, K., Grossman, M., Glass, J., Lah, J. J., Hales, C., et al. (2013). Reduced CSF p-Tau181 to Tau ratio is a biomarker for FTLD-TDP. *Neurology* 81, 1945–1952. doi: 10.1212/01.wnl.0000436625.63650.27

Huang, Y., Liu, Z., Wang, X. Q., Qiu, Y. H., and Peng, Y. P. (2014). A dysfunction of $CD4^+$ T lymphocytes in peripheral immune system of Parkinson's disease model mice. *Zhongguo ying yong sheng li xue za zhi* 30, 567–576. doi: 10.13459/j.cnki.cjap.2014.06.013

Huang, G., Wang, Y., Vogel, P., and Chi, H. (2015). Control of IL-17 receptor signaling and tissue inflammation by the p38α-MKP-1 signaling axis in a mouse model of multiple sclerosis. *Sci. Signal.* 8:ra24. doi: 10.1126/scisignal.aaa2147

Hymowitz, S. G., Filvaroff, E. H., Yin, J. P., Lee, J., Cai, L., Risser, P., et al. (2001). IL-17s adopt a cystine knot fold: structure and activity of a novel cytokine, IL-17F and implications for receptor binding. *EMBO J.* 20, 5332–5341. doi: 10.1093/emboj/20.19.5332

Infante-Duarte, C., Horton, H. F., Byrne, M. C., and Kamradt, T. (2000). Microbial lipopeptides induce the production of IL-17 in Th cells. *J. Immunol.* 165, 6107–6115. doi: 10.4049/jimmunol.165.11.6107

Ivanov, I. I., Atarashi, K., Manel, N., Brodie, E. L., Shima, T., Karaoz, U., et al. (2009). Induction of intestinal Th17 cells by segmented filamentous bacteria. *Cell* 139, 485–498. doi: 10.1016/j.cell.2009.09.033

Ivanov, I. I., McKenzie, B. S., Zhou, L., Tadokoro, C. E., Lepelley, A., Lafaille, J. J., et al. (2006). The orphan nuclear receptor RORγt directs the differentiation program of proinflammatory IL-17+ T helper cells. *Cell* 126, 1121–1133. doi: 10.1016/j.cell.2006.07.035

Jäkel, S., Agirre, E., Mendanha Falcão, A., van Bruggen, D., Lee, K. W., Knuesel, I., et al. (2019). Altered human oligodendrocyte heterogeneity in multiple sclerosis. *Nature* 566, 543–547. doi: 10.1038/s41586-019-0903-2

Ji, W., Shi, H., Zhang, H., Sun, R., Xi, J., Wen, D., et al. (2013). A formalized design process for bacterial consortia that perform logic computing. *PLoS One* 8:e57482. doi: 10.1371/journal.pone.0057482

Jin, J. J., Kim, H. D., Maxwell, J. A., Li, L., and Fukuchi, K. (2008). Toll-like receptor 4-dependent upregulation of cytokines in a transgenic mouse model of Alzheimer's disease. *J. Neuroinflammation* 5:23. doi: 10.1186/1742-2094-5-23

Kang, Z., Altuntas, C. Z., Gulen, M. F., Liu, C., Giltiay, N., Qin, H., et al. (2010). Astrocyte-restricted ablation of interleukin-17-induced Act1-mediated signaling ameliorates autoimmune encephalomyelitis. *Immunity* 32, 414–425. doi: 10.1016/j.immuni.2010.03.004

Kang, S. H., Li, Y., Fukaya, M., Lorenzini, I., Cleveland, D. W., Ostrow, L. W., et al. (2013). Degeneration and impaired regeneration of gray matter oligodendrocytes in amyotrophic lateral sclerosis. *Nat. Neurosci.* 16, 571–579. doi: 10.1038/nn.3357

Kang, Z., Wang, C., Zepp, J., Wu, L., Sun, K., Zhao, J., et al. (2013). Act1 mediates IL-17-induced EAE pathogenesis selectively in NG2+ glial cells. *Nat. Neurosci.* 16, 1401–1408. doi: 10.1038/nn.3505

Karlsen, J. R., Borregaard, N., and Cowland, J. B. (2010). Induction of neutrophil gelatinase-associated lipocalin expression by co-stimulation with

interleukin-17 and tumor necrosis factor-α is controlled by IκB-ζ but neither by C/EBP-β nor C/EBP-δ. *J. Biol. Chem.* 285, 14088–14100. doi: 10.1074/jbc.m109.017129

Kassmann, C. M., Lappe-Siefke, C., Baes, M., Brügger, B., Mildner, A., Werner, H. B., et al. (2007). Axonal loss and neuroinflammation caused by peroxisome-deficient oligodendrocytes. *Nat. Genet.* 39, 969–976. doi: 10.1038/ng2070

Kawanokuchi, J., Shimizu, K., Nitta, A., Yamada, K., Mizuno, T., Takeuchi, H., et al. (2008). Production and functions of IL-17 in microglia. *J. Neuroimmunol.* 194, 54–61. doi: 10.1016/j.jneuroim.2007.11.006

Kebir, H., Kreymborg, K., Ifergan, I., Dodelet-Devillers, A., Cayrol, R., Bernard, M., et al. (2007). Human TH17 lymphocytes promote blood-brain barrier disruption and central nervous system inflammation. *Nat. Med.* 13, 1173–1175. doi: 10.1038/nm1651

Kleinschek, M. A., Owyang, A. M., Joyce-Shaikh, B., Langrish, C. L., Chen, Y., Gorman, D. M., et al. (2007). IL-25 regulates Th17 function in autoimmune inflammation. *J. Exp. Med.* 204, 161–170. doi: 10.1084/jem.20061738

Kohlgruber, A. C., Gal-Oz, S. T., LaMarche, N. M., Shimazaki, M., Duquette, D., Koay, H. F., et al. (2018). γδ T cells producing interleukin-17A regulate adipose regulatory T cell homeostasis and thermogenesis. *Nat. Immunol.* 19, 464–474. doi: 10.1038/s41590-018-0094-2

Kolbinger, F., Huppertz, C., Mir, A., and Padova, F. D. (2016). IL-17A and multiple sclerosis: signaling pathways, producing cells and target cells in the central nervous system. *Curr. Drug Targets* 17, 1882–1893. doi: 10.2174/1389450117666160307144027

Kostic, M., Dzopalic, T., Zivanovic, S., Zivkovic, N., Cvetanovic, A., Stojanovic, I., et al. (2014). IL-17 and glutamate excitotoxicity in the pathogenesis of multiple sclerosis. *Scand. J. Immunol.* 79, 181–186. doi: 10.1111/sji.12147

Kostic, M., Zivkovic, N., Cvetanovic, A., Stojanovic, I., and Colic, M. (2017). IL-17 signalling in astrocytes promotes glutamate excitotoxicity: indications for the link between inflammatory and neurodegenerative events in multiple sclerosis. *Mult. Scler. Relat. Disord.* 11, 12–17. doi: 10.1016/j.msard.2016.11.006

Križaj, D., Ryskamp, D. A., Tian, N., Tezel, G., Mitchell, C. H., Slepak, V. Z., et al. (2014). From mechanosensitivity to inflammatory responses: new players in the pathology of glaucoma. *Curr. Eye Res.* 39, 105–119. doi: 10.3109/02713683.2013.836541

Kumar, P., Monin, L., Castillo, P., Elsegeiny, W., Horne, W., Eddens, T., et al. (2016). Intestinal interleukin-17 receptor signaling mediates reciprocal control of the gut microbiota and autoimmune inflammation. *Immunity* 44, 659–671. doi: 10.1016/j.immuni.2016.02.007

Kuwabara, T., Ishikawa, F., Kondo, M., and Kakiuchi, T. (2017). The role of IL-17 and related cytokines in inflammatory autoimmune diseases. *Mediators Inflamm.* 2017:3908061. doi: 10.1155/2017/3908061

Lai, Y., Li, D., Li, C., Muehleisen, B., Radek, K. A., Park, H. J., et al. (2012). The antimicrobial protein REG3A regulates keratinocyte proliferation and differentiation after skin injury. *Immunity* 37, 74–84. doi: 10.1016/j.immuni.2012.04.010

Laprevotte, E., Cochaud, S., du Manoir, S., Lapierre, M., Dejou, C., Philippe, M., et al. (2017). The IL-17B-IL-17 receptor B pathway promotes resistance to paclitaxel in breast tumors through activation of the ERK1/2 pathway. *Oncotarget* 8, 113360–113372. doi: 10.18632/oncotarget.23008

Levin, L. A., Crowe, M. E., and Quigley, H. A. (2017). Neuroprotection for glaucoma: requirements for clinical translation. *Exp. Eye Res.* 157, 34–37. doi: 10.1016/j.exer.2016.12.005

Li, Z., Li, K., Zhu, L., Kan, Q., Yan, Y., Kumar, P., et al. (2013). Inhibitory effect of IL-17 on neural stem cell proliferation and neural cell differentiation. *BMC Immunol.* 14:20. doi: 10.1186/1471-2172-14-20

Li, L., Xu, L., Chen, W., Li, X., Xia, Q., Zheng, L., et al. (2018). Reduced annexin A1 secretion by ABCA1 causes retinal inflammation and ganglion cell apoptosis in a murine glaucoma model. *Front. Cell. Neurosci.* 12:347. doi: 10.3389/fncel.2018.00347

Li, C., Zhao, B., Lin, C., Gong, Z., and An, X. (2019). TREM2 inhibits inflammatory responses in mouse microglia by suppressing the PI3K/NF-κB signaling. *Cell Biol. Int.* 43, 360–372. doi: 10.1002/cbin.10975

Liddelow, S. A., Guttenplan, K. A., Clarke, L. E., Bennett, F. C., Bohlen, C. J., Schirmer, L., et al. (2017). Neurotoxic reactive astrocytes are induced by activated microglia. *Nature* 541, 481–487. doi: 10.1038/nature21029

Liu, G., Guo, J., Liu, J., Wang, Z., and Liang, D. (2014). Toll-like receptor signaling directly increases functional IL-17RA expression in neuroglial cells. *Clin. Immunol.* 154, 127–140. doi: 10.1016/j.clim.2014.07.006

Liu, X., He, F., Pang, R., Zhao, D., Qiu, W., Shan, K., et al. (2014). Interleukin-17 (IL-17)-induced microRNA 873 (miR-873) contributes to the pathogenesis of experimental autoimmune encephalomyelitis by targeting A20 ubiquitin-editing enzyme. *J. Biol. Chem.* 289, 28971–28986. doi: 10.1074/jbc.m114.577429

Liu, Y., Holdbrooks, A. T., Meares, G. P., Buckley, J. A., Benveniste, E. N., and Qin, H. (2015). Preferential recruitment of neutrophils into the cerebellum and brainstem contributes to the atypical experimental autoimmune encephalomyelitis phenotype. *J. Immunol.* 195, 841–852. doi: 10.4049/jimmunol.1403063

Liu, Z., Huang, Y., Cao, B. B., Qiu, Y. H., and Peng, Y. P. (2017). Th17 cells induce dopaminergic neuronal death *via* LFA-1/ICAM-1 interaction in a mouse model of Parkinson's disease. *Mol. Neurobiol.* 54, 7762–7776. doi: 10.1007/s12035-016-0249-9

Liu, C., Swaidani, S., Qian, W., Kang, Z., Sun, P., Han, Y., et al. (2011). A CC' loop decoy peptide blocks the interaction between Act1 and IL-17RA to attenuate IL-17- and IL-25-induced inflammation. *Sci. Signal.* 4:ra72. doi: 10.1126/scisignal.2001843

Liu, Z., Qiu, A. W., Huang, Y., Yang, Y., Chen, J. N., Gu, T. T., et al. (2019). IL-17A exacerbates neuroinflammation and neurodegeneration by activating microglia in rodent models of Parkinson's disease. *Brain Behav. Immun.* 81, 630–645. doi: 10.1016/j.bbi.2019.07.026

Liu, X., Zhou, F., Yang, Y., Wang, W., Niu, L., Zuo, D., et al. (2019). MiR-409–3p and MiR-1896 co-operatively participate in IL-17-induced inflammatory cytokine production in astrocytes and pathogenesis of EAE mice *via* targeting SOCS3/STAT3 signaling. *Glia* 67, 101–112. doi: 10.1002/glia.23530

Locatelli, G., Theodorou, D., Kendirli, A., Jordão, M. J. C., Staszewski, O., Phulphagar, K., et al. (2018). Mononuclear phagocytes locally specify and adapt their phenotype in a multiple sclerosis model. *Nat. Neurosci.* 21, 1196–1208. doi: 10.1038/s41593-018-0212-3

Lock, C., Hermans, G., Pedotti, R., Brendolan, A., Schadt, E., Garren, H., et al. (2002). Gene-microarray analysis of multiple sclerosis lesions yields new targets validated in autoimmune encephalomyelitis. *Nat. Med.* 8, 500–508. doi: 10.1038/nm0502-500

Luzza, F., Parrello, T., Monteleone, G., Sebkova, L., Romano, M., Zarrilli, R., et al. (2000). Up-regulation of IL-17 is associated with bioactive IL-8 expression in Helicobacter pylori-infected human gastric mucosa. *J. Immunol.* 165, 5332–5337. doi: 10.4049/jimmunol.165.9.5332

Marino, M., Papa, S., Crippa, V., Nardo, G., Peviani, M., Cheroni, C., et al. (2015). Differences in protein quality control correlate with phenotype variability in 2 mouse models of familial amyotrophic lateral sclerosis. *Neurobiol. Aging* 36, 492–504. doi: 10.1016/j.neurobiolaging.2014.06.026

McGeachy, M. J., Cua, D. J., and Gaffen, S. L. (2019). The IL-17 family of cytokines in health and disease. *Immunity* 50, 892–906. doi: 10.1016/j.immuni.2019.03.021

McManus, R. M., Higgins, S. C., Mills, K. H., and Lynch, M. A. (2014). Respiratory infection promotes T cell infiltration and amyloid-β deposition in APP/PS1 mice. *Neurobiol. Aging* 35, 109–121. doi: 10.1016/j.neurobiolaging.2013.07.025

Molofsky, A. V., and Deneen, B. (2015). Astrocyte development: a guide for the perplexed. *Glia* 63, 1320–1329. doi: 10.1002/glia.22836

Momčilović, M., Stamenković, V., Jovanović, M., Andjus, P. R., Jakovčevski, I., Schachner, M., et al. (2017). Tenascin-C deficiency protects mice from experimental autoimmune encephalomyelitis. *J. Neuroimmunol.* 302, 1–6. doi: 10.1016/j.jneuroim.2016.12.001

Montine, T. J., Phelps, C. H., Beach, T. G., Bigio, E. H., Cairns, N. J., Dickson, D. W., et al. (2012). National Institute on Aging-Alzheimer's Association guidelines for the neuropathologic assessment of Alzheimer's disease: a practical approach. *Acta Neuropathol.* 123, 1–11. doi: 10.1016/j.jalz.2011.10.007

Moustafa, A. A., Chakravarthy, S., Phillips, J. R., Gupta, A., Keri, S., Polner, B., et al. (2016). Motor symptoms in Parkinson's disease: a unified framework. *Neurosci. Biobehav. Rev.* 68, 727–740. doi: 10.1016/j.neubiorev.2016.07.010

Naik, S., Bouladoux, N., Linehan, J. L., Han, S. J., Harrison, O. J., Wilhelm, C., et al. (2015). Commensal-dendritic-cell interaction specifies a unique protective skin immune signature. *Nature* 520, 104–108. doi: 10.1038/nature14052

Noh, M. Y., Cho, K. A., Kim, H., Kim, S. M., and Kim, S. H. (2014). Erythropoietin modulates the immune-inflammatory response of a SOD1(G93A) transgenic mouse model of amyotrophic lateral sclerosis (ALS). *Neurosci. Lett.* 574, 53–58. doi: 10.1016/j.neulet.2014.05.001

Novatchkova, M., Leibbrandt, A., Werzowa, J., Neubüser, A., and Eisenhaber, F. (2003). The STIR-domain superfamily in signal transduction, development and immunity. *Trends Biochem. Sci.* 28, 226–229. doi: 10.1016/s0968-0004(03)00067-7

Onishi, R. M., and Gaffen, S. L. (2010). Interleukin-17 and its target genes: mechanisms of interleukin-17 function in disease. *Immunology* 129, 311–321. doi: 10.1111/j.1365-2567.2009.03240.x

Orthmann-Murphy, J. L., Freidin, M., Fischer, E., Scherer, S. S., and Abrams, C. K. (2007). Two distinct heterotypic channels mediate gap junction coupling between astrocyte and oligodendrocyte connexins. *J. Neurosci.* 27, 13949–13957. doi: 10.1523/jneurosci.3395-07.2007

Owyang, A. M., Zaph, C., Wilson, E. H., Guild, K. J., McClanahan, T., Miller, H. R., et al. (2006). Interleukin 25 regulates type 2 cytokine-dependent immunity and limits chronic inflammation in the gastrointestinal tract. *J. Exp. Med.* 203, 843–849. doi: 10.1084/jem.20051496

Paintlia, M. K., Paintlia, A. S., Singh, A. K., and Singh, I. (2011). Synergistic activity of interleukin-17 and tumor necrosis factor-α enhances oxidative stress-mediated oligodendrocyte apoptosis. *J. Neurochem.* 116, 508–521. doi: 10.1111/j.1471-4159.2010.07136.x

Pavelka, K., Chon, Y., Newmark, R., Lin, S. L., Baumgartner, S., and Erondu, N. (2015). A study to evaluate the safety, tolerability, and efficacy of brodalumab in subjects with rheumatoid arthritis and an inadequate response to methotrexate. *J. Rheumatol.* 42, 912–919. doi: 10.3899/jrheum.141271

Pekny, M., and Pekna, M. (2016). Reactive gliosis in the pathogenesis of CNS diseases. *Biochim. Biophys. Acta* 1862, 483–491. doi: 10.1016/j.bbadis.2015.11.014

Pellerin, L., and Magistretti, P. J. (2004). Neuroenergetics: calling upon astrocytes to satisfy hungry neurons. *Neuroscientist* 10, 53–62. doi: 10.1177/1073858403260159

Peng, T., Chanthaphavong, R. S., and Sun, S. (2017). Keratinocytes produce IL-17c to protect peripheral nervous systems during human HSV-2 reactivation. *J. Exp. Med.* 214, 2315–2329. doi: 10.1084/jem.20160581

Puel, A., Cypowyj, S., Bustamante, J., Wright, J. F., Liu, L., Lim, H. K., et al. (2011). Chronic mucocutaneous candidiasis in humans with inborn errors of interleukin-17 immunity. *Science* 332, 65–68. doi: 10.1542/peds.2011-2107cccc

Qian, Y., Liu, C., Hartupee, J., Altuntas, C. Z., Gulen, M. F., Jane-Wit, D., et al. (2007). The adaptor Act1 is required for interleukin 17-dependent signaling associated with autoimmune and inflammatory disease. *Nat. Immunol.* 8, 247–256. doi: 10.1038/ni1439

Qin, Y., Garrison, B. S., Ma, W., Wang, R., Jiang, A., Li, J., et al. (2018). A milieu molecule for TGF-β required for microglia function in the nervous system. *Cell* 174, 156.e16–171.e16. doi: 10.1016/j.cell.2018.05.027

Quigley, H. A., and Broman, A. T. (2006). The number of people with glaucoma worldwide in 2010 and 2020. *Br. J. Ophthalmol.* 90, 262–267. doi: 10.1136/bjo.2005.081224

Ramirez-Carrozzi, V., Sambandam, A., Luis, E., Lin, Z., Jeet, S., Lesch, J., et al. (2011). IL-17C regulates the innate immune function of epithelial cells in an autocrine manner. *Nat. Immunol.* 12, 1159–1166. doi: 10.1038/ni.2156

Ransohoff, R. M. (2016). How neuroinflammation contributes to neurodegeneration. *Science* 353, 777–783. doi: 10.1126/science.aag2590

Ren, Y., Qi, Y., and Su, X. (2019). Th17 cells in glaucoma patients promote Ig production in IL-17A and IL-21-dependent manner. *Clin. Exp. Pharmacol. Physiol.* 46, 875–882. doi: 10.1111/1440-1681.13141

Rentzos, M., Rombos, A., Nikolaou, C., Zoga, M., Zouvelou, V., Dimitrakopoulos, A., et al. (2010). Interleukin-17 and interleukin-23 are elevated in serum and cerebrospinal fluid of patients with ALS: a reflection of Th17 cells activation? *Acta Neurol. Scand.* 122, 425–429. doi: 10.1111/j.1600-0404.2010.01333.x

Reynolds, J. M., Lee, Y. H., Shi, Y., Wang, X., Angkasekwinai, P., Nallaparaju, K. C., et al. (2015). Interleukin-17B antagonizes interleukin-25-mediated mucosal inflammation. *Immunity* 42, 692–703. doi: 10.1016/j.immuni.2015.03.008

Rieck, J. (2013). The pathogenesis of glaucoma in the interplay with the immune system. *Invest. Ophthalmol. Vis. Sci.* 54, 2393–2409. doi: 10.1167/iovs.12-9781

Rocha, N. P., Assis, F., Scalzo, P. L., Vieira, E. L. M., Barbosa, I. G., de Souza, M. S., et al. (2018). Reduced activated T lymphocytes (CD4+CD25+) and plasma levels of cytokines in Parkinson's disease. *Mol. Neurobiol.* 55, 1488–1497. doi: 10.1007/s12035-017-0404-y

Rodgers, J. M., Robinson, A. P., Rosler, E. S., Lariosa-Willingham, K., Persons, R. E., Dugas, J. C., et al. (2015). IL-17A activates ERK1/2 and enhances differentiation of oligodendrocyte progenitor cells. *Glia* 63, 768–779. doi: 10.1002/glia.22783

Rouvier, E., Luciani, M. F., Mattéi, M. G., Denizot, F., and Golstein, P. (1993). CTLA-8, cloned from an activated T cell, bearing AU-rich messenger RNA instability sequences and homologous to a herpesvirus saimiri gene. *J. Immunol.* 150, 5445–5456.

Ruddy, M. J., Wong, G. C., Liu, X. K., Yamamoto, H., Kasayama, S., Kirkwood, K. L., et al. (2004). Functional cooperation between interleukin-17 and tumor necrosis factor-α is mediated by CCAAT/enhancer-binding protein family members. *J. Biol. Chem.* 279, 2559–2567. doi: 10.1074/jbc.m308809200

Saddawi-Konefka, R., Seelige, R., Gross, E. T., Levy, E., Searles, S. C., Washington, A. Jr., et al. (2016). Nrf2 induces IL-17D to mediate tumor and virus surveillance. *Cell Rep.* 16, 2348–2358. doi: 10.1016/j.celrep.2016.07.075

Saksida, T., Koprivica, I., Vujičić, M., Stošić-Grujičić, S., Perović, M., Kanazir, S., et al. (2018). Impaired IL-17 production in gut-residing immune cells of 5xFAD mice with Alzheimer's disease pathology. *J. Alzheimers Dis.* 61, 619–630. doi: 10.3233/jad-170538

Sanadgol, N., Golab, F., Tashakkor, Z., Taki, N., Moradi Kouchi, S., Mostafaie, A., et al. (2017). Neuroprotective effects of ellagic acid on cuprizone-induced acute demyelination through limitation of microgliosis, adjustment of CXCL12/IL-17/IL-11 axis and restriction of mature oligodendrocytes apoptosis. *Pharm. Biol.* 55, 1679–1687. doi: 10.1080/13880209.2017.1319867

Saresella, M., Calabrese, E., Marventano, I., Piancone, F., Gatti, A., Alberoni, M., et al. (2011). Increased activity of Th-17 and Th-9 lymphocytes and a skewing of the post-thymic differentiation pathway are seen in Alzheimer's disease. *Brain Behav. Immun.* 25, 539–547. doi: 10.1016/j.bbi.2010.12.004

Schwandner, R., Yamaguchi, K., and Cao, Z. (2000). Requirement of tumor necrosis factor receptor-associated factor (TRAF)6 in interleukin 17 signal transduction. *J. Exp. Med.* 191, 1233–1240. doi: 10.1084/jem.191.7.1233

Segond von Banchet, G., Boettger, M. K., Konig, C., Iwakura, Y., Brauer, R., and Schaible, H. G. (2013). Neuronal IL-17 receptor upregulates TRPV4 but not TRPV1 receptors in DRG neurons and mediates mechanical but not thermal hyperalgesia. *Mol. Cell. Neurosci.* 52, 152–160. doi: 10.1016/j.mcn.2012.11.006

Shan, K., Pang, R., Zhao, C., Liu, X., Gao, W., Zhang, J., et al. (2017). IL-17-triggered downregulation of miR-497 results in high HIF-1α expression and consequent IL-1β and IL-6 production by astrocytes in EAE mice. *Cell. Mol. Immunol.* 14, 909–923. doi: 10.1038/cmi.2017.12

Shi, Y., Ullrich, S. J., Zhang, J., Connolly, K., Grzegorzewski, K. J., Barber, M. C., et al. (2000). A novel cytokine receptor-ligand pair. Identification, molecular characterization and *in vivo* immunomodulatory activity. *J. Biol. Chem.* 275, 19167–19176. doi: 10.1074/jbc.M910228199

Singh, N. P., Hegde, V. L., Hofseth, L. J., Nagarkatti, M., and Nagarkatti, P. (2007). Resveratrol (trans-3,5,4′-trihydroxystilbene) ameliorates experimental allergic encephalomyelitis, primarily *via* induction of apoptosis in T cells involving activation of aryl hydrocarbon receptor and estrogen receptor. *Mol. Pharmacol.* 72, 1508–1521. doi: 10.1124/mol.107.038984

Sommer, A., Marxreiter, F., Krach, F., Fadler, T., Grosch, J., Maroni, M., et al. (2018). Th17 lymphocytes induce neuronal cell death in a human iPSC-based model of Parkinson's disease. *Cell Stem Cell* 23, 123–131. doi: 10.1016/j.stem.2018.06.015

Spiller, K. J., Restrepo, C. R., Khan, T., Dominique, M. A., Fang, T. C., Canter, R. G., et al. (2018). Microglia-mediated recovery from ALS-relevant motor neuron degeneration in a mouse model of TDP-43 proteinopathy. *Nat. Neurosci.* 21, 329–340. doi: 10.1038/s41593-018-0083-7

St-Amour, I., Bosoi, C. R., Paré, I., Ignatius Arokia Doss, P. M., Rangachari, M., Hébert, S. S., et al. (2019). Peripheral adaptive immunity of the triple transgenic mouse model of Alzheimer's disease. *J. Neuroinflammation* 16:3. doi: 10.1186/s12974-018-1380-5

Starnes, T., Broxmeyer, H. E., Robertson, M. J., and Hromas, R. (2002). Cutting edge: IL-17D, a novel member of the IL-17 family, stimulates cytokine production and inhibits hemopoiesis. *J. Immunol.* 169, 642–646. doi: 10.4049/jimmunol.169.2.642

Stromnes, I. M., Cerretti, L. M., Liggitt, D., Harris, R. A., and Goverman, J. M. (2008). Differential regulation of central nervous system autoimmunity by T(H)1 and T(H)17 cells. *Nat. Med.* 14, 337–342. doi: 10.1038/nm1715

Sun, J., Zhang, S., Zhang, X., Zhang, X., Dong, H., and Qian, Y. (2015). IL-17A is implicated in lipopolysaccharide-induced neuroinflammation and cognitive impairment in aged rats *via* microglial activation. *J. Neuroinflammation* 12:165. doi: 10.1186/s12974-015-0394-5

Tian, K., Shibata-Germanos, S., Pahlitzsch, M., and Cordeiro, M. F. (2015). Current perspective of neuroprotection and glaucoma. *Clin. Ophthalmol.* 9, 2109–2118. doi: 10.2147/opth.s80445

Tzartos, J. S., Friese, M. A., Craner, M. J., Palace, J., Newcombe, J., Esiri, M. M., et al. (2008). Interleukin-17 production in central nervous system-infiltrating T cells and glial cells is associated with active disease in multiple sclerosis. *Am. J. Pathol.* 172, 146–155. doi: 10.2353/ajpath.2008.070690

Uyttenhove, C., Sommereyns, C., Théate, I., Michiels, T., and Van Snick, J. (2007). Anti-IL-17A autovaccination prevents clinical and histological manifestations of experimental autoimmune encephalomyelitis. *Ann. N Y Acad. Sci.* 1110, 330–336. doi: 10.1196/annals.1423.035

Vassar, R. (2004). BACE1: the β-secretase enzyme in Alzheimer's disease. *J. Mol. Neurosci.* 23, 105–114. doi: 10.1385/JMN:23:1-2:105

Waisman, A., Hauptmann, J., and Regen, T. (2015). The role of IL-17 in CNS diseases. *Acta Neuropathol.* 129, 625–637. doi: 10.1007/s00401-015-1402-7

Wang, J., Chen, F., Zheng, P., Deng, W., Yuan, J., Peng, B., et al. (2012). Huperzine A ameliorates experimental autoimmune encephalomyelitis *via* the suppression of T cell-mediated neuronal inflammation in mice. *Exp. Neurol.* 236, 79–87. doi: 10.1016/j.expneurol.2012.03.024

Wang, Y., Mei, Y., Feng, D., and Xu, L. (2008). Triptolide modulates T-cell inflammatory responses and ameliorates experimental autoimmune encephalomyelitis. *J. Neurosci. Res.* 86, 2441–2449. doi: 10.1002/jnr.21683

Wax, M. B., Tezel, G., Yang, J., Peng, G., Patil, R. V., Agarwal, N., et al. (2008). Induced autoimmunity to heat shock proteins elicits glaucomatous loss of retinal ganglion cell neurons *via* activated T-cell-derived fas-ligand. *J. Neurosci* 28, 12085–12096. doi: 10.1523/jneurosci.3200-08.2008

Wei, X., and Cho, K. S. (2019). Neuroinflammation and microglia in glaucoma: time for a paradigm shift. *J. Neurosci. Res.* 97, 70–76. doi: 10.1002/jnr.24256

Yan, Y., Ding, X., Li, K., Ciric, B., Wu, S., Xu, H., et al. (2012). CNS-specific therapy for ongoing EAE by silencing IL-17 pathway in astrocytes. *Mol. Ther.* 20, 1338–1348. doi: 10.1038/mt.2012.12

Yang, S. H., Kim, J., Lee, M. J., and Kim, Y. (2015). Abnormalities of plasma cytokines and spleen in senile APP/PS1/Tau transgenic mouse model. *Sci. Rep.* 5:15703. doi: 10.1038/srep15703

Yang, J., Kou, J., Lalonde, R., and Fukuchi, K. I. (2017). Intracranial IL-17A overexpression decreases cerebral amyloid angiopathy by upregulation of ABCA1 in an animal model of Alzheimer's disease. *Brain Behav. Immun.* 65, 262–273. doi: 10.1016/j.bbi.2017.05.012

Yang, X., Zeng, Q., Goktas, E., Gopal, K., Al-Aswad, L., Blumberg, D. M., et al. (2019). T-lymphocyte subset distribution and activity in patients with glaucoma. *Invest. Ophthalmol. Vis. Sci.* 60, 877–888. doi: 10.1167/iovs.18-26129

Yi, H., Bai, Y., Zhu, X., Lin, L., Zhao, L., Wu, X., et al. (2014). IL-17A induces MIP-1α expression in primary astrocytes *via* Src/MAPK/PI3K/NF-kB pathways: implications for multiple sclerosis. *J. Neuroimmune Pharmacol.* 9, 629–641. doi: 10.1007/s11481-014-9553-1

Zhang, J., Ke, K. F., Liu, Z., Qiu, Y. H., and Peng, Y. P. (2013). Th17 cell-mediated neuroinflammation is involved in neurodegeneration of aβ1–42-induced Alzheimer's disease model rats. *PLoS One* 8:e75786. doi: 10.1186/s12974-014-0201-8

Zhang, Y., Liu, M., Sun, H., and Yin, K. (2015). Matrine improves cognitive impairment and modulates the balance of Th17/Treg cytokines in a rat model of Aβ1–42-induced Alzheimer's disease. *Cent. Eur. J. Immunol.* 40, 411–419. doi: 10.5114/ceji.2015.56961

Zhang, J., Zeng, Y. Q., Zhang, J., Pan, X. D., Kang, D. Y., Huang, T. W., et al. (2015). Tripchlorolide ameliorates experimental autoimmune encephalomyelitis by down-regulating ERK1/2-NF-κB and JAK/STAT signaling pathways. *J. Neurochem.* 133, 104–112. doi: 10.1111/jnc.13058

Zhao, X., Kan, Q., Zhu, L., and Zhang, G. X. (2011). Matrine suppresses production of IL-23/IL-17 and ameliorates experimental autoimmune encephalomyelitis. *Am. J. Chinese Med.* 39, 933–941. doi: 10.1142/s0192415x11009317

Zhu, Y., Tan, W., Demetriades, A. M., Cai, Y., Gao, Y., Sui, A., et al. (2016). Interleukin-17A neutralization alleviated ocular neovascularization by promoting M2 and mitigating M1 macrophage polarization. *Immunology* 147, 414–428. doi: 10.1111/imm.12571

Zimmermann, J., Krauthausen, M., Hofer, M. J., Heneka, M. T., Campbell, I. L., and Muller, M. (2013). CNS-targeted production of IL-17A induces glial activation, microvascular pathology and enhances the neuroinflammatory response to systemic endotoxemia. *PLoS One* 8:e57307. doi: 10.1371/journal.pone.0057307

Zota, V., Nemirovsky, A., Baron, R., Fisher, Y., Selkoe, D. J., Altmann, D. M., et al. (2009). HLA-DR alleles in amyloid β-peptide autoimmunity: a highly immunogenic role for the DRB1*1501 allele. *J. Immunol.* 183, 3522–3530. doi: 10.4049/jimmunol.0900620

Conflict of Interest: The authors declare that the research was conducted in the absence of any commercial or financial relationships that could be construed as a potential conflict of interest.

frontiers in Neuroscience

PERSPECTIVE
published: 02 October 2020
doi: 10.3389/fnins.2020.577744

Antiviral Immune Response in Alzheimer's Disease: Connecting the Dots

*Ethan R. Roy and Wei Cao**

Huffington Center on Aging and Department of Molecular and Human Genetics, Baylor College of Medicine, Houston, TX, United States

Alzheimer's disease (AD) represents an enormous public health challenge currently and with increasing urgency in the coming decades. Our understanding of the etiology and pathogenesis of AD is rather incomplete, which is manifested in stagnated therapeutic developments. Apart from the well-established Amyloid Hypothesis of AD, gaining traction in recent years is the Pathogen Hypothesis, which postulates a causal role of infectious agents in the development of AD. Particularly, infection by viruses, among a diverse range of microorganisms, has been implicated. Recently, we described a prominent antiviral immune response in human AD brains as well as murine amyloid beta models, which has consequential effects on neuropathology. Such findings expectedly allude to the question about viral infections and AD. In this Perspective, we would like to discuss the molecular mechanism underlying the antiviral immune response, highlight how such pathway directly promotes AD pathogenesis, and depict a multilayered connection between antiviral immune response and other agents and factors relevant to AD. By tying together these threads of evidence, we provide a cohesive perspective on the uprising of antiviral immune response in AD.

Keywords: antiviral, interferon, Alzheimer's disease, innate immunity, amyloid, pathogen hypothesis, neuroinflammation

OPEN ACCESS

Edited by:
Xian-Le Bu,
Third Military Medical University, China

Reviewed by:
Eric Harold Frost,
Université de Sherbrooke, Canada
Dana Niedowicz,
University of Kentucky, United States

***Correspondence:**
Wei Cao
wei.cao@bcm.edu

Specialty section:
This article was submitted to Neurodegeneration, a section of the journal Frontiers in Neuroscience

Received: *29 June 2020*
Accepted: *08 September 2020*
Published: *02 October 2020*

Citation:
Roy ER and Cao W (2020) Antiviral Immune Response in Alzheimer's Disease: Connecting the Dots. Front. Neurosci. 14:577744. doi: 10.3389/fnins.2020.577744

INTRODUCTION

Hallmarked by the deposition of β-amyloid plaques and accumulation of neurofibrillary tangles, Alzheimer's disease (AD) manifests with complex pathophysiology and its etiology remains elusive. Among the many viewpoints for the underlying mechanisms, the Pathogen Hypothesis was proposed initially based on the clinical discoveries of Herpes Simplex Virus-1 (HSV-1) in association with AD, further expanded to include other microbes, and gained experimental support in recent years (Itzhaki et al., 1997, 2016; Itzhaki, 2018). In particular, Aβ has been shown to function as an antimicrobial peptide and, under experimental conditions, protect against microbial infection while seeding Aβ deposition (Kumar et al., 2016; Eimer et al., 2018). Separately, pathogenic involvement of proinflammatory responses in AD is also increasingly being appreciated (Heneka et al., 2015; Ransohoff, 2016). Because of the intimate association between infections and inflammation, the Pathogen Hypothesis putatively links to the neuroinflammation phenomenon in many aspects; however, the precise molecular correlation between these two processes in AD has yet to be established. Here, we intend to make the connections from multiple angles.

MOLECULAR MECHANISM UNDERLYING THE ANTIVIRAL IMMUNE RESPONSE IN AD

Mammalian antiviral innate immune defense mechanism utilize an array of nucleic acid innate immune sensors to detect viral genomes or their replication products, which activate a cascade of signaling events to induce rapid gene expression (Barrat et al., 2016). Among them, the type I IFN (IFN) cytokines, which include multiple IFNα subtypes, IFNβ, IFNε IFNκ, and IFNτω, instruct the frontline antiviral response (Capobianchi et al., 2015; McNab et al., 2015). All IFN species signal through a common receptor complex and drive the transcription of a large panel of IFN-stimulated genes (ISGs) (Schreiber and Piehler, 2015). ISGs operate in concert to interfere with viral replication through viral genome degradation and blockade of gene expression, protein synthesis and virion assembly, thus conveying protection.

Although normally non-immunogenic, host self-derived nucleic acids can provoke IFN response under pathological conditions such as autoimmune diseases. In systemic lupus erythematosus, immune complexes comprised of a patient's DNA or RNA and associated autoantibodies activate plasmacytoid dendritic cells (pDCs), a subset of innate immune cells, to stimulate IFN production and flares of systemic inflammation (Gilliet et al., 2008). In psoriasis, antimicrobial peptide cathelicidin LL-37 complexes with nucleic acids and similarly induces aberrant IFN production from pDCs (Lande et al., 2007). In both cases, nucleic acid-containing complexes gain immunogenicity by delivering nucleic acids to the intracellular innate immune sensors in pDCs to activate the signaling cascade for IFN production.

LL-37 and other antimicrobial peptides oligomerize and form pore structures on biological membranes (Arnusch et al., 2007; Xhindoli et al., 2014) (**Figure 1**). Similarly, oligomerization of Aβ exerts neuronal toxicity as well as antimicrobial function (Kayed et al., 2003; Soscia et al., 2010). By studying oligomers made from various proteins, we not only confirmed this fascinating gain-of-function but also discovered another intrinsic property of protein oligomers – affinity toward negatively charged molecules (Di Domizio et al., 2012b). Complexing soluble oligomers with nucleic acids or glycosaminoglycan, both negatively charged, expedite the formation of amyloid fibrils *in vitro*. More strikingly, nucleic acid-containing amyloid fibrils are potent inducers of IFN response from pDCs *in vitro* and *in vivo* (Di Domizio et al., 2012a). In short, Aβ and LL-37 share several characteristics: oligomerization, cytotoxicity to host and microbe cells, and binding to cofactors, the latter conveys interferongenicity (**Figure 1**). Not surprisingly then, amyloid-DNA composites present in bacterial biofilm stimulate an IFN response and promote autoimmunity (Gallo et al., 2015). To immune cells, these protein-nucleic acid complexes are indiscriminately sensed as virions to trigger an antiviral immune response.

Microglia, the brain resident immune cells, fulfill important functions in trophic support, cell debris removal and tissue surveillance under homeostatic conditions (Li and Barres, 2018; Prinz et al., 2019). However, microglial dysfunction can be a primary cause to neurological disorders, thus disease-associated microglia have received intense attention in recent years. Mouse primary microglia elicited a rapid IFN response to nucleic acid-containing amyloid fibrils *in vitro,* in a manner similar to that from peripheral immune cells (Roy et al., 2020). Activated microglia expressing Clec7a not only selectively surrounded the amyloid β plaques with sequestered DNA and RNA but also upregulated a large panel of ISGs, indicating profound IFN pathway activation in mouse models of amyloidosis. Thus, IFN constitutes a pivotal element within the neuroinflammatory network of AD. Most recently, the early and persistent IFN and antiviral response was confirmed by an analysis of microglial proteomes from Aβ models (Monasor et al., 2020).

ANTIVIRAL IMMUNE RESPONSE IN PROMOTING AD PATHOGENESIS

Microglia recruited to amyloid β plaques adopt a disease-associated phenotype, where they acquire a unique molecular state by downregulating homeostatic markers, upregulating immune effector molecules, and express a panel of genes that have been associated with increased risk for AD and other neurodegenerative disorders (Butovsky and Weiner, 2018; Hammond et al., 2018; Wang and Colonna, 2019). IFN was shown to be required for sustaining microglial activation since suppression of IFN signaling significantly reduced the levels of CD68 and Clec7a, markers for microglial activation, and shifted the morphology of microglia toward homeostatic form (Roy et al., 2020). Intriguingly, polymorphisms of ISGs, including *OAS1*, *ITGAM*, *LAPTM5,* and *LILRB4*, were conjointly identified as a significant risk factor for AD, implicating IFN pathway as a genetic modifier (Salih et al., 2019).

In AD tissue, ISG-expressing microglia preferentially associate with nucleic acid^{+} neuritic plaques (Roy et al., 2020). Furthermore, the IFN activation signature was correlated with amyloid load and disease severity across a large study cohort represented in the Mt. Sinai Brain Bank. These findings are in line with earlier reports of neuritic plaques sequestering self nucleic acids and microglia expressing IFNα in AD brains (Yamada et al., 1994; Ginsberg et al., 1997). Therefore, a prototypical antiviral immune response is manifested in both pre-clinic models and clinic AD cases. Interestingly, AD patients with rare TREM2 R47H variant, an AD risk factor, have increased presentation of proinflammatory microglia subsets including those enriched with IFN response (Sayed et al., 2020).

Although normal brain lacks detectable IFN expression, transient IFN production in CNS protects against opportunistic viral infections (Nallar and Kalvakolanu, 2014). However, chronic and dysregulated IFN expression is a major driver for type I interferonopathy, a group of hereditary CNS disorders (Hofer and Campbell, 2013; Rodero and Crow, 2016; Schwabenland et al., 2019). Separately, patients receiving systemic IFN treatment or with HIV-induced dementia display increased brain IFN activation, which is associated with cognitive and psychiatric dysfunctions (Gray et al., 1996; Hayley et al., 2013; Dipasquale et al., 2016; Wachholz et al., 2016). These observations collectively suggest a toxic influence of IFN on the brain. When

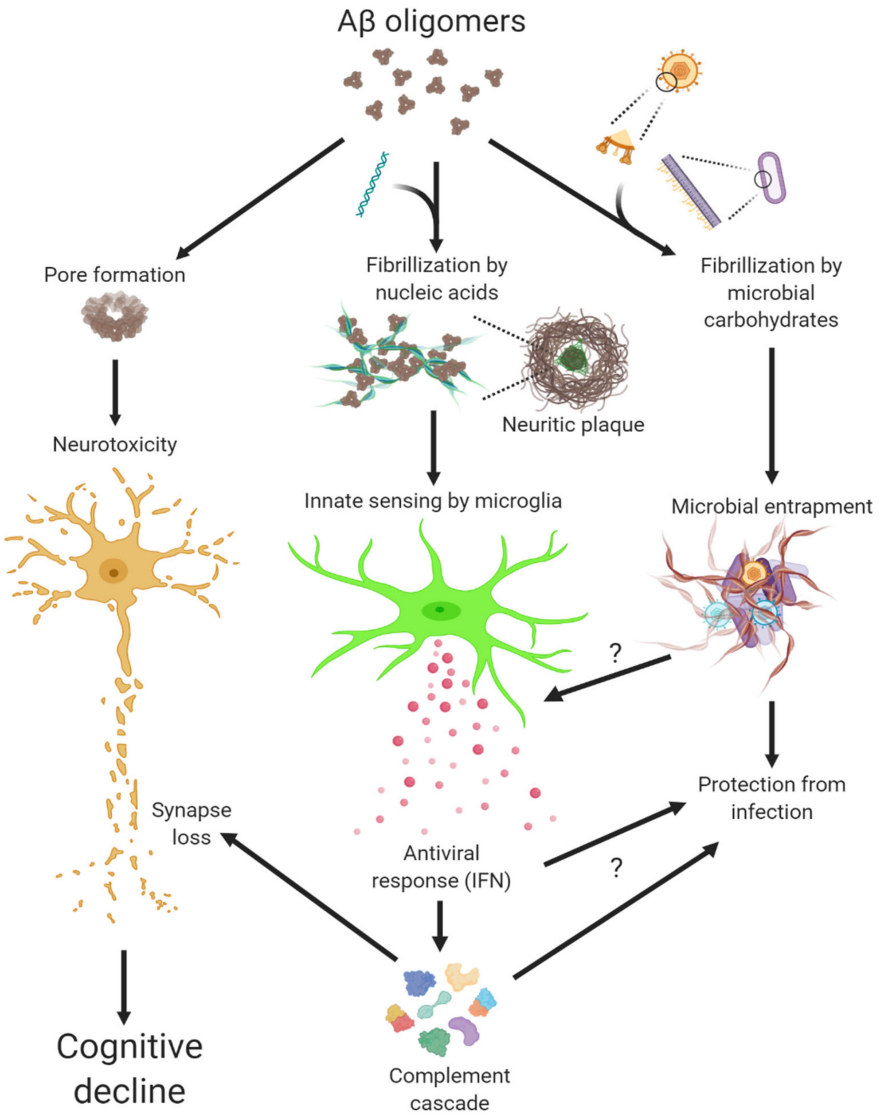

FIGURE 1 | Multiple actions of Aβ oligomers leading to neuropathogenesis in Alzheimer's disease.

delivered to the brain, IFNβ directly activates microglia, initiates neuroinflammation, and leads to microglia-mediated synapse loss (Roy et al., 2020). Conversely, suppression of IFN signaling in Aβ models rescued the synapse loss in the brain, supporting a direct role of IFN in synapse modification. Interestingly, IFN receptor ablation was previously shown to improve cognitive performance while altering glial phenotypes in $APP_{SWE}/PS1_{\Delta E9}$ mice (Minter et al., 2016).

Complement has been implicated in synaptic pathologies in diverse neurological and neuropsychiatric diseases, in particular neurodegeneration (Hong et al., 2016; Morgan, 2018; Tenner et al., 2018; Wu et al., 2019). Intriguingly, not only do a number of complement genes represent bona fide ISGs, but IFN-stimulated synapse elimination depends on the function of complement C3 (Roy et al., 2020). Not coincidently, synapse loss and memory impairment in mice recovered from West Nile Virus (WNV) infection was shown mediated by persistent microglial activation and the functional involvement of complement C3 (Vasek et al., 2016). Moreover, IFN pathway is robustly correlated with complement cascade in human AD (Roy et al., 2020). Given that synapse loss is clinically associated with cognitive decline (DeKosky and Scheff, 1990; Scheff et al., 1990; Terry et al., 1991), these findings highlight a pathogenic role of antiviral immune response in conjunction with complement cascade in modifying synapses in AD (**Figure 1**).

CONTRIBUTING FACTORS TO ANTIVIRAL IMMUNE RESPONSE IN AD

The central nervous system (CNS) is protected by a highly complex barrier structure, but is by no means invincible to

infections. Many neurotropic viruses can gain access to the brain through blood circulation or peripheral nerves (Swanson and McGavern, 2015). Acute viral infection in the CNS often triggers inflammatory response, where the IFN pathway plays a crucial role in the defense against a wide range of viral pathogens (Paul et al., 2007). However, strong immune reaction also leads to acute meningitis, encephalitis and myelitis, which manifest with behavioral and cognitive disruptions (Swanson and McGavern, 2015). In humans, WNV, HIV-1, Zika virus, and HSV-1 are the most common causes for viral encephalitis. Of note, the elderly population is susceptible to reactivation of latent varicella zoster virus (VZV), which results in shingles (Gilden et al., 2009). VZV is normally controlled by peripheral IFN response, but occasionally it can spread to CNS to cause encephalitis (Gilden et al., 2009; Kim et al., 2017). Fortunately, many people recover from these acute episodes; yet, a significant portion suffer from long term neurological sequelae (Swanson and McGavern, 2015; Klein et al., 2017). Rather than the irreversible damage caused by the pathogens, recent studies suggested a role of chronic inflammation that underlie neurological impairments, including conditions post WNV infection as mentioned earlier (Vasek et al., 2016). Therefore, prior exposure to CNS infections may have long-lasting neurocognitive consequences (**Figure 2**).

Although responsible for a common form of acute viral encephalitis, herpes simplex virus mostly carries out latent infection in the general population. Itzhaki et al. (1997) first detected HSV-1 DNA in the brain of 60% cases of apolipoprotein E gene (APOE-ε4) carriers and subsequently postulated the viral concept of AD: HSV-1 likely travels to the brain in middle age, where it remains in a latent state, and accumulation of damage from intermittent reactivation – direct viral action and major inflammatory effects – leads eventually to the development of AD (Itzhaki, 2018). Although the causal relationship between HSV-1 reactivation and AD is extremely difficult to prove in humans, the proposal is consistent with the concept of pathogenic chronic inflammation in CNS, as mentioned above. The IFN signaling, as a result of the cGAS-STING pathway activation in microglia, is indispensable for controlling HSV-1 infection in humans (Dupuis et al., 2003; Reinert et al., 2016). Therefore, IFN response required for resolving periodic HSV-1 activation may conceivably be a contributing factor in AD (**Figure 2**). Over the years, other viral pathogens have been detected in AD specimens and implicated in AD risk, among which noticeably are members of Herpesviridae. Increased human herpesvirus subtypes (HHV-6 and HHV-7) were independently identified from a multi-scale gene expression network analysis of late-onset AD (Readhead et al., 2018), though the study was later challenged (Jeong and Liu, 2019; Allnutt et al., 2020). On the other hand, while acute HSV-1 infection induced Aβ production in human induced neural stem cells (Cairns et al., 2020), Aβ was shown to play a protective role in brain against experimental infections by Herpesviridae, including HSV-1, and HHV-6 (Eimer et al., 2018). The interaction between Aβ and different types of microbes involves surface carbohydrate recognition, which rapidly seeds amyloid fibrils (Kumar et al., 2016; Eimer et al., 2018; **Figure 1**). In lieu of immune reaction,

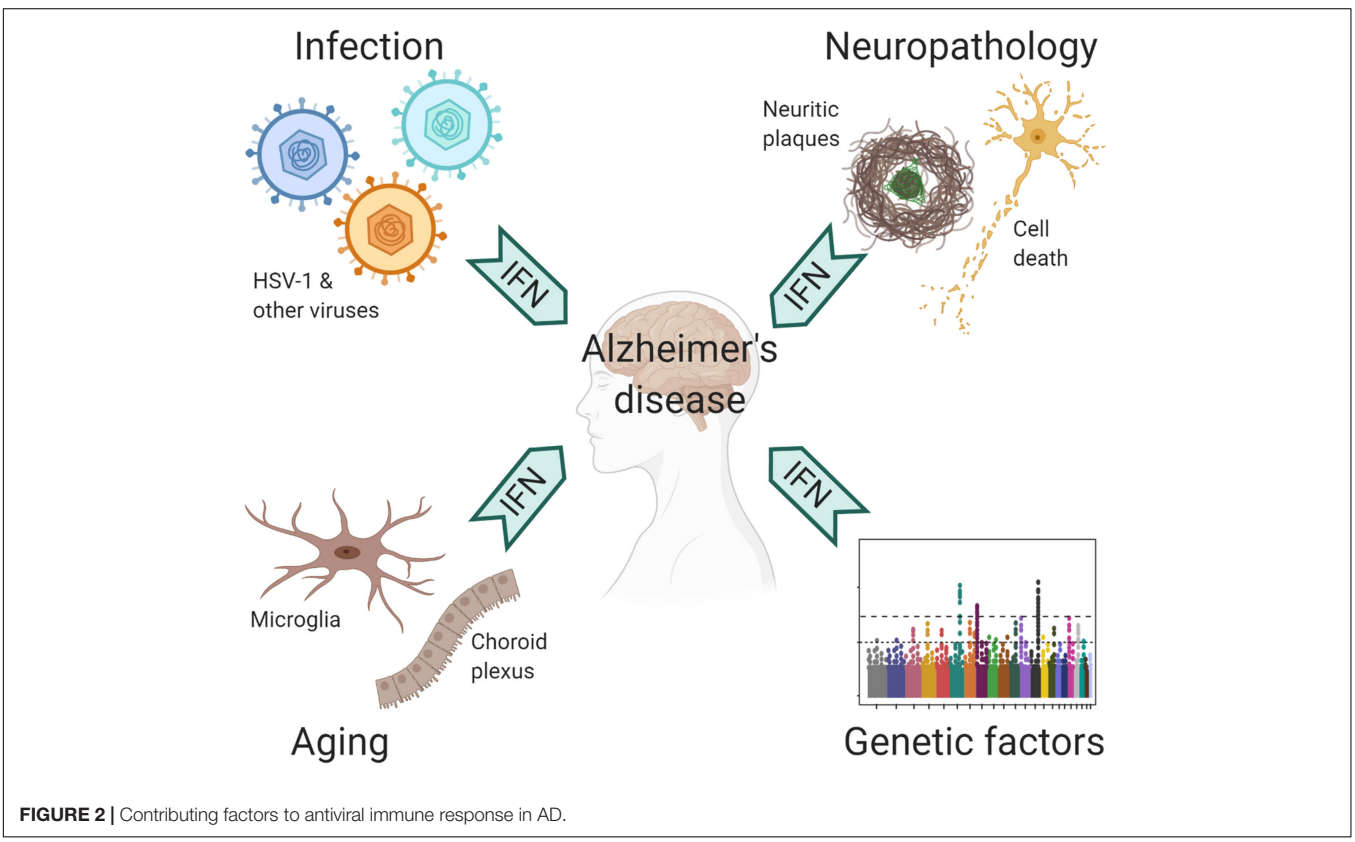

FIGURE 2 | Contributing factors to antiviral immune response in AD.

it remains to be shown if Aβ-entrapped viruses can be recognized by microglia and elicit effective IFN response.

Under pathological conditions, self-derived molecules can potently trigger inflammatory response in the absence of an infection. As discussed earlier, extracellular amyloid plaques with sequestered nucleic acids are recognized by microglia and elicit an antiviral response analogous to that during viral infection (**Figure 1**). Of note, sequence analysis of RNA isolated from AD neuritic plaques identified transcripts from cortical neurons, marking a self origin of plaque-associated nucleic acids (Ginsberg et al., 1999). Conceivably, such intrinsic IFN response would deter opportunistic viral infection or reactivation in AD brain, a point that awaits further investigation (**Figure 1**). On the other hand, dysregulated nucleic acid catabolism also results in aberrant IFN production. For example, mutations of deoxyribonuclease *TREX1* or ribonuclease *RNASEH2* lead to the accumulation of aberrant cytosolic nucleic acid species, IFN production, and encephalopathy in Aicardi-Goutieres syndrome (Rodero and Crow, 2016). Under neurodegenerative conditions, dead brain cells may release nucleic acids and other alarmin molecules thus stimulating an inflammation response. Although peripheral immune cells discern immunogenic vs. non-immunogenic cell death (Green et al., 2009), how microglia innately respond to different forms of CNS cell death is not known at this time. It is thus important to examine if additional endogenous agents stimulate innate IFN response in AD besides amyloid plaques.

It's well known that age is the most important risk factor for late-onset AD (LOAD). In normal aging brain, heightened IFN signaling from microglia inside the parenchyma and choroid plexus, an epithelial tissue located within the ventricles, has been shown to be detrimental to neurogenesis and cognitive function (Baruch et al., 2014; Deczkowska et al., 2017). On the other hand, LOAD is a polygenic disease, where a number of risk polymorphism and rare variants exert their functions from microglia and/or involved in immunity (Zhang et al., 2013; Huang et al., 2017; Kunkle et al., 2019). The implication of ISGs as risk factor of AD (Salih et al., 2019) together with IFN upregulation in aging brain suggest that IFN pathway may have a profound influence on AD pathogenesis (**Figure 2**).

Adult Down syndrome (DS) patients, who mostly carry trisomy 21 in their genome, unanimously develop the neuropathological changes of AD (Lott and Head, 2019). Besides amyloid precursor protein gene, four of the six IFN receptors, IFNAR1, IFNAR2, IFNGR2, and IL10RB, are encoded in the extra chromosome 21, which results in profound peripheral IFN response and autoinflammation in DS patients (Kola and Hertzog, 1997; Sullivan et al., 2016, 2017). Interestingly, mice bearing trisomy 16, which contains many orthologs from human trisomy 21, benefited from receiving antibodies blocking type I IFN (IFNα/β) and type II IFN (IFNγ) at development stage *in vivo*, whereas blocking IFNγ signaling rescued the premature death of trisomy 16 cortical neurons *in vitro* (Maroun, 1995; Hallam and Maroun, 1998; Hallam et al., 2000). By contrast, IFNγ blockade did not affect microglial activation nor synapse loss in amyloid β model (Roy et al., 2020). Since both type I and type II IFNs activate an overlapping JAK/STAT pathway to convey antiviral protection (Liu et al., 2012), these findings imply DS as a disease likely more affected by interferon activation.

In summary, we have described the IFN pathway activation, a prototypic antiviral immune response, as a major component of CNS neuroinflammatory network in AD and connected IFN response to various endogenous, pathological, infectious and genetic risk factors that have been implicated in AD pathogenesis. The discussion here is largely focused on the molecular events originated within CNS, but peripheral IFN, manifested as a result of viral infection, autoimmune condition or drug administration, nevertheless affects brain functions (Blank et al., 2016). Therefore, many important questions remain to be investigated to advance our fundamental understanding of AD more in the future.

DATA AVAILABILITY STATEMENT

The original contributions presented in the study are included in the article/supplementary material, further inquiries can be directed to the corresponding author.

AUTHOR CONTRIBUTIONS

WC formulated the concepts and wrote the manuscript. ER contributed to the manuscript writing and figure preparation. All authors contributed to the article and approved the submitted version.

FUNDING

This study was funded by the NIH grant AG057587, BrightFocus ADR, and Brown Foundation 2020 Healthy Aging Initiative to WC.

REFERENCES

Allnutt, M. A., Johnson, K., Bennett, D. A., Connor, S. M., Troncoso, J. C., Pletnikova, O., et al. (2020). Human herpesvirus 6 detection in Alzheimer's Disease cases and controls across multiple cohorts. *Neuron* 105, 1027.e2–1035.e2.

Arnusch, C. J., Branderhorst, H., de Kruijff, B., Liskamp, R. M., Breukink, E., and Pieters, R. J. (2007). Enhanced membrane pore formation by multimeric/oligomeric antimicrobial peptides. *Biochemistry* 46, 13437–13442. doi: 10.1021/bi7015553

Barrat, F. J., Elkon, K. B., and Fitzgerald, K. A. (2016). Importance of nucleic acid recognition in inflammation and autoimmunity. *Annu. Rev. Med.* 67, 323–336. doi: 10.1146/annurev-med-052814-023338

Baruch, K., Deczkowska, A., David, E., Castellano, J. M., Miller, O., Kertser, A., et al. (2014). Aging. Aging-induced type I interferon response at the choroid plexus

negatively affects brain function. *Science* 346, 89–93. doi: 10.1126/science.1252945

Blank, T., Detje, C. N., Spiess, A., Hagemeyer, N., Brendecke, S. M., Wolfart, J., et al. (2016). Brain endothelial- and epithelial-specific interferon receptor chain 1 drives virus-induced sickness behavior and cognitive impairment. *Immunity* 44, 901–912. doi: 10.1016/j.immuni.2016.04.005

Butovsky, O., and Weiner, H. L. (2018). Microglial signatures and their role in health and disease. *Nat. Rev. Neurosci.* 19, 622–635. doi: 10.1038/s41583-018-0057-5

Cairns, D. M., Rouleau, N., Parker, R. N., Walsh, K. G., Gehrke, L., and Kaplan, D. L. (2020). A 3D human brain-like tissue model of herpes-induced Alzheimer's disease. *Sci. Adv.* 6:eaay8828. doi: 10.1126/sciadv.aay8828

Capobianchi, M. R., Uleri, E., Caglioti, C., and Dolei, A. (2015). Type I IFN family members: similarity, differences and interaction. *Cytokine Growth Factor Rev.* 26, 103–111. doi: 10.1016/j.cytogfr.2014.10.011

Deczkowska, A., Matcovitch-Natan, O., Tsitsou-Kampeli, A., Ben-Hamo, S., Dvir-Szternfeld, R., Spinrad, A., et al. (2017). Mef2C restrains microglial inflammatory response and is lost in brain ageing in an IFN-I-dependent manner. *Nat. Commun.* 8:717.

DeKosky, S. T., and Scheff, S. W. (1990). Synapse loss in frontal cortex biopsies in Alzheimer's disease: correlation with cognitive severity. *Ann. Neurol.* 27, 457–464. doi: 10.1002/ana.410270502

Di Domizio, J., Dorta-Estremera, S., Gagea, M., Ganguly, D., Meller, S., Li, P., et al. (2012a). Nucleic acid-containing amyloid fibrils potently induce type I interferon and stimulate systemic autoimmunity. *Proc. Natl. Acad. Sci. U.S.A.* 109, 14550–14555. doi: 10.1073/pnas.1206923109

Di Domizio, J., Zhang, R., Stagg, L. J., Gagea, M., Zhuo, M., Ladbury, J. E., et al. (2012b). Binding with nucleic acids or glycosaminoglycans converts soluble protein oligomers to amyloid. *J. Biol. Chem.* 287, 736–747. doi: 10.1074/jbc.m111.238477

Dipasquale, O., Cooper, E. A., Tibble, J., Voon, V., Baglio, F., Baselli, G., et al. (2016). Interferon-alpha acutely impairs whole-brain functional connectivity network architecture - A preliminary study. *Brain Behav. Immun.* 58, 31–39. doi: 10.1016/j.bbi.2015.12.011

Dupuis, S., Jouanguy, E., Al-Hajjar, S., Fieschi, C., Al-Mohsen, I. Z., Al-Jumaah, S., et al. (2003). Impaired response to interferon-alpha/beta and lethal viral disease in human STAT1 deficiency. *Nat. Genet.* 33, 388–391. doi: 10.1038/ng1097

Eimer, W. A., Vijaya Kumar, D. K., Navalpur Shanmugam, N. K., Rodriguez, A. S., Mitchell, T., Washicosky, K. J., et al. (2018). Alzheimer's Disease-associated beta-amyloid is rapidly seeded by herpesviridae to protect against brain infection. *Neuron* 99, 56.e3–63.e3.

Gallo, P. M., Rapsinski, G. J., Wilson, R. P., Oppong, G. O., Sriram, U., Goulian, M., et al. (2015). Amyloid-DNA composites of bacterial biofilms stimulate autoimmunity. *Immunity* 42, 1171–1184. doi: 10.1016/j.immuni.2015.06.002

Gilden, D., Cohrs, R. J., Mahalingam, R., and Nagel, M. A. (2009). Varicella zoster virus vasculopathies: diverse clinical manifestations, laboratory features, pathogenesis, and treatment. *Lancet Neurol.* 8, 731–740. doi: 10.1016/s1474-4422(09)70134-6

Gilliet, M., Cao, W., and Liu, Y. J. (2008). Plasmacytoid dendritic cells: sensing nucleic acids in viral infection and autoimmune diseases. *Nat. Rev. Immunol.* 8, 594–606. doi: 10.1038/nri2358

Ginsberg, S. D., Crino, P. B., Hemby, S. E., Weingarten, J. A., Lee, V. M., Eberwine, J. H., et al. (1999). Predominance of neuronal mRNAs in individual Alzheimer's disease senile plaques. *Ann. Neurol.* 45, 174–181. doi: 10.1002/1531-8249(199902)45:2<174::aid-ana7>3.0.co;2-e

Ginsberg, S. D., Crino, P. B., Lee, V. M., Eberwine, J. H., and Trojanowski, J. Q. (1997). Sequestration of RNA in Alzheimer's disease neurofibrillary tangles and senile plaques. *Ann. Neurol.* 41, 200–209.

Gray, F., Scaravilli, F., Everall, I., Chretien, F., An, S., Boche, D., et al. (1996). Neuropathology of early HIV-1 infection. *Brain Pathol.* 6, 1–15. doi: 10.1007/978-1-4471-1957-9_1

Green, D. R., Ferguson, T., Zitvogel, L., and Kroemer, G. (2009). Immunogenic and tolerogenic cell death. *Nat. Rev. Immunol.* 9, 353–363. doi: 10.1038/nri2545

Hallam, D. M., Capps, N. L., Travelstead, A. L., Brewer, G. J., and Maroun, L. E. (2000). Evidence for an interferon-related inflammatory reaction in the trisomy 16 mouse brain leading to caspase-1-mediated neuronal apoptosis. *J. Neuroimmunol.* 110, 66–75. doi: 10.1016/s0165-5728(00)00289-7

Hallam, D. M., and Maroun, L. E. (1998). Anti-gamma interferon can prevent the premature death of trisomy 16 mouse cortical neurons in culture. *Neurosci. Lett.* 252, 17–20. doi: 10.1016/s0304-3940(98)00541-2

Hammond, T. R., Robinton, D., and Stevens, B. (2018). Microglia and the Brain: complementary partners in development and disease. *Annu. Rev. Cell. Dev. Biol.* 34, 523–544. doi: 10.1146/annurev-cellbio-100616-060509

Hayley, S., Scharf, J., and Anisman, H. (2013). Central administration of murine interferon-alpha induces depressive-like behavioral, brain cytokine and neurochemical alterations in mice: a mini-review and original experiments. *Brain Behav. Immun.* 31, 115–127. doi: 10.1016/j.bbi.2012.07.023

Heneka, M. T., Carson, M. J., El Khoury, J., Landreth, G. E., Brosseron, F., Feinstein, D. L., et al. (2015). Neuroinflammation in Alzheimer's disease. *Lancet Neurol.* 14, 388–405.

Hofer, M. J., and Campbell, I. L. (2013). Type I interferon in neurological disease-the devil from within. *Cytokine Growth Factor Rev.* 24, 257–267. doi: 10.1016/j.cytogfr.2013.03.006

Hong, S., Beja-Glasser, V. F., Nfonoyim, B. M., Frouin, A., Li, S., Ramakrishnan, S., et al. (2016). Complement and microglia mediate early synapse loss in Alzheimer mouse models. *Science* 352, 712–716. doi: 10.1126/science.aad8373

Huang, K. L., Marcora, E., Pimenova, A. A., Di Narzo, A. F., Kapoor, M., Jin, S. C., et al. (2017). A common haplotype lowers PU.1 expression in myeloid cells and delays onset of Alzheimer's disease. *Nat. Neurosci.* 20, 1052–1061. doi: 10.1038/nn.4587

Itzhaki, R. F. (2018). Corroboration of a major role for herpes simplex virus Type 1 in Alzheimer's Disease. *Front. Aging Neurosci.* 10:324. doi: 10.3389/fnagi.2018.00324

Itzhaki, R. F., Lathe, R., Balin, B. J., Ball, M. J., Bearer, E. L., Braak, H., et al. (2016). Microbes and Alzheimer's Disease. *J. Alzheimer's Dis.* 51, 979–984.

Itzhaki, R. F., Lin, W.-R., Shang, D., Wilcock, G. K., Faragher, B., and Jamieson, G. A. (1997). Herpes simplex virus type 1 in brain and risk of Alzheimer's disease. *Lancet* 349, 241–244. doi: 10.1016/s0140-6736(96)10149-5

Jeong, H. H., and Liu, Z. (2019). Are HHV-6A and HHV-7 really more abundant in Alzheimer's Disease? *Neuron* 104, 1034–1035. doi: 10.1016/j.neuron.2019.11.009

Kayed, R., Head, E., Thompson, J. L., McIntire, T. M., Milton, S. C., Cotman, C. W., et al. (2003). Common structure of soluble amyloid oligomers implies common mechanism of pathogenesis. *Science* 300, 486–489. doi: 10.1126/science.1079469

Kim, J.-A., Park, S.-K., Seo, S.-W., Lee, C.-H., and Shin, O. S. (2017). STING Is involved in antiviral immune response against VZV infection via the induction of Type I and III IFN pathways. *J. Invest. Dematol.* 137, 2101–2109. doi: 10.1016/j.jid.2017.03.041

Klein, R. S., Garber, C., and Howard, N. (2017). Infectious immunity in the central nervous system and brain function. *Nat. Immunol.* 18, 132–141. doi: 10.1038/ni.3656

Kola, I., and Hertzog, P. J. (1997). Animal models in the study of the biological function of genes on human chromosome 21 and their role in the pathophysiology of Down syndrome. *Hum. Mol. Genet.* 6, 1713–1727. doi: 10.1093/hmg/6.10.1713

Kumar, D. K., Choi, S. H., Washicosky, K. J., Eimer, W. A., Tucker, S., Ghofrani, J., et al. (2016). Amyloid-beta peptide protects against microbial infection in mouse and worm models of Alzheimer's disease. *Sci. Transl. Med.* 8:340ra372.

Kunkle, B. W., Grenier-Boley, B., Sims, R., Bis, J. C., Damotte, V., Naj, A. C., et al. (2019). Genetic meta-analysis of diagnosed Alzheimer's disease identifies new risk loci and implicates Abeta, tau, immunity and lipid processing. *Nat. Genet.* 51, 414–430.

Lande, R., Gregorio, J., Facchinetti, V., Chatterjee, B., Wang, Y. H., Homey, B., et al. (2007). Plasmacytoid dendritic cells sense self-DNA coupled with antimicrobial peptide. *Nature* 449, 564–569.

Li, Q., and Barres, B. A. (2018). Microglia and macrophages in brain homeostasis and disease. *Nat. Rev. Immunol.* 18, 225–242. doi: 10.1038/nri.2017.125

Liu, S. Y., Sanchez, D. J., Aliyari, R., Lu, S., and Cheng, G. (2012). Systematic identification of type I and type II interferon-induced antiviral factors. *Proc. Natl. Acad. Sci. U.S.A.* 109, 4239–4244. doi: 10.1073/pnas.1114981109

Lott, I. T., and Head, E. (2019). Dementia in down syndrome: unique insights for Alzheimer disease research. *Nat. Rev. Neurol.* 15, 135–147. doi: 10.1038/s41582-018-0132-6

Maroun, L. E. (1995). Anti-interferon immunoglobulins can improve the trisomy 16 mouse phenotype. *Teratology* 51, 329–335. doi: 10.1002/tera.1420510509

McNab, F., Mayer-Barber, K., Sher, A., Wack, A., and O'Garra, A. (2015). Type I interferons in infectious disease. *Nat. Rev. Immunol.* 15, 87–103. doi: 10.1038/nri3787

Minter, M. R., Moore, Z., Zhang, M., Brody, K. M., Jones, N. C., Shultz, S. R., et al. (2016). Deletion of the type-1 interferon receptor in APPSWE/PS1DeltaE9 mice preserves cognitive function and alters glial phenotype. *Acta Neuropathol. Commun.* 4:72.

Monasor, L. S., Muller, S. A., Colombo, A. V., Tanrioever, G., Konig, J., Roth, S., et al. (2020). Fibrillar Abeta triggers microglial proteome alterations and dysfunction in Alzheimer mouse models. *eLife* 9:e54083. doi: 10.7554/eLife.54083

Morgan, B. P. (2018). Complement in the pathogenesis of Alzheimer's disease. *Semin. Immunopathol.* 40, 113–124.

Nallar, S. C., and Kalvakolanu, D. V. (2014). Interferons, signal transduction pathways, and the central nervous system. *J. Interferon Cytokine Res.* 34, 559–576. doi: 10.1089/jir.2014.0021

Paul, S., Ricour, C., Sommereyns, C., Sorgeloos, F., and Michiels, T. (2007). Type I interferon response in the central nervous system. *Biochimie* 89, 770–778. doi: 10.1016/j.biochi.2007.02.009

Prinz, M., Jung, S., and Priller, J. (2019). Microglia biology: one century of evolving concepts. *Cell* 179, 292–311. doi: 10.1016/j.cell.2019.08.053

Ransohoff, R. M. (2016). How neuroinflammation contributes to neurodegeneration. *Science* 353, 777–783. doi: 10.1126/science.aag2590

Readhead, B., Haure-Mirande, J. V., Funk, C. C., Richards, M. A., Shannon, P., Haroutunian, V., et al. (2018). Multiscale analysis of independent Alzheimer's Cohorts finds disruption of molecular, genetic, and clinical networks by human herpesvirus. *Neuron* 99, 64.e7–82.e7.

Reinert, L. S., Lopusna, K., Winther, H., Sun, C., Thomsen, M. K., Nandakumar, R., et al. (2016). Sensing of HSV-1 by the cGAS-STING pathway in microglia orchestrates antiviral defence in the CNS. *Nat. Commun.* 7:13348.

Rodero, M. P., and Crow, Y. J. (2016). Type I interferon-mediated monogenic autoinflammation: the type I interferonopathies, a conceptual overview. *J. Exp. Med.* 213, 2527–2538. doi: 10.1084/jem.20161596

Roy, E. R., Wang, B., Wan, Y. W., Chiu, G., Cole, A., Yin, Z., et al. (2020). Type I interferon response drives neuroinflammation and synapse loss in Alzheimer disease. *J. Clin. Invest.* 130, 1912–1930. doi: 10.1172/jci133737

Salih, D. A., Bayram, S., Guelfi, S., Reynolds, R. H., Shoai, M., Ryten, M., et al. (2019). Genetic variability in response to amyloid beta deposition influences Alzheimer's disease risk. *Brain Commun.* 1:fcz022.

Sayed, F. A., Kodama, L., Udeochu, J. C., Fan, L., Carling, G. K., Le, D., et al. (2020). AD-linked R47H-TREM2 mutation induces disease-enhancing proinflammatory microglial states in mice and humans. *bioRxiv* [Preprint]. doi: 10.1101/2020.07.24.218719

Scheff, S. W., DeKosky, S. T., and Price, D. A. (1990). Quantitative assessment of cortical synaptic density in Alzheimer's disease. *Neurobiol. Aging* 11, 29–37. doi: 10.1016/0197-4580(90)90059-9

Schreiber, G., and Piehler, J. (2015). The molecular basis for functional plasticity in type I interferon signaling. *Trends Immunol.* 36, 139–149. doi: 10.1016/j.it.2015.01.002

Schwabenland, M., Mossad, O., Peres, A. G., Kessler, F., Maron, F. J. M., Harsan, L. A., et al. (2019). Loss of USP18 in microglia induces white matter pathology. *Acta Neuropathol. Commun.* 7:106.

Soscia, S. J., Kirby, J. E., Washicosky, K. J., Tucker, S. M., Ingelsson, M., Hyman, B., et al. (2010). The Alzheimer's disease-associated amyloid beta-protein is an antimicrobial peptide. *PLoS One* 5:e9505. doi: 10.1371/journal.pone.0009505

Sullivan, K. D., Evans, D., Pandey, A., Hraha, T. H., Smith, K. P., Markham, N., et al. (2017). Trisomy 21 causes changes in the circulating proteome indicative of chronic autoinflammation. *Sci. Rep.* 7:14818.

Sullivan, K. D., Lewis, H. C., Hill, A. A., Pandey, A., Jackson, L. P., Cabral, J. M., et al. (2016). Trisomy 21 consistently activates the interferon response. *eLife* 5:e16220.

Swanson, P. A., and McGavern, D. B. (2015). Viral diseases of the central nervous system. *Curr. Opin. Virol.* 11, 44–54.

Tenner, A. J., Stevens, B., and Woodruff, T. M. (2018). New tricks for an ancient system: physiological and pathological roles of complement in the CNS. *Mol. Immunol.* 102, 3–13. doi: 10.1016/j.molimm.2018.06.264

Terry, R. D., Masliah, E., Salmon, D. P., Butters, N., DeTeresa, R., Hill, R., et al. (1991). Physical basis of cognitive alterations in Alzheimer's disease: synapse loss is the major correlate of cognitive impairment. *Ann. Neurol.* 30, 572–580. doi: 10.1002/ana.410300410

Vasek, M. J., Garber, C., Dorsey, D., Durrant, D. M., Bollman, B., Soung, A., et al. (2016). A complement-microglial axis drives synapse loss during virus-induced memory impairment. *Nature* 534, 538–543. doi: 10.1038/nature18283

Wachholz, S., Esslinger, M., Plumper, J., Manitz, M. P., Juckel, G., and Friebe, A. (2016). Microglia activation is associated with IFN-alpha induced depressive-like behavior. *Brain Behav. Immun.* 55, 105–113. doi: 10.1016/j.bbi.2015.09.016

Wang, S., and Colonna, M. (2019). Microglia in Alzheimer's disease: a target for immunotherapy. *J. Leukoc Biol.* 106, 219–227.

Wu, T., Dejanovic, B., Gandham, V. D., Gogineni, A., Edmonds, R., Schauer, S., et al. (2019). Complement C3 is activated in human AD brain and is required for neurodegeneration in mouse models of amyloidosis and tauopathy. *Cell Rep.* 28, 2111.e6–2123.e6.

Xhindoli, D., Pacor, S., Guida, F., Antcheva, N., and Tossi, A. (2014). Native oligomerization determines the mode of action and biological activities of human cathelicidin LL-37. *Biochem. J.* 457, 263–275. doi: 10.1042/bj20131048

Yamada, T., Horisberger, M. A., Kawaguchi, N., Moroo, I., and Toyoda, T. (1994). Immunohistochemistry using antibodies to α-interferon and its induced protein, MxA, in Alzheimer's and Parkinson's disease brain tissues. *Neurosci. Lett.* 181, 61–64. doi: 10.1016/0304-3940(94)90560-6

Zhang, B., Gaiteri, C., Bodea, L. G., Wang, Z., McElwee, J., Podtelezhnikov, A. A., et al. (2013). Integrated systems approach identifies genetic nodes and networks in late-onset Alzheimer's disease. *Cell* 153, 707–720.

Conflict of Interest: The authors declare that the research was conducted in the absence of any commercial or financial relationships that could be construed as a potential conflict of interest.

frontiers in Neuroscience

ORIGINAL RESEARCH
published: 03 December 2020
doi: 10.3389/fnins.2020.587986

Dynamic Changes in the Gut Microbiome at the Acute Stage of Ischemic Stroke in a Pig Model

*Julie Jeon[1†], Jeferson Lourenco[2†], Erin E. Kaiser[2,3,4], Elizabeth S. Waters[2,3,4], Kelly M. Scheulin[2,3,4], Xi Fang[1], Holly A. Kinder[2,3,4], Simon R. Platt[3,5], Michael J. Rothrock Jr.[6], Todd R. Callaway[2], Franklin D. West[2,3,4] and Hea Jin Park[1]**

[1] Department of Foods and Nutrition, College of Family and Consumer Sciences, University of Georgia, Athens, GA, United States, [2] Department of Animal and Dairy Sciences, College of Agricultural and Environmental Sciences, University of Georgia, Athens, GA, United States, [3] Regenerative Bioscience Center, University of Georgia, Athens, GA, United States, [4] Neuroscience Program, Biomedical and Health Sciences Institute, University of Georgia, Athens, GA, United States, [5] Department of Small Animal Medicine and Surgery, University of Georgia, Athens, GA, United States, [6] Egg Safety and Quality Research Unit, U.S. National Poultry Research Center, USDA-ARS, Athens, GA, United States

OPEN ACCESS

Edited by:
Deng-Feng Zhang, Kunming Institute of Zoology, Chinese Academy of Sciences, China

Reviewed by:
Hongwei Zhou, Southern Medical University, China
Peiying Li, Shanghai Jiao Tong University School of Medicine, China

***Correspondence:**
Hea Jin Park
hjpark@uga.edu

[†]These authors have contributed equally to this work

Specialty section:
This article was submitted to Neurodegeneration, a section of the journal Frontiers in Neuroscience

Received: *27 July 2020*
Accepted: *02 November 2020*
Published: *03 December 2020*

Citation:
Jeon J, Lourenco J, Kaiser EE, Waters ES, Scheulin KM, Fang X, Kinder HA, Platt SR, Rothrock MJ Jr, Callaway TR, West FD and Park HJ (2020) Dynamic Changes in the Gut Microbiome at the Acute Stage of Ischemic Stroke in a Pig Model. Front. Neurosci. 14:587986. doi: 10.3389/fnins.2020.587986

Stroke is a major cause of death and long-term disability affecting seven million adults in the United States each year. Recently, it has been demonstrated that neurological diseases, associated pathology, and susceptibility changes correlated with changes in the gut microbiota. However, changes in the microbial community in stroke has not been well characterized. The acute stage of stroke is a critical period for assessing injury severity, therapeutic intervention, and clinical prognosis. We investigated the changes in the gut microbiota composition and diversity using a middle cerebral artery (MCA) occlusion ischemic stroke pig model. Ischemic stroke was induced by cauterization of the MCA in pigs. Blood samples were collected prestroke and 4 h, 12 h, 1 day, and 5 days poststroke to evaluate circulating proinflammatory cytokines. Fecal samples were collected prestroke and 1, 3, and 5 days poststroke to assess gut microbiome changes. Results showed elevated systemic inflammation with increased plasma levels of tumor necrosis factor alpha at 4 h and interleukin-6 at 12 h poststroke, relative to prestroke. Microbial diversity and evenness were reduced at 1 day poststroke compared to prestroke. Microbial diversity at 3 days poststroke was negatively correlated with lesion volume. Moreover, beta-diversity analysis revealed trending overall differences over time, with the most significant changes in microbial patterns observed between prestroke and 3 days poststroke. Abundance of the Proteobacteria was significantly increased, while Firmicutes decreased at 3 days poststroke, compared to prestroke populations. Abundance of the lactic acid bacteria *Lactobacillus* was reduced at 3 days poststroke. By day 5, the microbial pattern returned to similar values as prestroke, suggesting the plasticity of gut microbiome in an acute period of stroke in a pig model. These findings provide a basis for characterizing gut microbial changes during the acute stage of stroke, which can be used to assess stroke pathology and the potential development of therapeutic targets.

Keywords: MCAO, swine model, microbial diversity, inflammation, acute stroke

INTRODUCTION

An estimated seven million adults in the United States suffer from stroke each year, making it the fifth leading cause of death and the first leading cause of long-term disability (Benjamin et al., 2019). The immune response and inflammation are major stroke components effecting severity, as they can significantly exacerbate the primary stroke injury and cause further cell death in the brain (Deb et al., 2010; Borgens and Liu-Snyder, 2012). High levels of systemic inflammation are closely associated with poor stroke outcomes in stroke animal models and patients (Di Napoli et al., 2001; Audebert Heinrich et al., 2004; Elkind et al., 2004; McColl et al., 2007, 2008). Interestingly, it has recently been demonstrated that the gut microbiome changes in response to stroke (Swidsinski et al., 2012; Yin et al., 2015; Durgan et al., 2019) and that modulating the gut microbiome can alter the poststroke inflammatory response, leading to improved recovery in rodent models (Benakis et al., 2016; Singh et al., 2016; Yamashiro et al., 2017; Spychala et al., 2018). Few studies have assessed the changes in the microbial populations during the acute stage of stroke, making it critically important to better characterize these microbial alterations to identify potential biomarkers for injury severity, recovery, and therapeutic targets.

It has been demonstrated that adjustments in the gut microbiome influence ischemic brain injury by altering immune homeostasis (Benakis et al., 2016; Singh et al., 2016) and neuroprotective cytokine production (Benakis et al., 2016). This suggests that the gut microbiome is another potential therapeutic target for stroke (Benakis et al., 2016; Singh et al., 2016, 2018; Winek et al., 2016; Benakis et al., 2020). Studies of gut microbiome changes in stroke have demonstrated decreases in both commensal and beneficial genera, increases in pathogenic genera in human patients (Swidsinski et al., 2012; Yin et al., 2015), and substantial changes in the phylum Firmicutes, Bacteroidetes, and Actinobacteria in stroke mice (Singh et al., 2016). Imbalances of the intestinal microbiota can lead to gut barrier dysfunction and impairment of stroke outcomes. In a mouse middle cerebral artery occlusion (MCAO) ischemic stroke model, the stroke mouse exhibited an imbalance in microbial communities, resulting in a reduction in intestinal motility and increased protein leakage in the gut (Singh et al., 2016). These changes correlated with increased brain invasion of proinflammatory T cells from the gut and significantly increased brain infarction (Benakis et al., 2016). These findings in a rodent stroke model indicate that the gut microbiome is drastically affected by stroke and plays a pivotal role in stroke severity. However, recent failures to translate findings in rodent stroke models have led to the desire to study stroke pathophysiology and therapeutic targets in more translational large animal models such as the pig (Fisher et al., 2009; Saver et al., 2009; Albers et al., 2011).

Pigs are a robust translational animal model for biomedical research, especially gut and brain research, due to the myriad of similarities to humans in physiology, anatomy, pathology, and eating behavior (Watanabe et al., 2001; Lind et al., 2007; Swindle et al., 2012; Kaiser and West, 2020). They are omnivorous and have similar intestinal size and length in proportion to humans, contributing comparable transit time to humans (Clouard et al., 2012; Heinritz et al., 2013). The gut bacterial diversity of pigs are similar to that of humans showing higher richness and lower evenness than other animals (Lamendella et al., 2011), and 96% of the functional genes found in the human gut metagenome was present in the pig gut metagenome (Xiao et al., 2016), suggesting that the complexity of the pig microbiota is comparable to that of humans. Moreover, pigs have similar brain size, gray and white matter composition, and cytoarchitecture having a gyrencephalic brain like humans and unlike rodents (Baker et al., 2017). These similarities in the brain are predicted to lead to more human-like stroke pathology in the brain and brain–gut interactions. Due to gut homology between humans and pigs, a number of experiments have been conducted in pigs to study the interplay between the gut microbiome and the immune system (Foster et al., 2003; Scharek et al., 2005; Wilson et al., 2005; Zhang et al., 2013), yet never in a stroke pig.

In the current study, we investigated the changes in gut microbial diversity and composition in a MCAO stroke pig model developed by our research team (Duberstein et al., 2014; Platt et al., 2014; Baker et al., 2017). The results of this study conducted in a translational large animal model will help characterize patterns of bacterial changes during the acute stage of stroke, potentially providing future insight into stroke severity, recovery, and therapeutic targets.

MATERIALS AND METHODS

Stroke Induction and Confirmation Utilizing Magnetic Resonance Imaging

All experimental procedures were approved by the University of Georgia Institutional Animal Care and Use Committee, and the study was conducted in accordance with the recommendations of the NIH's guide for the Use and Care of Laboratory Animals (AUP approval number: A2017 07-019-Y2-A16). Seven castrated male Landrace pigs (5–6 months old, 48–56 kg) were individually housed in a room in which the temperature was kept at 27°C, with a 12-h light/dark cycle.

Ischemic stroke was induced in pigs by middle cerebral artery occlusion (MCAO) as previously described (Duberstein et al., 2014; Platt et al., 2014; Baker et al., 2017). Briefly, pigs were administered Excede [5 mg/kg intramuscularly and fentanyl patch (100 mcg/h transdermally)] 1 day prior to the stroke surgery to prevent infections and to manage pain. Midazolam (0.2 mg/kg) and xylazine (2 mg/kg) were administered intramuscularly for presurgery analgesia and sedation. For anesthesia, propofol was injected intravenously, and prophylactic lidocaine (1.0 ml of 2% lidocaine) was administered locally to the laryngeal folds to facilitate intubation. Anesthesia was maintained with 1.5% isoflurane in oxygen.

A curvilinear incision began from the superior right orbit and extended to the rostral aspect of the auricle. The temporalis muscle was retracted, and a craniectomy was performed at the exposed local dura mater. The middle cerebral artery located at the distal part of the Circle of Willis was permanently occluded using a bipolar electrocautery forceps. After postoperative recovery, pigs were returned to their respective pens and

monitored every 4 h. To reduce postoperative pain and fever, Banamine (2.2 mg/kg intramuscularly) was administered every 12 h for the first 24 h and every 24 h for the following 3 days poststroke.

Magnetic resonance imaging (MRI) was conducted 1 day poststroke using a General Electric 3.0 T MRI system to confirm ischemic stroke. Pigs were anesthetized using the aforementioned anesthesia protocol and placed in a supine position using an 8-channel torso coil. T2 fluid-attenuated inversion recovery (T2-FLAIR) and diffusion-weighted imaging (DWI) sequences were used in conjunction with apparent diffusion coefficient (ADC) maps to confirm the presence of ischemic lesions.

Blood Collection and Proinflammatory Cytokine Analysis

Peripheral blood was collected prestroke and 4 h, 12 h, 1 day, and 5 days poststroke, and plasma was separated and stored at −80°C. Circulating tumor necrosis factor alpha (TNF-α) and interleukin-6 (IL-6) were quantified by ELISAs (R&D systems, Minneapolis, MN, United States) to determine changes in inflammatory response.

Fecal Collection and Microbial DNA Extraction

Fecal samples were collected prestroke and 1, 3, and 5 days poststroke. Samples were obtained directly from the rectum using sterilized plastic fecal loops (5 cm within the rectum). To prevent any contamination during fecal collection, all materials were sterilized prior to sample collection. Pig anus was stimulated with a sterilized loop for defecation, and the stool was collected into a sterilized sample tube without any contact to the floor or body. The fecal samples were immediately frozen on dry ice and stored at −80°C until further analysis.

Bacterial DNA was extracted from fecal samples using a previously validated approach described by RothrockJr., Hiett et al. (2014). In this method, 330 mg of fecal material is subjected to a combination of mechanical and enzymatic processes using a modified version of the FastDNA Spin Kit for Feces (MP Biomedicals, Solon, OH, United States) and the QIAamp DNA Stool Mini Kit (QIAGEN, Valencia, CA, United States). DNA purification was carried out using the DNA Stool–Human Stool–Pathogen Detection Protocol of the QIAcube Robotic Workstation. Following purification, DNA concentrations were determined spectrophotometrically (Synergy H4 Hybrid Multimode Microplate Reader; BioTek, Winooski, VT, United States).

16S rRNA Gene Sequencing and Analysis

The extracted DNA samples were sent to the Georgia Genomics and Bioinformatics Core[1] to sequence the 16s ribosomal RNA (rRNA) gene. The V3–V4 region was amplified using the S-D-Bact-0341-b-S-17 (5′-CCTACGGGNGGCWGCAG-3′) and S-D-Bact-0785-a-A-21 (5′-GACTACHVGGGTATCTAATCC-3′) primer pair (Klindworth et al., 2013). Samples were sequenced using an Illumina MiSeq platform (Illumina, San Diego, CA, United States). Sequencing data were provided as FASTQ files, which were merged and converted into FASTA files, and further analyzed using the QIIME pipeline v1.9.1 (Caporaso et al., 2010). Sequences were clustered as operational taxonomic units (OTUs) at 97% similarity, and representative sequences were aligned to the Greengenes database (gg_13_8_otus). Singleton OTUs and OTUs whose representative sequences could not be aligned were excluded from the analysis. The computed alpha-diversity indexes are as follows: number of observed OTUs, Shannon index, and evenness. Beta-diversity was computed using the weighted UniFrac distance matrix. This metric was chosen because it accounts for the phylogenetic relationship when calculating beta-diversity.

[1]https://dna.uga.edu/

Statistical Analysis

Data were analyzed using GraphPad Prism (Version 8.1.1; GraphPad Software, Inc., San Diego, CA, United States) and are shown as mean ± SEM. Paired *t*-tests were used to measure the contrasts between pre- and poststroke time points. Differences in beta-diversity were accessed by two-sample *t*-tests between each individual time point, and the non-parametric *P*-values generated by the Bonferroni's multiple comparisons test were used for inferences. Regression analysis was performed to evaluate associations between microbiome changes and stroke severity. For all statistical tests, $P \leq 0.05$ were considered significant, and trends were declared when $0.05 < P < 0.10$.

RESULTS

Magnetic Resonance Imaging Confirmed Ischemic Lesions 1 Day Poststroke

Non-invasive MRI allows for real-time, longitudinal assessment of stroke pathophysiology and is a critical clinical tool commonly used to differentiate between stroke type and severity (González, 2012; Baker et al., 2017). We confirmed ischemic stroke 1 day poststroke in all animals in the study. Both T2-FLAIR and DWI sequences showed edematous lesions with bright hyperintense signal (**Figures 1A,B**), whereas ADC maps exhibited cytotoxic edema with dark hypointense regions due to restricted water diffusion (**Figure 1C**). Lesion volume, midline shift, and hemorrhage volume of the same cohort of pigs have been recently published (Kaiser et al., 2020). In brief, DWI sequences showed territorial hyperintense lesions at 1 day poststroke with an average volume of 9.9 ± 1.4 cm^3. Analysis of T2-weighted (T2W) sequences revealed a significant ($P < 0.01$) increase in ipsilateral hemisphere volume indicative of cerebral swelling when compared to the contralateral hemisphere (26.0 ± 1.8 cm^3 vs. 22.5 ± 1.4 cm^3, respectively) and an associated midline shift of 2.5 ± 0.6 mm. Acute intracerebral hemorrhage was observed via T2Star sequences with a mean hemorrhage volume of 1.7 ± 0.1 cm^3. Collectively, MRI results demonstrated that MCAO led to tissue-level damage including ischemic infarction, hemispheric swelling, pronounced midline shift, and intracerebral hemorrhage (Kaiser et al., 2020).

Circulating TNF-α and IL-6 Levels Were Increased During the Acute Stage of Stroke in a MCAO Pig Model

Elevated systemic inflammation has been associated with gut microbiome dysbiosis and correlated with increased brain infarction (McColl et al., 2007, 2008). Elevated systemic inflammation results in poor clinical outcomes and increased mortality in stroke patients (Di Napoli et al., 2001; Elkind et al., 2004), making it a key biomarker in stroke (Di Napoli and Papa, 2006). In MCAO pigs, plasma TNF-α was increased ∼28% at 4 h poststroke relative to prestroke levels (79.75 ± 6.00 pg/ml vs. 61.62 ± 6.38 pg/ml, respectively, $P = 0.003$, **Figure 2A**). Comparatively, TNF-α levels rapidly dropped following this peak and reached the lowest level at 1 day poststroke (43.75 ± 4.38 pg/ml, $P = 0.003$). TNF-α levels returned to prestroke levels by 5 days poststroke (53.36 ± 5.57 pg/ml). Similar to TNF-α, plasma IL-6 levels were significantly increased ∼20% at 12 h poststroke compared to prestroke (52.46 ± 2.44 pg/ml vs. 44.01 ± 0.85 pg/ml, respectively, $P = 0.01$) and returned to prestroke levels by 5 days poststroke (44.94 ± 1.07 pg/ml, **Figure 2B**), confirming an elevated inflammatory response during the acute stage of stroke in the pig model.

Diversity of Fecal Microbiota Was Altered During the Acute Stage of Ischemic Stroke

Changes in diversity of gut microbiome are often an indicator of dysbiosis associated with disease pathology (Kriss et al., 2018). In MCAO pigs, microbial diversity and evenness were altered during the acute stage of stroke as shown in **Table 1**. The Shannon and evenness indices were reduced ($P \leq 0.05$) at 1 day poststroke compared to prestroke but returned to prestroke levels at 3 days poststroke. However, the number of observed OTUs, which is an estimator of microbial richness, was not significantly affected ($P \geq 0.21$) during the course of the study. Consequently, poststroke values were not significantly different from prestroke values (**Table 1**).

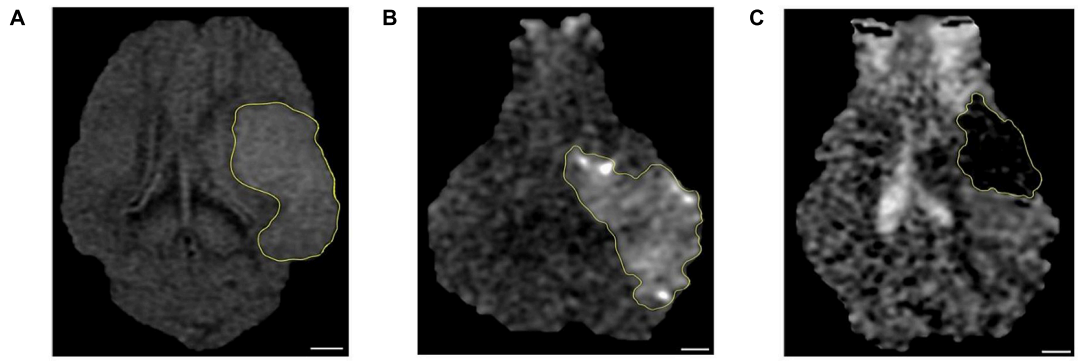

FIGURE 1 | Magnetic resonance imaging (MRI) confirmed ischemic stroke in pigs. The hyperintense regions seen in **(A)** T2 fluid-attenuated inversion recovery (T2-FLAIR) and **(B)** diffusion-weighted imaging (DWI) sequences corresponded to **(C)** apparent diffusion coefficient (ADC) map hypointense regions thus confirming the presence of ischemic infarction 1 day post-middle cerebral artery occlusion (post-MCAO) surgery ($n = 7$). A scale bar is provided in each picture (6 mm), and the lesion area was outlined by yellow line.

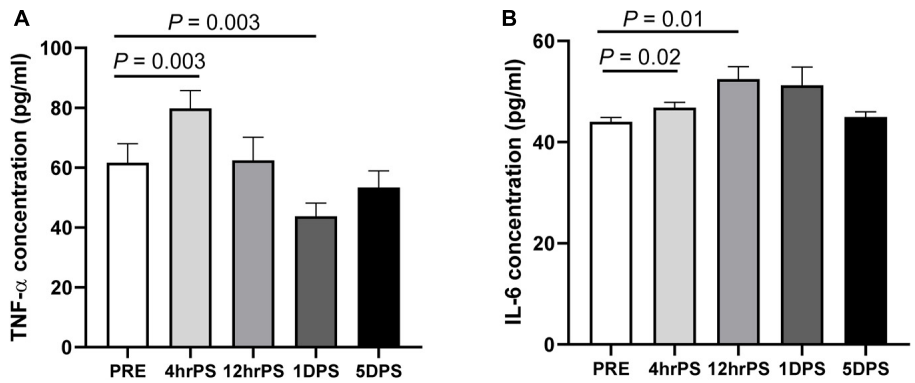

FIGURE 2 | Plasma concentrations of proinflammatory cytokines were increased during the acute stage of ischemic stroke in pigs. Plasma concentration (pg/ml) of **(A)** tumor necrosis factor alpha (TNF-α) and **(B)** interleukin-6 (IL-6) were measured prestroke (PRE, $n = 7$), 4 h poststroke (4 hrPS, $n = 7$ and 6, respectively), 12 h poststroke (12 hrPS, $n = 7$), 1 day poststroke (1DPS, $n = 7$), and 5 days poststroke (5DPS, $n = 5$). *P*-value: paired *t*-test comparing the mean prestroke values vs. each time point poststroke.

TABLE 1 | Alpha-diversity was changed during the acute stage of ischemic stroke in a pig model.

Alpha-diversity indices		Prestroke (n = 7)	Poststroke		
			1 day (n = 7)	3 days (n = 6)	5 days (n = 4)
Number of observed OTUs	Mean	7,110	5,824	6,140	5,744
	SEM	1,130	407	222	344
	P-value	–	NS	NS	NS
Shannon	Mean	8.14	7.46	7.92	7.93
	SEM	0.40	0.27	0.18	0.31
	P-value	–	0.05	NS	NS
Evenness	Mean	0.638	0.596	0.630	0.635
	SEM	0.022	0.017	0.013	0.022
	P-value	–	0.02	NS	NS

P-value, paired t-test comparing the mean prestroke values vs. each time point poststroke. SEM, standard error of mean; NS, not significant, P > 0.05.

To further investigate the association between the dysbiosis and stroke severity, the correlations between microbial diversity and MRI results were assessed. The correlative analysis indicated that Shannon (r = −0.9715, P = 0.0012), Evenness (r = −0.9395, P = 0.0054), and Chao 1 (r = −0.8902, P = 0.0174) at day 3 poststroke was negatively associated with lesion volume measured by a high resolution of MRI (**Figure 3**), suggesting the lower microbial diversity poststroke was related to increased stroke severity at the acute stage of stroke.

Beta-diversity was assessed using the weighted UniFrac distance matrix to investigate the similarity of microbial patterns among groups. There was a trend (P = 0.07) for overall differences across all time points (**Figure 4**). The most distinct separation in the UniFrac distance was observed between 3 days post- and prestroke (**Figure 4C**). Taken together, the alpha-diversity was decreased at 1 day poststroke, and beta-diversity was most distinctly different 3 days poststroke compared to prestroke.

Stroke Altered Fecal Microbiome Composition

The composition changes in gut microbiota were evaluated at different taxonomic levels (phylum, family, and genus) during the acute stage of ischemic stroke (**Figures 5–7**). The most prevalent phyla prestroke were Firmicutes (89.94 ± 1.65%), followed by Bacteroidetes (3.45 ± 1.02%), Actinobacteria (1.83 ± 0.70%), and Proteobacteria (1.13 ± 0.65%, **Figure 5**). The composition of these four major phyla changed during the acute stage of stroke. At 3 days poststroke, the abundance of Firmicutes was decreased by 27% (66.08 ± 7.35% vs. 89.94 ± 1.65%, P = 0.01), while Proteobacteria significantly increased 19-fold relative to prestroke levels (20.96 ± 5.50% vs. 1.13 ± 0.65%, P = 0.01). At 5 days poststroke, both phyla returned to prestroke levels (Firmicutes, 86.86 ± 3.70% and Proteobacteria, 0.68 ± 0.19%). Similar to Proteobacteria, Actinobacteria reached their highest abundance 3 days poststroke (3.78 ± 0.85% vs. 1.83 ± 0.70%, P = 0.02 compared to prestroke) and showed comparable levels to prestroke at 5 days poststroke (2.20 ± 0.93%). The second most abundant phylum at prestroke, Bacteroidetes, tended to increase 3 days poststroke (7.63 ± 1.53% vs. 3.45 ± 1.02%, P = 0.06) compared to prestroke and remained consistent at 5 days poststroke (7.13 ± 2.58%, **Figure 5B**). The ratio of Firmicutes to Bacteroidetes was decreased ∼60% at 1 day poststroke compared to that of prestroke (17.33 ± 4.69% vs. 43.18 ± 12.59%, P = 0.04, **Figure 5C**) and returned to the levels observed prestroke at 3 days poststroke and remained stable, suggesting a significant microbial shift occurred at the acute stage of stroke. Other significant changes in bacterial phyla were observed in bacteria with relatively low abundance, including TM7, Cyanobacteria, and Fusobacteria, yet their abundance remained below 0.15% during the entire study (**Figure 5B**).

Consistent with phyla changes, a significant change in abundance was observed at the family level 3 days poststroke (**Figure 6**). The most abundant family prestroke was *Lactobacillaceae*, making up 33.13 ± 5.66% of the population. However, the population rapidly dropped to 10.63 ± 2.67% 3 days poststroke (P < 0.001) and increased to 20.19 ± 10.98% 5 days poststroke. The abundance of *Enterobacteriaceae*, *Erysipelotrichaceae*, *Prevotellaceae*,

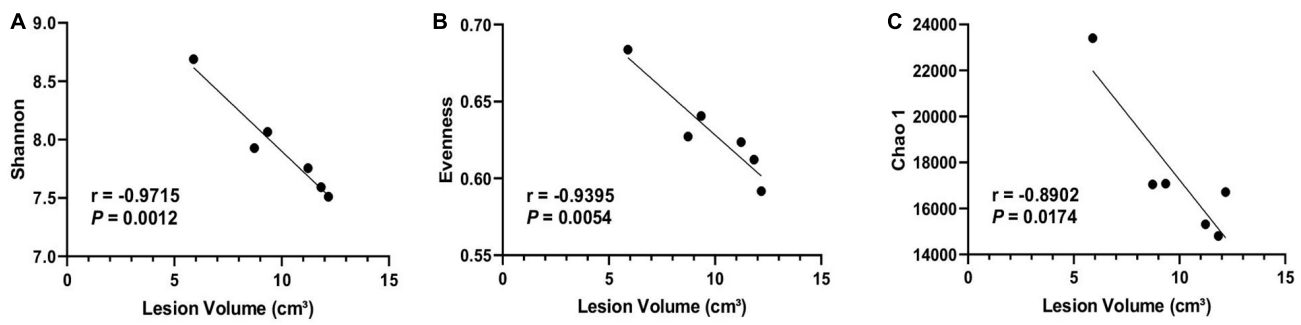

FIGURE 3 | Microbial diversity was negatively correlated with brain lesion volume. Brain lesion volume measured 1 day poststroke was negatively correlated with alpha-diversity indices including **(A)** Shannon, **(B)** Evenness, and **(C)** Chao1 at 3 days poststroke (n = 6). Regression analysis was performed to evaluate associations between microbial composition and stroke severity. Pearson correlation coefficient and *P*-values are shown.

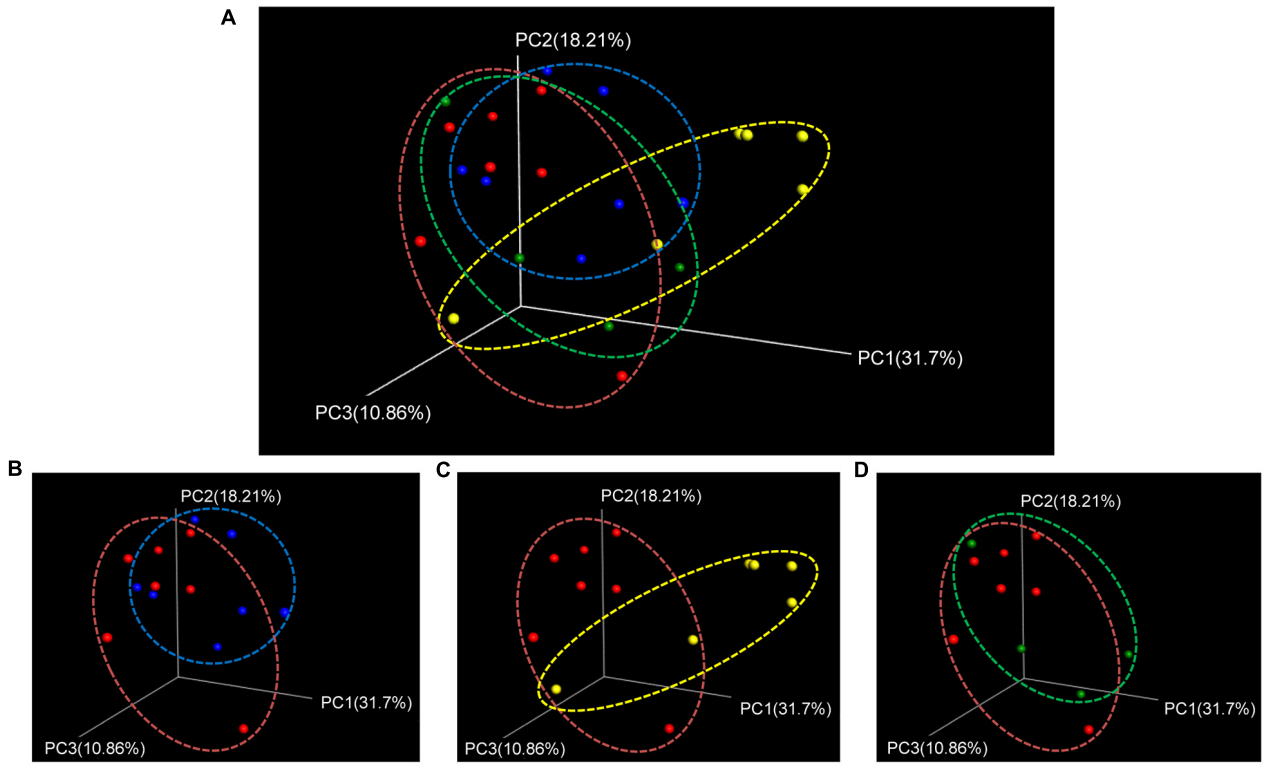

FIGURE 4 | Beta-diversity (weighted UniFrac PCoA plots) showed trending differences between pre- and poststroke in middle cerebral artery occlusion (MCAO) pig model. **(A)** Beta-diversity changes during the acute stage of stroke were shown by PCoA plots. Different bacterial communities were compared between **(B)** prestroke (n = 7) vs. 1 day poststroke (n = 7), **(C)** prestroke vs. 3 days poststroke (n = 6), and **(D)** prestroke vs. 5 days poststroke (n = 4). Trending differences were observed between prestroke and 3 days poststroke (non-parametric P-values generated by the Bonferroni's multiple comparisons test were used for inferences).

Coriobacteriaceae, *Desulfovibrionaceae*, *Peptostreptococcaceae*, and *Enterococcaceae* were increased up to 3 days poststroke and returned to prestroke levels at 5 days poststroke (**Figure 6**). **Supplementary Figures 1**, **2** show changes in the gut microbiome detected at the class and order levels, respectively.

Four bacterial genera were identified with relatively high abundance (>1%): *Lactobacillus*, *Prevotella*, *Parabacteroides*, and *Collinsella* (**Figure 7**). *Lactobacillus* had the greatest average abundance prestroke (33.13 ± 5.66%), and its presence reached the lowest point (10.63 ± 2.67%, $P < 0.001$) 3 days poststroke; however, it tended to return to prestroke levels at 5 days poststroke (20.19 ± 10.98%). Contrary to what was observed for *Lactobacillus*, the abundance of *Collinsella* (2.11 ± 0.59% vs. 0.79 ± 0.38%) and *Prevotella* (3.17 ± 0.81% vs. 0.84 ± 0.31%) were increased three to four times 3 days poststroke compared to prestroke levels ($P \leq 0.03$). *Parabacteroides* was significantly increased at 1 day poststroke (0.48 ± 0.18%) compared to prestroke (0.08 ± 0.05%). **Supplementary Figure 3** shows the 18 bacterial genera that were significantly altered during the acute stage of stroke in MCAO pigs. Stroke altered microbiota composition in MCAO pigs, with the majority of changes occurring 3 days poststroke as observed at the phylum, family, and genus levels.

Regression analysis conducted to better understand the changes in microbial composition between prestroke and 3 days poststroke and stroke severity at the acute stage of stroke indicates that changes in abundance of phylum Bacteroidetes, Proteobacteria, and Fusobacteria were positively correlated with lesion volume, MLS, and hemorrhage volume, while Firmicutes was negatively correlated with the stroke severity (**Table 2**). Moreover, changes in abundance of *Lactobacillaceae* and *Lactobacillus* were negatively related to the stroke severity (**Table 2**), supporting that the changes in microbial composition at the acute stage of stroke is closely related to stroke severity.

DISCUSSION

In this study, we investigated alterations in microbial composition during the acute stroke phase in a MCAO pig ischemic stroke model. The fecal microbiome was dynamically changed during this stage, as follows: (1) stroke reduced species diversity and evenness 1 day poststroke and changed bacterial community patterns (beta-diversity) among groups 3 days poststroke; (2) the ratio of Firmicutes to Bacteroidetes was decreased 1 day poststroke; (3) high abundance of Proteobacteria and low abundance of the genus *Lactobacillus* were observed 3 days poststroke. These results showed a dynamic compositional change in bacteria following a stroke event, particularly 3 days poststroke, and that this was transient with most microbiome

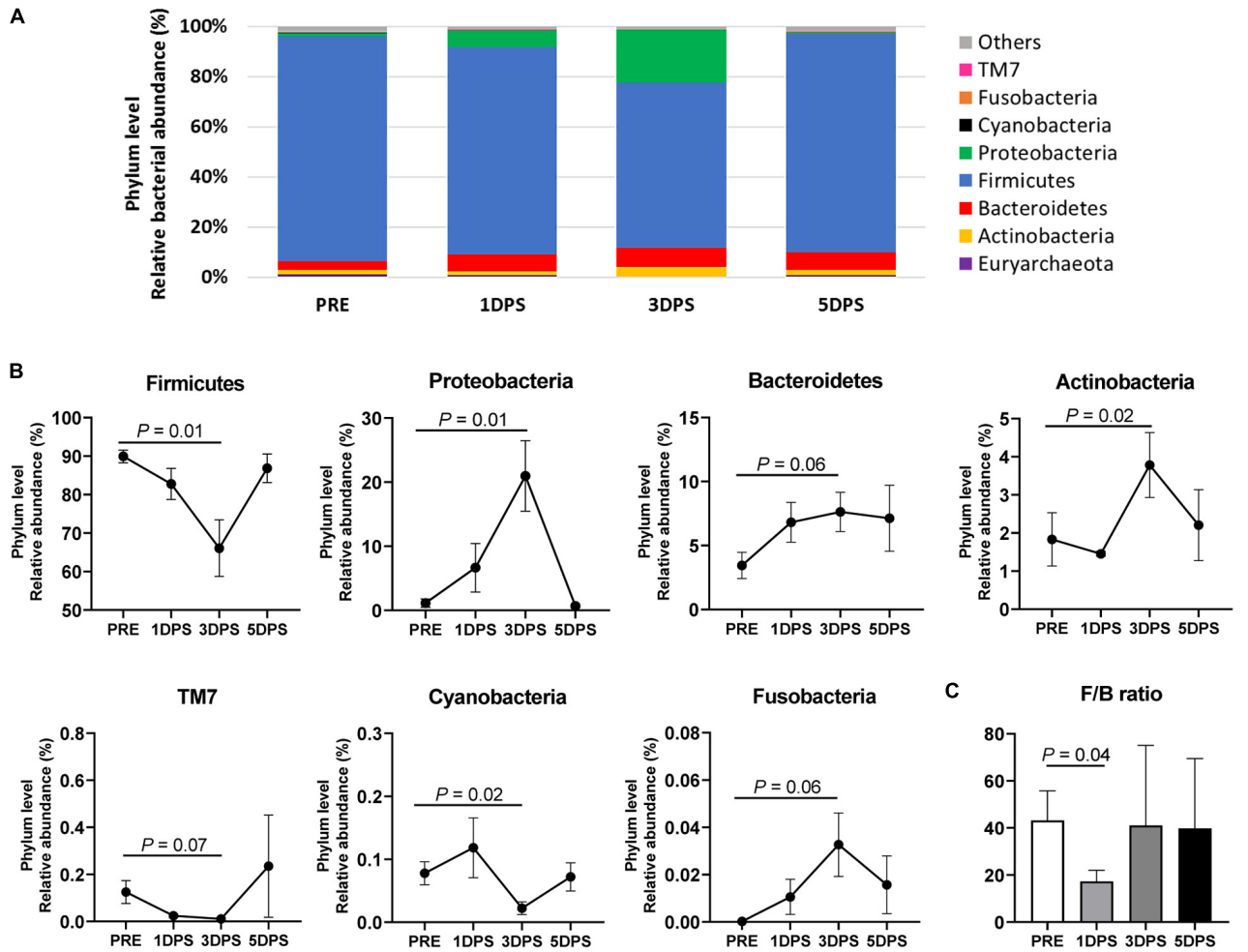

FIGURE 5 | Stroke resulted in phylum level perturbations in gut microbiota between pre- and poststroke in MCAO pig model. **(A)** Mean relative abundances of bacterial phylum prestroke (PRE, $n = 7$), 1 day poststroke (1 DPS, $n = 7$), 3 days poststroke (3 DPS, $n = 6$), and 5 days poststroke (5 DPS, $n = 4$) are shown. **(B)** Bacterial phyla showed changes in the abundance ($P < 0.10$) during acute stage of stroke. **(C)** The ratio of Firmicutes to Bacteroidetes (F/B) at 1 day poststroke (1 DPS) was lower than that at prestroke (PRE), 3 days poststroke (3 DPS), and 5 days poststroke (5 DPS). *P*-value: paired *t*-test comparing the mean prestroke values vs. each time point poststroke.

metrics returning to prestroke levels by 5 days poststroke. Interestingly, increases in the systemic inflammatory response measured by circulating TNF-α and IL-6 were observed along with changes in fecal microbiome at the acute stage of stroke. This initial study demonstrates the plasticity of the gut microbiome during the acute stage of stroke, which occurred concurrently with systemic inflammation.

Microbial dysbiosis of the gastrointestinal tract has been reported in a number of neurological injuries and diseases including stroke (Swidsinski et al., 2012; Yin et al., 2015; Benakis et al., 2016; Singh et al., 2016; Prehn-Kristensen et al., 2018; Nicholson et al., 2019). These compositional changes in the gut microflora can be assessed by using alpha- and beta-diversity indices (Wagner et al., 2018). Alpha-diversity, representing the richness and diversity of a community, has been shown to decrease in attention-deficit/hyperactivity disorder (Prehn-Kristensen et al., 2018), autism spectrum (Ma et al., 2019) as well as brain injury (Singh et al., 2016; Nicholson et al., 2019). In accordance with the previous studies, our results showed the rapid reduction in alpha-diversity (Shannon index and evenness) responding to MCAO-induced stroke. Likewise, the differences in beta-diversity, representing overall similarity of bacterial communities, have been reported in stroke (Yin et al., 2015; Singh et al., 2016) and brain injury models (Prehn-Kristensen et al., 2018; Nicholson et al., 2019). Consistent with the shifts shown in brain injury rodent models (Nicholson et al., 2019), our beta-diversity analysis revealed the greatest difference at 3 days poststroke compared to prestroke. By 5 days poststroke, the distinctive microbiome pattern overlapped with the prestroke pattern, suggesting that beta-diversity recovered during the acute stage of stroke, although the microflora profile is not identical to prestroke. Overall, our findings demonstrate a reduced species diversity and evenness and trending changes in beta-diversity between pre- and poststroke,

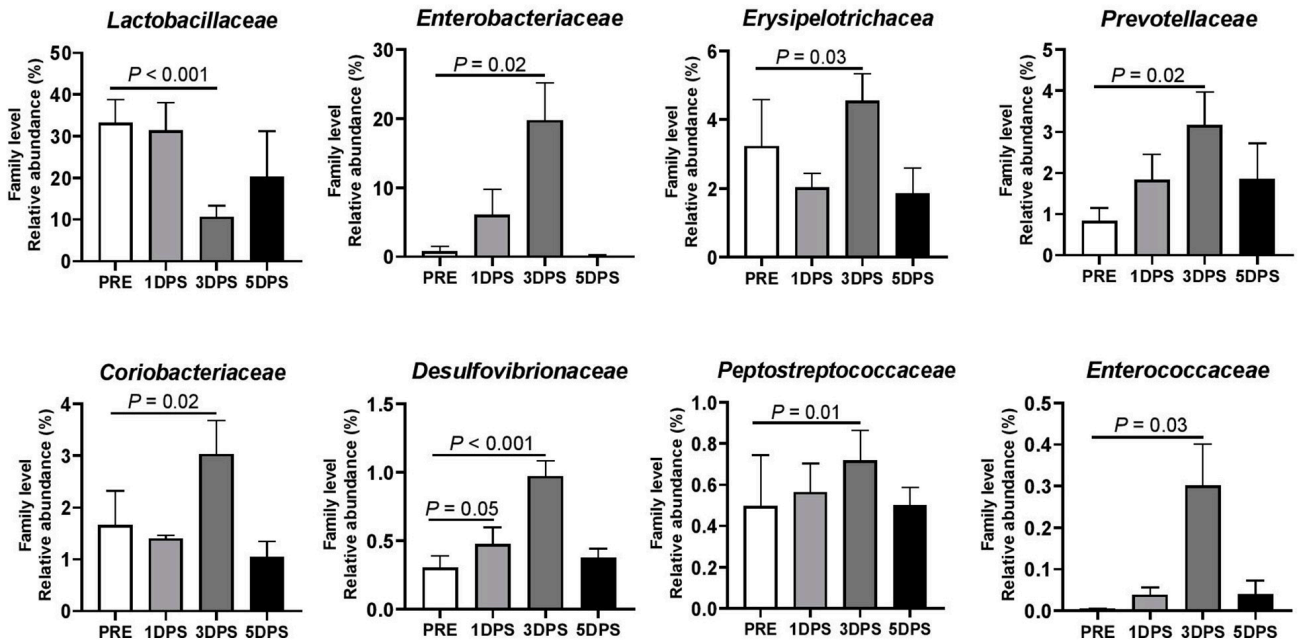

FIGURE 6 | Stroke resulted in family level perturbations in gut microbiota between pre- and poststroke in MCAO pig model. Bacterial families showed changes in abundance ($P \leq 0.05$) during the acute stage of stroke. *P*-value: Paired *t*-test comparing the mean prestroke values vs. each time point poststroke. Prestroke (PRE, $n = 7$), 1 day poststroke (1 DPS, $n = 7$), 3DPS ($n = 6$), and 5 DPS ($n = 4$).

indicating that stroke alters the gut microbiome during the acute stage.

Firmicutes and Bacteroidetes are the two predominant phyla in human gut bacteria, and the ratios between these phyla are often used as a marker of dysbiosis or is seen as indicative of energy availability in the lower gastrointestinal tract (Eckburg et al., 2005). A decrease in the ratio of Firmicutes to Bacteroidetes (F/B ratio) has been reported in neurological (Rowin et al., 2017; Vogt et al., 2017; Nicholson et al., 2019) and inflammatory bowel diseases (Kabeerdoss et al., 2015). Stroked pigs in this study also showed significantly reduced F/B ratio 1 day poststroke. Previous obesity studies showed increases in F/B ratio (Ley et al., 2006; Koliada et al., 2017), which suggested that obese individuals that had a high abundance of Firmicutes may be more efficient at extracting energy from the diet in the form of volatile fatty acids produced in the lower gastrointestinal tract microbial fermentation (Turnbaugh et al., 2006; Munukka et al., 2012). The reduction in the F/B ratio observed in the current study suggests that stroke pigs may not be able to produce as many volatile fatty acids following stroke. Consequently, the role of the F/B ratio in a disease pathology needs to be further investigated (Liang et al., 2018).

Proteobacteria is a well-known phyla containing opportunistic pathogenic bacteria such as *Escherichia*, *Salmonella*, *Helicobacter*, and others (Rizzatti et al., 2017), and increased abundances have been observed in type 2 diabetes (Lambeth et al., 2015), obesity (Fei and Zhao, 2012), inflammatory bowel disease (Morgan et al., 2012), and neurological conditions including stroke (Yin et al., 2015; Nicholson et al., 2019). A rapid increase in Proteobacteria was observed 3 days poststroke in the current study, indicating an increase in the phyla following stroke onset. Stroked pigs had a greater abundance of *Enterobacteriaceae* and *Desulfovibrionaceae* 3 days poststroke. Enriched levels of the families *Enterobacteriaceae* and *Desulfovibrionaceae* were previously found in patients with a high risk of stroke (Zeng et al., 2019), and higher level of *Desulfovibrionaceae* was detected in patients following stroke (Yin et al., 2015). The increased abundance of Proteobacteria at the acute stage of stroke may play an important role in the development of systemic inflammation in stroke, potentially leading to more deleterious outcomes.

Lactic acid bacteria (LAB) may help in reducing inflammation and in controlling pathogen populations through the production of lactic acids. In addition, LAB produce important gut-derived metabolites such as short-chain fatty acids (George et al., 2018), which act as signaling molecules in immune responses (Rizzetto et al., 2018). Talani et al. (2020) demonstrates that implementation of gut *Bifidobacteria* improved cognitive behavior and hippocampal plasticity with increases in hippocampal BDNF in rats, suggesting the probiotics as a potential therapeutic treatment in brain diseases associated with cognitive functions. *Lactobacillus* is a common component of commercial human and animal probiotics (Salvetti et al., 2012). Low populations of *Lactobacillus* were found in patients with irritable bowel syndrome, HIV, type 1 diabetes, and multiple sclerosis (Heeney et al., 2018). A decrease in relative abundance of *Lactobacillus* was also observed in the present study 3 days poststroke. Contrary to our findings, Zeng et al. (2019) found enrichment of LAB in high-risk stroke patients and suggested that the presence of LAB in the gastrointestinal tract compensates for the loss of butyrate-producing bacteria in these individuals.

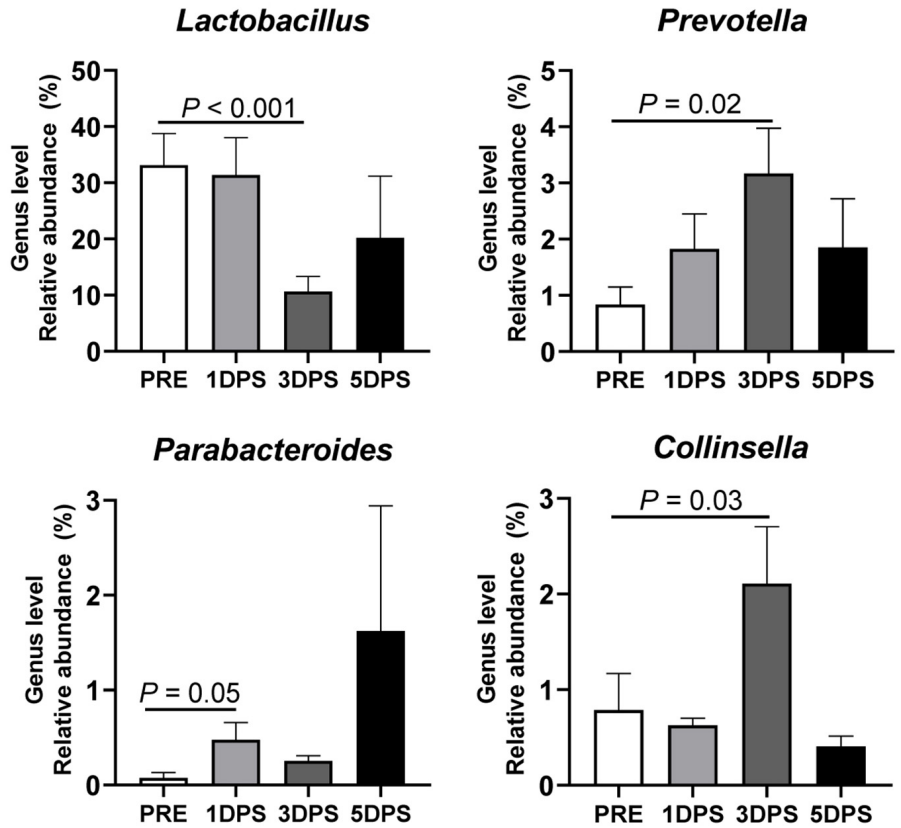

FIGURE 7 | Stroke resulted in genus-level perturbations in gut microbiota between pre- and poststroke in middle cerebral artery occlusion (MCAO) pig model. The abundance of *Lactobacillus*, *Prevotella*, *Parabacteroides*, and *Collinsella* showed >1% relative abundance and demonstrated a significant change in abundance during acute stroke. *P*-value: Paired *t*-test comparing the mean prestroke values vs. each time point poststroke. Prestroke (PRE, *n* = 7), 1 day poststroke (1DPS, *n* = 7), 3 DPS (*n* = 6), and 5DPS (*n* = 4).

Further research is needed to reconcile the discrepancies in the field. The results from this study suggest that the use of probiotics such as *Lactobacillus* at the acute stage may benefit stroke patients.

Increased populations of specific microflora may result in an increase in end products that are risk factors for stroke such as trimethylamine-N-oxide (TMAO). Trimethylamine, a precursor of TMAO, is produced by gut microbiota from dietary choline and is further metabolized to TMAO in the liver. Circulating TMAO has been reported to increase the buildup of atherosclerotic plaques in coronary vasculature, increasing the risks of stroke (Bennett et al., 2013; Tang et al., 2013). Specifically, the abundance of *Peptostreptococcaceae* and *Prevotella* were positively associated with circulating TMAO (Koeth et al., 2013). In the present study, pigs with stroke had increased abundances of both *Peptostreptococcaceae* and *Prevotella*, suggesting that the dysbiosis during the acute stage of stroke is potentially related to increased TMAO production. Additionally, a dysregulation of lipid profiles is considered as another risk factor for stroke. In stroke pigs, an increased abundance of *Coriobacteriaceae* was found, which was negatively correlated with blood triglycerides and low-density lipoprotein cholesterol in hyperlipidemia patients (Liu et al., 2018). The increase in *Coriobacteriaceae* observed in this study may be the result of compensatory mechanisms in response to stroke-induced changes in gastrointestinal conditions that alter the microbial ecology throughout the gut. Understanding the role of microflora on the regulation of metabolites associated with stroke may provide an insight on the development of novel therapeutic targets, as reviewed by Tonomura et al. (2020) indicating the role of bacterial metabolites such as TAMO and short-chain fatty acids in stroke.

Evidence on the interaction between the gut microbiota and stroke outcome have been cumulatively reported in humans and animal models. In humans, stroke dysbiosis was closely linked to severe stroke and unfavorable outcome (Yin et al., 2015; Xia et al., 2019). In mice model of stroke, disturbance of the gut microbiota increased intestinal proinflammatory T cells and have aggravated ischemic brain lesions (Benakis et al., 2016). In the current study, the changes in microbial diversity and microbiota composition were associated with stroke severity measured by high-resolution structural MRI at the acute stage of stroke. The lesion volume was negatively related with the alpha-diversity indexes suggesting that reduced microbial richness and evenness in stroke pigs are related

TABLE 2 | Changes in gut microbiota composition for 3 days poststroke were correlated with lesion volume, midline shift, and hemorrhage volume in ischemic stroke in a pig model (n = 6).

		Lesion volume	MLS	Hemorrhage volume
Phylum	Bacteroidetes	r = 0.6318	r = 0.5920	r = 0.6310
		P = 0.0205	P = 0.0330	P = 0.0207
	Firmicutes	r = −0.7999	r = −0.7415	r = −0.8202
		P = 0.0010	P = 0.0037	P = 0.0006
	Proteobacteria	r = 0.8500	r = 0.7837	r = 0.8856
		P = 0.0002	P = 0.0015	$P < 0.0001$
	Fusobacteria	r = 0.6817	r = 0.5170	r = 0.4576
		P = 0.0103	NS	NS
Family	*Lactobacillaceae*	r = −0.7057	r = −0.7150	r = −0.6911
		P = 0.0070	P = 0.0060	P = 0.0089
	Enterobacteriaceae	r = 0.8440	r = 0.7715	r = 0.8802
		P = 0.0003	P = 0.0020	$P < 0.0001$
	Prevotellaceae	r = 0.7355	r = 0.7120	r = 0.7905
		P = 0.0042	P = 0.0063	P = 0.0013
	Desulfovibrionaceae	r = 0.7141	r = 0.7966	r = 0.7107
		P = 0.0061	P = 0.0011	P = 0.0065
	Enterococcaceae	r = 0.8270	r = 0.7174	r = 0.8710
		P = 0.0005	P = 0.0058	P = 0.0001
Genus	*Lactobacillus*	r = −0.7056	r = −0.7150	r = −0.6910
		P = 0.0071	P = 0.0060	P = 0.0089
	Prevotella	r = 0.7355	r = 0.7120	r = 0.7904
		P = 0.0042	P = 0.0063	P = 0.0013
	Parabacteroides	r = 0.6110	r = 0.5803	r = 0.5573
		P = 0.0265	P = 0.0376	P = 0.0479

r, Pearson correlation coefficient; NS, not significant, P > 0.05.

to the high severity of stroke. Moreover, we found that potential pathogenic bacteria Proteobacteria, *Enterobacteriaceae*, and *Desulfovibrionaceae* were increased and beneficial bacteria *Lactobacillaceae* and *Lactobacillus* were decreased 3 days poststroke. Interestingly, abundance of the pathogenic bacteria was positively related to the lesion volume, MLS, and hemorrhage volume, while that of beneficial bacteria was negatively related to the stroke severity, proposing that gut dysbiosis may be a potential indicator to identify prognostic and therapeutic target for stroke.

The role of inflammation in neurological diseases has been widely recognized (Di Napoli et al., 2001; Audebert Heinrich et al., 2004; Elkind et al., 2004; McColl et al., 2007, 2008), and alterations in the bacterial community due to disease have been correlated with changes in inflammatory responses (Benakis et al., 2016; Winek et al., 2016; Yamashiro et al., 2017; Spychala et al., 2018; Zeraati et al., 2019). Consistent with previous findings, increased plasma levels of proinflammatory cytokines were observed in the current study, concurrent with the changes in gut microbiome composition. Increased gut permeability and translocation of bacteria to host tissues have been previously reported in stroke conditions (Crapser et al., 2016; Stanley et al., 2016), supporting the involvement of the gut microbial population in stroke pathophysiology. It is well known that lipopolysaccharides (LPS) from the cell wall of Gram-negative bacteria (Hurley, 1995) trigger an immune response by binding to Toll-like receptor 4 in endothelial cells, activating monocytes/macrophages, and nuclear factor kappa B signaling cascades, resulting in the production of proinflammatory cytokines such as TNF-α (Cario et al., 2002; Mafra et al., 2014). Proinflammatory cytokines contribute to the disruption of tight junction proteins between the epithelial cells, leading to an increase in gut permeability (Katzenberger et al., 2015) as well as translocation of bacteria and microbial-derived end products into the blood stream in what is known as "leaky gut syndrome." Leaky gut syndrome results in a cycle of increasing inflammation that is detrimental to stroke patients, which could potentially be mitigated by therapeutic treatments that alter the composition of the gut microbial composition.

CONCLUSION

The present study demonstrated, for the first time using a large translational animal model such as swine, the plasticity of the gut microbiome during the acute stage of stroke. These changes included significant shifts in microbial diversity, the ratio of Firmicutes to Bacteroidetes, and the abundance of Proteobacteria and *Lactobacillus*. Importantly, the microbial changes were significantly correlated with the severity of brain lesion measured by MRI. Given the significant degree of physiological similarities between swine and humans, findings from the current study contribute to increasing our understanding of the pathophysiology of stroke in human patients. Future studies investigating the role of the microbiome and its effect on the stroke immune response are warranted to understand the effect of therapeutic treatments on the gut microbiota in stroke patients.

DATA AVAILABILITY STATEMENT

The original contributions presented in the study are publicly available. This data can be found here: https://www.mg-rast.org, under accession number mgm4901524.3.

ETHICS STATEMENT

The animal study and experimental procedures were reviewed and approved by the University of Georgia Institutional Animal Care and Use Committee and the study was conducted in accordance with the recommendations of the NIH's guide for the Use and Care of Laboratory Animals (AUP approval number: A2017 07-019-Y2-A16).

AUTHOR CONTRIBUTIONS

JJ performed the experiments, collected the data, analyzed the data, and wrote the manuscript. JL analyzed the data and wrote the manuscript. EK and EW performed the experiments, collected the data, and administered the project. KS and

XF performed the experiments and collected the data. HK administered the project. SP and MR managed the experimental methodology. TC conceptualized the project. FW contributed to funding acquisition, administered the project, and wrote the manuscript. HP conceptualized the project, contributed to funding acquisition, administered the project, and wrote the manuscript. All authors contributed to the article and approved the submitted version.

FUNDING

This work was supported by the Georgia Experimental Agricultural Station, HATCH No. GEO00795 and the National Institutes of Health, NINDS grant R01NS093314.

ACKNOWLEDGMENTS

We would like to express our great appreciation to Park and West Laboratory undergraduate researchers in assisting with the many facets of animal work. We are also particularly grateful for the assistance given with handling of the fecal samples by Laura Lee Rutherford from the USDA-ARS US National Poultry Research Center.

SUPPLEMENTARY MATERIAL

The Supplementary Material for this article can be found online at: https://www.frontiersin.org/articles/10.3389/fnins.2020.587986/full#supplementary-material

REFERENCES

Albers, G. W., Goldstein, L. B., Hess, D. C., Wechsler, L. R., Furie, K. L., Gorelick, P. B., et al. (2011). Stroke treatment academic industry roundtable (STAIR) recommendations for maximizing the use of intravenous thrombolytics and expanding treatment options with intra-arterial and neuroprotective therapies. *Stroke* 42, 2645–2650. doi: 10.1161/STROKEAHA.111.618850

Audebert Heinrich, J., Rott Michaela, M., Eck, T., and Haberl Roman, L. (2004). Systemic inflammatory response depends on initial stroke severity but is attenuated by successful thrombolysis. *Stroke* 35, 2128–2133. doi: 10.1161/01.STR.0000137607.61697.77

Baker, E. W., Platt, S. R., Lau, V. W., Grace, H. E., Holmes, S. P., Wang, L., et al. (2017). Induced pluripotent stem cell-derived neural stem cell therapy enhances recovery in an ischemic stroke pig model. *Sci. Rep.* 7:10075. doi: 10.1038/s41598-017-10406-x

Benakis, C., Brea, D., Caballero, S., Faraco, G., Moore, J., Murphy, M., et al. (2016). Commensal microbiota affects ischemic stroke outcome by regulating intestinal gammadelta T cells. *Nat. Med.* 22, 516–523. doi: 10.1038/nm.4068

Benakis, C., Poon, C., Lane, D., Brea, D., Sita, G., Moore, J., et al. (2020). Distinct commensal bacterial signature in the gut is associated with acute and long-term protection from ischemic stroke. *Stroke* 51, 1844–1854. doi: 10.1161/STROKEAHA.120.029262

Benjamin, E. J., Muntner, P., Alonso, A., Bittencourt, M. S., Callaway, C. W., Carson, A. P., et al. (2019). Heart disease and stroke statistics-2019 update: a report from the American heart association. *Circulation* 139, e56–e528. doi: 10.1161/CIR.0000000000000659

Bennett, B. J., de Aguiar Vallim, T. Q., Wang, Z., Shih, D. M., Meng, Y., Gregory, J., et al. (2013). Trimethylamine-N-oxide, a metabolite associated with atherosclerosis, exhibits complex genetic and dietary regulation. *Cell Metab.* 17, 49–60. doi: 10.1016/j.cmet.2012.12.011

Borgens, R. B., and Liu-Snyder, P. (2012). Understanding secondary injury. *Q. Rev. Biol.* 87, 89–127. doi: 10.1201/b13492-11

Caporaso, J. G., Kuczynski, J., Stombaugh, J., Bittinger, K., Bushman, F. D., Costello, E. K., et al. (2010). QIIME allows analysis of high-throughput community sequencing data. *Nat. Methods* 7, 335–336. doi: 10.1038/nmeth.f.303

Cario, E., Brown, D., McKee, M., Lynch-Devaney, K., Gerken, G., and Podolsky, D. K. (2002). Commensal-associated molecular patterns induce selective toll-like receptor-trafficking from apical membrane to cytoplasmic compartments in polarized intestinal epithelium. *Am. J. Pathol.* 160, 165–173. doi: 10.1016/S0002-9440(10)64360-X

Clouard, C., Meunier-Salaun, M. C., and Val-Laillet, D. (2012). Food preferences and aversions in human health and nutrition: how can pigs help the biomedical research? *Animal* 6, 118–136. doi: 10.1017/s1751731111001315

Crapser, J., Ritzel, R., Verma, R., Venna, V. R., Liu, F., Chauhan, A., et al. (2016). Ischemic stroke induces gut permeability and enhances bacterial translocation leading to sepsis in aged mice. *Aging* 8, 1049–1063. doi: 10.18632/aging.100952

Deb, P., Sharma, S., and Hassan, K. M. (2010). Pathophysiologic mechanisms of acute ischemic stroke: an overview with emphasis on therapeutic significance beyond thrombolysis. *Pathophysiology* 17, 197–218. doi: 10.1016/j.pathophys.2009.12.001

Di Napoli, M., and Papa, F. (2006). Systemic inflammation, blood pressure, and stroke outcome. *J. Clin. Hypertens.* 8, 187–194. doi: 10.1111/j.1524-6175.2005.04590.x

Di Napoli, M., Papa, F., and Bocola, V. (2001). C-reactive protein in ischemic stroke: an independent prognostic factor. *Stroke* 32, 917–924. doi: 10.1161/01.str.32.4.917

Duberstein, K. J., Platt, S. R., Holmes, S. P., Dove, C. R., Howerth, E. W., Kent, M., et al. (2014). Gait analysis in a pre- and post-ischemic stroke biomedical pig model. *Physiol. Behav.* 125, 8–16. doi: 10.1016/j.physbeh.2013.11.004

Durgan, D. J., Lee, J., McCullough, L. D., and Bryan, R. M. Jr. (2019). Examining the role of the microbiota-gut-brain axis in stroke. *Stroke* 50, 2270–2277. doi: 10.1161/STROKEAHA.119.025140

Eckburg, P. B., Bik, E. M., Bernstein, C. N., Purdom, E., Dethlefsen, L., Sargent, M., et al. (2005). Diversity of the human intestinal microbial flora. *Science* 308, 1635–1638. doi: 10.1126/science.1110591

Elkind, M. S., Cheng, J., Rundek, T., Boden-Albala, B., and Sacco, R. L. (2004). Leukocyte count predicts outcome after ischemic stroke: the Northern Manhattan Stroke Study. *J. Stroke Cerebrovasc. Dis.* 13, 220–227. doi: 10.1016/j.jstrokecerebrovasdis.2004.07.004

Fei, N., and Zhao, L. (2012). An opportunistic pathogen isolated from the gut of an obese human causes obesity in germfree mice. *ISME J.* 7, 880–884. doi: 10.1038/ismej.2012.153

Fisher, M., Feuerstein, G., Howells, D. W., Hurn, P. D., Kent, T. A., Savitz, S. I., et al. (2009). Update of the stroke therapy academic industry roundtable preclinical recommendations. *Stroke* 40, 2244–2250. doi: 10.1161/STROKEAHA.108.541128

Foster, N., Lovell, M. A., Marston, K. L., Hulme, S. D., Frost, A. J., Bland, P., et al. (2003). Rapid protection of gnotobiotic pigs against experimental salmonellosis following induction of polymorphonuclear leukocytes by avirulent *Salmonella enterica*. *Infect. Immun.* 71, 2182–2191. doi: 10.1128/iai.71.4.2182-2191.2003

George, F., Daniel, C., Thomas, M., Singer, E., Guilbaud, A., Tessier, F. J., et al. (2018). Occurrence and dynamism of lactic acid bacteria in distinct ecological niches: a multifaceted functional health perspective. *Front. Microbiol.* 9:2899. doi: 10.3389/fmicb.2018.02899

González, R. G. (2012). Clinical MRI of acute ischemic stroke. *J. Magn. Reson. Imaging* 36, 259–271. doi: 10.1002/jmri.23595

Heeney, D. D., Gareau, M. G., and Marco, M. L. (2018). Intestinal *Lactobacillus* in health and disease, a driver or just along for the ride? *Curr. Opin. Biotechnol.* 49, 140–147. doi: 10.1016/j.copbio.2017.08.004

Heinritz, S. N., Mosenthin, R., and Weiss, E. (2013). Use of pigs as a potential model for research into dietary modulation of the human gut microbiota. *Nutr. Res. Rev.* 26, 191–209. doi: 10.1017/s0954422413000152

Hurley, J. C. (1995). Endotoxemia: methods of detection and clinical correlates. *Clin. Microbiol. Rev.* 8, 268–292. doi: 10.1128/cmr.8.2.268-292.1995

Kabeerdoss, J., Jayakanthan, P., Pugazhendhi, S., and Ramakrishna, B. S. (2015). Alterations of mucosal microbiota in the colon of patients with inflammatory bowel disease revealed by real time polymerase chain reaction amplification of 16S ribosomal ribonucleic acid. *Indian J. Med. Res.* 142, 23–32. doi: 10.4103/0971-5916.162091

Kaiser, E. E., Waters, E. S., Fagan, M. M., Scheulin, K. M., Platt, S. R., Jeon, J. H., et al. (2020). Characterization of tissue and functional deficits in a clinically translational pig model of acute ischemic stroke. *Brain Res.* 1736:146778. doi: 10.1016/j.brainres.2020.146778

Kaiser, E. E., and West, F. D. (2020). Large animal ischemic stroke models: replicating human stroke pathophysiology. *Neural Regen. Res.* 15, 1377–1387. doi: 10.4103/1673-5374.274324

Katzenberger, R. J., Ganetzky, B., and Wassarman, D. A. (2015). The gut reaction to traumatic brain injury. *Fly* 9, 68–74. doi: 10.1080/19336934.2015.1085623

Klindworth, A., Pruesse, E., Schweer, T., Peplies, J., Quast, C., Horn, M., et al. (2013). Evaluation of general 16S ribosomal RNA gene PCR primers for classical and next-generation sequencing-based diversity studies. *Nucleic Acids Res.* 41:e1. doi: 10.1093/nar/gks808

Koeth, R. A., Wang, Z., Levison, B. S., Buffa, J. A., Org, E., Sheehy, B. T., et al. (2013). Intestinal microbiota metabolism of L-carnitine, a nutrient in red meat, promotes atherosclerosis. *Nat. Med.* 19, 576–585. doi: 10.1038/nm.3145

Koliada, A., Syzenko, G., Moseiko, V., Budovska, L., Puchkov, K., Perederiy, V., et al. (2017). Association between body mass index and Firmicutes/Bacteroidetes ratio in an adult Ukrainian population. *BMC Microbiol.* 17:120. doi: 10.1186/s12866-017-1027-1

Kriss, M., Hazleton, K. Z., Nusbacher, N. M., Martin, C. G., and Lozupone, C. A. (2018). Low diversity gut microbiota dysbiosis: drivers, functional implications and recovery. *Curr. Opin. Microbiol.* 44, 34–40. doi: 10.1016/j.mib.2018.07.003

Lambeth, S. M., Carson, T., Lowe, J., Ramaraj, T., Leff, J. W., Luo, L., et al. (2015). Composition, diversity and abundance of gut microbiome in prediabetes and type 2 diabetes. *J. Diabetes Obes.* 2, 1–7. doi: 10.15436/2376-0949.15.031

Lamendella, R., Santo Domingo, J. W., Ghosh, S., Martinson, J., and Oerther, D. B. (2011). Comparative fecal metagenomics unveils unique functional capacity of the swine gut. *BMC Microbiol.* 11:103. doi: 10.1186/1471-2180-11-103

Ley, R. E., Turnbaugh, P. J., Klein, S., and Gordon, J. I. (2006). Human gut microbes associated with obesity. *Nature* 444, 1022–1023. doi: 10.1038/4441022a

Liang, D., Leung, R. K.-K., Guan, W., and Au, W. W. (2018). Involvement of gut microbiome in human health and disease: brief overview, knowledge gaps and research opportunities. *Gut Pathog.* 10:3.

Lind, N. M., Moustgaard, A., Jelsing, J., Vajta, G., Cumming, P., and Hansen, A. K. (2007). The use of pigs in neuroscience: modeling brain disorders. *Neurosci. Biobehav. Rev.* 31, 728–751. doi: 10.1016/j.neubiorev.2007.02.003

Liu, Y., Song, X., Zhou, H., Zhou, X., Xia, Y., Dong, X., et al. (2018). Gut microbiome associates with lipid-lowering effect of rosuvastatin in vivo. *Front. Microbiol.* 9:530. doi: 10.3389/fmicb.2018.00530

Ma, B., Liang, J., Dai, M., Wang, J., Luo, J., Zhang, Z., et al. (2019). Altered gut microbiota in Chinese children with autism spectrum disorders. *Front. Cell. Infect. Microbiol.* 9:40. doi: 10.3389/fcimb.2019.00040

Mafra, D., Lobo, J. C., Barros, A. F., Koppe, L., Vaziri, N. D., and Fouque, D. (2014). Role of altered intestinal microbiota in systemic inflammation and cardiovascular disease in chronic kidney disease. *Future Microbiol.* 9, 399–410. doi: 10.2217/fmb.13.165

McColl, B. W., Rothwell, N. J., and Allan, S. M. (2007). Systemic inflammatory stimulus potentiates the acute phase and CXC chemokine responses to experimental stroke and exacerbates brain damage via interleukin-1- and neutrophil-dependent mechanisms. *J. Neurosci.* 27, 4403–4412. doi: 10.1523/jneurosci.5376-06.2007

McColl, B. W., Rothwell, N. J., and Allan, S. M. (2008). Systemic inflammation alters the kinetics of cerebrovascular tight junction disruption after experimental stroke in mice. *J. Neurosci.* 28, 9451–9462. doi: 10.1523/jneurosci.2674-08.2008

Morgan, X. C., Tickle, T. L., Sokol, H., Gevers, D., Devaney, K. L., Ward, D. V., et al. (2012). Dysfunction of the intestinal microbiome in inflammatory bowel disease and treatment. *Genome Biol.* 13:R79. doi: 10.1186/gb-2012-13-9-r79

Munukka, E., Wiklund, P., Pekkala, S., Volgyi, E., Xu, L., Cheng, S., et al. (2012). Women with and without metabolic disorder differ in their gut microbiota composition. *Obesity* 20, 1082–1087. doi: 10.1038/oby.2012.8

Nicholson, S. E., Watts, L. T., Burmeister, D. M., Merrill, D., Scroggins, S., Zou, Y., et al. (2019). Moderate traumatic brain injury alters the gastrointestinal microbiome in a time-dependent manner. *Shock* 52, 240–248. doi: 10.1097/shk.0000000000001211

Platt, S. R., Holmes, S. P., Howerth, E. W., Duberstein, K. J. J., Dove, C. R., Kinder, H. A., et al. (2014). Development and characterization of a Yucatan miniature biomedical pig permanent middle cerebral artery occlusion stroke model. *Exp. Transl. Stroke Med.* 6:5. doi: 10.1186/2040-7378-6-5

Prehn-Kristensen, A., Zimmermann, A., Tittmann, L., Lieb, W., Schreiber, S., Baving, L., et al. (2018). Reduced microbiome alpha diversity in young patients with ADHD. *PLoS One* 13:e0200728. doi: 10.1371/journal.pone.0200728

Rizzatti, G., Lopetuso, L. R., Gibiino, G., Binda, C., and Gasbarrini, A. (2017). Proteobacteria: a common factor in human diseases. *Biomed Res. Int.* 2017:9351507. doi: 10.1155/2017/9351507

Rizzetto, L., Fava, F., Tuohy, K. M., and Selmi, C. (2018). Connecting the immune system, systemic chronic inflammation and the gut microbiome: the role of sex. *J. Autoimmun.* 92, 12–34. doi: 10.1016/j.jaut.2018.05.008

Rothrock, M. J. Jr., Hiett, K. L., Gamble, J., Caudill, A. C., Cicconi-Hogan, K. M., and Caporaso, J. G. (2014). A hybrid DNA extraction method for the qualitative and quantitative assessment of bacterial communities from poultry production samples. *J. Vis. Exp.* 94:52161. doi: 10.3791/52161

Rowin, J., Xia, Y., Jung, B., and Sun, J. (2017). Gut inflammation and dysbiosis in human motor neuron disease. *Physiol. Rep.* 5:e13443. doi: 10.14814/phy2.13443

Salvetti, E., Torriani, S., and Felis, G. E. (2012). The genus *Lactobacillus*: a taxonomic update. *Probiotics Antimicrob. Proteins* 4, 217–226. doi: 10.1007/s12602-012-9117-8

Saver, J. L., Albers, G. W., Dunn, B., Johnston, K. C., Fisher, M., and Consortium, S. V. (2009). Stroke therapy academic industry roundtable (STAIR) recommendations for extended window acute stroke therapy trials. *Stroke* 40, 2594–2600. doi: 10.1161/STROKEAHA.109.552554

Scharek, L., Guth, J., Reiter, K., Weyrauch, K. D., Taras, D., Schwerk, P., et al. (2005). Influence of a probiotic *Enterococcus faecium* strain on development of the immune system of sows and piglets. *Vet. Immunol. Immunopathol.* 105, 151–161. doi: 10.1016/j.vetimm.2004.12.022

Singh, V., Roth, S., Llovera, G., Sadler, R., Garzetti, D., Stecher, B., et al. (2016). Microbiota dysbiosis controls the neuroinflammatory response after stroke. *J. Neurosci.* 36, 7428–7440. doi: 10.1523/jneurosci.1114-16.2016

Singh, V., Sadler, R., Heindl, S., Llovera, G., Roth, S., Benakis, C., et al. (2018). The gut microbiome primes a cerebroprotective immune response after stroke. *J. Cereb. Blood Flow Metab.* 38, 1293–1298. doi: 10.1177/0271678X18780130

Spychala, M. S., Venna, V. R., Jandzinski, M., Doran, S. J., Durgan, D. J., Ganesh, B. P., et al. (2018). Age-related changes in the gut microbiota influence systemic inflammation and stroke outcome. *Ann. Neurol.* 84, 23–36. doi: 10.1002/ana.25250

Stanley, D., Mason, L., Mackin, K., Srikhanta, Y., Lyras, D., Prakash, M. D., et al. (2016). Translocation and dissemination of commensal bacteria in post-stroke infection. *Nat. Med.* 22, 1277–1284. doi: 10.1038/nm.4194

Swidsinski, A., Loening-Baucke, V., Krüger, M., and Kirsch, S. (2012). Central nervous system and the colonic bioreactor: analysis of colonic microbiota in patients with stroke unravels unknown mechanisms of the host defense after brain injury. *Intest. Res.* 10, 332–342. doi: 10.5217/ir.2012.10.4.332

Swindle, M. M., Makin, A., Herron, A. J., Clubb, F. J. Jr., and Frazier, K. S. (2012). Swine as models in biomedical research and toxicology testing. *Vet. Pathol.* 49, 344–356. doi: 10.1177/0300985811402846

Talani, G., Biggio, F., Mostallino, M. C., Locci, V., Porcedda, C., Boi, L., et al. (2020). Treatment with gut bifidobacteria improves hippocampal plasticity and cognitive behavior in adult healthy rats. *Neuropharmacology* 165:107909. doi: 10.1016/j.neuropharm.2019.107909

Tang, W. H., Wang, Z., Levison, B. S., Koeth, R. A., Britt, E. B., Fu, X., et al. (2013). Intestinal microbial metabolism of phosphatidylcholine and cardiovascular risk. *N. Engl. J. Med.* 368, 1575–1584. doi: 10.1056/NEJMoa1109400

Tonomura, S., Ihara, M., and Friedland, R. P. (2020). Microbiota in cerebrovascular disease: a key player and future therapeutic target. *J. Cereb. Blood Flow Metab.* 40, 1368–1380. doi: 10.1177/0271678X20918031

Turnbaugh, P. J., Ley, R. E., Mahowald, M. A., Magrini, V., Mardis, E. R., and Gordon, J. I. (2006). An obesity-associated gut microbiome with increased capacity for energy harvest. *Nature* 444, 1027–1031. doi: 10.1038/nature05414

Vogt, N. M., Kerby, R. L., Dill-McFarland, K. A., Harding, S. J., Merluzzi, A. P., Johnson, S. C., et al. (2017). Gut microbiome alterations in Alzheimer's disease. *Sci. Rep.* 7:13537. doi: 10.1038/s41598-017-13601-y

Wagner, B., Grunwald, G. K., Zerbe, G. O., Mikulich-Gilbertson, S., Robertson, C. E., Zemanick, E., et al. (2018). On the use of diversity measures in longitudinal sequencing studies of microbial communities. *Front. Microbiol.* 9:1037. doi: 10.3389/fmicb.2018.01037

Watanabe, H., Andersen, F., Simonsen, C. Z., Evans, S. M., Gjedde, A., Cumming, P., et al. (2001). MR-based statistical atlas of the Gottingen minipig brain. *Neuroimage* 14, 1089–1096. doi: 10.1006/nimg.2001.0910

Wilson, S., Norton, P., Haverson, K., Leigh, J., and Bailey, M. (2005). Development of the palatine tonsil in conventional and germ-free piglets. *Dev. Comp. Immunol.* 29, 977–987. doi: 10.1016/j.dci.2005.03.008

Winek, K., Dirnagl, U., and Meisel, A. (2016). The gut microbiome as therapeutic target in central nervous system diseases: implications for stroke. *Neurotherapeutics* 13, 762–774. doi: 10.1007/s13311-016-0475-x

Xia, G.-H., You, C., Gao, X.-X., Zeng, X.-L., Zhu, J.-J., Xu, K.-Y., et al. (2019). Stroke dysbiosis index (SDI) in gut microbiome are associated with brain injury and prognosis of stroke. *Front. Neurol.* 10:397. doi: 10.3389/fneur.2019.00397

Xiao, L., Estelle, J., Kiilerich, P., Ramayo-Caldas, Y., Xia, Z., Feng, Q., et al. (2016). A reference gene catalogue of the pig gut microbiome. *Nat. Microbiol.* 1:16161. doi: 10.1038/nmicrobiol.2016.161

Yamashiro, K., Tanaka, R., Urabe, T., Ueno, Y., Yamashiro, Y., Nomoto, K., et al. (2017). Gut dysbiosis is associated with metabolism and systemic inflammation in patients with ischemic stroke. *PLoS One* 12:e0171521. doi: 10.1371/journal.pone.0171521

Yin, J., Liao, S. X., He, Y., Wang, S., Xia, G. H., Liu, F. T., et al. (2015). Dysbiosis of gut microbiota with reduced trimethylamine-N-oxide level in patients with large-artery atherosclerotic stroke or transient ischemic attack. *J. Am. Heart Assoc.* 4:e002699. doi: 10.1161/jaha.115.002699

Zeng, X., Gao, X., Peng, Y., Wu, Q., Zhu, J., Tan, C., et al. (2019). Higher risk of stroke is correlated with increased opportunistic pathogen load and reduced levels of butyrate-producing bacteria in the gut. *Front. Cell. Infect. Microbiol.* 9:4. doi: 10.3389/fcimb.2019.00004

Zeraati, M., Enayati, M., Kafami, L., Shahidi, S. H., and Salari, A. A. (2019). Gut microbiota depletion from early adolescence alters adult immunological and neurobehavioral responses in a mouse model of multiple sclerosis. *Neuropharmacology* 157:107685. doi: 10.1016/j.neuropharm.2019.107685

Zhang, Q., Widmer, G., and Tzipori, S. (2013). A pig model of the human gastrointestinal tract. *Gut Microbes* 4, 193–200. doi: 10.4161/gmic.23867

Conflict of Interest: The authors declare that the research was conducted in the absence of any commercial or financial relationships that could be construed as a potential conflict of interest.

frontiers in Aging Neuroscience

ORIGINAL RESEARCH
published: 16 December 2020
doi: 10.3389/fnagi.2020.618538

Systematic and Comprehensive Automated Ventricle Segmentation on Ventricle Images of the Elderly Patients: A Retrospective Study

Xi Zhou[1†], Qinghao Ye[2,3†], Yinghui Jiang[2,3†], Minhao Wang[2,3], Zhangming Niu[4], Wade Menpes-Smith[4], Evandro Fei Fang[5], Zhi Liu[6], Jun Xia[1] and Guang Yang[7,8*]*

[1] Department of Radiology, Shenzhen Second People's Hospital, The First Affiliated Hospital of Shenzhen University Health Science Center, Shenzhen, China, [2] Hangzhou Ocean's Smart Boya Co., Ltd., Hangzhou, China, [3] Mind Rank Ltd., Hongkong, China, [4] Aladdin Healthcare Technologies Ltd., London, United Kingdom, [5] Department of Clinical Molecular Biology, University of Oslo, Oslo, Norway, [6] School of Information Science and Engineering, Shandong University, Qingdao, China, [7] Cardiovascular Research Centre, Royal Brompton Hospital, London, United Kingdom, [8] National Heart and Lung Institute, Imperial College London, London, United Kingdom

Background and Objective: Ventricle volume is closely related to hydrocephalus, brain atrophy, Alzheimer's, Parkinson's syndrome, and other diseases. To accurately measure the volume of the ventricles for elderly patients, we use deep learning to establish a systematic and comprehensive automated ventricle segmentation framework.

Methods: The study participation included 20 normal elderly people, 20 patients with cerebral atrophy, 64 patients with normal pressure hydrocephalus, and 51 patients with acquired hydrocephalus. Second, get their imaging data through the picture archiving and communication systems (PACS) system. Then use ITK software to manually label participants' ventricular structures. Finally, extract imaging features through machine learning.

Results: This automated ventricle segmentation method can be applied not only to CT and MRI images but also to images with different scan slice thicknesses. More importantly, it produces excellent segmentation results (Dice > 0.9).

Conclusion: This automated ventricle segmentation method has wide applicability and clinical practicability. It can help clinicians find early disease, diagnose disease, understand the patient's disease progression, and evaluate the patient's treatment effect.

Keywords: deep learning, neuroimage, magnetic resonance imaging, ventricular segmentation, image segmentation, convolutional neural network (CNN), computer tomography (CT)

OPEN ACCESS

Edited by:
Feiqi Zhu,
Shenzhen University, China

Reviewed by:
Lin Gu,
National Institute of Informatics, Japan
Xurui Jin,
Duke Kunshan University, China

***Correspondence:**
Jun Xia
xiajun@email.szu.edu.cn
Guang Yang
g.yang@imperial.ac.uk

[†] These authors have contributed equally to this work

Received: *17 October 2020*
Accepted: *23 November 2020*
Published: *16 December 2020*

Citation:
Zhou X, Ye Q, Jiang Y, Wang M, Niu Z, Menpes-Smith W, Fang EF, Liu Z, Xia J and Yang G (2020) Systematic and Comprehensive Automated Ventricle Segmentation on Ventricle Images of the Elderly Patients: A Retrospective Study. Front. Aging Neurosci. 12:618538. doi: 10.3389/fnagi.2020.618538

INTRODUCTION

The volume of the ventricle has always been closely related to degenerative brain diseases and traumatic brain injury. Researchers have also described that enlargement of the ventricles is an important characteristic of medical conditions such as schizophrenia, Parkinson's disease, Alzheimer's disease, hydrocephalus, and trauma to the brain (Silbert et al., 2003; Thompson et al., 2004; Chou et al., 2009; Liu et al., 2010; Cavedo et al., 2012; Khan et al., 2012; Anandh et al., 2016; Del et al., 2016; Owen et al., 2018; Kocaman et al., 2019; Lundervold et al., 2019). In some

disease diagnosis guidelines, EI $>$ 0.3 is often defined as ventricular enlargement (Relkin et al., 2005; Mori et al., 2012). However, some studies have shown that the correlation between EI and ventricle volume is only 0.619 (Toma et al., 2011). The measurement of EI is affected by different scan baselines and different measurement planes, which only reflects the local conditions of the ventricle at the selected level, and cannot fully assess the size of the ventricle (Ambarki et al., 2010). Moreover, EI is sensitive to the expansion of the ventricle to both sides, and the effect is not good when evaluating patients whose ventricle expands to the long axis (He et al., 2020). At the same time, in the normal elderly, the range of EI is relatively wide. Taking EI $=$ 0.3 as the cut-off value, it is difficult to effectively distinguish between normal and enlarged ventricles (Brix et al., 2017). Therefore, when we need the volume of the ventricle, and the volume of the ventricle is measurable, then we should use it (Ambarki et al., 2010). Because of this, research on ventricle segmentation methods has brought much attention, and researchers have continuously optimized algorithms to make better and more accurate estimation (Chen et al., 2009; Coupe et al., 2011; Kempton et al., 2011; Poh et al., 2012; Qiu et al., 2015; Tang et al., 2015, 2018; Qian et al., 2017; Cherukuri et al., 2018; Shao et al., 2019; Dubost et al., 2020).

Volumetric measurement is the only method to directly determine the ventricular size. It is realized by segmentation, which can be roughly categorized into automated segmentation and manual segmentation (Huff et al., 2019). The manual segmentation technique is the gold standard for volumetric quantification of regional brain structures (Kocaman et al., 2019), but when dealing with more data, manual segmentation of the ventricles is time-consuming, subjective, and less reproducible (Chou et al., 2008; Liu et al., 2009; Poh et al., 2012). Therefore, it is highly in demand for an automated ventricle segmentation method to be developed and machine and deep learning based methods have emerged as the new era.

In the previous automated ventricle segmentation methods, researchers often conducted single-mode studies, i.e., segment either on CT images (Liu et al., 2010; Poh et al., 2012; Qian et al., 2017; Cherukuri et al., 2018) or MRI images (Qiu et al., 2015; Tang et al., 2015, 2018). Therefore, the developed automated ventricle segmentation methods were rarely interchangeable. Moreover, various algorithms might perform differently in segmenting different sections of the ventricles (Chen et al., 2009; Coupe et al., 2011; Shao et al., 2019; Dubost et al., 2020). Most previous machine learning (including deep learning) based studies were developed using images with a slice thickness of $<$3 mm, because at the same scanning distance, the smaller of the image thickness, the more images could be obtained, which could be more conducive for machine/deep learning algorithms to extract more image features (Xia et al., 2004; Coupe et al., 2011; Kempton et al., 2011). However, in clinical practice, due to time constraints, images with larger slice thicknesses are more common. Therefore, the clinical usage of these methods is relatively limited.

The reproducibility of machine/deep learning based algorithms across different scanners and pulse sequences had not always been comprehensively examined (Kempton et al., 2011). Moreover, their accuracy in different clinical populations and sensitivity to real changes in brain volume could still be improved. A larger slice thickness would increase the partial volume effect, which could have a significant negative impact on the algorithm accuracy. For example, the intraventricular calcified area located at the border of the ventricle may not be recognized. Some cerebellar ventricle areas (anterior, posterior, and inferior horns of the lateral ventricle) may not be recognized because they are not connected to the core of the lateral ventricle (Liu et al., 2010). In some automated ventricle segmentation methods, pathological ventricles were not included (Huff et al., 2019), but pathological ventricles are common in the elderly, especially in patients with acquired hydrocephalus, because they may have brain trauma, brain tumors, subarachnoid hemorrhage, and it becomes extremely difficult to delineate the ventricle from these patients. Previous literature also reported the segmentation of the ventricle of idiopathic Normal Pressure Hydrocephalus (iNPH) patients (Shao et al., 2019). These patients are prone to segmentation failure due to the enlarged ventricle. Therefore, our purpose is not only to optimize the algorithm and obtain more accurate results but more importantly, to make this automated ventricle segmentation method be more widely used and be trustworthy for clinical practice.

In summary, the goal of this study is to establish a deep learning based automated ventricle segmentation method that can be generally used for both CT and MRI images, and is versatile for both thin-layer and thick-layer images.

METHODS

Participants

First, we selected the images of patients over 60 years old who underwent brain CT or MRI examinations at Shenzhen Second People's Hospital from January 1, 2016 to December 31, 2019. Second, as we aimed to delineate the ventricle and perform a comprehensive analysis, we chose the normal elderly, the elderly with brain atrophy, the elderly with idiopathic normal pressure hydrocephalus, and the elderly with acquired hydrocephalus people. Because the shape and size of the ventricles of these four types of patients are very representative, showing a trend from normal to severe, which can help us systematically and comprehensively analyze the ventricular system. Third, the diagnostic results of these patients were agreed upon by two radiologists with more than 10 years of work experience and strictly followed the disease diagnosis guidelines. Last but not least, due to a large number of normal elderly people and patients with brain atrophy, a large number of manual labeling would be infeasible. However, there is no obvious deformation of their ventricle structure, and it is easier for the automatic ventricle segmentation of the normal elderly and the elderly with brain atrophy. Therefore, we arranged the normal elderly and the elderly with brain atrophy in the order of the time of head imaging examination and numbered them, and made the numbers into small pieces of paper, and placed them in a large carton. Using a simple random sampling method, let 20 doctors in the radiology department randomly sample small pieces of paper. In the end, we randomly selected 20 normal elderly people

and elderly people with brain atrophy for manual marking. The flowchart of the admission and exclusion of patients is shown in **Figure 1**, and the basic study population description is shown in **Table 1**.

Ethics Statement

This study was carried out in accordance with the recommendations of the Ethics Committee of The First Affiliated Hospital of Shenzhen University and Shenzhen Second People's hospital. All subjects gave written informed consent in accordance with the Declaration of Helsinki.

Imaging Protocol and Label

First, a CT scan of the head was performed on two CT instruments, one of which was SOMATOM Definition Flash from Siemens, Germany, and the other was SOMATOM Emotion 16 from Siemens, Germany. Secondly, MRI examinations were conducted using a 1.5T MR scanner (Avanto, Siemens, Erlangen, Germany), and a 3.0T MRI scanner (Prisma, Siemens, Erlangen, Germany). All images were stored in the picture archiving and communication systems (PACS).

Then manually delineation of the ventricle was conducted. For MRI images, we chose T1WI for manual labeling. The specific manual labeling process is as follows: (1) two radiologists with 10 years of clinical experience used ITK software to label the ventricles; (2) a senior radiologist with 20 years of clinical experience evaluated the delineation results of the ventricles and made adjustment if inaccurate manual labeling was found; and (3) for the controversial annotated cases, we invited a neurology expert and a neurosurgery expert to discuss, and modifications and the final annotation results were approved by them.

We defined the thick layer image when the scan layer thickness was >3 mm, and otherwise, it was defined as the thin layer image. Therefore, all images were classified into four groups, i.e., thin-slice CT images, thick-slice CT images, thin-slice MRI images, and thick-slice MRI images.

The Proposed Deep Learning Framework

In real-world scenarios, the thick-slice images are more easily obtained, while thin-slices images are rare, and it is more difficult for clinicians to annotate them. Moreover, the distribution of different image thicknesses can result in the *domain shift* problem that can confuse the deep learning models (Yan et al., 2019). Therefore, we proposed a thickness agnostic image segmentation model, which only required the annotation of thick-slice images for the model training.

Our goal is to utilize the unlabeled thin-slice images to minimize the performance gap between thick-slice and thin-slice images. In our model, the thick-slice images are denoted as $D_S = \left\{\left(x_s, y_s\right) \middle|\ x_s \in R^{H\times W\times 3}, y_s \in R^{H\times W}\right\}$, and the thin-slices images are represented as $D_T = \{x_t | x_t \in R^{H\times W\times 3}\}$.

With the increased development and application of deep learning methods, encoder-decoder based architectures (Milletari et al., 2016; Zhou et al., 2018) are widely used in medical image segmentation. The workflow of our proposed deep learning based framework is presented in **Figure 2**. For image feature extraction and reconstruction, we adopted ResNet-34, which was pre-trained on ImageNet datasets as the encoder of input images. For the decoder, sub-pixel convolution was used for constructing segmentation results since the deconvolution operation was computationally heavy and interpolation-based methods could not bring additional information to improve the segmentation. The sub-pixel convolution can be then represented as

$$F^L = SP\left(W_L * F^{L-1} + b_L\right), \tag{1}$$

where $SP(\cdot)$ operator transforms and arranges a tensor with the shape of $H \times W \times C \times r^2$ into a tensor shaped in $rH \times rW \times C$, F^{L-1} and F^L are the input feature and output feature, W_L and b_L are the parameters of the sub-pixel convolution operator.

We took both thick-slice and thin-slice images as the input and optimized our model with the following objective function

$$L\left(x_s, x_t\right) = L_S\left(p_s, y_s\right) + \lambda L_T(p_t), \tag{2}$$

where λ is a hyper-parameter for weighting the impact of L_s and L_T, p_s and p_t are the model's predictions of the segmentation probability shaped of $H \times W \times C$. L_S is the cross-entropy loss defined as follows

$$L_S = -\frac{1}{HW}\sum_{n=1}^{HW}\sum_{c=1}^{C} y_s^{n,c} \log p_t^{n,c}. \tag{3}$$

Since we expect our model to learn an accurate segmentation paradigm for both thick-slice images and thin-slice images, the L_T can be regarded as the distance between the probability distribution of the target domain (thin-slice domain) p_t and the uniform distribution $U = \frac{1}{C}$. Therefore, minimizing the distance between the two distributions enables classes to be more separable. Because it implicitly pushes the image features away from the decision boundary and makes alignment between two distributions. Mathematically, the objective function of thin-slice images is formulated as

$$L_T = -D_f(p_t^{n,c} || U) = -\frac{1}{C}\sum_{c=1}^{C} f\left(C p_t^{n,c}\right). \tag{4}$$

Most existing methods (Vu et al., 2019) would choose $f(x) = x\log x$, which is alternatively named as the KL-divergence. However, one of the main obstacles is that when adopting KL-divergence for L_T as the objective function, the gradient of L_T would be extremely imbalanced between easy and hard samples. Taking the binary case as an example, the gradient can be computed as

$$\frac{\partial L_T}{\partial p_t^{n,i}} = \log\left(1 - p_t^{n,i}\right) - \log p_t^{n,i}, \tag{5}$$

of which the increasing speed is faster as $p_t^{n,i}$ becomes larger.

Therefore, to mitigate the unbalancing problem represented above, instead of choosing $f(x) = x\log x$, we select Pearson χ^2

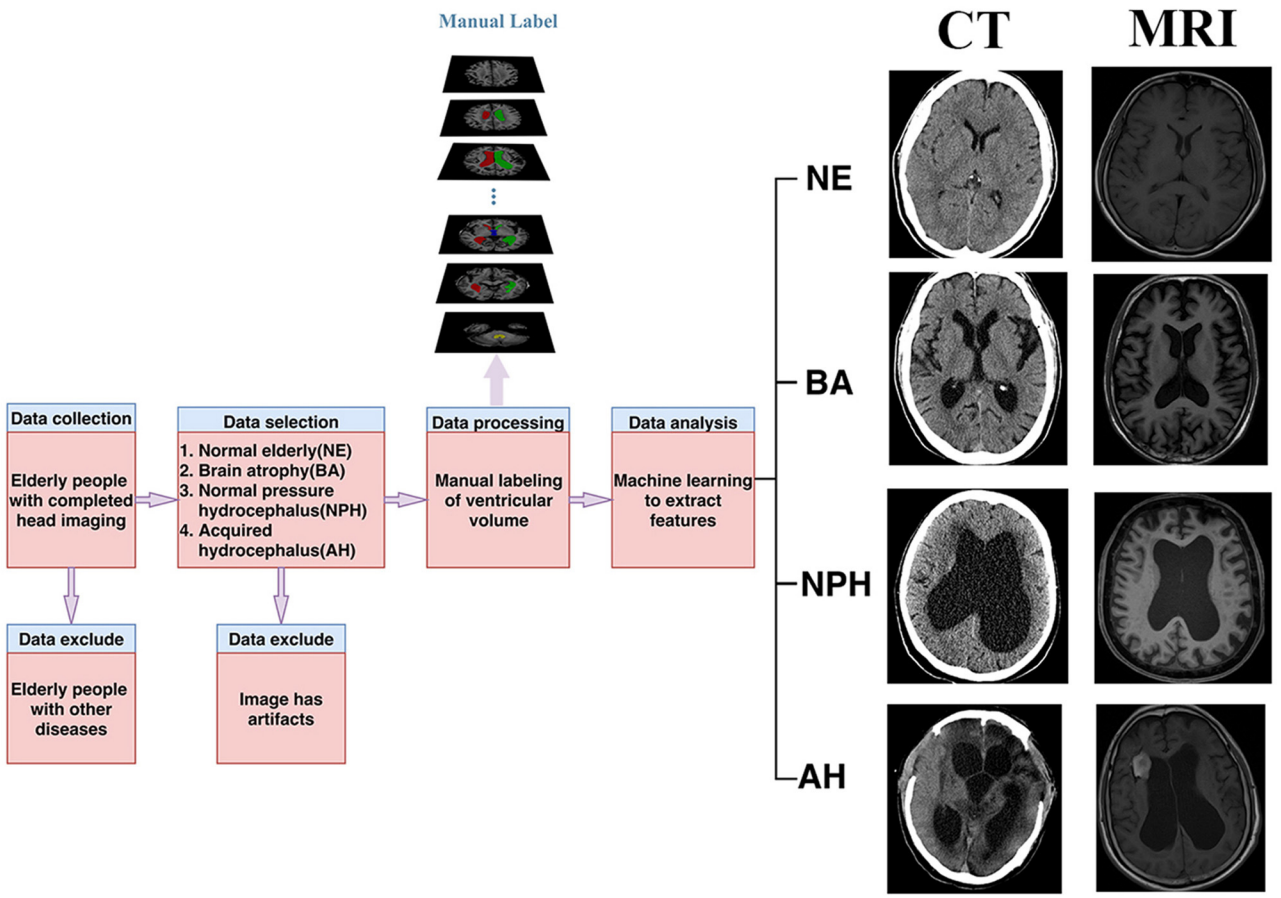

FIGURE 1 | Study flow chart for the inclusion of participants.

divergence [i.e., $f(x) = x^2 - 1$] for L_T. Therefore, the gradient of L_T can be noted as

$$\frac{\partial L_T}{\partial p_t^{n,i}} = 2 - 4p_t^{n,i}, \tag{6}$$

which balances the gradient between easy and hard samples. During model training, the above loss functions were optimized iteratively. For testing, we fed each slice of images as the input and get the predicted segmentation.

RESULT

Diagnostic Efficiency

For experiments, we collected thick-slice and thin-slice samples from iNPH patients with different modalities (MRI and CT) as **Table 2** shows. It is of note that we only used the annotations from thick-slice images for our supervised deep learning. We investigated the performance of U-Net (Ronneberger et al., 2015) and U-Net++ (Zhou et al., 2018) on thin-slice and thick-slice images. Both U-Net and U-Net++ adopted encoders and decoders structure while using the middle features to maintain the information of images. As shown in **Table 3**, compared to conventional and state-of-the-art models, our method achieved significant improvement on both thick-slice and thin-slice images. To further illustrate, our method outperformed U-Net and U-Net++, which are commonly used in medical segmentation, by a large margin. Besides, with the help of a pre-trained ResNet-34 encoder, our model could gain at most 0.1 Dice coefficient on thick-slice images.

Component Analysis

To examine the influence of each component in our method, we conducted ablation studies to verify the effectiveness of our method, and the results are summarized in **Table 4**. We can observe that if our model only trained on thick-slice images, we can get comparable results on thick slices but the model cannot perform well on thin-slice images as shown in the first row of **Table 4**. However, without the annotation from images, the prediction results would be extremely unreliable since the objective function reached the global minimum when the probability of each class was assigned the same value. Moreover, when incorporating both thick-slice and thin-slice images into the training under the proposed semi-supervised paradigm, our method could result in better performance on thin-slice images

TABLE 1 | Demographic information of subjects used in this study.

	Normal elderly (n = 20)	Brain atrophy (n = 20)	Normal pressure hydrocephalus (n = 64)	Acquired hydrocephalus (n = 51)
Age* (years)	64.81 ± 3.19	70.95 ± 5.55	70.77 ± 6.81	67.01 ± 5.41
Sex (male:female)	11:9	12:8	37:27	31:20
Scanning status of imaging equipment[#]				
CT-1	4	3	19	24
CT-2	6	7	28	16
MRI-1	5	4	23	18
MRI-2	5	6	31	20

Age reported as mean ± standard deviation.

[#]*CT-1 represents the CT instrument of SOMATOM Definition Flash from Siemens, Germany. CT-2 represents the CT instrument of SOMATOM Emotion 16 from Siemens, Germany. MRI-1 represents the 1.5T MR scanner (Avanto, Siemens, Erlangen, Germany). MRI-2 represents the 3.0T MRI scanner (Prisma, Siemens, Erlangen, Germany). The slice thickness of CT image includes: 0.5, 1.0, 1.5, 2.0, 4.8, 5.0 mm. The slice thickness of MRI image includes: 1.0, 7.8, 8.0 mm.*

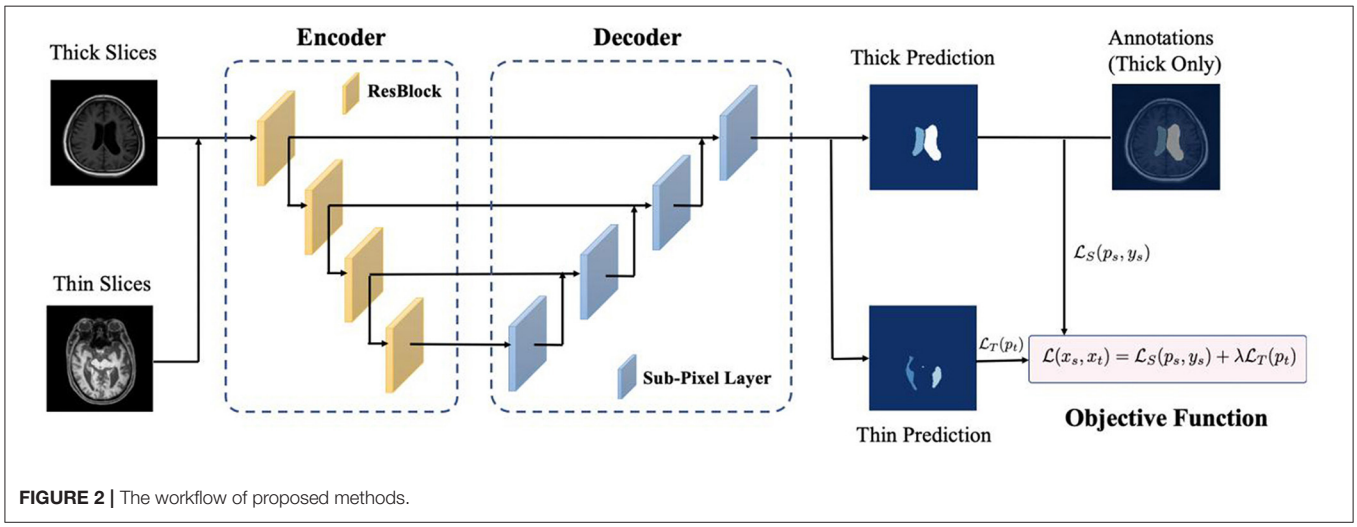

FIGURE 2 | The workflow of proposed methods.

TABLE 2 | The number of thick-slice and thin-slice images used for our study.

Modality	The number of the training set		The number of the testing set	
	Thick-slice	Thin-slice	Thick-slice	Thin-slice
MRI	1,013	1,629	189	982
CT	2,611	2,595	309	492

For CT and MRI datasets, each dataset is divided into two groups. The training set is only used for model training and optimization, while the testing set is used to validate the effectiveness of the trained model.

by at least 3.5% improvement on the Dice coefficient compared to the model in Exp 1, while it only sacrificed little performance on thick images. The rationale behind this is that our model can learn a shared feature representation for both thick-slice and thin-slice images, which can be beneficial for handling different types of images.

Qualitative Analysis

Figure 3 shows the example segmentation results on randomly selected thin-slice images from the testing set for both MRI and CT modalities. In the second column of each modality, it can be observed that U-Net performed poorly on MRI images. Meanwhile, U-Net++, which is the updated version of U-Net, showed better predictions compared to the U-Net while they were still not accurate. Compared with the U-Net and U-Net++, our method achieved accurate results and could segment both MRI and CT images with high precision. Particularly, in the last row of the CT example, although the original image had low contrast, our method was still able to recognize each part and segmented the data accurately, which has demonstrated the robustness of our method. Divide patients with acquired hydrocephalus into Subarachnoid hemorrhage group, brain trauma group, and brain tumor group according to the cause of the disease. Using our method to automatically segment the images of the three groups of patients, the results of CT images show that the Dice of the three groups are 0.94, 0.95, and 0.94, respectively. The results of the MRI image showed that the Dice of the three groups were 0.91, 0.89, 0.92, respectively (**Table 5**).

DISCUSSION

Through **Figures 2**, **3** and **Tables 2**–**4**, we can observe that our automated ventricle segmentation method can be successfully applied CT and MRI images with different thicknesses. More

TABLE 3 | Comparison results (Dice) of our method vs. other state-of-the-art methods.

Method	MRI			CT		
	Thick	Thin	Mixed	Thick	Thin	Mixed
U-Net (Ronneberger et al., 2015)	0.9226	0.7665	0.8353	0.9351	0.7987	0.8513
U-Net++ (Zhou et al., 2018)	0.9159	0.8495	0.8602	**0.9421**	0.7797	0.8424
Ours	**0.9323**	**0.9056**	**0.9099**	0.9365	**0.8697**	**0.8954**

For each trained model, we tested it on thick-slice data only, thin-slice data only, and the combination of these two data. We can see that our method outperforms the other two state-of-the-art methods by a large margin, especially on the thin-slice images. Bold values indicate the best performance.

TABLE 4 | Dice coefficient comparison for our ablation studies.

Exp.	Thick	Thin	MRI			CT		
			Thick	Thin	Mixed	Thick	Thin	Mixed
1	√		**0.9390**	0.8199	0.8391	**0.9438**	0.8345	0.8767
2		√	0.0034	0.0108	0.0110	0.0109	0.0006	0.0069
3	√	√	0.9323	**0.9056**	**0.9099**	0.9365	**0.8697**	**0.8954**

Trained our model with different thickness images. "Thick" represents our model is trained with labeled thick-slice images, and "Thin" means the model is trained with thin-slice images without annotations. We can see with the help of the semi-supervised training technique we proposed, our method can gain a significant improvement on thin-slice images. Bold values indicate the best performance.

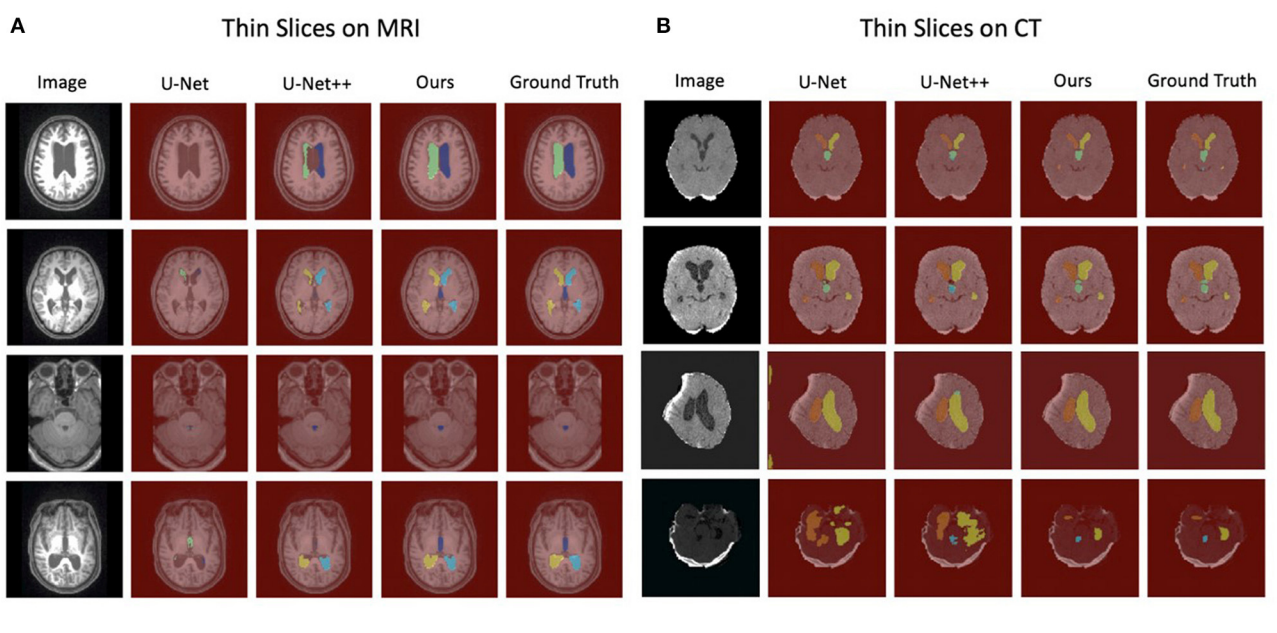

FIGURE 3 | The visualization of segmentation results for thin-slice with MRI images and CT images. **(A)** The completeness of segmentation indicates the performance of each model on MRI images in which our method achieves the best. **(B)** Our method is superior to other competing approaches on CT images, specifically for low contrast images (The last row).

importantly, the segmentation results obtained are better (Dice > 0.9) compared to widely used U-Net and its advanced version U-Net++. There is no doubt that the proposed method is promising for different clinical scenarios.

Clinical Significance of the Automated Ventricle Segmentation

Changes in the shape and size of the ventricles are associated with many diseases, and relevance ventricular enlargement is a crucial marker of brain atrophy associated with normal or pathological aging processes (Schoemaker et al., 2019). Ventricular enlargement also represents a feasible short-term marker of disease progression in mild cognitive impairment and Alzheimer's disease (Nestor et al., 2008). Ventricular enlargement can occur early in the course of Parkinson's disease and is associated with cognitive decline (Apostolova et al., 2012). New/enlarging T2w lesions adjacent to the ventricle wall and thalamic atrophy are independently associated with

TABLE 5 | Thick-slice image segmentation results(Dice) of acquired hydrocephalus.

Method	CT			MRI		
	Subarachnoid hemorrhage ($n = 24$)	Trauma ($n = 13$)	Tumor ($n = 3$)	Subarachnoid hemorrhage ($n = 24$)	Trauma ($n = 10$)	Tumor ($n = 4$)
U-Net	0.9091	0.9143	**0.9387**	0.9085	0.8729	0.92
U-Net++	0.8903	0.8835	0.9219	0.9004	0.8649	**0.9274**
Ours	**0.9407**	**0.9454**	0.9364	**0.9105**	**0.8919**	0.9231

Divide patients with acquired hydrocephalus into cerebral hemorrhage group, brain trauma group, and brain tumor group according to the cause of the disease. Using our method to automatically segment the images of the three groups of patients, the results of CT images show that the Dice of the three groups are 0.94, 0.95, and 0.94, respectively. The results of the MRI image showed that the Dice of the three groups were 0.91, 0.89, 0.92, respectively. Bold values indicate the best performance.

lateral ventricular enlargement in multiple sclerosis (Sinnecker et al., 2020). Ventricular enlargement is also arguably the most consistent neuroanatomical biomarker present in schizophrenia (Sayo et al., 2012). Whether it is to detect early disease (Dalaker et al., 2011), evaluate the condition of the patient (Ferrarini et al., 2008), diagnose the disease (Relkin et al., 2005), evaluate the effect of surgery (Neikter et al., 2020) or other aspects, accurate measurement of the size of the ventricles has very important clinical significance (Shi et al., 2015).

When following patients with hydrocephalus, the timing for intervention is difficult to decide for clinicians. Therefore, by providing clinicians with an accurate measure of increased ventricle volume, automated ventricular segmentation techniques would give them more information to make their decisions (Qiu et al., 2015). The segmentation of ventricles provides quantitative measures on the changes of ventricles in the brain that form vital diagnostics information (Chen et al., 2009). The automated segmentation of ventricles can assist in making a differential diagnosis of ischemic stroke. The quantitative measurement of the ventricles can be helpful in a treatment, recovery, and follow-up process. The segmented ventricles can also serve as the reference in determining the spatial position of the infarct, which can provide useful information for treatment planning (Poh et al., 2012). Accurate and automated segmentation and labeling tools enable more sophisticated evaluations of the ventricular system in neurodegenerative diseases, cerebrospinal fluid disorders, as well as in normal aging (Shao et al., 2019). Various diseases affect the size and morphology of the ventricles, and knowledge of the normal and abnormal ventricular system is essential in understanding various pathological states. For these reasons, it is critical to extract the ventricular system to ascertain its morphology and volume (Xia et al., 2004). By manually labeling the ventricles, the time required to measure the volume and relative ventricle volume of each subject is about 30 min, which is acceptable in research, but obviously not feasible in clinical practice (Ambarki et al., 2010). Using the automatic ventricle segmentation method can save time significantly. Besides, the unsupervised segmentation method can leverage the dependency of labeled data which is more practical for a real-world scenario. For instance, Liu et al. (2019) utilized the quality of merged segmentation results to update the ensemble weights of different segmentation results in order to achieve accurate segmentation results. Meanwhile, Ganaye et al. (2018) took advantage of the invariant nature of the anatomical structure to improve the robustness of the segmentation results by applying semantic constraints.

Comparison Studies and the Advantages of Our Proposed Method

Huff et al. mentioned the limitations of their research for an automated ventricle segmentation method that all the studies were performed on similar CT scanners with similar acquisition parameters and identical slice thicknesses. No pathological ventricles were included in this study other than simply enlarged ventricles (Huff et al., 2019). In our research, we can see that data acquired from different scanners were validated, the thickness of the scan layer was also different, and pathological ventricles were also included. Qiu et al. (2015) outlined the limitations of their study as validated on a limited number of images since MR images of preterm neonates were usually not performed at our center unless a severe disease was suspected. Because of this, we did not deliberately make requests when selecting patients. As our goal is to automatically segment the ventricles, the image we chose must be systematic and comprehensive. The shape and size of the ventricles of the four groups of patients can represent the ventricles of the elderly cohort. Kocaman et al. (2019) performed a study on a small number of individuals. The actual sample size of our four groups of patients is large, and in clinical practice, these patients are relatively common. As the sample size increased, the results of our automated ventricle segmentation method were also gradually stabilized.

Xia et al. pointed out the limitations of their research on automated extraction of the ventricular system: When the slice thickness, especially in coronal and axial directions, is too high, the algorithm could not work satisfactorily. Most of the subjects tested did not have any pathology or major distortion of the ventricles (Xia et al., 2004). In our research, the thickness of the scan slice was no longer a confounding factor. Both thick-slice and thin-slice images could be processed with better ventricle segmentation results. At the same time, our patients included not only normal elderly people but also brain atrophy elderly people with slight changes in the ventricle shape and size. Besides, our proposed framework also performed well for iNPH patients with significant changes in the shape and size of the ventricles. More importantly, the elderly with acquired

hydrocephalus with obvious changes in intracranial structures caused by trauma, tumor, hemorrhage, and other conditions were also included. Shao et al. mentioned in their brain ventricle parcellation work that the proposed network was also robust to white matter hyperintensities (WMH), which were often associated with NPH and located adjacent to the lateral ventricles. WMH can sometimes negatively affect the outcome of automated segmentation algorithms (Shao et al., 2019). Similarly, some of our patients were also NPH patients, and they had white matter hyperintensities around their lateral ventricles. Some patients with brain atrophy had a similar situation, but our ventricle segmentation framework could handle it.

Influence of Examination Type and Slice Thickness on Ventricle Segmentation

In clinical work, we often choose CT or MRI for head imaging examination. Both methods have their advantages and disadvantages. For CT, it is relatively convenient to operate, no need to worry about metal implantation, and the inspection speed is fast. But it has ionizing radiation to the human body, and it has a low signal to noise ratio and relatively low contrast. For MRI, it does not produce ionizing radiation and can provide better soft-tissue resolution, but its inspection time is long and may have considerable issues such as metal implantation and claustrophobia and other related problems (Chen et al., 2009; Liu et al., 2010; Coupe et al., 2011; Poh et al., 2012; Qian et al., 2017; Huff et al., 2019). It is well known that in medical images partial volume effect is inevitable. Reducing the slice thickness can reduce the partial volume effect. But for CT examinations, this means that patients have to receive more ionizing radiation, and for MRI examinations, the examination time will be longer. For deep learning, more content means more information, so thin-layer images are naturally the best choice. However, in clinical practice, because of the heavy burden for a large patient population, thick-slice scanning is still the most used acquisition method. But for the segmentation of the ventricles from thick-slice images, the number of images per patient is small, and the information that can be extracted is also limited. Coupled with the influence of the partial volume effect, it is often difficult to segment the boundaries of the ventricles from thick-slice images (Xia et al., 2004). The stroke area on the CT image is often adjacent or connected to the ventricle area, and the grayscale is similar, which increases the difficulty of accurately segmenting the ventricle (Qian et al., 2017). In addition, on the CT image, due to the noise and low contrast between the soft tissues, there is no obvious peak in the cerebrospinal fluid in the whole brain intensity histogram. This makes it difficult to find a suitable threshold for cerebrospinal fluid using traditional histogram-based segmentation methods (Liu et al., 2010). Part of the volume effect will affect the segmentation of the ventricle, especially on MR images with limited resolution (Coupe et al., 2011). Due to the partial volume effect, there exist transition regions between the Cerebrospinal fluid and gray matter, if these transition regions are completely excluded, the ventricular system is under-segmented, and some ventricular components, for example, the lateral ventricles, may be broken into several disconnected parts (Liu et al., 2009). The temporal horns and occipital poles of the ventricle can be separated from the main body. When the shape-based ventricle segmentation method and the ventricle segmentation method based on the regional growth technology are used, the results will be affected. In addition, the signal intensity of the choroidal plexus is similar to that of gray matter. When a simple threshold technique is used to segment the ventricle, the result will also be affected (Coupe et al., 2011). All in all, different imaging data and slice thickness have their advantages and disadvantages, and they also have a different impact on automated segmentation methods.

Limitations of Our Automated Ventricle Segmentation Framework

Because our current work was a retrospective study based on the elderly to establish a new systematic automated ventricle segmentation method. Therefore, our research might still have some limitations. First of all, because this study selected elderly patients, our method might have insufficient capacity to deal with pediatric patients. Secondly, because this was multi-center and multi-modal research, in terms of results, our goal was to perform well as a whole, so the expression of results in some respects was bound to be relatively weakened. When processing cross-hospital data, we need to handle extensive re-training of the model to ensure the accuracy of the running results. As a deep learning based model, the training data collected at one site are often unavailable to others due to privacy and legal issues (Wang et al., 2020a,b).

In future research, we will focus on extracting different imaging and biological features through deep learning of images, laboratory test results, and clinical information of patients with abnormal ventricles. We will achieve a systematic and comprehensive analysis of patients with ventricular abnormalities, and determine whether the patient has a certain disease that can cause ventricular abnormalities.

CONCLUSION

In order to systematically and comprehensively assess the size of the ventricle of elderly patients, we have established an automated ventricle segmentation method. This automated ventricle segmentation method can not only be applied to both CT and MRI images but can be also applied to images with different slice thicknesses. More importantly, it produces superior segmentation results. Deploying this automated ventricle segmentation method in the clinical scenarios can help doctors to find and diagnose early disease, evaluate the progress of the patient's condition, and inform the treatment planning for the patients. At the same time, the medical image scanning method and the slice thickness are no longer limitations for automated ventricle segmentation. There is no doubt that the proposed method will have a wide application in clinical studies.

DATA AVAILABILITY STATEMENT

The original contributions presented in the study are included in the article/supplementary material, further inquiries can be directed to the corresponding author/s.

ETHICS STATEMENT

The studies involving human participants were reviewed and approved by Ethics Committee of The First Affiliated Hospital of Shenzhen University and Shenzhen Second People's hospital. Written informed consent for participation was not required for this study in accordance with the national legislation and the institutional requirements.

AUTHOR CONTRIBUTIONS

XZ, QY, YJ, JX, and GY conceived and designed the study, contributed to data analysis, contributed to data interpretation, and contributed to the writing of the report. XZ, ZN, WM-S, EF, ZL, and JX contributed to the literature search. XZ and JX contributed to data collection. XZ, QY, YJ, and MW performed data curation and contributed to the tables and figures. All authors contributed to the article and approved the submitted version.

FUNDING

This work was supported in part by the Natural Science Foundation of Guangdong Province (2020A1515010918), in part by the Project of Shenzhen International Cooperation Foundation (GJHZ20180926165402083), in part by the Project of Shenzhen Basic Development Project (JCYJ 20190806164409040), in part by the Clinical Research Project of Shenzhen Health and Family Planning Commission (SZLY2018018), in part by the Hangzhou Economic and Technological Development Area Strategical Grant (Imperial Institute of Advanced Technology), in part by the European Research Council Innovative Medicines Initiative on Development of Therapeutics and Diagnostics Combatting Coronavirus Infections Award DRAGON: rapiD and secuRe AI imaging based diaGnosis, stratification, fOllow-up, and preparedness for coronavirus paNdemics (H2020-JTI-IMI2 101005122), and in part by the AI for Health Imaging Award CHAIMELEON: Accelerating the Lab to Market Transition of AI Tools for Cancer Management (H2020-SC1-FA-DT S-2019-1 952172).

ACKNOWLEDGMENTS

The authors would like to sincerely thank Meng-Yao Xu for her support and suggestions for the production of diagrams and tables throughout the entire project.

REFERENCES

Ambarki, K., Israelsson, H., Wahlin, A., Birgander, R., Eklund, A., and Malm, J. (2010). Brain ventricular size in healthy elderly: comparison between Evans index and volume measurement. *Neurosurgery 67*, 94–99. doi: 10.1227/01.NEU.0000370939.30003.D1

Anandh, K. R., Sujatha, C. M., and Ramakrishnan, S. (2016). A method to differentiate mild cognitive impairment and Alzheimer in MR images using Eigen value descriptors. *J. Med. Syst.* 40:25. doi: 10.1007/s10916-015-0396-y

Apostolova, L., Alves, G., Hwang, K. S., Babakchanian, S., Bronnick, K. S., and Larsen, J. P., et al. (2012). Hippocampal and ventricular changes in Parkinson's disease mild cognitive impairment. *Neurobiol. Aging* 33, 2113–2124. doi: 10.1016/j.neurobiolaging.2011.06.014

Brix, M. K., Westman, E., Simmons, A., Ringstad, G. A., Eide, P. K., and Wagner-Larsen, K., et al. (2017). The Evans' Index revisited: new cut-off levels for use in radiological assessment of ventricular enlargement in the elderly. *Eur. J. Radiol.* 95, 28–32. doi: 10.1016/j.ejrad.2017.07.013

Cavedo, E., Galluzzi, S., Pievani, M., Boccardi, M., and Frisoni, G. B. (2012). Norms for imaging markers of brain reserve. *J. Alzheimers Dis.* 31, 623–633. doi: 10.3233/JAD-2012-111817

Chen, W., Smith, R., Ji, S. Y., Ward, K. R., and Najarian, K. (2009). Automated ventricular systems segmentation in brain CT images by combining low-level segmentation and high-level template matching. *BMC Med. Inform. Decis. Mak.* 9 (Suppl. 1):S4. doi: 10.1186/1472-6947-9-S1-S4

Cherukuri, V., Ssenyonga, P., Warf, B. C., Kulkarni, A. V., Monga, V., and Schiff, S. J. (2018). Learning based segmentation of CT brain images: application to postoperative hydrocephalic scans. *IEEE Trans. Biomed. Eng.* 65, 1871–1884. doi: 10.1109/TBME.2017.2783305

Chou, Y. Y., Lepore, N., Avedissian, C., Madsen, S. K., Parikshak, N., and Hua, X., et al. (2009). Mapping correlations between ventricular expansion and CSF amyloid and tau biomarkers in 240 subjects with Alzheimer's disease, mild cognitive impairment and elderly controls. *Neuroimage* 46, 394–410. doi: 10.1016/j.neuroimage.2009.02.015

Chou, Y. Y., Lepore, N., de Zubicaray, G. I., Carmichael, O. T., Becker, J. T., and Toga, A. W., et al. (2008). Automated ventricular mapping with multi-atlas fluid image alignment reveals genetic effects in Alzheimer's disease. *Neuroimage* 40, 615–630. doi: 10.1016/j.neuroimage.2007.11.047

Coupe, P., Manjon, J. V., Fonov, V., Pruessner, J., Robles, M., and Collins, D. L. (2011). Patch-based segmentation using expert priors: application to hippocampus and ventricle segmentation. *Neuroimage* 54, 940–954. doi: 10.1016/j.neuroimage.2010.09.018

Dalaker, T. O., Zivadinov, R., Ramasamy, D. P., Beyer, M. K., Alves, G., and Bronnick, K. S., et al. (2011). Ventricular enlargement and mild cognitive impairment in early Parkinson's disease. *Mov. Disord.* 26, 297–301. doi: 10.1002/mds.23443

Del, R. E., Konishi, J., Bouix, S., Blokland, G. A., Mesholam-Gately, R. I., and Goldstein, J., et al. (2016). Enlarged lateral ventricles inversely correlate with reduced corpus callosum central volume in first episode schizophrenia: association with functional measures. *Brain Imaging Behav.* 10, 1264–1273. doi: 10.1007/s11682-015-9493-2

Dubost, F., Bruijne, M., Nardin, M., Dalca, A. V., Donahue, K. L., and Giese, A. K., et al. (2020). Multi-atlas image registration of clinical data with automated quality assessment using ventricle segmentation. *Med. Image Anal.* 63:101698. doi: 10.1016/j.media.2020.101698

Ferrarini, L., Palm, W. M., Olofsen, H., van der Landen, R., Jan, B. G., and Westendorp, R. G., et al. (2008). MMSE scores correlate with local ventricular enlargement in the spectrum from cognitively normal to Alzheimer disease. *Neuroimage* 39, 1832–1838. doi: 10.1016/j.neuroimage.2007.11.003

Ganaye, P. A., Sdika, M., and Benoit-Cattin, H. (2018). "Semi-supervised learning for segmentation under semantic constraint," in *International Conference on Medical Image Computing and Computer-Assisted Intervention* (Cham: Springer), 595–602.

He, W., Fang, X., Wang, X., Gao, P., Gao, X., and Zhou, X., et al. (2020). A new index for assessing cerebral ventricular volume in idiopathic normal-pressure hydrocephalus: a comparison with Evans' index. *Neuroradiology* 62, 661–667. doi: 10.1007/s00234-020-02361-8

Huff, T. J., Ludwig, P. E., Salazar, D., and Cramer, J. A. (2019). Fully automated intracranial ventricle segmentation on CT with 2D regional convolutional neural network to estimate ventricular volume. *Int. J. Comput. Assist. Radiol. Surg.* 14, 1923–1932. doi: 10.1007/s11548-019-02038-5

Kempton, M. J., Underwood, T. S., Brunton, S., Stylios, F., Schmechtig, A., and Ettinger, U., et al. (2011). A comprehensive testing protocol for MRI neuroanatomical segmentation techniques: evaluation of a novel lateral ventricle segmentation method. *Neuroimage* 58, 1051–1059. doi: 10.1016/j.neuroimage.2011.06.080

Khan, A. F., Drozd, J. J., Moreland, R. K., Ta, R. M., Borrie, M. J., and Bartha, R. (2012). A novel MRI-compatible brain ventricle phantom for validation of

segmentation and volumetry methods. *J. Magn. Reson. Imaging* 36, 476–482. doi: 10.1002/jmri.23612

Kocaman, H., Acer, N., Koseoglu, E., Gultekin, M., and Donmez, H. (2019). Evaluation of intracerebral ventricles volume of patients with Parkinson's disease using the atlas-based method: a methodological study. *J. Chem. Neuroanat.* 98, 124–130. doi: 10.1016/j.jchemneu.2019.04.005

Liu, B., Gu, L., and Lu, F. (2019). "Unsupervised ensemble strategy for retinal vessel segmentation," in *International Conference on Medical Image Computing and Computer-Assisted Intervention* (Cham: Springer).

Liu, J., Huang, S., Ihar, V., Ambrosius, W., Lee, L. C., and Nowinski, W. L. (2010). Automatic model-guided segmentation of the human brain ventricular system from CT images. *Acad. Radiol.* 17, 718–726. doi: 10.1016/j.acra.2010.02.013

Liu, J., Huang, S., and Nowinski, W. L. (2009). Automatic segmentation of the human brain ventricles from MR images by knowledge-based region growing and trimming. *Neuroinformatics* 7, 131–146. doi: 10.1007/s12021-009-9046-1

Lundervold, A. J., Vik, A., and Lundervold, A. (2019). Lateral ventricle volume trajectories predict response inhibition in older age-A longitudinal brain imaging and machine learning approach. *PLoS ONE* 14:e207967. doi: 10.1371/journal.pone.0207967

Milletari, F., Navab, N., and Ahmadi, S. A. (2016). "V-net: fully convolutional neural networks for volumetric medical image segmentation," in *2016 Fourth International Conference on 3D Vision (3DV)* (IEEE), 565–571.

Mori, E., Ishikawa, M., Kato, T., Kazui, H., Miyake, H., and Miyajima, M., et al. (2012). Guidelines for management of idiopathic normal pressure hydrocephalus: second edition. *Neurol. Med. Chir.* 52, 775–809. doi: 10.2176/nmc.52.775

Neikter, J., Agerskov, S., Hellstrom, P., Tullberg, M., Starck, G., and Ziegelitz, D., et al. (2020). Ventricular volume is more strongly associated with clinical improvement than the evans index after shunting in idiopathic normal pressure hydrocephalus. *AJNR Am. J. Neuroradiol.* 41, 1187–1192. doi: 10.3174/ajnr.A6620

Nestor, S. M., Rupsingh, R., Borrie, M., Smith, M., Accomazzi, V., and Wells, J. L., et al. (2008). Ventricular enlargement as a possible measure of Alzheimer's disease progression validated using the Alzheimer's disease neuroimaging initiative database. *Brain* 131 (Pt 9), 2443–2454. doi: 10.1093/brain/awn146

Owen, J. P., Bukshpun, P., Pojman, N., Thieu, T., Chen, Q., and Lee, J., et al. (2018). Brain MR imaging findings and associated outcomes in carriers of the reciprocal copy number variation at 16p11.2. *Radiology* 286, 217–226. doi: 10.1148/radiol.2017162934

Poh, L. E., Gupta, V., Johnson, A., Kazmierski, R., and Nowinski, W. L. (2012). Automatic segmentation of ventricular cerebrospinal fluid from ischemic stroke CT images. *Neuroinformatics* 10, 159–172. doi: 10.1007/s12021-011-9135-9

Qian, X., Lin, Y., Zhao, Y., Yue, X., Lu, B., and Wang, J. (2017). Objective ventricle segmentation in brain CT with ischemic stroke based on anatomical knowledge. *Biomed. Res. Int.* 2017:8690892. doi: 10.1155/2017/8690892

Qiu, W., Yuan, J., Rajchl, M., Kishimoto, J., Chen, Y., and de Ribaupierre, S., et al. (2015). 3D MR ventricle segmentation in pre-term infants with post-hemorrhagic ventricle dilatation (PHVD) using multi-phase geodesic level-sets. *Neuroimage* 118, 13–25. doi: 10.1016/j.neuroimage.2015.05.099

Relkin, N., Marmarou, A., Klinge, P., Bergsneider, M., and Black, P. M. (2005). Diagnosing idiopathic normal-pressure hydrocephalus. *Neurosurg.* 57, S4–S16. doi: 10.1227/01.NEU.0000168185.29659.C5

Ronneberger, O., Fischer, P., and Brox, T. (2015). "U-Net: convolutional networks for biomedical image segmentation," in: *Medical Image Computing and Computer-Assisted Intervention – MICCAI 2015*. Lecture notes in computer science, Vol. 9351, eds N. Navab, J. Hornegger, W. Wells, and A. Frangi (Cham: Springer).

Sayo, A., Jennings, R. G., and Van Horn, J. D. (2012). Study factors influencing ventricular enlargement in schizophrenia: a 20 year follow-up meta-analysis. *Neuroimage* 59, 154–167. doi: 10.1016/j.neuroimage.2011.07.011

Schoemaker, D., Buss, C., Pietrantonio, S., Maunder, L., Freiesleben, S. D., and Hartmann, J., et al. (2019). The hippocampal-to-ventricle ratio (HVR): Presentation of a manual segmentation protocol and preliminary evidence. *Neuroimage* 203:116108. doi: 10.1016/j.neuroimage.2019.116108

Shao, M., Han, S., Carass, A., Li, X., Blitz, A. M., and Shin, J., et al. (2019). Brain ventricle parcellation using a deep neural network: application to patients with ventriculomegaly. *Neuroimage Clin.* 23:101871. doi: 10.1016/j.nicl.2019.101871

Shi, J., Stonnington, C. M., Thompson, P. M., Chen, K., Gutman, B., and Reschke, C., et al. (2015). Studying ventricular abnormalities in mild cognitive impairment with hyperbolic Ricci flow and tensor-based morphometry. *Neuroimage* 104, 1–20. doi: 10.1016/j.neuroimage.2014.09.062

Silbert, L. C., Quinn, J. F., Moore, M. M., Corbridge, E., Ball, M. J., and Murdoch, G., et al. (2003). Changes in premorbid brain volume predict Alzheimer's disease pathology. *Neurology* 61, 487–492. doi: 10.1212/01.WNL.0000079053.77227.14

Sinnecker, T., Ruberte, E., Schadelin, S., Canova, V., Amann, M., and Naegelin, Y., et al. (2020). New and enlarging white matter lesions adjacent to the ventricle system and thalamic atrophy are independently associated with lateral ventricular enlargement in multiple sclerosis. *J. Neurol.* 267, 192–202. doi: 10.1007/s00415-019-09565-w

Tang, X., Crocetti, D., Kutten, K., Ceritoglu, C., Albert, M. S., and Mori, S., et al. (2015). Segmentation of brain magnetic resonance images based on multi-atlas likelihood fusion: testing using data with a broad range of anatomical and photometric profiles. *Front. Neurosci.* 9:61. doi: 10.3389/fnins.2015.00061

Tang, X., Luo, Y., Chen, Z., Huang, N., Johnson, H. J., and Paulsen, J. S., et al. (2018). A fully-automated subcortical and ventricular shape generation pipeline preserving smoothness and anatomical topology. *Front. Neurosci.* 12:321. doi: 10.3389/fnins.2018.00321

Thompson, P. M., Hayashi, K. M., De Zubicaray, G. I., Janke, A. L., Rose, S. E., and Semple, J., et al. (2004). Mapping hippocampal and ventricular change in Alzheimer disease. *Neuroimage* 22, 1754–1766. doi: 10.1016/j.neuroimage.2004.03.040

Toma, A. K., Holl, E., Kitchen, N. D., and Watkins, L. D. (2011). Evans' index revisited: the need for an alternative in normal pressure hydrocephalus. *Neurosurgery* 68, 939–944. doi: 10.1227/NEU.0b013e318208f5e0

Vu, T., Jain, H., Bucher, M., Cord, M., and Pérez, P. (2019). "ADVENT: adversarial entropy minimization for domain adaptation in semantic segmentation," in *2019 IEEE/CVF Conference on Computer Vision and Pattern Recognition (CVPR), Long Beach, CA, USA*, 2512–2521.

Wang, C., Dong, S., Zhao, X., Papanastasiou, G., Zhang, H., and Yang, G. (2020a). SaliencyGAN: deep learning semisupervised salient object detection in the fog of IoT. *IEEE Trans. Indus. Inform.* 16, 2667–2676. doi: 10.1109/TII.2019.2945362

Wang, C., Yang, G., Papanastasiou, G., Zhang, H., Rodrigues, J., and Albuquerque, V. (2020b). "Industrial cyber-physical systems-based cloud IoT edge for federated heterogeneous distillation," in *IEEE Transactions on Industrial Informatics*, 1.

Xia, Y., Hu, Q., Aziz, A., and Nowinski, W. L. (2004). A knowledge-driven algorithm for a rapid and automatic extraction of the human cerebral ventricular system from MR neuroimages. *Neuroimage* 21, 269–282. doi: 10.1016/j.neuroimage.2003.09.029

Yan, W., Wang, Y., Gu, S., Huang, L., Yan, F., Xia, L., et al. (2019). "The domain shift problem of medical image segmentation and vendor-adaptation by Unet-GAN," in *International Conference on Medical Image Computing and Computer-Assisted Intervention*: (Cham Springer), 623–631.

Zhou, Z., Siddicquee, M., Tajbakhsh, N., and Liang, J. (2018). UNet++: a nested U-Net architecture for medical image segmentation. *Deep Learn Med Image Anal Multimodal Learn Clin Decis Support* 11045, 3–11. doi: 10.1007/978-3-030-00889-5_1

Conflict of Interest: ZN and WM-S are employed by Aladdin Healthcare Technologies Ltd. QY, YJ, and MW are employed by Hangzhou Ocean's Smart Boya Co., Ltd., China and Mind Rank Ltd., China.

The remaining authors declare that the research was conducted in the absence of any commercial or financial relationships that could be construed as a potential conflict of interest.

frontiers in Aging Neuroscience

ORIGINAL RESEARCH
published: 21 December 2020
doi: 10.3389/fnagi.2020.604246

Aggregation of Vascular Risk Factors Modulates the Amplitude of Low-Frequency Fluctuation in Mild Cognitive Impairment Patients

Liying Zhuang[1,2], Huafu Ni[1,3], Junyang Wang[1], Xiaoyan Liu[1], Yajie Lin[1], Yujie Su[1], Kan Zhang[1], Yaguo Li[2], Guoping Peng[1] and Benyan Luo[1]**

[1] Department of Neurology, First Affiliated Hospital, Zhejiang University School of Medicine, Hangzhou, China, [2] Department of Neurology, Zhejiang Hospital, Hangzhou, China, [3] Department of Neurology, Beilun People's Hospital, Ningbo, China

Background: Several vascular risk factors, including hypertension, diabetes, body mass index, and smoking status are found to be associated with cognitive decline and the risk of Alzheimer's disease (AD). We aimed to investigate whether an aggregation of vascular risk factors modulates the amplitude of low-frequency fluctuation (ALFF) in patients with mild cognitive impairment (MCI).

Methods: Forty-three MCI patients and twenty-nine healthy controls (HCs) underwent resting-state functional MRI scans, and spontaneous brain activity was measured by the ALFF technique. The vascular risk profile was represented with the Framingham Heart Study general cardiovascular disease (FHS-CVD) risk score, and each group was further divided into high and low risk subgroups. Two-way ANOVA was performed to explore the main effects of diagnosis and vascular risk and their interaction on ALFF.

Results: The main effect of diagnosis on ALFF was found in left middle temporal gyrus (LMTG) and left superior parietal gyrus (LSPG), and the main effect of risk on ALFF was detected in left fusiform gyrus (LFFG), left precuneus (LPCUN), and left cerebellum posterior lobe (LCPL). Patients with MCI exhibited increased ALFF in the LMTG and LSPG than HCs, and participants with high vascular risk showed increased ALFF in the LFFG and LCPL, while decreased ALFF in the LPCUN. An interaction between diagnosis (MCI vs. HC) and FHS-CVD risk (high vs. low) regarding ALFF was observed in the left hippocampus (LHIP). HCs with high vascular risk showed significantly increased ALFF in the LHIP than those with low vascular risk, while MCI patients with high vascular risk showed decreased ALFF in the LHIP than HCs with high vascular risk. Interestingly, the mean ALFF of LHIP positively correlated with word recall test in HCs with high vascular risk (rho = 0.630, $P = 0.016$), while negatively correlated with the same test in MCI patients with high vascular risk (rho = −0.607, $P = 0.001$).

Conclusions: This study provides preliminary evidence highlighting that the aggregation of vascular risk factors modulates the spontaneous brain activity in MCI patients, and this may serve as a potential imaging mechanism underlying vascular contribution to AD.

Keywords: mild cognitive impairment, functional magnetic resonance imaging, amplitude of low frequency fluctuation, vascular risk, cognition

Edited by:
Xian-Le Bu,
Third Military Medical University, China

Reviewed by:
Zhigang Qi,
Capital Medical University, China
Zan Wang,
Southeast University, China

***Correspondence:**
Benyan Luo
luobenyan@zju.edu.cn
Guoping Peng
guopingpeng@zju.edu.cn

Received: *21 September 2020*
Accepted: *30 November 2020*
Published: *21 December 2020*

Citation:
Zhuang L, Ni H, Wang J, Liu X, Lin Y, Su Y, Zhang K, Li Y, Peng G and Luo B (2020) Aggregation of Vascular Risk Factors Modulates the Amplitude of Low-Frequency Fluctuation in Mild Cognitive Impairment Patients. Front. Aging Neurosci. 12:604246. doi: 10.3389/fnagi.2020.604246

INTRODUCTION

Alzheimer's disease (AD) is a cognitive continuous ranging from cognitively unimpaired, mild cognitive impairment (MCI) to dementia (McKhann et al., 2011; Dubois et al., 2014). Genetic susceptibility as well as environmental factors and their interaction over the life span contributes to a variety of pathological process in the clinical expression of dementia (Qiu et al., 2009). Several vascular risk factors such as hypertension, diabetes, dyslipidemia, and obesity appear to increase AD risk, which suggests the contribution of vascular factors to the pathogenesis of this condition (Breteler, 2000; Purnell et al., 2009). Previous clinical trials have demonstrated that about thirty percent of AD cases are attributed to seven controllable risk factors, including high blood pressure, diabetes, obesity, smoking, depression, low level of physical activity, and education (Barnes and Yaffe, 2011; Norton et al., 2014). Some studies have evaluated the effect of treatment of a single vascular risk factor on cognitive deterioration, however, results were controversial (Launer et al., 2000; Tan et al., 2003; Ninomiya et al., 2011; Safouris et al., 2015). The aggregative effects of vascular risk factors may better illustrate the role of vascular components in cognitive deterioration.

The Framingham Heart Study general cardiovascular disease (FHS-CVD) risk profile is a globally, well-validated and multivariable assessment of overall cardiovascular risk (D'Agostino et al., 2008). The FHS-CVD risk is quantified by weighting sex, age, systolic blood pressure (SBP), treatment for hypertension, current smoking status, diabetes, and body mass index (BMI) and predicts the risk of vascular events over a 10-year period. Furthermore, the FHS-CVD risk can represent the influence of vascular risk factors on structural and functional changes of macro- and micro-vessels. The FHS-CVD risk score can also predict the progression of cognitive decline in AD and the risk of progression from MCI to dementia (Viticchi et al., 2015, 2017). Moreover, vascular risk represented by FHS-CVD risk acts alone and synergistically with β-amyloid (Aβ) pathology to promote cognitive decline in cognitively normal elderly adults (Rabin et al., 2018). While there has been extensive evidence showing the effects of vascular risk factors on disease, the mechanisms of vascular involvement in cognitive impairment, as well as dementia and AD, remain not fully understood.

Functional neuroimaging techniques sensitive to spatial patterns of blood oxygenation or blood flow are important tools for investigating the functional organization of the human brain. Functional MRI (fMRI) is a good example of this field. In 1995, it has been demonstrated that blood oxygen level-dependent (BOLD) low frequency oscillations (<0.1 Hz) in resting-state fMRI were of physiological significance and were closely associated with brain spontaneous neuronal activity (Biswal et al., 1995). He et al. firstly introduced amplitude of low-frequency fluctuation (ALFF) to quantitatively measure regional BOLD signal variation in attention deficit hyperactivity disorder (He et al., 2007). To date, ALFF has been proved to be a reliable and useful indicator to characterize the spontaneous neuronal activity of the brain in MCI or AD patients (Wang et al., 2011; Cha et al., 2015). The purpose of our study was to explore whether the aggregation of vascular risk factors represented by FHS-CVD risk modulates the spontaneous brain activity in MCI patients.

MATERIALS AND METHODS

Participants and Clinical Evaluation

In this study, 43 MCI subjects and 29 healthy controls (HCs) were enrolled from the Memory Clinic of the First Affiliated Hospital, Zhejiang University School of Medicine. Written informed consent were collected from all the subjects prior to participating in the study, in accordance with protocols approved by the Ethics Committee of the First Affiliated Hospital of Zhejiang University (reference number: 2016-315).

Demographic data and medical history were collected from all of the participants. Each of them underwent general and neurological examination and a comprehensive neuropsychological battery assessment, including Clinical Dementia Rating (CDR), Mini-Mental State Examination (MMSE), Montreal Cognitive Assessment (MoCA), and the 14-item AD Assessment Scale-Cognitive (ADAS-Cog) subscale.

Inclusion and Exclusion Criteria

MCI patients met the following criteria (Winblad et al., 2004): (1) 54 to 80 years old; (2) years of education $\geq$ 6; (3) a subjective complaint of memory; (4) an objective memory impairment <1.5 SD for age adjusted and education adjusted norms; (5) CDR = 0.5; (6) MMSE score was 20 or higher for subjects with 6 years and 24 or higher for those with 9 years of education; (7) normal activities of daily living; (8) not demented. In addition, HCs met the following conditions: CDR = 0; MMSE score of 20 or higher for subjects with 6 years and 24 or higher for subjects with 9 years of education (Katzman et al., 1988).

Subjects with prior stroke (Hachinski ischemic score >4), traumatic brain injury, Parkinson's disease, epilepsy, alcoholism, major depression or other neuropsychiatric conditions, or severe visual or hearing loss were all excluded from this study.

FHS-CVD risk

For each participant, the FHS-CVD risk score was quantified by the calculator provided by the American Heart Association and the American College of Cardiology (https://framinghamheartstudy.org/fhs-risk-functions/cardiovascular-disease-10-year-risk/). The information required for FHS-CVD risk includes age, sex, SBP, antihypertensive treatment, diabetes, smoking, and BMI (D'Agostino et al., 2008). The FHS-CVD risk provides a 10-year risk prediction of future cardiovascular events (defined as coronary death, non-fatal myocardial infarction, angina, heart failure, fatal or non-fatal stroke, transient ischemic attack, and peripheral artery disease). Subjects were clustered into two subgroups based on FHS-CVD risk scores (low: <10%, high: $\geq$10%) as in a previous study (Hou et al., 2018), scince guidelines from the American Heart Association recommend aspirin for patients with a 10-year risk more than 10% (Pearson et al., 2002).

MRI Scanning

All subjects were scanned using a General Electric 3.0 Tesla scanner (General Electric Medical Systems, Waukesha, WI, United States) with a standard head coil. Functional images were obtained by a gradient-recalled echo-planar imaging (GRE-EPI) sequence: repetition time (TR) = 2,000 ms; echo time (TE) = 30 ms; flip angle (FA) = 90°; acquisition matrix = 64 × 64; field of view (FOV) = 220 × 220 mm^2; thickness = 3.2 mm; gap = 0 mm; number of slices = 43. T1-weighted anatomical images were acquired by a 3D-magnetization prepared rapid gradient-echo (MPRAGE) sequence: TR = 8.2 ms; TE = 3.18 ms; FA = 8°; acquisition matrix = 256 × 256; FOV = 256 × 256 mm^2; thickness = 1.0 mm; gap = 0 mm; number of slices = 176. During the scan, subjects were asked to keep their eyes closed, remain still, and not to fall asleep.

Imaging Pre-processing

Imaging preprocessing were performed with SPM12 (http://www.fil.ion.ucl.ac.uk/spm) and RESTplus V1.2 (http://www.restfmri.net/forum/RESTplusV1.2). The steps of imaging preprocessing were the same as described previously (Zhuang et al., 2019). The first 10 volumes were discarded for the participants' adaption to the scanner. Timing differences and head-motion effects of the remaining volumes were further corrected. Participants with head motion of translation or rotation parameters exceeding ± 3 mm or ± 3° were excluded. The head motion index estimated by a realignment algorithm was calculated for each participant, and the difference between groups was statistically analyzed. Next, the T1-weighted structural images were co-registered to the motion corrected mean functional images using a linear transformation. Gray matter, white matter and cerebrospinal fluid were further segmented for the transformed structural images with a unified segmentation algorithm (Ashburner and Friston, 2005). The corrected functional images were normalized to the Montreal Neurological Institute (MNI) space and re-sampled to a voxel size of 3 × 3 × 3 mm^3 voxels. The resulting images were spatially smoothed with the full width at half maximum (FWHM) of 6 mm. The last step was the removal of linear trend of time courses.

Calculation of ALFF

ALFF values were calculated using the RESTplus software as in previous studies (He et al., 2007; Zhuang et al., 2019). After data preprocessing, the time series were transformed to the frequency domain of 0.01∼0.08 Hz and the power spectrum was obtained for each given voxel. Secondly, the square root of the power spectrum obtained with the Fast Fourier Transform was averaged between 0.01 and 0.08 Hz. This averaged square root was considered as ALFF. Finally, standardization was performed by dividing the ALFF value of each voxel with the global mean ALFF value within a whole-brain mask.

Statistical Analysis

Two-way analysis of variance (ANOVA) was carried out for the comparison of continuous demographic and neuropsychological data, and chi-square test was applied for categorical variables. The main effects of diagnosis (MCI vs. HC) and FHS-CVD risk (high vs. low), and the interaction between diagnosis and risk were analyzed. All of the statistical analyses above were performed by SPSS 17.0, with $P < 0.05$ as statistically significant.

A voxel-wise ANOVA was performed to analyze the main effects of diagnosis, the main effects of FHS-CVD risk, and the interactions between diagnosis and FHS-CVD risk on ALFF maps using SPM12 (http://www.fil.ion.ucl.ac.uk/spm). The significant clusters of the main effects and interactions were further analyzed by *post-hoc* tests. Multiple comparison correction was carried out for the statistical maps, based on Gaussian random field theory (GRF) (voxel-wise $P < 0.01$, cluster-wise $P < 0.05$, two-tailed) as in previous studies (Yang et al., 2019; Zhou et al., 2019; Huang et al., 2020). At last, we performed a correlative analysis between the ALFF values of the significant clusters of interactions and the neuropsychological test scores ($P < 0.05$).

RESULTS

Demographics and Clinical Data

The excessive motion artifacts or distortions of the images were visually inspected to ensure adequate quality. The head motion index (framewise displacement, FD) was calculated for each participant (Power et al., 2013). The average FD values were compared across different subgroups using two-way ANOVA. Neither main effect of diagnosis ($F = 3.032$, $P = 0.086$), vascular risk ($F = 0.018$, $P = 0.893$), nor interaction between diagnosis and vascular risk ($F = 0.713$, $P = 0.401$) was found on FD.

The demographics profiles of MCI patients and HCs stratified by FHS-CVD risk were shown in **Table 1**. The demographics of MCI patients and HCs, including age, education years, gender ratio were all matched. There were no significant differences of each vascular risk factor and FHS-CVD risk between MCI patients and HCs. Subjects with high FHS-CVD risk got older age, more males, more diabetic patients, and more hypertensive patients with higher SBP. While, there were no significant differences of education years between different FHS-CVD risk subgroups in either MCI or HC groups. Compared with controls, MCI patients exhibited deficits as noted on MMSE, MoCA, word recall test, following commands, delayed word recall, and ADAS-Cog 14. There was no significant difference of neuropsychological test score except for MMSE and Construction scores between high and low FHS-CVD risk. We did not find any interaction between diagnosis and FHS-CVD risk on neuropsychological data (for details see **Supplementary Table 1**).

Diagnosis × FHS-CVD Risk Interaction on ALFF

The main effects of diagnosis on ALFF were identified in the left middle temporal gyrus (LMTG) and left superior parietal gyrus (LSPG). Compared with cognitively normal controls, patients with MCI exhibited higher value of ALFF in the LMTG and LSPG (see **Table 2** and **Figure 1**).

The main effects of FHS-CVD risk on ALFF were observed in the left fusiform gyrus (LFFG), left precuneus (LPCUN), and left cerebellum posterior lobe (LCPL). Compared with subjects

TABLE 1 | Demographics profiles of MCI patients and HCs stratified by FHS-CVD risk.

	MCI group (*N* = 43)		HC group (*N* = 29)		*P*		
	Low risk (*N* = 17)	High risk (*N* = 26)	Low risk (*N* = 15)	High risk (*N* = 14)	diagnosis	risk	interaction
Age (years)	60.71 ± 6.32	64.50 ± 5.64	58.20 ± 4.92	66.79 ± 3.68	0.933	<0.001*	0.070
Education (years)	9.35 ± 2.80	9.73 ± 3.27	10.40 ± 3.44	11.43 ± 2.79	0.074	0.355	0.668
Gender (male/female)	0/17	18/8	1/14	6/8	0.291	<0.001*	0.079
SBP (mmHg)	117.47 ± 7.75	125.58 ± 15.52	116.93 ± 10.84	126.21 ± 13.74	0.987	0.007*	0.850
BMI (Kg/m^2)	22.73 ± 3.12	24.10 ± 2.77	22.46 ± 1.78	23.94 ± 4.19	0.770	0.055	0.938
Antihypertension (yes/no)	0/17	11/15	0/15	8/6	0.423	<0.001*	0.423
Diabetes (yes/no)	0/17	5/21	0/15	3/11	0.883	0.008*	0.883
Current smoker (yes/no)	0/17	6/20	0/15	0/14	0.072	0.072	0.072
FHS-CVD risk	0.06 ± 0.02	0.24 ± 0.09	0.06 ± 0.02	0.20 ± 0.08	0.180	<0.001*	0.312

*Values were described as the mean ± standard deviation (SD). The P-values were obtained by two-way analysis of variance (ANOVA). *P < 0.05.*

TABLE 2 | Diagnosis × FHS-CVD risk interaction on ALFF.

Brain region	BA	Peak MNI coordinates (mm)			Peak *F*-value	Cluster size (mm3)
		X	Y	Z		
Main effect of diagnosis						
L middle temporal gyrus	21	−60	0	−24	3.59	1,134
L superior parietal gyrus	5	−33	−45	66	3.93	945
Main effect of risk						
L fusiform gyrus	20	−36	−9	−27	3.24	972
L precuneus	31	−2	−54	18	3.55	1,377
L cerebellum posterior lobe	/	−6	−75	−27	3.71	1,431
Diagnosis × risk interaction						
L hippocampus	/	−24	−6	−24	3.48	1458

All the regions survived the multiple comparisons based on Gaussian random field theory (GRF) (voxel-wise P < 0.01, cluster-wise P < 0.05, two-tailed). L, left; BA, Brodmann's area.

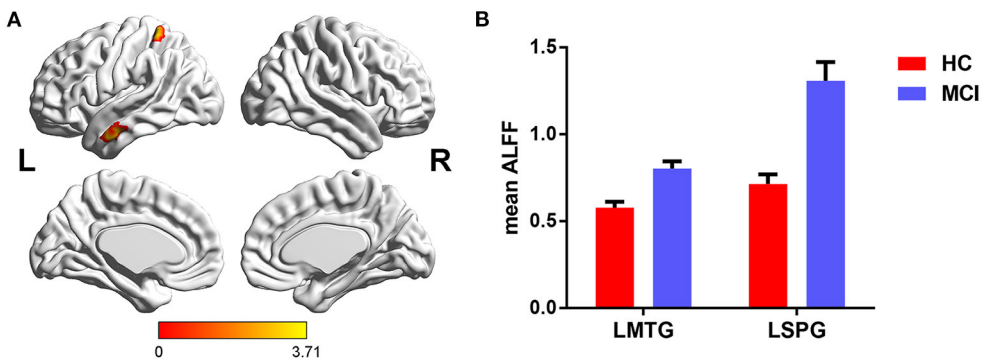

FIGURE 1 | The main effects of diagnosis on ALFF and *post-hoc* analysis. **(A)** The main effects were identified in the LMTG and LSPG. **(B)** Compared with cognitively normal controls, patients with MCI exhibited increased ALFF in the LMTG and LSPG. LMTG, left middle temporal gyrus; LSPG, left superior parietal gyrus.

with low FHS-CVD risk, those with high FHS-CVD risk showed significantly increased ALFF in the LFFG and LCPL, while decreased ALFF in the LPCUN (see **Table 2** and **Figure 2**).

Furthermore, significant interaction of diagnosis × FHS-CVD risk on ALFF was seen in the left hippocampus (LHIP). Interestingly, compared to subjects with low FHS-CVD risk, those with high risk produced opposite trajectory changes in the LHIP across HC and MCI. HCs with high vascular risk showed significantly increased ALFF in the LHIP than those with low vascular risk, while MCI patients with high vascular risk showed

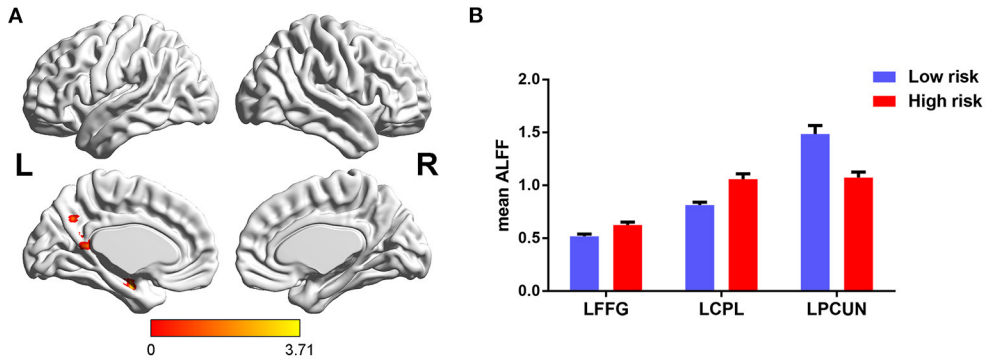

FIGURE 2 | The main effects of FHS-CVD risk on ALFF and *post-hoc* analysis. **(A)** The main effects were identified in the LFFG, LPCUN, and LCPL. **(B)** Compared with subjects with low FHS-CVD risk, those with high FHS-CVD risk showed significantly increased ALFF in the LFFG and LCPL, while decreased ALFF in the LPCUN. LFFG, left fusiform gyrus; LPCUN, left precuneus; LCPL, left cerebellum posterior lobe.

lower ALFF values in the LHIP than those with low vascular risk with no significance. MCI patients with high vascular risk showed decreased ALFF in the LHIP than HCs with high vascular risk (see **Table 2** and **Figure 3**).

Behavioral Significance

We further performed a correlation analysis to explore the behavioral significance of the interaction between diagnosis and FHS-CVD risk. We found that ALFF in the LHIP was positively correlated with word recall test in HCs with high vascular risk (rho $= 0.630$, $P = 0.016$), while negatively correlated with the same test in MCI patients with high vascular risk (rho $= -0.607$, $P = 0.001$; **Figure 4**).

DISCUSSION

In the present study, we aimed to explore whether an aggregation of vascular risk factors modulates the ALFF in patients with MCI and to identify whether it correlates with the behavioral characteristics in MCI. We found the main effects of vascular risk on ALFF were observed in the LFFG, LPCUN, and LCPL. Previous studies have demonstrated that each single vascular risk factor has an effect on the structure, function or metabolism of the brain. Subjects with hypertension showed decreased brain functional and effective connectivity (Bu et al., 2018). Hypertension was significantly associated with lower mean white matter fractional anisotropy, representing impaired integrity of the white matter microstructural (Haight et al., 2018). Many studies have demonstrated cognitive dysfunction, disruptions of functional connectivity, and white matter within the default mode network (Chen et al., 2015; Cui et al., 2015; Qi et al., 2017; Tan et al., 2019). There was significant hypoperfusion in multiple brain regions in smokers (Durazzo et al., 2015). The positive BOLD signal is known to indicate increased neuronal activity, while a negative BOLD signal indicates decreased neuronal activity, and therefor blood flow (Boorman et al., 2010). Based on this BOLD imaging principle, vascular factors themselves can cause a certain degree of abnormal signals in brain regions, and it's not surprising that the aggregation of all these vascular risk factors has an effect on the spontaneous brain activity in our present study. Further analysis showed participants with high vascular risk showed decreased ALFF in the LPCUN, while increased ALFF in the LFFG and LCPL. The predominant hypometabolism involving the precuneus was observed both in MCI and AD patients (Riederer et al., 2018). The decreased ALFF in the LPCUN in our study suggested that the precuneus is fragile to vascular damage, and participants with higher vascular risk may be in a vulnerability state for the development of neurodegenerative disorders, especially AD (Dai et al., 2008). Although the cerebellum was known to be a relatively preserved structure, studies have demonstrated the cerebellar posterior lobe contributes to higher cognitive function (Hoche et al., 2018). As the vascular risk increases, the cognitive cerebellum may be activated in compensation for deficit in the cerebral cortex (Bai et al., 2011).

Previous systematic reviews or meta-analyses of vascular risk factors for dementia and AD showed that the relative risk of diabetes, hypertension, smoking, obesity, and hyperlipemia for dementia and AD ranges from 1.24 to 3.1 (Ballard et al., 2011). As with metabolic syndrome, taking different vascular risk factors as a whole, may help to provide more comprehensive information (Frisardi et al., 2010). Few studies investigated the accumulating effect of different vascular risk factors on brain function based on resting-state fMRI. The FHS-CVD risk score is a simple and reliable tool for comprehensive assessment of the risk of cardiovascular events. In this study, we found the interaction of diagnosis and FHS-CVD risk on ALFF was in the LHIP. As the hub node of memory circuit, hippocampus plays an important role in the encoding, storage, and retrieval of memories, and it's thought to be one of the earliest brain regions to be affected in AD (Gliebus, 2018). Both fMRI and structural imaging studies have demonstrated hippocampus changes in patients with MCI, and the changes become more severe in AD patients (Leandrou et al., 2018; Xue et al., 2019). HCs with high FHS-CVD risk showed increased ALFF in the LHIP than those with low FHS-CVD risk and ALFF in the LHIP significantly positively correlated with word recall test in HCs with high FHS-CVD risk, this may represent brain

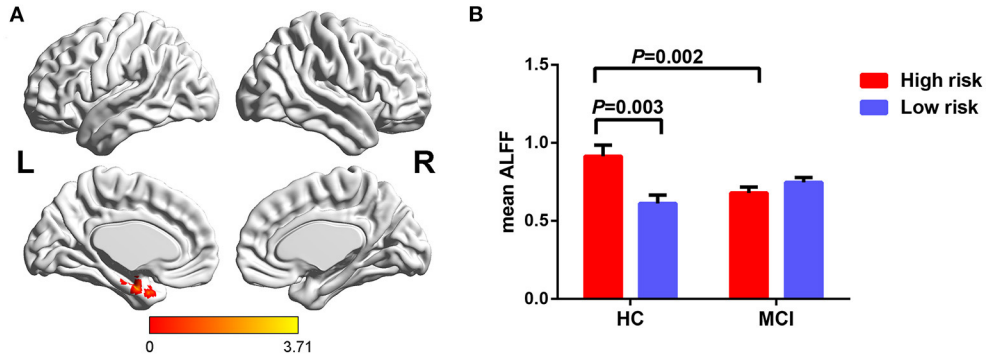

FIGURE 3 | The interaction of diagnosis × FHS-CVD risk on ALFF and *post-hoc* analysis. **(A)** The interaction was seen in the LHIP. **(B)** HCs with high risk showed significantly increased ALFF in the LHIP than those with low risk, while MCI patients with high risk showed decreased ALFF in the LHIP than HCs with high risk. LHIP, left hippocampus.

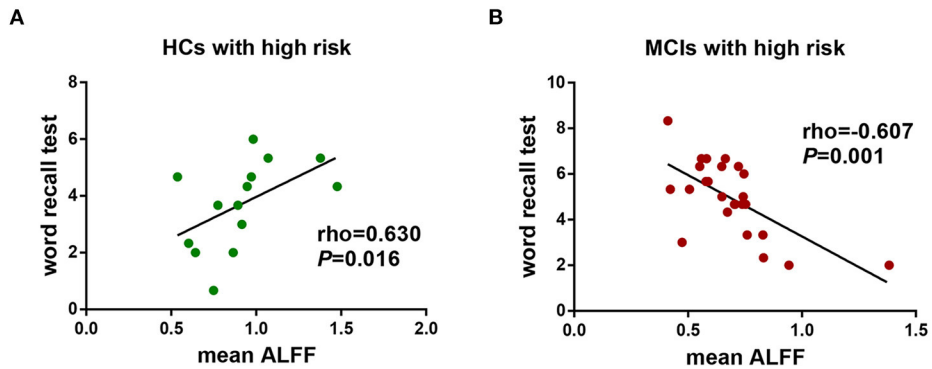

FIGURE 4 | The behavioral significance of the interaction of diagnosis × FHS-CVD risk on ALFF. **(A)** ALFF in the LHIP was positively correlated with word recall test in HCs with high vascular risk (rho = 0.630, $P = 0.016$). **(B)** ALFF in the LHIP was negatively correlated with word recall test in MCI patients with high vascular risk (rho = −0.607, $P = 0.001$). LHIP, left hippocampus.

function compensation in response to increased vascular risk effects. While MCI patients showed opposite trajectory changes of ALFF as the FHS-CVD risk increased and the ALFF value negatively correlated with the same test in MCI patients with high FHS-CVD risk. Compensation of early neural network connections was observed in the normal elderly and in MCI patients without vascular risk factors, while this compensation was inhibited in MCI as vascular risk factors increased (Chen et al., 2018), giving some support for our findings. Accumulating evidences highlight the significance of vascular dysfunction in AD. Neuropathological studies have found that nearly 80% of patients diagnosed with AD have vascular lesions such as microinfarcts and cerebral atherosclerosis (Toledo et al., 2013; Power et al., 2018). The animal models of AD driven by Aβ also showed microvascular morphological changes (Iadecola, 2010). Vascular risk factors, such as hypertension and diabetes may induce blood-brain barrier and neurovascular unit injury, thus causing chronic cerebral hypoperfusion to adversely affect the neuronal homeostasis and eventually lead to neuronal cell death (Goldwaser et al., 2016; Wang et al., 2018; Liesz, 2019). While individual vascular risk factors could specifically or primarily affect neurovascular unit to varying degrees, their aggregation in clusters may have a broader impact on the cerebrovascular system, including micro-vessels and macro-vessels. Vemuri et al. have demonstrated that vascular health can directly or indirectly affect neurodegeneration biomarkers, such as tau deposition in entorhinal cortex (Vemuri et al., 2017). It is identified recently that Aβ generating reactive oxygen species causes pericyte constriction of brain capillaries can lead to chronic hypoperfusion, exacerbating neurodegeneration and cognitive dysfunction in AD (Nortley et al., 2019). A clinical pathologic study found that the Aβ peptide load in MCI patients appeared intermediate between HCs and dementia due to AD (Mufson et al., 1999). In our study, one explanation for the lower ALFF of LHIP in MCI patients with high FHS-CVD risk might be that, in addition to the effects of neurodegenerative pathology, the higher FHS-CVD risk representing the greater aggregation of vascular factors may lead to more severe vascular dysfunction and reduction of cerebral blood flow in MCI, resulting in decompensation. Meta-analysis of fMRI studies has already concluded that patients with MCI showed decreased ALFF value than HCs in the LHIP (Pan et al., 2017). This kind of change may

imply weakening of the activities of neurons in the hippocampus, reflecting the pathophysiological transition process of MCI to AD (Yang et al., 2018). Further longitudinal studies are needed to clarify this in the future.

Our study possessed several biological and technical limitations. First, we did not measure Aβ deposition, a major pathological biomarker of AD. There has been increasing evidence of interaction between vascular pathology and Aβ pathology, with cerebral ischemia promoting the aggregation of Aβ, which in turn further reduces cerebral blood flow (Popa-Wagner et al., 2015). Aβ deposition and the presence of cerebrovascular pathologies often co-exist in the brains of the elderly population (Attems and Jellinger, 2014; Love and Miners, 2016). Thus, although the present study demonstrated that FHS-CVD risk modulates the effect of diagnosis on cognition and cerebral function, there may be convergent pathologies that contribute to altered brain function. Second, due to the sample size of this study, further repeated studies with large sample in independent samples are needed. Finally, since it's is a cross-sectional study, we were unable to draw any causal conclusions. Longitudinal studies of the effects of FHS-CVD risk on cerebral function are still needed in the future.

In conclusion, we first assessed the vascular-imaging-behavior relationship involving the FHS-CVD risk profile in MCI patients and HCs. This study provides preliminary evidence highlighting that the aggregation of vascular risk factors modulates the spontaneous brain activity in MCI, and this may serve as a potential imaging mechanism underlying vascular contribution to AD.

DATA AVAILABILITY STATEMENT

The datasets generated for this study are available on request to the corresponding authors.

ETHICS STATEMENT

The studies involving human participants were reviewed and approved by the Research Ethics Committee of the First Affiliated Hospital of Zhejiang University. The patients/participants provided their written informed consent to participate in this study. Written informed consent was obtained from the individual(s) for the publication of any potentially identifiable images or data included in this article.

AUTHOR CONTRIBUTIONS

LZ contributed to the conception and design of the work, the analysis and interpretation of data, and the manuscript writing. HN and XL helped analyze the data. JW, XL, YLin, YS, and KZ contributed to the conception, design and acquisition data. YLi contributed to the conception and design of the work. GP and BL revised the work critically. All authors reviewed and approved the submitted manuscript.

FUNDING

This work was supported by the Science Technology Department of Zhejiang Province (2017C03011), the Ministry of Science and Technology of the People's Republic of China (2016YFC1306402), Zhejiang Provincial Natural Science Foundation (LY20H090014 and LQ19H090006), and Zhejiang Science and Technology Project (2018KY195, WKJ-ZJ-2024, and WKJ-ZJ-1809).

SUPPLEMENTARY MATERIAL

The Supplementary Material for this article can be found online at: https://www.frontiersin.org/articles/10.3389/fnagi.2020.604246/full#supplementary-material

REFERENCES

Ashburner, J., and Friston, K. J. (2005). Unified segmentation. *Neuroimage* 26, 839–851. doi: 10.1016/j.neuroimage.2005.02.018

Attems, J., and Jellinger, K. A. (2014). The overlap between vascular disease and Alzheimer's disease–lessons from pathology. *BMC Med.* 12:206. doi: 10.1186/s12916-014-0206-2

Bai, F., Liao, W., Watson, D. R., Shi, Y., Yuan, Y., Cohen, A. D., et al. (2011). Mapping the altered patterns of cerebellar resting-state function in longitudinal amnestic mild cognitive impairment patients. *J. Alzheimers Dis.* 23, 87–99. doi: 10.3233/JAD-2010-101533

Ballard, C., Gauthier, S., Corbett, A., Brayne, C., Aarsland, D., and Jones, E. (2011). Alzheimer's disease. *Lancet* 377, 1019–1031. doi: 10.1016/S0140-6736(10)61349-9

Barnes, D. E., and Yaffe, K. (2011). The projected effect of risk factor reduction on Alzheimer's disease prevalence. *Lancet Neurol.* 10, 819–828. doi: 10.1016/S1474-4422(11)70072-2

Biswal, B., Yetkin, F. Z., and Haughton, V. M., Hyde, J. S. (1995). Functional connectivity in the motor cortex of resting human brain using echo-planar MRI. *Magn. Reson. Med.* 34, 537–541. doi: 10.1002/mrm.1910340409

Boorman, L., Kennerley, A. J., Johnston, D., Jones, M., Zheng, Y., Redgrave, P., et al. (2010). Negative blood oxygen level dependence in the rat: a model for investigating the role of suppression in neurovascular coupling. *J. Neurosci.* 30, 4285–4294. doi: 10.1523/JNEUROSCI.6063-09.2010

Breteler, M. M. (2000). Vascular risk factors for Alzheimer's disease: an epidemiologic perspective. *Neurobiol. Aging* 21, 153–60. doi: 10.1016/S0197-4580(99)00110-4

Bu, L., Huo, C., Xu, G., Liu, Y., Li, Z., Fan, Y., et al. (2018). Alteration in brain functional and effective connectivity in subjects with hypertension. *Front. Physiol.* 9:669. doi: 10.3389/fphys.2018.00669

Cha, J., Hwang, J. M., Jo, H. J., Seo, S. W., Na, D. L., and Lee, J. M. (2015). Assessment of functional characteristics of amnestic mild cognitive impairment and alzheimer's disease using various methods of resting-state FMRI analysis. *Biomed. Res. Int.* 2015:907464. doi: 10.1155/2015/907464

Chen, H., Su, F., Ye, Q., Wang, Z., Shu, H., and Bai, F. (2018). The dose-dependent effects of vascular risk factors on dynamic compensatory neural processes in mild cognitive impairment. *Front. Aging Neurosci.* 10:131. doi: 10.3389/fnagi.2018.00131

Chen, Y., Liu, Z., Zhang, J., Tian, G., Li, L., Zhang, S., et al. (2015). Selectively disrupted functional connectivity networks in type 2 diabetes mellitus. *Front. Aging Neurosci.* 7:233. doi: 10.3389/fnagi.2015.00233

Cui, Y., Jiao, Y., Chen, H. J., Ding, J., Luo, B., Peng, C. Y., et al. (2015). Aberrant functional connectivity of default-mode network in type 2 diabetes patients. *Eur Radiol.* 25, 3238–3246. doi: 10.1007/s00330-015-3746-8

D'Agostino, R. S., Vasan, R. S., Pencina, M. J., Wolf, P. A., Cobain, M., Massaro, J. M., et al. (2008). General cardiovascular risk profile for use in primary care: the framingham heart study. *Circulation* 117, 743–753. doi: 10.1161/CIRCULATIONAHA.107.699579

Dai, W., Lopez, O. L., Carmichael, O. T., Becker, J. T., Kuller, L. H., and Gach, H. M. (2008). Abnormal regional cerebral blood flow in cognitively normal elderly subjects with hypertension. *Stroke* 39, 349–354. doi: 10.1161/STROKEAHA.107.495457

Dubois, B., Feldman, H. H., Jacova, C., Hampel, H., Molinuevo, J. L., Blennow, K., et al. (2014). Advancing research diagnostic criteria for Alzheimer's disease: the IWG-2 criteria. *Lancet Neurol.* 13, 614–629. doi: 10.1016/S1474-4422(14)70090-0

Durazzo, T. C., Meyerhoff, D. J., and Murray, D. E. (2015). Comparison of regional brain perfusion levels in chronically smoking and non-smoking adults. *Int. J. Environ. Res. Public Health* 12, 8198–8213. doi: 10.3390/ijerph120708198

Frisardi, V., Solfrizzi, V., Seripa, D., Capurso, C., Santamato, A., Sancarlo, D., et al. (2010). Metabolic-cognitive syndrome: a cross-talk between metabolic syndrome and Alzheimer's disease. *Ageing Res. Rev.* 9, 399–417. doi: 10.1016/j.arr.2010.04.007

Gliebus, G. P. (2018). Memory dysfunction continuum (Minneap Minn). *Behav. Neurol. Psychiatry* 24, 727–744. doi: 10.1212/CON.0000000000000619

Goldwaser, E. L., Acharya, N. K., Sarkar, A., Godsey, G., and Nagele, R. G. (2016). Breakdown of the cerebrovasculature and blood-brain barrier: a mechanistic link between diabetes mellitus and Alzheimer's disease. *J. Alzheimers Dis.* 54, 445–456. doi: 10.3233/JAD-160284

Haight, T., Nick, B. R., Erus, G., Hsieh, M. K., Davatzikos, C., Nasrallah, I., et al. (2018). White matter microstructure, white matter lesions, and hypertension: an examination of early surrogate markers of vascular-related brain change in midlife. *Neuroimage Clin.* 18, 753–761. doi: 10.1016/j.nicl.2018.02.032

He, Y., Wang, L., Zang, Y., Tian, L., Zhang, X., Li, K., et al. (2007). Regional coherence changes in the early stages of Alzheimer's disease: a combined structural and resting-state functional MRI study. *Neuroimage* 35, 488–500. doi: 10.1016/j.neuroimage.2006.11.042

Hoche, F., Guell, X., Vangel, M. G., Sherman, J. C., and Schmahmann, J. D. (2018). The cerebellar cognitive affective/Schmahmann syndrome scale. *Brain* 141, 248–270. doi: 10.1093/brain/awx317

Hou, J., Sun, H., Guo, Y., Zhou, Y., Yin, W., Xu, T., et al. (2018). Associations between urinary monohydroxy polycyclic aromatic hydrocarbons metabolites and framingham risk score in Chinese adults with low lung function. *Ecotoxicol. Environ. Saf.* 147, 1002–1009. doi: 10.1016/j.ecoenv.2017.09.058

Huang, X., Wen, Z., Qi, C. X., Tong, Y., Dan, H. D., Xie, B. J., et al. (2020). Altered temporal dynamic intrinsic brain activity in late blindness. *Biomed. Res. Int.* 2020:1913805. doi: 10.1155/2020/1913805

Iadecola, C. (2010). The overlap between neurodegenerative and vascular factors in the pathogenesis of dementia. *Acta Neuropathol.* 120, 287–296. doi: 10.1007/s00401-010-0718-6

Katzman, R., Zhang, M. Y., Ya-Qu, O., Wang, Z. Y., Liu, W. T., Yu, E., et al. (1988). A Chinese version of the mini-mental state examination; impact of illiteracy in a Shanghai dementia survey. *J. Clin. Epidemiol.* 41, 971–978. doi: 10.1016/0895-4356(88)90034-0

Launer, L. J., Ross, G. W., Petrovitch, H., Masaki, K., Foley, D., White, L. R., et al. (2000). Midlife blood pressure and dementia: the Honolulu-Asia aging study. *Neurobiol Aging.* 21, 49–55. doi: 10.1016/S0197-4580(00)00096-8

Leandrou, S., Petroudi, S., Kyriacou, P. A., Reyes-Aldasoro, C. C., and Pattichis, C. S. (2018). Quantitative MRI brain studies in mild cognitive impairment and alzheimer's disease: a methodological review. *IEEE Rev. Biomed. Eng.* 11, 97–111. doi: 10.1109/RBME.2018.2796598

Liesz, A. (2019). The vascular side of Alzheimer's disease. *Science* 365, 223–224. doi: 10.1126/science.aay2720

Love, S., and Miners, J. S. (2016). Cerebrovascular disease in ageing and Alzheimer's disease. *Acta Neuropathol.* 131, 645–658. doi: 10.1007/s00401-015-1522-0

McKhann, G. M., Knopman, D. S., Chertkow, H., Hyman, B. T., Jack, C. J., Kawas, C. H., et al. (2011). The diagnosis of dementia due to Alzheimer's disease: recommendations from the National Institute on aging-Alzheimer's association workgroups on diagnostic guidelines for Alzheimer's disease. *Alzheimers Dement.* 7, 263–269. doi: 10.1016/j.jalz.2011.03.005

Mufson, E. J., Chen, E. Y., Cochran, E. J., Beckett, L. A., Bennett, D. A., and Kordower, J. H. (1999). Entorhinal cortex beta-amyloid load in individuals with mild cognitive impairment. *Exp. Neurol.* 158, 469–490. doi: 10.1006/exnr.1999.7086

Ninomiya, T., Ohara, T., Hirakawa, Y., Yoshida, D., Doi, Y., Hata, J., et al. (2011). Midlife and late-life blood pressure and dementia in Japanese elderly: the Hisayama study. *Hypertension* 58, 22–28. doi: 10.1161/HYPERTENSIONAHA.110.163055

Nortley, R., Korte, N., Izquierdo, P., Hirunpattarasilp, C., Mishra, A., Jaunmuktane, Z., et al. (2019). Amyloid beta oligomers constrict human capillaries in Alzheimer's disease via signaling to pericytes. *Science* 365:eaav9518. doi: 10.1126/science.aav9518

Norton, S., Matthews, F. E., Barnes, D. E., Yaffe, K., and Brayne, C. (2014). Potential for primary prevention of Alzheimer's disease: an analysis of population-based data. *Lancet Neurol.* 13, 788–794. doi: 10.1016/S1474-4422(14)70136-X

Pan, P., Zhu, L., Yu, T., Shi, H., Zhang, B., Qin, R., et al. (2017). Aberrant spontaneous low-frequency brain activity in amnestic mild cognitive impairment: a meta-analysis of resting-state fMRI studies. *Ageing Res. Rev.* 35, 12–21. doi: 10.1016/j.arr.2016.12.001

Pearson, T. A., Blair, S. N., Daniels, S. R., Eckel, R. H., Fair, J. M., Fortmann, S. P., et al. (2002). AHA guidelines for primary prevention of cardiovascular disease and stroke: 2002 update: consensus panel guide to comprehensive risk reduction for adult patients without coronary or other atherosclerotic vascular diseases. american heart association science advisory and coordinating committee. *Circulation* 106, 388–391. doi: 10.1161/01.CIR.0000020190.45892.75

Popa-Wagner, A., Buga, A. M., Popescu, B., and Muresanu, D. (2015). Vascular cognitive impairment, dementia, aging and energy demand a vicious cycle. *J. Neural Transm.* 122 (Suppl. 1), S47–S54. doi: 10.1007/s00702-013-1129-3

Power, J. D., Barnes, K. A., Snyder, A. Z., Schlaggar, B. L., and Petersen, S. E. (2013). Steps toward optimizing motion artifact removal in functional connectivity MRI; a reply to carp. *Neuroimage* 76, 439–441. doi: 10.1016/j.neuroimage.2012.03.017

Power, M. C., Mormino, E., Soldan, A., James, B. D., Yu, L., Armstrong, N. M., et al. (2018). Combined neuropathological pathways account for age-related risk of dementia. *Ann. Neurol.* 84, 10–22. doi: 10.1002/ana.25246

Purnell, C., Gao, S., Callahan, C. M., and Hendrie, H. C. (2009). Cardiovascular risk factors and incident Alzheimer disease: a systematic review of the literature. *Alzheimer Dis. Assoc. Disord.* 23, 1–10. doi: 10.1097/WAD.0b013e318187541c

Qi, D., Wang, A., Chen, Y., Chen, K., Zhang, S., Zhang, J., et al. (2017). Default mode network connectivity and related white matter disruption in type 2 diabetes mellitus patients concurrent with amnestic mild cognitive impairment. *Curr. Alzheimer Res.* 14, 1238–1246. doi: 10.2174/1567205014666170417113441

Qiu, C., Kivipelto, M., and von Strauss, E. (2009). Epidemiology of Alzheimer's disease: occurrence, determinants, and strategies toward intervention. *Dialogues Clin. Neurosci.* 11, 111–128. doi: 10.31887/DCNS.2009.11.2/cqiu

Rabin, J. S., Schultz, A. P., Hedden, T., Viswanathan, A., Marshall, G. A., Kilpatrick, E., et al. (2018). Interactive Associations of vascular risk and beta-amyloid burden with cognitive decline in clinically normal elderly individuals: findings from the harvard aging brain study. *JAMA Neurol.* 75, 1124–1131. doi: 10.1001/jamaneurol.2018.1123

Riederer, I., Bohn, K. P., Preibisch, C., Wiedemann, E., Zimmer, C., Alexopoulos, P., et al. (2018). Alzheimer disease and mild cognitive impairment: integrated pulsed arterial spin-labeling MRI and (18).F-FDG PET. *Radiology* 288, 198–206. doi: 10.1148/radiol.2018170575

Safouris, A., Psaltopoulou, T., Sergentanis, T. N., Boutati, E., Kapaki, E., and Tsivgoulis, G. (2015). Vascular risk factors and Alzheimer's disease pathogenesis: are conventional pharmacological approaches protective for cognitive decline progression? *CNS Neurol. Disord. Drug Targets* 14, 257–269. doi: 10.2174/1871527314666150217123147

Tan, X., Liang, Y., Zeng, H., Qin, C., Li, Y., Yang, J., et al. (2019). Altered functional connectivity of the posterior cingulate cortex in type 2 diabetes with cognitive impairment. *Brain Imaging Behav.* 13, 1699–1707. doi: 10.1007/s11682-018-0017-8

Tan, Z. S., Seshadri, S., Beiser, A., Wilson, P. W., Kiel, D. P., Tocco, M., et al. (2003). Plasma total cholesterol level as a risk factor for

Alzheimer disease: the framingham study. *Arch. Intern. Med*. 163, 1053–1057. doi: 10.1001/archinte.163.9.1053

Toledo, J. B., Arnold, S. E., Raible, K., Brettschneider, J., Xie, S. X., Grossman, M., et al. (2013). Contribution of cerebrovascular disease in autopsy confirmed neurodegenerative disease cases in the national Alzheimer's coordinating centre. *Brain*. 136 (Pt. 9), 2697–2706. doi: 10.1093/brain/awt188

Vemuri, P., Lesnick, T. G., Przybelski, S. A., Knopman, D. S., Lowe, V. J., Graff-Radford, J., et al. (2017). Age, vascular health, and Alzheimer disease biomarkers in an elderly sample. *Ann. Neurol*. 82, 706–718. doi: 10.1002/ana.25071

Viticchi, G., Falsetti, L., Buratti, L., Boria, C., Luzzi, S., Bartolini, M., et al. (2015). Framingham risk score can predict cognitive decline progression in Alzheimer's disease. *Neurobiol. Aging* 36, 2940–2945. doi: 10.1016/j.neurobiolaging.2015.07.023

Viticchi, G., Falsetti, L., Buratti, L., Sajeva, G., Luzzi, S., Bartolini, M., et al. (2017). Framingham risk score and the risk of progression from mild cognitive impairment to dementia. *J. Alzheimers Dis*. 59, 67–75. doi: 10.3233/JAD-170160

Wang, Y., Zhang, R., Tao, C., Xu, Z., Chen, W., Wang, C., et al. (2018). Blood-brain barrier disruption and perivascular beta-amyloid accumulation in the brain of aged rats with spontaneous hypertension: evaluation with dynamic contrast-enhanced magnetic resonance imaging. *Korean J. Radiol*. 19, 498–507. doi: 10.3348/kjr.2018.19.3.498

Wang, Z., Yan, C., Zhao, C., Qi, Z., Zhou, W., Lu, J., et al. (2011). Spatial patterns of intrinsic brain activity in mild cognitive impairment and Alzheimer's disease: a resting-state functional MRI study. *Hum. Brain Mapp*. 32, 1720–1740. doi: 10.1002/hbm.21140

Winblad, B., Palmer, K., Kivipelto, M., Jelic, V., Fratiglioni, L., Wahlund, L. O., et al. (2004). Mild cognitive impairment–beyond controversies, towards a consensus: report of the International working group on mild cognitive impairment. *J. Intern. Med*. 256, 240–246. doi: 10.1111/j.1365-2796.2004.01380.x

Xue, J., Guo, H., Gao, Y., Wang, X., Cui, H., Chen, Z., et al. (2019). Altered directed functional connectivity of the hippocampus in mild cognitive impairment and Alzheimer's disease: a resting-state fMRI study. *Front. Aging Neurosci*. 11:326. doi: 10.3389/fnagi.2019.00326

Yang, L., Yan, Y., Wang, Y., Hu, X., Lu, J., Chan, P., et al. (2018). Gradual disturbances of the Amplitude of Low-Frequency Fluctuations (ALFF). and fractional ALFF in Alzheimer spectrum. *Front. Neurosci*. 12:975. doi: 10.3389/fnins.2018.00975

Yang, Y., Lin, X., Li, J., Han, L., Li, Z., Liu, S., et al. (2019). Aberrant brain activity at early delay stage post-radiotherapy as a biomarker for predicting neurocognitive dysfunction late-delayed in patients with nasopharyngeal carcinoma. *Front. Neurol*. 10:752. doi: 10.3389/fneur.2019.00752

Zhou, F., Wu, L., Guo, L., Zhang, Y., and Zeng, X. (2019). Local connectivity of the resting brain connectome in patients with low back-related leg pain: a multiscale frequency-related Kendall's coefficient of concordance and coherence-regional homogeneity study. *Neuroimage Clin*. 21:101661. doi: 10.1016/j.nicl.2019.101661

Zhuang, L., Liu, X., Shi, Y., Liu, X., and Luo, B. (2019). Genetic variants of PICALM rs541458 modulate brain spontaneous activity in older adults with amnestic mild cognitive impairment. *Front. Neurol*. 10:494. doi: 10.3389/fneur.2019.00494

Conflict of Interest: The authors declare that the research was conducted in the absence of any commercial or financial relationships that could be construed as a potential conflict of interest.

frontiers in Aging Neuroscience

ORIGINAL RESEARCH
published: 11 January 2021
doi: 10.3389/fnagi.2020.621298

Lymphocyte and NK Cell Counts Can Predict Sepsis-Associated Delirium in Elderly Patients

*Dongkai Li, Jiahui Zhang, Guangxu Bai, Jianwei Chen, Wei Cheng and Na Cui**

Department of Critical Care Medicine, Peking Union Medical College Hospital, Beijing, China

Background: Sepsis-associated delirium (SAD) is prevalent in elderly patients and is recognized as brain dysfunction associated with increased inflammatory response in the central nervous system during sepsis. Neuroinflammation was demonstrated to be part of its mechanism and we aimed to validate the role of immunity imbalance in a combined retrospective and prospective cohort study.

Methods: We performed a retrospective study analyzing the association between SAD and lymphocyte counts in the peripheral blood, alongside a prospective trial evaluating the quantitative changes in lymphocyte subsets and their predictive value for early diagnosis of SAD.

Results: In the retrospective study, among 1,010 enrolled adult patients (age ≥65 years), 297 patients were diagnosed with delirium during intensive care unit (ICU) stay and lymphocyte counts at ICU admission in the SAD group were significantly higher than in non-delirious counterparts (1.09 ± 0.32 vs. 0.82 ± 0.24, respectively, $p = 0.001$). In the prospective study, lymphocyte counts [0.83 (0.56, 1.15) vs. 0.72 (0.40, 1.06) × 10^9/L, $p = 0.020$] and natural killer (NK) cell counts [96 (68, 118) vs. 56 (26, 92) cells/μl, $p = 0.024$] were significantly higher in the SAD group. The area under the curve value of NK cell count was 0.895 [95% confidence interval (CI): 0.857, 0.933] and of lymphocyte count was 0.728 (95% CI: 0.662, 0.795). An NK cell count cut-off value of 87 cells/ml in septic patients at ICU admission was predictive of delirium with a sensitivity of 80.2% and specificity of 80.8%.

Conclusions: We found that lymphocyte and NK cell counts were significantly higher in senior patients with SAD and that NK cell count may be valuable for the prediction of SAD within elderly patient cohorts.

Keywords: delirium, sepsis-associated delirium, lymphocyte subsets, NK cell, elderly people

OPEN ACCESS

Edited by:
Feiqi Zhu,
Shenzhen University, China

Reviewed by:
Peter Keyel,
Texas Tech University, United States
Beita Zhao,
Northwest A and F University, China

****Correspondence:***
Na Cui
pumchcn@163.com

Received: *26 October 2020*
Accepted: *15 December 2020*
Published: *11 January 2021*

Citation:
Li D, Zhang J, Bai G, Chen J, Cheng W and Cui N (2021) Lymphocyte and NK Cell Counts Can Predict Sepsis-Associated Delirium in Elderly Patients. Front. Aging Neurosci. 12:621298. doi: 10.3389/fnagi.2020.621298

INTRODUCTION

Delirium is a common diagnosis in hospitalized elderly patients (Devlin et al., 2018). As characterized as a mental disorder presenting with global cognitive dysfunction and altered consciousness, sleep cycle, and psychomotor activity (Cole et al., 2009; Devlin et al., 2018), delirium is associated with prolonged intensive care unit (ICU) and hospital stay and

increased morbidity (Iwashyna et al., 2010; Sonneville et al., 2017). Among various predisposing and precipitating factors of delirium, infection, which may lead to organ dysfunction or sepsis, is highlighted in the management of delirium of elderly patients in ICU (Eidelman et al., 1996). The signs of neurological involvement including confusion, agitation, and coma occurring during sepsis are summarized as sepsis-associated delirium (SAD), of which the incidence is approximately 50% (Young et al., 1990). Previous studies demonstrated that sustained systemic inflammation may contribute to prolonged or aggravated brain dysfunction (Ely et al., 2004; McGrane et al., 2011; van den Boogaard et al., 2011; Sonneville et al., 2013). Although the impact of increased inflammatory responses and numerous inflammatory biomarkers in SAD diagnosis, prediction, and interventions have been investigated, solid evidence remains insufficient for the clinical aid in the management of SAD (Toft et al., 2019).

In recent years, extensive studies have indicated that the balance between SAD and peripheral immunity is of great importance in the development of neurological damage (Ren et al., 2020). The present study aimed to investigate the role of immune imbalance in elderly patients with SAD using clinical data from combined retrospective and prospective cohorts. We hypothesized that imbalance in the peripheral immunity could be observed from peripheral lymphocyte counts, which are included in standard blood examinations. We then designed a prospective study to compare changes in immunity in senior sepsis patients with or without SAD, along with the predictive value of lymphocyte counts for diagnosis of SAD.

MATERIALS AND METHODS

Study Design

The study consisted of two parts: a retrospective study analyzed the incidence of SAD in critical care settings and its potential association with lymphocyte counts and neutrophil to lymphocyte ratios (NLR) in the peripheral blood, while a prospective trial evaluated quantitative changes in immune status along with their predictive value for early diagnosis of SAD. This study was approved by the institutional review board of Peking Union Medical College Hospital (PUMCH; approval number: JS-1170). Informed consent was obtained from all patients, and the study was registered at chictr.org.cn (identifier ChiCTR-ROC-17010750).

Retrospective Study

A retrospective analysis of prospectively collected data was carried out on 1,061 consecutive adult patients (aged ≥65 years) diagnosed with sepsis that were admitted to the Department of Critical Care Medicine between May 2013 and Dec 2016. The data collected included complete past medical history; clinical evaluation including records of vital signs and clinical scores; lab tests at admission, 24 and 48 h after ICU admission including complete blood counts and C-reactive protein (CRP). All patients underwent routine blood analysis at admission using a fully automated cell counter in the local hematology laboratory. The NLR was calculated by dividing the absolute neutrophil count by the absolute lymphocyte count from the same sample. We excluded patients who survived less than 24 h in the ICU (25 patients), those with a history of recognition dysfunction (nine patients), and those with neutropenia at ICU admission (16 patients). Follow-up data were extracted from medical records. The primary endpoint was delirium diagnosed within the first 7 days from admission in patients with sepsis.

Prospective Study

The prospective arm of the study evaluated sepsis patients admitted to the PUMCH between January 2017 and December 2019. Inclusion criteria were: (1) age ≥65 years; (2) ICU stay >24 h; and (3) diagnosis of Sepsis 3.0 (Shankar-Hari et al., 2016). Exclusion criteria were: (1) any condition causing neutropenia; (2) any condition causing primary or acquired immunodeficiency, such as HIV, autoimmune disease at an active stage, hematological disease, or malignant tumors receiving chemotherapy or glucocorticoids within the previous 3 months; (3) life expectancy of <24 h; and (4) failure to meet the inclusion criteria or obtain written consent.

Delirium Monitoring

We used the simplified Chinese version of the confusion assessment method for the ICU (CAM-ICU) assessment tool to screen all patients for delirium at ICU admission, twice a day (morning and evening) and upon changes or fluctuations in mental status after ICU admission (Wang et al., 2013). In the retrospective study, a detailed review of medical and nursing notes was performed by the investigators for a full evaluation of delirium. CAM-ICU positivity was considered as delirium and the corresponding duration was recorded. Similarly, in the prospective study, delirium was diagnosed by the same method and its onset and duration were the primary outcomes of the study.

Data Collection

In both the retrospective and prospective studies, patient demographics, clinical data such as mean arterial pressure, heart rate, duration of ventilator treatment, acute physiology and chronic health evaluation (APACHE) II score and sequential organ failure assessment (SOFA) score, and outcomes, such as the duration of ICU and in-hospital stays, ICU and in-hospital mortality, and 28-day mortality were recorded.

Blood samples were obtained at ICU admission and for a routine examination, including complete blood counts, CRP, procalcitonin, and blood gas analysis. Measurement of immunological parameters was performed on peripheral blood samples in the PUMCH laboratories as previously described (Jalla et al., 2004). In brief, freshly collected EDTA anti-coagulated whole blood was incubated and tested with a panel of monoclonal antibodies labeled with fluorescein isothiocyanate/phycoerythrin/peridinin chlorophyl protein and directed against combinations of CD3/CD8/CD4, CD3/CD16CD56/CD19, and isotype controls (Immunotech,

France), then subjected to flow cytometric analysis using a three-color EPICS-XL flow cytometer (Beckman Coulter, Brea, CA, USA) to detect T-cells ($CD3^+$), $CD4^+$ and $CD8^+$ T-cell subgroups, B-cells ($CD19^+$), and natural killer (NK) cells (CD3-$CD16^+$ $CD56^+$). The following fluorescent monoclonal antibodies were used in this study: CD45-FITC/CD4-RD1/CD8-ECD/CD3-PC5, CD45-FITC/CD56-RD1/CD19-ECD/CD3-PC5, and CD16-PE (Beckman Coulter, Brea, CA, USA). The gating strategy of flow cytometry experiments is shown in **Figure 1**. Rate nephelometry (Array 360; Beckman Coulter, Brea, CA, USA) was used to measure serum levels of immunoglobulin (Ig)A, IgG, and IgM and of complement factors C3 and C4.

Statistical Analysis

Statistical analysis was conducted using SPSS v19.0 software (IBM SPSS, Armonk, NY, USA). Measurement data were expressed as mean ± SD and compared using independent *t*-tests. Enumeration data were compared using a χ^2 test or with Fisher's exact test, as appropriate. For detection of correlation, Pearson's correlation analysis was performed. $P < 0.05$ was considered to indicate a statistically significant difference. Statistically significant variables were subsequently analyzed using a binary logistic regression to identify risk factors associated with the onset of delirium. Only variables markedly associated with SAD ($p < 0.05$) were included in the final model. Receiver operating characteristic (ROC) curves and the area under the curves (AUCs) were examined in significant variables associated with the onset of delirium, to determine a cut-off level and to predict mortality.

RESULTS

Retrospective Study

The number of eligible and excluded sepsis patients is shown in **Figure 2**. Among 1,010 included adult patients (aged ≥65 years), 297 patients were recorded as CAM-ICU positive and diagnosed with delirium during ICU stay. Patient characteristics of the two groups are provided in **Table 1**. No significant differences were identified between the groups in age, sex, SOFA score, or lactate at ICU admission ($p > 0.05$), while patients with delirium had higher APACHE II scores. In terms of vital signs, patients with delirium had a significantly higher heart rate and lower temperature and oxygenation index, and a higher proportion received life-sustaining treatments (**Table 1**).

Inflammatory parameters, source of infection, and co-morbidities in the two groups of patients are shown in **Table 2**. The delirium group had a higher proportion of underlying stroke history [56 (18.9%) vs. 92 (12.9%), $p = 0.007$]. No significant difference was identified in the infection source between the two groups, nor any different proportion of other co-morbidities including hypertension, diabetes, or chronic kidney disease. The outcome result is shown in **Table 3**. Patients with delirium had longer ICU (14.2 ± 14.6 vs. 5.9 ± 10.9 days, $p < 0.005$) and hospitalization times [22.4 (12.1, 40.0) vs. 16.1 (9.8, 27.9) days, $p < 0.005$] and duration of mechanical ventilation (243.0 ± 309.6 vs. 100.1 ± 246.2 h, $p < 0.005$) and vasopressor usage (247.2 ± 304.8 vs. 144.5 ± 274.4 h, $p < 0.005$). However, the 28-day mortality between the two groups showed no statistically significant differences.

Common inflammatory markers and their time courses were also compared. At ICU admission, higher levels of procalcitonin [1.2 (0.29, 7.3) vs. 0.88 (0.21, 4.29) ng/ml, $p = 0.003$], neutrophils (11.3 ± 4.8 vs. 10.6 ± 4.2 × 10^9/L, $p = 0.083$) and lymphocytes (1.09 ± 0.32 vs. 0.82 ± 0.24 × 10^9/L, $p = 0.001$) were observed in delirious patients while differences in 1, 3-β-D-glucan (BDG) and CRP were not significant. Comparison at 24 and 48 h after ICU admission showed that the differences in neutrophil counts tended to become non-significant while lymphocyte counts remained statistically significant between the two groups (**Table 2**, **Figure 3**). As a derived parameter, the NLR showed similar trends to the neutrophil counts.

Multivariable logistic regression analysis was conducted for all parameters that were statistically different in the univariate analysis. The results indicated that APACHE II score [OR 1.024 (1.008, 1.040), $p = 0.003$], NLR [OR 1.013 (1.003, 1.023), $p = 0.018$], lymphocyte count [OR 1.586 (1.228, 2.047), $p < 0.005$] and history of stroke [OR 1.403 (1.024, 1.922), $p = 0.035$] showed significant associations with delirium (**Table 4**).

Prospective Study

As shown in **Figure 2**, 275 patients who were over 65 years of age were eligible for enrolment into the study from January 2018 to December 2019 and 247 patients were enrolled. The clinical characteristics of the 247 patients, of which 96 patients were diagnosed with SAD, are shown in **Table 5**. No significant differences were identified between the two groups in age, sex, APACHE II score, SOFA score, or lactate at ICU admission ($p > 0.05$). The patients who died in 28-day after ICU admission in the prospective cohort were 18 in the non-delirium group and 12 in the delirium group, which correspond to the 28-day mortality of 11.9% and 12.5%, respectively. For inflammatory markers, the patients with delirium had higher levels of procalcitonin [1.1 (0.45, 6.5) vs. 0.81 (0.2, 5.1) ng/ml, $p = 0.021$], lymphocyte counts [0.83 (0.56, 1.15) vs. 0.72 (0.40, 1.06) × 10^9/L, $p = 0.020$] and lower NLR [13.5 (7.7, 22.0) vs. 17.1 (9.6, 26.4), $p = 0.028$], while the difference in neutrophil counts between the two groups was non-significant.

The lymphocyte subset results are shown in **Table 6** and the demonstration of sample data in the flow cytometry experiment is shown in **Figure 4**. NK cell counts in the SAD group were significantly higher than those of the non-SAD group [96 (68, 118) vs. 56 (26, 92) cells/μl, $p = 0.024$] while the differences in B lymphocyte, $CD4^+$ T lymphocyte, and $CD8^+$ T lymphocyte counts between the two groups were not. No significant differences in other studied immune parameters (C3, C4, IgA, IgG, and IgM) were found between SAD and non-SAD patients. We also performed a ROC analysis. Compared with lymphocyte counts and APACHE II score, NK cell counts had the greatest discriminatory ability, with an AUC value of 0.895 (95% CI: 0.857, 0.933),

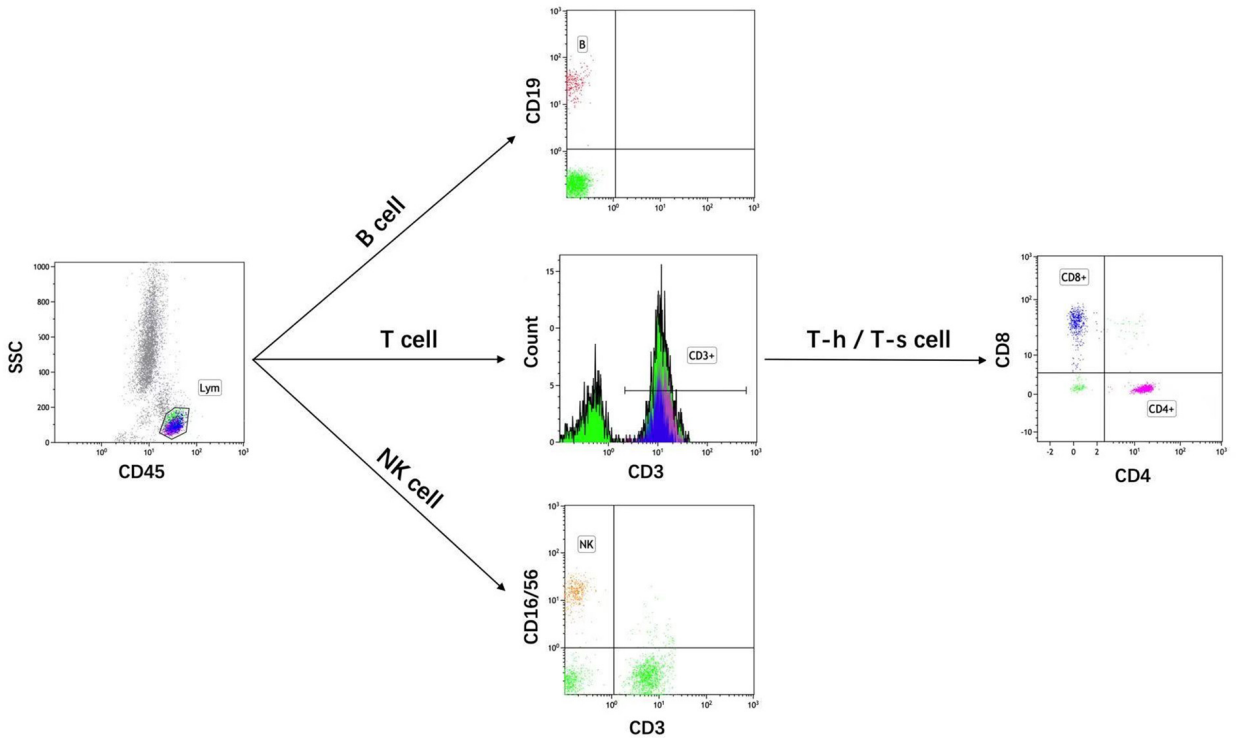

FIGURE 1 | The gating strategy of flow cytometry experiments.

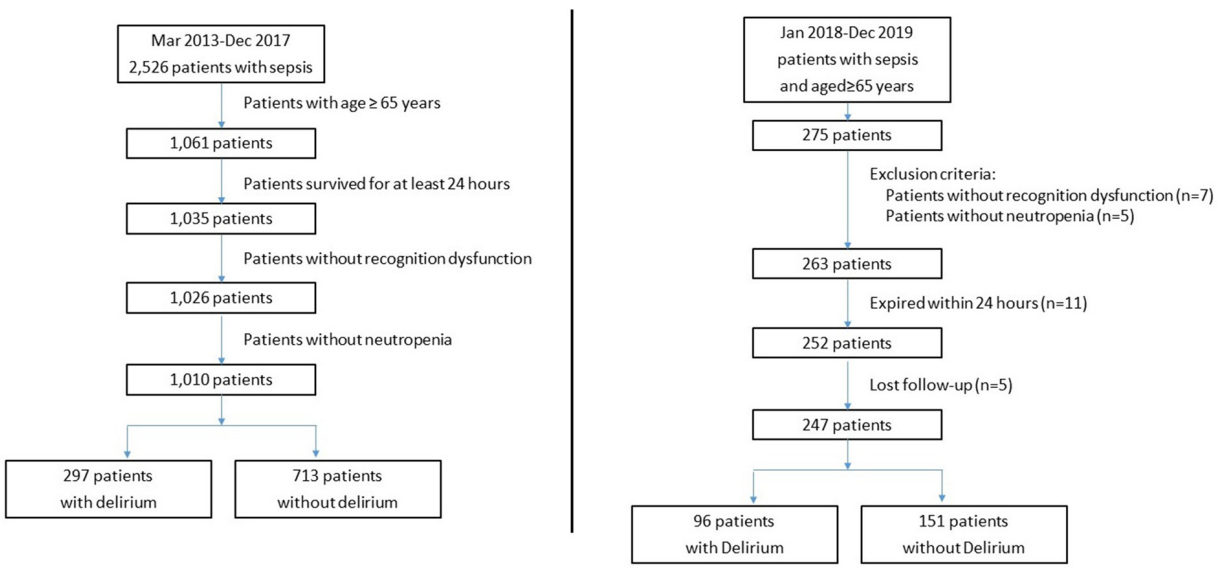

FIGURE 2 | Flowchart comparison of the retrospective and prospective studies.

while that of lymphocyte counts was 0.728 (95% CI: 0.662, 0.795) and the APACHE II score was 0.611 (95% CI: 0.540, 0.682; **Figure 5**). According to the ROC curves, an NK cell count cut-off value of 87 cells/μl in senior septic patients at ICU admission was predictive of a diagnosis of delirium with a sensitivity of 80.2% and specificity of 80.8%, while the cut-off values of APACHE II and lymphocyte count were 21 points and 0.96 × 10^9/L, respectively. The discriminatory powers of the above three parameters are shown in **Table 7**.

TABLE 1 | Baseline characteristics of the retrospective cohort.

Variables	Delirium (*n* = 297)	Non-delirium (*n* = 713)	*p*-value
Age	74.6 ± 7.1	74.3 ± 7.0	0.315
Sex, male	173 (58.2%)	388 (52.2%)	0.152
APACHE II	20.5 ± 6.6	18.9 ± 7.9	<0.005
SOFA	5.9 ± 4.6	6.0 ± 4.7	0.562
Vital sign			
Heart rate	96.8 ± 20.5	92.5 ± 21.8	<0.005
Temperature	36.5 ± 1.0	36.7 ± 0.9	<0.005
Respiratory rate	18.5 ± 6.8	18.5 ± 7.0	0.944
PFO2	293.3 ± 163.3	341.8 ± 181.4	<0.005
Vital sign			
Lactate	2.4 ± 2.3	2.3 ± 2.7	0.626
Treatment received			
Vasopressor	222 (74.7%)	321 (45.0%)	<0.005
Mechanical ventilation	259 (87.2%)	607 (85.1%)	0.014
Early mobilization	159 (53.5%)	149 (20.1%)	<0.005

APACHE II, acute physiology, and chronic health evaluation II; SOFA, sequential organ failure assessment.

TABLE 2 | Inflammatory markers, infection source, and co-morbidities of the retrospective cohort.

Variables	Delirium (*n* = 297)	Non-delirium (*n* = 713)	*p*-value
At ICU admission			
PCT level, ng/ml	1.2 (0.29 ± 7.3)	0.88 (0.21 ± 4.29)	0.039
BDG, pg/ml	72.4 (32.2, 142.2)	73.6 (51.3, 137.4)	0.113
CRP, mg/L	117.9 ± 84.4	129.2 ± 79.8	0.574
Neutrophil count ($\times 10^9$/L)	11.3 ± 4.8	10.6 ± 4.2	0.083
Lymphocyte count ($\times 10^9$/L)	1.09 ± 0.32	0.82 ± 0.24	0.001
NLR	13.5 (7.7, 22.0)	17.1 (9.6, 26.4)	0.028
Vital sign			
At 24 h after admission			
Neutrophil count ($\times 10^9$/L)	11.9 ± 3.9	10.9 ± 3.7	0.084
Lymphocyte count ($\times 10^9$/L)	1.06 ± 0.26	0.84 ± 0.18	0.013
NLR	12.7 (8.0, 23.6)	12.8 (7.8, 18.9)	0.318
At 48 h after admission			
Neutrophil count ($\times 10^9$/L)	11.4 ± 3.6	10.9 ± 3.5	0.235
Lymphocyte count ($\times 10^9$/L)	1.07 ± 0.15	0.83 ± 0.19	0.003
NLR	12.5(7.9 ± 23.7)	14.2(8.1 ± 24.1)	0.455
Infection source			<0.005
Lung	120 (40.4%)	233 (32.7%)	
Bloodstream	25 (8.4%)	63 (8.8%)	
Abdominal cavity	87 (29.3%)	254 (35.6%)	
Thoracic and mediastinum	9 (3.0%)	15 (2.1%)	
UTI	10 (3.4%)	42 (5.9%)	
Bile duct	11 (3.7%)	44 (6.2%)	
CNS	2 (0.7%)	6 (0.8%)	
Other	13 (4.4%)	26 (3.6%)	
Co-morbidities			
Hypertension	172 (57.9%)	402 (56.4%)	0.324
Stroke history	56 (18.9%)	92 (12.9%)	0.007
Diabetes mellitus	83 (27.9%)	206 (28.9%)	0.495
Chronic kidney disease	21 (7.1%)	49 (6.9%)	0.659

ICU, intensive care unit; PCT, procalcitonin, BDG, 1, 3-β-D-glucan; NLR, neutrophil to lymphocyte ratio; UTI, urinary tract infection; CNS, central nervous system.

TABLE 3 | Outcomes of the retrospective cohort.

Variables	Delirium (*n* = 297)	Non-delirium (*n* = 713)	*p*-value
ICU stay time, day	14.2 ± 14.6	5.9 ± 10.9	<0.005
Hospitalization time, day	22.4 (12.1, 40.0)	16.1 (9.8, 27.9)	<0.005
28-day mortality	51 (10.9%)	91 (11.1%)	0.458
Duration of mechanical ventilation, hour	243.0 ± 309.6	100.1 ± 246.2	<0.005
Duration of vasopressor usage, hour	247.2 ± 304.8	144.5 ± 274.4	<0.005

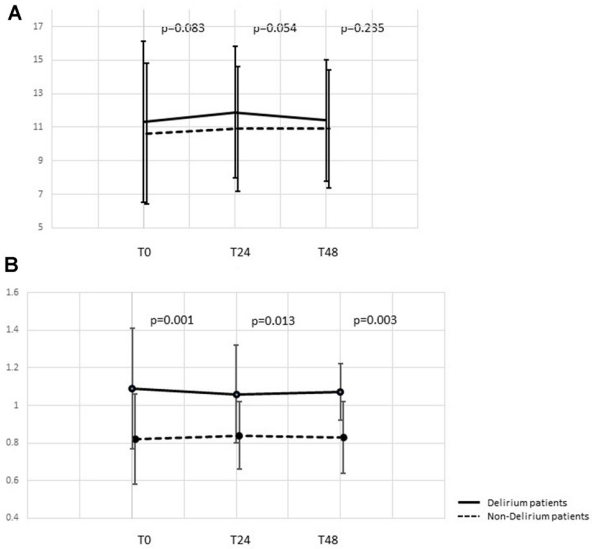

FIGURE 3 | Time course of neutrophil and lymphocyte count dynamic changes. **(A)** Time course of neutrophil counts at 0, 24, and 48 h after ICU admission. **(B)** Time course of lymphocyte counts at 0, 24, and 48 h after ICU admission. ICU, intensive care unit.

DISCUSSION

To our knowledge, this is the first study to show that immune imbalance, as measured by peripheral lymphocyte counts and lymphocyte subsets, is independently associated with SAD in elderly patients in critical care settings. We demonstrated significantly higher lymphocyte counts in patients with SAD, of which increased NK cell count was independently associated with a higher incidence of SAD. This finding supports the role of NK cells and potential neuroinflammation in the development of SAD in senior sepsis patients and provides evidence that evaluation of lymphocyte subtyping is important for early diagnosis and prediction of this pathophysiological process.

In this combined study, a retrospective study was first performed to compare common inflammatory parameters between advanced age patients with and without SAD. Our results showed significantly increased lymphocyte counts in the SAD group during the first 48 h after ICU admission (**Figure 3**), and multivariable analysis showed that lymphocyte count was independently associated with SAD (**Table 4**). To further explain this difference, we performed the prospective part of the study, focusing on lymphocyte subsets. Specifically, we found high NK cell counts at ICU admission were associated with a higher incidence of SAD and the ROC analysis confirmed its good predictive performance.

In senior patients, delirium was demonstrated to be associated with a poorer prognosis compared with non-delirious counterparts. In a cohort of ICU patients ≥60 years of age, Pisani et al. (2009) reported a 1-year mortality rate of 40% with a delirium duration of 1–2 days, which rose to 70% if delirium persisted for ≥5 days. As a common complication of sepsis and

TABLE 4 | Multivariable logistic regression analysis on sepsis-associated delirium.

	Unadjusted		Adjusted	
	OR (95% CI)	***p*-value**	**OR (95% CI)**	***p*-value**
Age	1.240 (0.988, 1.554)	0.063	1.004 (0.988, 1.021)	0.624
APACHE II	1.028 (1.013, 1.044)	<0.005	1.024 (1.008, 1.040)	0.003
PCT	1.002 (0.997, 1.007)	0.532	1.000 (0.995, 1.006)	0.845
Neutrophil	1.014 (0.997, 1.031)	0.105	1.008 (0.988, 1.028)	0.435
NLR	1.006 (1.000, 1.011)	0.061	1.013 (1.003, 1.023)	0.018
Lymphocyte	1.366 (1.124, 1.660)	0.002	1.586 (1.228, 2.047)	<0.005
Stroke history	1.527 (1.124, 2.075)	0.007	1.403 (1.024, 1.922)	0.035

APACHE II, acute physiology, and chronic health evaluation II; PCT, procalcitonin; NLR, neutrophil to lymphocyte ratio; CI, confidence interval.

TABLE 5 | Baseline characteristics of the prospective cohort.

Variables	**Delirium (*n* = 96)**	**Non-delirium (*n* = 151)**	***p*-value**
Age	74.7 ± 6.4	73.8 ± 5.9	0.305
Sex, male	61 (63.5%)	93 (61.6%)	0.758
APACHE II	22.0 ± 7.1	23.1 ± 7.0	0.700
SOFA	5.1 ± 4.6	5.8 ± 4.3	0.622
Lactate	2.6 ± 2.8	2.5 ± 2.3	0.728
At ICU admission			
PCT level, ng/ml	1.1 (0.45, 6.5)	0.81 (0.2, 5.1)	0.021
BDG, pg/ml	82.4 (52.2, 112.2)	91.6 (41.3, 156.2)	0.245
CRP, mg/L	101.2 ± 54.4	135.2 ± 92.8	0.334
Neutrophil count ($\times 10^9$/L)	11.2 ± 7.3	13.0 ± 8.7	0.369
Lymphocyte count ($\times 10^9$/L)	0.83 (0.56, 1.15)	0.72 (0.40, 1.06)	0.020
NLR	13.6 (7.8, 25.9)	15.7 (9.2, 27.0)	0.399

APACHE II, acute physiology and chronic health evaluation II; SOFA, sequential organ failure assessment; PCT, procalcitonin; BDG, 1,3-β-D-glucan; CRP, C-reactive protein; NLR, neutrophil to lymphocyte ratio.

TABLE 6 | Lymphocyte subsets of prospective cohort.

Cell count (cells/μl)	Delirium (*n* = 96)	Non-delirium (*n* = 151)	*p*-value
B lymphocyte	89 (45, 144)	96 (45, 181)	0.109
T lymphocyte	509 (289, 799)	483 (302, 734)	0.118
$CD4^+$ T	302 (196, 473)	294 (186, 463)	0.120
$CD8^+$ T	148 (75, 301)	135 (72, 236)	0.686
NK cell	96 (68, 118)	56 (26, 92)	0.024
C3, g/L	0.726 ± 0.332	0.781 ± 0.369	0.363
C4, g/L	0.181 ± 0.065	0.167 ± 0.062	0.128
IgA, g/L	2.58 ± 1.23	2.48 ± 1.27	0.602
IgG, g/L	11.2 ± 4.4	10.76 ± 4.9	0.509
IgM, g/L	0.77 ± 0.49	0.77 ± 0.44	0.930

C3, complement factor 3; C4, complement factor 4; Ig, immunoglobulin; LB, B lymphocyte; LY, lymphocyte; NK cell, natural killer cell.

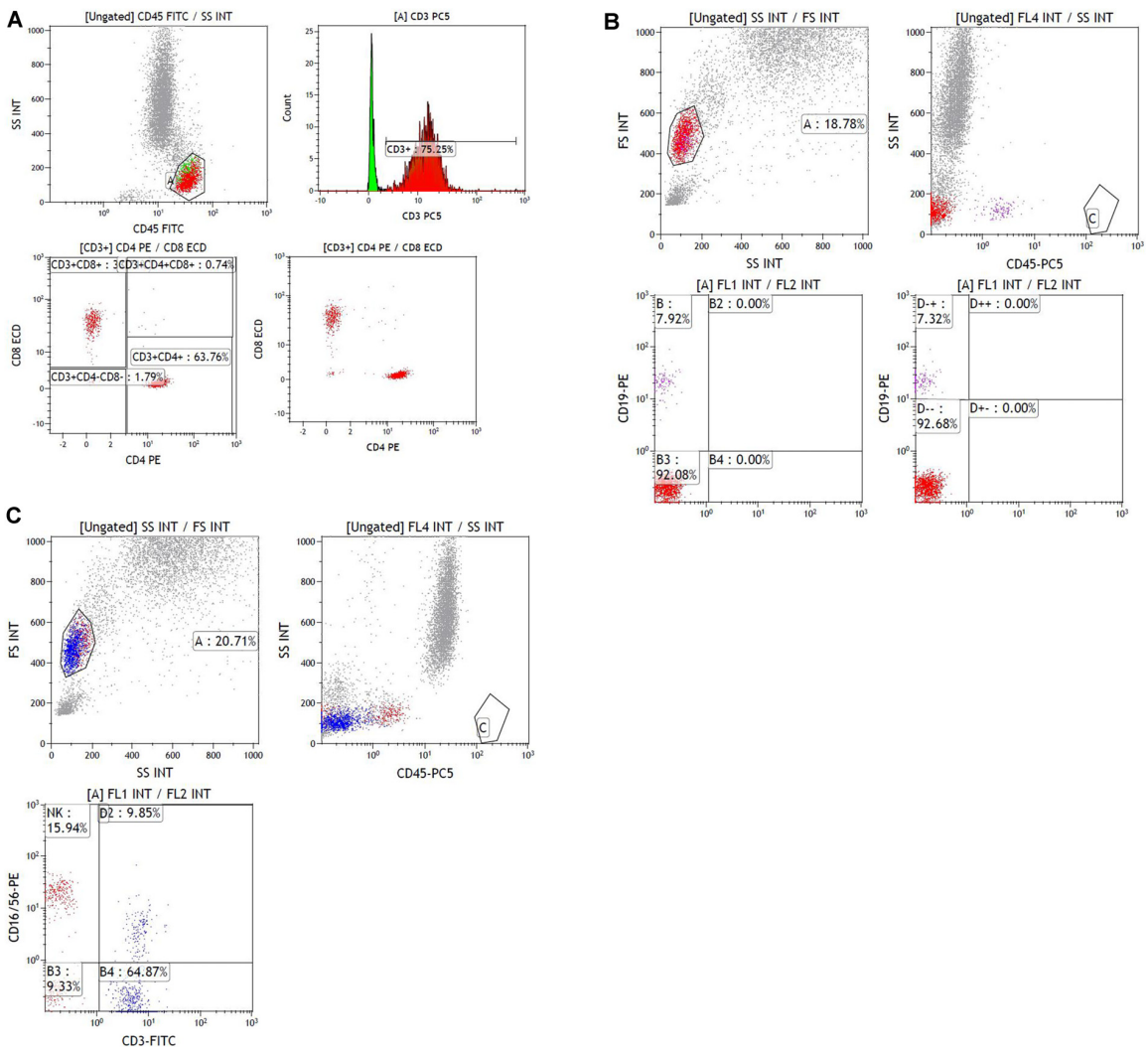

FIGURE 4 | Sample data of flow cytometry experiment. **(A)** Sample data of gating data on T lymphocytes. The gating percentage of [$CD3^+$], [$CD3^+CD4^+$] and [$CD3^+$ $CD8^+$] were 75.25, 47.98 and 25.36%, respectively. **(B)** Sample data of gating data on B lymphocytes. The gating percentage of [$CD19^+$] was 7.92%. **(C)** Sample data of gating data on NK lymphocyte. The gating percentage of [$CD16^+CD56^+$] was 15.94%.

an independent predictor of death (Ebersoldt et al., 2007), SAD is reported to have an incidence of 70% and its mechanism is incompletely understood, especially in patients of advanced age (Eidelman et al., 1996; Zauner et al., 2002; Simone and Tan, 2011). In this study, our results showed that the SAD was associated with prolonged ICU/hospitalization and ventilation

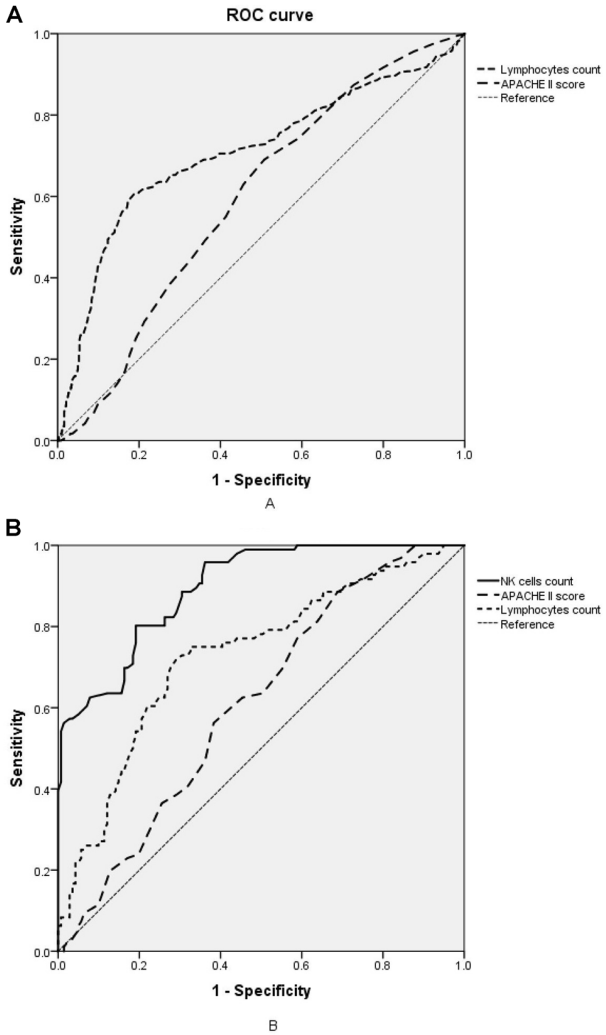

FIGURE 5 | Receiver operating characteristic (ROC) analysis of immune parameters predicting sepsis-associated delirium (SAD). **(A)** ROC curves of APACHE II score and lymphocyte counts in the retrospective cohort. **(B)** ROC curves of NK cell counts, APACHE II score and lymphocyte counts in the prospective cohort. APACHE II, acute physiology and chronic health evaluation II; NK cell, natural killer cell.

duration while the 28-day mortality between the SAD and non-SAD groups was non-significant. Our results correspond with the inconsistent association between delirium and mortality, especially for 28-day mortality. However, considering the majority of the patients mainly suffered from pulmonary and abdominal infection and the weaning on mechanical ventilation and rehabilitation relied on good compliance and consciousness, it is reasonable that the patients with delirium were associated with significantly prolonged duration of mechanical ventilation and ICU stay time.

Recently, the impact of CNS inflammation has been a key area of investigation in delirium of senior patients (Godbout et al., 2005; Yiru and Xia, 2018; Berger et al., 2019). Although multiple studies have demonstrated the damage from excessive inflammation to the CNS and the association between SAD and "cytokine storm" that manifests as immune factor imbalance (Munford and Pugin, 2001; Oberholzer et al., 2001; Abraham and Singer, 2007), the significance and impact of lymphocyte counts on SAD remain undetermined (Inoue et al., 2015; Egberts and Mattace-Raso, 2017; Kotfis et al., 2019). Our findings support that the lymphocytes, as well as NK cells, may play an important role in the mechanism of SAD, irrespective of the presence or absence of other inflammatory mediators or the influence of inflammation on survival and other organ dysfunctions. Previous studies have demonstrated that NK cells can be swiftly mobilized by danger signals and are among the earliest arrivals at target organs including the inflamed CNS (Shi et al., 2011). Noteworthy, the results of a previous study showed that severe sepsis patients with high levels of NK cells at admission had higher mortality (Andaluz-Ojeda et al., 2011). Hatta et al. (2014) also demonstrated the association between increasing blood NK cell activity and the occurrence of delirium. In the present study, lymphocyte and NK cell counts were significantly higher in SAD patients while other immune parameters including $CD4^+$, $CD8^+$, and other inflammatory factors were not, suggesting innate immune activation and potential neuroinflammation played an important role in elderly patients with sepsis. According to our results, increased peripheral NK cell counts are an independent predictor of delirium in sepsis patients of advanced age and close monitoring for the occurrence of delirium would be necessary.

Since Macdonald et al. (2007) first reported that high levels of CRP independently predicted the incidence of delirium, attention has been paid to the inflammatory response and the association between delirium and numerous inflammatory biomarkers (McGrane et al., 2011; Toft et al., 2019). However, none of them were demonstrated to effectively assist in diagnosing and predicting delirium. Intriguingly,

TABLE 7 | Discriminatory powers of APACHE II, lymphocyte count, and NK cell count in the retrospective and prospective cohorts.

		Area under ROC curve (95% CI)	Sensitivity	Specificity	Predictive positive value	Predictive negative value	Relative risk for delirium (95% CI)
Retrospective cohort	APACHE II	0.595 (0.564, 0.626)	38.40%	72.70%	45.40%	72.70%	1.661 (1.605, 2.114)
	Lymphocyte count	0.707 (0.676, 0.739)	60.80%	78.50%	62.20%	79.40%	5.986 (4.671, 7.669)
Prospective cohort	APACHE II	0.611 (0.540, 0.682)	56.30%	61.70%	50.00%	67.40%	2.071 (1.223, 3.509)
	Lymphocytes count	0.728 (0.662, 0.795)	71.90%	69.50%	60.00%	79.50%	5.833 (3.319, 10.253)
	NK cells count	0.895 (0.857, 0.933)	80.20%	80.80%	72.60%	86.50%	17.049 (8.945, 32.495)

The cut-off values of NK cell count, APACHE II score, and lymphocyte count were 87 cells/μl, 21 points, and 0.96 × 10^9/L, respectively. APACHE II, acute physiology, and chronic health evaluation II; NK cell, natural killer cell; ROC, receiver operating characteristic; CI, confidence interval.

growing evidence suggests that the non-specific immune system activation may be the initial response during sepsis, leading to an immune imbalance between neutrophils and lymphocytes in the peripheral circulation and acute inflammation including neuroinflammation in delirium among senior patients (Egberts and Mattace-Raso, 2017; Kotfis et al., 2019). Our results show that the levels of peripheral lymphocytes significantly increased in senior patients with delirium and remained elevated during the first 48 h after ICU admission. Hence, as one of the most common and routine tests in clinical practice, complete blood cell tests and differential subset counts should be highly valued in the management of delirium.

This study had several limitations. First, owing to the nature of the retrospective analysis, our study on delirium accepted the most widely used and simple diagnostic criteria of CAM-ICU, instead of the CAM-ICU-7 released in 2017 to improve its performance regarding delirium severity (Khan et al., 2017). Second, our study did not conduct dynamic monitoring of lymphocyte subsets over time to illustrate dynamic changes, which could be improved in future studies. Third, this intervention was performed at a single medical center, and the relatively small sample size might have obscured the detection of some real changes, which may consist of differences in lymphocyte subsets and inflammatory parameters due to a lack of statistical power. Besides, the neuroinflammatory agents such as cerebrospinal fluid analysis or acetylcholinesterase-activity measurement were not investigated in our study since the practical difficulties in clinical. Future work on larger cohorts and multicenter controlled study and deep research on neuroinflammatory reaction is warranted to confirm our conclusions.

CONCLUSIONS

In this combined retrospective and prospective study, we found that the lymphocyte and NK cell counts were significantly higher in senior patients with SAD, compared with age-matched non-SAD patients, and that NK cell counts may be valuable for the prediction of SAD within patient cohorts of advanced age. Our findings highlighted the importance of NK cells and potential neuroinflammation in the progression of SAD in elderly patients and support the addition of lymphocyte subset analysis to the prediction and diagnosis of SAD.

DATA AVAILABILITY STATEMENT

The raw data supporting the conclusions of this article will be made available by the authors, without undue reservation.

ETHICS STATEMENT

The studies involving human participants were reviewed and approved by institutional review board of Peking Union Medical College Hospital (PUMCH; approval number: JS-1170). The patients/participants provided their written informed consent to participate in this study.

AUTHOR CONTRIBUTIONS

DL designed the study and prepared the drafting of this article. NC conceived the study and made final approval of this manuscript. GB and JZ analyzed all data and helped revise this manuscript. WC contributed to the acquisition of laboratory data and JC was in charge of the acquisition of clinical data. All authors contributed to the article and approved the submitted version.

FUNDING

The work was supported by the Non-profit Central Research Institute Fund of Chinese Academy of Medical Sciences (No. 2019XK320040), National Natural Science Foundation of China (No. 81601657), Tibet Natural Science Foundation (No. XZ2019ZR-ZY12(Z)), and Wu Jieping Medical Foundation (No. 320.6750.18419).

REFERENCES

Abraham, E., and Singer, M. (2007). Mechanisms of sepsis-induced organ dysfunction. *Crit. Care Med.* 35, 2408–2416. doi: 10.1097/01.ccm.0000282072.56245.91

Andaluz-Ojeda, D., Iglesias, V., Bobillo, F., Almansa, R., Rico, L., Gandía, F., et al. (2011). Early natural killer cell counts in blood predict mortality in severe sepsis. *Crit. Care* 15:R243. doi: 10.1186/cc10501

Berger, M., Oyeyemi, D., Olurinde, M. O., Whitson, H. E., Weinhold, K. J., Woldorff, M. G., et al. (2019). The INTUIT study: investigating neuroinflammation underlying postoperative cognitive dysfunction: neuroinflammation in postop cognitive dysfunction. *J. Am. Geriatr. Soc.* 67, 794–798. doi: 10.1111/jgs.15770

Cole, M. G., Ciampi, A., Belzile, E., and Zhong, L. (2009). Persistent delirium in elderly hospital patients: a systematic review of frequency and prognosis. *Age Ageing* 38, 19–26. doi: 10.1093/ageing/afn253

Devlin, J. W., Skrobik, Y., Gélinas, C., Needham, D. M., Slooter, A. J. C., Pandharipande, P. P., et al. (2018). Clinical practice guidelines for the prevention and management of pain, agitation/sedation, delirium, immobility and sleep disruption in adult patients in the ICU. *Crit. Care Med.* 46, e825–e873. doi: 10.1097/CCM.0000000000003299

Ebersoldt, M., Sharshar, T., and Annane, D. (2007). Sepsis-associated delirium. *Intensive Care Med.* 33, 941–950. doi: 10.1007/s00134-007-0622-2

Egberts, A., and Mattace-Raso, F. U. (2017). Increased neutrophil-lymphocyte ratio in delirium: a pilot study. *Clin. Interv. Aging* 12, 1115–1121. doi: 10.2147/CIA.S137182

Eidelman, L. A., Putterman, D., Putterman, C., and Sprung, C. L. (1996). The spectrum of septic encephalopathy. Definitions, etiologies and mortalities. *JAMA* 275, 470–473.

Ely, E. W., Shintani, A., Truman, B., Speroff, T., Gordon, S. M., Harrell, F. E., et al. (2004). Delirium as a septic-associated encephalopathy: a comprehensive review predictor of mortality in mechanically ventilated patients in the intensive care unit. *JAMA* 291, 1753–1762. doi: 10.1001/jama.291.14.1753

Godbout, J. P., Chen, J., Abraham, J., Richwine, A. F., Berg, B. M., Kelley, K. W., et al. (2005). Exaggerated neuroinflammation and sickness behavior in aged

mice following activation of the peripheral innate immune system. *FASEB J.* 19, 1329–1331. doi: 10.1096/fj.05-3776fje

Hatta, K., Kishi, Y., Takeuchi, T., Wada, K., Odawara, T., Usui, C., et al. (2014). The predictive value of a change in natural killer cell activity for delirium. *Progr. Neuropsychopharmacol. Biol. Psychiatry* 48, 26–31. doi: 10.1016/j.pnpbp.2013.09.008

Inoue, S., Vasilevskis, E. E., Pandharipande, P. P., Girard, T. D., Graves, A. J., Thompson, J., et al. (2015). The impact of lymphopenia on delirium in ICU patients. *PLoS One* 10:e0126216. doi: 10.1371/journal.pone.0126216

Iwashyna, T. J., Ely, E. W., Smith, D. M., and Langa, K. M. (2010). Long-term cognitive impairment and functional disability among survivors of severe sepsis. *JAMA* 304, 1787–1794. doi: 10.1001/jama.2010.1553

Jalla, S., Sazawal, S., Deb, S., Black, R. E., Das, S. N., Sarkar, A., et al. (2004). Enumeration of lymphocyte subsets using flow cytometry: effect of storage before and after staining in a developing country setting. *Indian J. Clin. Biochem.* 19, 95–99. doi: 10.1007/BF02894264

Kotfis, K., Bott-Olejnik, M., Szyll Nska, A., Rotter, I., and Szylińska, A. (2019). Clinical medicine could neutrophil-to-lymphocyte ratio (NLR) serve as a potential marker for delirium prediction in patients with acute ischemic stroke? A prospective observational study. *J. Clin. Med.* 8:1075. doi: 10.3390/jcm8071075

Khan, B. A., Perkins, A. J., Gao, S., Hui, S. L., Campbell, N. L., Farber, M. O., et al. (2017). The confusion assessment method for the ICU-7 delirium severity scale. *Crit. Care Med.* 45, 851–857. doi: 10.1097/CCM.0000000000002368

Macdonald, A., Adamis, D., Treloar, A., and Martin, F. (2007). C-reactive protein levels predict the incidence of delirium and recovery from it. *Age Aging* 36, 222–225. doi: 10.1093/ageing/afl121

McGrane, S., Girard, T. D., Thompson, J. L., Shintani, A. K., Woodworth, A., Ely, E. W., et al. (2011). Procalcitonin and C-reactive protein levels at admission as predictors of duration of acute brain dysfunction in critically ill patients. *Crit. Care* 15:R78. doi: 10.1186/cc10070

Munford, R. S., and Pugin, J. (2001). Normal responses to injury prevent systemic inflammation and can be immunosuppressive. *Am. J. Respir. Crit. Care Med.* 163, 316–321. doi: 10.1164/ajrccm.163.2.2007102

Oberholzer, A., Oberholzer, C., and Moldawer, L. L. (2001). Sepsis syndromes: understanding the role of innate and acquired immunity. *Shock* 16, 83–96. doi: 10.1097/00024382-200116020-00001

Pisani, M. A., Kong, S. Y., Kasl, S. V., Murphy, T. E., Araujo, K. L. B., and Van Ness, P. (2009). Days of delirium are associated with 1-year mortality in an elderly intensive care unit population. *Am. J. Respir. Crit. Care Med.* 180, 1092–1097. doi: 10.1164/rccm.200904-0537OC

Ren, C., Yao, R. Q., Zhang, H., Feng, Y.-W., and Yao, Y.-M. (2020). Sepsis-associated encephalopathy: a vicious cycle of immunosuppression. *J. Neuroinflammation* 17:14. doi: 10.1186/s12974-020-1701-3

Shankar-Hari, M., Phillips, G. S., Levy, M. L., Seymour, C. W., Liu, V. X., Deutschman, C. S., et al. (2016). Developing a new definition and assessing new clinical criteria for septic shock. *JAMA* 315, 775–787. doi: 10.1001/jama.2016.0289

Shi, F. D., Ljunggren, H. G., La Cava, A., and Van Kaer, L. (2011). Organ-specific features of natural killer cells. *Nat. Rev. Immunol.* 11, 658–671. doi: 10.1038/nri3065

Simone, M. J., and Tan, Z. S. (2011). The role of inflammation in the pathogenesis of delirium and dementia in elderly adults: a review. *CNS Neurosci. Ther.* 17, 506–513. doi: 10.1111/j.1755-5949.2010.00173.x

Sonneville, R., de Montmollin, E., Poujade, J., Garrouste-Orgeas, M., Souweine, B., Darmon, M., et al. (2017). Potentially modifiable factors contributing to sepsis associated encephalopathy. *Intensive Care Med.* 43, 1075–1084. doi: 10.1007/s00134-017-4807-z

Sonneville, R., Verdonk, F., Rauturier, C., Klein, I. F., Wolff, M., Annane, D., et al. (2013). Understanding brain dysfunction in sepsis. *Ann. Intensive Care* 3:15. doi: 10.1186/2110-5820-3-15

Toft, K., Tontsch, J., Abdelhamid, S., Steiner, L., Siegemund, M., and Hollinger, A. (2019). Serum biomarkers of delirium in the elderly: a narrative review. *Ann. Intensive Care* 9:76. doi: 10.1186/s13613-019-0548-1

van den Boogaard, M., Kox, M., Quinn, K. L., van Achterberg, T., van der Hoeven, J. G., Schoonhoven, L., et al. (2011). Biomarkers associated with delirium in critically ill patients and their relation with long-term subjective cognitive dysfunction; indications for different pathways governing delirium in inflamed and noninflamed patients. *Crit. Care* 15:R297. doi: 10.1186/cc10598

Wang, C., Wu, Y., Yue, P., Wesley Ely, E., Huang, J., Yang, X., et al. (2013). Delirium assessment using confusion assessment method for the intensive care unit in chinese critically ill patients. *J. Crit. Care.* 28, 223–229. doi: 10.1016/j.jcrc.2012.10.004

Young, G. B., Bolton, C. F., Austin, T. W., Archibald, Y. M., Gonder, J., Wells, G. A., et al. (1990). The encephalopathy associated with septic illness. *Clin. Invest. Med.* 13, 297–304.

Yiru, W., and Xia, S. (2018). Postoperative delirium in the elderly: the potential neuropathogenesis. *Aging Clin. Exp. Res.* 30, 1287–1295. doi: 10.1007/s40520-018-1008-8

Zauner, C., Gendo, A., Kramer, L., Funk, G. C., Bauer, E., Schenk, P., et al. (2002). Impaired subcortical and cortical sensory evoked potential pathways in septic patients. *Crit. Care Med.* 30, 1136–1139. doi: 10.1097/00003246-200205000-00030

Conflict of Interest: The authors declare that the research was conducted in the absence of any commercial or financial relationships that could be construed as a potential conflict of interest.

frontiers in Aging Neuroscience

ORIGINAL RESEARCH
published: 01 February 2021
doi: 10.3389/fnagi.2020.625166

Systemic Inflammation Increases the Susceptibility to Levodopa-Induced Dyskinesia in 6-OHDA Lesioned Rats by Targeting the NR2B-Medicated PKC/MEK/ERK Pathway

*Aijuan Yan, Lu Song, Yu Zhang, Xijin Wang and Zhenguo Liu**

Department of Neurology, Xinhua Hospital Affiliated to Shanghai Jiao Tong University School of Medicine, Shanghai, China

Background: The long-term administration of levodopa (L-dopa), the gold-standard treatment for Parkinson's disease (PD), is irreparably associated with L-dopa-induced dyskinesia (LID), which dramatically affects the quality of life of patients. However, the underlying molecular mechanisms of how LID exacerbates remain unknown. Neuroinflammation in the striatum plays an active role in LID. These findings prompt an investigation of non-neuronal mechanisms of LID. This study will examine the effects of systemic inflammation in the development and progression of LID.

Methods: To evaluate the possible influence of systemic inflammation in the appearance of LID, the PD rats received an intraperitoneal (IP) injection of various concentrations of lipopolysaccharides (LPS, 1, 2, and 5 mg/kg) or saline. One day later, these PD rats started to receive daily treatment with L-dopa (6 mg/kg) along with benserazide (6 mg/kg) or saline for 21 days, and dyskinesia was evaluated at several time points. Moreover, the activation of microglia and astrocytes and the molecular changes in NR2B and mGLUR5 signaling pathways were measured.

Results: We found that systemic inflammatory stimulation with LPS exacerbated the intensity of abnormal involuntary movements (AIMs) induced by L-dopa treatment in 6-hydroxydopamine (6-OHDA) lesioned rats. The LPS injection activated the gliocytes and increased the levels of proinflammatory cytokines in the striatum in LID rats. The PD rats that received the LPS injection showed the overexpression of p-NR2B and NR2B, as well as activated PKC/MEK/ERK and NF-κB signal pathways in response to the L-dopa administration. On the contrary, clodronate-encapsulated liposomes (Clo-lipo), which could suppress the inflammatory response induced by peripheral LPS injection, improved behavioral dysfunction, inhibited neuroinflammation, prevented NR2B overexpression, and decreased the phosphorylation of PKC/MEK/ERK and NF-κB signaling pathways.

OPEN ACCESS

Edited by:
Xian-Le Bu,
Third Military Medical University, China

Reviewed by:
Qian Liu,
Northwest University, China
Sachchida Nand Rai,
University of Allahabad, India

****Correspondence:***
Zhenguo Liu
liuzhenguo@xinhuamed.com.cn

Received: *02 November 2020*
Accepted: *30 December 2020*
Published: *01 February 2021*

Citation:
Yan A, Song L, Zhang Y, Wang X and Liu Z (2021) Systemic Inflammation Increases the Susceptibility to Levodopa-Induced Dyskinesia in 6-OHDA Lesioned Rats by Targeting the NR2B-Medicated PKC/MEK/ERK Pathway. Front. Aging Neurosci. 12:625166. doi: 10.3389/fnagi.2020.625166

Conclusion: This study suggests that systemic inflammation, by exacerbating preexisting neuroinflammation and facilitating NR2B subunit activity, may play a crucial role in the development of LID. The administration of Clo-lipo restores the effects of LPS and decreases the susceptibility to LID in 6-OHDA lesioned rats.

Keywords: L-dopa induced dyskinesia, Parkinson's disease, systemic inflammation, NR2B, neuroinflammation

INTRODUCTION

Parkinson's disease (PD) is characterized by the progressive loss of dopaminergic neurons in the substantia nigra (SN) and leads to bradykinesia, rigidity, and tremor (Kalia and Lang, 2015). Levodopa (L-dopa), the gold-standard treatment for PD, alleviates the motor symptoms of PD. However, its long-term administration is irreparably associated with abnormal involuntary movements (AIMs), termed L-dopa-induced dyskinesia (LID) (Espay et al., 2018), which dramatically affects the quality of life of patients. Treatment of high doses of L-dopa and the severity of PD mainly contributed to the development and progression of dyskinesia (Cilia et al., 2014).

Recently, non-neuronal mechanisms have been proposed to play important roles in the development of LID (Del-Bel et al., 2016). The immune system has emerged as an important player in LID and was a potential target for pharmacological therapy (Pisanu et al., 2018). Glial cells are significant in the immune reaction of the brain to noxious insults by establishing the inflammatory milieu surrounding activated glial cells (Bortolanza et al., 2015a). Previous researches showed that the L-dopa chronic treatment eliciting AIMs were associated with microgliosis, astrocytosis, and an increased expression of proinflammatory cytokines (Bortolanza et al., 2015a; Del-Bel et al., 2016; Carta et al., 2017). The study of Mulas et al. (2016) showed that a pulsatile treatment with L-dopa resulted in a neuroinflammatory response in the striatum, while continuous delivery of the drug was void of any inflammatory response and dyskinetic outcome. Neuroinflammation is a shared feature of LID in the human brain and in animal models. Conditions that induce neuroinflammatory response and cytokine release could facilitate LID (Mulas et al., 2016). Several reports revealed that peripheral inflammatory response could induce neuroinflammation *via* the activation of microglia and the production of proinflammatory cytokines, including interleukin-6 (IL-6), interleukin-1β (IL-1β), and tumor necrosis factor-α (TNF-α) in the brain (Murta et al., 2015). A well-studied model of systemic inflammation in rodents is the intraperitoneal (IP) injection of *Escherichia coli* lipopolysaccharide (LPS) from Gram-negative bacteria to induce the innate immune response (Wu et al., 2012). Whether the systematic inflammatory response is involved in LID is unclear.

N-methyl-D-aspartate (NMDA) is a heterotetramer ion channel assembled from a combination of GluN1, GluN2, and GluN3 subunits (Yang et al., 2018). NR2A and NR2B are the most common subtypes of NMDA receptors (NMDARs) found in the central nervous system (CNS) of mammals. Neuronal apoptosis is prevented when NR2A is selectively activated, whereas the activation of NR2B is associated with the inflammatory response (Zhang et al., 2018). NR2B is best characterized as a regulatory subunit that plays an important role in the inflammatory response (Chen et al., 2008). The proinflammatory cytokines in the brain have been shown to facilitate the NR2B subunit of the NMDA receptor activity (Viviani et al., 2003). The phosphorylation of the NR2B subunit plays a very important role in the regulation of NMDA receptor function and has been connected to alterations of synaptic efficacy of the NMDA receptor. CP-101,606, an NR2B-selective antagonist, has been reported to reduce dyskinesia as measured by clinical scoring (Ba et al., 2019). A possible role for the NR2B receptor in dyskinesia in patients with PD (Herring et al., 2017) or Parkinsonian animals (Gan et al., 2014) has been highlighted. However, whether the activation of NR2B in the striatum plays a contributing role in the exacerbation of LID susceptibility after systemic inflammation is currently unknown.

How systematic inflammation aggravated LID remains unclear. Based on the above evidence, we proposed that the systematic inflammatory response, through its actions on NR2B, would influence the development of LID. Furthermore, based on the existence of a correlation between LID and NR2B receptor-dependent signaling pathways, we performed the biochemical analysis in order to elucidate the molecular mechanisms of LPS on LID. To achieve systematic inflammation, we used a model of IP injection of LPS in 6-hydroxydopamine (6-OHDA)-lesioned rats. This study will discuss how systematic inflammation affects LID in 6-OHDA lesioned rats.

MATERIALS AND METHODS

Animals

Adult male Sprague-Dawley rats in Specific Pathogen Free (SPF) grade (mean weight 200–250 g) were purchased from the Shanghai Laboratory Animal Center (SLAC; Shanghai, China). The production license number is SCXK 2017-0005. The rats were housed five per cage under a temperature of 22.0 ± 2.0°C and humid conditions, in a 12 h-light/dark cycle with free access to food and water. All animal works were performed in accordance with the guidelines of the National Institutes of Health for the care and use of laboratory animals as stipulated by the Institutional Animal Care and Use Committee of the School of Medicine, Shanghai Jiao Tong University, Shanghai, China. All experimental animal procedures followed the Animal Research: Reporting of *In Vivo* Experiments (ARRIVE) guidelines (https://www.nc3rs.org.uk/arrive-guidelines), and the guidelines of the Regulation for the Administration of

Affairs Concerning Experimental Animals of China enacted in 1988.

Rat Model of PD

6-hydroxydopamine-lesioned PD rat models were performed according to our previous study (Xie et al., 2014). Briefly, rats were anesthetized with ketamine (100 mg/kg) by IP injection. Then, the rats received 6-OHDA (16 μg dissolved in 4 μl of 0.9% saline containing 0.2% L-ascorbic acid; Sigma-Aldrich, St. Louis, MO, USA) injection into the right middle forebrain bundle (MFB) at the following coordinates relative to the bregma: (1) anterior-posterior (AP), 3.7 mm; medial-lateral (ML), 1.7 mm; and dorsal-ventral (DV), 7.8 mm and (2) AP, 4.4 mm; ML, 1.2 mm; and DV, 7.8 mm. The injection speed was 1 μl/min. The needle was withdrawn 5 min after infusion. After 21 days, rats exhibiting >7 contralateral turns over 1 min in response to IP injections of apomorphine (0.5 mg/kg) were selected as successful PD rat models and could be used for subsequent experiments.

Drug Treatment and LID

In the first part of our study, the successful PD rats were divided into four groups randomly. Systemic inflammation was induced by one injection of LPS from *E. coli* O26:B6 (Sigma, St. Louis, MO, USA). These PD rats received a single IP injection of LPS (1, 2, and 5 mg/kg; Sigma-Aldrich Chemical, M O, USA; Cho et al., 2015; Ho et al., 2015; Kosyreva et al., 2018) or 0.9% saline. After 24 h, they were administered with L-dopa (6 mg/kg, IP.) along with benserazide (6 mg/kg, i.p.) once daily for 21 days to induce a model of dyskinesia (Tronci et al., 2017; **Figure 1A**).

Clodronate-encapsulated liposomes (Clo-lipo) were widely used to deplete peripheral macrophages (Ma et al., 2016; Yan et al., 2018). Clodronate was encapsulated in liposomes with a concentration of 5 mg clodronate/ml, a concentration that ensures the depletion of 80% of macrophages within 72 h after systemic administration (Seiler et al., 1997). Our study found that Clo-lipo can deplete 82% of macrophages in the spleen 72 h after injection (**Supplementary Figure 1**). In the second part, the successful PD rats received IP injections of phosphate-buffered saline (PBS) liposomes (1 ml/100 g of the order preparation; Nico van Rooijen; Amsterdam, The Netherlands) or Clo-lipo (1 ml/100 g of the order preparation; Nico van Rooijen; Amsterdam, The Netherlands). After 72 h, the two rat groups were administered with LPS (2 mg/kg, IP) and then treated with an administration of L-dopa/benserazide (6/6 mg/kg, IP) once daily for 21 days (**Figure 1B**). Two hours after the final L-dopa/benserazide treatment, the rats were sacrificed by CO_2 euthanization, and brain samples were stored at −80°C until analysis.

Abnormal Involuntary Movement Ratings

Abnormal involuntary movements were evaluated according to the rat dyskinesia scale described in our previous publications (Gan et al., 2015). On days 1, 2, 4, 6, 9, 13, 17, and 21 of the L-dopa/benserazide treatment, AIMs were individually observed in the 6-OHDA-lesioned PD rats after the L-dopa/benserazide injection by an experimenter who was unaware of the pharmacological intervention. Rats were placed individually in plastic cages and observed for 1 min at 20 min intervals for a duration of 120 min. AIMs were classified into three subtypes according to their distribution as axial movement, limb movement, and orolingual movement. The severity of each AIM subtype was assessed using scores from 0 to 4 (0: absent, 1: present <50% of the time; 2: present >50% of the time; 3: present all the times but interrupted by external stimuli; and 4: present all the times, and not interrupted by external stimuli). For every rat, the ALO (Axical, Limb, Orolingual) AIMs score was calculated by adding each of the three individual scores.

Immunohistochemistry

Immunohistochemical staining of rat brain sections was performed as previously described (Xie et al., 2014). The brains were removed, postfixed for 24 h in 4% paraformaldehyde (PFA), and then cryoprotected in 30% sucrose in PBS (pH 7.4). Subsequently, serial coronal sections (cut thickness: 20 μm) were cut on a freezing microtome. The brain sections were fixed with 4% PFA for 15 min and then incubated in PBS for 10 min. Slides were blocked for 1 h in 10% normal donkey serum and then incubated in a primary antibody at 4°C overnight. Primary antibodies included rabbit anti-iba1 (1:200, Abcam) and rabbit anti-glial fibrillary acidic protein (GFAP; 1:400, Abcam). After being washed three times with PBS, the sections were incubated with the corresponding donkey anti-rabbit secondary antibody conjugated to Alexa Fluor 594 (1:400 dilution, Life Technologies) for 1 h at room temperature. The brain sections were viewed using a fluorescence microscope (Leica, Solms, Germany). Three fields measuring 150 × 150 μm in the lesioned striatum were imaged in each section. A total of 10 sections (taking every other section spaced 200 μm apart) were evaluated for each rat as previously described (Ma et al., 2016). The mean integrated optical density (IOD) was measured by the ImageJ software (Media Cybernetics, Bethesda, MO). The ratio of the mean IOD between the different groups was used for further analysis.

Quantitative PCR

The rats from each group were sacrificed by anesthetic overdose 21 days after L-dopa injection. Total RNA was isolated from rat brains using Trizol Reagent (Life Technologies, Rockville, MD, USA) and was reverse transcribed to cDNA using the PrimeScript RT Reagent kit (Takara Bio, Inc., Otsu, Japan). qPCR was performed using an SYBR Green kit (Takara Bio, Inc., Otsu, Japan) according to the manufacturer's instructions. The outcome was expressed as the fold-difference normalized to glyceraldehyde-3-phosphate dehydrogenase (GAPDH). Q-PCR was detected using an ABI PRISM 7500 Sequence Detection system (Thermo Fisher Scientific, Inc., Waltham, USA). The sequences of the primer pairs for proinflammatory cytokine genes are as follows:

IL-1β (F: AGCTGCACTGCAGGCTTCGAGATG, R: GAA CTGTGCAGACTCAAA CTCCAC); IL-6 (F: TCCTACC CCAACTTCCAATGCTC, R: TTGGATGGTCTT GGTCCTT AGCC); TNF-α (F: CACGCTCTTCTGTCTACTG AACTTC G, R: TGCTCC TCCGCTTGGTGGTT); and GAPDH (F: TTC CTACC CCCAATGTATCCG, R: CATGAG GTCCACCAC CCTGTT).

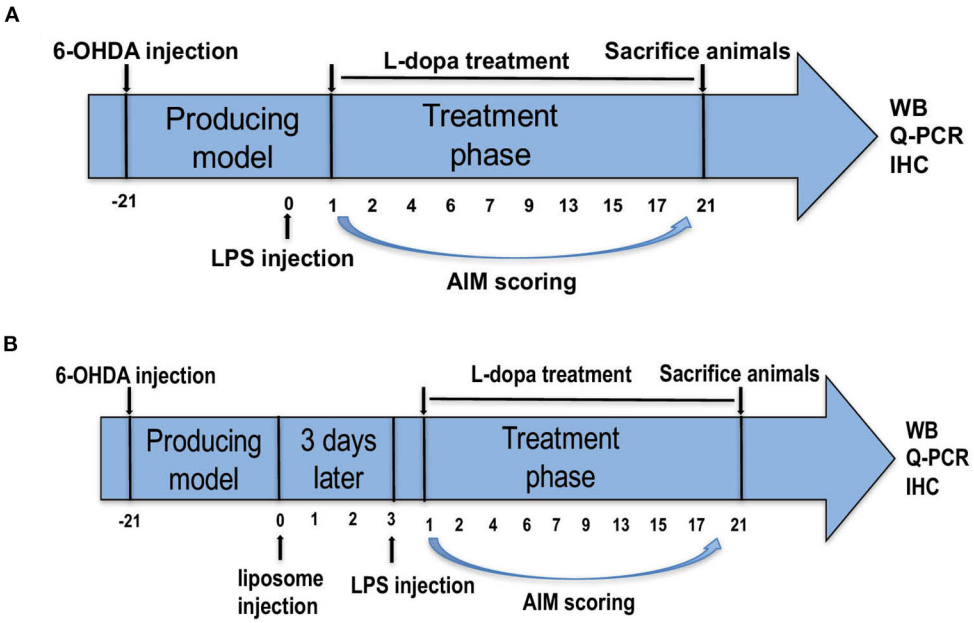

FIGURE 1 | Experimental design of the study. **(A)** Parkinson's disease (PD) rats were unilaterally injected with 6-hydroxydopamine (6-OHDA) in the middle forebrain bundle (MFB). Contralateral turning behaviors after apomorphine injection were tested. Rats in the PD+LPS+L-dopa group were administrated with lipopolysaccharide (LPS). Twenty four hours later, rats in the PD+saline+L-dopa and PD+LPS+L-dopa group were administrated with L-dopa (6 mg/kg, IP) plus benserazide [6 mg/kg, intraperitoneal (IP)] for 21 days. Abnormal involuntary movements (AIMs) were evaluated during this period, at days 1, 2, 4, 6, 7, 9, 13, 15, 17, and 21. **(B)** The successful PD rats were divided into two groups and received IP injections of phosphate-buffered saline (PBS) liposomes (1 ml/100 g) or clodronate-liposomes (Clo-lipos, 1 ml/100 g), respectively. After 3 days, the animals received a single injection of LPS (2 mg/kg, IP) and were then treated with L-dopa/benserazide (6/6 mg/kg, IP) once daily for 21 days. The animals were sacrificed 2 h after the last injection for Western blot, quantitative PCR (q-PCR), and immunofluorescence.

Western Blotting

Tissue samples were prepared by homogenizing the brain in a standard lysis buffer. The protein concentration was measured using a Pierce BCA Protein Assay Kit (ThermoFisher Scientific). Forty micrograms of protein per well were separated by Sodium dodecyl sulphate polyacrylamide gel electrophoresis (SDS-PAGE) and transferred onto a nitrocellulose membrane. The membranes were blocked with 5% non-fat dried milk for 1 h and incubated with primary antibodies against iba1 (1:1,000, Abcam), GFAP (1:2,000, Abcam), p-NR2B (1:1,000, Abcam), NR2B (1:1,000, Abcam), mGLUR5 (1:1,000, Abcam), p-PKC (1:1,000, Cell Signaling Technology), PKC (1:1,000, Cell Signaling Technology), p-MEK (1:1000, Cell Signaling Technology), MEK (1:1,000, Cell Signaling Technology), p-pERK (1:1,000, Cell Signaling Technology), ERK (1:1,000, Cell Signaling Technology), and β-actin (1:1,000, Cell Signaling Technology) overnight at 4°C. After being washed with Tris-buffered saline with TWEEN 20 (TBST) buffer, the membranes were incubated with horseradish peroxidase (HRP)-conjugated secondary antibody (1:2,000, Cell Signaling Technology) for 1 h at room temperature and then subjected to chemiluminescent detection according to the manufacturer's instructions (Millipore).

Statistical Analysis

Behavioral data were non-parametric and analyzed using the Kruskal–Wallis test followed by the Dunn's test for multiple comparisons in the case of comparing data over multiple days, or the Mann–Whitney *U*-test. Group comparisons were performed using one-way ANOVA with a Tukey's multiple comparisons test. We reported actual values of p from the ANOVA. All values are presented in the study as means ± SEM. Values of $p < 0.05$ were considered statistically significant. The statistical analysis was performed using the GraphPad software (GraphPad Software, Inc., La Jolla, USA).

RESULTS

Effect of Peripheral LPS Injection on LID

To evaluate whether systematic inflammation can produce an effect on dyskinesia in LID, the successful PD rats received a single IP injection of LPS used at 1 mg/kg, 2 mg/kg, and 5 mg/kg. A lower dose of L-dopa (6 mg/kg, plus 6 mg/kg benserazide, IP) was used in an attempt to better highlight the differences in the AIM score between LPS- and saline-treated PD rats during the L-dopa treatment (Tronci et al., 2017). Our results revealed that 5 mg/kg LPS resulted in the death of PD rats. The sham and PD groups received the saline for 21 days, and these rats did not develop LID. Administration of L-dopa for 21 days induced dyskinesia in both LPS and saline-treated PD rats. In terms of the ALO AIM score, PD+2 mg/kg LPS and PD+1 mg/kg LPS rats were obviously increased

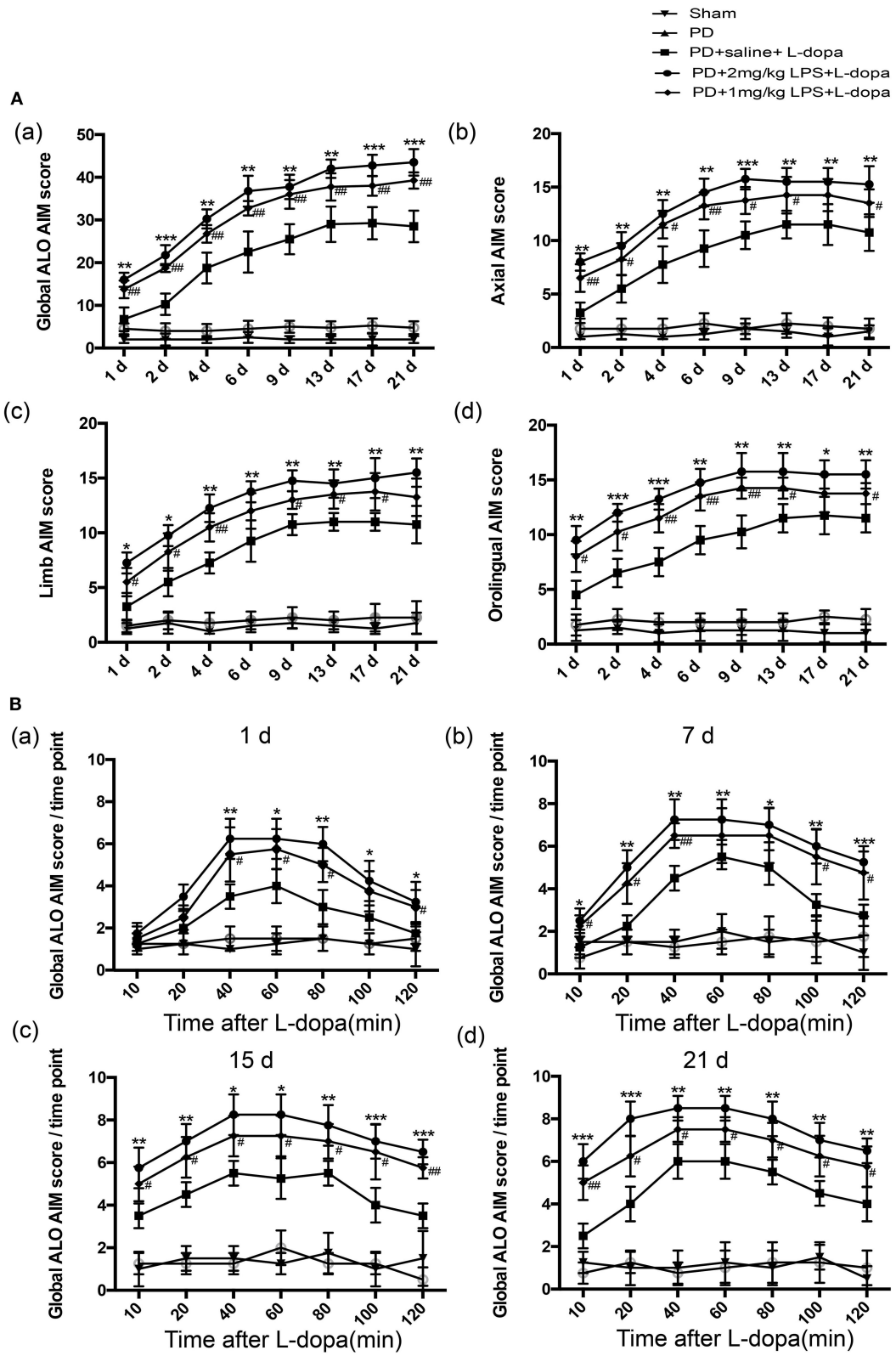

FIGURE 2 | Effect of peripheral LPS injection on the ALO AIMs during a 3-week treatment with L-dopa. Rats were rated for ALO AIMs for 120 min post injection. **(A)** (a) sum of axial, limb, and orolingual, (b) axial, (c) limb, and (d) orolingual AIMs. **(B)** the global ALO AIM score at different time points at 1 day (a), 7 days (b), 15 days (c), and 21 days (d). Values are presented as the mean ± SEM. $^{*}p < 0.05$, $^{**}p < 0.01$, and $^{***}p < 0.001$: PD+2 mg/kg LPS+L-dopa vs. PD+saline+L-dopa; $^{\#}p < 0.05$ and $^{\#\#}p < 0.01$: PD+1 mg/kg LPS+L-dopa vs. PD+saline+L-dopa.

compared with the PD+saline rats at the same time point during the course of the L-dopa treatment ($^{*}p < 0.05$, $^{**}p < 0.01$, $^{***}p < 0.001$ vs. PD+saline+L-dopa. $^{\#}p < 0.05$, $^{\#\#}p < 0.01$, vs. PD+saline+L-dopa, **Figure 2A**a, $n = 12$/group). This was the same trend in axial AIM (**Figure 2A**b), limb AIM (**Figure 2A**c), and orolingual AIM (**Figure 2A**d). On the L-dopa treatment days 1, 7, 15, and 21, we also analyzed the ALO AIM score of these five groups at 10, 20, 40, 60, 80, 100, and 120 min after the L-dopa treatment. Interestingly, since day 7 of using L-dopa, an increased ALO AIM score was observed in the LPS-treated rats at 10 min after the L-dopa treatment as compared with the PD+saline+L-dopa group ($^{*}p < 0.05$, $^{**}p < 0.01$, $^{***}p < 0.001$ vs. PD+saline+L-dopa. $^{\#}p < 0.05$, $^{\#\#}p < 0.01$, vs. PD+saline+L-dopa; **Figure 2B**, $n = 12$/group), indicating that LPS exacerbates LID. A higher dose of LPS (2 mg/kg) had a greater effect on LID than the lower dose (1 mg/kg). These data suggested that peripheral LPS injection into PD rats showed a higher susceptibility to develop dyskinesia as compared to the saline-treated PD rats during the L-dopa treatment.

Peripheral LPS Injection Produces Long-Lasting Effects on Neuroinflammation in the Striatum of LID Rats

To investigate if only a single IP injection of LPS is involved in neuroinflammation in normal rats, the inflammatory response in the striatum was tested. Our study found that LPS could significantly increase the expression of glia markers Iba-1 (**Supplementary Figure 2A**a,b) and GFAP (**Supplementary Figure 2A**a,c) and the mRNA levels of IL-1β, IL-6, and TNF-α (**Supplementary Figure 2B**) in the striatum of 24 h after injecting the normal rats. Furthermore, we investigated the effects of one IP injection of LPS on neuroinflammation in the striatum of LID rats. As shown in **Figure 3**, in the PD+saline+L-dopa group, the microglia and astrocytes in the lesioned hemispheres were activated as compared to the PD group and the sham group ($^{\#}p < 0.05$, $^{\#\#}p < 0.01$ vs. sham, $n = 4$/group). To characterize the effect of peripheral LPS injection on neuroinflammation in the striatum, the activation of microglia and astrocytes, IL-1β, IL-6, and TNF-α mRNA levels were quantified. The PD rats pretreated with a challenge with LPS showed an increase of Iba1+ and GFAP+ cells in the lesioned striatum as compared to the PD+saline+L-dopa group after the last L-dopa treatment, ($^{*}p < 0.05$, $^{**}p < 0.01$, $^{***}p < 0.001$ vs. PD+saline+L-dopa, **Figures 3A,B**, $n = 4$/group). Moreover, the Q-PCR analysis of mRNA for the proinflammatory cytokines was performed on day 21 of the L-dopa chronic administration. Results showed the release of peripheral LPS-infusion induced inflammatory cytokines IL-1β, IL-6, and TNF-α in the PD+LPS+L-dopa group ($^{*}p < 0.05$, $^{**}p < 0.01$ vs. PD+saline+L-dopa, **Figure 3C**). These results showed that IP infusion of LPS induced neuroinflammation in the striatum, characterized by significant activation of microglia and astrocytes, and increased in the expression of IL-1β, IL-6, and TNF-α.

LPS Treatments Increased the Expressions of p-NR2B and NR2B in the Striatum of LID Rats

Our study found that LPS-treated rats showed significantly higher levels of phosphorylation of NR2B and total NR2B in the striatum 24 h after the injection (**Supplementary Figures 3A,B**). No differences were found in the mGluR5 levels in the striatum injected with LPS compared to the saline-injected group (**Supplementary Figure 3C**). To examine whether a single IP injection of LPS to the PD rats influenced the protein expression of NR2B and mGluR5 in the striatum in L-dopa induced animals, we performed Western blotting on the striatum tissue collected at 2 h after the last L-dopa injection. The LPS-treated PD rats showed significantly higher levels of phosphorylation of NR2B and total NR2B, in response to L-dopa, compared with the PD+saline+L-dopa group ($^{*}p < 0.05$ vs. PD + saline+ L-dopa, **Figures 4A,B**, $n = 4$/group). No difference was found in the expression of mGLUR5 levels in the lesioned striatum injected with LPS compared with the PD+saline+L-dopa group (**Figure 4C**; $n = 4$/group). We thought that the overexpression of the NR2B subunit induced by a single IP injection of LPS might play an important role in the induction of dyskinesia during the course of the L-dopa injection.

Lipopolysaccharide Treatments Further Activated the Striatal PKC/MEK/ERK and NF-κB Signal Pathways in the Striatum After Pulsatile L-Dopa Treatment

Consistent with the previous report, we found the phosphorylation of PKC/MEK/ERK was significantly increased in the lesioned striatum of the PD+saline+L-dopa group as compared to the PD group ($^{\#}p < 0.05$, $^{\#\#}p < 0.01$ vs. sham, **Figure 5**, $n = 4$/group). Our data showed that peripheral LPS injection could increase the expression of phosphorylation of NR2B and total NR2B in the striatum of the L-dopa-treated group. Thus, the impact of LPS injection on the striatal NR2B receptor was evaluated by measuring PKC/MEK/ERK and NF-κB signal pathways. Our results demonstrated that the administration of peripheral LPS to the PD rats could significantly increase the phosphorylation of PKC/MEK/ERK and NF-κB compared with the saline-treated PD rats during the course of the L-dopa injection ($^{*}p < 0.05$, $^{***}p < 0.001$ vs. PD+saline+L-dopa, **Figure 5**, $n = 4$/group). These results showed that a single acute intraperitoneal LPS administration to the PD rats could further activate PKC/MEK/ERK and NF-κB signaling pathways in the striatum during the L-dopa treatment.

Clo-lipo Administration Attenuated the AIM Score and Suppressed LPS-Induced Striatal Neuroinflammation in LID Rats

A previous study has shown that this unselective macrophage depletion by Clo-lipo administration reduced the experimental acute inflammatory response induced by the LPS injection (Villaran et al., 2010; Xie et al., 2017; Pervin et al., 2018). In this study, we found that systematic inflammatory stimulation with LPS exacerbated the intensity of the ALO AIM score

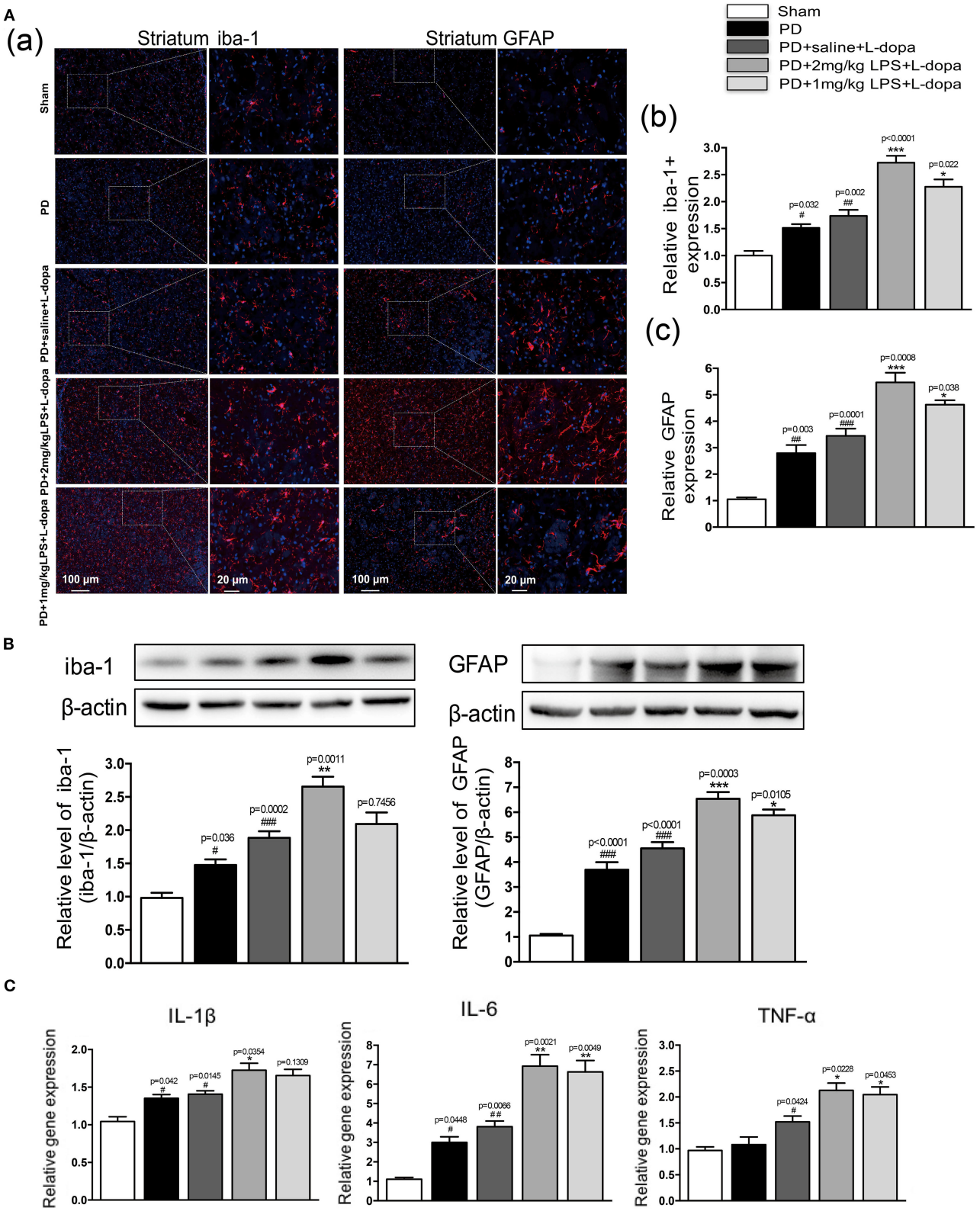

FIGURE 3 | Effect of peripheral LPS injection on the striatal neuroinflammation after the pulsatile L-dopa treatment. **(A)** (a) Microglia and astrocytes were determined in the striatum by immunohistochemical analysis of Iba1 and GFAP. Scale bar = 100 μm in left panels and 20 μm in right panels. (b) The quantity of microglia in the striatum was quantified by the intensity of iba-1+immunofluorescence. (c) The number of astrocytes in the striatum was quantified by the intensity of

(Continued)

FIGURE 3 | GFAP+immunofluorescence. **(B)** Expression levels of iba-1 and GFAP were analyzed by Western blotting. **(C)** The mRNA levels of the proinflammatory mediators IL-1β, IL-6, and TNF-α normalized to GAPDH in the striatum. Values are presented as the mean ± SEM. $n = 4$ per group. $^{\#}p < 0.05$, $^{\#\#}p < 0.01$, and $^{\#\#\#}p < 0.001$ vs. sham. $^{*}p < 0.05$, $^{**}p < 0.01$, and $^{***}p < 0.001$ vs. PD+saline+L-dopa.

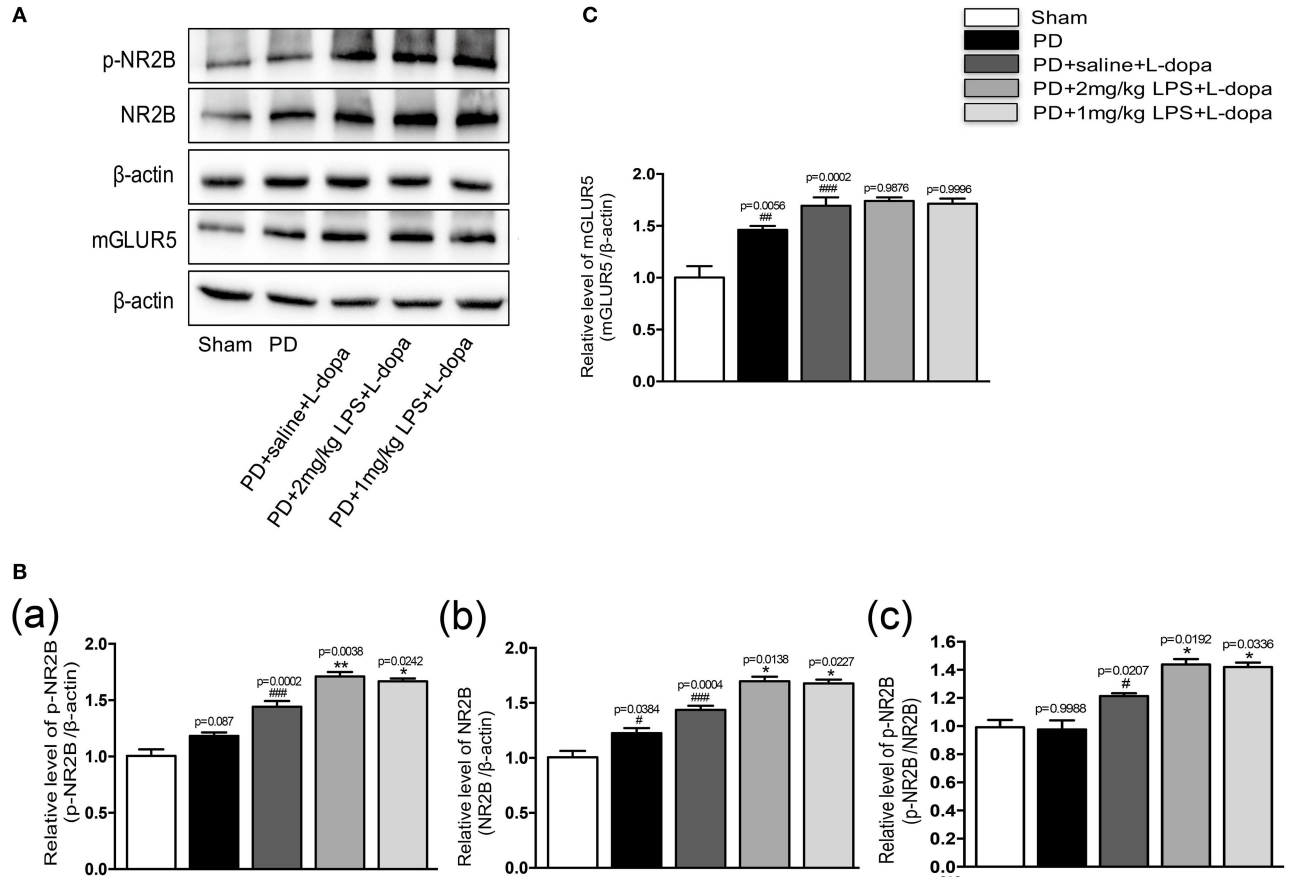

FIGURE 4 | Effect of peripheral LPS injection on the expression of NR2B and mGluR5 in the striatum of LID rats. **(A)** Expression levels of p-NR2B, NR2B, and mGLUR5 in the striatum were analyzed by Western blotting. **(B)** (a) Quantification of the densitometric value of the p-NR2B protein bands is shown, normalized to β-actin. (b) Quantification of the densitometric value of the NR2B protein bands is shown, normalized to β-actin. (c) Quantification of the densitometric value of the p-NR2B protein bands is shown, normalized to NR2B. **(C)** Quantification of the densitometric value of the mGLUR5 protein bands is shown, normalized to β-actin. Values are presented as mean ± SEM. $n = 4$ per group. $^{\#}p < 0.05$, $^{\#\#}p < 0.01$, and $^{\#\#\#}p < 0.001$ vs. sham. $^{*}p < 0.05$, $^{**}p < 0.01$ vs. PD+saline+L-dopa.

induced by the L-dopa treatment in the 6-OHDA-lesioned rats. To verify whether inhibiting LPS-induced inflammatory reaction may reduce the ALO AIM score in the 6-OHDA-lesioned rats treated with L-dopa, we used Clo-lipos to inhibit systemic inflammation induced by LPS. We found that the administration of Clo-lipo in the PD+Clo lipo+LPS+L-dopa group reduced the ALO AIM (**Figure 6A**a), axial AIM (**Figure 6A**b), limb AIM (**Figure 6A**c), and orolingual AIM (**Figure 6A**d) score compared with the PD+PBS lipo+LPS+L-dopa group ($^{*}p < 0.05$, $^{**}p < 0.01$ vs. PD+Clo lipo+LPS+L-dopa, $n = 12$/group).

To evaluate whether the administration of Clo-lipo can attenuate peripheral LPS injection-induced neuroinflammation in the striatum, we used the immunohistochemical analysis and the Western blot of Iba-1 and GFAP to determine the microglia and astrocyte response in 21 days after the L-dopa treatment. The PD+PBS lipo+LPS+L-dopa group showed clear microglial and astrocyte activation compared with the PD+Clo lipo+LPS+L-dopa group ($^{**}p < 0.01$, $^{***}p < 0.001$, vs. PD+ saline +L-dopa, $^{\#}p < 0.05$, $^{\#\#}p < 0.01$ vs. PD+PBS lipo+LPS+L-dopa, **Figures 6B,C**, $n = 4$/group). The administration of Clo-lipo can inhibit the release of neuroinflammatory cytokines IL-1β, IL-6, and TNF-α in the lesioned striatum compared with the PD+PBS lipo+LPS+L-dopa group ($^{***}p < 0.001$, vs. PD+ saline +L-

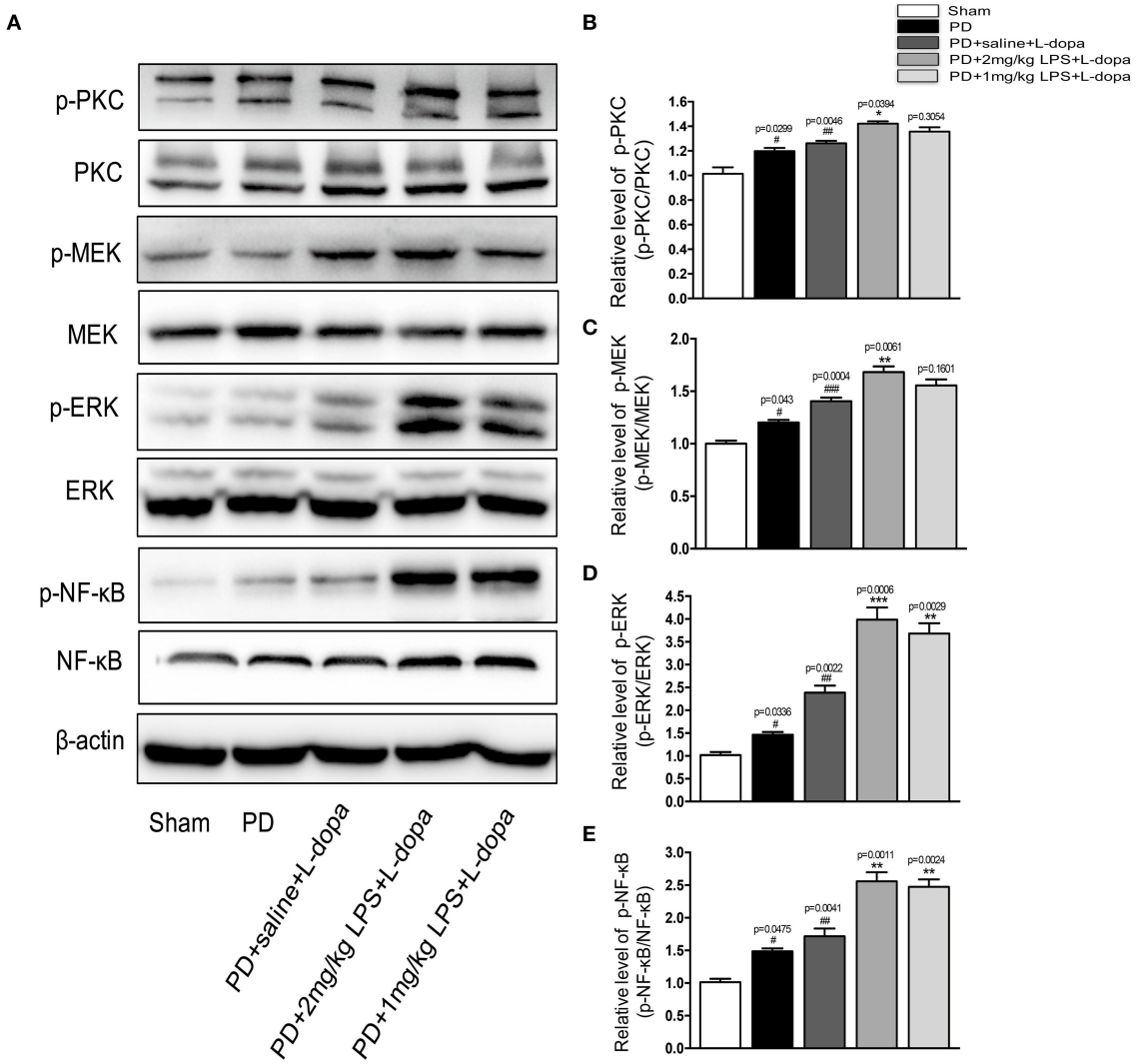

FIGURE 5 | Effects of peripheral LPS injection on striatal PKC/MEK/ERK and NF-κB signaling pathways in LID rats. **(A)** Expression levels of p-PKC, PKC, p-MEK, MEK, p-ERK, ERK, p-NF-κB, and NF-κB in the striatum were analyzed by Western blotting. **(B)** Quantification of the densitometric value of the p-PKC protein bands is shown, normalized to PKC. **(C)** Quantification of the densitometric value of the p-MEK protein bands is shown, normalized to MEK. **(D)** Quantification of the densitometric value of the p-ERK protein bands is shown, normalized to ERK. **(E)** Quantification of the densitometric value of the p- p-NF-κB protein bands is shown, normalized to NF-κB. Values are presented as the mean ± SEM. $n = 4$ per group. $^{\#}p < 0.05$, $^{\#\#}p < 0.01$, and $^{\#\#\#}p < 0.001$ vs. sham. $^{*}p < 0.05$, $^{**}p < 0.01$, $^{***}p < 0.001$ vs. PD+saline+L-dopa.

dopa, $^{\#}p < 0.05$, vs. PD+PBS lipo+LPS+L-dopa, **Figure 6D**, $n = 4$/group).

Clo-lipo Administration Prevents the Activation of Striatal NR2B-Mediated PKC/MEK/ERK and NF-κB Signaling Pathways Induced by Peripheral LPS Injection in LID Rats

In our study, the results showed that peripheral LPS injection markedly upregulated the striatal NR2B expression and activated its downstream PKC/MEK/ERK and NF-κB signaling pathways in the lesioned striatum as compared to the PD+saline+L-dopa group. Thus, we further examined the effects of Clo-lipo administration on the upregulation of p-NR2B and NR2B expression in the striatum of the LPS-treated LID rats. Firstly, we studied the effects of Clo-lipos on the LPS-treated rats. We found that the administration of Clo-lipos decreased LPS-stimulated p-NR2B and NR2B overexpression as compared to the PBS lipo+LPS group (**Supplementary Figure 4**). Furthermore, the Western blot analysis revealed that administration with Clo-lipos decreased p-NR2B and NR2B expression in the lesioned striatum of the PD+clo lipo+saline+L-dopa group as compared with the PD+PBS lipo+saline+L-dopa group ($^{*}p < 0.05$, $^{**}p < 0.01$, $^{***}p < 0.001$, vs. PD+saline+L-dopa, $^{\#}p < 0.05$, $^{\#\#}p < 0.01$

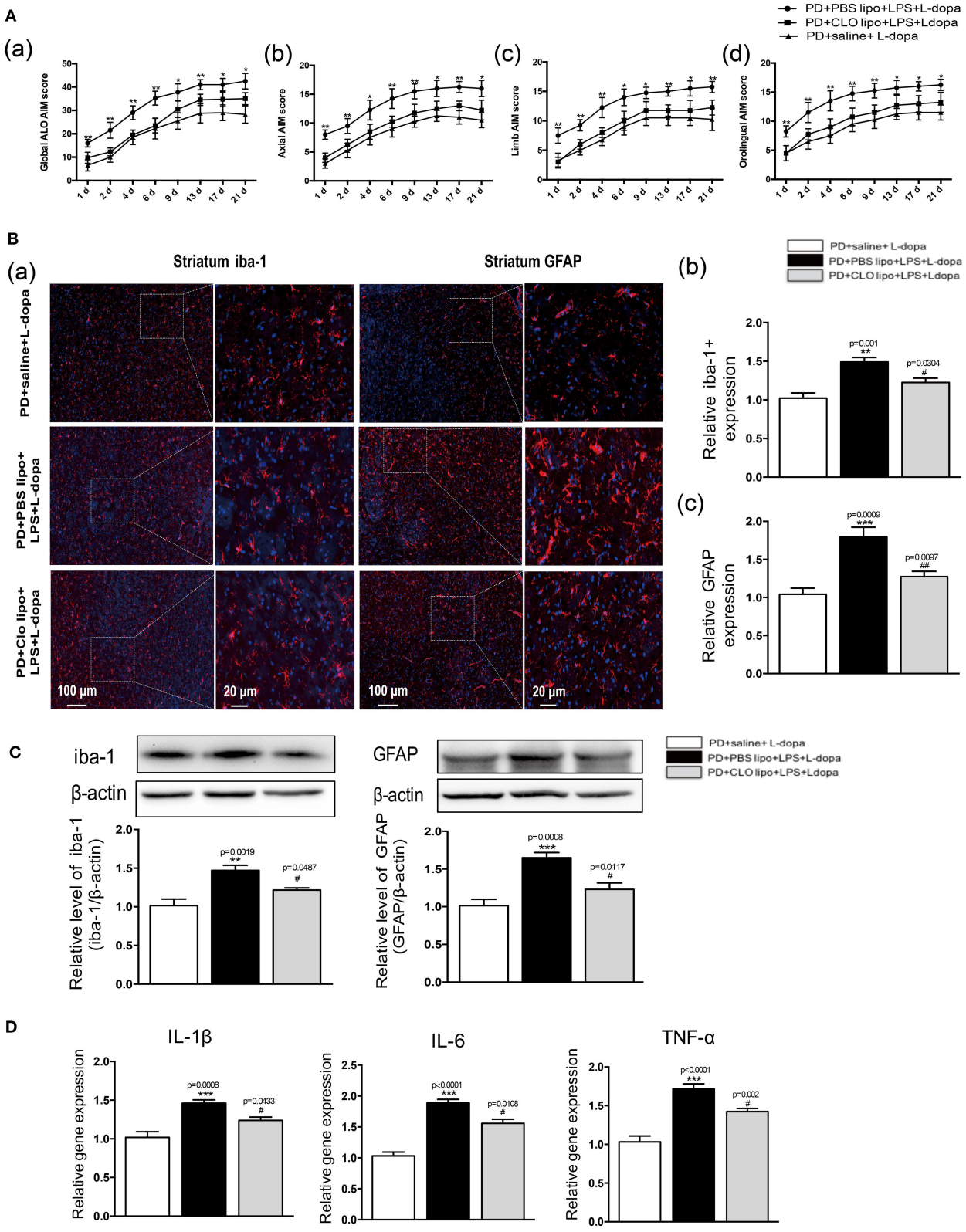

FIGURE 6 | Effects of Clodronate liposome treatments on ALO AIMs score and LPS-induced activation of neuroinflammation in the striatum of LID rats. **(A)** (a) A sum of axial, limb, and orolingual, (b) axial, (c) limb, and (d) orolingual AIMs. **(B)** (a) Microglia and astrocyte were determined in the striatum by immunohistochemical analysis of Iba-1 and GFAP. Scale bar = 100 μm in left panels and 20 μm in right panels. (b) The quantity of microglia in the striatum was quantified by the intensity of

(Continued)

FIGURE 6 | iba-1+immunofluorescence. (c) The number of astrocytes in the striatum was quantified by the intensity of GFAP+immunofluorescence. **(C)** Expression levels of iba-1 and GFAP were analyzed by Western blotting. **(D)** The mRNA levels of the proinflammatory mediators IL-1β, IL-6, and TNF-α normalized to GAPDH in the striatum. Values are presented as the mean ± SEM. $n = 4$ per group. $^{*}p < 0.05$, $^{**}p < 0.01$, $^{***}p < 0.001$ vs. PD+saline+L-dopa. $^{\#}p < 0.05$, $^{\#\#}p < 0.01$ vs. PD+ PBS lipo+LPS+L-dopa.

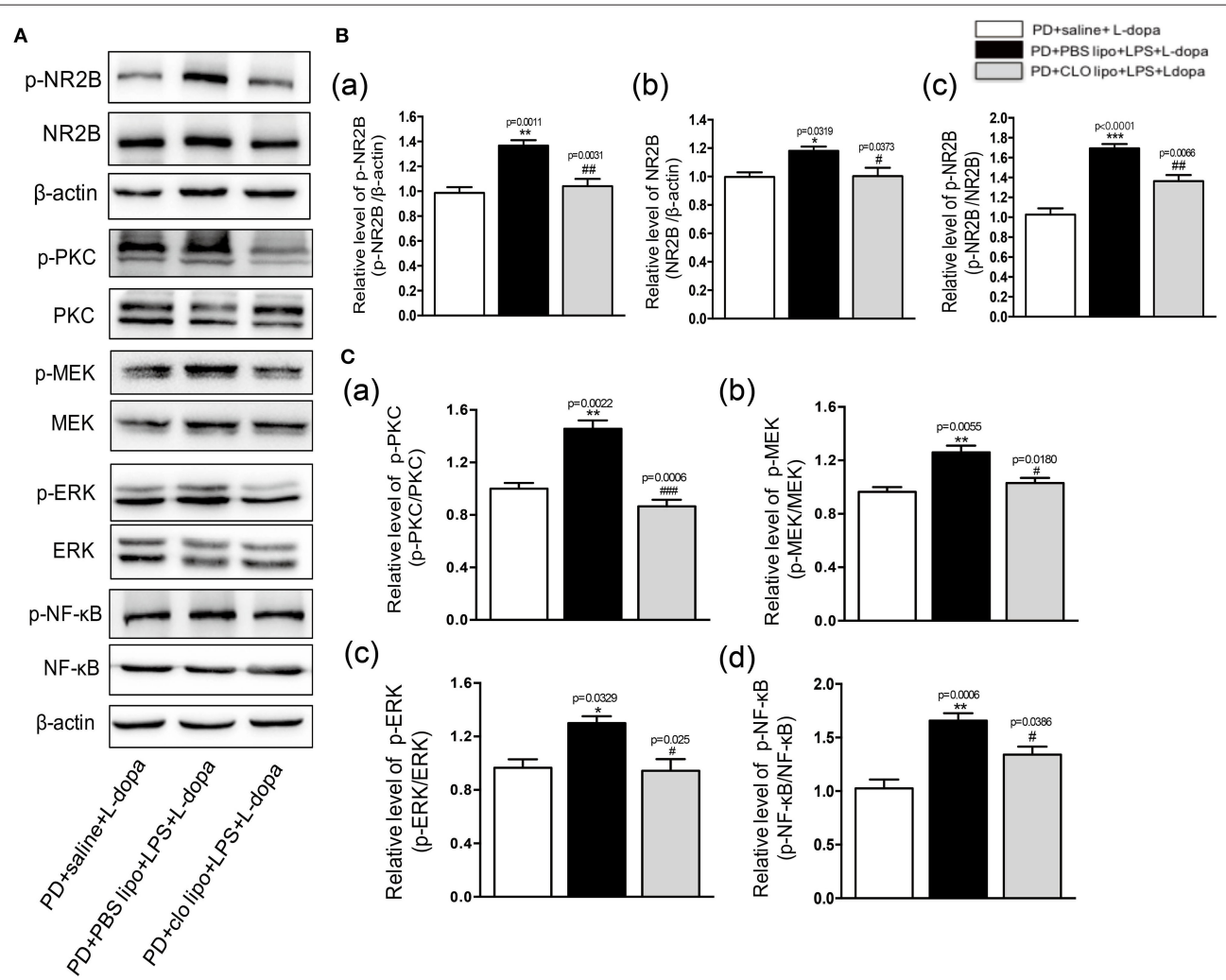

FIGURE 7 | Effects of Clodronate liposome treatments on striatal NR2B, PKC/MEK/ERK, and NF-κB signaling pathways in LPS-treated LID rats. **(A)** Expression levels of p-NR2B, NR2B, p-PKC, PKC, p-MEK, MEK, p-ERK, ERK, p-NF-κB, and NF-κB in the striatum were analyzed by Western blotting. **(B)** (a) Quantification of the densitometric value of the p-NR2B protein bands is shown, normalized to β-actin. (b) Quantification of the densitometric value of the NR2B protein bands is shown, normalized to β-actin. (c) Quantification of the densitometric value of the p-NR2B protein bands is shown, normalized to NR2B. **(C)** (a) Quantification of the densitometric value of the p-PKC protein bands is shown, normalized to PKC. (b) Quantification of the densitometric value of the p-MEK protein bands is shown, normalized to MEK. (c) Quantification of the densitometric value of the p-ERK protein bands is shown, normalized to ERK. (d) Quantification of the densitometric value of the p-NF-κB protein bands is shown, normalized to NF-κB. Values are presented as mean ± SEM. $n = 4$ per group. $^{*}p < 0.05$, $^{**}p < 0.01$, and $^{***}p < 0.001$ vs. PD+saline+L-dopa. $\#p < 0.05$, $\#\#p < 0.01$, $\#\#\#p < 0.001$, vs. PD+ PBS lipo+LPS+L-dopa.

vs. PD+PBS lipo+LPS+L-dopa, **Figures 7A,B**, $n = 4$/group). We next observed that the phosphorylation of PKC/MEK/ERK and NF-κB induced by peripheral LPS injection was largely inhibited by Clo-lipo administration as compared to the PD+PBS lipo+saline+L-dopa group ($^{*}p < 0.05$, $^{**}p < 0.01$, vs. PD+saline+L-dopa, $^{\#}p < 0.05$, $^{\#\#\#}p < 0.001$ vs. PD+PBS lipo+LPS+L-dopa, **Figures 7A,C**, $n = 4$/group).

DISCUSSION

A growing body of studies demonstrated that the systemic inflammatory response could strongly influence the CNS (Holmes, 2013; Anthony and Couch, 2014). In our study, we used a single peripheral LPS injection to mimic the systemic inflammatory response to research the relationship

between the periphery and the brain. Our study showed that systemic inflammation could increase the susceptibility to LID in 6-OHDA lesioned rats. Several findings are of interest in our study. Firstly, the peripheral LPS administration could induce neuroinflammation in the striatum of LID rats as demonstrated by the activation of glia cells and the increase in proinflammatory cytokines. Secondly, the exacerbation of LID in the LPS-induced systemic inflammation was also accompanied by the upregulation of both phosphorylated and total forms of NR2B in the striatum. Thirdly, systemic inflammation activated the PKC/MEK/ERK and NF-κB signaling pathways in LID rats. Clo-lipos ameliorated the effect of peripheral LPS injection, improved behavioral dysfunction, prevented NR2B overexpression, and decreased the phosphorylation of PKC/MEK/ERK and NF-κB signaling pathways.

There is increasing evidence that neuroinflammation may play a critical role in the etiogenesis of LID (Pisanu et al., 2018). Researches showed that inflammatory cytokines in the peripheral immune system might amplify neuroinflammation and contribute to the pathogenesis of a neurodegenerative disease (Perry et al., 2007; Cunningham et al., 2009; Ferrari and Tarelli, 2011). However, the role of systemic inflammation is unknown in LID. Thus, we wanted to study whether systemic inflammation would worsen the L-dopa-induced neuroinflammatory response in the striatum and exacerbate LID. To achieve this, systemic inflammation was induced by a single IP injection of LPS, an easy and well-characterized model of systemic inflammation. LPS is a major Gram-negative bacterial endotoxin that can trigger various cellular activities that contribute to the pathogenesis of inflammatory responses and induce the production of proinflammatory cytokines, such as TNF-α and IL-1β (Fu et al., 2014). Our study found that administration of LPS to the PD rats resulted in an increased susceptibility to the development of AIMs during the L-dopa treatment. In addition, several previous studies demonstrated that neuronal proinflammatory factors have been found to correlate with the LID expression in the 6-OHDA rat models of PD, where the development of AIM was accompanied by an increased immunoreactivity for the microglial marker OX-42, together with GFAP and with increases of nNOS, cyclooxygenase-2 (COX2), and NF-κB levels in the striatum (Bortolanza et al., 2015a,b; Dos-Santos-Pereira et al., 2016). Therefore, we analyzed the activation of striatal glial cells and the expression of pre-inflammatory cytokines in LPS-pretreated LID rats and controls. Our results revealed that LPS administration increased the number of activated microglia and astrocytes and promoted the pre-inflammatory cytokines TNF-a, IL-1β, and IL-6 in the striatum of LID rats.

Another striking finding of this study was the role of NR2B, a subunit of the NMDA receptor, in the LPS-treated LID rats. NMDARs are one of the major excitatory receptors within the CNS and have been the focus of potential therapeutics in a variety of neurological disorders (Yang et al., 2018). In the adult mammalian brain, NMDARs are comprised of different combinations of subunits of two classes, NR2A and NR2B, that are differentially distributed throughout the brain. Glycine confers neuroprotection through non-ionotropic activation of NR2A and subsequent enhancement of Akt activation (Zhang et al., 2018). On the other hand, the activation of NR2B plays an important role in the development and maintenance of chronic inflammatory response (Chen et al., 2008). NR2B was also found involved in the occurrence of LID (Blandini and Armentero, 2012). Many early studies performed in animals with dyskinetic conditions found an increase in the expression of NR2B in the striatum (Ahmed et al., 2011). NR2B antagonist CP-101,606 inhibits NR2B phosphorylation and provides benefit for the therapy of the LID rat model (Kong et al., 2015). A previous study showed that a single acute IP injection of LPS to postnatal male rats caused long-lasting (over 2 months) and possibly permanent changes in both the hippocampal and the cortex at the mRNA level of NR2B (subunit of NMDA; Harre et al., 2008). Our study found that the expression of phosphorylated and total forms of NR2B was markedly increased in the PD+LPS+L-dopa group compared with the PD+saline-L-dopa group. Thus, our findings confirmed that LPS-induced systemic inflammation could activate the NR2B submit. In addition, there is other evidence showing that peripheral inflammation can induce the activation of NR2B. For example, IL-1β can directly alter NR2B function *via* tyrosine kinase-mediated phosphorylation of NR2B (Viviani et al., 2003). NR2B subunits are overexpressed in an inflammatory model of Alzheimer's disease (AD; Maher et al., 2014). Therefore, we can speculate that a single IP injection of LPS would alter the NR2B subunit expression in the striatum of PD rats and lead to an increase in the susceptibility to LID in 6-OHDA lesioned rats. The downstream molecules resulting from NR2B activation may be responsible for behavioral deficits in the LPS-treated LID rats. Previous researches demonstrated that NMDA receptors could activate the PKC/ERK signaling pathway (Jia et al., 2007; Rodriguez-Duran and Escobar, 2014; Jiang et al., 2018), which may be due to positive coupling of the NR2B subunit to ERK (Sava et al., 2012). Furthermore, it was reported that hyperactivation of PKC/ERK and NF-κB by prolonged L-dopa treatment contributed to the development of LID (Bishnoi et al., 2008; Lin et al., 2017). Our results demonstrated that the administration of peripheral LPS could further increase the phosphorylation of PKC/MEK/ERK and NF-κB in LID rats.

Clodronate-liposome administration is a well-described method of depleting macrophages and reducing the experimental acute inflammatory response in an animal model. In the following experiment, we used Clo-lipos to ameliorate systemic inflammation induced by an LPS injection. Our results indicated that Clo-lipo administration significantly attenuated the AIM score of the LPS-treated LID rats. Furthermore, Clo-lipos decreased the LPS-induced activation of glial cells and the production of proinflammatory factors in the striatum. In addition, Clo-lipo administration reduced the overexpression of both phosphorylated and total forms of NR2B, which inhibited the phosphorylation of PKC/MEK/ERK and NF-κB signal pathways in the LPS-treated LID rats. These data suggested that Clo-lipos, which ameliorated the effect of LPS, improved behavioral dysfunction, prevented NR2B activation, and decreased the phosphorylation of PKC/MEK/ERK and NF-κB signaling pathways.

Our data indicated that systemic inflammation, by exacerbating neuroinflammation and facilitating the NR2B

subunit activity, increased the susceptibility to LID in 6-OHDA lesioned rats, suggesting a possible pathophysiological role of the systemic inflammatory response in the appearance of dyskinesia, at least in the 6-OHDA-lesioned rat model of PD. On the other hand, the administration of Clo-lipo restored the effects of LPS, which further attenuated dyskinesia in the LPS-treated PD rats during the L-dopa treatment.

DATA AVAILABILITY STATEMENT

The original contributions presented in the study are included in the article/**Supplementary Material**, further inquiries can be directed to the corresponding author/s.

ETHICS STATEMENT

The animal study was reviewed and approved by the Institutional Animal Care and Use Committee of the School of Medicine, Shanghai Jiao Tong University, Shanghai, China.

AUTHOR CONTRIBUTIONS

ZL and AY designed experiments. AY, LS, YZ, and XW performed the experiments. AY analyzed the results. AY wrote the manuscript with contributions from ZL. All authors read and approved the final manuscript.

FUNDING

This study was supported by the National Key R&D Programmes of China (2017YFC1310300), the projects of the National Natural Science Foundation of China (81974173, 81771211, 81703852, and 81671273), the projects of the Shanghai Committee of Science and Technology (17401901000), the innovation research team of high-level local universities in Shanghai, Shanghai Municipal Commission of Health (2019SY024), the projects of the Shanghai Committee of Science and Technology (19401932100), Shanghai Health and Family Planning Commission Foundation Special Plan for Clinical Research in Health Industry (201940021).

SUPPLEMENTARY MATERIAL

The Supplementary Material for this article can be found online at: https://www.frontiersin.org/articles/10.3389/fnagi.2020.625166/full#supplementary-material

Supplementary Figure 1 | Clodronate liposome treatment depleted macrophages in the spleen. **(A)** Immunohistochemistry analysis shows the CD68+ macrophages in the spleen of PD+PBS lipo and PD+CLP lipo groups at 3 days after liposome injection. **(B)** Bar graph shows quantification of the percentage of CD68+macrophages in the spleen of PD+PBS lipo and PD+CLP lipo groups.

Supplementary Figure 2 | Effect of peripheral only one LPS injection on the striatal neuroinflammation of normal rats. **(A)** Expression levels of iba-1 (a,b) and GFAP (a,c) were analyzed by Western blotting. **(B)** The mRNA levels of the proinflammatory mediators IL-1β (a), IL-6 (b), and TNF-α (c) normalized to GAPDH in the striatum. Values are presented as mean ± SEM. $n = 4$ per group. $^{*}p < 0.05$, $^{**}p < 0.01$, and $^{***}p < 0.001$ vs. saline.

Supplementary Figure 3 | LPS treatments increased the expressions of p-NR2B and NR2B in the striatum of normal rats. **(A)** Expression levels of p-NR2B, NR2B, and mGLUR5 in the striatum were analyzed by Western blotting. **(B)** (a) Quantification of the densitometric value of the p-NR2B protein bands is shown, normalized to β-actin. (b) Quantification of the densitometric value of the NR2B protein bands is shown, normalized to β-actin. (c) Quantification of the densitometric value of the p-NR2B protein bands is shown, normalized to NR2B. **(C)** Quantification of the densitometric value of the mGLUR5 protein bands is shown, normalized to β-actin. Values are presented as mean ± SEM. $n = 4$ per group. $^{*}p < 0.05$, $^{**}p < 0.01$, and $^{***}p < 0.001$ vs. saline.

Supplementary Figure 4 | Effects of Clodronate liposome treatments on striatal p-NR2B, NR2B, and mGLUR5 in LPS-treated rats. **(A)** Expression levels of p-NR2B, NR2B, and mGLUR5 in the striatum were analyzed by Western blotting. **(B)** Quantification of the densitometric value of the p-NR2B protein bands is shown, normalized to β-actin. **(C)** Quantification of the densitometric value of the NR2B protein bands is shown, normalized to β-actin. **(D)** Quantification of the densitometric value of the mGLUR5 protein bands is shown, normalized to β-actin. Values are presented as the mean ± SEM. $n = 4$ per group. $^{*}p < 0.05$, $^{**}p < 0.01$, and $^{***}p < 0.001$ vs. PBS lipo+LPS. $^{\&\&}p < 0.01$, $^{\&\&\&}p < 0.001$ vs. PBS lipo+saline.

REFERENCES

Ahmed, I., Bose, S. K., Pavese, N., Ramlackhansingh, A., Turkheimer, F., Hotton, G., et al. (2011). Glutamate NMDA receptor dysregulation in Parkinson's disease with dyskinesias. *Brain* 134 (Pt. 4), 979–986. doi: 10.1093/brain/awr028

Anthony, D. C., and Couch, Y. (2014). The systemic response to CNS injury. *Exp. Neurol.* 258, 105–111. doi: 10.1016/j.expneurol.2014.03.013

Ba, M., Ding, W., Guan, L., Lv, Y., and Kong, M. (2019). S-nitrosylation of Src by NR2B-nNOS signal causes Src activation and NR2B tyrosine phosphorylation in levodopa-induced dyskinetic rat model. *Hum. Exp. Toxicol.* 38, 303–310. doi: 10.1177/0960327118806633

Bishnoi, M., Chopra, K., and Kulkarni, S. K. (2008). Differential striatal levels of TNF-alpha, NFkappaB p65 subunit and dopamine with chronic typical and atypical neuroleptic treatment: role in orofacial dyskinesia. *Prog. Neuropsychopharmacol. Biol. Psychiatry* 32, 1473–1478. doi: 10.1016/j.pnpbp.2008.05.003

Blandini, F., and Armentero, M. T. (2012). New pharmacological avenues for the treatment of L-DOPA-induced dyskinesias in Parkinson's disease: targeting glutamate and adenosine receptors. *Expert Opin. Investig. Drugs* 21, 153–168. doi: 10.1517/13543784.2012.651457

Bortolanza, M., Cavalcanti-Kiwiatkoski, R., Padovan-Neto, F. E., da-Silva, C. A., Mitkovski, M., Raisman-Vozari, R., et al. (2015a). Glial activation is associated with l-DOPA induced dyskinesia and blocked by a nitric oxide synthase inhibitor in a rat model of Parkinson's disease. *Neurobiol. Dis.* 73, 377–387. doi: 10.1016/j.nbd.2014.10.017

Bortolanza, M., Padovan-Neto, F. E., Cavalcanti-Kiwiatkoski, R., Dos Santos-Pereira, M., Mitkovski, M., Raisman-Vozari, R., et al. (2015b). Are cyclooxygenase-2 and nitric oxide involved in the dyskinesia of Parkinson's disease induced by L-DOPA? *Philos. Trans. R. Soc. Lond. B. Biol. Sci.* 370:20140190. doi: 10.1098/rstb.2014.0190

Carta, A. R., Mulas, G., Bortolanza, M., Duarte, T., Pillai, E., Fisone, G., et al. (2017). l-DOPA-induced dyskinesia and neuroinflammation: do microglia and astrocytes play a role? *Eur. J. Neurosci* 45, 73–91. doi: 10.1111/ejn.13482

Chen, L., Liu, J. C., Zhang, X. N., Guo, Y. Y., Xu, Z. H., Cao, W., et al. (2008). Down-regulation of NR2B receptors partially contributes to analgesic effects of Gentiopicroside in persistent inflammatory pain. *Neuropharmacology* 54, 1175–1181. doi: 10.1016/j.neuropharm.2008.03.007

Cho, C. H., Kim, J., Ahn, J. Y., Hahn, H. G., and Cho, S. W. (2015). N-adamantyl-4-methylthiazol-2-amine suppresses lipopolysaccharide-induced brain

inflammation by regulating NF-kappaB signaling in mice. *J. Neuroimmunol* 289, 98–104. doi: 10.1016/j.jneuroim.2015.10.016

Cilia, R., Akpalu, A., Sarfo, F. S., Cham, M., Amboni, M., Cereda, E., et al. (2014). The modern pre-levodopa era of Parkinson's disease: insights into motor complications from sub-Saharan Africa. *Brain* 137 (Pt. 10), 2731–2742. doi: 10.1093/brain/awu195

Cunningham, C., Campion, S., Lunnon, K., Murray, C. L., Woods, J. F., Deacon, R. M., et al. (2009). Systemic inflammation induces acute behavioral and cognitive changes and accelerates neurodegenerative disease. *Biol. Psychiatry* 65, 304–312. doi: 10.1016/j.biopsych.2008.07.024

Del-Bel, E., Bortolanza, M., Dos-Santos-Pereira, M., Bariotto, K., and Raisman-Vozari, R. (2016). l-DOPA-induced dyskinesia in Parkinson's disease: are neuroinflammation and astrocytes key elements? *Synapse* 70, 479–500. doi: 10.1002/syn.21941

Dos-Santos-Pereira, M., da-Silva, C. A., Guimaraes, F. S., and Del-Bel, E. (2016). Co-administration of cannabidiol and capsazepine reduces L-DOPA-induced dyskinesia in mice: Possible mechanism of action. *Neurobiol. Dis.* 94, 179–195. doi: 10.1016/j.nbd.2016.06.013

Espay, A. J., Morgante, F., Merola, A., Fasano, A., Marsili, L., Fox, S. H., et al. (2018). Levodopa-induced dyskinesia in Parkinson disease: current and evolving concepts. *Ann. Neurol.* 84, 797–811. doi: 10.1002/ana.25364

Ferrari, C. C., and Tarelli, R. (2011). Parkinson's disease and systemic inflammation. *Parkinsons. Dis.* 2011:436813. doi: 10.4061/2011/436813

Fu, Y. Y., Zhang, F., Zhang, L., Liu, H. Z., Zhao, Z. M., Wen, X. R., et al. (2014). Mangiferin regulates interleukin-6 and cystathionine-b-synthase in lipopolysaccharide-induced brain injury. *Cell. Mol. Neurobiol.* 34, 651–657. doi: 10.1007/s10571-014-0039-8

Gan, J., Qi, C., and Liu, Z. (2015). Roles of Ca(2+)/calmodulin-dependent protein kinase II in subcellular expression of striatal N-methyl-D-aspartate receptors in l-3, 4-dihydroxyphenylalanine-induced dyskinetic rats. *Drug Des. Devel. Ther.* 9, 2119–2128. doi: 10.2147/DDDT.S73868

Gan, J., Qi, C., Mao, L. M., and Liu, Z. (2014). Changes in surface expression of N-methyl-D-aspartate receptors in the striatum in a rat model of Parkinson's disease. *Drug Des. Devel. Ther.* 8, 165–173. doi: 10.2147/DDDT.S51559

Harre, E. M., Galic, M. A., Mouihate, A., Noorbakhsh, F., and Pittman, Q. J. (2008). Neonatal inflammation produces selective behavioural deficits and alters N-methyl-D-aspartate receptor subunit mRNA in the adult rat brain. *Eur. J. Neurosci.* 27, 644–653. doi: 10.1111/j.1460-9568.2008.06031.x

Herring, W. J., Assaid, C., Budd, K., Vargo, R., Mazenko, R. S., Lines, C., et al. (2017). A Phase Ib randomized controlled study to evaluate the effectiveness of a single-dose of the NR2B selective N-Methyl-D-aspartate antagonist MK-0657 on levodopa-induced dyskinesias and motor symptoms in patients with Parkinson disease. *Clin. Neuropharmacol.* 40, 255–260. doi: 10.1097/WNF.0000000000000241

Ho, Y. H., Lin, Y. T., Wu, C. W., Chao, Y. M., Chang, A. Y., and Chan, J. Y. (2015). Peripheral inflammation increases seizure susceptibility via the induction of neuroinflammation and oxidative stress in the hippocampus. *J. Biomed. Sci.* 22:46. doi: 10.1186/s12929-015-0157-8

Holmes, C. (2013). Review: systemic inflammation and Alzheimer's disease. *Neuropathol. Appl. Neurobiol.* 39, 51–68. doi: 10.1111/j.1365-2990.2012.01307.x

Jia, J., Wang, X., Li, H., Han, S., Zu, P., and Li, J. (2007). Activations of nPKCepsilon and ERK1/2 were involved in oxygen-glucose deprivation-induced neuroprotection via NMDA receptors in hippocampal slices of mice. *J. Neurosurg. Anesthesiol.* 19, 18–24. doi: 10.1097/01.ana.0000211020.88431.e2

Jiang, S., Li, X., Jin, W., Duan, X., Bo, L., Wu, J., et al. (2018). Ketamine-induced neurotoxicity blocked by N-Methyl-d-aspartate is mediated through activation of PKC/ERK pathway in developing hippocampal neurons. *Neurosci. Lett.* 673, 122–131. doi: 10.1016/j.neulet.2018.02.051

Kalia, L. V., and Lang, A. E. (2015). Parkinson's disease. *Lancet* 386, 896–912. doi: 10.1016/S0140-6736(14)61393-3

Kong, M., Ba, M., Liu, C., Zhang, Y., Zhang, H., and Qiu, H. (2015). NR2B antagonist CP-101,606 inhibits NR2B phosphorylation at tyrosine-1472 and its interactions with Fyn in levodopa-induced dyskinesia rat model. *Behav. Brain Res* 282, 46–53. doi: 10.1016/j.bbr.2014.12.059

Kosyreva, A. M., Makarova, O. V., Kakturskiy, L. V., Mikhailova, L. P., Boltovskaya, M. N., and Rogov, K. A. (2018). Sex differences of inflammation in target organs, induced by intraperitoneal injection of lipopolysaccharide, depend on its dose. *J. Inflamm. Res* 11, 431–445. doi: 10.2147/JIR.S178288

Lin, J. Y., Liu, Z. G., Xie, C. L., Song, L., and Yan, A. J. (2017). Antidyskinetic treatment with MTEP affects multiple molecular pathways in the parkinsonian striatum. *Parkinsons. Dis.* 2017:5798734. doi: 10.1155/2017/5798734

Ma, Y., Li, Y., Jiang, L., Wang, L., Jiang, Z., Wang, Y., et al. (2016). Macrophage depletion reduced brain injury following middle cerebral artery occlusion in mice. *J. Neuroinflammation* 13:38. doi: 10.1186/s12974-016-0504-z

Maher, A., El-Sayed, N. S., Breitinger, H. G., and Gad, M. Z. (2014). Overexpression of NMDAR2B in an inflammatory model of Alzheimer's disease: modulation by NOS inhibitors. *Brain Res. Bull* 109, 109–116. doi: 10.1016/j.brainresbull.2014.10.007

Mulas, G., Espa, E., Fenu, S., Spiga, S., Cossu, G., Pillai, E., et al. (2016). Differential induction of dyskinesia and neuroinflammation by pulsatile versus continuous l-DOPA delivery in the 6-OHDA model of Parkinson's disease. *Exp. Neurol.* 286, 83–92. doi: 10.1016/j.expneurol.2016.09.013

Murta, V., Farias, M. I., Pitossi, F. J., and Ferrari, C. C. (2015). Chronic systemic IL-1beta exacerbates central neuroinflammation independently of the blood-brain barrier integrity. *J. Neuroimmunol* 278, 30–43. doi: 10.1016/j.jneuroim.2014.11.023

Perry, V. H., Cunningham, C., and Holmes, C. (2007). Systemic infections and inflammation affect chronic neurodegeneration. *Nat. Rev. Immunol.* 7, 161–167. doi: 10.1038/nri2015

Pervin, M., Karim, M. R., Kuramochi, M., Izawa, T., Kuwamura, M., and Yamate, J. (2018). Macrophage populations and expression of regulatory inflammatory factors in hepatic macrophage-depleted rat livers under lipopolysaccharide (LPS) treatment. *Toxicol. Pathol.* 46, 540–552. doi: 10.1177/0192623318776898

Pisanu, A., Boi, L., Mulas, G., Spiga, S., Fenu, S., and Carta, A. R. (2018). Neuroinflammation in L-DOPA-induced dyskinesia: beyond the immune function. *J Neural Transm (Vienna)*. doi: 10.1007/s00702-018-1874-4

Rodriguez-Duran, L. F., and Escobar, M. L. (2014). NMDA receptor activation and PKC but not PKA lead to the modification of the long-term potentiation in the insular cortex induced by conditioned taste aversion: differential role of kinases in metaplasticity. *Behav. Brain Res.* 266, 58–62. doi: 10.1016/j.bbr.2014.02.049

Sava, A., Formaggio, E., Carignani, C., Andreetta, F., Bettini, E., and Griffante, C. (2012). NMDA-induced ERK signalling is mediated by NR2B subunit in rat cortical neurons and switches from positive to negative depending on stage of development. *Neuropharmacology* 62, 925–932. doi: 10.1016/j.neuropharm.2011.09.025

Seiler, P., Aichele, P., Odermatt, B., Hengartner, H., Zinkernagel, R. M., and Schwendener, R. A. (1997). Crucial role of marginal zone macrophages and marginal zone metallophils in the clearance of lymphocytic choriomeningitis virus infection. *Eur. J. Immunol.* 27, 2626–2633. doi: 10.1002/eji.1830271023

Tronci, E., Napolitano, F., Munoz, A., Fidalgo, C., Rossi, F., Bjorklund, A., et al. (2017). BDNF over-expression induces striatal serotonin fiber sprouting and increases the susceptibility to l-DOPA-induced dyskinesia in 6-OHDA-lesioned rats. *Exp. Neurol.* 297, 73–81. doi: 10.1016/j.expneurol.2017.07.017

Villaran, R. F., Espinosa-Oliva, A. M., Sarmiento, M., De Pablos, R. M., Arguelles, S., Delgado-Cortes, M. J., et al. (2010). Ulcerative colitis exacerbates lipopolysaccharide-induced damage to the nigral dopaminergic system: potential risk factor in Parkinson's disease. *J. Neurochem.* 114, 1687–1700. doi: 10.1111/j.1471-4159.2010.06879.x

Viviani, B., Bartesaghi, S., Gardoni, F., Vezzani, A., Behrens, M. M., Bartfai, T., et al. (2003). Interleukin-1beta enhances NMDA receptor-mediated intracellular calcium increase through activation of the Src family of kinases. *J. Neurosci.* 23, 8692–8700. doi: 10.1523/JNEUROSCI.23-25-08692.2003

Wu, K. L., Chan, S. H., and Chan, J. Y. (2012). Neuroinflammation and oxidative stress in rostral ventrolateral medulla contribute to neurogenic hypertension induced by systemic inflammation. *J. Neuroinflammation* 9:212. doi: 10.1186/1742-2094-9-212

Xie, C. L., Wang, W. W., Zhang, S. F., Yuan, M. L., Che, J. Y., Gan, J., et al. (2014). Levodopa/benserazide microsphere (LBM) prevents L-dopa induced dyskinesia by inactivation of the DR1/PKA/P-tau pathway in 6-OHDA-lesioned Parkinson's rats. *Sci. Rep.* 4:7506. doi: 10.1038/srep07506

Xie, X., Luo, X., Liu, N., Li, X., Lou, F., Zheng, Y., et al. (2017). Monocytes, microglia, and CD200-CD200R1 signaling are essential in the transmission of inflammation from the periphery to the central nervous system. *J. Neurochem.* 141, 222–235. doi: 10.1111/jnc.13972

Yan, A., Zhang, Y., Lin, J., Song, L., Wang, X., and Liu, Z. (2018). Partial depletion of peripheral M1 macrophages reverses motor deficits in MPTP-treated mouse

by suppressing neuroinflammation and dopaminergic neurodegeneration. *Front. Aging Neurosci.* 10:160. doi: 10.3389/fnagi.2018.00160

Yang, L., Bai, H. H., Zhang, Z. Y., Liu, J. P., Suo, Z. W., Yang, X., et al. (2018). Disruption of SHP1/NMDA receptor signaling in spinal cord dorsal horn alleviated inflammatory pain. *Neuropharmacology* 137, 104–113. doi: 10.1016/j.neuropharm.2018.04.029

Zhang, Z., Liu, J., Fan, C., Mao, L., Xie, R., Wang, S., et al. (2018). The GluN1/GluN2B NMDA receptor and metabotropic glutamate receptor 1 negative allosteric modulator has enhanced neuroprotection in a rat subarachnoid hemorrhage model. *Exp. Neurol.* 301 (Pt. A), 13–25. doi: 10.1016/j.expneurol.2017.12.005

Conflict of Interest: The authors declare that the research was conducted in the absence of any commercial or financial relationships that could be construed as a potential conflict of interest.

frontiers in Aging Neuroscience

ORIGINAL RESEARCH
published: 01 March 2021
doi: 10.3389/fnagi.2021.600484

Elamipretide (SS-31) Improves Functional Connectivity in Hippocampus and Other Related Regions Following Prolonged Neuroinflammation Induced by Lipopolysaccharide in Aged Rats

Yang Liu[1†], Huiqun Fu[1†], Yan Wu[2], Binbin Nie[3], Fangyan Liu[1], Tianlong Wang[1], Wei Xiao[1], Shuyi Yang[1], Minhui Kan[1] and Long Fan[1]*

[1] Department of Anesthesiology, Xuanwu Hospital, Capital Medical University, Beijing, China, [2] Department of Anatomy, Capital Medical University, Beijing, China, [3] Institue of High Energy Physics, Chinese Academy of Sciences, Beijing, China

OPEN ACCESS

Edited by:
Feiqi Zhu,
Shenzhen University, China

Reviewed by:
Marta Llansola,
Principe Felipe Research Center (CIPF), Spain
Qian Liu,
Northwest University, China

***Correspondence:**
Tianlong Wang
w_tl5595@hotmail.com

[†] *These authors have contributed equally to this work*

Received: *30 August 2020*
Accepted: *01 February 2021*
Published: *01 March 2021*

Citation:
Liu Y, Fu H, Wu Y, Nie B, Liu F, Wang T, Xiao W, Yang S, Kan M and Fan L (2021) Elamipretide (SS-31) Improves Functional Connectivity in Hippocampus and Other Related Regions Following Prolonged Neuroinflammation Induced by Lipopolysaccharide in Aged Rats. Front. Aging Neurosci. 13:600484. doi: 10.3389/fnagi.2021.600484

Neuroinflammation has been recognized as a major cause for neurocognitive diseases. Although the hippocampus has been considered an important region for cognitive dysfunction, the influence of hippocampal neuroinflammation on brain functional connectivity (FC) has been rarely studied. In this study, lipopolysaccharide (LPS) was used to induce systemic inflammation and neuroinflammation in the aged rat brain, while elamipretide (SS-31) was used for treatment. Systemic and hippocampal inflammation were determined using ELISA, while astrocyte responses during hippocampal neuroinflammation were determined by interleukin 1 beta (IL-1β)/tumor necrosis factor alpha (TNFα) double staining immunofluorescence. Oxidative stress was determined by reactive oxidative species (ROS), electron transport chain (ETC) complex, and superoxide dismutase (SOD). Short- (<7 days) and long-term (>30 days) learning and spatial working memory were tested by the Morris water maze (MWM). Resting-state functional magnetic resonance imaging (rs-fMRI) was used to analyze the brain FC by placing seed voxels on the left and right hippocampus. Compared with the vehicle group, rats with the LPS exposure showed an impaired MWM performance, higher oxidative stress, higher levels of inflammatory cytokines, and astrocyte activation in the hippocampus. The neuroimaging examination showed decreased FC on the right orbital cortex, right olfactory bulb, and left hippocampus on day 3, 7, and 31, respectively, after treatment. In contrast, rats with SS-31 treatment showed lower levels of inflammatory cytokines, less astrocyte activation in the hippocampus, and improved MWM performance. Neuroimaging examination showed increased FC on the left-parietal association cortex (L-PAC), left sensory cortex, and left motor cortex on day 7 with the right flocculonodular lobe on day 31 as compared with those without SS-31 treatment. Our study demonstrated that inhibiting neuroinflammation in the hippocampus not only reduces inflammatory responses in the hippocampus but also improves

the brain FC in regions related to the hippocampus. Furthermore, early anti-inflammatory treatment with SS-31 has a long-lasting effect on reducing the impact of LPS-induced neuroinflammation.

Keywords: lipopolysaccharide, neuroinflammation, functional connectivity, elamipretide, cognition

INTRODUCTION

Neuroinflammation has been proved to be a major cause for post-operative cognitive dysfunction (POCD) and other perioperative neurocognitive disorders (Subramaniyan and Terrando, 2019). As a crucial region to learning and memory, the hippocampus has traditionally been considered as a classic region for studying neuroinflammation and neurodegenerative diseases in many clinical studies and preclinical experiments. The recent studies demonstrated that although various regions may also participate, the hippocampus, both morphology and function, is one of the most sensitive regions that is affected by aging, neuroinflammation, and chronic stress (Fjell et al., 2014; Bartsch and Wulff, 2015). Meanwhile, clinical studies have reported that the disruption of the brain–blood barrier (BBB), an early event in the aging brain, begins in the hippocampus (Montagne et al., 2015). These findings suggest that the hippocampus in the aging brain is more likely to be affected by peripheral inflammatory cytokines triggered by surgery and other perioperative stress events. Therefore, the hippocampus is a brain region of great importance in understanding the development and molecular mechanisms of cognitive dysfunction.

Acute and chronic inflammation in the hippocampus has already been associated with cognitive dysfunction in neurocognitive diseases (Schwalm et al., 2014; Chesnokova et al., 2016). In our previous work, we reported the specific roles of interleukin-1beta (IL-1β) secretion and the nuclear factor-kappa B (NF-κB) signaling pathway in the long-term astrocyte activation after lipopolysaccharide (LPS) exposure in aged rats (Fu et al., 2014; Kan et al., 2016). These results suggest that astrocyte-derived inflammatory cytokines are important in the long-term neuroinflammation in aged rats, contributing to neuron homeostasis, BBB function, improving local synapse transmission and plasticity, and in the regulation of structural remodeling (Abbott et al., 2006; Santello et al., 2019). The aged brain is known to form many more neurotoxic A1 type astrocytes in response to LPS in neuroinflammation (Clarke et al., 2018); thus, the aged rats are more suitable to be used for studying mechanisms for neuroinflammation induced by POCD. However, a variety of preclinical, clinical, and neuroimaging studies has indicated that the hippocampus is not only the region affected by neurocognitive disease (Teipel et al., 2015; Mitchell et al., 2018; Zhang et al., 2019), besides the hippocampus neuroinflammation, the brain functions in other related regions may also be affected in disease development.

Oxidative stress has been reported to coexisted with neuroinflammation, and mitochondria play an important role in cognitive dysfunction (Wu et al., 2017; Zhao et al., 2019). Recent study showed that reducing the level of mitochondrial reactive oxygen species (mtROS) triggered by LPS also reduced the inflammatory responses in BV-2 cell (microglia cell line) (Park et al., 2015). Meanwhile, there are also studies supporting the evidence that mtROS also induce inflammatory responses in the astrocyte (Alfonso-Loeches et al., 2014). Elamipretide (SS-31), a mitochondria targeted antioxidant, functions by removing excessive reactive oxygen species (ROS) produced during the oxidative stress. However, whether reducing the ROS level also reduces inflammatory responses in the astrocytes and improves the long-term cognitive function in aged brains still need further investigation.

Resting state functional magnetic resonance imaging (rs-fMRI) enabled a non-invasive method for studying the brain function in each pathological phase for the disease development *in vivo* (Lopes et al., 2017; Hardcastle et al., 2019; Passamonti et al., 2019). Using a seed voxel, the hippocampus revealed decreased functional connectivity (FC) in Alzheimer's disease (AD) (Qian et al., 2019), mild cognitive impairment (MCI) (Chirles et al., 2017), and POCD (Browndyke et al., 2017), suggesting that apart from the hippocampus, other brain regions are also affected because they show decreased correlations with the hippocampus. Recently, rs-fMRI also has been conducted to detect the long-term change of the brain function in rats after repeated mild traumatic brain (Pham et al., 2021). However, the cellular and molecular mechanisms underlying these changes are unclear. In rodents, recent studies found that neuroinflammation, microglia, and astrocyte activation, and changes in spatial working memory coexisted with alteration in the brain function (Nasrallah et al., 2016; Griffin et al., 2019), indicating that rodent models are highly attractive options for simultaneous study of neuroimaging changes and molecular mechanisms.

In the present study, we investigated the effects of hippocampal neuroinflammation on the brain FC in aged rats by removing excessive oxidative stress after LPS exposure. We combined neuroimaging and neuroscience to assess both the hippocampal neuroinflammation and brain function in regions related to cognition. The model was chosen based on our previous findings that LPS exposure causes long-term neuroinflammation characterized by cognitive dysfunction and astrocyte activation in aged rats (Fu et al., 2014; Kan et al., 2016). Because elamipretide (SS-31), has been reported to be able to improve cognitive dysfunction and inflammatory responses in the hippocampus caused by LPS and inhalational anesthetics (Wu et al., 2017; Zhao et al., 2019), it was used to inhibit inflammatory response after LPS exposure. We hypothesize that anti-inflammatory protection provided by SS-31 treatment will both improve the short-term (within 7 days) and long-term (after 30 days) brain FC and ameliorate the hippocampal neuroinflammation after LPS exposure.

MATERIALS AND METHODS

Ethical Approval

This experiment was approved by the ethical committee of Capital Medical University (Approved number: AEEI-2018-166) and complied with the Guide for the Care and Use of Laboratory Animals prepared by the Institute of Laboratory Animal Resources and published by the National Institute of Health. All efforts were used to minimize the pain and suffering of animals.

Animals and Treatments

two-hundred and forty male rats (Wistar, 20 months old, 500–700 g, SPF grade, Chengdu Dossy Experimental Animals Co., Ltd., Sichuan Province, China) were used in this study. All rats were housed in standardized and controlled laboratory conditions (21–25°C in temperature and 50–60% in humidity on a 12-h light/dark cycle with food and water provided *ad libitum*). The detailed processing line is shown in **Figure 1A**.

Rats were randomly divided into four groups:

1. Vehicle group (V group, $n = 50$): Rats were treated with 0.9% normal saline intraperitoneal (i.p.) injection.
2. SS-31-treated group (S group, $n = 50$): Rats were treated with SS-31 (5 mg/kg i.p. at a volume of 0.4 ml/kg, dissolved in normal saline, and synthesized by China Peptides Co., Ltd, Shanghai, China).
3. LPS-treated group (L group, $n = 70$): Rats were treated with LPS (2 mg/kg i.p., dissolved in normal saline, 055:B5, Sigma-Aldrich, St. Louis, MO, USA).
4. LPS + SS-31-treated group (L + S group, $n = 70$): Rats were treated with SS-31 (5 mg/kg) for 30 min before the LPS injection (both i.p. injections).

The doses of LPS and SS-31 were determined based on the previous studies (Fu et al., 2014; Wu et al., 2016). All time points were selected according to our previous work (Fu et al., 2014; Kan et al., 2016).

Tissue Preparation

A cohort of rats were randomly selected in each group and sacrificed at 3, 7, and 30 days ($n = 5$ per time point per group) after treatment. Under deep isoflurane anesthesia (Forene, Abbott Laboratories, Queenborough, UK), the rat brains were rapidly dissected following decapitation. All dissections were performed on a chilled-ice glass plate. The entire dissected brain was immediately mounted in optimum cutting temperature (OCT) compound (Sakura Finetek USA, Inc., Torrance, CA, USA), frozen in liquid nitrogen, and then stored at −80°C subsequent to immunofluorescence. Another cohort of rats (n = 5 per time point per group) were sacrificed at the same time points mentioned above for measuring inflammatory cytokines in hippocampus. The blood samples were extracted from the inferior vena cava. After clotting at 4°C, the blood sample was centrifuged for 20 min at 1,000 × *g*. The serum was collected and stored at −80°C for subsequent ELISA analysis.

For another cohort of rats ($n = 5$ per time point per group), the hippocampus was collected for doing real-time PCR (RT-PCR) and mitochondria isolating (the left for RT-PCR and the right for isolating mitochondria). The hippocampus mitochondria were isolated using the Mitochondria Isolation Reagent Kit (C3606, Beyotime Institute of Biotechnology Co., Shanghai, China) according to the manufacturer's instructions. All the procedures were done on chilled cold ice, and the whole procedure was finished within 1 h. After isolation, the mitochondria sediments were resuspended by appropriate amount of Mitochondrial Stock Solution (GMS 12198.2, GenMed Scientific, Shanghai, China).

Immunofluorescence and Microscopy

The coronal hippocampus sections were cut at a thickness of 20 μm with a freezing microtome (CM1850, Leica Microsciences, Mannheim, Germany). The sections were selected according to the landmarks corresponding to the Paxino & Watson's rat brain atlas (bregma −2.80 to −3.60) for subsequent immunofluorescence staining. The selected sections were first fixed in ice-cold 4% paraformaldehyde (CM-0055, Lifeline Cell Technology, Frederick, MD, USA) for 15 min then washed with 10 mM phosphate buffered saline (PBS; ZLI-9062, Zhongshan Goldbridge Biotech, Co, Ltd, Beijing, China) for three times. After permeabilizing using 0.3% Triton-X 100 (T9284, Sigma-Aldrich, St Louis, MO, USA) for 1 h at room temperature, sections were blocked by 10% horse serum (8178102 Gibco New Zealand Origin) for 1 h. The sections were then incubated in primary antibodies for 2 h at room temperature and then overnight at 4°C: goat anti-IL-1β immunoglobulin G (IgG) (1:100, AF-501-NA, R&D Systems, Inc., Minneapolis, MN, USA), goat anti-tumor necrosis factor alpha (anti-TNFα) IgG (1:100, AF-510-NA, R&D Systems, Inc., Minneapolis, MN, USA), and mouse anti-glial fibrillary acidic protein (anti-GFAP)-IgG (1:1,000, MAB360, Millipore Corp., Billerica, MA, USA), respectively. The sections were washed with PBS for three times and then incubated in secondary antibodies in a dark room at room temperature for 2 h: Alexa Fluor 594 donkey anti-goat IgG (1:500, A11058, Invitrogen, Paisley, UK) and Alexa Fluor 488 donkey anti-mouse IgG (1:500, A21202, Invitrogen, Paisley, UK). Finally, all sections were counter-stained and then covered with fluorescent mounting medium with 4′,6-diamidino-2-phenylindole (DAPI; ZLI-9557, Zhongshan Goldbridge Biotech, Co., Ltd, Beijing, China) and anti-fading reagents. For negative control treatments, the primary and secondary antibodies were replaced by PBS, while other procedures remained the same.

Fluorescent images were analyzed using a confocal microscopy (Leica TCS2, Leica Microsystems, Mannheim, Germany) and image analyzing system (Optimas 6.5, CyberMetrics, Scottsdale, AZ, USA) by an independent observer who was blinded from the entire study. Cells were counted in the hippocampus DG region using the NIH ImageJ software (National Institutes of Health, Bethesda, MD, USA), from which the percentages of double stained GFAP (IL-1β and TNFα positive) in total GFAP were calculated.

ELISA Measurement

Inflammatory factors, including IL-1β and TNFα in serum, were measured using ELISA kits (RLB00 and RTA00, R&D Systems,

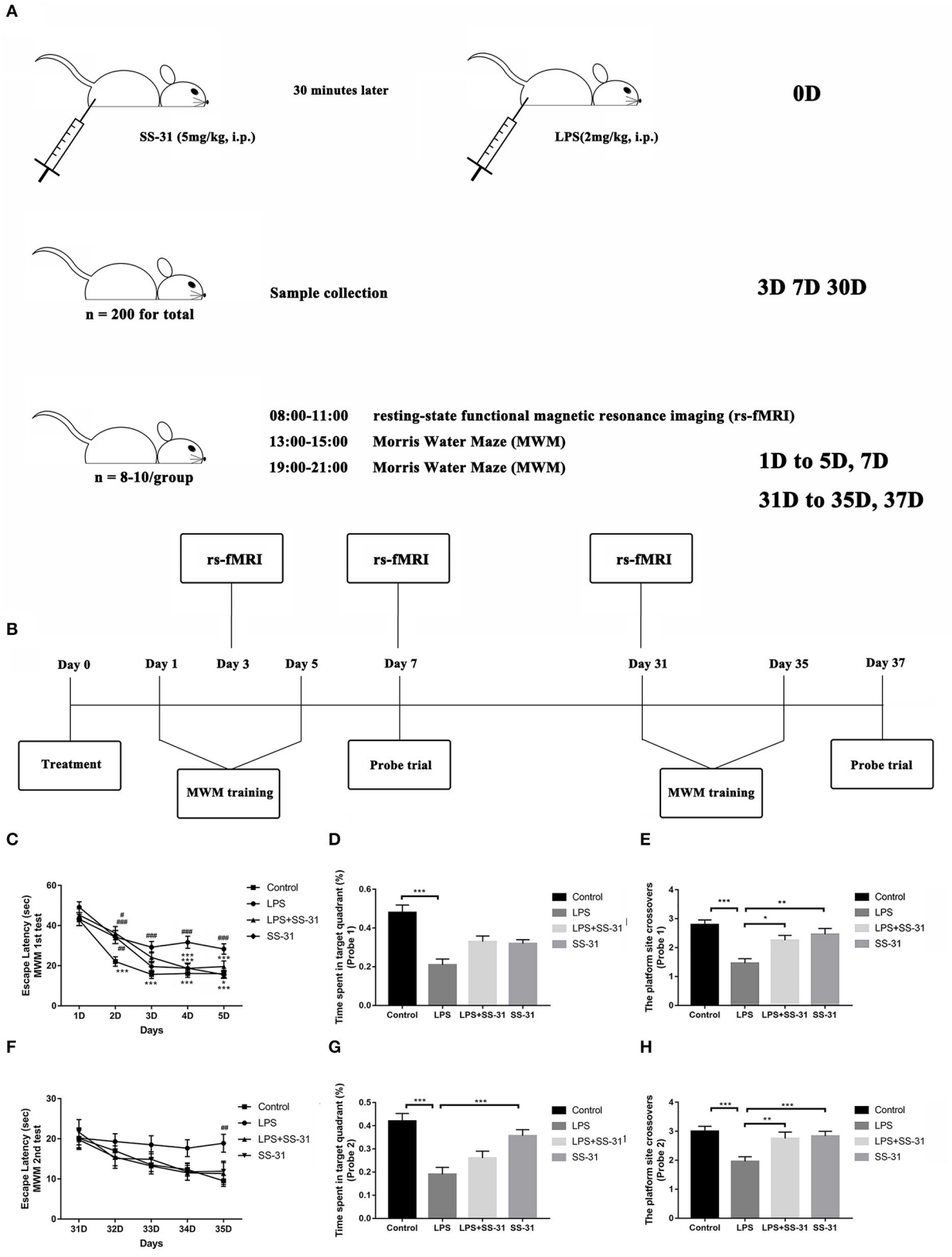

FIGURE 1 | Elamipretide (SS-31) improved cognitive dysfunction induced by lipopolysaccharide (LPS) in the aged rat brain. **(A)** Detailed processing line. **(B)** Morris water maze (MWM) training protocol. Spatial acquisition trials and probe trials were performed on both short term (day 1–7) and long term (day 31–37). **(C)** Rats

(Continued)

FIGURE 1 | treated with LPS showed a significant prolonged escape latency compared with those in vehicle (V) group and SS-31 (S) group from day 2 to 5, which was improved by SS-31 treatment from day 4 in LPS + SS-31 (L + S) group. **(D,E)** Rats treated with LPS showed reduced time spent in the target quadrant and fewer crossovers to this quadrant compared with V group. The reduction in crossovers was improved by SS-31 treatment. **(F)** In the long term, a significant difference in escape latency was observed on day 35 with rats treated with LPS seemed to have prolonged escape latency. **(G,H)** Rats treated with LPS spent significantly less time in the target quadrant compared to rats in the V and S groups, as well as showing significantly fewer crossovers than all other groups. Data are presented as mean ± SEMs, and escape latency was analyzed by two-way ANOVA for repeated measurements with the Bonferroni *post-hoc* analysis. Time spent in the target quadrant and crossovers were analyzed by one-way ANOVA followed with the Bonferroni *post-hoc* analysis. $^{\#}p < 0.05$, $^{\#\#}p < 0.01$, $^{\#\#\#}p < 0.001$ as indicated or vs. V; $^{*}p < 0.05$, $^{**}p < 0.01$, $^{***}p < 0.001$ vs. L group.

TABLE 1 | Sequences of primers in RT-PCT.

mRNA	Forward primer (5′ → 3′)	Reverse primer (5′ → 3′)
IL-1β	5′-ATGAGAGCATCCAGCTTCAAATC-3′	5′-CACACTAGCAGGTCGTCATCATC-3′
TNFα	5′-CAAGAGCCCTTGCCCTAA-3′	5′-CAGAGCAATGACTCCAAAGTA-3′
β-actin	5′-CCCATCTATGAGGGTTACGC-3′	5′-TTTAATGTCACGCACGATTTC-3′

Inc., Minneapolis, MN, USA) following the manufacturer's instructions. The proteins collected from the hippocampus were first analyzed using the BCA Protein Assay Kit (23227, Thermo Fisher Scientific, Waltham, MA, USA).

mRNA and RT-PCR

Total RNA was extracted from the hippocampus using Trizol (Invitrogen, Paisley, UK) and purified by RNase Away Reagent (catalog number 18270466, Invitrogen, Paisley, UK). The total amount of RNA was measured by NanoDrope 2000 (Thermo Fisher Scientific, Waltham, MA, USA), and the building of cDNA was synthesized using the M-MLV Reverse Transcriptase Kit (Promega, Madison, WI, USA) according to the manufacturer's instructions. The cDNA amplification was carried out using ABI 7500 Fast Real-Time PCR System (Applied Biosystems, Waltham, MA, USA) for 45 cycles (each for a duration of 2 min at 94°C, annealing for 5 s at 94°C and for 30 s at 60°C and finally extension for 10 min at 72°C). The primer sequences and amplification for IL-1β and TNFα were described in **Table 1**. The level of mRNA expression was evaluated by the SYBR Green detection method. Data were analyzed using the 2-ΔΔCt method by the expression of target gene in the rat hippocampus that is corrected by the expression of endogenous control (β-actin) and relative to the vehicle group.

Oxidative Stress

The mtROS were measured using the ROS Assay Kit (GMS 10104.1, GenMed Scientifics, Shanghai, China) according to the manufacturer's instructions. The serum and hippocampus SOD activity were measured using the SOD Assay Kit (Jiacheng Biological Technology Co., Ltd., Nanjing, China) according to the manufacturer's instructions. The enzyme activity was converted to units per milligram of protein. One unit of SOD activity was defined as the amount of that reduced the absorbance at 450 nm by 50%. The levels of electron transport chain (ETC) components—I/III/IV were also measured using the ETC Analyzing Kit (GMS 50007 for ETC-I, GMS 50009 for ETC-III and GMS 50010 for ETC-IV, GenMed Scientifics, Shanghai, China). All the above procedures were conducted on ice in a dark room. The results were collected by a microplate reader (SpectraMax iD5, Molecular Devices, San Jose, CA, USA).

Resting-State fMRI Acquisition

On day 3, 7, and 31 after treatment, 8–10 rats in each group were randomly selected for rs-fMRI data acquisition. The animal MRI measurements were performed using the 7.0-T Bruker PharmaScan System (70/16 PharmaScan, Bruker BioSpin GmbH, Rheinstetten, Germany), operated *via* the ParaVision 5.1 software. The same coils, including a rat brain surface coil and a quadrature resonator volume coil, were adopted in all the rats. Shimming was optimized for the cerebrum (40 × 40 × 40 mm voxel) using a three-dimensional field map-based automatic shimming method.

The animal anesthesia was conducted as Lu et al. (2012) described elsewhere. Briefly, animals were first anesthetized using isoflurane (3%) in oxygen and air (1:1) followed by dexmedetomidine (0.015 mg/kg, intramuscular injection) in an anesthesia induction chamber. When the animal was fully anesthetized, it was gently fixed in prone position on the MRI scanning bed, and anesthesia was maintained using isoflurane with enriched oxygen *via* a nose mask with a bite-bar and continuous intramuscular infusion of dexmedetomidine (0.03 mg/kg/h). The rat was fixed to a custom-made holder to minimize the head motion during the whole scanning process. After the anatomical localization scans were acquired, the isoflurane concentration was decreased to 0.20–0.25% to keep the respiration rate at the range of 60–85/min throughout the scanning process. A small animal monitoring system (Model 1025, Small Animal Instruments Inc., New York, NY, USA), including a rectal temperature probe, respiration pneumonic sensor, and fiber optic oximetry sensor or cardiogram electrodes, was adopted for real-time monitoring. The core body temperature was maintained at 37°C *via* a warm water circulation system. If the respiration rate increased to 90/min, the concentration of isoflurane was increased to 0.5%.

Anatomical images (T2WI) were acquired with fast-spin–echo sequence using TurboRARE with the following parameters: repetition time (TR) 5000.0 ms, echo time (TE) 36.0 ms, echo spacing 12 ms, echo-train length 8, field of view 3.50 × 3.50 cm, matrix size 256 × 256, and 28 slices with a thickness of 1.0 mm. For blood-oxygen-level-dependent (BOLD) images, EPI-SE-FOVsat sequence was used with the following parameters: matrix size 64 × 64, flip angle = 90°, resolution = 0.55 × 0.55 mm, 28

slices with a thickness of 1.0 mm, slice gap = 0, TR = 2000.0 ms, TE = 18.0 ms, volume = 180.

Data Processing and Analysis

The data were preprocessed using spmratIHEP software based on the statistical parametric mapping (SPM12) software and rs-fMRI Data Analysis Toolkit (REST) software, and statistically analyzed by spmratIHEP based on SPM12. The data were carefully examined for completeness and truncation artifacts. The FC values were analyzed and compared between the V group, SS-31 group, LPS group, and LPS + SS-31 group. All the functional images post-processing was performed by a single experienced observer, unaware to whom the scans belonged. The preprocessing and data analysis were performed using spmratIHEP (Nie et al., 2013, 2014) based on SPM12 (Welcome Department of Imaging Science; http://www.fil.ion.ucl.ac.uk/spm) and REST software (http://restfmri.net/Forum/Index.php?~q=rest).

The voxel size of the functional datasets of all individuals was first multiplied by a factor of 5 to better approximate human dimensions, and then preprocessed using the following main steps: (1) slice timing: The differences of slice acquisition times of each individual were corrected using slice timing. (2) Realign: The temporal processed volumes of each subject were realigned to the first volume to remove any head motion, and a mean image was created over the 180 realigned volumes. All participants had < 1 mm of translation in the x, y, or z axis and a 1° of rotation in each axis. (3) Spatial normalization: The realigned volumes were spatially standardized into the Paxino and Watson space (Liang et al., 2017) by normalizing with the EPI template *via* their corresponding mean image. Subsequently, all the normalized images were resliced by $1.0 \times 1.5 \times 1.0$ mm voxels (after zooming). (4) Smooth: The normalized functional series were smoothed with a Gaussian kernel of 2 mm^3 full width at half-maximum (FWHM). (5) Removal of the linear trend: The smoothed images had any systematic drift or trend removed using a linear model. (6) Filtering: The band pass was filtered at 0.01–0.08 Hz as the physiological spontaneous BOLD fluctuation mainly focused on this band, and to remove the very low frequency drift and high frequency noise. The pre-processed images were analyzed within spmratIHEP in SPM12 based on the framework of the general linear model.

The FC analysis was performed by REST software (http://restfmri.net/Forum/index.php? q=rest) by placing seed regions at the left and right hippocampus (L- and R-hip). Pearson's correlation was computed between each voxels of the L- and R-hip, and the other intercranial voxels to obtain FC maps for each rat. To identify differences in the FC maps between groups V, S, L, and L + S, a one-way ANOVA and *post-hoc* two-sample *t*-test were performed. Regions with significant FC changes between each two groups were yielded based on voxel-level height threshold of $p < 0.001$ and a cluster-extent threshold of 20 voxels.

Morris Water Maze

One day after treatment, learning and spatial working memory were assessed by the Morris water maze (MWM) with the same group of animals subjected to rs-fMRI scanning (n = 8–10 per group). Detailed description of the training protocols can be found in our previous study (Kan et al., 2016). Briefly, the MWM test was divided into two parts: spatial acquisition trials (day 1–5) and probe trial (day 7). On day 6, the rats were allowed for a rest. The water maze is a black painted circular tank with 150 cm in diameter and 60 cm in height, placing at the center of a quiet room. On the wall of the tank, there were four different visual clues, dividing it into four quadrants. A black curtain was held in place by a rectangular scaffold around the water maze to minimize harsh lights entering the room. A video camera mounted to the ceiling above the water tank was used to track the rat swimming speed, latency to find the platform, and target quadrant crossovers with an animal activity tracking system (Ethovision, Noldus Information Technologies, Wageningen, The Netherlands). For each training session, the tank was filled with clean water for about 35 cm in depth (23 $\pm$ 2°C) with a hidden circle platform 1.5 cm below the water surface at the third quadrant. On day 1–5, the rat was gently placed in one quadrant facing the wall of the MWM before each spatial acquisition trials. Then, the rat was allowed to swim freely for up to 60 s in the water maze to locate the platform. If the rat succeeded, it was allowed to stay for 5 s on the platform. Otherwise, the rat was physically placed on the platform for 20 s. Four spatial acquisition trials were performed on each rat per day and continued for 5 consecutive days. A 3–5 min interval was allowed between each trial. On day 7, a probe trial was conducted in which the platform was removed and the rat was placed at the quadrant opposite to the platform and allowed to swim for 30 s. The times the rat crossover the platform location and the percentage of time spent in the platform quadrant were recorded. From day 31–35, spatial acquisition trials were repeated followed by a probe trial on day 37. The time line for the MWM testing is shown in **Figure 1B**.

Statistical Analysis

All data were analyzed using IBM SPSS 25.0 (IBM, Chicago, IL, USA). Data are presented as mean ± SEM. Results in the MWM spatial acquisition trials were analyzed by two-way ANOVA for repeated measurements. Results in the MWM probe trials were analyzed by one-way ANOVA. The above data were further analyzed by the Bonferroni *post-hoc* analysis. Other data were analyzed by two-way ANOVA followed by the Bonferroni *post-hoc* analysis.

For rs-fMRI data, the analyzing method is mentioned in section Data Processing and Analysis. To further determine the relationship between FC and performances in the behavior test, Pearson's correlation was performed. Prior to the correlation analysis, *t-value*s with statistical significance were transformed to Z-scores using the Fisher transformation.

RESULTS

Lipopolysaccharide Exposure Impairs While Elamipretide (SS-31) Preserves Learning and Spatial Working Memory

The MWM was used to test the effects of LPS exposure and SS-31 treatment on learning and spatial working memory in

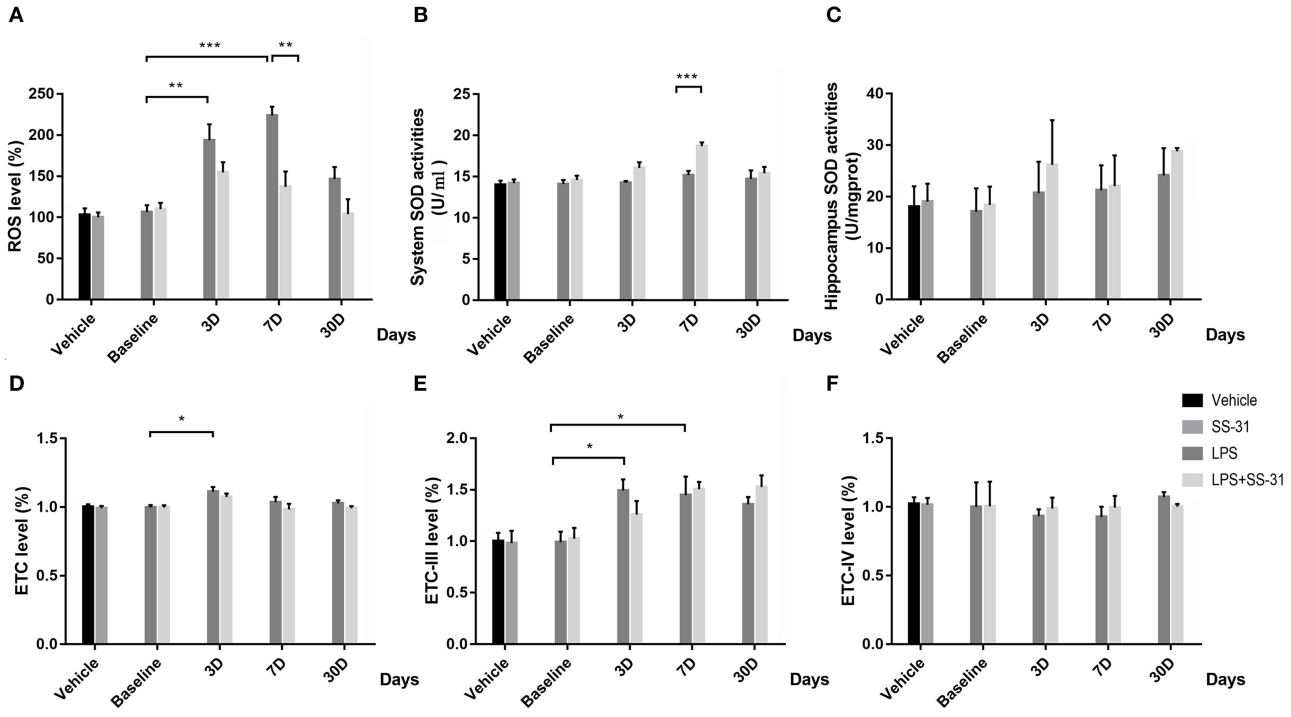

FIGURE 2 | Effects of lipopolysaccharide (LPS) exposure and elamipretide (SS-31) treatment on oxidative stress. **(A)** LPS exposure caused a significant mitochondrial ROS (mtROS) increase while rats with SS-31 treatment have lower level. **(B,C)** LPS exposure and SS-31 treatment caused superoxide dismutase (SOD) changes in the hippocampus. **(D–F)** LPS exposure and SS-31 treatment caused electron transport chain (ETC) complex I/III/IV changes in the hippocampus. Data are presented as mean ± SEMs ($n = 5$). Comparisons were made by two-way ANOVA followed by the Bonferroni *post-hoc* analysis. $^{*}p < 0.05$, $^{**}p < 0.01$, $^{***}p < 0.001$ vs. LPS (L) group.

both the short (< 7 days) and long terms (>30 days). From day 1 to 5, all rats showed significantly improved escape latency during the 5 days training [$F_{(3,141)} = 11.237$ for treatments and $F_{(4,188)} = 73.179$ for training days, $p < 0.001$, repeated measures two-way ANOVA; **Figure 1C**]. Significant interactions between training days and treatments were also observed [$F_{(12,564)} = 1.791$, $p = 0.046$, repeated measures ANOVA]. The *post-hoc* analysis indicated that LPS caused a significant increased escape latency from day 2 ($p < 0.001$), while SS-31 showed a significant improved escape latency from day 4 compared with the LPS group ($p < 0.001$). For the probe trial on day 7, a significant difference in the time spent in the target quadrant (one-way ANOVA, $F = 12.152$, $p < 0.001$, **Figure 1D**) and platform crossovers (one-way ANOVA, $F = 11.525$, $p < 0.001$, **Figure 1E**) was observed. The *post-hoc* analysis revealed that the the LPS-treated rats spent significantly less time in the platform crossovers than vehicle, LPS + SS-31, and SS-31 treated rats ($p < 0.001$, $p = 0.013$, and $p = 0.004$, **Figure 1E** respectively). However, there was no difference in the time spent in target quadrant when comparing LPS exposure rats with either SS-31- ($p = 0.159$) or LPS + SS-31-treated rats ($p = 0.063$, **Figure 1D**).

For the second acquisition trials from day 31 to 35, there was no interaction between training days and treatments [$F_{(12,468)} = 0.732$, $p = 0.720$; **Figure 1F**]; however, there was a significant difference among training days [$F_{(4,156)} = 6.790$, $p < 0.001$]. The *post-hoc* analysis revealed that rats with the LPS exposure had a significantly different escape latency on day 35 compared with other groups ($p = 0.002$). For the probe trial on day 37, there was a significant difference in the time spent in the target quadrant (one-way ANOVA, $F = 12.926$, $p < 0.001$; **Figure 1G**) and platform crossovers (one-way ANOVA, $F = 7.568$, $p < 0.001$; **Figure 1H**). The *post-hoc* analysis revealed that the LPS-exposed rats performed fewer platform crossovers than rats treated with vehicle ($p < 0.001$), rats treated with SS-31 ($p = 0.004$), and rats treated with LPS + SS-31 ($p = 0.017$). In addition, the LPS-treated rats spent significantly less time in target quadrant compared with vehicle- ($p < 0.001$) and SS-31-treated ($p < 0.001$) rats.

Oxidative Responses at the Systemic Level and Hippocampus After LPS Exposure and SS-31 Treatment

To determine the effect of SS-31 treatment in systemic level and aged rat hippocampus, oxidative stress was measured. For the hippocampus ROS, no interactive effect was observed [$F_{(3, 32)} = 0.111$, $p = 0.111$]; however, significant effects were seen in treatments and training days separately [$F_{(1, 32)} = 10.775$, $p = 0.002$ for treatment and $F_{(3, 32)} = 8.167$, $p < 0.001$, for days respectively; two-way ANOVA, **Figure 2A**]. Furthermore,

the Bonferroni *post-hoc* analysis revealed that the hippocampus ROS started to increase 3 days after the LPS exposure ($p = 0.009$) and reached a peak level on day 7 ($p < 0.001$). On day 30, the ROS fell back to the baseline level ($p = 0.705$). Meanwhile, the hippocampus ROS was significantly higher as compared with rats receiving SS-31 treatment on day 7 ($p = 0.002$). For rats in L + S group, no significant change in the ROS level has been observed after the LPS exposure. For the SOD level, no interactive effect was observed [$F_{(3, 32)} = 2.392$, $p = 0.087$]; however, significant effects were seen in treatment and training days separately [$F_{(1, 32)} = 13.212$, $p = 0.001$ for treatment and $F_{(3, 32)} = 6.040$, $p = 0.002$, respectively; two-way ANOVA, **Figure 2B**]. No difference has been observed in the hippocampus SOD activities [$F_{(3, 32)} = 0.523$, $p = 0.811$, respectively; two-way ANOVA, **Figure 2C**]. Furthermore, a significant higher SOD level in the system level was observed in day 7 as compared with rats without SS-31 treatment ($p < 0.001$, the Bonferroni *post-hoc* analysis, **Figure 2B**).

For the ETC-I level, no interactive effect was observed [$F_{(3,27)} = 0.444$, $p = 0.723$, respectively; two-way ANOVA, **Figure 2D**], while a significant effect was found in days [$F_{(3, 27)} = 0.004$, $p = 0.723$]. A significant rise of ETC-I level was observed on day 3 ($p = 0.027$, the Bonferroni *post-hoc* analysis), whereas no difference was observed on other time points. For rats with SS-31 treatment, no significant change in ETC-I was observed. For the ETC-III level, no interactive effect was observed [$F_{(3, 32)} = 1.099$, $p = 0.364$, respectively; two-way ANOVA, **Figure 2E**], whereas, a significant effect was observed in days [$F_{(3, 32)} = 7.075$, $p = 0.001$]. The ETC-III started to increase on day 3 and reached a peak level on day 7 after the LPS exposure ($p = 0.025$ and $p = 0.05$, the Bonferroni *post-hoc* analysis, respectively). On day 30, no significant difference could be observed ($p = 0.182$). For rats with SS-31 treatment, no significant effect could be observed.

No interactive effect or separative effect was observed in ETC-IV in both groups of rats [$F_{(3, 32)} = 0.180$, $p = 0.909$ for interactive effect, $F_{(1, 32)} = 0.042$, $p = 0.840$ for treatment and $F_{(3, 32)} = 0.240$, $p = 0.868$ for days, respectively; two-way ANOVA, **Figure 2F**].

Inflammatory Responses at the Systemic Level and Hippocampus After the LPS Exposure and SS-31 Treatment

To determine the effect of the LPS exposure and SS-31 treatment, proinflammatory cytokines in the serum and hippocampus and the mRNA expressions were measured.

No interaction effects were seen in systemic levels in both IL-1β and TNFα [$F_{(3, 48)} = 0.800$, $p = 0.500$ and $F_{(3, 40)} = 1.167$, $p = 0.334$, respectively; two-way ANOVA]; while a significant effect was seen in days [$F_{(3, 48)} = 6.514$, $p = 0.001$ and $F_{(3, 40)} = 1.167$, $p = 0.040$, respectively; two-way ANOVA]. Furthermore, the Bonferroni *post-hoc* analysis revealed that the serum levels of IL-1β significantly increased and reached a peak level on day 7 ($p = 0.001$; **Figure 3A**) in rats with LPS. For rats with LPS + SS-31, no significant change in serum IL-1β levels was observed. When considering SS-31 treatment, a higher level of IL-1β was observed in the L group ($p = 0.049$, respectively). For TNFα, a significant increase was observed on day 7 (the highest increase, $p = 0.034$, respectively; **Figure 3D**). For rats with LPS + SS-31, no significant change in TNFα level was observed. On day 7, higher level of TNFα was observed in the L group ($p = 0.030$, respectively).

Further, proinflammatory cytokines in the hippocampus were analyzed for inflammatory responses in the central nervous system (CNS). No interactive effects were seen in both inflammatory cytokines [$F_{(3, 35)} = 0.865$, $p = 0.469$ for IL-1β and $F_{(3, 40)} = 1.167$, $p = 0.334$ for TNFα, respectively; two-way ANOVA], whereas significant effects in days were observed [$F_{(3, 35)} = 5.260$, $p = 0.004$ for IL-1β and $F_{(3, 40)} = 3.033$, $p = 0.040$ for TNFα, respectively; two-way ANOVA]. Furthermore, the Bonferroni *post-hoc* analysis revealed that the LPS exposure resulted in significantly increased levels of IL-1β on day 7 and 30 ($p = 0.002$ and $p = 0.047$, respectively, **Figure 3B**) as compared with the baseline level. For the effect of SS-31, significant lower levels of IL-1β were observed on day 7 and 30 after the LPS exposure ($p = 0.041$ and $p = 0.034$, respectively) when compared with the rats without SS-31 treatment. For TNFα, no significant change was observed though there was a tendency that the levels of TNFα seemed to be increased after the LPS exposure (**Figure 3E**).

When checking the mRNA expression in the aged rat hippocampus, a significant interactive effect in levels of IL-1β mRNA expression was observed [$F_{(3, 32)} = 20.514$, $p < 0.001$]. No interactive effect was seen in TNFα [$F_{(3, 32)} = 1.651$, $p = 0.197$, respectively; two-way ANOVA], whereas a significant effect was seen in days [$F_{(3,32)} = 4.251$, $p = 0.012$]. To further determine the differences, the IL-1β mRNA expression reached a peak at day 3 after the LPS exposure ($p < 0.001$, the Bonferroni *post-hoc* analysis). When considering the effect of SS-31, a significant lower level of mRNA expression was observed on day 3 as compared with rats in L group ($p < 0.001$, **Figure 3C**). For TNFα, a significant difference of mRNA expression was observed on day 7 ($p = 0.021$, the Bonferroni *post-hoc* analysis, **Figure 3F**) when considering the SS-31 effect. For other time points, no significant differences in mRNA expression were observed for both groups of rats.

Activation of Astrocytes in the Aged Rat Hippocampus After the LPS Exposure and SS-31 Treatment

To determine whether neuroinflammation in the aged rat hippocampus resulted in impaired behavior performances, the astrocyte activation in the inflammatory responses was measured.

In the hippocampus, both levels of IL-1β and TNFα secreted by astrocyte activation were affected by the LPS exposure and SS-31 treatment [$F_{(3, 72)} = 3.371$, $p = 0.023$ for IL-1β and $F_{(3, 72)} = 4.691$, $p = 0.005$ for TNFα, two-way ANOVA, **Figures 4A,B**]. When considering LPS exposure, the Bonferroni *post-hoc* analysis revealed that levels of IL-1β positive astrocytes were significantly increased on day 3, 7, and 30 in L group ($p < 0.001$, $p < 0.001$, and $p < 0.001$, respectively) and day 3 and 7 in L + S group ($p < 0.001$ and $p = 0.001$, respectively) compared with baseline. When considering SS-31 treatment, reduced levels

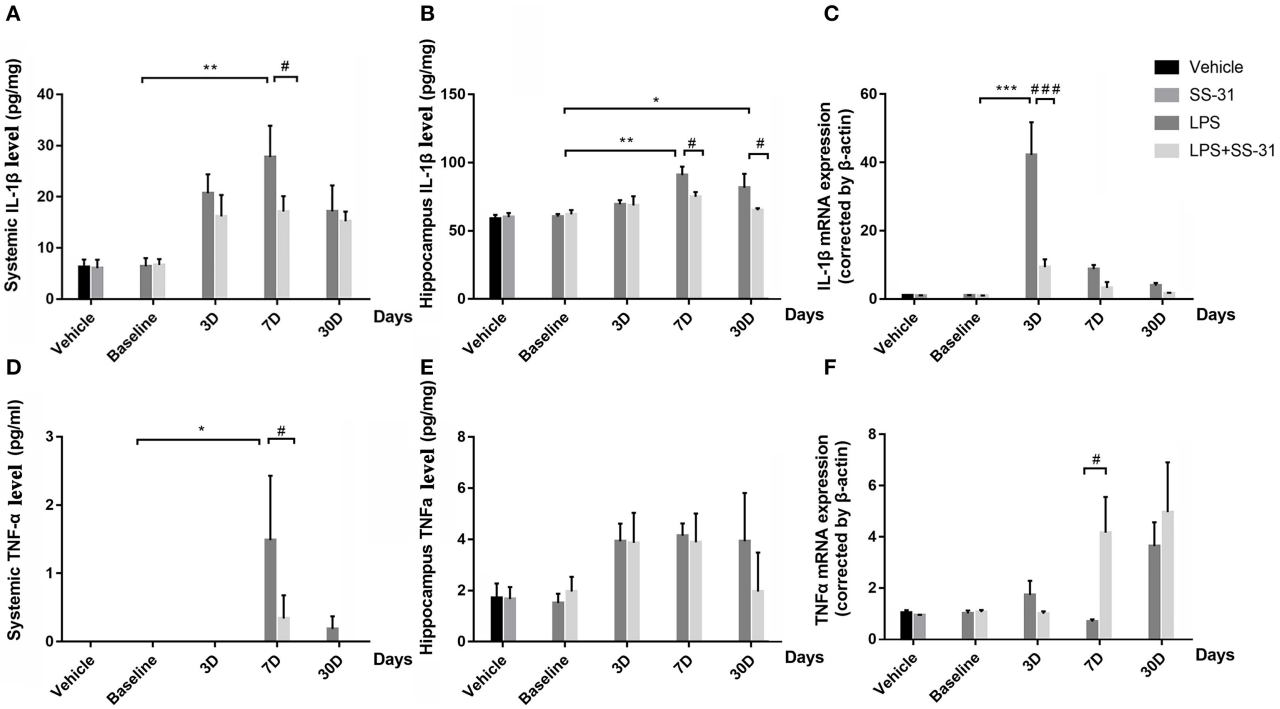

FIGURE 3 | Effects of lipopolysaccharide (LPS) exposure and elamipretide (SS-31) treatment. ELISA showed differences in **(A,D)** the systemic and **(B,E)** the hippocampus IL-1β and TNFα expression. RT-PCR showed differences in mRNA expression for **(C)** IL-1β and **(F)** TNFα Data are presented as mean ± SEMs ($n = 5$). Comparisons were made by two-way ANOVA followed by the Bonferroni *post-hoc* analysis. $^{\#}p < 0.05$, $^{\#\#}p < 0.01$, $^{\#\#\#}p < 0.001$ as indicated or vs. V; $^{*}p < 0.05$, $^{**}p < 0.01$, $^{***}p < 0.001$ vs. L group.

of IL-1β positive astrocytes were observed on day 7 and 30 as compared with L group ($p < 0.001$ and $p < 0.001$, respectively; **Figure 4E**). For TNFα positive astrocyte, a significantly increased level was observed on day 3, 7, and 30 in L group ($p < 0.001$, $p < 0.001$, and $p < 0.001$, respectively) and L + S group ($p < 0.001$, $p < 0.001$, and $p < 0.001$, respectively). When considering the treatment effect, lower levels of TNFα positive astrocytes were observed in L + S group compared with rats in L group ($p = 0.003$, $p < 0.001$, and $p < 0.001$, respectively; **Figure 4F**).

For the treatment of SS-31, no significant difference has been found in IL-1β/TNFα positive astrocytes [$F_{(3, 56)} = 0.187$, $p = 0.987$ for IL-1β and $F_{(3,56)} = 0.060$, $p = 0.981$ for TNFα, respectively; two-way ANOVA, **Figures 4C,D,G,H**].

Hippocampal Neuroinflammation Affects the Hippocampus-Related Brain Function in Aged Rat

To further understand the effects of inflammatory responses in the hippocampus on the brain function in other regions, we used rs-fMRI scanning with L- and R-hip as seed voxels.

Compared with rats in the V group, those exposed to the LPS showed both decreased L-hip-seeded and R-hip-seeded FC on the right orbital cortex (R-OC), right olfactory bulb (R-Ob), and L-hip on day 3, 7, and 31, respectively (**Figures 5A–C**; **Table 2**). Using the same method, increased FC was observed on the right visual cortex (R-VC), right sensory cortex (R-SC), left retrosplenial cortex (L-RSC), and left parietal association cortex (L-PAC) on day 3 with the R-SC on day 31 (one-way ANOVA followed by the *post-hoc* two-sample *t*-test, $p < 0.001$, cluster 20; **Figures 5A,C**; **Table 2**). No FC increase was observed on day 7. Localizations in transverse plane are also presented (**Figures 5D–F**).

Compared with rats treated with LPS, those treated with LPS + SS-31 showed both increased L-hip-seeded and R-hip-seeded FC on the L-PAC, left sensory cortex (L-SC), and left motor cortex (L-MC) on day 7, and the right flocculonodular lobe (R-PFL) on day 31 (one-way ANOVA followed by the *post-hoc* two-sample *t*-test, $p < 0.001$, cluster 20; **Figures 6B,C**; **Table 3**). Using the same method, decreased FC was observed on the right olfactory cortex (R-OFC) and R-VC on day 3 (one-way ANOVA followed by the *post-hoc* two-sample *t*-test, $p < 0.001$, cluster 20; **Figures 6A,C**; **Table 3**). Localizations in transverse plane are also presented (**Figures 6D–F**).

No significant FC change was found in V group and S group.

Altered Brain Function Affected Learning and Spatial Working Memory

To further determine if altered brain function in aged rat resulted in differences in learning and spatial working memory, the Pearson's correlation was used. On day 7, a significant correlation

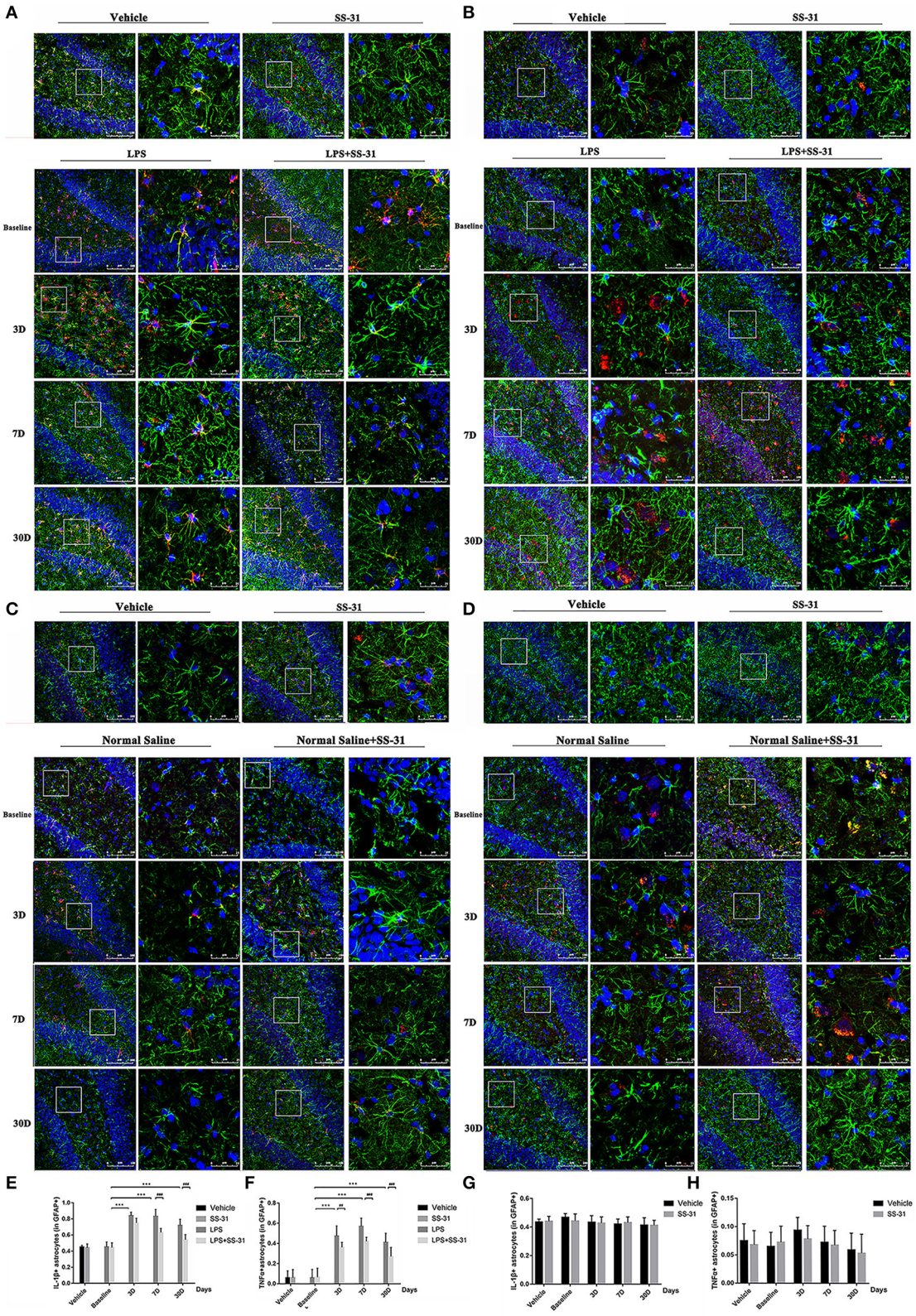

FIGURE 4 | Astrocytes activation induced by lipopolysaccharide (LPS) exposure and elamipretide (SS-31) treatment. **(A,B)** LPS exposure induced a significant increase in IL-1β/TNFα secretion and astrocyte activation both in the LPS (L) and LPS + SS-31 (L + S) groups. SS-31 treatment improved the inflammatory response *(Continued)*

FIGURE 4 | in the aged rat brain. **(C,D)** SS-31 treatment induced no significant inflammatory responses and astrocyte activation. **(E,F)** Double-stained immunofluorescence cell count showed that SS-31 treatment reduced the inflammatory response from day 3 to 30, whereas LPS caused prolonged IL-1β/TNFα secretion and astrocyte activation. **(G,H)** SS-31 treatment induced no significant change in IL-1β/TNFα positive astrocytes. Data are presented as mean ± SEMs (n = 5). Comparisons were made by two-way ANOVA followed by the Bonferroni *post-hoc* analysis. $^{\#}p < 0.05$, $^{\#\#}p < 0.01$, $^{\#\#\#}p < 0.001$ as indicated or vs. V; $^{*}p < 0.05$, $^{**}p < 0.01$, $^{***}p < 0.001$ vs. L group.

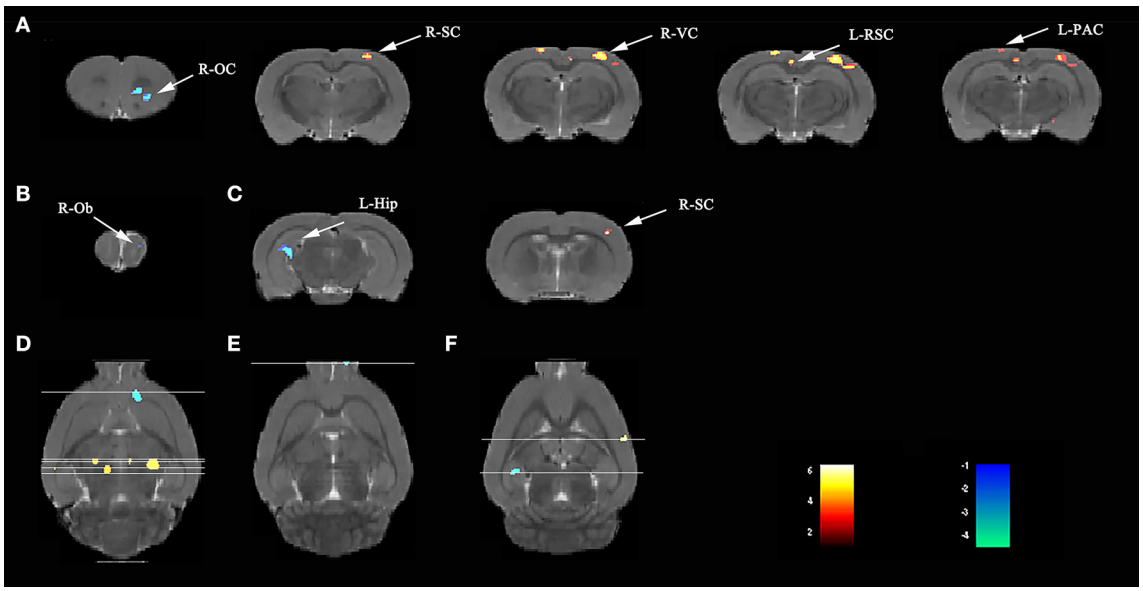

FIGURE 5 | Lipopolysaccharide (LPS) exposure induced both short- and long-term functional connectivity (FC) changes in the aged rat brain. LPS exposure caused FC changes in **(A)** 3 days, **(B)** 7 days, and **(C)** 31 days. **(D–F)** Localization for different regions of interest (ROIs) on day 3, 7, and 31. Data were analyzed by one-way ANOVA followed by the *post-hoc* two-sample *t*-test. A voxel-level height threshold of $p < 0.001$ and a cluster-extent threshold of 20 were considered as statistically significant. Both the left and right hippocampus were used as seed voxels.

TABLE 2 | LPS exposure caused significant functional connectivity (FC) changes in the aged rat brain in short and long term.

Day	Cluster (Total)	Sub-regions	Cluster size	*t*-value	Paxino's atlas		
					x	y	z
3	Cluster 1		80	−4.2917	2.4818	4.9159	3.0021
		Right-orbital cortex	80	−4.2917	2.4818	4.9159	3.0021
	Cluster 2		402	5.4930	3.2489	0.8785	−3.7179
		Right-visual cortex	87	5.1701	3.1171	1.0547	−4.1979
		Right-sensory cortex	110	5.4734	3.5018	0.7093	−3.2379
	Cluster 3		248	4.2736	−0.6197	1.1396	−4.1979
		Left-retrosplenial cortex	163	4.2736	−0.6197	1.1396	−4.1979
	Cluster 4		99	4.7769	−2.1034	−0.1988	−3.2379
		Left-parietal association cortex	69	4.7769	−2.1034	−0.1988	−3.2379
7	Cluster 1		164	−5.5104	1.4882	2.8678	7.3221
		Right-olfactory bulb	144	−5.5104	1.4882	2.8678	7.3221
31	Cluster 1		154	−5.1868	−4.4751	3.5214	−5.6379
		Left-hippocampus	154	−5.1868	−4.4751	3.5214	−5.6379
	Cluster 2		53	4.4788	5.6206	2.6984	−1.3179
		Right-sensory cortex	53	4.4788	5.6206	2.6984	−1.3179

**L, left; R, right. The regions of interest (ROIs) were drawn according to the rat anatomic atlas (Paxino and Watson, 4th edition).*

† The t-values were the maximum values of the two-sample t-tests for the ROIs with statistical significance (showing the greatest statistical significance within a cluster). A positive t-value means increased FC, while a negative t-value means the opposite. Comparison was performed for L and CON groups, with the V group as baseline. $p < 0.001$ and a cluster size of 20 was considered as statistically significant.

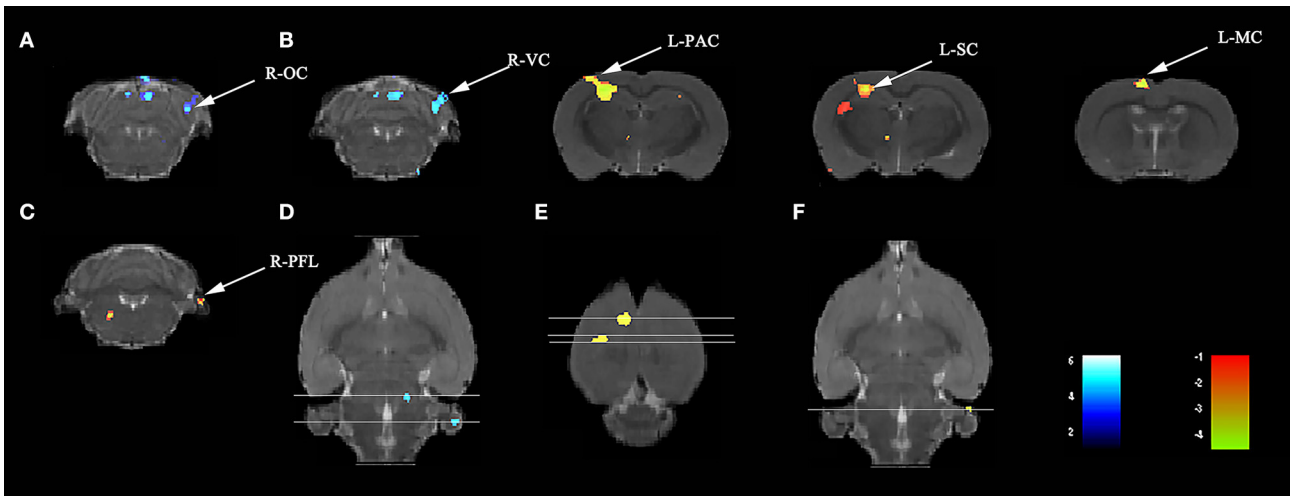

FIGURE 6 | SS-31 treatment induced both short- and long-term functional connectivity (FC) changes in the aged rat brain. **(A)** SS-31 treatment caused FC changes in 3 days. SS-31 treatment improved FC connectivity in **(B)** 7 days and **(C)** 31 days. **(D–F)** Localization for different regions of interest (ROIs) on day 3, 7, and 31. Data were analyzed by one-way ANOVA followed by the *post-hoc* two-sample *t*-test. A voxel-level height threshold of $p < 0.001$ and a cluster-extent threshold of 20 were considered as statistically significant. Both the left and right hippocampus were used as seed voxels.

TABLE 3 | Elamipretide (SS-31) treatment improved functional connectivity (FC) connectivity in the aged rat brain.

Day	Cluster (Total)	Sub-regions	Cluster size	*t*-value	Paxino's atlas		
					x	y	z
3	Cluster 1		507	−5.9723	4.6668	3.1200	−9.9579
		Right-olfactory cortex	83	−5.3672	4.6602	3.2190	−9.4779
		Right-visual cortex	31	−4.4835	4.6536	2.8755	−8.9979
7	Cluster 1		709	5.9146	−3.1826	1.2896	−2.7579
		Left-parietal association cortex	61	5.3679	−3.3144	1.1826	−3.2379
		Left-sensory cortex	373	5.9146	−3.1826	1.2896	−2.7579
	Cluster 2		165	5.9085	−1.3406	0.2183	−0.8379
		Left-motor cortex	158	5.9085	−1.3406	0.2183	−0.8379
31	Cluster 1		32	4.781	5.7394	6.5273	−9.9579
		Right-flocculonodular lobe	21	4.781	5.7394	6.5273	−9.9579

**L, left; R, right. The ROIs were drawn according to the rat anatomic atlas (Paxino and Watson, 4th edition).*

† The t-values were the maximum values of the two-sample t-tests for the ROIs with statistical significance (showing the greatest statistical significance within a cluster). A positive t-value means increased FC, while a negative t-value means the opposite. Comparison was performed for L and L + S groups, with the L group as baseline. $p < 0.001$ and a cluster size of 20 was considered as statistically significant.

was observed in R-Ob in the L group ($p = 0.0002$, $r^2 = 0.6014$ for time spent and $p < 0.0001$, $r^2 = 0.742$ for crossovers, **Figure 7A**) as compared with rats in V group. Meanwhile, L-PAC, L-SC, and L-MC were also observed significant correlations with behavior performances ($p = 0.0008$ and $p = 0.0187$ with $r^2 = 0.4931$ and $r^2 = 0.2997$ for time spent; $p = 0.00065$, $p = 0.015$, and $p = 0.0041$ with $r^2 = 0.3615$, $r^2 = 0.4762$, and $r^2 = 0.4118$ for crossovers, **Figure 7B**). However, no significant correlation was observed for L-MC on day 7 ($p = 0.3603$). On day 31, no significant correlations were observed for L-hip, R-SC, and R-PFL on latency ($p = 0.0543$, $p = 0.1497$, and $p = 0.1997$, **Figure 8**).

DISCUSSION

Our result revealed that oxidative stress induced by a single dose of LPS injection may be able to cause long-term expression of astrocyte-derived inflammatory cytokines in the hippocampus, long-term FC change in the hippocampus, and other related regions, as well as impaired learning and spatial working memory. By removing excessive ROS triggered by the LPS exposure, elamipretide (SS-31) significantly reverse the above effects. Our study, therefore, demonstrates LPS-induced oxidative stress has long-term effects on the prolonged hippocampus neuroinflammation, cognitive function,

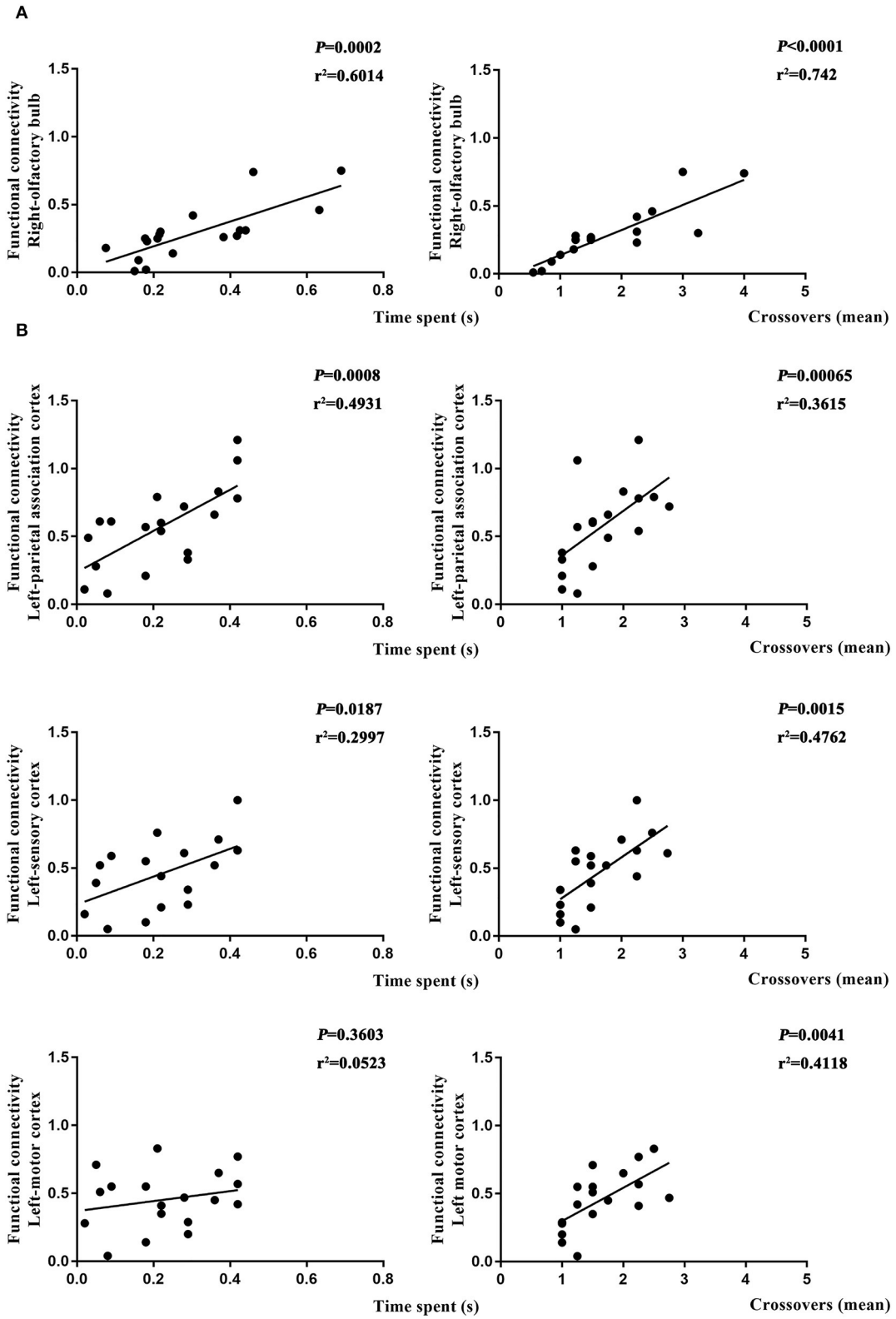

FIGURE 7 | Relationship between functional connectivity (FC) and behavior performances on day 7. **(A)** Correlation analysis in L and NS groups. **(B)** Correlation analysis in L and L + S groups. Pearson's correlation was used with $p < 0.05$ for statistical significance and r^2 for correlation.

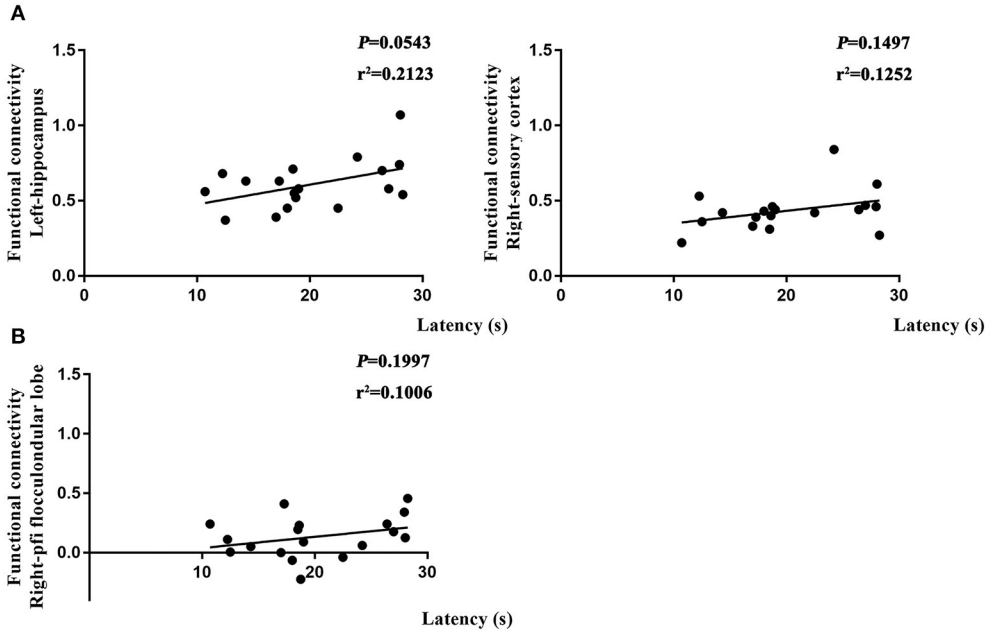

FIGURE 8 | Relationship between functional connectivity (FC) and behavior performances on day 31. **(A)** Correlation analysis in L and NS groups. **(B)** Correlation analysis in L and L + S groups. Pearson's correlation was used with $p < 0.05$ for statistical significance and r^2 for correlation.

and network connection between the hippocampus and other regions in aged rats.

The MWM is a classical approach to assess spatial learning and working memory. The spatial learning is assessed across repeated trials, and the reference memory is determined by preference for the platform area when the platform is absent (Vorhees and Williams, 2006). In our study, there is a significantly increased latency for rats in the L group as compared with rats in the other three groups, suggesting that the LPS exposure caused impaired learning ability in both short (<7 days) and long term (>30 days), and SS-31 treatment has a significant effect on improving the cognitive function. For reference memory, significantly decreased time spent in target quadrant showed cognitive dysfunction in both short (<7 days) and long term (>30 days). For rats with SS-31 treatment, significantly higher times for platform crossovers showed improved cognitive function. Although a higher time spent in target quadrant was observed, for rats in the S group, no significant difference was observed in time spent in target quadrant as compared with the rats with the LPS exposure. Considering the fact that the rats in the S group had already shown significantly higher times for platform crossovers and latency, with no significant difference in L-1β/TNFα positive astrocytes, the reason may be due to a rather strict correction in statistical analysis. Significant lower times for crossovers showed that the rats in the L group had significantly impaired reference memory.

Traditionally, astrocytes have been considered as a major contributor for neuron homeostasis, functional outcomes of local synaptic transmission and plasticity, and BBB constructing (Abbott et al., 2006; Santello et al., 2019). However, astrocytes have also recently been reported to play a pivotal role in the neuroinflammation and cognitive function (Habbas et al., 2015; Santello et al., 2019). We previously reported that a single systemic injection of LPS (2 mg/kg) activated NF-κB signaling pathway in astrocytes and induced long-term expression of IL-1β and TNFα mRNA in the aged rat hippocampus, which caused prolonged neuroinflammation (Fu et al., 2014; Kan et al., 2016). In addition, our study also reported that the LPS exposure caused decreased expression of post-synaptic density protein-95 (PSD-95) in neurons while blocking NF-κB signaling pathway in astrocytes improved the phenomenon (Kan et al., 2016). This demonstrated that the LPS exposure resulted in impaired synaptic plasticity, which further induced impaired learning and spatial working memory. In the present study, long-term neuroinflammation was inhibited by SS-31 treatment. Interestingly, SS-31 was specially designed to remove excessive ROS from mitochondria rather than inhibiting NF-κB signaling pathway (Wu et al., 2017; Zhao et al., 2019), suggesting that anti-oxidant treatment is also effective for inhibiting neuroinflammation in aged rat. Our result demonstrated that the SS-31 treatment inhibited LPS induced long-term astrocyte activation and enhanced expression of astrocyte-derived proinflammatory cytokines in the aged rat hippocampus, and it improved learning and spatial working memory. Although the A1 type astrocytes (neurotoxic and may contribute to neurodegenerative diseases) have been proved to be activated by microglia (Liddelow et al., 2017), recent studies also showed that astrocytes may trigger microglial activation (Jha et al., 2018). The present study showed that the LPS exposure induced astrocytes activation followed with long-term

inflammatory responses in the hippocampus, suggesting that the astrocytes may play an important role in long-term inflammatory response in the aged brain. The previous studies revealed that mtROS generation may induce inflammasome activation in astrocytes (Alfonso-Loeches et al., 2014). The use of SS-31 treatment removed excessive ROS from the CNS, which helps to reduce the inflammatory response of the astrocytes, and further improved cognitive function in the long term. Overall, our findings suggested that anti-oxidant treatment may be a potential method for preventing POCD in elderly patients in clinical practice.

Mitochondrial reactive oxygen species induce the activation of NF-κB and the nucleotide-binding oligomerization domain (NOD)-like receptor family, pyrindomain containing 3 (NLRP3) inflammasome (Bauernfeind et al., 2009), which activate caspase 1 and result processing and secretion of IL-1β, IL-18, and TNF-α in the hippocampus of aged mice and cognitive impairments (Fu et al., 2020). For ROS, significant increase can be observed from day 3 to 7 with the treatment effect can only be seen on day 7. Our result demonstrated that the SS-31 treatment has a significant effect on the short term (within 7 days). For the SOD level, no significant effect can be observed in the hippocampus, though rats with SS-31 treatment seemed to have a higher level. The levels of ETC-I/III/IV have similar change, which is consistent with the previous findings that the ROS correlated with ETC-I/III/IV levels (Yan et al., 2020). The previous study on ROS level in the hippocampus also indicated a similar effect on ROS within 3 days after the LPS exposure (Zhao et al., 2019). Another study based on rat pups (7 days after birth) reported a similar effect on ROS production 6 h after isoflurane exposure (Wu et al., 2017). However, no results for long term were reported for both studies. Our result suggested that the inflammatory responses in the hippocampus last longer than oxidative stress. Early prevention of oxidative stress has a long-term effect on preventing inflammatory response in the aged rat hippocampus. However, the mechanism for oxidative induced long-term astrocytes activation still need further investigations.

It is an interesting phenomenon that although the compounds (LPS and SS-31) are no longer exist 30 days after administration, the inflammatory effect and treatment effect still exist in the aged rat hippocampus. Meanwhile, no long-term effect can be seen in solely SS-31 administration, but the effect of the LPS exposure is prevented. However, the mechanism should be further studied. The previous study reported a single dose of LPS injection (1 mg/kg, i.p.) is enough to make a long-term dysfunction of hypothalamic–pituitary–adrenal (HPA) axis in adult rats (2 months old), including a significantly increased TNFα in peripheral and corticosterone 4 weeks after the initial dose of LPS injection, which may likely to involve some kind of learning-like brain plasticity (Valles et al., 2002). In the present study, we used aged rats (20 months) with weaker BBB and less tolerance to peripheral stressors, and higher dose of LPS injection (2 mg/kg), the above which may cause a more severe inflammatory response. Another study based on single dose of LPS injection (2 mg/kg) reported that the neuronal function followed by systemic inflammation is NLRP3 inflammasome dependent (14 days after injection) in which the spine density of basal cell in the hippocampus CA1 region still remains significantly decreased even 3 months after the LPS exposure (Beyer et al., 2020). Meanwhile, a great number of evidence has shown that the NLRP3 inflammasome activation also contributes to aging process (Meyers and Zhu, 2020), which also supports our result that the inflammatory responses in the aged rat hippocampus may be long-lasting even the LPS and SS-31 no longer exist. Although we did not measure the level of NLRP3 inflammasome, we used the same doses and administration method of LPS. The long-term neuroinflammation may also be induced by the NLRP3 inflammasome. Based on the findings that the difference in oxidative stress only lasted for 7 days (ROS level and ETC-III level), there may conclude that early prevention of excessive oxidative stress may have a long-term effect in the inflammation prevention.

Although the rs-fMRI has been widely used to study cognitive function and neurodegenerative disease in human subjects, the functional basis of BOLD signal is still under debate. The previous studies in both resting or task fMRI revealed that the neural activity required for the execution of cognitive tasks corresponds to flow within a low-dimensional state space, which is further assumed to reflect the BOLD responses (Hutchison et al., 2013; Shine et al., 2019). Because studies found that the intrinsic connectivity networks under neural activity are likely shaped but not fully determined by structural connectivity (Damoiseaux and Greicius, 2009), other mechanisms may responsible for neural network activity. A clinical study based on post-mortem data revealed that the spatial pattern of neurotransmitter receptors density (e.g., dopaminergic D_1 and cholinergic M_1) and topology factors are closely related to neural activity at the network level (Shine et al., 2019), which suggests that the FC in rs-fMRI may also be related to neural activities from chemical transmitters besides axon and dendrites. The previous studies showed that the LPS exposure resulted in decreased amounts of PSD-95 (Kan et al., 2016), loss of neural transmitter receptors (Zhang et al., 2017), and swollen astrocytes (Fan et al., 2014), all of which may further impair synaptic plasticity (Santello et al., 2019). Therefore, as previously mentioned, the intrinsic connectivity networks under neural activity are likely shaped but not fully determined by structural connectivity (Hutchison et al., 2013), which indicates that changes in the brain function may occur in remote areas due to FC *via* neurotransmitters. In our study, rats exposed to LPS showed changes in FC not only in cognitive-related regions (e.g., L-RSC and L-hip) but also in regions distant from the hippocampus (e.g., R-Ob and R-OC); thus, neuroinflammation in the hippocampus may also affect remote regions *via* neurotransmitters rather than anatomical connectivity. This may also explain why the flocculonodular lobe is also engaged in the hippocampus-related brain function in aged rat despite located in cerebellum. Furthermore, our results suggest that anti-inflammatory treatment not only inhibits hippocampal neuroinflammation but also protects the brain function in other regions in the long term.

The default mode network (DMN) has been proved to be an important neural network, which activates during mind-wondering and becomes less active during task-acquisition

(Raichle, 2015). The disruption of DMN is mostly seen in human neurocognitive disorders (Greicius et al., 2004; Qian et al., 2019). Meanwhile, the recent studies also found that the rat brain has DMN, and it has similar components as human beings (Lu et al., 2012). In the present study, rats with the LPS exposure showed changed FC in R-OC, L-RSC on day 3 and L-hip on day 31 with both sides of the hippocampus as seed regions. These regions are all major components of rat DMN. Imaging studies had already proven that different brain regions function as networks (Biswal et al., 1995; Wang et al., 2010), and a disruption of the brain connectivity suggested a long-term disruption for neural correlation between the hippocampus and target brain region. The RSC is situated at the crossroads between the hippocampus and neocortex (Wyss and Van Groen, 1991). Change in FC between Hip and RSC may result in information disruption in the aged rat brain. These may also explain why the rats still had impaired cognitive function 30 days after the LPS exposure. The prefrontal cortex (PFC) has been proved to be both significant in DMN and the hippocampus-prefrontal afferents that are critical for encoding memory (Raichle, 2015; Spellman et al., 2015). However, we did not observe a significant difference in FC between PFC and Hip. This indicated that the LPS exposure did not disrupt correlation between PFC and Hip. Considering that there are still significant differences in IL-1β secretion in the hippocampus, we hypothesize that this phenomenon may be resulted from the excessive IL-1β in the hippocampus. This is also consistent with the previous findings that IL-1β played a significant role in cognitive function (Huang and Sheng, 2010). However, in rats with SS-31 treatment, no significant change was observed in rat DMN though the improved MWM performance was observed. These results indicated that SS-31 may improve the brain FC by improving other regions, instead of DMN. It also suggested that DMN may not be the only network important in cognitive function. For the SS-31 treatment, FC change in the cerebellum was observed. Recent studies revealed that the cerebellum participates in both motor and cognitive aspects of navigation (Igloi et al., 2015; Wang et al., 2016). Our result is consistent with these findings and showed that improving FC between the hippocampus and cerebellum may also improve learning and spatial working memory.

Despite application of the latest medical practices, most of the neurodegenerative diseases remain difficult to cure and show irreversible development. Few studies have investigated whether inhibiting the hippocampus neuroinflammation or interrupting related signaling pathway improves the brain function in other regions. In one of our clinical studies, we reported improvements in cognitive test performance after anti-inflammatory treatment in elderly patients following spinal surgery (Zhang et al., 2018). However, rs-fMRI was not applied in this study so the function in other brain regions could not be fully assessed. In the present study, as consistent with improved behavior performances in the MWM, we observed increased FC from day 7 to 31 in the other brain regions using the bilateral hippocampus as seed voxels in rats treated with SS-31. Accordingly, we demonstrated that inhibiting inflammation in the hippocampus also improves the brain functions in other regions. Furthermore, IL-1β expression in the astrocytes on day 30 did not differ in rats with SS-31 treatment as compared with baseline data; however, a significant difference was observed on day 30 in L group. This indicates that SS-31 produces long-term protective effects against prolonged neuroinflammation in aged rat.

For the correlation analysis, our result demonstrated that the LPS exposure caused altered brain function is highly correlated with impaired behavior performances in the short term (<7 days). Interestingly, in the long term, altered brain function could be observed in both L and L + S groups as compared with rats in the NS group with no difference in behavior performances found. Moreover, a significant difference could still be found in probe trial (day 37) after the second MWM training session (day 31–35). Previous studies in human subjects reported abnormal PET or fMRI change at preclinical stage of cognitive diseases (Jack et al., 2010; Sperling et al., 2011), indicating that altered brain function may appear early than abnormal cognitive function as disease develops. For the present study, our result indicated that altered brain function may still exist in the long term after LPS exposure although the behavior may already seem to be back to normal. Moreover, our result suggested that these subjects (normal cognitive function with altered brain function) survived from neuroinflammation are still likely to have a worse cognitive function as compared with rats with SS-31 treatment or without LPS exposure.

There are several limitations for the present study. First, learning effect cannot be fully excluded. For groupwise comparisons at the same time point, the learning effect is minimized because each group underwent same training procedure; however, for the time-wise comparisons, the learning effect is a possibility. Studies demonstrated that the MWM training altered FC within DMN for up to 7 days in adult rat (Nasrallah et al., 2016). Whether 23 days (from day 7 to 31) is a sufficient test period for aged rat requires further investigations. Second, anesthesia could potentially influence FC patterns. Although a recent study demonstrated that combined isoflurane and dexmedetomidine anesthesia is an appropriate anesthesia method (Paasonen et al., 2018), data on the aged rat brain are still lacking because aging has also been reported to have influence on FC patterns (Ash et al., 2016). Third, the correlation analysis was done on time spent and crossovers in the short term (<7 days) and latency in the long term (>30 days). The reason for doing this is that the FC and behavior performance have to be at the same time so that the individual difference can be largely avoided.

In conclusion, our study demonstrated that the LPS-induced hippocampal neuroinflammation causes impaired brain function in other regions in aged rats, while inhibiting the inflammatory response in the hippocampus improves brain function in hippocampus and other related regions. The protective effect of inhibiting inflammatory responses coexisted with the improved behavior performance, fewer IL-1β- and TNFα-positive astrocytes in the hippocampus DG region, and lower IL-1β and TNFα secretion at the systemic level.

DATA AVAILABILITY STATEMENT

The raw data supporting the conclusions of this article will be made available by the authors, without undue reservation.

ETHICS STATEMENT

The animal study was reviewed and approved by Ethical Committee of Capital Medical University.

AUTHOR CONTRIBUTIONS

YL, HF, and TW: author study design. YL, HF, FL, MK, and SY: experiments performance. YL, BN, and YW: data analysis. YL and HF: manuscript writing. TW, LF, and WX: manuscript revision. All authors contributed to the article and approved the submitted version.

FUNDING

This work was supported by grants from Beijing Municipal Administration of Hospitals' Ascent Plan (Code: DFL20150802), Beijing Municipal Administration of Hospitals Clinical Medicine Development of Special Funding Support (Code: ZYLX201706), and Beijing 215 High Level Healthcare Talent Plan Academic Leader (Code: 008-0027).

ACKNOWLEDGMENTS

The authors express their appreciation to Profs. Lirong Chang and Yizhi Song from Department of Anatomy, Capital Medical University for their generous help with the study design. The authors also express their appreciation to the staff of Beijing Area Major Laboratory of Peptide and Small Molecular Drugs, Engineering Research Center of Endogenous Prophylactic of Ministry of Education of China.

SUPPLEMENTARY MATERIAL

The Supplementary Material for this article can be found online at: https://www.frontiersin.org/articles/10.3389/fnagi.2021.600484/full#supplementary-material

REFERENCES

Abbott, N. J., Ronnback, L., and Hansson, E. (2006). Astrocyte-endothelial interactions at the blood-brain barrier. *Nat. Rev. Neurosci.* 7, 41–53. doi: 10.1038/nrn1824

Alfonso-Loeches, S., Urena-Peralta, J. R., Morillo-Bargues, M. J., Oliver-De La Cruz, J., and Guerri, C. (2014). Role of mitochondria ROS generation in ethanol-induced NLRP3 inflammasome activation and cell death in astroglial cells. *Front. Cell. Neurosci.* 8:216. doi: 10.3389/fncel.2014.00216

Ash, J. A., Lu, H., Taxier, L. R., Long, J. M., Yang, Y., Stein, E. A., et al. (2016). Functional connectivity with the retrosplenial cortex predicts cognitive aging in rats. *Proc. Natl. Acad. Sci. U.S.A.* 113, 12286–12291. doi: 10.1073/pnas.1525309113

Bartsch, T., and Wulff, P. (2015). The hippocampus in aging and disease: From plasticity to vulnerability. *Neuroscience* 309, 1–16. doi: 10.1016/j.neuroscience.2015.07.084

Bauernfeind, F. G., Horvath, G., Stutz, A., Alnemri, E. S., MacDonald, K., Speert, D., et al. (2009). Cutting edge: NF-kappaB activating pattern recognition and cytokine receptors license NLRP3 inflammasome activation by regulating NLRP3 expression. *J. Immunol.* 183, 78—791. doi: 10.4049/jimmunol.0901363

Beyer, M. M. S., Lonnemann, N., Remus, A., Latz, E., Heneka, M. T., and Korte, M. (2020). Enduring changes in neuronal function upon systemic inflammation are NLRP3 inflammasome dependent. *J. Neurosci.* 40, 5480–5494. doi: 10.1523/JNEUROSCI.0200-20.2020

Biswal, B., Yetkin, F., Haughton, V., and Hyde, J. (1995). Functional connectivity in the motor cortex of resting human brain using echo-planar MRI. *Magn. Reson. Med.* 34, 537–541. doi: 10.1002/mrm.1910340409

Browndyke, J. N., Berger, M., Harshbarger, T. B., Smith, P. J., White, W., Bisanar, T. L., et al. (2017). Resting-state functional connectivity and cognition after major cardiac surgery in older adults without preoperative cognitive Impairment: preliminary findings. *J. Am. Geriatr. Soc.* 65:e6–e12. doi: 10.1111/jgs.14534

Chesnokova, V., Pechnick, R. N., and Wawrowsky, K. (2016). Chronic peripheral inflammation, hippocampal neurogenesis, and behavior. *Brain Behav. Immun.* 58, 1–8. doi: 10.1016/j.bbi.2016.01.017

Chirles, T. J., Reiter, K., Weiss, L. R., Alfini, A. J., Nielson, K. A., and Smith, J. C. (2017). Exercise training and functional connectivity changes in mild cognitive impairment and healthy elders. *J. Alzheimers Dis.* 57, 845–856. doi: 10.3233/JAD-161151

Clarke, L. E., Liddelow, S. A., Chakraborty, C., Munch, A. E., Heiman, M., and Barres, B. A. (2018). Normal aging induces A1-like astrocyte reactivity. *Proc. Natl. Acad. Sci. U.S.A.* 115:E1896–E1905. doi: 10.1073/pnas.1800165115

Damoiseaux, J. S., and Greicius, M. D. (2009). Greater than the sum of its parts: a review of studies combining structural connectivity and resting-state functional connectivity. *Brain Struct. Funct.* 213, 525–533. doi: 10.1007/s00429-009-0208-6

Fan, L., Wang, T., Chang, L., Song, Y., Wu, Y., and Ma, D. (2014). Systemic inflammation induces a profound long term brain cell injury in rats. *Acta Neurobiol. Exp.* 74, 298–306.

Fjell, A. M., McEvoy, L., Holland, D., Dale, A. M., Walhovd, K. B., and Alzheimer's Disease Neuroimaging Initiative. (2014). What is normal in normal aging? Effects of aging, amyloid and Alzheimer's disease on the cerebral cortex and the hippocampus. *Prog. Neurobiol.* 117, 20–40. doi: 10.1016/j.pneurobio.2014.02.004

Fu, H. Q., Yang, T., Xiao, W., Fan, L., Wu, Y., Terrando, N., et al. (2014). Prolonged neuroinflammation after lipopolysaccharide exposure in aged rats. *PLoS ONE* 9:e106331. doi: 10.1371/journal.pone.0106331

Fu, Q., Li, J., Qiu, L., Ruan, J., Mao, M., Li, S., et al. (2020). Inhibiting NLRP3 inflammasome with MCC950 ameliorates perioperative neurocognitive disorders, suppressing neuroinflammation in the hippocampus in aged mice. *Int. Immunopharmacol.* 82:106317. doi: 10.1016/j.intimp.2020.106317

Greicius, M. D., Srivastava, A., Reiss, A., and Menon, V. (2004). Default-mode network activity distinguishes Alzheimer's disease from healthy aging: Evidence from functional MRI. *Proc. Natl. Acad. Sci. U.S.A.* 101, 4637–4642. doi: 10.1073/pnas.0308627101

Griffin, P., Dimitry, J. M., Sheehan, P. W., Lananna, B. V., Guo, C., Robinette, M. L., et al. (2019). Circadian clock protein Rev-erbalpha regulates neuroinflammation. *Proc. Natl. Acad. Sci. U.S.A.* 116, 5102–5107. doi: 10.1073/pnas.1812405116

Habbas, S., Santello, M., Becker, D., Stubbe, H., Zappia, G., Liaudet, N., et al. (2015). Neuroinflammatory TNFalpha impairs memory via astrocyte signaling. *Cell* 163, 1730–1741. doi: 10.1016/j.cell.2015.11.023

Hardcastle, C., Huang, H., Crowley, S., Tanner, J., Hernaiz, C., Rice, M., et al. (2019). Mild cognitive impairment and decline in resting state functional connectivity after total knee arthroplasty with general anesthesia. *J. Alzheimers Dis.* 69, 1003–1018. doi: 10.3233/JAD-180932

Huang, Z. B., and Sheng, G. Q. (2010). Interleukin-1beta with learning and memory. *Neurosci. Bull.* 26, 455–468. doi: 10.1007/s12264-010-6023-5

Hutchison, R. M., Womelsdorf, T., Allen, E. A., Bandettini, P. A., Calhoun, V. D., Corbetta, M., et al. (2013). Dynamic functional connectivity: promise, issues, and interpretations. *NeuroImage* 80, 360–378. doi: 10.1016/j.neuroimage.2013.05.079

Igloi, K., Doeller, C. F., Paradis, A. L., Benchenane, K., Berthoz, A., Burgess, N., et al. (2015). Interaction between hippocampus and cerebellum crus I in sequence-based but not place-based navigation. *Cereb. Cortex.* 25, 4146–4154. doi: 10.1093/cercor/bhu132

Jack, C. R., Knopman, D. S., Jagust, W. J., Shaw, L. M., Aisen, P. S., Weiner, M. W., et al. (2010). Hypothetical model of dynamic biomarkers of the Alzheimer's pathological cascade. *Lancet Neurol.* 9, 119–128. doi: 10.1016/S1474-4422(09)70299-6

Jha, M. K., Jo, M., Kim, J. H., and Suk, K. (2018). Microglia-astrocyte crosstalk: an intimate molecular conversation. *Neuroscientist* 25, 227–240. doi: 10.1177/1073858418783959

Kan, M. H., Yang, T., Fu, H. Q., Fan, L., Wu, Y., Terrando, N., et al. (2016). Pyrrolidine Dithiocarbamate prevents neuroinflammation and cognitive dysfunction after endotoxemia in rats. *Front. Aging Neurosci.* 8:175. doi: 10.3389/fnagi.2016.00175

Liang, S., Wu, S., Huang, Q., Duan, S., Liu, H., Li, Y., et al. (2017). Rat brain digital stereotaxic white matter atlas with fine tract delineation in Paxinos space and its automated applications in DTI data analysis. *Magn. Reson. Imaging* 43, 122–128. doi: 10.1016/j.mri.2017.07.011

Liddelow, S. A., Guttenplan, K. A., Clarke, L. E., Bennett, F. C., Bohlen, C. J., Schirmer, L., et al. (2017). Neurotoxic reactive astrocytes are induced by activated microglia. *Nature* 541, 481–487. doi: 10.1038/nature21029

Lopes, R., Delmaire, C., Defebvre, L., Moonen, A. J., Duits, A. A., Hofman, P., et al. (2017). Cognitive phenotypes in Parkinson's disease differ in terms of brain-network organization and connectivity. *Hum. Brain Mapp.* 38, 1604–1621. doi: 10.1002/hbm.23474

Lu, H., Zou, Q., Gu, H., Raichle, M. E., Stein, E. A., and Yang, Y. (2012). Rat brains also have a default mode network. *Proc. Natl. Acad. Sci. U.S.A.* 109, 3979–3984. doi: 10.1073/pnas.1200506109

Meyers, A. K., and Zhu, X. (2020). The NLRP3 inflammasome: metabolic regulation and contribution to inflammaging. *Cells* 9:1808. doi: 10.3390/cells9081808

Mitchell, A. S., Czajkowski, R., Zhang, N., Jeffery, K., and Nelson, A. J. D. (2018). Retrosplenial cortex and its role in spatial cognition. *Brain Neurosci. Adv.* 2:2398212818757098. doi: 10.1177/2398212818757098

Montagne, A., Barnes, S. R., Sweeney, M. D., Halliday, M. R., Sagare, A. P., Zhao, Z., et al. (2015). Blood-brain barrier breakdown in the aging human hippocampus. *Neuron* 85, 296–302. doi: 10.1016/j.neuron.2014.12.032

Nasrallah, F. A., To, X. V., Chen, D. Y., Routtenberg, A., and Chuang, K. H. (2016). Resting state functional connectivity data supports detection of cognition in the rodent brain. *Data Brief* 7, 1156–1164. doi: 10.1016/j.dib.2016.03.041

Nie, B., Chen, K., Zhao, S., Liu, J., Gu, X., Yao, Q., et al. (2013). A rat brain MRI template with digital stereotaxic atlas of fine anatomical delineations in paxinos space and its automated application in voxel-wise analysis. *Hum. Brain. Mapp.* 34, 1306–1318. doi: 10.1002/hbm.21511

Nie, B., Liu, H., Chen, K., Jiang, X., and Shan, B. (2014). A statistical parametric mapping toolbox used for voxel-wise analysis of FDG-PET images of rat brain. *PLoS ONE* 9:e108295. doi: 10.1371/journal.pone.0108295

Paasonen, J., Stenroos, P., Salo, R. A., Kiviniemi, V., and Grohn, O. (2018). Functional connectivity under six anesthesia protocols and the awake condition in rat brain. *NeuroImage* 172, 9–20. doi: 10.1016/j.neuroimage.2018.01.014

Park, J., Min, J. S., Kim, B., Chae, U. B., Yun, J. W., Choi, M. S., et al. (2015). Mitochondrial ROS govern the LPS-induced pro-inflammatory response in microglia cells by regulating MAPK and NF-kappaB pathways. *Neurosci. Lett.* 584, 191–196. doi: 10.1016/j.neulet.2014.10.016

Passamonti, L., Tsvetanov, K. A., Jones, P. S., Bevan-Jones, W. R., Arnold, R., Borchert, R. J., et al. (2019). Neuroinflammation and functional connectivity in Alzheimer's disease: interactive influences on cognitive performance. *J. Neurosci.* 39, 7218–7226. doi: 10.1523/JNEUROSCI.2574-18.2019

Pham, L., Wright, D. K., O'Brien, W. T., Bain, J., Huang, C., Sun, M., et al. (2021). Behavioral, axonal, and proteomic alterations following repeated mild traumatic brain injury: novel insights using a clinically relevant rat model. *Neurobiol. Dis.* 148:105151. doi: 10.1016/j.nbd.2020.105151

Qian, W., Fischer, C. E., Churchill, N. W., Kumar, S., Rajji, T., and Schweizer, T. A. (2019). Delusions in Alzheimer disease are associated with decreased default mode network functional connectivity. *Am. J. Geriatr. Psychiatry* 27, 1060–1068. doi: 10.1016/j.jagp.2019.03.020

Raichle, M. E. (2015). The brain's default mode network. *Annu. Rev. Neurosci.* 38, 433–447. doi: 10.1146/annurev-neuro-071013-014030

Santello, M., Toni, N., and Volterra, A. (2019). Astrocyte function from information processing to cognition and cognitive impairment. *Nat. Neurosci.* 22, 154–166. doi: 10.1038/s41593-018-0325-8

Schwalm, M. T., Pasquali, M., Miguel, S. P., Dos Santos, J. P., Vuolo, F., Comim, C. M., et al. (2014). Acute brain inflammation and oxidative damage are related to long-term cognitive deficits and markers of neurodegeneration in sepsis-survivor rats. *Mol. Neurobiol.* 49, 380–385. doi: 10.1007/s12035-013-8526-3

Shine, J. M., Breakspear, M., Bell, P. T., Ehgoetz Martens, K. A., Shine, R., Koyejo, O., et al. (2019). Human cognition involves the dynamic integration of neural activity and neuromodulatory systems. *Nat. Neurosci.* 22, 289–296. doi: 10.1038/s41593-018-0312-0

Spellman, T., Rigotti, M., Ahmari, S. E., Fusi, S., Gogos, J. A., and Gordon, J. A. (2015). Hippocampal-prefrontal input supports spatial encoding in working memory. *Nature* 522, 309–314. doi: 10.1038/nature14445

Sperling, R. A., Aisen, P. S., Beckett, L. A., Bennett, D. A., Craft, S., Fagan, A. M., et al. (2011). Toward defining the preclinical stages of Alzheimer's disease: recommendations from the National Institute on Aging-Alzheimer's Association workgroups on diagnostic guidelines for Alzheimer's disease. *Alzheimers Dement.* 7, 280–292. doi: 10.1016/j.jalz.2011.03.003

Subramaniyan, S., and Terrando, N. (2019). Neuroinflammation and perioperative neurocognitive disorders. *Anesth. Analg.* 128, 781–788. doi: 10.1213/ANE.0000000000004053

Teipel, S., Drzezga, A., Grothe, M. J., Barthel, H., Chételat, G., Schuff, N., et al. (2015). Multimodal imaging in Alzheimer's disease: validity and usefulness for early detection. *Lancet Neurol.* 14, 1037–1053. doi: 10.1016/S1474-4422(15)00093-9

Valles, A., Marti, O., Harbuz, M. S., and Armario, A. (2002). A single lipopolysaccharide administration is sufficient to induce a long-term desensitization of the hypothalamic-pituitary-adrenal axis. *Neuroscience* 112, 383–389. doi: 10.1016/S0306-4522(02)00047-7

Vorhees, C. V., and Williams, M. T. (2006). Morris water maze: procedures for assessing spatial and related forms of learning and memory. *Nat. Protoc.* 1, 848–858. doi: 10.1038/nprot.2006.116

Wang, J., Zuo, X., and He, Y. (2010). Graph-based network analysis of resting-state functional MRI. *Front. Syst. Neurosci.* 4:16. doi: 10.3389/fnsys.2010.00016

Wang, L., Almeida, L. E. F., de Souza Batista, C. M., Khaibullina, A., Xu, N., Albani, S., et al. (2016). Cognitive and behavior deficits in sickle cell mice are associated with profound neuropathologic changes in hippocampus and cerebellum. *Neurobiol. Dis.* 85, 60–72. doi: 10.1016/j.nbd.2015.10.004

Wu, J., Hao, S., Sun, X. R., Zhang, H., Li, H., Zhao, H., et al. (2017), Elamipretide (SS-31) ameliorates isoflurane-induced long-term impairments of mitochondrial morphogenesis and cognition in developing rats. *Front. Cell. Neurosci.* 11:119. doi: 10.3389/fncel.2017.00119

Wu, J., Zhang, M., Li, H., Sun, X., Hao, S., Ji, M., et al. (2016). BDNF pathway is involved in the protective effects of SS-31 on isoflurane-induced cognitive deficits in aging mice. *Behav. Brain Res.* 305, 115–121. doi: 10.1016/j.bbr.2016.02.036

Wyss, J. M., and Van Groen, T. (1991). Connections between the retrosplenial cortex and the hippocampal formation in the rat a review. *Hippocampus* 2, 1–11. doi: 10.1002/hipo.450020102

Yan, J., Jiang, J., He, L., and Chen, L. (2020). Mitochondrial superoxide/hydrogen peroxide: An emerging therapeutic target for metabolic diseases. *Free Rad. Biol. Med.* 152, 33–42. doi: 10.1016/j.freeradbiomed.2020.02.029

Zhang, M., Zhang, Y. H., Fu, H. Q., Zhang, Q. M., and Wang, T. L. (2018). Ulinastatin may significantly improve postoperative cognitive function of

elderly patients undergoing spinal surgery by reducing the translocation of lipopolysaccharide and systemic inflammation. *Front. Pharmacol.* 9:1007. doi: 10.3389/fphar.2018.01007

Zhang, S., Wang, X., Ai, S., Ouyang, W., Le, Y., and Tong, J. (2017). Sepsis-induced selective loss of NMDA receptors modulates hippocampal neuropathology in surviving septic mice. *PLoS ONE* 12:e0188273. doi: 10.1371/journal.pone.0188273

Zhang, Y., Xu, H., Zhang, F., Shao, F., Ellenbroek, B., Wang, J., et al. (2019). Deficiencies of microglia and TNFα in the mPFC-mediated cognitive inflexibility induced by social stress during adolescence. *Brain Behav. Immun.* 79, 256–266. doi: 10.1016/j.bbi.2019.02.010

Zhao, W., Xu, Z., Cao, J., Fu, Q., Wu, Y., Zhang, X., et al. (2019). Elamipretide (SS-31) improves mitochondrial dysfunction, synaptic and memory impairment induced by lipopolysaccharide in mice. *J. Neuroinflammation* 16:230. doi: 10.1186/s12974-019-1627-9

Conflict of Interest: The authors declare that the research was conducted in the absence of any commercial or financial relationships that could be construed as a potential conflict of interest.

frontiers in Neuroscience

GENERAL COMMENTARY
published: 23 March 2021
doi: 10.3389/fnins.2021.645694

Commentary: Urinary Neopterin, a New Marker of the Neuroinflammatory Status in Amyotrophic Lateral Sclerosis

Gisele Espíndola[1,2,3], *Débora da Luz Scheffer*[1] and *Alexandra Latini*[1]*

[1] Laboratório de Bioenergética e Estresse Oxidativo, Departamento de Bioquímica, Centro de Ciências Biológicas, Universidade Federal de Santa Catarina, Florianópolis, Brazil, [2] Ambulatório de Doenças Neuromusculares e Neurogenéticas Hospital Universitário Polydoro Ernani de São Thiago, Universidade Federal de Santa Catarina, Florianópolis, Brazil, [3] Programa de Pós-Graduação em Ciências Médicas, Universidade Federal de Santa Catarina, Florianópolis, Brazil

Keywords: inflammation, biomarkers, neurodegenerative diseases, amyotrophic lateral sclerosis, urine

A Commentary on

Urinary neopterin, a new marker of the neuroinflammatory status in amyotrophic lateral sclerosis

by Lunetta, C., Lizio, A., Gerardi, F., Tarlarini, C., Filippi, M., Riva, N., et al. (2020). J. Neurol. 267, 3609–3616. doi: 10.1007/s00415-020-10047-7

OPEN ACCESS

Edited by:
Xian-Le Bu,
Third Military Medical University, China

Reviewed by:
Sumru Savas,
Ege University, Turkey
Dietmar Fuchs,
Innsbruck Medical University, Austria

***Correspondence:**
Alexandra Latini
alatinilabox@gmail.com

Specialty section:
This article was submitted to Neurodegeneration, a section of the journal Frontiers in Neuroscience

Received: *23 December 2020*
Accepted: *11 February 2021*
Published: *23 March 2021*

Citation:
Espíndola G, Scheffer DL and Latini A (2021) Commentary: Urinary Neopterin, a New Marker of the Neuroinflammatory Status in Amyotrophic Lateral Sclerosis. Front. Neurosci. 15:645694. doi: 10.3389/fnins.2021.645694

Amyotrophic lateral sclerosis (ALS) is a heterogeneous progressive neurodegenerative disorder characterized by weakness and muscle atrophy in different areas of the body. The diagnosis is based on (i) the presence of signs of impairment of the lower and upper motor neurons in the cerebral motor cortex, brainstem, and spinal cord, (ii) electrophysiological evidence for chronic neurogenic changes, and on (iii) the exclusion of other diagnostic possibilities (Brooks, 1994; de Carvalho et al., 2008). The physiopathology of the disease is still not completely defined; however, chronic neuroinflammation is a hallmark of ALS (Takeda et al., 2020). So far, there is no cure or effective treatment for ALS and the lack of reliable biomarkers in peripheral biological fluids compromises the monitoring of the progression of the disease.

Lunetta et al. in an elegant work evaluated whether urinary neopterin levels could be used as a surrogate marker to predict the neuroinflammatory status of ALS (Lunetta et al., 2020). The authors found a negative association between the severity of the disease and urinary neopterin concentrations, claiming that those levels would represent the degree of inflammation in the nervous system of ALS patients. Indeed, neopterin levels have been used as a sensitive marker of immune system activation for decades (for a review see Ghisoni et al., 2015b). Neopterin is a byproduct of tetrahydrobiopterin (BH4) metabolism, which is stimulated under inflammation to generate more BH4 and enhance nitric oxide synthesis, catecholaminergic neurotransmitters production, and the metabolism of ether lipids (for a review see Ghisoni et al., 2015b). As stated by the authors, it has been traditionally understood that neopterin is formed and secreted by immune cells upon stimulation by inflammatory mediators, namely interferon gamma (IFN-γ) and interleukin 1 beta, hydrogen peroxide, and others (for a review see Ghisoni et al., 2015b); compounds known to be increased in the biological fluids of patients affected by ALS (Vu and Bowser, 2017; Jin et al., 2020).

Believed for decades to be an inert metabolic byproduct, the functional role and the origin of neopterin in the human nervous system are still not fully understood. The evidence available in the literature suggested that neopterin crosses the blood-brain barrier (BBB), and therefore, neopterin

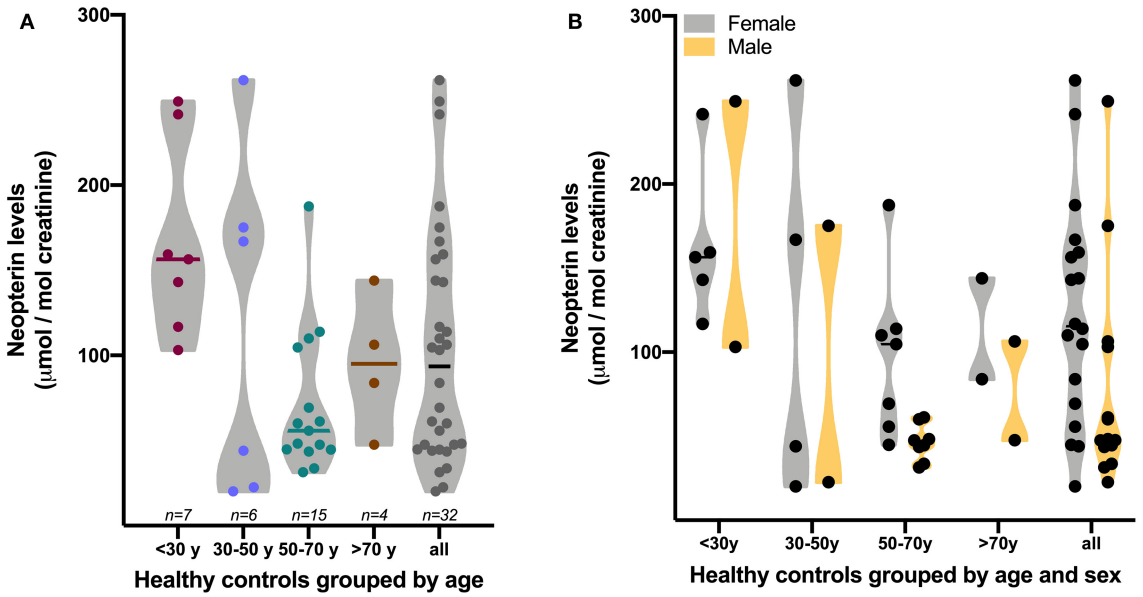

FIGURE 1 | Levels of neopterin in the urine of healthy controls grouped by age **(A)** or age and sex **(B)**. Neopterin levels were assessed in urine samples collected in the morning with a minimum of 2 h retention in a collector plastic cup. Neopterin quantification was performed by liquid chromatography coupled with fluorescent detection as previously reported by our group (Scheffer et al., 2019). Graph was generated with GraphPad Software version 9.

cerebrospinal fluid (CSF) levels might reflect peripheral neopterin concentrations (Fuchs et al., 1989). However, this process would occur at a very low quotient (1/40) (Hagberg et al., 1993), suggesting that CSF neopterin might have a local origin and be independently synthesized in the nervous system. This is supported by the lack of correlation between CSF and blood neopterin concentrations in patients with neurological-neuroinflammatory chronic conditions with normal BBB function (Kuehne et al., 2013). Additionally, our group recently demonstrated that neopterin is secreted by primary human brain cells, neurons, astrocytes and microglia, after being challenged with lipopolysaccharide or IFN-γ, supporting that neopterin CSF levels represent the central production of the compound (de Paula Martins et al., 2018). We also showed in experimental studies that intracellular neopterin has cytoprotective and memory enhancing effects mainly by activating *NRF-2*, the master regulator of cellular anti-oxidative responses (Moi et al., 1994; Itoh et al., 1999). The demonstrated capacity of neopterin to enhance the activity of the antioxidant system and the mitochondrial function to favor the anti-inflammatory facet of the immune system, and to facilitate the triggering of long-term potentiation–a molecular mechanism involved in hippocampal memory formation–allowed us to propose that neopterin is an endogenous cytoprotective compound with the specific role of increasing cellular resistance against stress; e.g., during chronic inflammatory conditions (Ghisoni et al., 2015a,b, 2016). This new data support that intracellular neopterin in non-immune cells is associated with cytoprotective functions, while increased levels of neopterin in peripheral fluids would likely represent the degree of inflammation. Therefore, the peripheral levels of this pterin might not necessarily reflect the local nervous system inflammatory status–that would require increased BBB permeability - but might instead reflect the degree of systemic activation of the inflammatory response.

It is widely understood that biomarkers are necessary for the development, testing, and ongoing positioning of new drugs and also for monitoring the evolution of a disease (*fda.org*). In this context, the quantification of neopterin levels in the urine has the potential value of revealing the degree of systemic inflammation. Indeed, Lunetta et al. showed a positive correlation between urinary neopterin levels and C-reactive protein concentrations (although not stated in Lunetta et al., 2020) it is assumed the levels were assessed in the blood). However, according to the box-plot shown in Lunetta's **Figure 1** (Lunetta et al., 2020), 75% of ALS urinary samples shared similar levels of neopterin with the healthy control group, which compromise the use of urinary neopterin as a surrogate marker of the degree of neuroinflammation in this condition. Additionally, levels of urinary neopterin are more prone to show higher variability than in plasma, since they are shaped by age, retention time at the moment of sample collection, and others factors (Kampmann and Hansen, 1981). Although the sample size is small, **Figure 1** shows the greatest variability of neopterin levels in the urine in young healthy adults, an age-group not included in Lunetta's work (Lunetta et al., 2020).

Finally, Lunetta's work was a pioneer in demonstrating that systemic inflammation can be followed in urine samples of ALS-affected individuals. In addition, the authors stressed that this measurement might become a useful surrogate

endpoint for classifying ALS candidates for future drugs aimed at intervening in the chronically exacerbated inflammatory response characteristics of ALS.

AUTHOR CONTRIBUTIONS

Material preparation and data collection were performed by GE and AL. The biochemical analyses were performed by DS. The first draft of the manuscript was written by AL. All authors contributed to the study conception and design, read, and approved the final manuscript.

FUNDING

This work was supported by CAPES/PROAP (Coordenação de Aperfeiçoamento de Pessoal de Nível Superior/Programa de Apóio à Pós-Graduação, Brazil). AL was a CNPq (Conselho Nacional de Desenvolvimento Científico e Tecnológico, Brazil) fellow.

ACKNOWLEDGMENTS

The authors are grateful to Theodore Griswold for language editing.

REFERENCES

Brooks, B. R. (1994). El escorial World Federation of Neurology criteria for the diagnosis of amyotrophic lateral sclerosis. *J. Neurol. Sci.* 124, 96–107. doi: 10.1016/0022-510X(94)90191-0

de Carvalho, M., Dengler, R., Eisen, A., England, J. D., Kaji, R., Kimura, J., et al. (2008). Electrodiagnostic criteria for diagnosis of ALS. *Clin. Neurophysiol.* 119, 497–503. doi: 10.1016/j.clinph.2007.09.143

de Paula Martins, R., Ghisoni, K., Lim, C. K., Aguiar, A. S., Guillemin, G. J., Latini, A., et al. (2018). Neopterin preconditioning prevents inflammasome activation in mammalian astrocytes. *Free Radic. Biol. Med.* 115, 371–382. doi: 10.1016/j.freeradbiomed.2017.11.022

Fuchs, D., Chiodi, F., Albert, J., Asjö, B., Hagberg, L., Hausen, A., et al. (1989). Neopterin concentrations in cerebrospinal fluid and serum of individuals infected with HIV-1. *Aids* 3, 285–288. doi: 10.1097/00002030-198905000-00006

Ghisoni, K., Aguiar, A. S., de Oliveira, P. A., Matheus, F. C., Gabach, L., Perez, M., et al. (2016). Neopterin acts as an endogenous cognitive enhancer. *Brain. Behav. Immun.* 56, 156–164. doi: 10.1016/j.bbi.2016.02.019

Ghisoni, K., de Martins, R. D. P. R., Barbeito, L., and Latini, A. (2015b). Neopterin as a potential cytoprotective brain molecule. *J. Psychiatr. Res.* 71, 134–139. doi: 10.1016/j.jpsychires.2015.10.003

Ghisoni, K., Latini, A., Kuehne, L. K., Reiber, H., Bechter, K., Hagberg, L., et al. (2015a). Cerebrospinal fluid neopterin is brain-derived and not associated with blood-CSF barrier dysfunction in non-inflammatory affective and schizophrenic spectrum disorders. Letter to the Editor. *J. Psychiatr. Res.* 63, 141–142. doi: 10.1016/j.jpsychires.2015.02.002

Hagberg, L., Dotevall, L., Norkrans, G., Larsson, M., Wachter, H., and Fuchs, D. (1993). Cerebrospinal fluid neopterin concentrations in central nervous system infection. *J. Infect. Dis.* 168, 1285–1288. doi: 10.1093/infdis/168.5.1285

Itoh, K., Wakabayashi, N., Katoh, Y., Ishii, T., Igarashi, K., Engel, J. D., et al. (1999). Keap1 represses nuclear activation of antioxidant responsive elements by Nrf2 through binding to the amino-terminal Neh2 domain. *Genes Dev.* 13, 76–86. doi: 10.1101/gad.13.1.76

Jin, M., Günther, R., Akgün, K., Hermann, A., and Ziemssen, T. (2020). Peripheral proinflammatory Th1/Th17 immune cell shift is linked to disease severity in amyotrophic lateral sclerosis. *Sci. Rep.* 10:5941. doi: 10.1038/s41598-020-62756-8

Kampmann, J., and Hansen, J. (1981). Glomerular filtration rate and creatinine clearance. *Br. J. Clin. Pharmacol.* 12, 7–14. doi: 10.1111/j.1365-2125.1981.tb01848.x

Kuehne, L. K., Reiber, H., Bechter, K., Hagberg, L., and Fuchs, D. (2013). Cerebrospinal fluid neopterin is brain-derived and not associated with blood-CSF barrier dysfunction in non-inflammatory affective and schizophrenic spectrum disorders. *J. Psychiatr. Res.* 47, 1417–1422. doi: 10.1016/j.jpsychires.2013.05.027

Lunetta, C., Lizio, A., Gerardi, F., Tarlarini, C., Filippi, M., Riva, N., et al. (2020). Urinary neopterin, a new marker of the neuroinflammatory status in amyotrophic lateral sclerosis. *J. Neurol.* 267, 3609–3616. doi: 10.1007/s00415-020-10047-7

Moi, P., Chan, K., Asunis, I., Cao, A., and Kan, Y. W. (1994). Isolation of NF-E2-related factor 2 (Nrf2), a NF-E2-like basic leucine zipper transcriptional activator that binds to the tandem NF-E2/AP1 repeat of the beta-globin locus control region. *Proc. Natl. Acad. Sci. U.S.A.* 91, 9926–9930. doi: 10.1073/pnas.91.21.9926

Scheffer, D., da, L. D. D. L., Ghisoni, K., Aguiar, A. S. A. S., and Latini, A. (2019). Moderate running exercise prevents excessive immune system activation. *Physiol. Behav.* 204, 248–255. doi: 10.1016/j.physbeh.2019.02.023

Takeda, T., Kitagawa, K., and Arai, K. (2020). Phenotypic variability and its pathological basis in amyotrophic lateral sclerosis. *Neuropathology* 40, 40–56. doi: 10.1111/neup.12606

Vu, L. T., and Bowser, R. (2017). Fluid-based biomarkers for amyotrophic lateral sclerosis. *Neurotherapeutics* 14, 119–134. doi: 10.1007/s13311-016-0503-x

Conflict of Interest: The authors declare that the research was conducted in the absence of any commercial or financial relationships that could be construed as a potential conflict of interest.

frontiers in Aging Neuroscience

ORIGINAL RESEARCH
published: 19 May 2021
doi: 10.3389/fnagi.2021.655667

White Matter Integrity Involvement in the Preclinical Stage of Familial Creutzfeldt–Jakob Disease: A Diffusion Tensor Imaging Study

*Donglai Jing[1,2†], Yaojing Chen[3†], Kexin Xie[1†], Yue Cui[1], Chunlei Cui[4], Li Liu[1], Hui Lu[1], Jing Ye[1], Ran Gao[1], Lin Wang[1], Zhigang Liang[4], Zhanjun Zhang[3] and Liyong Wu[1]**

[1] Department of Neurology, Xuanwu Hospital, Capital Medical University, Beijing, China, [2] Department of Neurology, Rongcheng People's Hospital, Hebei, China, [3] State Key Laboratory of Cognitive Neuroscience and Learning, Beijing Normal University, Beijing, China, [4] Department of Nuclear Medicine, Xuanwu Hospital, Capital Medical University, Beijing, China

Objective: The objective of the study was to explore patterns of white matter (WM) alteration in preclinical stage familial Creutzfeldt–Jakob disease (fCJD) using diffusion tensor imaging (DTI).

Methods: Seven asymptomatic carriers of the *PRNP* G114V mutation and six non-carriers were recruited from the same fCJD kindred and follow-up obtained from all asymptomatic carriers and two non-carriers 2 years later. Overlapping WM patterns were also explored in asymptomatic carriers and symptomatic CJD patients. All participants underwent clinical and neuropsychological assessments and DTI at baseline and follow-up. DTI data were subjected to whole-brain voxel-wise analysis of fractional anisotropy (FA) and mean diffusivity (MD) in WM using tract-based spatial statistics. Three comparisons were conducted: baseline carriers against non-carriers (baseline analysis), changes after 2 years in carriers (follow-up analysis), and differences between patients with symptomatic CJD and healthy controls (CJD patient analysis).

Results: Neither carriers nor non-carriers developed any neurological symptoms during 2 years of follow-up. Baseline analysis showed no differences between the carrier and non-carrier groups in MD and FA. Follow-up analysis showed significantly increased MD in multiple WM tracts, among which increased MD in the bilateral superior longitudinal fasciculus, bilateral anterior thalamic radiation, bilateral cingulate gyrus, and left uncinate fasciculus overlapped the patterns observed in patients with symptomatic CJD.

Conclusion: Changes in integrity within multiple WM tracts can be detected during the preclinical stage of fCJD.

Keywords: Creutzfeldt–Jakob disease, preclinical stage, diffusion tensor imaging, tract-based spatial statistics, white matter

OPEN ACCESS

Edited by:
Deng-Feng Zhang, Key Laboratory of Animal Models and Human Disease Mechanisms, Kunming Institute of Zoology (CAS), China

Reviewed by:
Jiu Chen, Nanjing Medical University, China
Maurizio Pocchiari, National Institute of Health (ISS), Italy

****Correspondence:***
Liyong Wu
wmywly@hotmail.com

† These authors have contributed equally to this work and share first authorship

Received: *19 January 2021*
Accepted: *06 April 2021*
Published: *19 May 2021*

Citation:
Jing D, Chen Y, Xie K, Cui Y, Cui C, Liu L, Lu H, Ye J, Gao R, Wang L, Liang Z, Zhang Z and Wu L (2021) White Matter Integrity Involvement in the Preclinical Stage of Familial Creutzfeldt–Jakob Disease: A Diffusion Tensor Imaging Study. Front. Aging Neurosci. 13:655667. doi: 10.3389/fnagi.2021.655667

Abbreviations: WM, white matter; DTI, diffusion tensor imaging; CJD, Creutzfeldt-Jakob disease; fCJD, familial Creutzfeldt-Jakob disease; sCJD, sporadic Creutzfeldt–Jakob disease; PRNP, prion protein gene; EEG, electroencephalogram; TBSS, Tract based spatial statistics; FA, fractional anisotropy; MD, mean diffusivity; MMSE, Mini Mental State Examination; MoCA, Montreal Cognitive Assessment; CDR, Clinical Dementia Rating; NPI-Q, neuropsychiatric inventory questionnaire; FWE, family-wise error; MR, magnetic resonance; FSL, FMRIB Software Library; GLM, general linear model; EYO, Estimated years from expected symptom onset.

INTRODUCTION

Creutzfeldt–Jakob disease (CJD) is a rare, fatal neurodegenerative disorder characterized by rapidly progressive dementia, motion disturbances, and akinetic mutism. Familial CJD (fCJD), which is caused by mutations in the prion protein gene, *PRNP*, and sporadic CJD (sCJD) are two major forms of CJD that share similar pathophysiological features (Jeong and Kim, 2014). Given the completely dominant and fully penetrant inheritance pattern of fCJD (Takada and Geschwind, 2013), asymptomatic *PRNP* mutation carriers provide an ideal preclinical model for research, while non-carriers from the same kindred represent the best control group for exploring the disease process. By investigating asymptomatic carriers and patients, previous studies have identified structural and metabolic alterations in individuals with both preclinical and symptomatic CJD.

Diffusion tensor imaging (DTI) is a non-invasive MRI technique that can determine the orientation and integrity of white matter (WM) fibers *in vivo* and has been widely used to show WM changes in the early stages of CJD. Previous DTI studies in CJD cases have demonstrated mean diffusivity (MD) changes in multiple WM tracts (Lee et al., 2012; Wang et al., 2013). A pathological study including 26 patients with CJD applying DTI and post-mortem analysis demonstrated reduced MD and reactive astrocytic gliosis in WM, suggesting WM pathological involvement in symptomatic CJD (Caverzasi et al., 2014b); however, there has been little research investigating WM integrity in the preclinical stage of CJD, although gray matter involvement has been proven (Lee et al., 2009). An FDG-PET study conducted by our research group revealed hypometabolism in the parietal and temporal lobes of the same individual with preclinical CJD (Lu et al., 2020), suggesting that metabolic changes may occur at least 10 years before the estimated onset of clinical symptoms. Therefore, further observations of changes in WM in preclinical CJD are of great significance in studying CJD pathogenesis, as such changes may jointly contribute to disease onset, along with alterations in gray matter.

To investigate changes in WM, we conducted a prospective DTI study in asymptomatic carriers and non-carriers of the *PRNP* G114V mutation from the same fCJD kindred, which were the same individuals as those included in our previous FDG-PET study (Lu et al., 2020). The purpose of the current study was to investigate the patterns of WM changes in the brains of individuals with preclinical CJD.

MATERIALS AND METHODS

Ethics Statement

The study protocols outlined in this manuscript were approved by the Ethics Committee and local Institutional Review Board of Xuanwu Hospital, Capital Medical University, Beijing. All methods and experiments were performed following the relevant guidelines and regulations. All participants enrolled in the study or their guardians signed an informed written consent giving specific approval for this study before the study commenced.

Participants

Data used in this study were from a Chinese Han fCJD kindred with a G114V mutation in *PRNP*, which has been followed since 2008. Post-mortem analysis was performed in the proband, confirming the diagnosis of CJD (Ye et al., 2008). Details of the clinical findings and genetic analysis of this family have already been published in our FDG-PET study (Liu et al., 2010). Thirteen asymptomatic family members aged > 18 years and one of whose parents was an fCJD patient or G114V mutation carrier were enrolled. Asymptomatic participants were defined as those who did not report any neurological complaints and were normal on neurological examination. Detailed exclusion criteria are provided in our previous FDG-PET study (Lu et al., 2020). Participants were divided into two groups: seven asymptomatic carriers of the *PRNP* V mutation and six non-carriers. All participants underwent clinical examination, neuropsychological assessment, electroencephalogram (EEG) testing, and DTI at baseline. All evaluations were double blind to the genotypes (i.e., neither physicians examining participants nor the participants themselves were aware of their gene mutation status).

Follow-up evaluation was carried out a mean of 2 years after the baseline interview in seven carriers and two non-carriers, and consisted of in-depth clinical examination, neuropsychological assessment, EEG testing, and DTI. Follow-up was not obtained for five non-carriers due to refusal to participate further in the study. All carriers and non-carriers for whom follow-up was obtained had received no treatment for cognitive impairment or neurological symptoms in the previous 2 years.

For comparison with the subset of carriers and non-carriers who were followed-up, from 2018 to 2019, 10 patients with symptomatic CJD who were not from the *PRNP* G114V fCJD kindred were enrolled from the clinic at Xuanwu Hospital, along with age-, and sex-matched healthy controls enrolled from the community. All patients with symptomatic CJD were diagnosed according to the European probable CJD criteria (Zerr et al., 2009). The exclusion criteria were as follows: (1) presence of other causes of cognitive impairment, including small vessel disease, stroke, infection, autoimmune diseases, metabolic diseases, and neurodegenerative diseases other than CJD; (2) incapable of cooperation; (3) history of traumatic brain injury; (4) history of psychosis or congenital mental growth retardation; or (5) contradiction for MRI. Controls were recruited if they had cognitive symptoms, normal general cognitive functioning, and no active neurological or psychiatric disease. The exclusion criteria for healthy controls were the same as those for asymptomatic family members (described above).

Neurological Assessments

All participants received standardized clinical and cognitive assessments including Mini Mental State Examination (MMSE), Montreal Cognitive Assessment (MoCA), Clinical Dementia Rating (CDR), and neuropsychiatric inventory questionnaire assessments (NPI-Q). Clinicians who performed the assessments were unaware of the mutation status of participants.

Genetic Analysis for *PRNP* Gene Mutation

Venous blood samples (5 ml) were collected from 10 patients with symptomatic CJD in EDTA anticoagulant vessels and stored at -20°C. A blood extraction kit was used to extract blood DNA. DNA concentration and purity were determined using a NanoDrop2000. Specific primers were used to amplify DNA fragments in the region of the mutation site. Reaction system: 2 × Phanta Max Buffer 12.5 μl, Phanta Max Super-Fidelity DNA Polymerase (1 U/μl) 0.5 μl, dNTP Mix (10 mM each) 0.5 μl, Primer-F (10 μM) 1 μl, Primer-R (10 μM) 1 μl, DNA 1 μl, and water to 25 μl. Reaction procedure: 95°C denaturation 5 min; 95°C denaturation for 30 s, 65°C annealing for 30 s, 72°C extension for 30 s, 25 cycles, each cycle reduced by 0.6; 95°C denaturation for 30 s, 50°C annealing for 30 s, 72°C extension for 1 min, 20 cycles; 72°C extension 10 min. After PCR, 3 μl aliquots of products were analyzed by 2.5% agarose gel electrophoresis, and PCR products were also sequenced using an ABI 3730XL DNA Analyzer.

Electroencephalogram

All participants received a 2-h EEG at baseline and follow-up using 18-lead electroencephalographic transducers (Micromed, Italy). Electrodes were placed according to the international standard 10–20 system. Conventional single lead, double lead, and sphenoid lead were traced. Eyes closed and deep breathing experiments were performed.

MRI Acquisition and Imaging Parameters

Magnetic resonance (MR) scanning was performed on a GE Signa PET/MR 3.0 Tesla scanner (GE Healthcare, Milwaukee, WI, United States) in Xuanwu Hospital, Capital Medical University. All 13 asymptomatic family members received their first PET/MR scans in March 2017. Nine of them received follow-up scans in March 2019. All 10 patients with symptomatic CJD received their scans on the same scanner during their hospital stays from 2018 to 2020. DTI data were acquired using a spin echo-echo planar imaging sequence (TR/TE = 16,500/97.6 m) with a *b*-value of 1,000 s/mm^2, applying diffusion gradients along 30 directions. Seventy axial slices, with no slice gap, were acquired (FOV = 220 × 220 mm^2, matrix = 112 × 112, slice thickness = 2 mm, and number of excitations = 1).

Diffusion Tensor Imaging Processing

Diffusion tensor imaging data were preprocessed using the PANDA software package (a pipeline tool for analyzing brain diffusion images, PANDA; http://www.nitrc.org/projects/panda/), which was independently developed by the state key laboratory of cognitive neuroscience and learning of Beijing Normal University. Briefly, preprocessing involved correction of eddy current and head movement, creating a brain mask, and fitting the diffusion tensor model. Outputs were voxel-wise maps of fractional anisotropy (FA) and mean diffusivity (MD). The FA index of DTI is a sensitive neuroimaging measure of degeneration and describes overall WM health, maturation, and organization. MD is another index representing the average dispersion level and dispersion resistance of water molecules overall, which can reflect changes in brain tissue. Higher MD values indicate more free water molecules in the tissue, which influence the information transmission speed to some extent.

Tract-Based Spatial Statistics Analysis

Tract-based spatial statistics (TBSS) analysis was performed to explore the influence of CJD pathology on WM integrity. In TBSS, all participant FA and MD data were projected onto a mean FA tract skeleton before applying voxel-wise cross-participant statistics. Voxel-wise statistical analyses were conducted using a non-parametric permutation-based inference tool ["randomize," part of FMRIB Software Library (FSL)] with the general linear model for statistical modeling. Paired *t*-tests, based on voxels, were used for comparisons between carriers at baseline versus follow-up. Student *t*-tests, based on voxels, were used for comparisons between carriers versus non-carriers at baseline, and CJD patients versus healthy controls. The DTI parameters at each voxel were modeled as linear combinations of predictors (five grouping variables) and covariates (age and sex), which were stored in the columns of a "design matrix"; significance thresholds were set at family-wise error (FWE) corrected $P < 0.05$ using the threshold-free cluster enhancement option.

Statistical Analysis

In this study, SPSS 23.0 software was used to evaluate statistical significance. Differences in age, education, and cognitive scores were assessed using the Student's *t*-test. Sex differences were assessed using the Chi-square test. Results were considered statistically significant at $p < 0.05$.

Estimated years from expected symptom onset (EYO) values were calculated as the age of the participant at the time of assessment in this study minus the age of the parent at symptom onset; if the parent of the participant had not developed CJD symptoms, the age of the grandparent was used to calculate EYO. For example, if the participant was 35 years old, and the parent's age at onset was 45 years, then the EYO value would be 10. Parental age at onset was determined using a semi-structured interview in which family members were asked about the age of first progressive cognitive decline.

RESULTS

General Characteristics of Study Participants

Asymptomatic family members (n = 13) were recruited from the same kindred [the same participants were reported in our previous FDG-PET study (Lu et al., 2020)]. A detailed family tree was published in the report of the FDG-PET and is provided in **Supplementary Figure 1** (Lu et al., 2020). In this kindred, nine family members (four males and five females) have passed away due to CJD. Details of the clinical features and examination results of family members are summarized in **Supplementary Table 1**.

At baseline, seven asymptomatic carriers and six non-carriers from this kindred were examined. Demographic data and

neurological assessment scores are summarized in **Table 1**. There was no significant difference in age, sex, years of education, MMSE score, or MoCA score between the seven asymptomatic carriers and six non-carriers. NPI-Q scores were 0 in all participants. Mean EYO was 13.7 ± 8.4 years in asymptomatic carriers. Details of clinical features and examination results are presented in **Supplementary Table 2**.

All seven carriers and two of the six non-carriers underwent follow-up 2 years after baseline assessment. Neither the carriers nor the non-carriers had developed any neurological symptoms during the 2-year follow-up period. No signs of lesions were detected on EEG or regular MRI. Furthermore, there were no significant differences between baseline and follow-up MMSE and MoCA scores in the seven carriers. NPI-Q and CDR scores were 0 in all participants. Detailed clinical features are shown in **Supplementary Table 2**. Comparisons of the MRI analysis results of asymptomatic carriers at follow-up and baseline are shown in **Supplementary Figure 2**.

Among 10 patients with symptomatic CJD, three were familial cases with *PRNP* E200K mutations, and the other seven patients were sporadic cases with no mutations detected. Demographic data and neurological assessment scores for patients with symptomatic CJD are summarized in **Table 2**. There were no significant differences in age, sex, or years of education between patients with CJD and controls. Details of the clinical features and examination results for the 10 patients with symptomatic CJD are presented in **Supplementary Table 3**. The results of MRI analysis of patients with CJD and healthy controls are shown in **Supplementary Figure 2**.

TABLE 1 | Demographic data of mutation non-carriers and carriers at baseline.

	Non-carriers	Carriers	*p* value
Number of participants	6	7	–
Age (years)	32 ± 8.0	33 ± 10.4	0.77
Sex (male/female)	4/2	2/5	0.29
Years of education	11 ± 3.3	10 ± 2.9	0.80
MMSE	29 ± 1.2	29 ± 0.8	1.00
MoCA	27 ± 2.7	26 ± 5.1	0.77
NPI-Q	0	0	–

Data are presented as mean ± standard deviation.
MMSE, mini-mental state examination; MoCA, Montreal cognitive assessment; and NPI-Q, neuropsychiatric inventory questionnaire.

TABLE 2 | Demographic data of patients with Creutzfeldt–Jacob disease (CJD) and healthy controls.

	CJD patients	Healthy controls	*p* value
Number of participants	10	10	–
Age (years)	61 ± 7.7	56 ± 5.2	0.146
Sex (male/female)	4/6	5/5	0.661
Years of education	10 ± 4.8	11 ± 3.2	0.394
MMSE	4.4 ± 7.5	28 ± 0.8	<0.001
MoCA	1.7 ± 3.9	26 ± 2.7	<0.001
NPI-Q	NA	0	–

Data are presented as mean ± standard deviation.
MMSE, mini-mental state examination; MoCA, Montreal cognitive assessment; NPI-Q, neuropsychiatric inventory questionnaire; and NA, not available.

Group Differences in WM Diffusion Metrics Among the Groups

At baseline, TBSS analysis showed that there was no significant difference in MD and FA between asymptomatic carriers of the *PRNP* G114V mutation and non-carriers (FWE correction, $p < 0.05$). After 2 years, TBSS analysis showed that asymptomatic carriers had increased MD across multiple WM tracts, including the left inferior fronto-occipital fasciculus, left uncinate fasciculus, bilateral anterior thalamic radiation, bilateral cingulate gyrus, bilateral superior longitudinal fasciculus, and bilateral corticospinal tracts (FWE correction, $p < 0.05$; **Figure 1**). No reduced FA was observed in any WM tract.

Furthermore, significant differences were detected between patients with symptomatic CJD and matched controls (FWE correction, $p < 0.05$; **Figure 2**). TBSS analysis showed that patients with CJD had increased MD across multiple WM tracts, including the bilateral cingulate gyrus, forceps major, bilateral anterior thalamic radiation, left uncinate fasciculus, and bilateral superior longitudinal fasciculus. No reduced FA was observed in any WM tracts.

Among WM tracts with increased MD in patients with symptomatic CJD, asymptomatic carriers showed overlapping patterns in the bilateral superior longitudinal fasciculus, bilateral anterior thalamic radiation, cingulate gyrus, and left uncinate

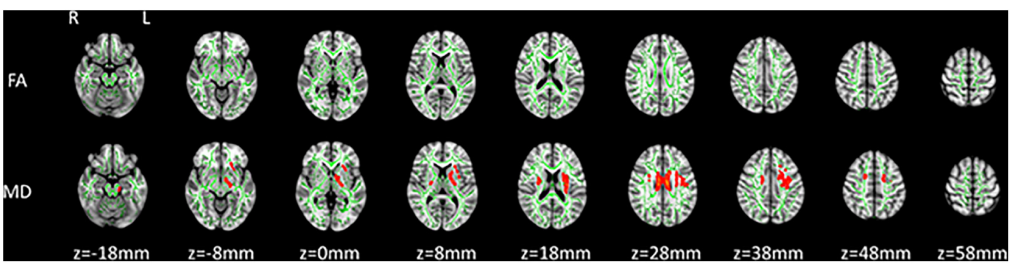

FIGURE 1 | Tract-based spatial statistics (TBSS) analysis of asymptomatic carriers at baseline compared with follow-up. Increased mean diffusivity (MD) was detected by TBSS analysis in asymptomatic prion protein gene (*PRNP*) G114V mutation carriers at follow-up relative to baseline [family-wise error (FWE) correction, $P < 0.05$]. Significant areas of increased MD (red code) in asymptomatic carriers at follow-up relative to baseline are shown with the skeleton (green code).

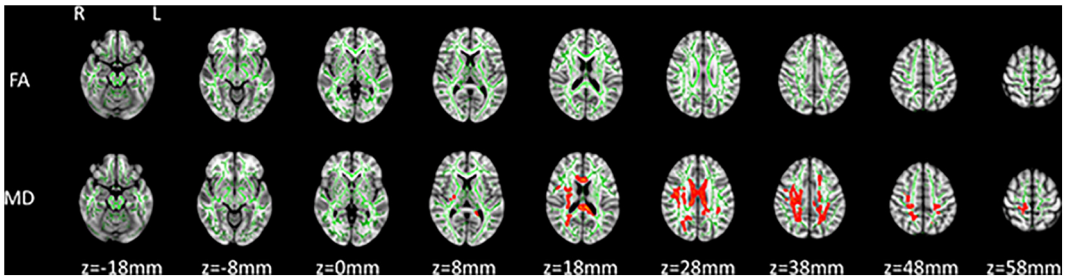

FIGURE 2 | TBSS analysis of symptomatic patients with Creutzfeldt–Jacob disease (CJD) compared with healthy controls. Increased MD was detected in patients with CJD compared with healthy controls (FWE correction, $P < 0.05$). Significant areas of increased MD (red code) in patients with CJD versus healthy controls are shown with the skeleton (green).

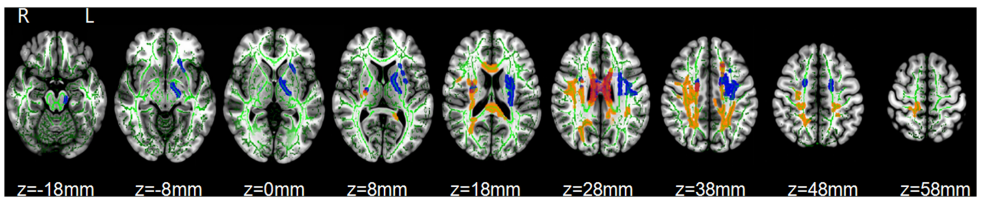

FIGURE 3 | Overlapping patterns of increased MD were found between asymptomatic carriers and patients with CJD. Overlapping areas of increased MD (red code), significant areas of increase MD (blue code) in asymptomatic carriers at follow-up relative to baseline, and significant areas of increased MD (yellow code) in CJD patients versus healthy controls are shown with the skeleton (green code).

fasciculus (**Figure 3**). Details of the observed changes in MD are presented in **Figure 4**.

DISCUSSION

In this prospective study, we applied DTI to detect global WM involvement in asymptomatic *PRNP* G114V mutation carriers. We found that changes in WM were characterized by increased MD, accompanied by FA within the normal range. The observed alterations were mainly focused in several WM tracts in asymptomatic carriers, which included patterns overlapping those of patients with symptomatic CJD. Notably, the changes in WM tracts were also correlated with the gray matter metabolic alterations identified in our previous FDG-PET study. To our knowledge, our findings provide the first description of WM abnormalities in the preclinical stage of fCJD, which, together with the gray matter changes revealed by the FDG-PET study, describe pathological imaging changes occurring during the asymptomatic stage of CJD.

In our study, changes were found at follow-up in multiple WM tracts in asymptomatic carriers. Among the detected changes, those in the bilateral superior longitudinal fasciculus, bilateral anterior thalamic radiation, bilateral cingulate gyrus, and left uncinate fasciculus overlapped the patterns detected in patients with CJD. Previous investigations have also detected WM alterations in similar areas, consistent with our data. A DTI study of 26 patients with CJD found MD changes in WM, including in the uncinate fasciculus, superior longitudinal fasciculus, and anterior thalamic radiation (Caverzasi et al., 2014b). Another study applying DTI in 26 patients with CJD identified MD alteration in the cingulate gyrus (Caverzasi et al., 2014a). Notably, related gray matter changes were found in the same participants as those in this study in our previous investigation, which further supports our results.

An FDG-PET study was previously conducted in the same participants included in this investigation. The FDG-PET study focused on gray matter alterations, and the results suggested hypometabolic changes in the parietal and temporal lobes in the preclinical stage of CJD (Lu et al., 2020). Although there is limited evidence supporting WM changes in non-affected carriers, preclinical gray matter changes in the same participants could suggest the involvement of WM. In our FDG-PET study, hypometabolism was observed in the parietal and temporal lobes, while increased MD was found in the superior longitudinal fasciculus, cingulate gyrus, and uncinate gyrus, which are connected to the temporal and parietal lobes (Vogt et al., 2004; Price et al., 2008; Merchant, 2018). These data infer possible metabolic decline in the parietal and temporal lobes, suggesting potential impairment of these WM tracts. Overall, these findings suggest that WM pathological changes occur in patients with preclinical CJD and are potentially correlated with CJD onset.

In our study, increased MD and normal FA were detected in the WM of asymptomatic carriers, while the same alterations were also detected in patients with CJD, and represent pathological imaging changes in the clinical stage of the disease. It may be assumed that the imaging patterns detected in asymptomatic carriers are preclinical pathological changes rather than being secondary to aging; however, the DTI alterations detected differ from those usually reported in patients with CJD

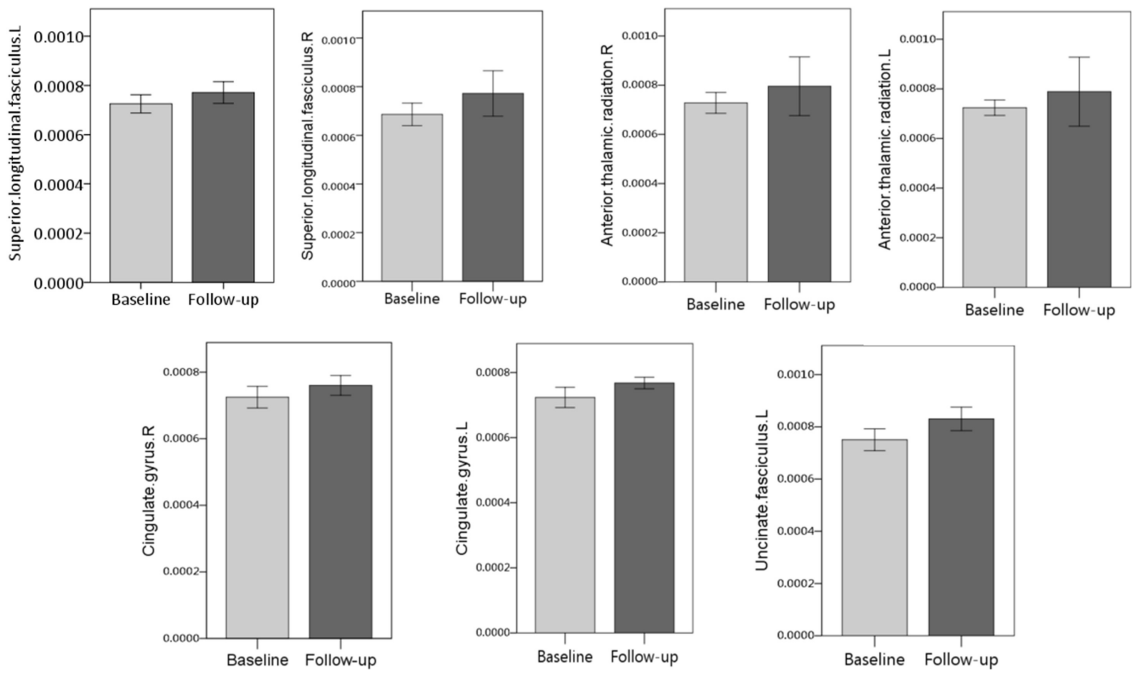

FIGURE 4 | Detailed MD changes (FWE correction, $P < 0.05$) in overlapping white matter (WM) tracts between asymptomatic carriers and patients with CJD are shown. Overlapping patterns were detected in the bilateral superior longitudinal fasciculus, bilateral thalamic radiation, bilateral cingulate gyrus, and left uncinate fasciculus.

(Wang et al., 2013; Caverzasi et al., 2014b), although they are consistent with some other studies with findings that support our results. Notably, a DTI study in patients with familial CJD detected increased MD in several WM tracts, which is consistent with our findings (Lee et al., 2012). Other DTI investigations in patients with sCJD patients also found increased MD in WM (Grau-Rivera et al., 2017). Elevated MD usually appears in patients with demyelination or axonal degeneration, which leads to less restricted movement of water (Lee et al., 2012; Wang et al., 2013; Tromp, 2016); this interpretation is supported by previous histopathological studies, which suggested patchy foci of demyelination in WM (Park et al., 1980; Macchi et al., 1983; Antoine et al., 1996), similar to the pathological changes associated with the second stage of the Braak hypothesis in CJD (Caverzasi et al., 2014b; Iwasaki, 2020). Therefore, we speculate that the increased MD in both asymptomatic carriers and symptomatic patients could be explained by demyelination in the WM. FA reflects the ratio of axial to radial diffusitivity (Wang et al., 2013). We hypothesize that, as the observed WM changes may impair water diffusion in all directions (Matsusue et al., 2004; Wang et al., 2013), which may be attributed to both demyelination and axonal degeneration (Wang et al., 2013), similar alterations in both axial and radial diffusion could account for the observed relative preservation of FA. A previous study of patients with CJD also found that FA was within the normal range, consistent with our findings (Wang et al., 2013). Furthermore, FA preservation was observed in both patients with CJD and asymptomatic carriers, which could further implicate the clinical imaging changes.

A strength of this study is that it shows the earliest known brain changes detected by DTI in the asymptomatic stage of fCJD, which were correlated with the gray matter alterations determined by FDG-PET; however, these results require further confirmation, as the study was limited by the small sample size, since fCJD is a very rare disease. Additionally, the symptomatic patients included in this study were not from the same kindred as the asymptomatic carriers and non-carriers. As our data were collected as part of an ongoing research project, we anticipate that further analyses will be conducted, to investigate the dynamic changes of indices between the asymptomatic and clinical disease stages.

CONCLUSION

In conclusion, the preliminary results from our TBSS analysis indicate increased MD in several WM tracts and suggest the involvement of WM integrity in the preclinical stage of fCJD. Overall, this study may provide new insights into CJD pathogenesis.

DATA AVAILABILITY STATEMENT

The original contributions presented in the study are included in the article/**Supplementary Material**, further inquiries can be directed to the corresponding author/s.

ETHICS STATEMENT

The studies involving human participants were reviewed and approved by Ethics Committee and local Institutional Review Board of Xuanwu Hospital, Capital Medical University, Beijing. The patients/participants provided their written informed consent to participate in this study.

AUTHOR CONTRIBUTIONS

DJ, YCh, ZZ, and LWa were responsible for the study concept and design. CC, HL, LL, JY, ZL, RG, and LWa were responsible for clinical data collection. YCh and ZZ analyzed the image results. DJ, KX, and YCu were the major contributors in writing the manuscript. ZZ and LWu were responsible for critical revision of the manuscript for important intellectual content. All authors contributed to the article and approved the submitted version.

FUNDING

This work was supported by the Ministry of Science and Technology of China (2019YFC0118600), the National Natural Science Foundation of China (No. 81971011), and Funding from Beijing Municipal Science and Technology Committee (D171100008217005 and 7202060). 333 talent project of Hebei Province as our funders and the grant numbers is A202001116.

ACKNOWLEDGMENTS

We are grateful to the patients and their families for granting us the permission to publish this information.

SUPPLEMENTARY MATERIAL

The Supplementary Material for this article can be found online at: https://www.frontiersin.org/articles/10.3389/fnagi.2021.655667/full#supplementary-material

REFERENCES

Antoine, J. C., Laplanche, J. L., Mosnier, J. F., Beaudry, P., Chatelain, J., and Michel, D. (1996). Demyelinating peripheral neuropathy with Creutzfeldt-Jakob disease and mutation at codon 200 of the prion protein gene. *Neurology* 46, 1123–1127. doi: 10.1212/wnl.46.4.1123

Caverzasi, E., Henry, R. G., Vitali, P., Lobach, I. V., Kornak, J., Bastianello, S., et al. (2014a). Application of quantitative DTI metrics in sporadic CJD. *Neuroimage Clin.* 4, 426–435. doi: 10.1016/j.nicl.2014.01.011

Caverzasi, E., Mandelli, M. L., DeArmond, S. J., Hess, C. P., Vitali, P., Papinutto, N., et al. (2014b). White matter involvement in sporadic Creutzfeldt-Jakob disease. *Brain* 137(Pt 12), 3339–3354.

Grau-Rivera, O., Calvo, A., Bargallo, N., Monte, G. C., Nos, C., Llado, A., et al. (2017). Quantitative magnetic resonance abnormalities in Creutzfeldt-Jakob disease and fatal insomnia. *J. Alzheimers Dis.* 55, 431–443. doi: 10.3233/jad-160750

Iwasaki, Y. (2020). The braak hypothesis in prion disease with a focus on Creutzfeldt-Jakob disease. *Neuropathology* 40, 436–449. doi: 10.1111/neup.12654

Jeong, B. H., and Kim, Y. S. (2014). Genetic studies in human prion diseases. *J. Korean Med. Sci.* 29, 623–632.

Lee, H., Cohen, O. S., Rosenmann, H., Hoffmann, C., Kingsley, P. B., Korczyn, A. D., et al. (2012). Cerebral white matter disruption in Creutzfeldt-Jakob disease. *AJNR Am. J. Neuroradiol.* 33, 1945–1950. doi: 10.3174/ajnr.a3125

Lee, H., Rosenmann, H., Chapman, J., Kingsley, P. B., Hoffmann, C., Cohen, O. S., et al. (2009). Thalamo-striatal diffusion reductions precede disease onset in prion mutation carriers. *Brain* 132(Pt 10), 2680–2687. doi: 10.1093/brain/awp064

Liu, Z., Jia, L., Piao, Y., Lu, D., Wang, F., Lv, H., et al. (2010). Creutzfeldt-Jakob disease with PRNP G114V mutation in a Chinese family. *Acta Neurol. Scand.* 121, 377–383. doi: 10.1111/j.1600-0404.2009.01236.x

Lu, H., Jing, D., Chen, Y., Cui, C., Gao, R., Wang, L., et al. (2020). Metabolic changes detected by 18F-FDG PET in the preclinical stage of familial Creutzfeldt-Jakob disease. *J. Alzheimers Dis.* 77, 1513–1521. doi: 10.3233/jad-200576

Macchi, G., Abbamondi, A. L., Di Trapani, G., and Sbriccoli, A. (1983). On the white matter lesions of the Creutzfeldt-Jakob disease. *J. Neurol. Sci.* 63, 197–206. doi: 10.1016/0022-510x(84)90196-5

Matsusue, E., Kinoshita, T., Sugihara, S., Fujii, S., Ogawa, T., and Ohama, E. (2004). White matter lesions in panencephalopathic type of Creutzfeldt-Jakob disease: MR imaging and pathologic correlations. *AJNR Am. J. Neuroradiol.* 25, 910–918.

Merchant, R. E. (2018). "Superior longitudinal fasciculus," in *Encyclopedia of Clinical Neuropsychology*, eds J. S. Kreutzer, J. DeLuca, and B. Caplan (New York, NY: Springer).

Park, T. S., Kleinman, G. M., and Richardson, E. P. (1980). Creutzfeldt-Jakob disease with extensive degeneration of white matter. *Acta Neuropathol. (Berl.)* 52, 239–242. doi: 10.1007/bf00705813

Price, G., Cercignani, M., Parker, G. J., Altmann, D. R., Barnes, T. R., Barker, G. J., et al. (2008). White matter tracts in first-episode psychosis: a DTI tractography study of the uncinate fasciculus. *Neuroimage* 39, 949–955. doi: 10.1016/j.neuroimage.2007.09.012

Takada, L. T., and Geschwind, M. D. (2013). Prion diseases. *Semin. Neurol.* 33, 348–356.

Tromp, D. (2016). *DTI Scalars (FA, MD, AD, RD) – How Do They Relate to Brain Structure?*. Roanoke, VA: The Winnower.

Vogt, B. A., Hof, P., and Vogt, L. J. (2004). "Cingulate gyrus," in *The Human Nervous System. Chapter 24*, eds G. Paxinos and J. K. Mai (Cambridge, MA: Academic Press), 915–949. doi: 10.1016/b978-012547626-3/50025-9

Wang, L. H., Bucelli, R. C., Patrick, E., Rajderkar, D., Alvarez Iii, E., Lim, M. M., et al. (2013). Role of magnetic resonance imaging, cerebrospinal fluid, and electroencephalogram in diagnosis of sporadic Creutzfeldt-Jakob disease. *J. Neurol.* 260, 498–506. doi: 10.1007/s00415-012-6664-6

Ye, J., Han, J., Shi, Q., Zhang, B. Y., Wang, G. R., Tian, C., et al. (2008). Human prion disease with a G114V mutation and epidemiological studies in a Chinese family: a case series. *J. Med. Case Rep.* 2:331.

Zerr, I., Kallenberg, K., Summers, D. M., Romero, C., Taratuto, A., Heinemann, U., et al. (2009). Updated clinical diagnostic criteria for sporadic Creutzfeldt-Jakob disease. *Brain* 132(Pt 10), 2659–2668.

Conflict of Interest: The authors declare that the research was conducted in the absence of any commercial or financial relationships that could be construed as a potential conflict of interest.

Advantages of publishing in Frontiers

OPEN ACCESS
Articles are free to read for greatest visibility and readership

FAST PUBLICATION
Around 90 days from submission to decision

HIGH QUALITY PEER-REVIEW
Rigorous, collaborative, and constructive peer-review

TRANSPARENT PEER-REVIEW
Editors and reviewers acknowledged by name on published articles

Frontiers
Avenue du Tribunal-Fédéral 34
1005 Lausanne | Switzerland

Visit us: www.frontiersin.org
Contact us: frontiersin.org/about/contact

REPRODUCIBILITY OF RESEARCH
Support open data and methods to enhance research reproducibility

DIGITAL PUBLISHING
Articles designed for optimal readership across devices

FOLLOW US
@frontiersin

IMPACT METRICS
Advanced article metrics track visibility across digital media

EXTENSIVE PROMOTION
Marketing and promotion of impactful research

LOOP RESEARCH NETWORK
Our network increases your article's readership